IUSS
Scuola Universitaria Superiore Pavia

Università di Camerino

ANTARCTIC BACTERIA: HARNESSING NATURE-BASED INNOVATION TO ADVANCE HUMAN HEALTH AND ENVIRONMENTAL SUSTAINABILITY

A Thesis Submitted in Partial Fulfilment of the Requirements
for the Degree of Doctor of Philosophy in

Sustainable Development and Climate change

Doctoral Programme of National Interest

PhD SDC
SUSTAINABLE DEVELOPMENT
AND CLIMATE CHANGE

In the Curriculum
HEALTH AND ECOSYSTEMS

Maria Chiara Biondini

May, 2026

IUSS
Scuola Universitaria Superiore Pavia

Università di Camerino

ANTARCTIC BACTERIA: HARNESSING NATURE-BASED INNOVATION TO ADVANCE HUMAN HEALTH AND ENVIRONMENTAL SUSTAINABILITY

A Thesis Submitted in Partial Fulfilment of the Requirements
for the Degree of Doctor of Philosophy in

Sustainable Development and Climate change

Doctoral Programme of National Interest

PhD SDC
SUSTAINABLE DEVELOPMENT
AND CLIMATE CHANGE

In the Curriculum
HEALTH AND ECOSYSTEMS

by

Maria Chiara Biondini

Supervisor: Prof. Sandra Pucciarelli

Co-Supervisor(s): Prof. Rita Giovannetti

Abstract

Antarctica offers an exceptional natural laboratory for studying the evolutionary mechanisms underlying environmental adaptation. Antarctic microorganisms have developed remarkable survival strategies to withstand extreme conditions such as cold temperatures, oxidative stress, UV radiation, and limited nutrient availability. In response to these environmental stressors, they evolved unique features, including the ability to detoxify hazardous compounds (e.g. heavy metals and pollutants), scavenge iron, and produce pigments, biofilms, and biopolymers that protect against UV damage and confer environmental defence.

The research focused on the exploitation of Antarctic bacterial metabolism to provide nature-based alternatives in favour of human health and environmental sustainability. The strains of interest, recently isolated from a consortium associated with the marine ciliate *E. focardii*, were identified and characterized, offering insights into their biotechnological potential.

The microorganisms were screened for the production of bacterial cellulose (BC), an emerging polymer with broad biotechnological applications. BC can be obtained through entirely eco-friendly biosynthetic process and exhibits higher purity, water holding capacity, and tensile strength resistance compared to plant-derived cellulose. The putative cellulose synthase responsible for BC synthesis was identified and characterized in comparison with that of the standard cellulose producer *K. xylinus*. Depending on the culture conditions, bacterial cellulose was obtained with different morphologies enabling diverse applications. A product for packaging is being developed in collaboration with

papermills, based on foil-shaped BC applied as a surface coating on conventional paper.

Furthermore, the strains were able to synthesize pigments with potential iron scavenging, antioxidant, antibacterial, and UV protective properties. Two novel bioactive molecules, including a pyocyanin derivative and a pyoverdine, were biosynthesised, extracted, and characterized.

The pyocyanin derivative, in particular, was employed as a reducing agent for AgNPs synthesis and as bioactive agent in combination with biomaterials for tissue engineering, including 3D printed scaffolds for bone restoration and electrospun nanofiber membranes for wound healing and skin regeneration. Based on genomic sequencing data, the putative structure of the operon responsible for the synthesis of the pigment was proposed.

Finally, novel Antarctic strains belonging to the family *Halomonadaceae* were isolated and characterized, showing the potential to produce polymers similar to bioplastics, opening new opportunities for future research and applications.

Acknowledgements

I would like to spend a few words to thank all the people who made the achievement of this goal possible.

This research work have been conducted during and with the support of the Italian inter-university PhD Programme in Sustainable Development and Climate Change (PhD-SDC; link: www.phd-sdc.it), to which I sincerely express my gratitude.

I would like to thank my supervisor, Prof. Sandra Pucciarelli, for having guided me throughout this journey with kindness and generosity, transmitting to me her passion for research. We developed a constructive relationship that allowed me to work always in a welcoming, encouraging, and positive environment.

I would also like to thank the people who collaborated with me over these years, in particular my co-supervisor, Prof. Rita Giovannetti, and her research group in the Chemistry Department, including Prof. Marco Zannotti and my colleague of the 39th cycle, Martina Di Sessa. We constantly cooperated and supported each other. Moreover, I would like to thank the researcher Alberto Vassallo and Prof. Cristina Miceli for their kindness and invaluable advice.

My gratitude also goes to Prof. Ilídio Joaquim Sobreira Correia for having welcomed me in his laboratory during my research period abroad, to the master's students David Lopes and Domenica Acosta, who constantly worked alongside me, to Prof. Duarte Miguel de Melo Diogo and the other students of UBI who were always ready to help. I also warmly thank all the wonderful people I met

during my time abroad, who made me feel at home even in moments when everything felt overwhelming.

A special mention goes to my colleagues of the 38th cycle, with whom I shared the entire experience, to the CU6 coordinator Prof. Marina Boido, and to all those who have supported us throughout these three years.

Finally, I particularly want to thank my family, Luca, my friends and all my loved ones for having taken care of me even in the most difficult times. Your role has been and continues to be fundamental in every aspect of my life, and it is to you that I dedicate this achievement.

Table of contents

List of figures

List of tables

General introduction

Research in a Changing Planet: Sustainability, Climate and Health

The profound environmental changes currently affecting the Earth have drawn increasing attention to the measures required to safeguard both planetary health and human well-being, highlighting the need for multidisciplinary approaches to understand these processes and to develop effective response strategies. The urgency to achieve sustainability in a context of decreasing resources and constantly increasing human population led to the formulation of the 2030 Agenda for Sustainable Development, with the adoption of seventeen Sustainable Development Goals in 2015 *(Cowan et al., 2024)*.

After ten years, the SDGs have improved the lives of millions of people worldwide. However, escalating conflicts, climate change, inequalities and insufficient financing mean that progress remains below what is required to meet the Goals by 2030. Only 35% of SDG targets with available data are showing progress, nearly 50% are moving too slowly, and 18%, instead, are regressing. In particular, the Goal 13 (Climate Action) remains critically off track. Global temperatures exceeded the 1.5 °C threshold in 2024, the hottest year on record, atmospheric carbon dioxide has reached a concentration equal to 151% of pre-industrial levels, and acidification of the oceans and biodiversity loss are intensifying *(United Nations, 2025)*. The most recent Intergovernmental Panel on Climate Change (IPCC) reports have also highlighted the critical state of the planet, outlining multiple future climate scenarios that depend on the mitigation and adaptation measures adopted. Several high-risks scenarios are projected for the next future, involving increases in climate hazards, including heat-related

human mortality and morbidity, the spread of food-, water-, and vector-borne diseases, mental health challenges, more frequent flooding events, biodiversity loss, decrease in food production and water availability across multiple regions. These risks could be limited through timely and effective mitigation and adaptation strategies within a rapidly narrowing window of opportunity (*Figure 1*). Therefore, coordinated action among institutions at global, national, and local levels is essential *(Calvin et al., 2023)*.

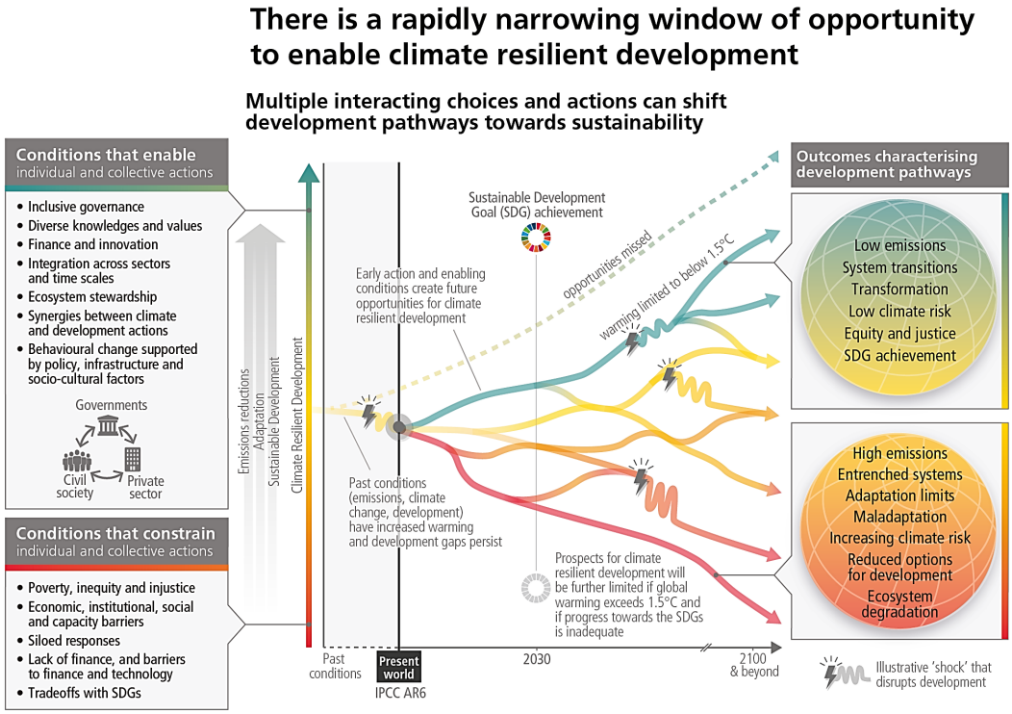

Figure 1 - The illustrative development pathways (red to green) and associated outcomes (right panel) show that there is a rapidly narrowing window of opportunity to secure a liveable and sustainable future for all (Calvin et al., 2023).

In this context, scientific research plays a crucial role by improving the understanding of climate-driven processes, supporting environmental monitoring and risk assessment, and developing innovative and sustainable solutions. In particular, universities contribute by connecting fundamental knowledge to applied innovation, by supporting institutional decision making, and by promoting education and awareness among people *(Blasco et al., 2020)*.

Thus, my contribution within the Doctoral Course of National Interest "Sustainable Development and Climate Change", focusing on the "Health and Ecosystems" themes of my curriculum, has followed these principles. Formation and education were constantly valorised through experimental investigations, educational activities for students, and participation in workshops, training courses, and conferences aimed at sharing ideas, knowledge, and achieved results. In parallel, efforts have been made to develop scientific collaborations in Italy and abroad and to involve industrial partners in order to build a bridge between research and industry. The final goal was to translate innovative research solutions into concrete applications, thanks to the support of our dedicated spin-off IrIdES with which I had the chance to collaborate during these three years.

In particular, the focus of my research was on extremophilic microorganisms as green and almost inexhaustible sources of bioactive molecules, innovative polymers, unique metabolic features and molecular pathways that remain largely unexplored. In the following section, an overview of scientific relevance of such organisms is provided, together with a summary of the background and development of the research projects in which I participated during the Doctoral course.

Extremophiles and extreme survival strategies: the case of the consortium associated with the Antarctic ciliate *Euplotes focardii*

In the context of an increasingly uncertain and rapidly changing climate, marked by the intensification of extreme events, extremophilic organisms have attracted growing interest within the scientific community. These organisms inhabit a wide range of inhospitable ecological niches worldwide, from polar regions and deep-sea hydrothermal vents to geothermal hot spring and the stratosphere (*Figure 2*) (Gallo & Aulitto, 2024). The remarkable adaptive strategies developed by these organisms to survive under harsh environmental conditions have been investigated to understand the origins of life and the potential for life on another planets *(Cowan et al., 2024)*. They can contribute to a deeper understanding of species adaptation to climate change and provide innovative biotechnological tools to address it, based on nature-inspired mechanisms. It has been recently shown that their conscious employment can significantly support sustainable development *(Cowan et al., 2024)*. Extremophiles can produce enzymes with unique characteristics (e. g. Taq polymerase), as they have evolved alternative pathways even for common metabolic functions, often relying on non-canonical genes or enzymatic strategies (Marzban & Tesei, 2025). In addition, they synthesize distinctive bioactive molecules with potent antioxidant, bioindicator, antimicrobial, antimalarial, antifungal, and anticancer activities *(Rather et al., 2023; T. R. e Silva et al., 2021)*, representing environmentally sustainable sources for biomedical applications of considerable value. Moreover, they can provide solutions for renewable energy production, including alternative energy sources *(Passarini et al., 2022)*, and biofuels *(Barnard et al., 2010)*, and have numerous applications in bioremediation, such

as heavy metal reduction *(Du et al., 2022)*. In some cases, the production of high-value compounds is coupled with efficient CO_2 fixation strategies, enhancing their contribution to sustainable biotechnology *(Cowan et al., 2024)*.

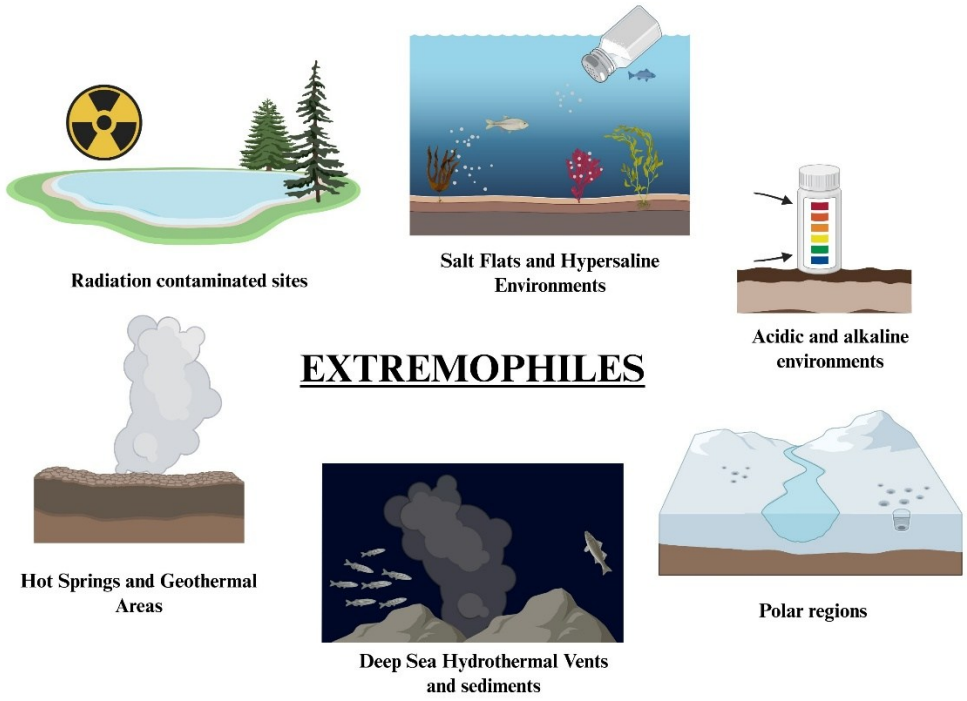

Figure 2 - Principal environments where the extremophilic microorganisms are found. Created in https://BioRender.com based on Gallo & Aulitto, 2024.

Among extremophilic ecological niches, polar regions harbour an extraordinary microbial diversity, thriving in hostile environments such as permafrost, glaciers, and polar seas. The evolution and structure of these microbial communities have been driven by multiple environmental factors, including persistently low temperatures, salinity fluctuations associated with sea-ice melting and formation processes, variable photoperiod influencing

photosynthetic processes, nutrient availability, and ocean currents (*Figure 3*) *(Gallo & Aulitto, 2024)*.

Southern Ocean, characterized by thermally stable and persistently cold environmental conditions, offers unique opportunities for studying speciation and evolutionary processes. This is largely due to the geographical isolation of the Antarctic continent following its separation from Gondwanaland and the formation of the Antarctic Polar Front approximately 25 million years ago, which has strongly limited gene flow from lower latitudes *(Pucciarelli et al., 2015)*.

Antarctic seawater hosts numerous microbial ecosystems. Among these, ciliated protozoa, heterotrophic unicellular eukaryotes, inhabit shallow coastal sediments. These organisms play a distinctive ecological role, as they provide niches for bacterial associations within different cellular compartments, including the nucleus, cytoplasm, perinuclear space, and cortical surface. It is believed that their relatively large size and their phagocytosis-based feeding strategy facilitate the establishment of bacterial symbiosis. These symbiotic relationships confer selective advantages to both partners, enhancing survival in extreme conditions *(John, Nagoth, Ramasamy, Ballarini, et al., 2020)*. For example, ciliates inhabiting anaerobic environments often depend on bacteria capable of using hydrogen as a primary metabolic substrate. While some interactions are obliged for both the ciliate hosts and the bacterial components, others appear to be facultative, providing benefits without being essential for host survival *(Pucciarelli et al., 2015)*.

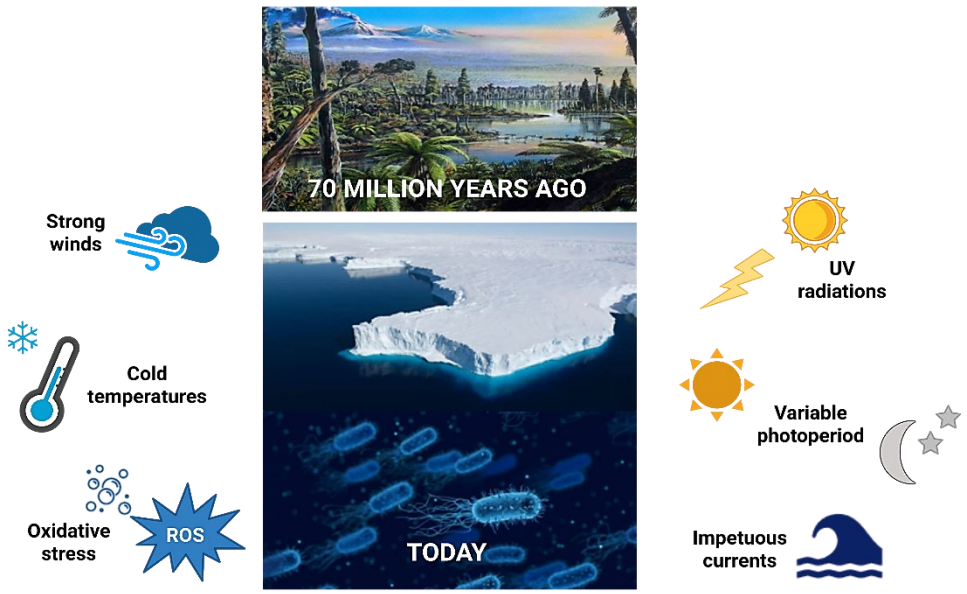

Figure 3 – The Antarctic continent, an exceptional environment to study adaptation under extreme conditions. Created in https://BioRender.com.

My scientific investigation journey began several years ago, when my predecessors discovered a new Antarctic marine protozoan, named *Euplotes focardii*. *E. focardii* is a free-swimming endemic ciliate inhabiting the oligotrophic coastal sediments of Terra Nova Bay (*Figure 4*). Its natural habitat is characterized by temperatures of −1.8 °C, salinity levels of 35‰, pH value ranging from 8.1 to 8.2. This ciliate is an obligate stenothermal psychrophilic microorganism, with optimal growth temperature of 4-5 °C under laboratory conditions *(John, Nagoth, Ramasamy, Ballarini, et al., 2020)*. Thus, *E. focardii* represents a valuable model for studying adaptation to low temperatures and elevated oxidative stress typical of marine polar environments, where the

increased solubility of oxygen at low temperatures leads to higher intracellular levels of reactive oxygen species *(Pucciarelli et al., 2015)*.

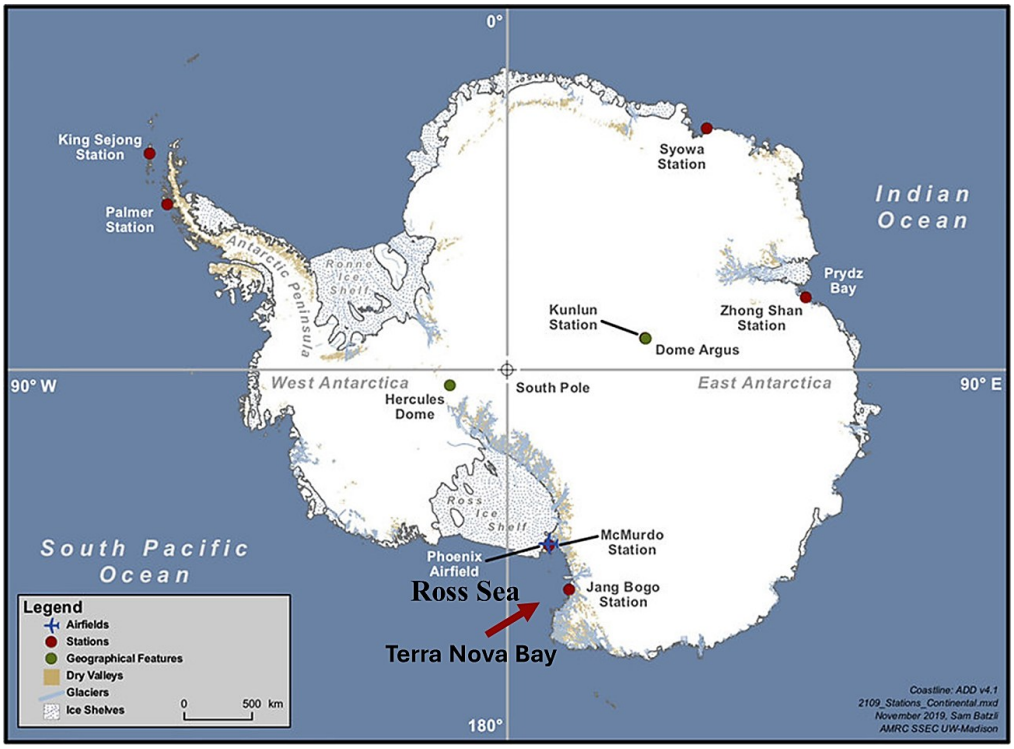

Figure 4 – Image of the Antarctic continent showing the location of Terra Nova Bay where the samples with E. focardii were collected (Lazzara et al., 2020).

The bacterial consortium associated with *E. focardii* has been firstly characterized through Illumina-based metagenomic analyses, identifying 11,179 contigs of putative prokaryotic origin. Within this community, *Bacteroidetes* (16 %), and *Proteobacteria* (78%) were predominant. Proteobacteria were mainly represented by *gamma-Proteobacteria* (39%), and *alpha-Proteobacteria* (30%) (*Figure 5*) *(Pucciarelli et al., 2015).* Genomic analyses revealed several distinctive genomic features of this bacterial consortium, including the ability to

use alternative carbon sources, store energy in high molecular weight compounds, such as polyhydroxyalkanoates, degrade aromatic compounds, synthesise anti-freeze and ice-binding proteins, and also numerous enzymes with oxidoreductase activity. Therefore, the consortium may play a key ecological role in coping with the prohibitive temperatures, high oxygen levels, and limited nutrient availability in these extreme environmental conditions *(Pucciarelli et al., 2015)*.

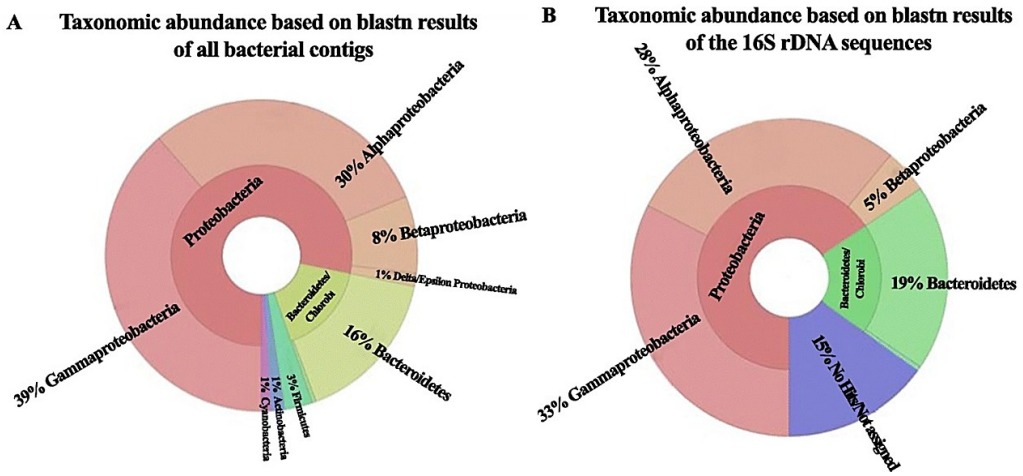

Figure 5 - Pie charts of the taxonomic abundance of the bacterial consortium based on BLASTn results of all the contigs (a) and of the 16S rDNA sequences (b) (Pucciarelli et al., 2015).

In subsequent years, several bacterial strains were isolated from the consortium and characterized in detail.

The first bacterial strain to be isolated was *Marinomonas* sp. ef1, which was shown to efficiently synthesise silver, copper and nickel nanoparticles with antimicrobial activity, degrade diesel and utilize biodiesel to produce a pigment belonging to the pyoverdine family of siderophores *(John et al., 2021a; John,*

Nagoth, Ramasamy, Ballarini, et al., 2020; Nagoth et al., 2024; Zannotti et al., 2023). The ability to degrade hydrocarbons and detoxify heavy metals through the synthesis of metallic nanoparticles with antimicrobial effect may represent an additional adaptive strategy which contributes to protecting both the bacterium and its ciliate host from environmental toxicity and pathogens.

Pseudomonas sp. ef1 also attracted particular interest due to its predicted capacity to remove toxic heavy metals and degrade aromatic hydrocarbons, as inferred from genome analyses. This bacterial strain presented 107 genes potentially associated with the metabolism of aromatic compounds and contains multiple genes involved in metal resistance and metal transport *(Ramasamy et al., 2019)*. Subsequently, *Pseudomonas* sp. ef1 was shown to be capable of producing silver, copper and nickel nanoparticles with antimicrobial activity, highlighting its potential application in bioremediation and biomedical fields *(John et al., 2021a; John, Nagoth, Ramasamy, Mancini, et al., 2020; Nagoth et al., 2024)*.

Other bacterial strains of interest are represented by *Bacillus* sp. ef1, *Brevundimonas* sp. ef1, and *Rhodococcus* sp. ef1, which have been also characterized as metallic nanoparticles producers with effective antimicrobial activity *(John et al., 2021a; Nagoth et al., 2024).*

Thesis aims, contents, and contributions to SDGs

The aim of this Doctoral Thesis is to advance knowledge of the bacterial consortium associated with *E. focardii*, with the goal of uncovering novel biotechnological and industrial potentials in favour of human health and ecosystem protection.

In continuity with previous research, this work provides additional insights into the microbial consortium through further biotechnological characterization of the bacterial strains and genome sequencing approach. Thus, *Pseudomonas* sp. ef1 was demonstrated to produce bacterial cellulose (BC) and novel pyoverdines, as reported in two scientific publications in which I contributed *(Biondini et al., 2025; Zannotti et al., 2026)*. *Rhodococcus* sp. ef1 was shown to be capable of producing a novel pyocyanin derivative and of potentially accumulating polyhydroxyalkanoates. Moreover, the bacterial strains previously isolated by my research group were subjected to further biotechnological characterization, including *Bacillus* sp. ef1 and *Brevundimonas* sp. ef1. Additionally, other members of the consortium were identified, isolated, and characterized, including several strains belonging to the *Halomonadaceae* family, as well as a novel Antarctic strain named *Brevundimonas* sp. #2. This latter is not part of the consortium associated with *E. focardiii*, but it was isolated from a sample of Antarctic water collected at Edmonson point during the 37th expedition of the PNRA (National Program of Antarctic Research).

Figure 6 provides an overview of the biotechnological potential of the microbial consortium unravelled to date.

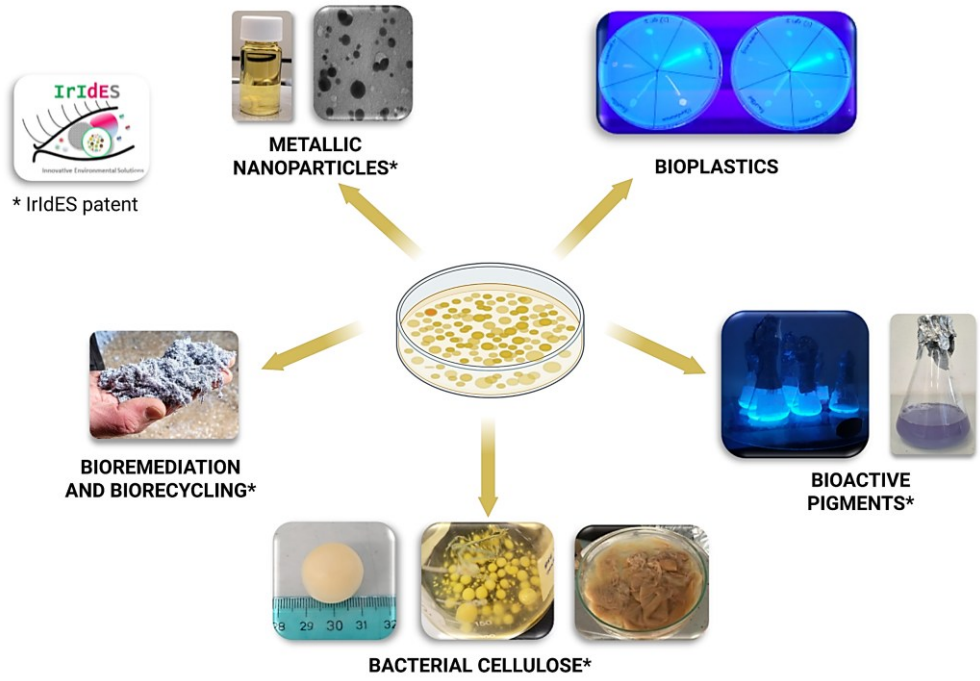

Figure 6 - Biotechnological potential of Antarctic bacterial strains isolated in our laboratory.

Overall, this research is aligned with the Sustainable Development Goals (SDGs) assigned to my research project, in particular SDG 3 (Good Health and Well-Being), SDG 6 (Clean Water and Sanitation), and SDG 13 (Climate Action).

The increasing demand for sustainable and environmentally friendly materials has guided research into biological alternatives capable of reducing the dependence on fossil resources and mitigating ecosystem degradation. In this context, microbial-derived biopolymers and bioactive molecules are emerging as promising solutions due to their renewable nature, low environmental impact, and versatility across different industrial sectors *(Hu et al., 2025)*.

Globally, the planet is losing approximately 5 million hectares of forests every year. Deforestation is dramatically associated with increasing concentrations of carbon dioxide, soil erosion, and biodiversity loss. A significant fraction of forest loss is driven by the high demand for forestry goods such as paper and wood *(Curtis et al., 2018)*. Consequently, the research for alternative materials capable of partially replacing conventional materials associated with ecosystem degradation has become a priority. Within this framework, part of this doctoral research focused on the synthesis and optimization of bacterial cellulose (BC), a biopolymer obtained through entirely green protocols. This emerging material has numerous biotechnological, industrial, and medical applications *(Raghavendran, 2020)*. Thus, optimization of BC production at an industrial scale could contribute to partially mitigating forest exploitation. The use of unexpensive media including waste recycling can help reduce production costs *(Kadier et al., 2021)*.

Among the possible applications, BC is remarkably appreciated in the food industry, serving as a novel biomaterial and as a degradable and edible packaging *(Sayah et al., 2024)*. This application is relevant considering the environmental impact of plastic packaging, linked to high CO_2 emissions during plastic production, short life-span and poor recyclability of these products, leading to waste accumulation in terrestrial and marine ecosystems. Around 8 million tons of plastic are estimated to enter the ocean every year *(García Rellán et al., 2023)*. Besides, fragmentation of plastic debris is associated to the formation of microplastics that can be detected even in the most pristine environments and can easily enter the food chain affecting human health *(Islam et al., 2024)*. Since packaging accounts for nearly 40% of plastic usage, the development of sustainable alternatives is crucial. Moreover, plastic packaging materials are

known to release chemicals such as phthalates and bisphenol A, and most food contact materials are estimated to contain non-intentionally added substances (NIAS), a major part of which remains unidentified *(Horodytska et al., 2020; Sheriff et al., 2025)*.

In this regard, the accumulation of bioplastics by microorganisms in the form of polyhydroxyalkanoates (PHAs) was investigated in this thesis. PHAs represent valuable eco-friendly substitutes for conventional plastics *(Sirohi et al., 2021)*. Evidence suggests that bioplastics can reduce carbon footprint and dependence on fossil fuels, particularly in sectors characterized by high consumption of disposable plastics such as the medical and food-packaging sectors. Since approximately 90% of plastic waste ultimately ends up in landfills, contaminating soil and groundwater and threatening ecosystems, application of biodegradable and biocompatible PHAs contributes both to environmental and human health protection *(Bhatia et al., 2021; J. Lee et al., 2021)*.

Moreover, bacterial pigments and other bioactive secondary metabolites are emerging as high-value biomolecules due to their sustainable production and unique properties. Since these metabolites can be produced through low-impact bioprocesses, they represent attractive alternatives to synthetic molecules traditionally used in food, cosmetic, and pharmaceutic industry *(Celedón & Díaz, 2021)*. In addition to their chromatic properties, many bacterial pigments exhibit antioxidant, antimicrobial, anticancer, and cytoprotective activities, particularly efficient in case of extremophilic producers *(Rather et al., 2023; T. R. e Silva et al., 2021)*. In the context of climate change-driven increasing antimicrobial resistance and growing incidence of infectious and neurodegenerative diseases *(Abbass et al., 2022; Bongioanni et al., 2021)*, the identification of novel non-toxic bioactive compounds is essential to support

human health while minimizing environmental impact. Therefore, efforts were made in the synthesis, optimization, and characterization of novel bacterial pigments, with preliminary characterization studies of their biotechnological potential.

Finally, the study of extremophilic microorganisms offers unique opportunities in the fields of bioremediation and CO_2 fixation *(Cowan et al., 2024)*. Carbon dioxide rising levels, largely driven by fossil fuel combustion and human-related activities, are having a profound impact on the balance of the planet, threatening ecosystem stability *(Nunes, 2023)*. Microbial processes capable of capturing carbon or contributing to pollutant degradation may represent innovative tools to mitigate climate change effects and improve environmental quality *(Cavicchioli et al., 2019)*.

Overall, extremophilic microorganisms with their unique metabolic pathways and survival strategies offer a unique perspective of adaptation and resilience under extreme conditions and can represent an exceptional biological resource for the development of sustainable biotechnological applications.

Thesis structure and organization

According to the different themes addressed, this work is organized into five chapters, each focusing on a specific aspect of my research.

The first chapter focuses on bacterial cellulose production mediated by different Antarctic strains, with particular attention to the two most efficient producers, *Pseudomonas* sp. ef1 and *Brevundimonas* sp. #2.

The second chapter investigates the ability of *Rhodococcus* sp. ef1 to produce a novel pyocyanin derivative, including its chemical characterization, molecular

elucidation of putative biosynthetic pathways involved, and a preliminary exploration of its biotechnological potential.

The third chapter is dedicated to the research conducted during the period abroad, during which the pigment was tested for biomedical applications in collaboration with the University of Beira Interior (Portugal). The bioactive pigment was employed to synthesise silver nanoparticles (AgNPs) using an innovative protocol. Both pyocyanin derivative and the resulting AgNPs were incorporative as bioactive agents into electrospun nanofiber membranes for skin regeneration and 3D-printed scaffolds for bone tissue restoration and regeneration.

In the fourth chapter, the synthesis and chemical characterization of two siderophores produced by *Pseudomonas* sp. ef1, including a novel pyoverdine, was reported.

Finally, the fifth and last chapter provides insights into novel strains belonging to the *Halomonadaceae* taxonomic group isolated from the consortium during the PhD research, presenting their preliminary characterization and an initial assessment of their biotechnological potential.

In the following sections, further information is provided in detail on each theme addressed in this research.

References

Abbass, K., Qasim, M. Z., Song, H., Murshed, M., Mahmood, H., & Younis, I. (2022). A review of the global climate change impacts, adaptation, and sustainable mitigation measures. *Environmental Science and Pollution Research*, *29*(28), 42539–42559. https://doi.org/10.1007/s11356-022-19718-6

Barnard, D., Casanueva, A., Tuffin, M., & Cowan, D. (2010). Extremophiles in biofuel synthesis. *Environmental Technology*, *31*(8–9), 871–888. https://doi.org/10.1080/09593331003710236

Bhatia, S. K., Otari, S. V., Jeon, J.-M., Gurav, R., Choi, Y.-K., Bhatia, R. K., Pugazhendhi, A., Kumar, V., Rajesh Banu, J., Yoon, J.-J., Choi, K.-Y., & Yang, Y.-H. (2021). Biowaste-to-bioplastic (polyhydroxyalkanoates): Conversion technologies, strategies, challenges, and perspective. *Bioresource Technology*, *326*, 124733. https://doi.org/10.1016/j.biortech.2021.124733

Biondini, M. C., Di Sessa, M., Vassallo, A., Chiappori, F., Zannotti, M., Mancini, A., Giovannetti, R., & Pucciarelli, S. (2025). Cellulose and Cellulose Synthase in a Marine Pseudomonas Strain from Antarctica: Characterization, Adaptive Implications, and Biotechnological Potential. *Marine Drugs*, *23*(10), 410. https://doi.org/10.3390/md23100410

Blasco, N., Brusca, I., & Labrador, M. (2020). Drivers for Universities' Contribution to the Sustainable Development Goals: An Analysis of Spanish Public Universities. *Sustainability*, *13*(1), 89. https://doi.org/10.3390/su13010089

Bongioanni, P., Del Carratore, R., Corbianco, S., Diana, A., Cavallini, G., Masciandaro, S. M., Dini, M., & Buizza, R. (2021). Climate change and

neurodegenerative diseases. *Environmental Research*, *201*, 111511. https://doi.org/10.1016/j.envres.2021.111511

Calvin, K., Dasgupta, D., Krinner, G., Mukherji, A., Thorne, P. W., Trisos, C., Romero, J., Aldunce, P., Barret, K., Blanco, G., Cheung, W. W. L., Connors, S. L., Denton, F., Diongue-Niang, A., Dodman, D., Garschagen, M., Geden, O., Hayward, B., Jones, C., … Ha, M. (2023). *IPCC, 2023: Climate Change 2023: Synthesis Report, Summary for Policymakers. Contribution of Working Groups I, II and III to the Sixth Assessment Report of the Intergovernmental Panel on Climate Change [Core Writing Team, H. Lee and J. Romero (eds.)]. IPCC, Geneva, Switzerland.* https://doi.org/10.59327/IPCC/AR6-9789291691647.001

Cavicchioli, R., Ripple, W. J., Timmis, K. N., Azam, F., Bakken, L. R., Baylis, M., Behrenfeld, M. J., Boetius, A., Boyd, P. W., Classen, A. T., Crowther, T. W., Danovaro, R., Foreman, C. M., Huisman, J., Hutchins, D. A., Jansson, J. K., Karl, D. M., Koskella, B., Mark Welch, D. B., … Webster, N. S. (2019). Scientists' warning to humanity: microorganisms and climate change. *Nature Reviews Microbiology*, *17*(9), 569–586. https://doi.org/10.1038/s41579-019-0222-5

Celedón, R. S., & Díaz, L. B. (2021). Natural Pigments of Bacterial Origin and Their Possible Biomedical Applications. *Microorganisms*, *9*(4), 739. https://doi.org/10.3390/microorganisms9040739

Cowan, D. A., Albers, S. V., Antranikian, G., Atomi, H., Averhoff, B., Basen, M., Driessen, A. J. M., Jebbar, M., Kelman, Z., Kerou, M., Littlechild, J., Müller, V., Schönheit, P., Siebers, B., & Vorgias, K. (2024). Extremophiles in a changing world. *Extremophiles*, *28*(2), 26. https://doi.org/10.1007/s00792-024-01341-7

Curtis, P. G., Slay, C. M., Harris, N. L., Tyukavina, A., & Hansen, M. C. (2018). Classifying drivers of global forest loss. *Science*, *361*(6407), 1108–1111. https://doi.org/10.1126/science.aau3445

Du, R., Gao, D., Wang, Y., Liu, L., Cheng, J., Liu, J., Zhang, X.-H., & Yu, M. (2022). Heterotrophic Sulfur Oxidation of Halomonas titanicae SOB56 and Its Habitat Adaptation to the Hydrothermal Environment. *Frontiers in Microbiology*, *13*. https://doi.org/10.3389/fmicb.2022.888833

Gallo, G., & Aulitto, M. (2024). Advances in Extremophile Research: Biotechnological Applications through Isolation and Identification Techniques. *Life*, *14*(9), 1205. https://doi.org/10.3390/life14091205

García Rellán, A., Vázquez Ares, D., Vázquez Brea, C., Francisco López, A., & Bello Bugallo, P. M. (2023). Sources, sinks and transformations of plastics in our oceans: Review, management strategies and modelling. *Science of The Total Environment*, *854*, 158745. https://doi.org/10.1016/j.scitotenv.2022.158745

Horodytska, O., Cabanes, A., & Fullana, A. (2020). Non-intentionally added substances (NIAS) in recycled plastics. *Chemosphere*, *251*, 126373. https://doi.org/10.1016/j.chemosphere.2020.126373

Hu, S., Shi, Z., Chen, K., Chen, X., Zhou, H., Yan, N., & Yang, G. (2025). Bacterial cellulose as green matrix material for environmental-friendly electronic devices. *Carbohydrate Polymers*, *368*, 124075. https://doi.org/10.1016/j.carbpol.2025.124075

Islam, M., Xayachak, T., Haque, N., Lau, D., Bhuiyan, M., & Pramanik, B. K. (2024). Impact of bioplastics on environment from its production to end-of-life. *Process*

Safety and Environmental Protection, *188*, 151–166. https://doi.org/10.1016/j.psep.2024.05.113

John, M. S., Nagoth, J. A., Ramasamy, K. P., Ballarini, P., Mozzicafreddo, M., Mancini, A., Telatin, A., Liò, P., Giuli, G., Natalello, A., Miceli, C., & Pucciarelli, S. (2020). Horizontal gene transfer and silver nanoparticles production in a new Marinomonas strain isolated from the Antarctic psychrophilic ciliate Euplotes focardii. *Scientific Reports*, *10*(1), 10218. https://doi.org/10.1038/s41598-020-66878-x

John, M. S., Nagoth, J. A., Ramasamy, K. P., Mancini, A., Giuli, G., Natalello, A., Ballarini, P., Miceli, C., & Pucciarelli, S. (2020). Synthesis of Bioactive Silver Nanoparticles by a Pseudomonas Strain Associated with the Antarctic Psychrophilic Protozoon Euplotes focardii. *Marine Drugs*, *18*(1), 38. https://doi.org/10.3390/md18010038

John, M. S., Nagoth, J. A., Zannotti, M., Giovannetti, R., Mancini, A., Ramasamy, K. P., Miceli, C., & Pucciarelli, S. (2021). Biogenic Synthesis of Copper Nanoparticles Using Bacterial Strains Isolated from an Antarctic Consortium Associated to a Psychrophilic Marine Ciliate: Characterization and Potential Application as Antimicrobial Agents. *Marine Drugs*, *19*(5), 263. https://doi.org/10.3390/md19050263

Kadier, A., Ilyas, R. A., Huzaifah, M. R. M., Harihastuti, N., Sapuan, S. M., Harussani, M. M., Azlin, M. N. M., Yuliasni, R., Ibrahim, R., Atikah, M. S. N., Wang, J., Chandrasekhar, K., Islam, M. A., Sharma, S., Punia, S., Rajasekar, A., Asyraf, M. R. M., & Ishak, M. R. (2021). Use of Industrial Wastes as Sustainable Nutrient Sources for Bacterial Cellulose (BC) Production: Mechanism,

Advances, and Future Perspectives. *Polymers*, *13*(19), 3365. https://doi.org/10.3390/polym13193365

Lazzara, M. A., Orendorf, S. A., Norton, T. P., Powers, J. G., Bromwich, D. H., Carpentier, S., Cassano, J. J., Colwell, S. R., Cayette, A. M., & Werner, K. (2020). The 13th and 14th Workshops on Antarctic Meteorology and Climate. *Advances in Atmospheric Sciences*, *37*(5), 423–430. https://doi.org/10.1007/s00376-019-9215-6

Lee, J., Park, H. J., Moon, M., Lee, J.-S., & Min, K. (2021). Recent progress and challenges in microbial polyhydroxybutyrate (PHB) production from CO2 as a sustainable feedstock: A state-of-the-art review. *Bioresource Technology*, *339*, 125616. https://doi.org/10.1016/j.biortech.2021.125616

Marzban, G., & Tesei, D. (2025). The Extremophiles: Adaptation Mechanisms and Biotechnological Applications. *Biology*, *14*(4), 412. https://doi.org/10.3390/biology14040412

Nagoth, J. A., John, M. S., Ramasamy, K. P., Mancini, A., Zannotti, M., Piras, S., Giovannetti, R., Rathnam, L., Miceli, C., Biondini, M. C., & Pucciarelli, S. (2024). Synthesis of Bioactive Nickel Nanoparticles Using Bacterial Strains from an Antarctic Consortium. *Marine Drugs*, *22*(2), 89. https://doi.org/10.3390/md22020089

Nunes, L. J. R. (2023). The Rising Threat of Atmospheric CO2: A Review on the Causes, Impacts, and Mitigation Strategies. *Environments*, *10*(4), 66. https://doi.org/10.3390/environments10040066

Órdenes-Aenishanslins, N., Anziani-Ostuni, G., Vargas-Reyes, M., Alarcón, J., Tello, A., & Pérez-Donoso, J. M. (2016). Pigments from UV-resistant Antarctic

bacteria as photosensitizers in Dye Sensitized Solar Cells. *Journal of Photochemistry and Photobiology B: Biology*, *162*, 707–714. https://doi.org/10.1016/j.jphotobiol.2016.08.004

Passarini, M. R. Z., Duarte, A. W. F., Rosa, L. H., de Oliveira, V. M., & Ottoni, J. R. (2022). Extremofuels: production of biofuels by extremophile microbes as an alternative to avoid climate change effects. In *Microbiome Under Changing Climate* (pp. 237–256). Elsevier. https://doi.org/10.1016/B978-0-323-90571-8.00010-9

Pucciarelli, S., Devaraj, R. R., Mancini, A., Ballarini, P., Castelli, M., Schrallhammer, M., Petroni, G., & Miceli, C. (2015). Microbial Consortium Associated with the Antarctic Marine Ciliate Euplotes focardii: An Investigation from Genomic Sequences. *Microbial Ecology*, *70*(2), 484–497. https://doi.org/10.1007/s00248-015-0568-9

Raghavendran, V. , A. E. , and R. I. (2020). Bacterial cellulose: Biosynthesis, production, and applications. In *Advances in Microbial Physiology* (Vol. 77, pp. 89–138). https://doi.org/10.1016/bs.ampbs.2020.07.002

Ramasamy, K. P., Telatin, A., Mozzicafreddo, M., Miceli, C., & Pucciarelli, S. (2019). Draft Genome Sequence of a New Pseudomonas sp. Strain, ef1, Associated with the Psychrophilic Antarctic Ciliate Euplotes focardii. *Microbiology Resource Announcements*, *8*(41). https://doi.org/10.1128/MRA.00867-19

Rather, L. J., Mir, S. S., Ganie, S. A., Shahid-ul-Islam, & Li, Q. (2023). Research progress, challenges, and perspectives in microbial pigment production for industrial applications - A review. *Dyes and Pigments*, *210*, 110989. https://doi.org/10.1016/j.dyepig.2022.110989

Sayah, I., Gervasi, C., Achour, S., & Gervasi, T. (2024). Fermentation Techniques and Biotechnological Applications of Modified Bacterial Cellulose: An Up-to-Date Overview. *Fermentation*, *10*(2), 100. https://doi.org/10.3390/fermentation10020100

Sheriff, S. S., Yusuf, A. A., Akiyode, O. O., Hallie, E. F., Odoma, S., Yambasu, R. A., Thompson-Williams, K., Asumana, C., Gono, S. Z., & Kamara, M. A. (2025). A comprehensive review on exposure to toxins and health risks from plastic waste: Challenges, mitigation measures, and policy interventions. *Waste Management Bulletin*, *3*(3), 100204. https://doi.org/10.1016/j.wmb.2025.100204

Silva, T. R. e, Silva, L. C. F., de Queiroz, A. C., Alexandre Moreira, M. S., de Carvalho Fraga, C. A., de Menezes, G. C. A., Rosa, L. H., Bicas, J., de Oliveira, V. M., & Duarte, A. W. F. (2021). Pigments from Antarctic bacteria and their biotechnological applications. *Critical Reviews in Biotechnology*, *41*(6), 809–826. https://doi.org/10.1080/07388551.2021.1888068

Sirohi, R., Kumar Gaur, V., Kumar Pandey, A., Jun Sim, S., & Kumar, S. (2021). Harnessing fruit waste for poly-3-hydroxybutyrate production: A review. *Bioresource Technology*, *326*, 124734. https://doi.org/10.1016/j.biortech.2021.124734

United Nations. (2025). *Progress towards the Sustainable Development Goals. Report of the Secretary-General*. https://doi.org/A/80/81-E/2025/62

Zannotti, M., Di Sessa, M., Biondini, M. C., Vassallo, A., Ferraro, S., Angeloni, S., Ricciutelli, M., Pucciarelli, S., & Giovannetti, R. (2026). Towards an easy production of novel pyoverdines by an antarctic Pseudomonas strain: a

spectroscopic and HPLC-MS/MS characterization study. *Dyes and Pigments*, *244*, 113096. https://doi.org/10.1016/j.dyepig.2025.113096

Zannotti, M., Ramasamy, K. P., Loggi, V., Vassallo, A., Pucciarelli, S., & Giovannetti, R. (2023). Hydrocarbon degradation strategy and pyoverdine production using the salt tolerant Antarctic bacterium *Marinomonas* sp. ef1. *RSC Advances*, *13*(28), 19276–19285. https://doi.org/10.1039/D3RA02536E

CHAPTER 1

Bacterial cellulose synthesis using Antarctic bacteria

This chapter is extensively based on the following publication, to which I contributed as the leading author, primarily to the methodology and formal analysis:

Biondini, M.C., Di Sessa, M., Vassallo, A., Chiappori, F., Zannotti, M., Mancini, A., Giovannetti, R., Pucciarelli, S. (2025). Cellulose and Cellulose Synthase in a Marine Pseudomonas Strain from Antarctica: Characterization, Adaptive Implications, and Biotechnological Potential. https://doi.org/10.3390/md23100410

Abstract

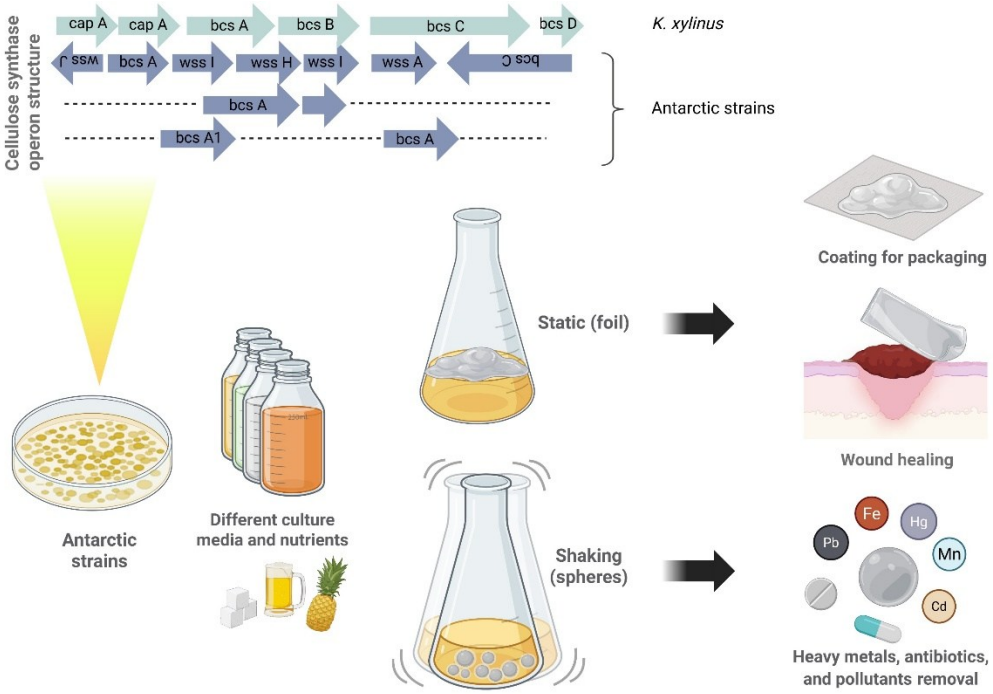

Figure 7- Graphical abstract of bacterial cellulose synthesis and applications. Created in https://BioRender.com.

This section of the thesis focuses on the synthesis of bacterial cellulose (BC) using recently isolated Antarctic bacterial strains.

Cellulose is the most abundant polymer on Earth, but its industrial use is often associated with environmental exploitation and deforestation. Although it is difficult to claim that bacterial cellulose is capable of fully replacing its vegetal counterpart, the search for alternative sources may nonetheless contribute significantly to ecosystem protection. Beyond its potential use as a substitute for paper film - currently limited by low production yields – bacterial cellulose

exhibits unique physicochemical properties which make it a promising material for innovative applications in packaging, biomedicine, and bioremediation.

Due to their remarkable evolutionary history, Antarctic bacteria have evolved unique survival strategies to cope with extreme environmental conditions, including the ability to produce cellulose-based biofilms. These biofilms may confer several advantages, such as facilitating surface colonization and preventing desiccation. Evolutionary pressure has often led to the activation of alternative biosynthetic pathways which may be exploited for biotechnological applications. Thus, these organisms represent valuable natural sources of innovative compounds and biopolymers with exclusive properties, opening the way to a wide range of potential applications.

The research investigated the potential of different Antarctic strains to produce BC under different culture conditions, to identify the most suitable parameters and culture media for each strain. *K. xylinus*, a well-established cellulose producer, was used as a reference standard. Analytical investigations conducted in collaboration with the Chemistry Department confirmed BC production and provided a chemical characterization of the polymer. Genetic studies were also conducted to elucidate the structure of the operon involved in the biosynthetic process, comparing the organization of the Antarctic microorganisms with that of *K. xylinus*.

Finally, the biosynthetic BC was tested in collaboration with papermills to develop a material suitable for packaging application. Future perspectives also include the application of bacterial cellulose for wound healing and

bioremediation to remove environmental pollutants, antibiotics, and heavy metals.

State of the art

Antarctica provides a unique natural laboratory to investigate the evolutionary processes behind environmental adaptation. Antarctic microorganisms have developed extraordinary survival strategies, including the ability to resist cold temperatures, oxidative stress, and UV radiation, to scavenge iron present in limited concentrations, and to detoxify hazardous compounds, such as heavy metals and pollutants *(Ramasamy et al., 2023)*. They have also shown the ability to produce different pigments and biopolymers in response to environmental stress factors *(Ramasamy et al., 2023)*. Cellulose forms the basic structural foundation of the primary cell wall of green plants, algae, and fungi *(Brigham, 2018)* and it is the main constituent of natural fibers such as cotton *(Felgueiras et al., 2021)*. It is a polysaccharide consisting of a linear chain of several β (1→4) linked D-glucose units and represents the most abundant organic polymer on Earth *(Felgueiras et al., 2021)*. Cellulose is also present in bacteria, the so-called nanocellulose *(Krasteva et al., 2017; Lahiri et al., 2021a)*. The biosynthesis of Bacterial cellulose (BC) has been observed many years ago by ancient Chinese growing the Kombucha tea mushroom, a syntrophic colony of acetic acid bacteria and yeast, which metabolizes sugar to produce a slightly acidic tea-colored drink and forms a thick cellulosic mat at its surface *(Marsh et al., 2014)*. BC was then reported by Brown in 1886, who identified the growth of a non-branched pellicle with a structure chemically equivalent to that of plant cellulose *(Poddar & Dikshit, 2021)*. Despite the similarities in the chemical structures, BC showed higher purity, water holding capacity, and tensile strength resistance compared to the vegetal counterpart *(Gorgieva & Trček, 2019a)*. While plant-derived cellulose is typically associated with lignin and hemicelluloses, thus

requiring component separation prior to use, BC consists of highly pure, parallel cellulose chains composed of -D-glucopyranose units interconnected by intermolecular hydrogen bonds *(Mohammadkazemi et al., 2015)*. Additionally, BC fibrils are 100 times smaller than those produced by the plants, a feature of particular relevance for biomedical applications, as it enables the mimicry of the extracellular matrix in tissue engineering *(I. G. R. da Silva et al., 2022)*. Moreover, BC can be obtained through entirely green protocols, respecting the integrity of ecosystems and the principles of the circular economy*(Raghavendran, 2020)*. According to global assessment, the world is losing 5 million hectares of forests every year, with an estimated 13% of deforestation driven by the demand for forestry goods such as paper and wood *(H. Ritchie, 2021)*. In this context, the optimization of BC production at an industrial scale could contribute to partially mitigating forest exploitation. Therefore, consistently with the growing demand for natural biopolymers in industrial applications aimed at minimizing the impact of petroleum-based materials, BC is emerging as a promising sustainable alternative *(Hu et al., 2025)*.

In recent year, BC has been evaluated as a promising polymer for biotechnological application. For example, it can be used in the food industry, serving as a novel biological material and edible packaging *(Sayah et al., 2024)*. In the medical field, BC finds use as a wound dressing material, artificial skin, vascular grafts, scaffolds for tissue engineering, artificial blood vessels, wound pads, and dental implants. Furthermore, BC has industrial applications, such as acting as sponges to collect leaking oil and as materials for absorbing toxins *(J. Wang et al., 2019)*. The versatility of BC in terms of molecular weight,

crystallinity, and hydrophilicity, together with its compatibility with several modification strategies, allows fine modulation of BC properties, including morphology, biodegradability or biostability, to meet the specific requirements of diverse applications (Torgbo & Sukyai, 2020).

In both plants and bacteria, cellulose is synthesized by cellulose synthase enzymes (CesAs). This complex varies considerably by kingdom; however, it shares a conserved catalytic subunit termed BcsA (bacterial cellulose synthase subunit A) in prokaryotes and CesA in eukaryotes *(McNamara et al., 2015)*. Plants' CesA derived from the bacterial cellulose synthase upon the endosymbiosis event that led to the formation of chloroplasts *(Little et al., 2018)*. Very few bacterial species can synthesize BC, with *Komagataeibacter xylinus* (previously known as *Gluconacetobacter xylinus*), as the most studied and the most efficient producer *(El-Saied et al., 2004; Lahiri et al., 2021a)*. *K. xylinus* is an aerobic gram-negative bacterium with fermentation activity in the pH range of 3-7 and a growth temperature range of 25-30°C, using saccharides as a carbon source *(Castro et al., 2011)*. *K. xylinus* can use various sugars and produces relatively high yields of cellulose in liquid medium *(Ross et al., 1991; Sani & Dahman, 2010)*. This organism produces cellulose extracellularly through a complex biosynthetic machinery involving the bcs operon, which comprises four protein-encoding genes, namely bcsA, bcsB, bcsC, and bcsD (*Figure 8*).

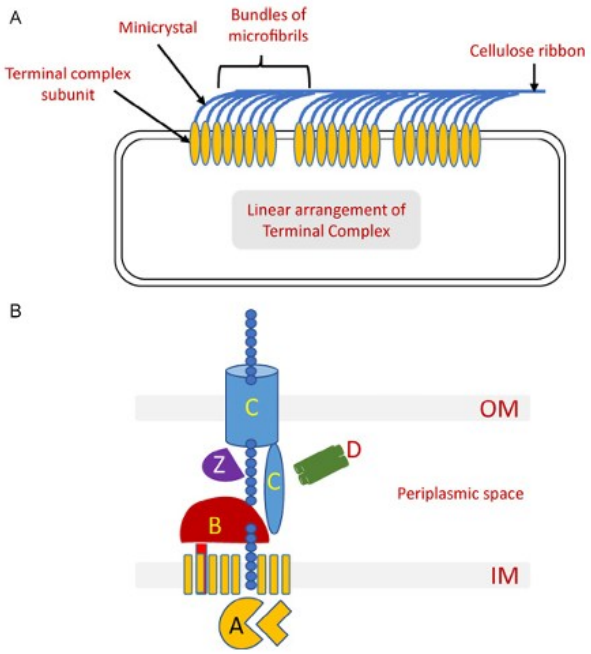

*Figure 8 - **BC synthesis**. From Raghavendran, 2020), https://doi.org/10.1016/bs.ampbs.2020.07.002.*

Briefly, glucose monomers are linked into linear β-1,4 glucan chains with approximately 15.000 glucose units per chain, through the activity of BcsA, the catalytic subunit, in association to BcsB, both located in the inner membrane. BcsC instead spans the periplasm and outer membrane and contributes to the translocation, assembly and crystallization of the glucan chains, whereas BcsD participates in glucan chains organization and transport outside the cell by forming a periplasmic pore-like structure *(Raghavendran, 2020; Ross et al., 1991)*. Once outside the cell, the linear β–1,4–glucan chains assemble in subfibrils consisting of 10-15 nascent glucan chains. The subfibrils crystallize into microfibrils, which associate into bundles, and later into ribbons composed

of about 1000 individual glucan chains. This hierarchical assembly leads to the formation of a thick, gelatinous pellicle at the air-liquid interface under static culture conditions *(Poddar & Dikshit, 2021)*. Most cellulose synthase operons also include a periplasmic cellulase, BcsZ, belonging to the GH family 8, whose biological role remains unknown, however, it is suggested that it may enhance cellulose production in vivo by regulating glucan chain length or preventing premature crystallization *(Berlemont et al., 2009; Omadjela et al., 2013)*.

Beside *K. xylinus*, other reported BC producers are represented by some *Agrobacterium* spp., *Azotobacter*, *Rhizobium* spp., *Sarcina*, *Alcaligenes*, and *Pseudomonas* genera *(Lahiri et al., 2021a)*. From an ecological point of view, the ability to produce BC can confer adaptive advantages, including the colonization of surfaces to have access to oxygen and nutrients and protection against desiccation, UV irradiation and heavy metals *(Ardré et al., 2019; K.-Y. Lee et al., 2014; Raghavendran V, 2020).*

In the present study, the potential of different Antarctic strains to produce BC under different culture conditions was investigated, providing insights on the optimal parameters and culture media for each strain. In particular, two Antarctic strains were selected for further analyses, *Pseudomonas* sp. ef1 and *Brevundimonas* sp. #2. *Pseudomonas* sp. ef1 is a marine strain isolated from a bacterial consortium associated with the Antarctic ciliate *Euplotes focardii (Pucciarelli et al., 2015; Ramasamy et al., 2019)*, previously demonstrated to be able to transform heavy metals such as copper, nickel, and silver into nanoparticles showing antibiotic activity *(John et al., 2021a, 2022a; Nagoth et al., 2024)*, and to produce unique pyoverdines *(Zannotti et al., 2026)*. This strain produced BC using synthesis media conditions that are unique. BC was

characterized through chemical analyses and compared with that obtained from the most efficient BC producer *K. xylinus*. *Pseudomonas* BC was synthesized with different shapes and structural characteristics as visualized under SEM analysis. Additionally, a putative *Pseudomonas* sp. ef1 cellulose synthase was identified and characterized. *Brevundimonas* sp. #2 is an Antarctic organism recently isolated from a sample of Antarctic water collected at Edmonson point during the 37th expedition of the PNRA and still under characterization. Its biosynthetic BC was tested in collaboration with papermaking industries to develop an innovative packaging application.

Materials and methods

Strains culturing and genome sequencing

DNA used for sequencing was extracted from the bacterial strains of interest, including *Bacillus* sp. ef1, *Brevundimonas* sp. ef1, *Brevundimonas* sp. #2, *Halomonas* sp., and *Pseudomonas* sp. ef1. The microbial cultures were grown overnight in 10 mL of LB (10 g/L tryptone, 5 g/L yeast extract, 10 g/L NaCl) at 23°C under shaking. Cells were harvested by centrifugation and DNA was extracted by using the 'DNeasy PowerSoil Pro Kit' (Qiagen), following the protocol provided by the manufacturer. Genomic DNA was sequenced with Nanopore technology using a native barcoding approach. For *Bacillus* sp. ef1, *Brevundimonas* sp. ef1 and *Pseudomonas* sp. ef1, sequencing was carried out using a MinION Mk1B and a R9.4 flow cell (Oxford Nanopore Technology, ONT). Basecalling was performed with MinKNOW (v24.02.16) using the super accurate model. Sequencing reads were assembled using EPI2ME (v5.1.14) and the workflow 'wf-bacterial-genomes' (v1.2.0) provided by ONT (GenBank acc. N. VAUR00000000). Genomic DNA of *Brevundimonas* sp. #2 and *Halomonas* sp., instead, was sequenced using a GridION equipped with a R 10.4 flow cell though a native barcoding approach (Oxford Nanopore Technology, ONT). Basecalling was performed with MinKNOW v23.11.3 using the super accurate model. A minimum Q score of 10 and a minimum read length of 200 b were applied as filtering criteria. Sequencing reads were assembled using EPI2ME v5.1.8 and the workflow 'wf-bacterial-genomes' v1.0.0.

The putative genes responsible for BC production were identified by aligning the protein sequences of *K. xylinus* with the genomes of the Antarctic bacterial strains using BLASTx.

Antarctic bacteria strains BC production, purification and characterization

The Antarctic strains of interest, including *Bacillus* sp. ef1, *Brevundimonas* sp. ef1, *Brevundimonas* sp. #2, *Halomonas* sp., and *Pseudomonas* sp. ef1 were screened for BC production testing different culture media:

- Hestrin-Schramm (HS) medium (pH 6 to 6.5), containing 20 g/L glucose, 5 g/L yeast extract, 5 g/L peptone, 2.7 g/L disodium hydrogen phosphate, 1.15 g/L citric acid, supplemented with sugars (glucose 1.5-2% or sucrose 2%), or alternatively, with waste from beer and ananas juice.
- Minimal medium 9 (M9) (pH 7.4), containing 6 g/L Na_2HPO_4, 3 g/L KH_2PO_4, 0.5 g/L NaCl, 1 g/L NH_4Cl, 2 mM $MgSO_4$, 0.1 mM $CaCl_2$, 1.5% glucose
- Artificial seawater (22 ‰) supplemented with 1 to 5% (w/v) glucose
- Deionized water supplemented with 1-3% glucose or sucrose
- Urea-based medium (pH 6.8), containing 5 g/L yeast extract, 5 g/L urea, 3 g/L KH_2PO_4, 0,05 g/L $MgSO_4$, supplemented with 2% glucose

Antarctic strains were inoculated in the selected media starting from LB agar plates culture grown overnight at 22 °C. Bacterial cultures were incubated both in static and shaking conditions at 22-24 °C for 10 days or until BC production had occurred.

Only the most suitable media were selected for further analyses, depending on the preferences of each Antarctic bacteria strain. The resulting biofilms were collected using a filter, washed multiple times with sterile deionized water, and incubated at 80°C for 4 hours while soaked in sterile deionized water to completely clean BC from bacteria.

Functional groups identification of the bacterial cellulose material was characterized by FT-IR analysis using a Perkin-Elmer System 2000 spectrometer (Waltham, MA, USA) equipped with Pike GladiATR technology. Prior to the analysis, the samples were dried in an oven at 40 °C.

Pseudomonas sp. ef1 BC production, purification, and characterization

Since it was one of the most efficient strains in terms of BC synthesis, *Pseudomonas* sp. ef1 was employed to produce BC of different shapes and to investigate the enzyme responsible for BC synthesis. BC production was conducted in HS medium at pH 6.5, testing both static and shaking conditions for 3-5 day, at temperatures of 22-24°C. Alternatively, *Pseudomonas* sp. ef1 BC was produced in artificial seawater (22 ‰) supplemented with 1.5% (w/v) glucose at 22-24°C, comparing static and shaking conditions, starting from cultures grown in yeast extract (1% w/v) or nutrient broth liquid medium. *K. xylinus* BC production was conducted in HS medium at pH 6 and temperatures of 28-30°C. The inoculum consisted of *Pseudomonas* sp. ef1 cells obtained from LB agar plates. The resulting biofilm was collected using a filter, washed multiple times with sterile deionized water, and incubated at 80°C for 4 hours while soaked in sterile deionized water to completely clean BC from bacteria. To evaluate how cultivation conditions affect BC production, the ratio of starting glucose (in grams) to producing cellulose (in grams) was calculated. The results showed a consistent production efficiency of approximately 30% across all conditions.

Functional groups identification of the bacterial cellulose material was characterized by FT-IR analysis using a Perkin-Elmer System 2000 spectrometer

(Waltham, MA, USA) equipped with Pike GladiATR technology. Prior to the analysis, the samples were dried in an oven at 40 °C.

Surface morphology and microstructural features of the dried bacterial cellulose samples, coated with a thin layer of chromium, were examined using a Sigma FE-SEM (Zeiss, Germany), operated at 5–15 kV.

X-ray diffractometry (XRD) patterns of the samples were recorded using a Bruker D6 powder diffractometer equipped with a Cu source (kα1 = 1.54060 Å) and Lynxeye SSD 160-2 detector (Bruker, Billerica, Massachusetts, U.S.). The bacterial celluloses were dried and ground to a powder before analysis. The samples were scanned over a 2θ range between 5 and 50° and a θ range between 2.5 and 25° for 15 min, with each step recorded at 0.2 s interval. Generator voltage and filament emission were set to 40 kV and 15 mA, respectively.

DSC measurements were performed using a Netzsch DSC 200 calorimeter with a scanning rate of 10 °C/min. The calorimeter cell was purged with dry nitrogen gas. The samples were analyzed as powder, and the mass of the powder samples was about 5 mg. DSC experiments were done in a temperature range from about 20 to 300 °C.

Identification of the *Pseudomonas* sp. ef1 Cellulose Synthase Enzymes, Transmembrane (TM) Regions Prediction and Homology Modeling

Pseudomonas sp. ef1 putative cellulose synthase was identified by local TBLASTN search in the corresponding genome using the BC synthase operon protein sequences from *K. xylinus* as the query. The accession numbers of the query sequences are available at the link https://www.mdpi.com/article/10.3390/md23100410/s1. The prediction of transmembrane (TM) proteins was conducted using DeepTMHMM, a tool that

utilizes deep neural networks *(Hallgren et al., 2022)*. To obtain the structural model of cellulose synthase, the corresponding sequence was divided into three regions corresponding to three structural domains: the extracellular (residues 1 to 350), transmembrane (residues 300 to 490), and the intracellular domain (residues 420 to 860). A model for each domain was obtained using RoseTTaFold, the deep learning tool of Rosetta *(Baek et al., 2021)*. The resulting models were manually overlapped using PyMol 3.1 (https://www.pymol.org/, accessed on 10 October 2025).

Brevundimonas sp. #2 BC production, characterization and application in the papermaking industry

Brevundimonas sp. ef1 was tested for BC production using HS medium pH 6.5 supplemented with 2% glucose. After 5 to 7 days of static incubation, a thin layer of cellulose-based biofilm was detectable. The BC was collected by centrifugation of the bacterial culture at 3.000 rpm for 10 minutes. The BC collected was washed with sterile deionized water multiple times to remove residual salts. The yield of the produced cellulose was calculated as follows:

$Yield\ (\%) = m0/C \times 100$,

where m0 is dry weight of cellulose (g) and C is the weight of carbon source (g) *(Mohammadkazemi et al., 2015)*.

Functional groups identification of the bacterial cellulose material was characterized by FT-IR analysis using a Perkin-Elmer System 2000 spectrometer (Waltham, MA, USA) equipped with Pike GladiATR technology. Prior to the analysis, the samples were dried in an oven at 40 °C.

Surface morphology and microstructural features of the dried bacterial cellulose samples, coated with a thin layer of chromium, were examined using a Sigma FE-SEM (Zeiss, Germany), operated at 5–15 kV.

An application of BC produced by this novel Antarctic strain was developed in collaboration with papermills. Preliminary tests were conducted in our laboratory. The synthesised BC was applied onto a standard paper sheet and dried in an oven at 40 °C. Subsequently, drops of oil and water were placed on the surface of both the paper treated with BC and the untreated paper to assess whether the treatment conferred additional oleophobic and/or hydrophobic properties. The Antarctic cellulose was tested both as a surface coating and as a bulk additive. For surface applications, BC was sprayed onto a paper foil of standard cellulose, whereas for bulk applications, BC was mixed with the vegetal pulp prior to sheet formation. Bacterial cellulose produced by *K. xylinus* was used as a reference standard. FT-IR spectra and SEM images were collected from the obtained samples, as previously described. The hydrophobic and oleophobic properties were evaluated by measuring the time required for water and oil droplets to be completely absorbed by the paper foil.

Two whitening protocols were also tested to meet the optical properties required by papermaking industry. Briefly, the first method tested was based on 20 ml of H_2O_2 5% (V/V) addition for each gram of dried cellulose. After overnight incubation, BC was washed several times with distilled water until pH value turned to 7. The second treatment occurred through NaOH 1% addition and overnight incubation.

Results

Different Antarctic strains are capable of producing cellulose

Bacillus sp. ef1, *Brevundimonas* sp. ef1, *Brevundimonas* sp. #2, *Halomonas* spp., and *Pseudomonas* sp. ef1 were inoculated into media with different compositions and incubated at 22-24 °C under static and/or shaking conditions. Depending on the bacterial strain, the medium, and the culture conditions, BC with different characteristics was obtained (*Table 1*). Subsequent FT-IR analyses allowed to confirm that cellulose was produced by the Antarctic strains tested (*Figure 9*). *K. xylinus* was used as a reference standard for cellulose production.

Table 1 – Bacterial cellulose obtained from the Antarctic strains tested. In the table above, the selected media together with the characteristics of the collected bacterial cellulose and the type of incubation (static or under shaking) are reported.

Medium	Bacterial strain	Characteristics of collected BC	Incubation and additional info	Picture
Seawater containing 1 to 4% glucose or sucrose	***Pseudomonas sp. ef1***	***Big compact aggregate, partially pigmented (orange)***	***Incubation under shaking***	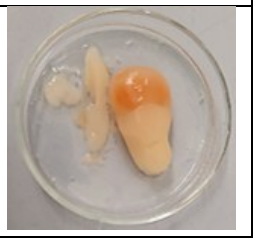

”	”	*Spherical (from few mm to 2 cm in diameter), white/yellow, from 2 to 4.25 g/sphere (wet weight)*	*Incubation under shaking*	 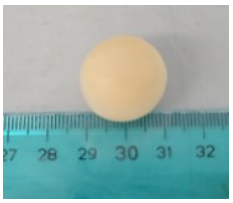
HS containing 2% glucose	”	*Foil-shaped*	*Static incubation*	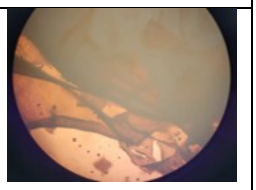
M9 containing 1.5 or 2% glucose	”	*Spherical, yellow (probably coated with pyoverdine)*	*Incubation under shaking*	
HS containing 2% sucrose	*Bacillus sp. ef1*	*Foil-shaped, white/brown or pigmented (yellow)*	*Static incubation*	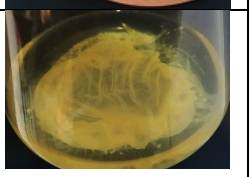
HS (pH 6.00) containing 2% ananas juice waste	”	*Foil-shaped, white/brown*	*Static incubation*	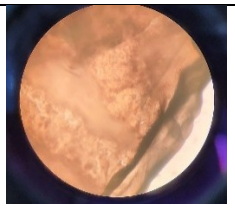

HS (pH 6.00) containing 2% sucrose	*”*	*Spherical, white, **0.37 g/sphere***	*Incubation under shaking*	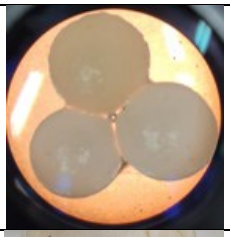
Urea (pH 6.7) containing 2% glucose	*”*	*Foil-shaped/dispersed*	*Static incubation*	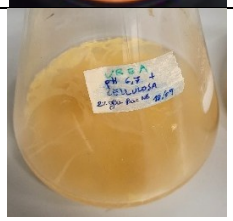
dH_2O containing 2% glucose	*Brevundimonas sp. ef1*	*Spherical, white, 1 to 3, 2 g/sphere (wet weight)*	*Incubation under shaking*	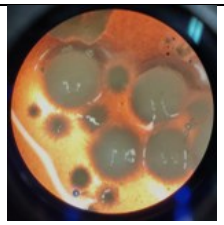
”	*”*	*Dispersed*	*Static incubation*	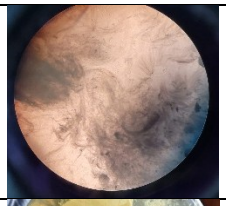
Seawater containing 1.5% glucose	*Brevundimonas sp. #2*	*Foil-shaped*	*Static incubation*	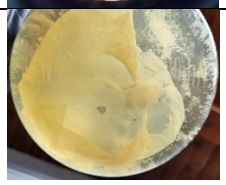
HS containing 1.5% to 3% glucose or sucrose	*”*	*Foil-shaped*	*Static incubation*	

HS containing 2% sucrose	*Halomonas sp. #1*	*Dispersed*	*Static incubation*	
HS medium (pH 6.5) containing 1% glucose	*Halomonas sp. #2CG*	*Dispersed*	*Static incubation*	
HS medium (pH 6.5) containing 2% sucrose	*Halomonas sp. #7*	*Dispersed*	*Static incubation*	
HS medium (pH 6.5) containing 1% lactose	*Halomonas sp. #12*	*Spherical, white*	*Incubation under shaking*	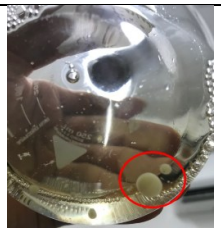
”	”	*Foil-shaped, white/yellow*	*Static incubation*	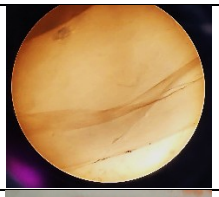
HS medium (pH 6.5) containing 2% sucrose	”	*Foil-shaped, pigmented (orange)*	*Static incubation*	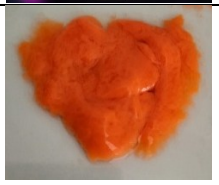

HS medium (pH 6.5) containing 2% sucrose	*Halomonas sp. #14*	*Dispersed*	*Static incubation*	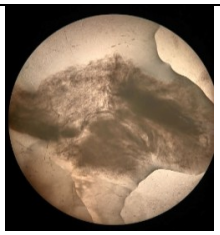
HS medium (pH 6.5) containing 2% glucose	*”*	*Irregular fragments*	*Static incubation*	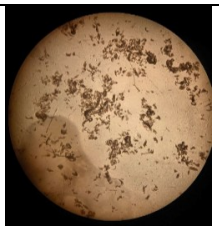
HS (pH 6) containing 1.5% glucose	*K. xylinus*	*Foil-shaped (compact disk)*	*Static incubation, no oxygen flow*	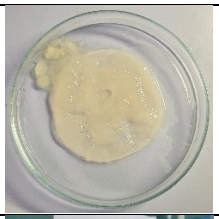
HS (pH 6) containing 1.5% glucose	*”*	*Compact aggregate*	*Static incubation, with oxygen flow*	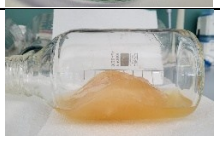

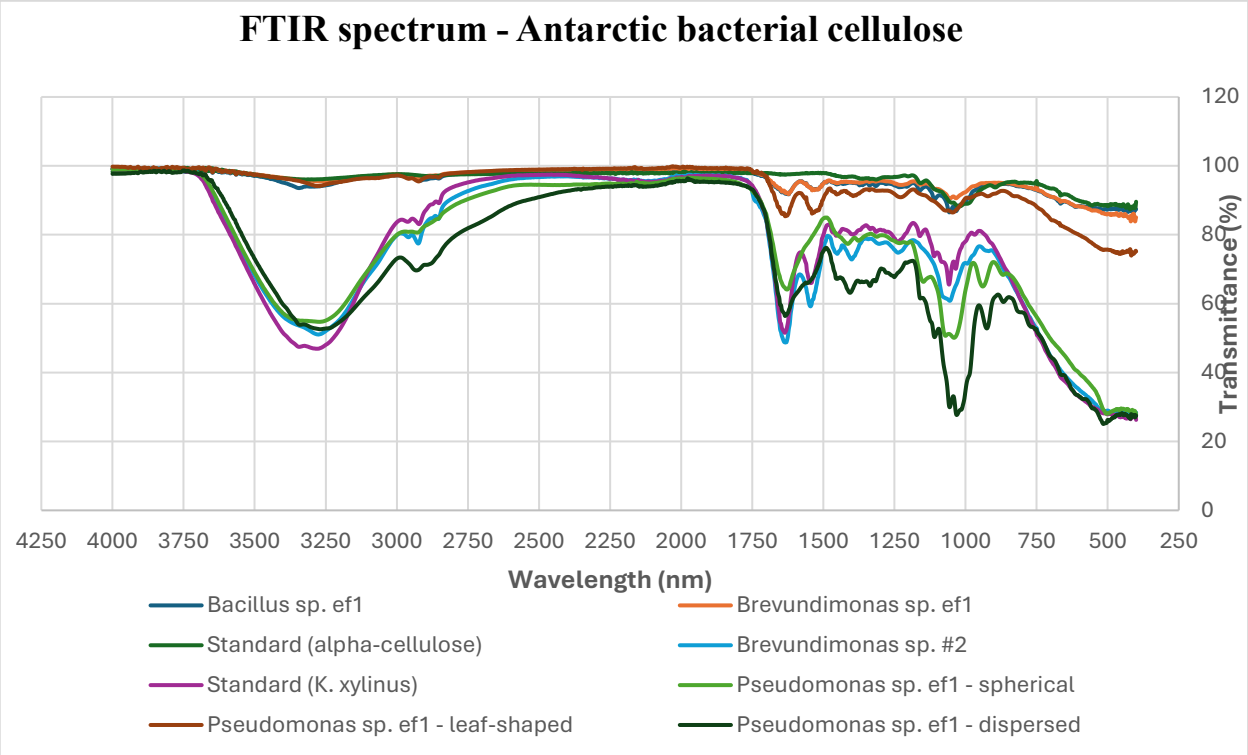

Figure 9 – FT-IR spectra confirming that BC was produced by the different Antarctic strains. K. xylinus (in violet) was used as a reference standard.

Putative genes responsible for BC production

By analysing the sequenced genomes of the Antarctic bacterial strains, the putative genes responsible for BC production were identified by aligning the protein sequences of *K. xylinus* with the genomes of the Antarctic bacterial strains using BLASTx. As shown in *Figure 10*, the putative operon structure of the Antarctic strains differed from the typical organization observed in *K. xylinus*. All the putatively involved protein sequences are reported in the Supplementary Material, Chapter I.

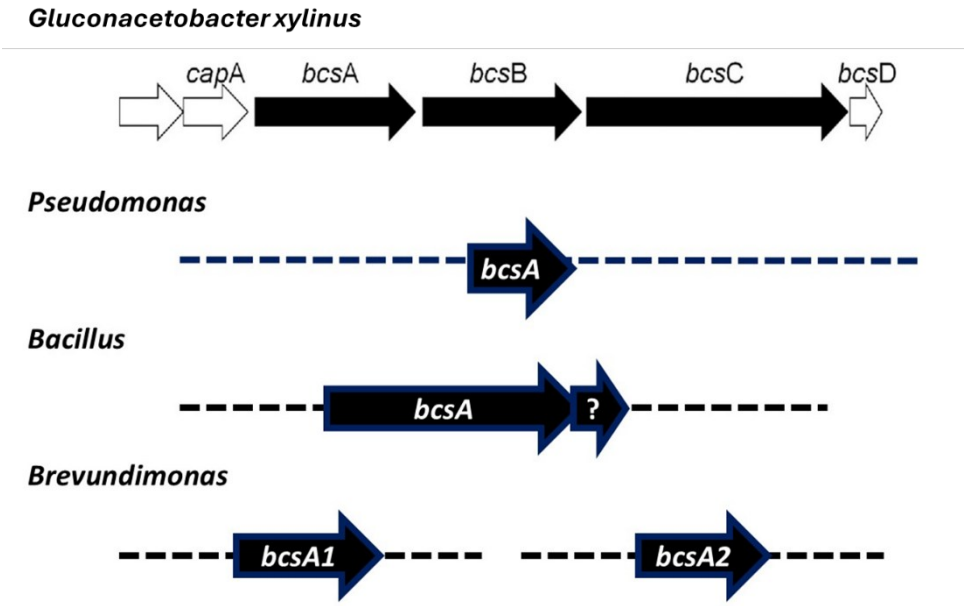

Figure 10 – Putative genes involved in BC production from the Antarctic bacterial strains tested. The operon structure of K. xylinus, the most studied BC producer, was used as a reference standard.

Different culture conditions leaded to different cellulose shapes (*Pseudomonas*)

The capacity of *Pseudomonas* sp. ef1 to synthesize BC was evaluated through fermentation in standard HS medium containing 1.5% glucose, which is commonly utilized for *K. xylinus*, the most well-known BC producer. BC production by *Pseudomonas* sp. ef1 was assessed in both static and shaking conditions. Under static conditions, the BC produced by *Pseudomonas* sp. ef1 exhibited a sheet-like form and was more dispersed in water (*Figure 11a*), differing from the BC produced by *K. xylinus*, which had a more gelatinous appearance (*Figure 11b*). *Pseudomonas* sp. ef1 can generate BC at a pH 6.5 and temperatures ranging from 22 to 24°C. In contrast, the optimal conditions for

BC production in *K. xylinus* are a pH 6 and temperatures between 28 and 30°C. Conversely, no BC production was detected under shaking conditions.

Since *Pseudomonas* sp. ef1 is a marine bacterium, BC production was also examined in artificial seawater supplemented with 1.5% glucose at 22-24°C, both in static and shaking conditions starting from cultures grown in yeast extract (1%) or nutrient broth liquid medium (as described under Material and Methods). After 5-6 days of incubation under shaking at 100 rpm, the formation of spherical flocculates was observed (*Figure 11c-d)*, with sizes ranging from 3 to 20 mm in diameter. The water content was estimated to be 79%. In contrast, the use of this medium resulted in no detectable BC production under static incubation.

(a)

(b)

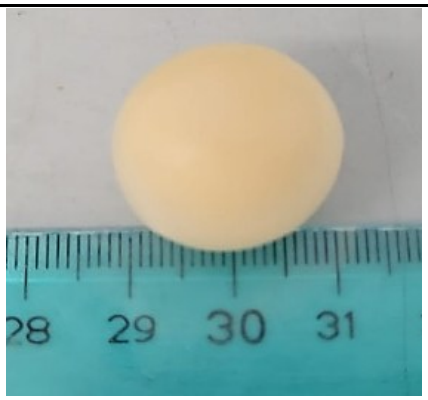

(c) ***(d)***

To evaluate how cultivation conditions affect BC production, the ratio of starting glucose (in grams) to producing cellulose (in grams) was calculated. The results showed a consistent production efficiency of approximately 30% across all conditions.

Figure 11 - Cellulose produced by Pseudomonas sp. ef1 (a) and K. xylinus (b) in HS medium under static conditions, and cellulose synthesized by Pseudomonas sp. ef1 in artificial marine water under agitation (c, d).

Fourier-Transform Infrared (FTIR) Spectroscopic Characterization of BC

To confirm that the obtained products correspond to BC, Fourier-Transform Infrared Spectroscopy (FTIR) analysis was performed. FTIR spectra were acquired from solid samples after drying both the spherical BC (*Figure 12*, gray line) and the dispersed sheet-like BC (*Figure 12*, orange line) and compared to cellulose produced by *K. xylinus* (*Figure 12*, blue line). Both cellulose types, spherical and dispersed, exhibited IR spectra comparable to those of *K. xylinus*

and standard plant-derived cellulose, as reported by *(Abderrahim et al., 2015)*. The broad adsorption band at 3330 cm cm^{-1} is attributed to the -OH stretching, the vibrations in the range 2850–2940 cm^{-1} are relative to the C-H stretching in the bacterial cellulose structure. The peak at around 1600 cm^{-1} can be attributed to the residual water, present in the cellulose network. Several bands have been detected at 1460, 1390, 1320, and 930 cm^{-1} attributed to C−H stretching of CH_2 and CH_3 groups, that could indicate the possibility of a methylated cellulose. Furthermore, a strong band is visible at around 1050 cm^{-1} that corresponds to C-O-C and C-O-H vibrations *(Fatima et al., 2023; Oliveira et al., 2015; Yim et al., 2017)*.

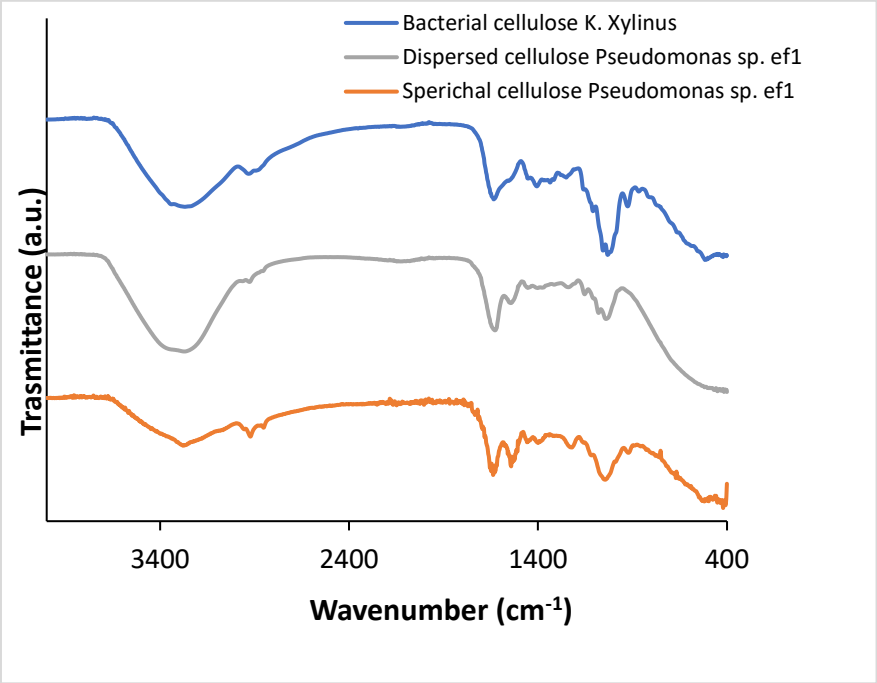

Figure 12 -FTIR spectra of bacterial cellulose (BC) produced by K. xylinus (blue line) and Pseudomonas sp. ef1 (gray and orange lines). The gray line represents the spectrum of sheet-like BC, while orange line corresponds to spherical-shaped BC.

Scanning Electron Microscope (SEM) Analysis of Bacterial Cellulose

The morphologies of the BC produced by *Pseudomonas* sp. ef1 and *K. xylinus* samples were evaluated by FE-SEM measurements (*Figure 13*).

SEM images reveal that the spherical BC produced by *Pseudomonas* sp. ef1 (*Figure 13a-b*) consists of filamentous structures with diameters below 1 µm, similar those observed in BC synthesized by *K. xylinus* (*Figure 13d*). However, the fibrous network of *Pseudomonas* sp. ef1 appears less uniform and less

distinctly organized compared to the well-defined and homogeneous architecture of *K. xylinus*-derived BC.

In contrast, the sheet-like BC morphology observed in *Pseudomonas* sp. ef1 (*Figure 13c*) presents a disordered and loosely connected structure. This irregular arrangement may contribute to its enhanced dispersibility in aqueous environments, suggesting potential advantages for applications requiring high water solubility or colloidal stability.

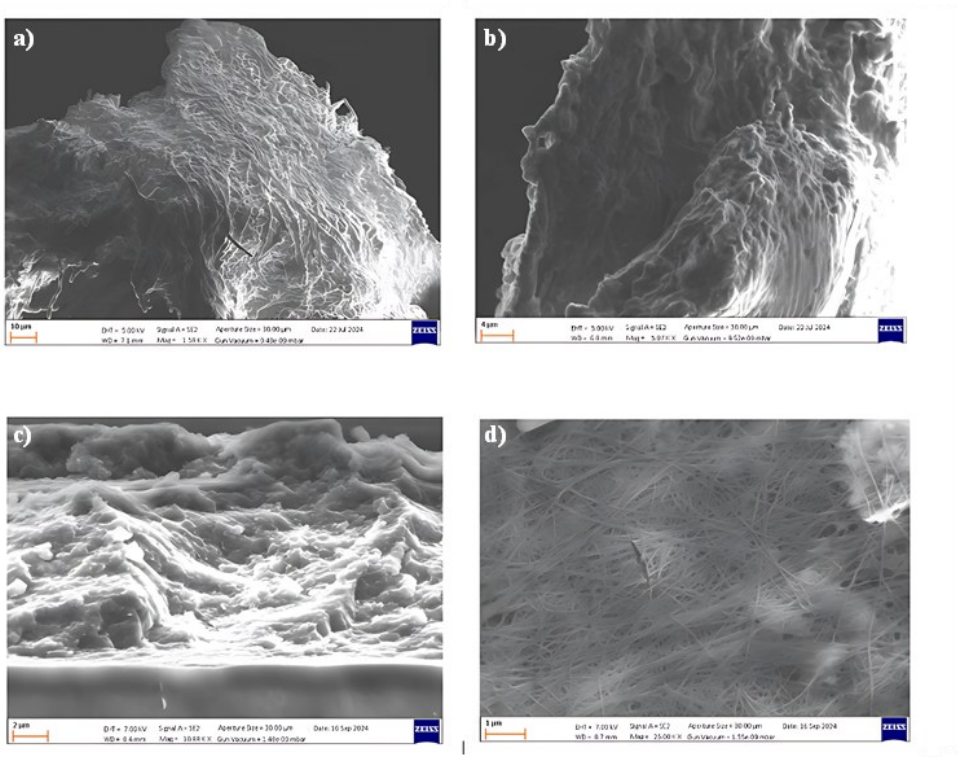

Figure 13 - SEM images of A, B) the spherical shaped BC from Pseudomonas sp. ef1, C) dispersed sheet-like BC from Pseudomonas sp. ef1. D) BC produced by K. xylinus.

Powder X-Ray Diffraction (XRD) Analysis

XRD was then used to analyse the crystal structure of BC samples. Various polymorphic forms of cellulose are possible; cellulose Iα is typically synthesized by microorganisms, while cellulose Iβ, which is the predominant form, is found in higher plants *(Stanciu et al., 2025)*. Despite both cellulose Iα and Iβ consisting of parallel molecular chains, they exhibit distinct crystal lattice structures: Iα is triclinic, whereas Iβ adopts a monoclinic configuration *(Nagarajan et al., 2017)*. Cellulose II can be obtained from either cellulose Iα or Iβ through specific treatments: alkali treatment (mercerization) or dissolution followed by recrystallization (regeneration), respectively (*Figure 14*).

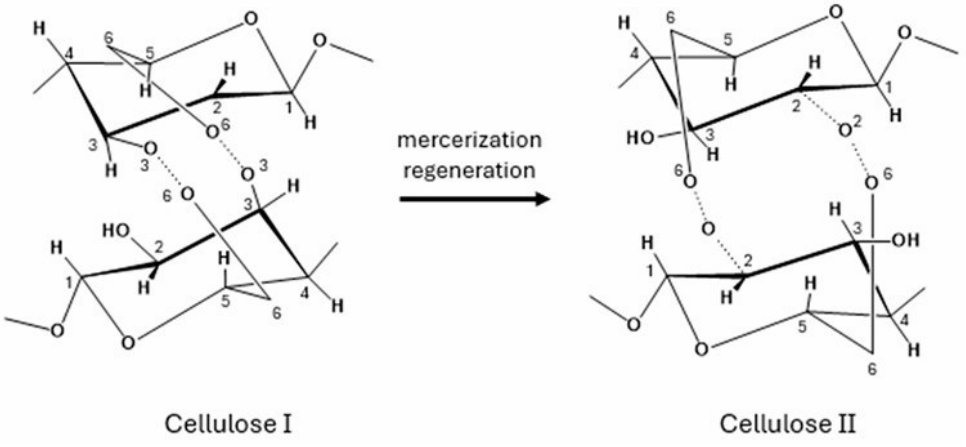

Figure 14 - Conversion of Cellulose I to Cellulose II.

In some cases, cellulose II has also been found in nature *(Kuga et al., 1993; O'Sullivan, 1997; Shibazaki et al., 1998)*; unlike cellulose I, which features parallel chains, cellulose II is characterized by an antiparallel chain arrangement and a monoclinic crystal lattice *(Nagarajan et al., 2017)*.

Figure 15 shows the XRD diffractograms of the different BCs. In the XRD spectra, the standard model of cellulose II, Iα, and Iβ are also reported. The diffraction pattern for dispersed sheet-like cellulose (yellow plot) shows three distinct peaks at 2θ = 14.6°, 16.6°, and 22.6°, in agreement with cellulose I structure, as also reported for cellulose produced by *K. xylinus (Vazquez et al., 2013)*. These peaks are assigned to the (1 0 0), (0 1 0), and (1 1 0) planes of cellulose Iα or the (1 1 0), (1 1 0), and (2 0 0) planes of cellulose Iβ *(C. M. Lee et al., 2015; Wada et al., 1997)*. Usually, cellulose produced by microorganisms is Iα, but distinguishing between the two allomorphs based solely on XRD peak positions is challenging due to their close proximity.

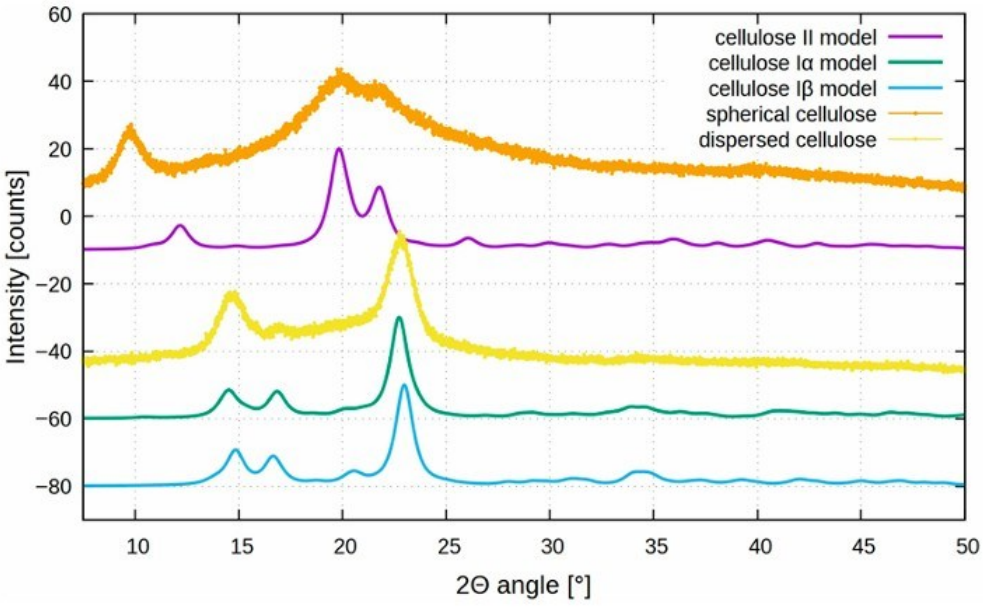

Figure 15 - X-ray diffraction patterns of dispersed (yellow) and spherical (orange) bacterial cellulose produced by Pseudomonas sp. ef1 in static and

agitation conditions, respectively, compared with cellulose Iα (green), cellulose Iβ (blue light), and cellulose II models (violet).

Analysing the spherical BC, the XRD pattern (orange plot) is quite different, showing distinct peaks at 2θ around 9.5◦, 19.5◦, and 21.5◦ that could be assigned to (1-1 0), (1 1 0), and (0 2 0) planes of the cellulose II structure, which is more thermodynamically stable but less ordered compared to cellulose I *(Chiriac et al., 2014; Gong et al., 2017; Nabeela et al., 2020)*.

The formation of cellulose II mediated by bacteria under agitation may be attributed to localized thermal effects induced by mechanical stirring. This shift confirms a rearrangement in the cellulose crystalline lattice due to agitation-induced structural changes; agitation not only enhances oxygen and nutrient distribution, but also generates mild heat and mechanical stress, which can promote partial rearrangement of glucan chains with the formation of disordered microdomains or transitional phases. These structural irregularities, including the presence of other compounds, such as bacterial metabolites or salts (high concentration in seawater), could be manifested as atypical reflections in the XRD profile, including the signal below 10°.

Differential Scanning Calorimetry (DSC)

DSC analyses were performed to thermically characterize these bacterial celluloses. As can be seen in *Figure 16*, during the increase in temperature from 20 to 300 °C, the decrease in the weight takes place in the two samples at about 100 °C, according to reference *(Martins et al., 2024)*. This process corresponds to loss of water from the cellulose samples; during the successive temperature

increase, further loss of sample mass cannot be observed in the two samples indicating a thermal stability up to 300 °C.

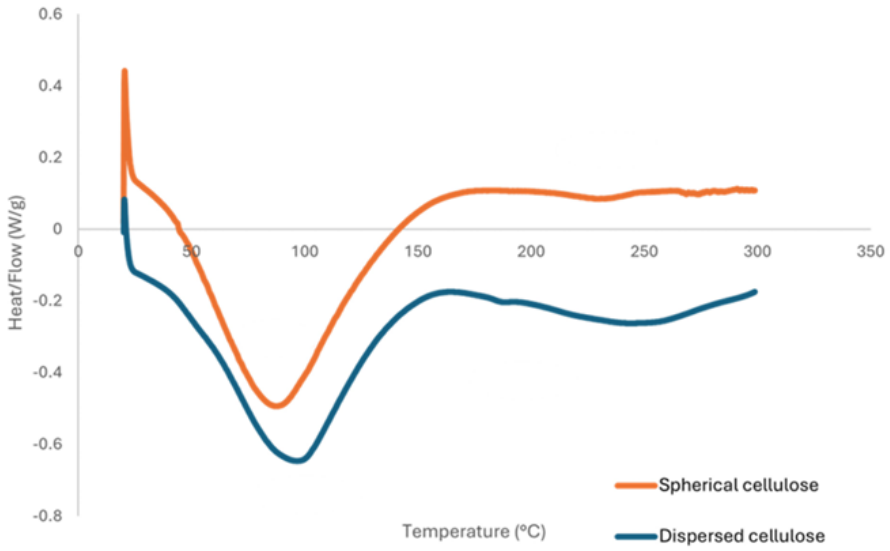

Figure 16 - DSC curves for dispersed and spherical bacterial cellulose produced by Pseudomonas sp. ef1 in static and agitation condition, respectively.

Genome sequencing and identification of *Pseudomonas* sp. ef1 cellulose synthase and structural predictions

Genome sequencing of *Pseudomonas* sp. ef1 DNA was successfully achieved using Nanopore technology. Mash's output showed, for each comparison between *Pseudomonas* sp. ef1 genome and the reference genome NZ_JAHSTX010000002 (corresponding to *P. triticicola*), two key values:

- id:f:0.966939 → estimate of the average nucleotide similarity (≈96.7% identity),

- kc:f:1.00442 → fraction of the genome "covered" by the sketch (≈100% coverage).

Since the Average Nucleotide Identity (ANI) estimated by Mash was ~96.7% and the coverage was nearly total, it exceeded the standard thresholds (ANI ≥95–96%, coverage ≥65%). These results suggest that *Pseudomonas* sp. ef1 belongs to the same species as *Pseudomonas triticicola*.

To identify the enzyme(s) involved in *Pseudomonas* sp. ef1 BC synthesis, a TBLASTN (2.2.28+) search was conducted on the corresponding genome using the BC synthase operon protein sequences from *K. xylinus* as the query. The accession numbers of the query sequences are listed in *Table S1* available through the following link: https://www.mdpi.com/article/10.3390/md23100410/s1. Only the *K. xylinus* cellulose synthase catalytic subunit (acc. # AHI24410.1), putative cellulose synthase 2 (acc. # AHI24410.1), and cellulose synthase 2 (AHI26282.1) showed a confident match with a single sequence in the *Pseudomonas* sp. ef1 genome in TBLASTN result that correspond to the catalytic subunit A. The other sequences from the *K. xylinus* operon did not show any confident matches. These findings are summarized in *Table S1* (https://www.mdpi.com/article/10.3390/md23100410/s1). Therefore, attention was focused on the characterization of this sequence. Blast search analysis revealed that the identified protein is composed of two different domains: the Scw11 superfamily, which includes the Exo-beta-1,3-glucanase family, and the BcsA superfamily, which includes cellulose synthase catalytic subunit A (*Figure* S2, https://www.mdpi.com/article/10.3390/md23100410/s1). The prediction has an E-value of 4 × 10−17, indicating a highly reliable result. Therefore, we named

the protein putative cellulose synthase catalytic subunit A (hereafter called pBCSA) from Pseudomonas sp. ef1. Since the cellulose synthase is known to be a transmembrane (TM) protein, the next step in characterizing the *Pseudomonas* sp. ef1 pBCSA involved predicting the topology of the TM regions. This prediction was carried out using DeepTMHMM, a deep learning model designed to calculate the likelihood of each residue being part of the extracellular, transmembrane, or intracellular region *(Hallgren et al., 2022)*. According to the prediction, along extracellular domain spanning the first 300 residues (blue line, *Figure 17*), three TM-helixes spanning residues from 300 to 400 (red squares in *Figure 17a*), a long intracellular domain (pink line in *Figure 17a*), and an additional four TM-helixes at the C-terminal domain were identified. The prediction of the long extracellular domain in the N-terminus was unexpected. To confirm the presence of this domain, the prediction of the 3D structure was carried out using the RoseTTaFold deep learning tool. The model shows very low error for most residues, with the median error at 1.01 Å, as shown in the *Figure S3* available at *https://www.mdpi.com/article/10.3390/md23100410/s1)* , Error vs. Residue Plot.

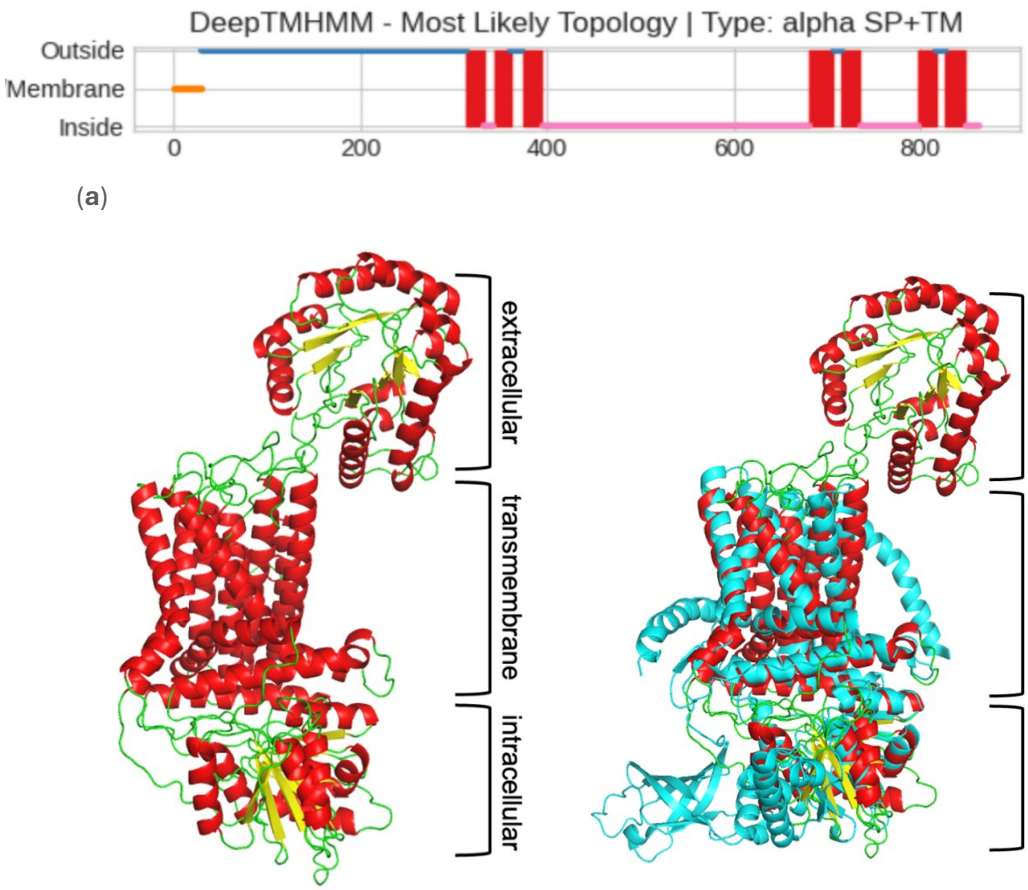

Figure 17- (a) Prediction of transmembrane regions of the putative Pseudomonas sp. ef1 cellulose synthase subunit A (pBCSA). The plot obtained with DeepTMHMM shows a signal peptide in orange, in blue and pink the extra-intracellular portion, respectively, and in red the transmembrane helixes. (b) Pseudomonas sp. ef1 pBCSA three-D model, coloured according to the secondary structures: helixes in red, strand in yellow and loop in green. (c) Superposed Pseudomonas sp. ef1 pBCSA and C. sphaeroides cellulose synthase subunit A model, the latter all coloured in cyan.

Given the constraints on residue length for the protein 3D modelling capabilities of this tool, the *Pseudomonas* sp. ef1 pBCSA amino acid sequence was segmented into three distinct overlapping sections based on transmembrane region predictions. These segments are defined as residues 1–350, 300–490, and 420–860, corresponding respectively to the extracellular domain, the initial three transmembrane helices, and the intracellular domain linked to the final four transmembrane helices. The final 3D model is reported in *Figure 17b*: the modelling confirmed the presence of the additional extracellular domain, not usually present in most of the BCS subunit A. The presence of this additional domain is even more evident in the superposition of the model with cellulose synthase A subunit of *Cereibacter sphaeroides (Morgan et al., 2014)*, which has been used as model template (5EJZ(MMDB) in iCn3D), reported in *Figure 17c.*

Some strains of *K. xylinus* possess operons which encodes a single long BcsAB fusion protein. By contrast, the extracellular domain of the putative *Pseudomonas* sp. ef1 pBCSA corresponds to the Exo-beta-1,3-glucanase family. These enzymes are known to play a key role in the degradation of beta-1,3-glucans, which are polysaccharides found in the cell walls of fungi, some bacteria, and plants. However, these proteins have also a role in biofilm formation and modification.

Brevundimonas sp. #2 BC synthesis, characterization and application in the papermaking industry

Brevundimonas sp. #2 was cultured in HS medium (pH 6.5) supplemented with 2% glucose. After 5 to 7 days of static incubation, a thin layer of cellulose-based

biofilm was collected and washed multiple times with deionized water (*Figure 18a*). The yield of the obtained BC was approximately 20%.

The BC collected was subsequently tested both as a surface coating and as a bulk additive.

Preliminary tests were conducted in our laboratory. The synthesised BC was applied onto a standard paper sheet and dried in an oven at 40 °C. Subsequently, drops of oil and water were placed on the surface of both treated and untreated paper. The surface treated with BC appeared impermeable to both water and oil for at least 48 hours (*Figure 18 b, c, d*).

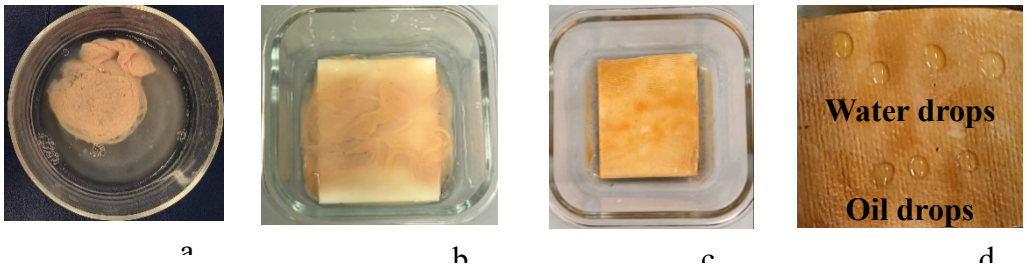

Figure 18 – BC of Brevundimonas sp. #2 was collected (a) and applied as a coating onto a standard paper sheet (b). After drying, additional oleophobic and hydrophobic properties were evaluated by measuring the time for water and oil absorption (d).

Subsequent tests were performed in collaboration with papermaking industries. BC obtained from *Brevundimonas* sp. #2 and from *K. xylinus* was applied to standard paper sheets made from vegetal pulp, both as bulk additives and surface coatings. The resulting samples were analysed through FT-IR and SEM (*Figure 19 and 20*). Application of BC from *K. xylinus* resulted particularly challenging due to the excessive compactness of its structure, which resisted the homogenization steps required to fragment the cellulose prior to its application.

In contrast, BC from *Brevundimonas* sp. #2 was more easily processable. Application of BC as a surface coating proved more promising than its application as a bulk additive, as the latter required a high material concentration. Hydrophobicity and oleophobicity tests showed encouraging results when BC was present on the surface of the paper (images not shown); however, the coating was not homogeneous (*Figure 20, panel c and d*), suggesting that a higher amount of material is required to achieve more effective and uniform results.

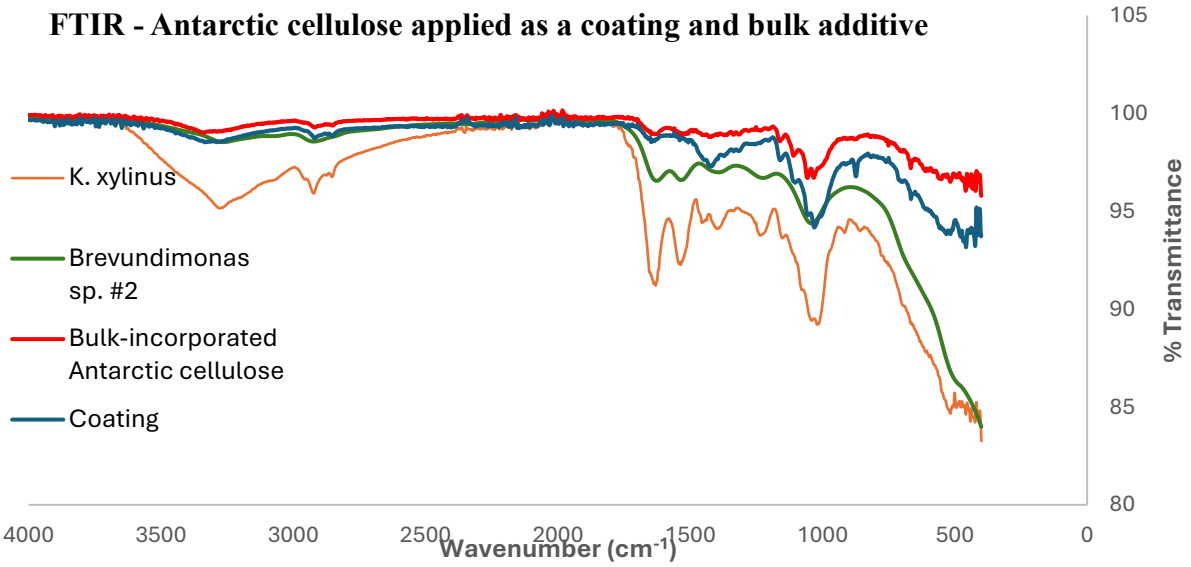
FTIR - Antarctic cellulose applied as a coating and bulk additive
K. xylinus
Brevundimonas sp. #2
Bulk-incorporated Antarctic cellulose
Coating
105
100
95
90
85
80
% Transmittance
4000
3500
3000
2500
2000
1500
1000
500
0
Wavenumber (cm-1)

a)

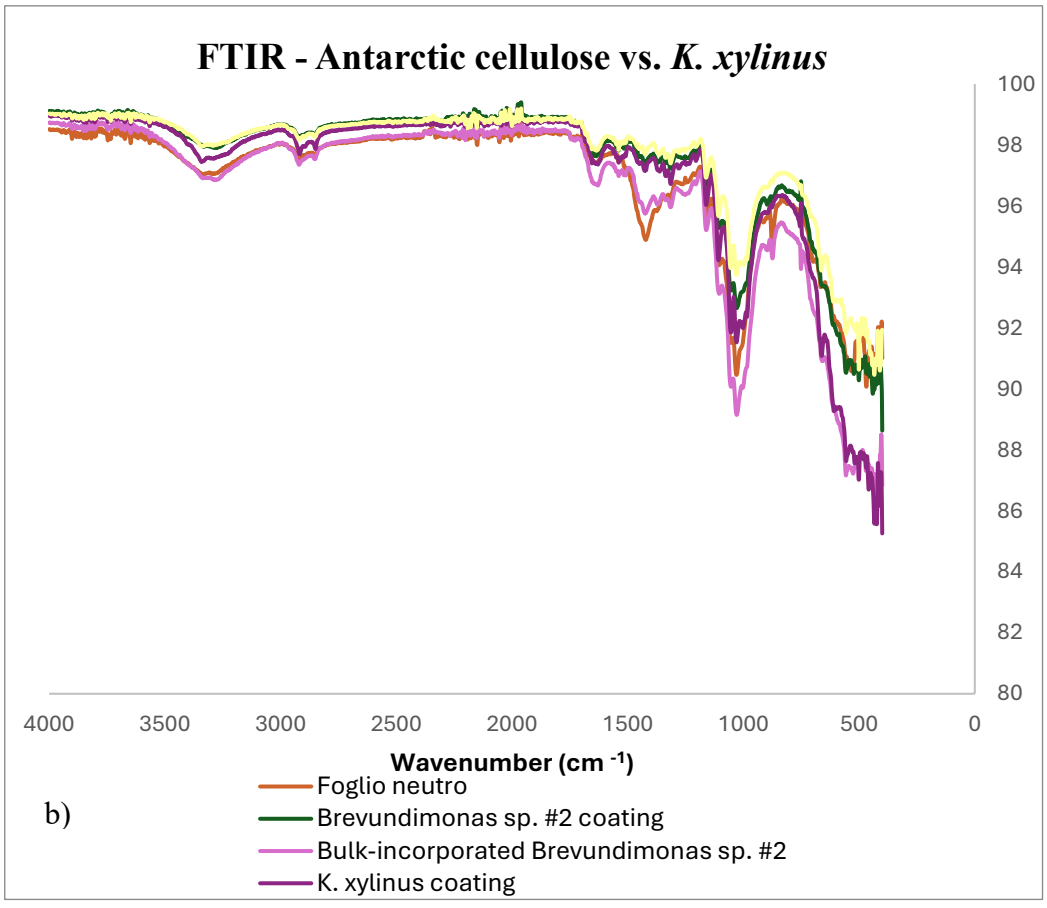
FTIR - Antarctic cellulose vs. K. xylinus
100
98
96
94
92
90
88
86
84
82
80
4000
3500
3000
2500
2000
1500
1000
500
0
Wavenumber (cm -1)
Foglio neutro
Brevundimonas sp. #2 coating
Bulk-incorporated Brevundimonas sp. #2
K. xylinus coating

b)

Figure 19 – ***FT-IR spectrum of BC from Brevundimonas sp. #2 and K. xylinus tested in papermaking industry applications, applied as a coating and bulk additive.***

The panel a of the figure shows the spectra of Antarctic bacterial cellulose applied as a coating (blue) or as a bulk additive (red) in collaboration with the papermaking industry. Spectra of BC obtained from Brevundimonas sp. #2 before application (green) and control BC from K. xylinus (orange) were also reported.

The panel b of the figure shows BC obtained from Brevundimonas sp. #2 applied as a coating (green) or as a bulk additive (pink) compared with BC produced from K. xylinus employed as a coating (purple) or incorporated as a bulk additive (yellow).

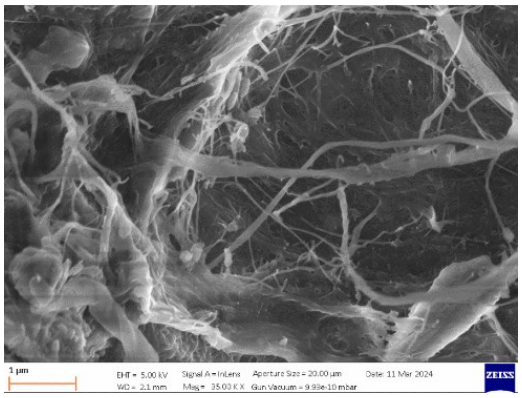
1 µm
ZEISS

a)

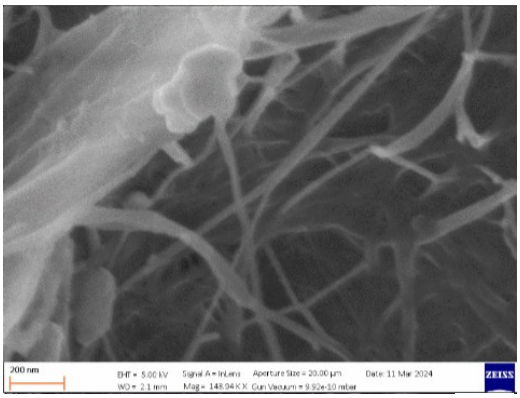
200 nm
ZEISS

b)

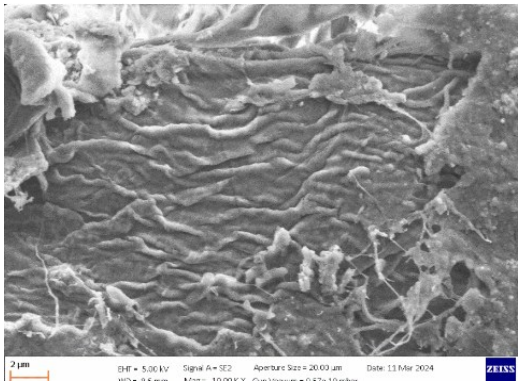
2 µm
ZEISS

c)

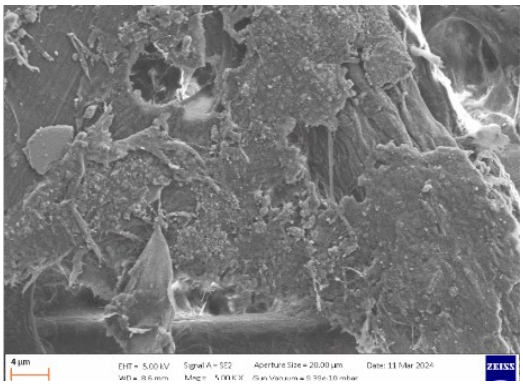
4 µm
ZEISS

d)

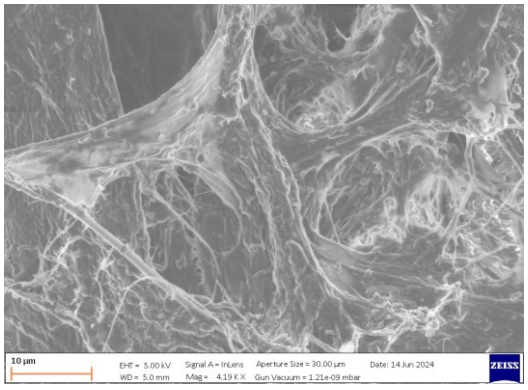
10 µm
ZEISS

e)

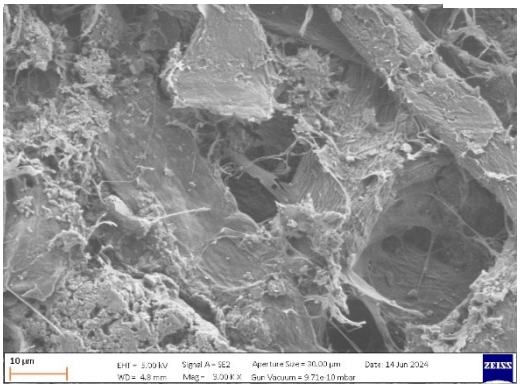
10 µm
ZEISS

f)

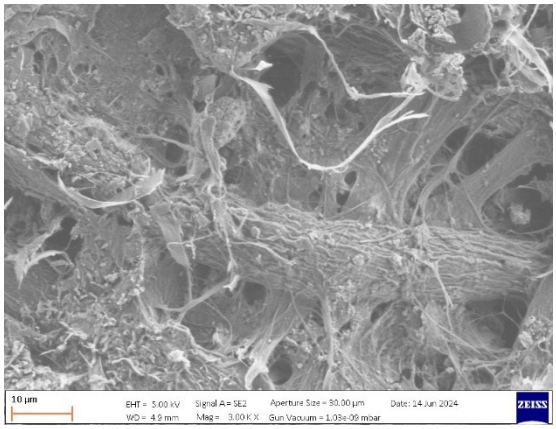

g

Figure 20 - ***SEM images of BC tested in papermaking industry applications.*** *The figure shows a standard paper foil without coating (a, b), a paper foil with Antarctic BC coating (c, d), Antarctic BC applied as a bulk additive within the vegetal pulp (e), paper foil with BC from K. xylinus applied as a coating (f) and BC from K. xylinus as a bulk additive within the vegetal pulp (g).*

Whitening treatments were performed by treating Antarctic BC with either NaOH 1% or with H_2O_2 5% to meet the requirements of the papermaking industry in terms of organoleptic properties. In both cases, BC appeared whiter after overnight incubation (*Figure 21*); however, due to the multiple washing steps required, it also became less compact and less concentrated, suggesting a partial loss of material. These observations were confirmed by FTIR spectra and SEM images (*Figures 22 and 23*). These latter analyses also showed that the surface of the treated BC exhibited pores (*Figure 23 a, b*), indicating that these treatments may compromise cellulose structure integrity.

Figure 21 - BC sample before (on the left) and after treatment with H_2O_2 (on the right).

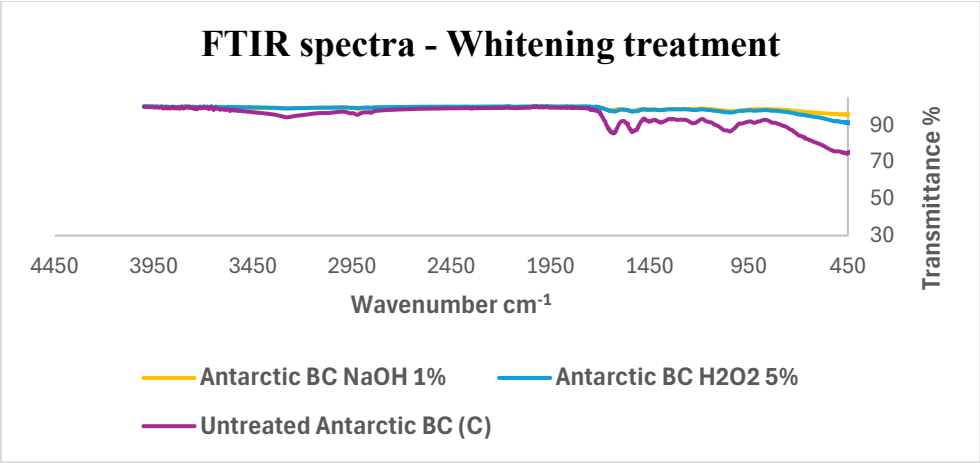

*Figure 22 – **FTIR spectra of Antarctic BC exposed to the whitening treatment**.*

The figure shows BC treated with NaOH 1% (yellow), H_2O_2 5% (blue), and untreated (purple). The differences in the spectra between treated and untreated samples suggested that the whitening treatments seem to affect the cellulose structure.

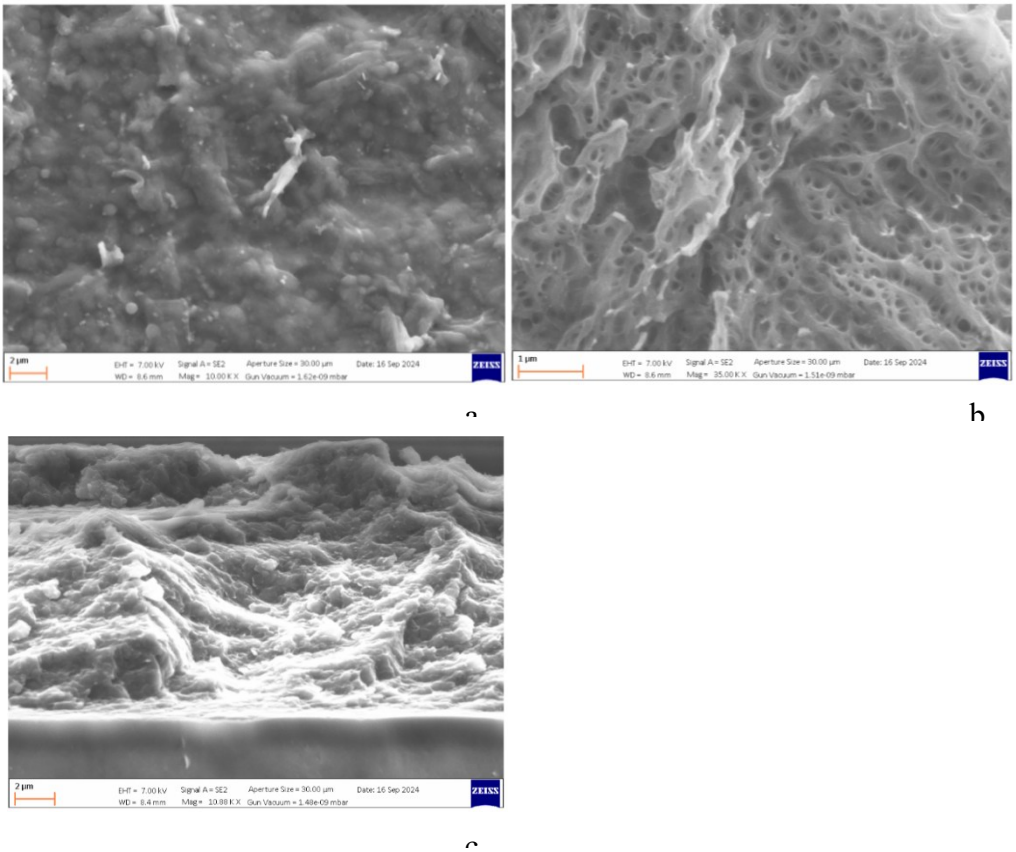

Figure 23 – ***SEM images of treated Antarctic BC to improve its optical properties****.*

a) Antarctic cellulose bleached with 1% NaOH. The structure appears to be fibrous but less compact. b) Antarctic cellulose treated with 5% H_2O_2. Several

pores are visible through the fibers revealing that the BC structure has been altered by the whitening treatment. c) Untreated BC (control).

Discussion

Bacterial cellulose was successfully produced using different Antarctic strains which are still under characterization. The morphology of the resulting BC varies depending on the bacterial strain, culture medium and incubation conditions, including spherical, foil-shaped, dispersed and fragmented BC. Under static incubation, indeed, it is possible to achieve a leaflet film at the liquid-air interface, whereas under shaking conditions, multiple morphologies can form, such as spheres, stars, and irregular shape *(Raghavendran V, 2020)*. Numerous factors have been identified that influence both the microbial capability of producing BC and the properties of the final product, including composition of the medium, temperature, pH, oxygen availability, humidity, light exposure, shape of the flask *(Almihyawi et al., 2024; Lahiri et al., 2021b)*. Several Antarctic strains were reported to produce BC, including species of *Bacillus* and *Pseudomonas*. Recent literature showed that *Bacillus* strains isolated from the soil can produce BC, with the highest yields observed in HS medium supplemented with sucrose as the carbon source *(Bektas & Yildirim, 2025)* consistent with our findings. *Pseudomonas* spp. has also been reported to produce cellulose to favour bacterial colonization of the air-liquid interface *(Ardré et al., 2019b)*. Despite their proven ability to produce exopolysaccharides, *Brevundimonas* and *Halomonas* spp., in contrast, are not reported among BC producers in the literature *(Ruiz-Ruiz et al., 2011; Verhoef et al., 2002)*.

A main limitation of the use of BC is constituted by the high related production costs which limit the large-scale operation of this bioprocess *(Raghavendran, 2020)*. However, the use of inexpensive media, such as seawater, and of food industry waste, including pineapple juice, dairy processing effluents, beer and sugar waste, expired food products, can contribute to the circular economy while reducing production costs *(Kadier et al., 2021)*. The use of bioreactors with controlled parameters, including oxygen and nutrient availability, temperature, pH, can also favour the scale-up to an industrial level *(V. Girard et al., 2024)*. Development of genetically engineered strains and the use of cell-free system can further improve the yield and the reproducibility of the process *(M. W. Ullah et al., 2017)*.

Reported BC yield in the literature ranged from 0,11 to 23,4 g/L, depending on the bacterial strains, the culture medium composition, and the fermentation conditions used *(Abouelkheir et al., 2020; V. Girard et al., 2024; Gullo et al., 2017; Mishra et al., 2022)*. In the present study, the Antarctic bacterial strains produced approximately 2,3 g/L of BC (dry weight), showing potential for further optimization under controlled fermentation conditions.

BC typically contains up to 98-99% water and exhibits a water retention capacity up to 300 times its dry weight *(V. Girard et al., 2024)*. In this work, the estimated water content was 79%.

After purification, BC purity approach 100%, as treatments such as NaOH washing efficiently remove bacterial cells and residual medium components. This high purity is also related to the absence of lignin, hemicellulose, pectin and waxes which are commonly found in plant-derived cellulose *(V. Girard et al., 2024)*. In the present work, NaOH treatment was omitted because it negatively

affected the BC structure. Purification was performed though repeated washing steps with distilled water. However, XRD analyses suggested the possible presence of bacterial and salt residues, indicating that additional crystallinity and purity analyses should be performed to better characterize the material.
Among the main functional properties reported for BC, the crystallinity index generally ranges between 60-90% *(Gullo et al., 2017; Kadier et al., 2021)*, while the Young's modulus is estimated up to 114-115 Gpa, reflecting the high mechanical strength of the material *(V. Girard et al., 2024)*. These parameters were not determined in the present study and should be investigated in future analyses.
BC also exhibits high thermal stability, generally up to 200-300 °C on average *(Gullo et al., 2017)*. This is consistent with the results reported in this study. Furthermore, BC is widely recognised as non-toxic and highly biocompatible, making it a promising biomaterial for biomedical and industrial applications *(V. Girard et al., 2024)*. Nevertheless, these properties were not directly assessed in this work and should be confirmed though dedicated experimental analyses.

While most cellulose is produced by plant cellulose synthase complexes, this enzyme clearly has a bacterial origin: there is no doubt that its genes have been acquired by plants from cyanobacterial ancestors of their chloroplasts *(Nobles & Brown, 2004)*. A marine Antarctic *Pseudomonas* strain capable of producing bacterial cellulose from glucose under energy-safe conditions was isolated. Genomic analyses suggested that this strain belongs to *Pseudomonas triticicola*, a recently discovered species clustering within the *P. fluorescens* group, isolated from the rhizosphere of wheat, and characterized by a G + C content of 59.99 mol% *(L. Girard et al., 2021)*. The produced BC exhibited different morphology,

according to the protocol used. In HS medium, the produced BC appeared as a sheet-like product, whereas in medium containing either yeast extract or nutrient broth and sea water under shaking conditions, the product appeared as spherical flocculates. *K. xylinus* cultures grown in liquid media are remarkably efficient at producing a surface pellicle composed entirely of pure cellulose fibers *(Lahiri et al., 2021a)*. The cellulose biosynthesis process in this bacterium is controlled by a four-gene bcsABCD operon. Among the corresponding proteins, BcsA and BcsB are essential for in vitro cellulose-synthesizing (BCS) activity. However, all four proteins—BcsA, BcsB, BcsC, and BcsD—are necessary to achieve optimal cellulose production in vivo. This suggests that BcsC and BcsD play critical roles in exporting glucan chains and organizing them into fibers at the cell surface. Certain strains of *K. xylinus* also possess a second bcs operon, which encodes a single, elongated BcsAB fusion protein, along with two additional genes, bcsX and bcsY, whose functions remain uncharacterized *(Morgan et al., 2014)*. Genomic data revealed unexpected diversity of cellulose synthase operons even in closely related bacteria, indicating substantial differences in cellulose secretion mechanisms *(Nobles & Brown, 2004)*.

Extremophiles, in particular, have evolved alternative pathways also for common metabolic functions, often relying on non-canonical genes or enzymatic strategies *(Marzban & Tesei, 2025)*. Accordingly, genomic analyses suggested that the Antarctic strains produce BC by using unusual genes or non-canonical pathways. In *Bacillus* sp. ef1, sequences likely corresponding to bcsA and bcsB were identified. In *Brevundimonas* sp. ef1, two sequences potentially involved in BC biosynthesis were found, the first encoding a protein with a glycoside hydrolase family 9 and a cellulase domain, and the second carrying a PEP-CTERM system TPR-repeat lipoprotein, likely participating in protein secretion

pathways. These proteins may contribute to the remodelling of the polysaccharidic chain and its transport outside the cell *(Haft et al., 2006; Petrushin et al., 2020)*. The localization of both sequences within a wss operon, notably involved in biofilm formation, further supports their potential involvement in BC synthesis. Gene products of wssA-J were reported to share homology with cellulose (bcsABZC) and alginate (algX/FIJ) biosynthetic genes, encoding proteins responsible for both the synthesis and acetylation of cellulose containing biofilms *(Burnett et al., 2023)*. In particular, wssI may be responsible for cellulose acetylation, influencing the architecture and the properties of the biofilm as an adaptive response to environmental conditions *(Burnett et al., 2023)*.

A putative cellulose synthase subunit A was identified in *Pseudomonas* sp. ef1, possessing an extracellular domain represented by a member of the Exo-beta-1,3-glucanase family, differently from some *K. xylinus* strains that possess a single long BcsAB fusion protein. The Exo-beta 1,3-glucanase family are enzymes that play a key role in the degradation of beta-1,3-glucans, which are polysaccharides found in the cell walls of fungi, some bacteria, and plants. However, these proteins have additional biological roles, including antifungal defense mechanisms by degrading fungal cell walls, or in biofilm formation and modulation. Notably, a study on Antarctic soil sample reported the discovery of a novel cold-adapted protein (RBcel1) classified as an endoglucanase belonging to the glycosyl hydrolase family 5 (GH5). This enzyme was shown to be involved in BC synthesis by synthetising non-reticulated cellulose using cellobiose as a substrate *(Berlemont et al., 2009)*. The unusual structure of the putative BCS A subunit may account for the sheet-like and water-soluble cellulose organization that is obtained by incubating *Pseudomonas* sp. ef1 in HS

medium at pH 6.5. This BCSA subunit structure is shared also by other cellulose-producing *Pseudomonas* strains. However, these strains also possess a standard operon organization. By contrast, *Pseudomonas* sp. ef1 appears to have lost the standard operon organization, likely following its adaptation to the Antarctic host environment. The water-soluble form of the *Pseudomonas* ef1 BC makes it particularly well-suited for coating applications, especially in food packaging, as it eliminates the need for additional processing steps—such as homogenization—before spreading it onto other materials. Bacterial synthesis of cellulose is seen as a convenient and effective way to produce stable recyclable fibers for use in wound dressing and in a variety of emerging nanotechnologies. Furthermore, BC has industrial applications, such as acting as sponges to collect leaking oil and as materials for absorbing toxins *(J. Wang et al., 2019)*. Exploring new methods for cellulose synthesis, beyond traditional vegetable sources, will aid in the development of innovative and renewable materials.

In addition, Antarctic BC was tested in collaboration with papermaking industry, for the development of an innovative packaging product.

Being able to scale-up BC production represents a key factor for its transition from laboratory research to commercial applications. Indeed, some BC-based products have already been developed and are currently available on the market. For instance, BC-based wound dressings are commercialized as moist membranes composed of 1.5-4.3% BC or as dry films with a thickness of 0.05 mm. These BC films have been also functionalized with chemically reduced AgNPs to enhance their antimicrobial properties *(Zhong, 2020a)*.

Moreover, as BC has been considered as a "generally recognized as safe" food additives by FDA since 1992, it has been applied in food sector as food additive and in the packaging industry *(Shi et al., 2014)*. One of the most established commercial applications of BC in this sector is nata de coco, a fermented cellulose gel marketed in Asian countries as a traditional dessert. BC is produced through the natural fermentation of coconut water by *K. xylinus*, forming a hydrated pellicle and used as a low-calorie and fiber-rich food ingredient *(Shi et al., 2014; Zhong, 2020b)*. Moreover, BC has been proposed as a thickening, suspending and stabilizing agent in beverage and food *(Lin et al., 2020)*.
Although industrial-scale BC production is already established for some products, its application in commercial food packaging is still emerging, mainly due to production costs, scalability limitations and the necessity to further tailor its physicochemical properties for packaging requirements *(J. Li et al., 2022)*.
However, recent literature has demonstrated that the incorporation of BC into paper can improve its properties in terms of tensile strength, hydrophobicity, fire-resistance *(Fillat et al., 2018; Janbade et al., 2022)*. The characteristics of the final product depend on several factors, including the bacterial strain employed, the type of paper substrate, and the method chosen for BC incorporation into paper supports *(Fillat et al., 2018)*. BC has been successfully incorporated into composite paper for durable goods such as banknotes and Bible paper, and it can be functionalized to produce paper with specific properties such as electrical conductivity, through the incorporation of metallic nanoparticles *(Janbade et al., 2022)*.

In agreement with these findings, the preliminary results obtained from BC incorporation as a coating material on traditional paper showed promising

hydrophobic and oleophobic properties, highly appreciated in packaging applications. However, further improvements in terms of surface coverage and coating homogeneity are still required to improve coating performance and to achieve an efficient and scalable product. Overall, the results obtained support the potential of BC as a sustainable functional coating for paper-based packaging materials, highlighting promising application prospects while also emphasizing the need for further process optimization to enable industrial implementation.

Conclusions

In this study, the production of bacterial cellulose by novel Antarctic strains was investigated. Microorganisms belonging to *Bacillus*, *Brevundimonas*, *Halomonas* and *Pseudomonas* spp. were proved to be BC producers. BC biosynthesis was examined in detail using *Pseudomonas* sp. ef1. When grown with glucose as sole carbon source, this strain resulted capable of producing BC with different morphologies, depending on the culture conditions: a sheet-like form of BC in Hestrin–Schramm (HS) medium under static conditions, and spherical BC flocculates in media containing yeast extract or nutrient broth with seawater under shaking conditions. The different BC morphologies were characterized by FT-IR, XRD, and DSC analysis confirming the presence of bacterial cellulose, and specifically cellulose I for dispersed sheet-like BC and cellulose II for spherical BC, with thermal stability up to 300 °C. Genomic analysis revealed a putative cellulose synthase subunit A with an extracellular domain belonging to the Exo-beta-1,3-glucanase family, which is unusual and likely contributes to the unique organization and water solubility of the BC produced by this strain. This structural peculiarity maybe the result of adaptation to the Antarctic environment. Lastly, Antarctic BC was employed to develop an

innovative product for biopackaging in collaboration with the papermaking industry, with ongoing efforts aimed at further optimization.

References

Abouelkheir, S. S., Kamara, M. S., Atia, S. M., Amer, S. A., Youssef, M. I., Abdelkawy, R. S., Khattab, S. N., & Sabry, S. A. (2020). Novel research on nanocellulose production by a marine Bacillus velezensis strain SMR: a comparative study. *Scientific Reports*, *10*(1), 14202. https://doi.org/10.1038/s41598-020-70857-7

Almihyawi, R. A. H., Musazade, E., Alhussany, N., Zhang, S., & Chen, H. (2024). Production and characterization of bacterial cellulose by Rhizobium sp. isolated from bean root. *Scientific Reports*, *14*(1), 10848. https://doi.org/10.1038/s41598-024-61619-w

Ardré, M., Dufour, D., & Rainey, P. B. (2019a). Causes and Biophysical Consequences of Cellulose Production by Pseudomonas fluorescens SBW25 at the Air-Liquid Interface. *Journal of Bacteriology*, *201*(18). https://doi.org/10.1128/JB.00110-19

Baek, M., DiMaio, F., Anishchenko, I., Dauparas, J., Ovchinnikov, S., Lee, G. R., Wang, J., Cong, Q., Kinch, L. N., Schaeffer, R. D., Millán, C., Park, H., Adams, C., Glassman, C. R., DeGiovanni, A., Pereira, J. H., Rodrigues, A. V., van Dijk, A. A., Ebrecht, A. C., … Baker, D. (2021). Accurate prediction of protein structures and interactions using a three-track neural network. *Science*, *373*(6557), 871–876. https://doi.org/10.1126/science.abj8754

Bektas, I., & Yildirim, N. B. (2025). Molecular Characterization of Bacterial Cellulose Producing *Bacillus* Strains Isolated From Soil. *Journal of Basic Microbiology*, *65*(6). https://doi.org/10.1002/jobm.70026

Berlemont, R., Delsaute, M., Pipers, D., D'Amico, S., Feller, G., Galleni, M., & Power, P. (2009). Insights into bacterial cellulose biosynthesis by functional metagenomics on Antarctic soil samples. *The ISME Journal*, *3*(9), 1070–1081. https://doi.org/10.1038/ismej.2009.48

Brigham, C. (2018). Biopolymers. In *Green Chemistry* (pp. 753–770). Elsevier. https://doi.org/10.1016/B978-0-12-809270-5.00027-3

Burnett, A. J. N., Rodriguez, E., Constable, S., Lowrance, B., Fish, M., & Weadge, J. T. (2023). WssI from the Gram-negative bacterial cellulose synthase is an O-acetyltransferase that acts on cello-oligomers with several acetyl donor substrates. *Journal of Biological Chemistry*, *299*(7), 104849. https://doi.org/10.1016/j.jbc.2023.104849

Castro, C., Zuluaga, R., Putaux, J.-L., Caro, G., Mondragon, I., & Gañán, P. (2011). Structural characterization of bacterial cellulose produced by Gluconacetobacter swingsii sp. from Colombian agroindustrial wastes. *Carbohydrate Polymers*, *84*(1), 96–102. https://doi.org/10.1016/j.carbpol.2010.10.072

Chiriac, A. I., Pastor, F. I. J., Popa, V. I., Aflori, M., & Ciolacu, D. (2014). Changes of supramolecular cellulose structure and accessibility induced by the processive endoglucanase Cel9B from Paenibacillus barcinonensis. *Cellulose*, *21*(1), 203–219. https://doi.org/10.1007/s10570-013-0118-x

El-Saied, H., Basta, A. H., & Gobran, R. H. (2004). Research Progress in Friendly Environmental Technology for the Production of Cellulose Products (Bacterial Cellulose and Its Application). *Polymer-Plastics Technology and Engineering*, *43*(3), 797–820. https://doi.org/10.1081/PPT-120038065

Fatima, A., Ortiz-Albo, P., Neves, L. A., Nascimento, F. X., & Crespo, J. G. (2023). Biosynthesis and characterization of bacterial cellulose membranes presenting relevant characteristics for air/gas filtration. *Journal of Membrane Science*, *674*, 121509. https://doi.org/10.1016/j.memsci.2023.121509

Felgueiras, C., Azoia, N. G., Gonçalves, C., Gama, M., & Dourado, F. (2021). Trends on the Cellulose-Based Textiles: Raw Materials and Technologies. *Frontiers in Bioengineering and Biotechnology*, *9*. https://doi.org/10.3389/fbioe.2021.608826

Fillat, A., Martínez, J., Valls, C., Cusola, O., Roncero, M. B., Vidal, T., Valenzuela, S. V., Diaz, P., & Pastor, F. I. J. (2018). Bacterial cellulose for increasing barrier properties of paper products. *Cellulose*, *25*(10), 6093–6105. https://doi.org/10.1007/s10570-018-1967-0

Girard, L., Lood, C., Höfte, M., Vandamme, P., Rokni-Zadeh, H., van Noort, V., Lavigne, R., & De Mot, R. (2021). The Ever-Expanding Pseudomonas Genus: Description of 43 New Species and Partition of the Pseudomonas putida Group. *Microorganisms*, *9*(8), 1766. https://doi.org/10.3390/microorganisms9081766

Girard, V., Chaussé, J., & Vermette, P. (2024). Bacterial cellulose: A comprehensive review. *Journal of Applied Polymer Science*, *141*(15). https://doi.org/10.1002/app.55163

Gong, J., Li, J., Xu, J., Xiang, Z., & Mo, L. (2017). Research on cellulose nanocrystals produced from cellulose sources with various polymorphs. *RSC Advances*, *7*(53), 33486–33493. https://doi.org/10.1039/C7RA06222B

Gorgieva, S., & Trček, J. (2019). Bacterial Cellulose: Production, Modification and Perspectives in Biomedical Applications. *Nanomaterials*, *9*(10), 1352. https://doi.org/10.3390/nano9101352

Gullo, M., Sola, A., Zanichelli, G., Montorsi, M., Messori, M., & Giudici, P. (2017). Increased production of bacterial cellulose as starting point for scaled-up applications. *Applied Microbiology and Biotechnology*, *101*(22), 8115–8127. https://doi.org/10.1007/s00253-017-8539-3

H. Ritchie. (2021). *Drivers of Deforestation*. Our World in Data. https://archive.ourworldindata.org/20251125-173858/drivers-of-deforestation.html

Haft, D. H., Paulsen, I. T., Ward, N., & Selengut, J. D. (2006). Exopolysaccharide-associated protein sorting in environmental organisms: the PEP-CTERM/EpsH system. Application of a novel phylogenetic profiling heuristic. *BMC Biology*, *4*(1), 29. https://doi.org/10.1186/1741-7007-4-29

Hallgren, J., Tsirigos, K. D., Pedersen, M. D., Almagro Armenteros, J. J., Marcatili, P., Nielsen, H., Krogh, A., & Winther, O. (2022). *DeepTMHMM predicts alpha and beta transmembrane proteins using deep neural networks*. https://doi.org/10.1101/2022.04.08.487609

Hu, S., Shi, Z., Chen, K., Chen, X., Zhou, H., Yan, N., & Yang, G. (2025). Bacterial cellulose as green matrix material for environmental-friendly electronic devices. *Carbohydrate Polymers*, *368*, 124075. https://doi.org/10.1016/j.carbpol.2025.124075

Janbade, A., Zaidi, S., Vats, M., Kumar, N., Dhiman, J., & Gupta, M. K. (2022). A Mini Review on Current Advancement in Application of Bacterial Cellulose in

Pulp and Paper Industry. In *Proceedings of International Conference on Innovative Technologies for Clean and Sustainable Development (ICITCSD – 2021)* (pp. 435–445). Springer International Publishing. https://doi.org/10.1007/978-3-030-93936-6_36

John, M. S., Nagoth, J. A., Ramasamy, K. P., Mancini, A., Giuli, G., Miceli, C., & Pucciarelli, S. (2022). Synthesis of Bioactive Silver Nanoparticles Using New Bacterial Strains from an Antarctic Consortium. *Marine Drugs*, *20*(9), 558. https://doi.org/10.3390/md20090558

John, M. S., Nagoth, J. A., Zannotti, M., Giovannetti, R., Mancini, A., Ramasamy, K. P., Miceli, C., & Pucciarelli, S. (2021). Biogenic Synthesis of Copper Nanoparticles Using Bacterial Strains Isolated from an Antarctic Consortium Associated to a Psychrophilic Marine Ciliate: Characterization and Potential Application as Antimicrobial Agents. *Marine Drugs*, *19*(5), 263. https://doi.org/10.3390/md19050263

Kadier, A., Ilyas, R. A., Huzaifah, M. R. M., Harihastuti, N., Sapuan, S. M., Harussani, M. M., Azlin, M. N. M., Yuliasni, R., Ibrahim, R., Atikah, M. S. N., Wang, J., Chandrasekhar, K., Islam, M. A., Sharma, S., Punia, S., Rajasekar, A., Asyraf, M. R. M., & Ishak, M. R. (2021). Use of Industrial Wastes as Sustainable Nutrient Sources for Bacterial Cellulose (BC) Production: Mechanism, Advances, and Future Perspectives. *Polymers*, *13*(19), 3365. https://doi.org/10.3390/polym13193365

Krasteva, P. V., Bernal-Bayard, J., Travier, L., Martin, F. A., Kaminski, P.-A., Karimova, G., Fronzes, R., & Ghigo, J.-M. (2017). Insights into the structure

and assembly of a bacterial cellulose secretion system. *Nature Communications*, *8*(1), 2065. https://doi.org/10.1038/s41467-017-01523-2

Kuga, S., Takagi, S., & Brown, R. M. (1993). Native folded-chain cellulose II. *Polymer*, *34*(15), 3293–3297. https://doi.org/10.1016/0032-3861(93)90404-X

Lahiri, D., Nag, M., Dutta, B., Dey, A., Sarkar, T., Pati, S., Edinur, H. A., Abdul Kari, Z., Mohd Noor, N. H., & Ray, R. R. (2021a). Bacterial Cellulose: Production, Characterization, and Application as Antimicrobial Agent. *International Journal of Molecular Sciences*, *22*(23), 12984. https://doi.org/10.3390/ijms222312984

Lee, C. M., Gu, J., Kafle, K., Catchmark, J., & Kim, S. H. (2015). Cellulose produced by Gluconacetobacter xylinus strains ATCC 53524 and ATCC 23768: Pellicle formation, post-synthesis aggregation and fiber density. *Carbohydrate Polymers*, *133*, 270–276. https://doi.org/10.1016/j.carbpol.2015.06.091

Lee, K.-Y., Buldum, G., Mantalaris, A., & Bismarck, A. (2014). More Than Meets the Eye in Bacterial Cellulose: Biosynthesis, Bioprocessing, and Applications in Advanced Fiber Composites. *Macromolecular Bioscience*, *14*(1), 10–32. https://doi.org/10.1002/mabi.201300298

Li, J., Zhang, F., Zhong, Y., Zhao, Y., Gao, P., Tian, F., Zhang, X., Zhou, R., & Cullen, P. (2022). Emerging Food Packaging Applications of Cellulose Nanocomposites: A Review. *Polymers*, *14*(19), 4025. https://doi.org/10.3390/polym14194025

Lin, D., Liu, Z., Shen, R., Chen, S., & Yang, X. (2020). Bacterial cellulose in food industry: Current research and future prospects. *International Journal of Biological Macromolecules*, *158*, 1007–1019. https://doi.org/10.1016/j.ijbiomac.2020.04.230

Little, A., Schwerdt, J. G., Shirley, N. J., Khor, S. F., Neumann, K., O'Donovan, L. A., Lahnstein, J., Collins, H. M., Henderson, M., Fincher, G. B., & Burton, R. A. (2018). Revised Phylogeny of the *Cellulose Synthase* Gene Superfamily: Insights into Cell Wall Evolution. *Plant Physiology*, *177*(3), 1124–1141. https://doi.org/10.1104/pp.17.01718

Marsh, A. J., O'Sullivan, O., Hill, C., Ross, R. P., & Cotter, P. D. (2014). Sequence-based analysis of the bacterial and fungal compositions of multiple kombucha (tea fungus) samples. *Food Microbiology*, *38*, 171–178. https://doi.org/10.1016/j.fm.2013.09.003

Martins, P. H. S., Barros, M. A., Silva, C. L., Ricci, P., Castilho, L. M. B., Santos, A. L. R., Rodrigues, H. S., Assunção, R. M. N., & Faria, A. M. (2024). A cellulose monolithic stir bar for sorptive extraction of glycerol from biodiesel. *RSC Advances*, *14*(25), 17380–17388. https://doi.org/10.1039/D4RA02985B

Marzban, G., & Tesei, D. (2025). The Extremophiles: Adaptation Mechanisms and Biotechnological Applications. *Biology*, *14*(4), 412. https://doi.org/10.3390/biology14040412

McNamara, J. T., Morgan, J. L. W., & Zimmer, J. (2015). A Molecular Description of Cellulose Biosynthesis. *Annual Review of Biochemistry*, *84*(1), 895–921. https://doi.org/10.1146/annurev-biochem-060614-033930

Mishra, S., Singh, P. K., Pattnaik, R., Kumar, S., Ojha, S. K., Srichandan, H., Parhi, P. K., Jyothi, R. K., & Sarangi, P. K. (2022). Biochemistry, Synthesis, and Applications of Bacterial Cellulose: A Review. *Frontiers in Bioengineering and Biotechnology*, *10*. https://doi.org/10.3389/fbioe.2022.780409

Mohammadkazemi, F., Azin, M., & Ashori, A. (2015). Production of bacterial cellulose using different carbon sources and culture media. *Carbohydrate Polymers*, *117*, 518–523. https://doi.org/10.1016/j.carbpol.2014.10.008

Morgan, J. L. W., McNamara, J. T., & Zimmer, J. (2014). Mechanism of activation of bacterial cellulose synthase by cyclic di-GMP. *Nature Structural & Molecular Biology*, *21*(5), 489–496. https://doi.org/10.1038/nsmb.2803

Nabeela, K., Thomas, R. T., Nair, R. V., Namboorimadathil Backer, S., Mohan, K., Chandran, P. R., & Pillai, S. (2020). Direct Visualization of Crystalline Domains in Carboxylated Nanocellulose Fibers. *ACS Omega*, *5*(21), 12136–12143. https://doi.org/10.1021/acsomega.0c00410

Nagarajan, S., Skillen, N. C., Irvine, J. T. S., Lawton, L. A., & Robertson, P. K. J. (2017). Cellulose II as bioethanol feedstock and its advantages over native cellulose. *Renewable and Sustainable Energy Reviews*, *77*, 182–192. https://doi.org/10.1016/j.rser.2017.03.118

Nagoth, J. A., John, M. S., Ramasamy, K. P., Mancini, A., Zannotti, M., Piras, S., Giovannetti, R., Rathnam, L., Miceli, C., Biondini, M. C., & Pucciarelli, S. (2024). Synthesis of Bioactive Nickel Nanoparticles Using Bacterial Strains from an Antarctic Consortium. *Marine Drugs*, *22*(2), 89. https://doi.org/10.3390/md22020089

Nobles, D. R., & Brown, R. M. (2004). The pivotal role of cyanobacteria in the evolution of cellulose synthases and cellulose synthase-like proteins. *Cellulose*, *11*(3–4), 437–448. https://doi.org/10.1023/B:CELL.0000046339.48003.0e

Oliveira, R. L., Vieira, J. G., Barud, H. S., Assunção, R. M. N., Rodrigues Filho, G., Ribeiro, S. J. L., & Messadeqq, Y. (2015). Synthesis and Characterization of

Methylcellulose Produced from Bacterial Cellulose under Heterogeneous Condition. *Journal of the Brazilian Chemical Society*. https://doi.org/10.5935/0103-5053.20150163

Omadjela, O., Narahari, A., Strumillo, J., Mélida, H., Mazur, O., Bulone, V., & Zimmer, J. (2013). BcsA and BcsB form the catalytically active core of bacterial cellulose synthase sufficient for in vitro cellulose synthesis. *Proceedings of the National Academy of Sciences*, *110*(44), 17856–17861. https://doi.org/10.1073/pnas.1314063110

O'Sullivan, A. C. (1997). Cellulose: the structure slowly unravels. *Cellulose*, *4*(3), 173–207. https://doi.org/10.1023/A:1018431705579

Petrushin, I., Belikov, S., & Chernogor, L. (2020). Cooperative Interaction of Janthinobacterium sp. SLB01 and Flavobacterium sp. SLB02 in the Diseased Sponge Lubomirskia baicalensis. *International Journal of Molecular Sciences*, *21*(21), 8128. https://doi.org/10.3390/ijms21218128

Poddar, M. K., & Dikshit, P. K. (2021). Recent development in bacterial cellulose production and synthesis of cellulose based conductive polymer nanocomposites. *Nano Select*, *2*(9), 1605–1628. https://doi.org/10.1002/nano.202100044

Pucciarelli, S., Devaraj, R. R., Mancini, A., Ballarini, P., Castelli, M., Schrallhammer, M., Petroni, G., & Miceli, C. (2015). Microbial Consortium Associated with the Antarctic Marine Ciliate Euplotes focardii: An Investigation from Genomic Sequences. *Microbial Ecology*, *70*(2), 484–497. https://doi.org/10.1007/s00248-015-0568-9

Raghavendran, V. , A. E. , and R. I. (2020). Bacterial cellulose: Biosynthesis, production, and applications. In *Advances in Microbial Physiology* (Vol. 77, pp. 89–138). https://doi.org/10.1016/bs.ampbs.2020.07.002

Ramasamy, K. P., Mahawar, L., Rajasabapathy, R., Rajeshwari, K., Miceli, C., & Pucciarelli, S. (2023). Comprehensive insights on environmental adaptation strategies in Antarctic bacteria and biotechnological applications of cold adapted molecules. *Frontiers in Microbiology*, *14*. https://doi.org/10.3389/fmicb.2023.1197797

Ramasamy, K. P., Telatin, A., Mozzicafreddo, M., Miceli, C., & Pucciarelli, S. (2019). Draft Genome Sequence of a New Pseudomonas sp. Strain, ef1, Associated with the Psychrophilic Antarctic Ciliate Euplotes focardii. *Microbiology Resource Announcements*, *8*(41). https://doi.org/10.1128/MRA.00867-19

Ross, P., Mayer, R., & Benziman, M. (1991). Cellulose biosynthesis and function in bacteria. *Microbiological Reviews*, *55*(1), 35–58. https://doi.org/10.1128/mr.55.1.35-58.1991

Ruiz-Ruiz, C., Srivastava, G. K., Carranza, D., Mata, J. A., Llamas, I., Santamaría, M., Quesada, E., & Molina, I. J. (2011). An exopolysaccharide produced by the novel halophilic bacterium Halomonas stenophila strain B100 selectively induces apoptosis in human T leukaemia cells. *Applied Microbiology and Biotechnology*, *89*(2), 345–355. https://doi.org/10.1007/s00253-010-2886-7

Sani, A., & Dahman, Y. (2010). Improvements in the production of bacterial synthesized biocellulose nanofibres using different culture methods. *Journal of Chemical Technology & Biotechnology*, *85*(2), 151–164. https://doi.org/10.1002/jctb.2300

Sayah, I., Gervasi, C., Achour, S., & Gervasi, T. (2024). Fermentation Techniques and Biotechnological Applications of Modified Bacterial Cellulose: An Up-to-Date Overview. *Fermentation*, *10*(2), 100. https://doi.org/10.3390/fermentation10020100

Shi, Z., Zhang, Y., Phillips, G. O., & Yang, G. (2014). Utilization of bacterial cellulose in food. *Food Hydrocolloids*, *35*, 539–545. https://doi.org/10.1016/j.foodhyd.2013.07.012

Shibazaki, H., Saito, M., Kuga, S., & Okano, T. (1998). Native Cellulose II Production by Acetobacter Xylinum Under Physical Constraints. *Cellulose*, *5*(3), 165–173. https://doi.org/10.1023/A:1009277122329

Silva, I. G. R. da, Pantoja, B. T. dos S., Almeida, G. H. D. R., Carreira, A. C. O., & Miglino, M. A. (2022). Bacterial Cellulose and ECM Hydrogels: An Innovative Approach for Cardiovascular Regenerative Medicine. *International Journal of Molecular Sciences*, *23*(7), 3955. https://doi.org/10.3390/ijms23073955

Stanciu, M.-C., Tanasă, F., & Teacă, C.-A. (2025). Crystallinity Changes in Modified Cellulose Substrates Evidenced by Spectral and X-Ray Diffraction Data. *Polysaccharides*, *6*(2), 30. https://doi.org/10.3390/polysaccharides6020030

Torgbo, S., & Sukyai, P. (2020). Biodegradation and thermal stability of bacterial cellulose as biomaterial: The relevance in biomedical applications. *Polymer Degradation and Stability*, *179*, 109232. https://doi.org/10.1016/j.polymdegradstab.2020.109232

Ullah, M. W., Ul Islam, M., Khan, S., Shah, N., & Park, J. K. (2017). Recent advancements in bioreactions of cellular and cell-free systems: A study of

bacterial cellulose as a model. *Korean Journal of Chemical Engineering*, *34*(6), 1591–1599. https://doi.org/10.1007/s11814-017-0121-2

Vazquez, A., Foresti, M. L., Cerrutti, P., & Galvagno, M. (2013). Bacterial Cellulose from Simple and Low Cost Production Media by Gluconacetobacter xylinus. *Journal of Polymers and the Environment*, *21*(2), 545–554. https://doi.org/10.1007/s10924-012-0541-3

Verhoef, R., de Waard, P., Schols, H. A., Rättö, M., Siika-aho, M., & Voragen, A. G. J. (2002). Structural elucidation of the EPS of slime producing Brevundimonas vesicularis sp. isolated from a paper machine. *Carbohydrate Research*, *337*(20), 1821–1831. https://doi.org/10.1016/S0008-6215(02)00280-X

Wada, M., OKANO, T., & SUGIYAMA, J. (1997). Synchrotron-radiated X-ray and neutron diffraction study of native cellulose. *Cellulose*, *4*(3), 221–232. https://doi.org/10.1023/A:1018435806488

Wang, J., Tavakoli, J., & Tang, Y. (2019). Bacterial cellulose production, properties and applications with different culture methods – A review. *Carbohydrate Polymers*, *219*, 63–76. https://doi.org/10.1016/j.carbpol.2019.05.008

Yim, S. M., Song, J. E., & Kim, H. R. (2017). Production and characterization of bacterial cellulose fabrics by nitrogen sources of tea and carbon sources of sugar. *Process Biochemistry*, *59*, 26–36. https://doi.org/10.1016/j.procbio.2016.07.001

Zannotti, M., Di Sessa, M., Biondini, M. C., Vassallo, A., Ferraro, S., Angeloni, S., Ricciutelli, M., Pucciarelli, S., & Giovannetti, R. (2026). Towards an easy production of novel pyoverdines by an antarctic Pseudomonas strain: a spectroscopic and HPLC-MS/MS characterization study. *Dyes and Pigments*, *244*, 113096. https://doi.org/10.1016/j.dyepig.2025.113096

Zhong, C. (2020a). Industrial-Scale Production and Applications of Bacterial Cellulose. *Frontiers in Bioengineering and Biotechnology*, *8*. https://doi.org/10.3389/fbioe.2020.605374

Zhong, C. (2020b). Industrial-Scale Production and Applications of Bacterial Cellulose. *Frontiers in Bioengineering and Biotechnology*, *8*. https://doi.org/10.3389/fbioe.2020.605374

CHAPTER 2

A novel *Rhodococcus* sp. ef1 – mediated biosynthetic pigment

Abstract

This study characterizes a novel pigment produced by the Antarctic bacterium *Rhodococcus* sp. ef1. The molecule exhibited pH-dependent colour changes, appearing blue under alkaline conditions and pink under acidic conditions. Chemical characterization enabled its identification as a pyocyanin derivative. To date, no *Rhodococcus* spp. have been reported to produce this pigment, which is typically synthesised by *Pseudomonas* spp., including *Pseudomonas aeruginosa*, although several *Rhodococcus* species possess genes putatively involved in its biosynthesis.

Genome sequencing of *Rhodococcus* sp. ef1 allowed the identification of genes typically present in the operon of *P. aeruginosa*. Despite further analyses are required to detail the chemical structure and verify operon organization, differences were observed in gene arrangement compared with the operon of *P. aeruginosa*, which may explain the different molecular structure and the behaviour of the pigment. Preliminary assessment of its bioactivity was also performed by evaluating the antimicrobial activity against common pathogenic species.

State of the art

In nature, microbes commonly synthesize pigments in response to several environmental factors *(Orlandi et al., 2022)*. Some of these molecules participate in the photosynthetic process of autotrophic bacteria, including chlorophyll, carotene and xanthene *(H. Agarwal et al., 2023)*. Coloured secondary metabolites protect cells against UV and oxidative stress induced damage *(Órdenes-Aenishanslins et al., 2016; Sandmann, 2019)*. Among the major representatives, carotenoids are efficient scavengers of reactive oxygen species *(Reis-Mansur et al., 2019)*. In several species, pigments also offer competitive advantages by inhibiting other hostile species or acting as virulence factors that contribute to host damage and colonization *(G. Y. Liu & Nizet, 2009)*. Siderophores, such as pyoverdines, are involved in iron chelation and transport, whereas phenazines play a pivotal role in modulating the redox state of the cell, regulating gene expression and promoting biofilm formation (Pierson & Pierson, 2010; Visca et al., 2007).

Bacterial pigments are emerging biomolecules due to their sustainable production and their valuable properties (*Figure 24*). Since these metabolites can be produced through entirely green protocols and low-impact bioprocesses, they represent an attractive alternative to synthetic molecules *(Celedón & Díaz, 2021)*. Their chromatic properties enable their employment in the food industry, cosmetics, and in textiles. Moreover, these compounds exhibit a broad spectrum of biological activities which ensure remarkable biotechnological applications in a wide range of sectors. Their photoprotective, antimicrobial, antioxidant, anticancer, and biostimulating activities are highly appreciated in biomedicine,

pharmaceutical industry, and agriculture *(Choi et al., 2021; Orlandi et al., 2022; Venil et al., 2020)*.

The market for natural pigments is currently expanding, with the natural β-carotene market estimated to be worth approximately USD 1.28 billion in 2024, compared to USD 256 million for the synthetic β-carotene. Similarly, the astaxanthin market is predicted to reach a value of USD 3,4 billion by 2027 *(Chavan et al., 2025)*. In contrast, the production of bacterial pigments has a more limited commercial resonance; however, this sector is expected to grow significantly in the following years *(Venil et al., 2020)*. Therefore, this emerging field with a wide diversity of compounds and considerable unexplored potential represents a promising sector to invest in. Moreover, bacterial pigments offer several advantages over synthetic counterparts. Life cycle assessments reveal that they have smaller environmental impacts, including reduced gas emissions and fossil resource depletion, as well as reduced toxicity and carcinogenicity *(Chavan et al., 2025)*.

The main limitations of microbial pigments include scale-up and stability of the compounds *(Venil et al., 2020)*. Wild-type strains typically produce pigments at low concentrations, making large-scale production challenging. Therefore, optimization of the culture conditions is pivotal to enhance the biosynthetic process. The use of agro-industrial waste as growth substrates can significantly contribute to reducing the production costs *(Chavan et al., 2025)*. In addition, genetic engineering, recombinant DNA technology, and enzyme isolation for in vitro synthesis represent promising strategies to overcome low productivity *(Orlandi et al., 2022)*. Regarding stability, natural pigments are often sensitive to environmental factors such as pH, light, temperature, and oxygen

concentration. However, several protective approaches have been recently developed, including pigment microencapsulation or production of nano emulsions with surfactants which can improve both resistance to degradation and solubility. *(Orlandi et al., 2022).*

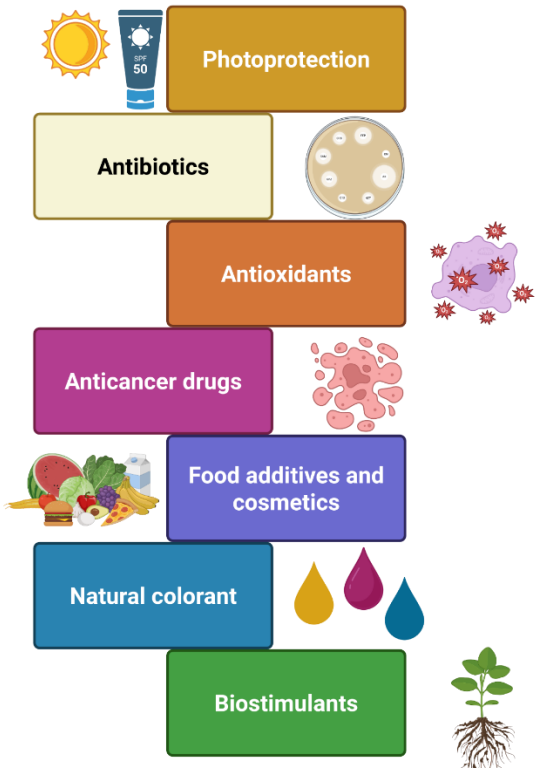

Figure 24 - Bacterial pigments can be employed in a broad range of applications, including cosmetics, biomedicine, food industry, textiles, and agriculture. Created with BioRender.com. Publication license obtained.

Overall, microbial pigments enhance bacterial survival and play essential ecological functions *(Garcia-Lopez et al., 2021)*. Their investigation provides important insights into microbial intra- and interspecific communication and

adaptation strategies. Moreover, the study of bacterial pigments expands the potential for discovering novel applications and driving biotechnological innovation. Despite recent advances, indeed, a multitude of pigment diversity remains still unexplored *(Anshi et al., 2024)*. In particular, bacteria inhabiting extreme environments represent a promising source of unique chemical structures and functions *(Órdenes-Aenishanslins et al., 2016)*.

Pyocyanin is a particular class of pigments belonging to the phenazine family, which comprises heterocyclic compounds containing nitrogen atoms *(Abdelaziz et al., 2023)*. Pyocyanin is a redox-active molecule, and its colour depends on its redox state: in neutral or alkaline conditions, the oxidized form exhibits a bright blue colour, in acidic conditions, instead, protonation leads to a deep pink-red colour. At pH of 7.0, pyocyanin generally exists in the zwitterionic form, appearing blue in colour *(Mudaliar & Bharath Prasad, 2024)*. The reduced form, instead, is colourless *(Price-Whelan et al., 2007)*. Pyocyanin is typically synthesized by *Pseudomonas* spp., with *P. aeruginosa* being the most widely studied representative *(Eltarahony et al., 2025a)*. Other genera, including *Streptomyces* spp., *Vibrio* spp., *Burkholderia* spp., *Brevibacterium* spp., etc., have also been recognized as potential producers *(W. Huang et al., 2024a)*. In *P. aeruginosa* strains, this molecule functions as a virulence factor involved in iron acquisition from the extracellular environment, by promoting reduction mechanisms which facilitate the liberation of iron from transferrin *(Shouman et al., 2023)*. The phenazine biosynthetic pathway typically consists of two homologous seven-gene phenazine operons, phz A1B1C1D1E1F1G1 and phz A2B2C2D2E2F2G2, responsible for the synthesis of phenazine-1-carboxylic acid, and three accessory genes, phzM, phzS, and phzH, encoding tailoring

enzymes involved in enzymatic modifications *(Mavrodi et al., 2001)*. phz operon can also be preceded by two regulatory genes, phzR and phzI *(S. R. Khan et al., 2005)*. Phenazines, including pyocyanin and its derivatives, comprise a multitude of molecules with a broad spectrum of biological activities, including antibacterial, fungicidal, antibiofilm, antitumoral, biopesticidal effects. *(W. Huang et al., 2024a).* Pyocyanin therapeutic potential seems related to its ability to generate reactive oxygen species (ROS), including superoxide ($O_2^{\cdot-}$) and hydrogen peroxide (H_2O_2) *(Marey et al., 2024; Mudaliar & Bharath Prasad, 2024).* The zwitterionic nature of the molecule enables pyocyanin to accept the electrons from reducing agents, like NADH or reduced glutathione, and to transport them to electron acceptors, such as oxygen. This redox activity of pyocyanin may play a dual role. On one side, it is involved in bactericidal, anticancer and antidegenerative effects, by altering the electron transfer pathways, leading to the generation of excess intracellular oxygen reduction products and subsequent cell death *(Marey et al., 2024)*. On the other side, the same activity may also impact normal mammalian cells, raising concerns regarding cytotoxicity. Studies suggested that the selective effect of pyocyanin on cancer cells is based on their increased basal levels of ROS compared to normal cells, and that cytotoxicity strictly depends on pyocyanin concentration.*(Abdelaziz et al., 2022; Marey et al., 2024).* Moreover, the producing strain plays an important role: while the pigment synthesised by *P. aeruginosa* may negatively affect mammalian cells, phenazines produced by other non-canonical organisms, such as *Streptomyces* spp., do not appear cytotoxic in eukaryotes and instead show promise as anticancer and anti-infective agents *(Mavrodi et al., 2010a)*. Despite its therapeutic potential, assessment of pyocyanin's toxicity remains essential to exclude any deleterious

effect or interference with normal cellular functions *(Mudaliar & Bharath Prasad, 2024).*

In this work, we report the synthesis of a novel pink-blue pigment from an Antarctic strain isolated from a bacterial consortium associated with the Antarctic ciliate *Euplotes focardii (Pucciarelli et al., 2015)* and named *Rhodococcus* sp. ef1. *E. focardii* is a free-swimming protozoan endemic to the oligotrophic coastal sediments of Terra Nova Bay, classified as an obligate psychrophilic stenotherm *(Mozzicafreddo et al., 2021; Pischedda et al., 2018; Pucciarelli et al., 2009; Yang et al., 2013)*. The bacterial strains within this consortium have previously demonstrated remarkable biotechnological potential. They are capable of transforming heavy metals, including copper, nickel, and silver, into nanoparticles, producing unique pyoverdines, and synthesizing bacterial cellulose with distinctive properties *(Biondini et al., 2025; John et al., 2021a, 2021b, 2022b; Nagoth et al., 2024; Zannotti et al., 2026)*. *Rhodococcus* is a genus of actinomycetes widely studied for its bioremediation potential *(Nazari et al., 2022)*. The novel *Rhodococcus* strain ef1 has already been successfully employed for the synthesis of metallic nanoparticles with antimicrobial activity *(John et al., 2022b; Nagoth et al., 2024)*. Here, we demonstrated that it is also capable of producing a novel pigment identified as a pyocyanin derivative. To our knowledge, this is the first report of a *Rhodococcus* strain synthesizing phenazine molecules.

In the following sections, insights on biosynthesis and chemical identification of a novel pyocyanin derivative are provided. The characterization occurred by UV-Vis spectroscopy, infrared spectroscopy, liquid chromatography coupled to a mass-mass spectrometer, and NMR spectroscopy. Finally, genome sequencing

of *Rhodococcus* sp. ef1 provided preliminary information about the structure of the putative operon involved in the synthesis of the molecule.

Materials and methods

Bacterial strain

The microbial organism used in this work, *Rhodococcus* sp. ef1, was isolated from a bacterial consortium associated with the Antarctic ciliate *E. focardii*. For its maintenance, this strain was plated from a glycerol stock onto a Lysogeny Broth Agar (LBA) medium (Tryptone 10 g/L, Yeast extract 5 g/L, NaCl 5 g/L, microbiological Agar 12 g/l) and grown overnight at 22 °C.

Pigment production and harvesting

A loop of bacterial culture was inoculated in 100 ml of modified Davis Minimal Medium (MMD) liquid medium in 500 ml flasks. The medium was prepared with the following composition:

- $(NH_4)_2SO_4$ 1g/l
- K_2HPO_4 7 g/l
- KH_2PO_4 2 g/l
- Na_3 citrate $2H_2O$ 1.5 g/l
- $MgSO_4$ $7H_2O$ 0.1 g/l

The pH was adjusted to 7.2 and the medium was autoclaved for 15 minutes at 121 °C to achieve sterilization. $MgSO_4$ was prepared, filtered and added post-sterilization to prevent precipitation.

Different concentrations of citrate were tested to identify the best culture conditions. Growth curves of bacterial culture supplemented with different

citrate concentrations were constructed by monitoring the OD 600 for two days, using a VWR UV-1600 PC spectrophotometer.

Since the use of 1.5 g/l citrate resulted in the fastest pigment production, this concentration was selected to enhance the biosynthetic process. Glucose, originally present in the medium, was removed as its presence favored bacterial growth over pigment production. Bacterial culture was incubated in a thermal shaker (110 rpm) at 24.5 °C. After two days, the production of the pigment was visible, as shown by the change in color of the microbial suspension. Pigment harvesting occurred after 4 days of culturing, on average.

The blue bacterial suspension was collected and centrifuged for 20 minutes at 3.000 rpm. The pellet was washed with distilled water to remove residual salts. Extraction was performed by adding chloroform (400 µl per 100 mg pellet) and incubating the sample overnight at 4 °C. Centrifugation at 14.000 rpm for 1 minute enabled the separation of the cell debris (white layer) from the pink chloroform layer, which was collected for subsequent steps. The solvent was then evaporated, and the dry pigment was weighed to estimate the crude yield of the pyocyanin derivative produced by *Rhodococcus* p. ef1.

Solubilization in water occurred by adding double distilled H_2O and NaOH 1 M (10% V/V) to the chloroform-extracted pigment under mild heating. Neutralization of pH was achieved by the gradual addition of HCl, drop by drop.

Genome sequencing

DNA used for sequencing was extracted from a culture of *Rhodococcus* sp. ef1 grown overnight in 10 mL of LB (10 g/L tryptone, 5 g/L yeast extract, 10 g/L NaCl) at 23°C under shaking. Cells were harvested by centrifugation and DNA was extracted by using the ‘DNeasy PowerSoil Pro Kit’ (Qiagen), following the

protocol provided by the manufacturer. Genomic DNA of *Rhodococcus* sp. ef1 was sequenced with nanopore technology and using a native barcoding approach, according to the protocol Ligation sequencing gDNA – Native Barcoding Kit 24 V14 (SQK-NBD114.24), version NBE_9169_v114_revQ_15Sep2022. The quality, purity and concentration of the DNA sample after extraction and in all the subsequent steps of library preparation were checked using NanoDrop (Thermo Scientific™), Qubit Fluorometer and Agilent TapeStation.

Sequencing was carried out using a GridION equipped with a R10.4 flow cell (Oxford Nanopore Technology, ONT). Basecalling was performed with MinKNOW v23.11.3 using the super accurate model. A minimum Q score of 10 and a minimum read length of 200 b were applied as filtering criteria. Sequencing reads were assembled using EPI2ME v5.1.8 and the workflow 'wf-bacterial-genomes' v1.0.0.

The putative coding regions (CDSs) were annotated by the software PROKKA (version 1.14.5). The annotated genome was analyzed to identify the operon responsible for the synthesis of pyocyanin-derivative. The predicted genes were aligned against *Pseudomonas aeruginosa* PAO1 operon sequences using Basic Local Alignment Search Tool (BLAST). Sequence alignments, SnapGene, and Operon Mapper were useful tools for the identification and the preliminary characterization of the putative operon responsible for the synthesis of the pigment in the analyzed strain.

The identification of the operon in the *Rhodococcus* genome was performed using Circoletto (Circoletto @ the BAT cave).

Multiple alignments were performed for each putative protein involved using Clustal Omega, provided by EMBL-EBI. Sequences belonging to *Pseudomonas*, *Streptomyces*, and *Actinobacteria* were selected based on the parameters given by BLASTx alignments. Information about sequence ID, organisms, e value, identities (%), positives (%), and gaps (%) are reported below for each alignment. The complete sequences of each alignment are provided in the last section of the thesis (Supplementary Material).

These are the sequences used in the multiple alignment of putative PhzS from *Rhodococcus* sp. ef1:

Sequence ID	*Organism*	*E - value*	*Identities*	*Positives*	*Gaps*
WP_100882555.1	*P. aeruginosa*	$1e^{-109}$	*49%*	*61%*	*3%*
VEE50093.1	*P. fluorescens*	$3e^{-109}$	*48%*	*61%*	*3%*
WP_256065518.1	*Rhodococcus erythropolis*	*0,0*	*99%*	*99%*	*0%*
WP_217019072.1	*Rhodococcus qingshengii*	*0,0*	*96%*	*97%*	*1%*
WP_372409467.1	*Streptomyces luteireticuli*	$4e^{-121}$	*54%*	*66%*	*3%*
WP_097866731.1	*Streptomyces sp. rh34*	$4e^{-124}$	*53%*	*64%*	*2%*

The sequences were selected from BLASTx alignments matches having an e value ≤ $1e^{-109}$, identities > 48%, gaps ≤ 3%.

These are the sequences used in the multiple alignment with the putative Antibiotic biosynthesis monooxygenase:

Sequence ID	*Organism*	*E - value*	*Identities*	*Positives*	*Gaps*
WP_433107589.1	*Microbispora sp. CA-102843*	*$1e^{-46}$*	*68%*	*84%*	*0%*
WP_143486620.1	*Pseudomonas mangiferae*	*$2e^{-26}$*	*53%*	*73%*	*1%*
WP_021334645.1	*Rhodococcus (multispecies)*	*$2e^{-72}$*	*100%*	*100%*	*0%*
WP_256065519.1	*Rhodococcus erythropolis*	*$9e^{-72}$*	*99%*	*99%*	*0%*
WP_433496940.1	*Sphaerimonospora sp. CA-214678*	*$5e^{-45}$*	*67%*	*80%*	*0%*
WP_344023404.1	*Streptomyces luteireticuli*	*$4e^{-42}$*	*65%*	*79%*	*0%*

The sequences were selected from BLASTx alignments matches having an e value ≤ $4e^{-42}$, identities ≥ 65%, gaps = 0%, excluding *Pseudomonas mangiferae*. While the alignments with the other *Pseudomonas* spp. did not show any similarity and produced unreliable matches, *Pseudomonas mangiferae*, instead,

showed a significant match (e value of $2e^{-26}$, identities of 53%, gaps of 1%) and was chosen as genus representative.

These are the sequences used in the multiple alignment with the putative PhzA/B from *Rhodococcus* sp. ef1:

Sequence ID	*Organism*	*E - value*	*Identities*	*Positives*	*Gaps*
HHW1969258.1	*Pseudomonas aeruginosa*	*$9e^{-59}$*	*70%*	*80%*	*0%*
WP_124339061.1	*Pseudomonas chlororaphis*	*$5e^{-59}$*	*68%*	*81%*	*0%*
WP_214992101.1	*Pseudomonas fluorescens*	*$3e^{-59}$*	*68%*	*81%*	*0%*
WP_053129818.1	*Pseudomonas sp. CMR5c*	*$1e^{-59}$*	*71%*	*79%*	*0%*
WP_030537981.1	*Rhodococcus (multispecies)*	*$1e^{-91}$*	*99%*	*99%*	*0%*
WP_397525121.1	*Rhodococcus qingshengii*	*$3e^{-88}$*	*96%*	*97%*	*0%*
WP_086157042.1	*Streptomyces marincola*	*$5e^{-65}$*	*79%*	*86%*	*0%*
WP_359815293.1	*Streptomyces niveus*	*$1e^{-64}$*	*80%*	*84%*	*0%*

The sequences were selected from BLASTx alignments matches having an e value < $9e^{-59}$, identities ≥ 68%), gaps = 0%.

These are the sequences used in the multiple alignment with the putative PhzC from *Rhodococcus* sp. ef1:

Sequence ID	*Organism*	*E - value*	*Identities*	*Positives*	*Gaps*
WP_209098778.1	*Pseudomonas aeruginosa*	$1e^{-106}$	*49%*	*60%*	*1%*
WP_214992101.1	*Pseudomonas fluorescens*	$3e^{-59}$	*68%*	*81%*	*0%*
WP_143486210.1	*Pseudomonas mangiferae*	$4e^{-103}$	*47%*	*57%*	*2%*
WP_186698045.1	*Pseudomonas shirazensis*	$7e^{-72}$	*39%*	*52%*	*2%*
WP_336505324.1	*Rhodococcus erythropolis*	*0,0*	*99%*	*99%*	*0%*
KSU60285.1	*Rhodococcus qingshengii*	$3e^{-88}$	*96%*	*97%*	*0%*
WP_314250358.1	*Streptomyces kutzneri*	$8e^{-124}$	*51%*	*64%*	*0%*
WP_226074269.1	*Streptomyces marincola*	$3e^{-121}$	*53%*	*64%*	*1%*
GAB2331875.1	*Streptomyces variabilis*	$4e^{-124}$	*53%*	*64%*	*1%*

The sequences were selected from BLASTx alignments matches having an e value $\leq 3e^{-59}$, identities of at least 39% (only in one case, in the other cases identities were $\geq 47\%$), gaps $\leq 2\%$.

These are the sequences used in the multiple alignment with the putative PhzD from *Rhodococcus* sp. ef1:

Sequence ID	Organism	E - value	Identities	Positives	Gaps
WP_153341071.1	*Nocardia aurantia*	$4e^{-84}$	61%	71%	0%
WP_203328712.1	*Pseudomonas aeruginosa*	$6e^{-76}$	55%	65%	0%
WP_075121686.1	*Pseudomonas chlororaphis*	$1e^{-75}$	54%	66%	0%
VEE46437.1	*Pseudomonas fluorescens*	$2e^{-75}$	54%	65%	0%
WP_336505323.1	*Rhodococcus erythropolis*	$2e^{-150}$	99%	99%	0%
WP_217019070.1	*Rhodococcus qingshengii*	$9e^{-149}$	99%	99%	0%
WP_055721456.1	*Streptomyces niveiscabiei*	$5e^{-77}$	56%	70%	0%

The sequences were selected from BLASTx alignments matches having an e value ≤ $1e^{-75}$, identities ≥ 54%), gaps = 0%.

These are the sequences used in the multiple alignment with the putative PhzE from *Rhodococcus* sp. ef1:

Sequence ID	*Organism*	*E - value*	*Identities*	*Positives*	*Gaps*
WP_026343200.1	*Nocardia sp. BMG111209*	*0,0*	*58%*	*70%*	*2%*
OLF51938.1	*Pseudomonas chlororaphis*	*0,0*	*54%*	*68%*	*2%*
VEE46436.1	*Pseudomonas fluorescens*	*0,0*	*59%*	*71%*	*0%*

WP_336505322.1	*Rhodococcus erythropolis*	*0,0*	*99%*	*99%*	*0%*
WP_047269922	*Rhodococcus qingshengii*	*0,0*	*100%*	*100%*	*0%*
WP_355064226.1	*Streptomyces rubiginosohelvolus*	*0,0*	*56%*	*70%*	*2%*
MGW0882928.1	*Streptomyces sp. NPDC002671*	*0,0*	*56%*	*69%*	*2%*

The sequences were selected from BLASTx alignments matches with an e value of 0,0, identities ≥ 54%, and gaps ≤ 2%.

These are the sequences used in the multiple alignment with the putative PhzF from *Rhodococcus* sp. ef1:

Sequence ID	*Organism*	*E - value*	*Identities*	*Positives*	*Gaps*
WP_319942845.1	*Nocardia aurantia*	$2e^{-104}$	*50%*	*61%*	*2%*
WP_315558930.1	*Pseudomonas aeruginosa*	$8e^{-91}$	*56%*	*66%*	*2%*
WP_150770788.1	*Pseudomonas fluorescens*	$4e^{-42}$	*35%*	*47%*	*5%*
WP_143486207.1	*Pseudomonas mangiferae*	$2e^{-91}$	*56%*	*67%*	*2%*
WP_276117756.1	*Rhodococcus sp. C3V*	*0,0*	*98%*	*98%*	*0%*
WP_071367550.1	*Streptomyces colonosanans*	$1e^{-94}$	*59%*	*69%*	*2%*
WP_398714565.1	*Streptomyces rubiginosohelvolus*	$6e^{-108}$	*51%*	*64%*	*1%*

The sequences were selected from BLASTx alignments matches having an e value ≤ $4e^{-42}$, identities ≥35%, gaps ≤ 5% (only in the alignment with *P. fluorescence*, in the other cases the gaps were ≤ 2%).

These are the sequences used in the multiple alignment with the putative PhzG from *Rhodococcus* sp. ef1:

Sequence ID	*Organism*	*E - value*	*Identities*	*Positives*	*Gaps*
WP_328709570.1	*Microbispora hainanensis*	$4e^{-66}$	*54%*	*66%*	*0%*
WP_128663115.1	*Pseudomonas aeruginosa*	$5e^{-45}$	*42%*	*56%*	*1%*
WP_075121689.1	*Pseudomonas chlororaphis*	$5e^{-53}$	*44%*	*62%*	*0%*
WP_248798019.1	*Pseudomonas sp. MWU13-2105*	$1e^{-54}$	*46%*	*61%*	*0%*
WP_217019068.1	*Rhodococcus qingshengii*	$2e^{-141}$	*96%*	*97%*	*0%*
WP_173874215.1	*Streptomyces albus*	$9e^{-73}$	*58%*	*69%*	*0%*
WP_355064222.1	*Streptomyces rubiginosohelvolus*	$1e^{-69}$	*56%*	*65%*	*0%*

The sequences were selected from BLASTx alignments matches having an e value ≤ $1e^{-54}$, identities ≥ 42%, gaps ≤ 1%.

These are the sequences used in the multiple alignment with the putative Baeyer-Villiger monooxygenase from *Rhodococcus* sp. ef1:

Sequence ID	*Organism*	*E - value*	*Identities*	*Positives*	*Gaps*
WP_261985629.1	*Microbispora sp. CSR-4*	*0,0*	*61%*	*75%*	*0%*
WP_420757901.1	*Pseudomonas aeruginosa*	*$8e^{-91}$*	*56%*	*66%*	*2%*
WP_150644880.1	*Pseudomonas fluorescens*	*0,0*	*56%*	*70%*	*0%*
TRX76844.1	*Pseudomonas mangiferae*	*$4e^{-164}$*	*48%*	*74%*	*0%*
WP_011331502.1	*Rhodococcus (multispecies)*	*0,0*	*97%*	*97%*	*0%*
WP_164247642.1	*Streptomyces sp S4.7*	*0,0*	*60%*	*74%*	*0%*
WP_344023394.1	*Streptomyces luteireticuli*	*0,0*	*60%*	*74%*	*0%*

The sequences were selected from BLASTx alignments matches having an e value $\leq 4e^{-164}$, identities $\geq$*48%, gaps* $\leq$ *2%.*

Chemical characterization

The following analyses were performed by a research group of the Chemical Department of the University of Camerino, including Martina Di Sessa, PhD student of IUSS/UNICAM of the 39th cycle, Prof. Rita Giovannetti and Prof. Marco Zannotti.

The pigment was characterized by UV-Vis spectroscopy using an Agilent 8454 Cary UV-Visible Diode Array Spectrophotometer (Agilent, Santa Clara, USA). The UV-Vis spectral features was tested at different pH by micro-additions of

HCl and NaOH 1M (Carlo Erba reagents, Cornaredo, MI, Italy). The infrared analysis was performed on a Perkin-Elmer System 2000 FT-IR instrument (Waltham, MA, USA). FT-IR analysis was performed on dry pigment by using a Perkin-Elmer System 2000 spectrometer (Waltham, MA, USA equipped with Pike GladiATR technology).

HPLC analysis has been performed using Agilent Technologies 1200 series, with a C-18 reversed phase column. (ALTIMA C18 150 x 4.6 mm, particles size 5 µm, ALLTECH). The separation was performed in isocratic condition with 100% acetonitrile as mobile phase, with a flux of 1 ml/min. The injection volume was 5 µL and the temperature of the column set at 30°C. The wavelength selected for the DAD detector were: 288 nm, 301 nm, 348 nm, 360 nm, 515 nm and 617 nm.

HPLC-MS/MS analysis were performed using an HPLC Agilent 1290 Infinity coupled with a Triple Quadrupole 6420 (Agilent, Santa Clara, USA) with an electrospray (ESI) source operating in positive mode. The column used was a C-18 reversed phase column. (ALTIMA C18 150 x 4.6 mm, particles size 5 µm, ALLTECH), with a mobile phase of 70% of acetonitrile and 30% of water. The source parameters were set as follow: the temperature of the drying gas was 350 °C; the gas flow was 12 L/min−1; the nebulizer pressure was 55 psi; and the capillary voltage was 4000V. The wavelength selected for the DAD detector were: 288 nm, 301 nm, 348 nm, 360 nm, 515 nm. The acquisitions were performed in scan mode and once identified some interesting precursor ions the acquisitions were carried out in product ion scan mode. For each selected precursor ion, the fragmentation of the investigated compounds was monitored at different collision energy: 10, 20 and 40 eV.

For all the analysis, the sample was filtered through a 0.2 μm single use syringe filter from Phenomenex (Bologna, Italy).
The ^{1}H NMR analysis was performed on a 500 MHz Bruker Ascend 500 Avance III HD, in deuterated chloroform ($CDCl_3$).

Antibiotic activity tests

Due to the very well-known antimicrobial properties of phenazines and their derivatives *(W. Huang et al., 2024a)*, the compound was tested against some common microbial species. A first screening was performed against *S. aureus* and the Antarctic strain *Bacillus* sp. ef1 as Gram-positive model organisms, and *E. coli* as a Gram-negative representative. The activity was evaluated against *S. aureus* and *E. coli* during the period abroad (as reported in the following chapter). The antimicrobial activity was evaluated against *Bacillus* sp. ef1 in the University of Camerino, both using the pigment extracted at basic pH and after pH neutralization through the addition of HCl, as previously described. Sterile filter paper discs (8 mm in diameter) were soaked with the pigment and placed on Mueller-Hinton Agar (MHA) plates uniformly spread with *Bacillus* sp. ef1.
Then, the antimicrobial potential was also evaluated against common pathogens, including *C. albicans, S. aureus*, *E. faecium*, *S. pyogenes, S. pneumoniae*, *S. agalactiae*, *P. aeruginosa*, *E. coli*, and *K. pneumoniae*. This study was performed in the Analysis Laboratory of the Hospital of Senigallia, under the supervision of Dr. Alessio Mancini, which isolated the species of interest and provided the material to perform the test. The pigment was tested under different concentrations, including 900, 600, 300, and 150 μg /ml. These concentrations were estimated based on the μg of pigment after chloroform evaporation per mL of water used during the solubilization step. Since not all the pigment present in

the chloroform layer could be completely solubilized in the aqueous phase, and due to the further dilution introduced by the process of neutralization, these concentrations are likely underestimated. The microbial species were cultured in their respective optimal solid media, including Candida brilliance for *C. albicans*, MacConkey Agar for Gram negative species, and colistin nalidixic acid (CNA) Agar for Gram positives. Arousing colonies were collected and resuspended in physiological solutions or LB medium, adjusting the final concentration to 0,5 McFarland units. The bacterial suspensions were spread onto plates containing the appropriate solid media for each strain. Filter paper discs (8 mm in diameter), previously sterilized under UV light for 30 minutes, were subsequently placed on the inoculated plate surfaces. The effects were observed after 48 hours of incubation by visual inspection of an inhibition halo surrounding the discs. The inhibition area (%) was calculated with the help of ImageJ software.

The antimicrobial activity test was subsequently repeated on a subset of pathogens, including *C. albicans, S. aureus*, *P. aeruginosa*, *E. coli*, and *K. pneumoniae*, by performing broth microdilution assay. Briefly, the pyocyanin derivative was extracted in basic environment (pH ~ 10) and diluted in sterile Brain Heart Infusion Broth (BHI broth, Scharlau) to final concentrations of 600, 200 and 60 μg /ml. The selected microbial strains were inoculated into the broth, adjusting the final concentration to 0,5 McFarland units. Microorganisms inoculated in BHI alone and in BHI with the addition of the same concentrations (V/V) of H_2O (pH ~ 10) used during pigment extraction were used as control samples, to check, respectively, the suitability of the selected culture medium for the growth of all strains and the potential impact of basic environment on

microbial growth. The effects were evaluated after 48 hours of incubation by visual inspection of tube turbidity.

Lastly, pigment activity was also evaluated against *Bacillus* sp. ef1 by soaking discs obtained from spherical bacterial cellulose (BC) produced by the Antarctic strain *Pseudomonas* sp. ef1 (as previously reported in Chapter 1) and discs obtained from Kombucha cellulose synthesised from a consortium of acetic cellulose producers. This was a preliminary test performed to explore the possibility to combine different Antarctic bacteria-derived biomaterials the bioactive pigment and the bacterial cellulose, for biomedical purposes.

Results

Biosynthesis of pyocyanin

After two days of bacterial culture in MMD medium, blue bacterial suspension was present in the flask, revealing that the synthesis had occurred. Color intensity increased with time (*Figure 25*).

Figure 25 - Pyocyanin-derivative production after 4 days of bacterial culturing in MMD medium

Different concentration of sodium citrate affects the synthesis speed and yield

Different concentrations of sodium citrate were tested, including 0, 0,5, 1, 1,5, 2 g/L. The bacterial growth was monitored until the production of pyocyanin-derivative became visible. After two days of incubation, pigment synthesis was observed only in the cultures supplemented with 1.5 g/L and 2g/L sodium citrate, with 1,5 g/L showing the highest and the fastest production *(Figures 26-27)*.

Figure 26 -Different concentration of Na_3-citrate affects pyocyanin-derivative production.

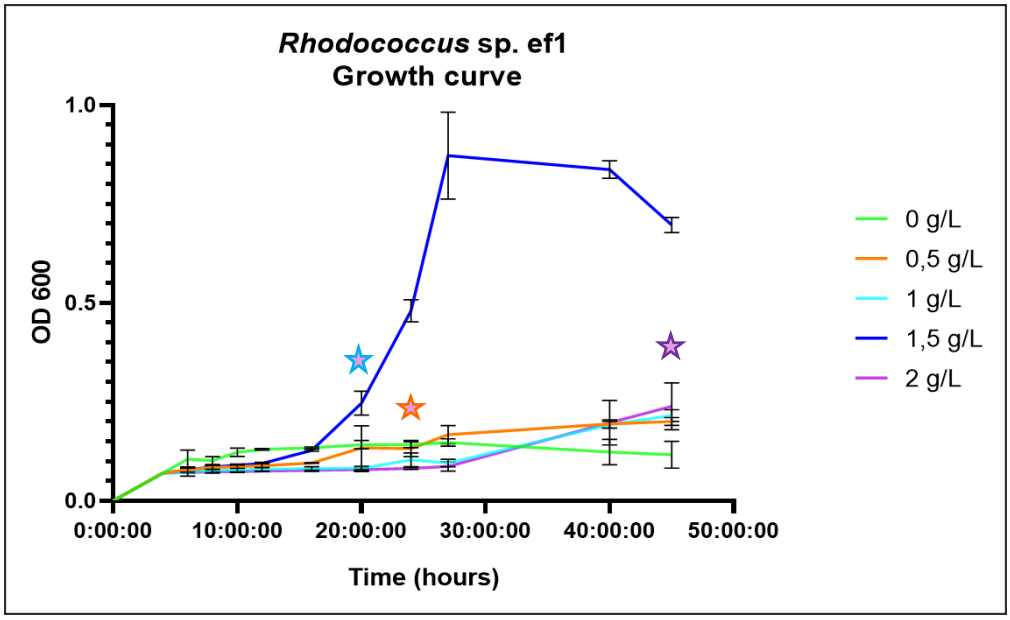

Figure 27 - Growth curve with different Na_3-citrate concentrations. The stars indicate the time at which the synthesis of the pigment became detectable

Pigment harvesting and solubilization in water

Blue bacterial suspension was centrifuged to collect the pellet containing cell-associated pigment. Chloroform was added to the sample to help the extraction process. Following overnight incubation, chloroform layer turned pink, indicating a successful extraction of the pigment *(Figure 28)*. The estimated crude yield of the pyocyanin derivative was 31 mg/L.

Figure 28 – Chloroform phase containing the extracted pigment.

Solubilization in water occurred under alkaline pH, by adding double distilled H_2O and NaOH 1 M (10% V/V) to the chloroform-extracted pigment. This step was performed under mild heating of the sample. The water upper layer became dark blue, whereas the chloroform layer at the bottom became gradually transparent *(Figure 29)*.

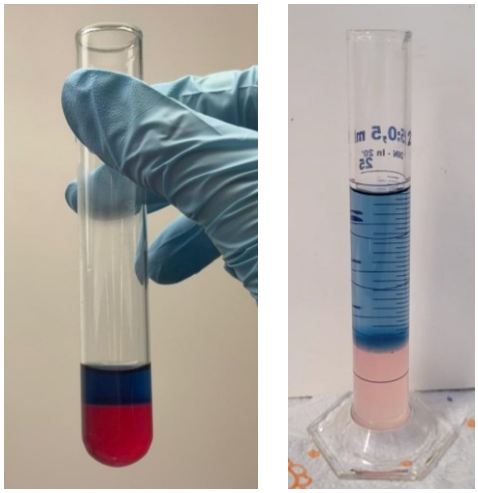

Figure 29 - Water solubilization of the pigment starting from chloroform extraction.

Neutralization of the pigment was performed by adding HCl drop by drop under mild heating of the sample. The color shifted to light grey-violet at pH 7.0 *(Figure 30)*.

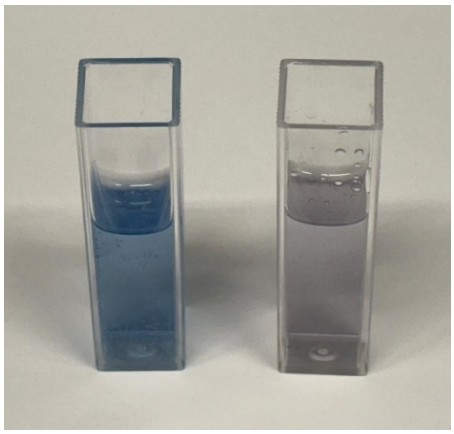

Figure 30 - Pigment displays an intense blue colour in an alkaline environment (on the left), whereas it appears mild grey/violet in neutral pH conditions.

DNA extraction and sequencing results

The extracted DNA concentration was 870,7 ng/µl. The purity of the sample was adequate for the following analyses, with an A_{260}/A_{280} ratio of 1.92 and an A_{260}/A_{230} ratio of 2.02. The library had an optimal length distribution of the fragments, with a main peak at 26722 bp, as shown in *Table 2*. 5 Gb of data were obtained from the sequencing process, with a coverage of 328,42 per base, on average. Information derived from genome assembly is resumed in *Table 3*. Three contigs were identified, corresponding to a putative circular chromosome and two plasmids (Contig 3, 1 and 2 in the *Table 4,* respectively).

Table 2 - Length distribution of the fragments after library preparation.

Size (bp)	***Calibrated Conc.***	***% Integrated Area***	***From (bp)***	***To (bp)***
100	*8.50*	*-*	*70*	*143*
26722	*47.6*	*99.80*	*6165*	*>60.000*

Table 3 - The table shows the number of contigs identified, the sequenced bases, the number of identified coding regions (CDS), rRNA, tRNA and tmRNA sequences.

Contigs	*3*
Bases	*7089123*
CDS	*6734*

rRNA	*15*
Repeat region	*1*
tRNA	*55*
tmRNA	*1*

Table 4 - The table below shows the identified coding regions with length, coverage, circularity.

#seq_name	***Length***	***Coverage***	***Circularity***
contig_3	*6.467.287*	*317*	*Yes*
contig_2	*496.104*	*392*	*No*
contig_1	*125.735*	*665*	*No*

Chemical characterization

Chemical characterization was performed in parallel by the PhD student of the 39th Martina Di Sessa, under the supervision of Prof. Rita Giovannetti and Prof. Marco Zannotti of the Chemical Department. The FT-IR spectrum confirmed that this molecule containing aromatic ring was a pyocyanin derivative (data not shown). HPLC data confirmed the purity of the sample, and the results from HPLC-MS/MS and H NMR spectra further confirmed the identity of the pigment, in agreement with the literature (data not shown) *(Koyun et al., 2022; Shouman et al., 2023).*

UV-vis spectrum and FTIR analyses executed by me during the period abroad are reported in Chapter 3, *Figure 40-41*.

The putative operon structure

The genes putatively involved in the pyocyanin derivative synthesis were identified among the annotated coding regions. These sequences were analyzed through BLAST alignments and compared with the well-characterized phenazine operon of *P. aeruginosa* PAO1, used as a reference standard *(Mavrodi et al., 2001)*.
The biosynthetic genes are present in a clustered region on Contig 1, previously recognized as a plasmid. This genomic organization is consistent with an operon arrangement, as also suggested by Operon Mapper predictions. The putative operon structure was reconstructed *(Figure 31)*. Six genes were identified as part of the biosynthetic core, including phzB, phzC, phzD, phzE, phzF, phzG.

Moreover, few other putative phenazine related sequences were identified, likely encoding tailoring enzymes involved in chemical modifications of pyocyanin precursors. phzS was located in the upstream region, followed by a predicted coding sequence potentially encoding an antibiotic biosynthesis monooxygenase. Downstream phzG, instead, a Baeyer-Villiger monooxygenase was identified. Interestingly, phzM and phzH, responsible for pyocyanin decoration in *P. aeruginosa*, were apparently absent in this bacterial strain. These differences in the additional genes associated with pyocyanin modification could explain the differences in the chemical structure of the novel phenazine derivative.

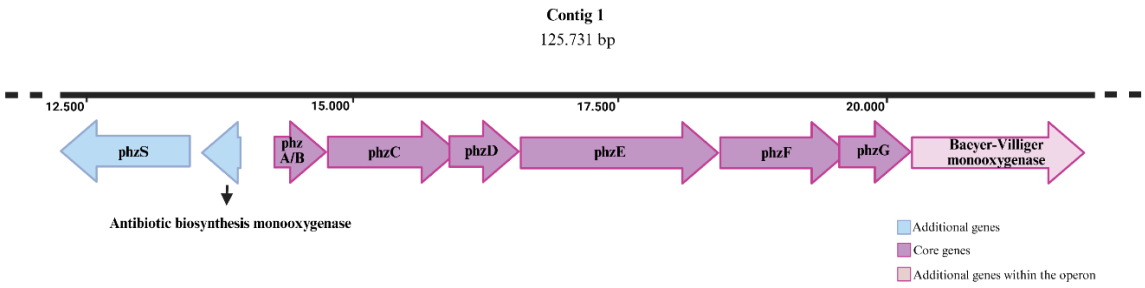

Figure 31 - The putative operon structure involved in the phenazine biosynthesis present in the contig 1.

The protein sequences of the six genes of the core are reported in the Supplementary Material section, followed by the protein sequences likely corresponding to the tailoring enzymes.

Interestingly, only a single gene putatively associated with pigment biosynthesis was identified on Contig 3, corresponding to the main chromosome. This gene was annotated as phzG1 and is potentially responsible for encoding the enzyme PhzG. This sequence was not apparently part of an operon. Adjacent genes in the same strand are involved in iron binding and transportation. BLAST alignments revealed the presence of a conserved domain of a pyridoxine/pyridoxamine 5'-phosphate oxidase, consistent with the PhzG protein family. BLASTp alignment with PhzG2 of the reference strains *P. aeruginosa* PAO1 revealed 35% of protein sequence identity, with a E value of $2e^{-33}$ and 92% of coverage. The alignment with PhzG1 of P. aeruginosa PAO1 showed similar results with 35,55% of identity, $1e^{-33}$ of E value, and 92% of query coverage The corresponding protein sequence is provided in the Supplementary Material section.

In the following section, the outputs (alignments and phylogenetic trees) of Clustal Omega alignments are reported among the putatively involved sequences and the selected reference sequences reported in the Supplementary Material section – Chapter II.

Multiple alignment output for the putative PhzS:

```
CLUSTAL O(1.2.4) multiple sequence alignment


Rhodococcus_qingshengiiWP_217019072.1       MASKDLTTIRPPISTTTRPPISIAGAGIGGLSAALALHERGHEA-ALFESAPEIVPLGVG     59
Rho_PhzS                                    MASKDL--------TTTRPPISIAGAGIGGLSAALALHERGHEA-ALFESAPEIVPLGVG     51
Rhodococcus_erythropolisWP_256065518.1      MASKDL--------TTTRPPISIAGAGIGGLSAALALHERGHEA-ALFESAPEIVPLGVG     51
Pseudomonas_aeruginosaWP_100882555.1        --------------MSEPIDILIAGAGIGGLSCALALHQAGIGKVTLLESSSEIRPLGVG     46
Pseudomonas_fluorescensVEE50093.1           --------------MSEPIDILIAGAGIGGLSCALALHQAGIGKVTLLESSSEIRPLGVG     46
Streptomyces_sp.rh34WP_097866731.1          ------------MSKAAQTAIVIAGAGIGGLTAALALHARGLPA-TVLETAAEIRPLGVG     47
Streptomyces_luteireticuliWP_372409467.1    ------------MTTADTAGFVIAGAGIGGLTAALALHARGIGA-TVLEAAEEILPLGVG     47
                                                        :    : *********:.*****  *    :::*:: ** *****

Rhodococcus_qingshengiiWP_217019072.1       INVQPTAIAELSRLGLADQLARIGVATQAHRYVDHRGRTLWTEPRGIAAGHDYPQYSVHR     119
Rho_PhzS                                    INVQPTAIAELSRLGLADQLARIGVATQAHRYVDHRGRTLWTEPRGIAAGHDYPQYSVHR     111
Rhodococcus_erythropolisWP_256065518.1      INVQPTAIAELSRLGLADQLARIGVATQAHRYVDHRGRTLWTEPRGIAAGHDYPQYSVHR     111
Pseudomonas_aeruginosaWP_100882555.1        INIQPAAVEALAELGLGPALAATAIPTHELRYIDQSGATVWSEPRGVEAGNAYPQYSIHR     106
Pseudomonas_fluorescensVEE50093.1           INIQPAAVEALAELGLGPALAATAIPTHELRYIDQSGATVWSEPRGVEAGNAYPQYSIHR     106
Streptomyces_sp.rh34WP_097866731.1          INIQPTAVAELIGLGLGDALAATGIPTREHRYLNHRGATLWTEPRGAAAGHAAPQYSLHR     107
Streptomyces_luteireticuliWP_372409467.1    INIQPAAIAELTALGFADALAATGIATREHLYVDHRGTTLWTEPRGLAAGYGHPQYSLHR     107
                                            **:**:*:  *  **:.  **  .: *:   *::: * *:*:****  **   ****:**

Rhodococcus_qingshengiiWP_217019072.1       GHLQMMLLDAVTERLGPGAVHSDARLSNISGSGETAIRLTVVNSDGRSRILDTDVLVGAD     179
Rho_PhzS                                    GHLQMMLLDAVTERLGPGAVHSDARLSNISGSGETAIQLTVVNSDGRSRILDTDVLVGAD     171
Rhodococcus_erythropolisWP_256065518.1      GHLQMMLLDAVTERLGPGAVHSDARLSNISGSGETAIQLTVVNSDGRSRTLDTDVLVGAD     171
Pseudomonas_aeruginosaWP_100882555.1        GELQMILLAAVRERLGQQAVRTDLGVERIEERDGR-VLIGARDGHGKPQALGADVLVGAD     165
Pseudomonas_fluorescensVEE50093.1           GELQMILLAAVRERLGQQAVRTGLGVERIEERDGR-VLIGARDGHGKPLALGGDVLVGAD     165
Streptomyces_sp.rh34WP_097866731.1          GELQMLLLEAVKERLGARAIRTATEVRGFHQAGDR-VFVHTTTPSGEAEVAEADVLIGAD     166
Streptomyces_luteireticuliWP_372409467.1    GELQMMLLDAVRERLGPGAVRTGLRVHGFERTADG-VRVEARDPSDSAVLLEATALIGAD     166
                                            *.***:** ** ****  *:::   :  :       : : .    .        .*:***

Rhodococcus_qingshengiiWP_217019072.1       GLHSTVRRWLHPDEAPVSVAGTTMWRGLADLPYTFLDGVTMIIANDGTGTRMVAYPCSEQ     239
Rho_PhzS                                    GLHSTVRRWLHPDEAPVSVAGTTMWRGLADLPYIFLDGVTMIIANDGTGTRLVAYPCSEQ     231
Rhodococcus_erythropolisWP_256065518.1      GLHSTVRRWLHPDEAPVSVAGTTMWRGLADLPYTFLDGVTMIIANDGTGTRLVAYPCSEQ     231
Pseudomonas_aeruginosaWP_100882555.1        GIHSAVRAHLHPDQGPLSHGGITMWRGVTELD-RFLDGKTMIVANDEHWSRLVAYPISAR     224
Pseudomonas_fluorescensVEE50093.1           GIHSAVRAHLHPDQGPLSHGGITMWRGVTEFD-RFLDGKTMIVANDEHWSRLVAYPISAR     224
Streptomyces_sp.rh34WP_097866731.1          GLRSAVRSQLHPDEPPLRTTAVRMWRGLTELP-AFIDGRTMIIAADDRAGRFVAYPCSRR     225
Streptomyces_luteireticuliWP_372409467.1    GVRSTVRDRLHPGRSGLSTGGTRMWRGLTELD-GFLDGRTMIVAADDRATRLIAYPVSTR     225
                                            *::*:**  ***..  :   .  ****::::   *:** ***:* *    *::*** * :

Rhodococcus_qingshengiiWP_217019072.1       ASVEGRTLLNWVCLTPPDRRSPSE--------DERTGLVNALAEWDFDWFALTELAARSP     291
Rho_PhzS                                    ASVEGRTLLNWVCLTPSDRRSPSE--------DERTGLVNALAEWDFDWFDLTELAARSP     283
Rhodococcus_erythropolisWP_256065518.1      ASVEGRTLLNWVCLTPSDRRSPSE--------DERTGLVNALAEWDFDWFDLTELAARSP     283
Pseudomonas_aeruginosaWP_100882555.1        HAAEGKSLVNWVCMVPSAAVGQLDNEADWNRDGRLEDVLPFFADWDLGWFDIRDLLTRNQ     284
Pseudomonas_fluorescensVEE50093.1           HAAEGKSLVNWVCMVPSAAVGQLDNEADWNRNGRLEDVLPFFADWDLGWFDIRDLLTRNQ     284
Streptomyces_sp.rh34WP_097866731.1          HAERGTVLLNWVCLAAVEGGDP-G---SGVEPGRLEDLLPHFADWEFDWLDIRGTLAASP     281
Streptomyces_luteireticuliWP_372409467.1    AAARGKALLNWVCLVPDPAGGA-AGDPRLSRPGDPEEVLPHLAHWSFDWLDLRAMVLGSP     284
                                             : .*  *:****:.     .           .    ::  :*.*.:.*: :      .
```

```
Rhodococcus_qingshengiiWP_217019072.1       QVSVYPMVDRDPLSHWGSGRVTLLGDAAHPMYPIGANGASQAIIDAGALAECFTRATDPV   351
Rho_PhzS                                    QVSVYPMVDRDPLSHWGSGRVTLLGDAAHPMYPIGANGASQAIIDAGALAECFTRATDPV   343
Rhodococcus_erythropolisWP_256065518.1      QVSVYPMVDRDPLSHWGSGRVTLLGDAAHPMYPIGANGASQAIIDAGALAECFTRATDPV   343
Pseudomonas_aeruginosaWP_100882555.1        LILQYPMVDRDPLPHWGRGRITLLGDAAHLMYPMGANGASQAILDGIELAAALARNADVA   344
Pseudomonas_fluorescensVEE50093.1           LILQYPMVDRDPLPHWGRGRITLLGDAAHLMYPMGANGASQAILDGIELAAALARNADVA   344
Streptomyces_sp.rh34WP_097866731.1          EILHYPMVDRDPLPTWGDSRVTILGDAAHPMYPIGANGASQAVLDGVAVAAELSGGGDPA   341
Streptomyces_luteireticuliWP_372409467.1    QILHYPMVDRDPLDRWGDGRVTLLGDAAHLMYPIGANGASQAVLDAAALADHCAEHADPA   344
                                             :  *********  ** .*:*:****** ***:********::*.  :*   :   * .

Rhodococcus_qingshengiiWP_217019072.1       SALRSYEAMRIIPTTSIVEANRAMNESEKKTASRAGDPASAPARRLREITTEYRTVVDRS   411
Rho_PhzS                                    SALRSYEAMRIIPTTSIVEANRAMNESEKKTASRAGDPAAAPVRRLREITTEYRTVVDRS   403
Rhodococcus_erythropolisWP_256065518.1      SALRSYEAMRIIPTTSIVEANRAMNESEKKTASRAGDPAAAPARRLREITTEYRTVVDRS   403
Pseudomonas_aeruginosaWP_100882555.1        AALREYEEARRPTANKIILANRERERKEEWAAASRPKTEK---SAALEAITGSYRNQVERP   401
Pseudomonas_fluorescensVEE50093.1           AALREYEEARRPTANKIILANRERERKEEWAAASRPKTEK---SAALEAITGSYRNQVERP   401
Streptomyces_sp.rh34WP_097866731.1          AALHRYEAARRPATTAIVEANRAMDRSERALAERLDGDV---SAELRTITDDYRAAVERS   398
Streptomyces_luteireticuliWP_372409467.1    VALERYEAVRRPATTAIVLANREMDHAEKALAARPDGDK---SATLAEVTTAYRTTVERR   401
                                             **. **  *   :. *: ***  :. *   * *          *  :*  **  *:*

Rhodococcus_qingshengiiWP_217019072.1       TAR--     414
Rho_PhzS                                    TAR--     406
Rhodococcus_erythropolisWP_256065518.1      TAR--     406
Pseudomonas_aeruginosaWP_100882555.1        R----     402
Pseudomonas_fluorescensVEE50093.1           R----     402
Streptomyces_sp.rh34WP_097866731.1          -----     398
Streptomyces_luteireticuliWP_372409467.1    PSAGR     406
```

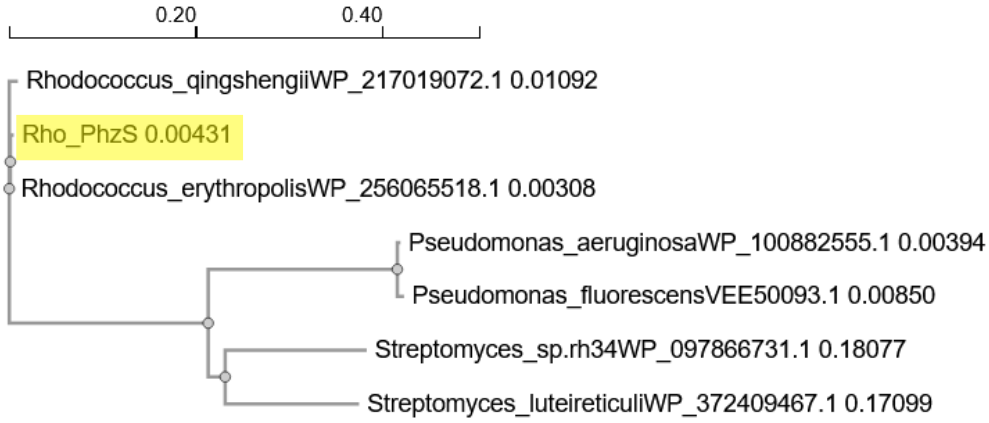

Multiple alignment output for the putative antibiotic biosynthesis monooxygenase:

```
CLUSTAL O(1.2.4) multiple sequence alignment

Pseudomonas_mangiferaeWP_143486620.1_antibiotic_biosynthesis_monooxygenase                -------MSGSEVTFINVIDV-DPSKQAEVIKLLQEGTESVISKRPGFVSVTLLASKDGS     52
Rhodococcus_erythropolisWP_256065519.1_antibiotic_biosynthesis_monooxygenase_family_protein MTETVIREGDKVATFINILELKDPAKQQDLIDVLNEGTEKVIKHQPGFISVNLFASRDGS     60
RhodococcusMULTISPECIESWP_021334645.1_MULTISPECIES:_antibiotic_biosynthesis_monooxygenase_family_protein MTETVIREGDKVATFINILELKDPAKQQDLIDVLNEGTEKVIKHQPGFISVNLFASRDGS     60
Rho_Antibiotic_biosynthesis_monooxygenase                                                 MTETVIREGDKVATFINILELKDPAKQQDLIDVLNEGTEKVIKHQPGFISVNLFASRDGS     60
Sphaerimonospora_sp.                                                                      MSETVIRVEDQVVTFINILDV-DPTKQQELIDVLNEGTEKVMSHRPGFVSVNILASLDGT     59
Microbispora_sp.                                                                          MSETVIRVGDQVATFINVFDV-DPSQQQELIGILNEGAEKVMRHRPGFISVNILASADGT     59
Streptomyces_luteireticuliWP_344023404.1_antibiotic_biosynthesis_monooxygenase_family_protein MSETVIRVGDEVATLINVFDV-EPSKQQELIAVLNEGTEKVMRHRPGFISVNLLASADGT     59
                                                                                                 .. .*:**:::: :*::* ::* :*:**:*.*: ::***:**.::** **:

Pseudomonas_mangiferaeWP_143486620.1_antibiotic_biosynthesis_monooxygenase                RVVNIAKWKSAADIQATQGDPAAAEFAKRTAALAKASPGIFEVVGEYSA 101
Rhodococcus_erythropolisWP_256065519.1_antibiotic_biosynthesis_monooxygenase_family_protein RVVNLAQWSSPDDIKAVATNPDAQAFAKKAAELATPAPGPYSVASVTQA 109
RhodococcusMULTISPECIESWP_021334645.1_MULTISPECIES:_antibiotic_biosynthesis_monooxygenase_family_protein RVVNLAQWSSPDDIKAVATNPDAQVFAKKAAELATPAPGPYSVASVTQA 109
Rho_Antibiotic_biosynthesis_monooxygenase                                                 RVVNLAQWSSPDDIKAVATNPDAQVFAKKAAELATPAPGPYSVASVTQA 109
Sphaerimonospora_sp.                                                                      RVVNLAQWRSLDDIKATMSDPEAQTFAKRTAEIAKAAPSPYRVVSVHHA 108
Microbispora_sp.                                                                          RVVNLAQWRSPDDIKATAGDPEAQVFAKRAAEIAKAAPQPYKVVSVYHA 108
Streptomyces_luteireticuliWP_344023404.1_antibiotic_biosynthesis_monooxygenase_family_protein RVVNYAQWRSPDDIKATLGDPEAGAFAKRAAELAKAAPLVYKVVAVHHA 108
                                                                                          **** *:* *  **:*.  :* *  ***::* :*. :*  : *..   *
```

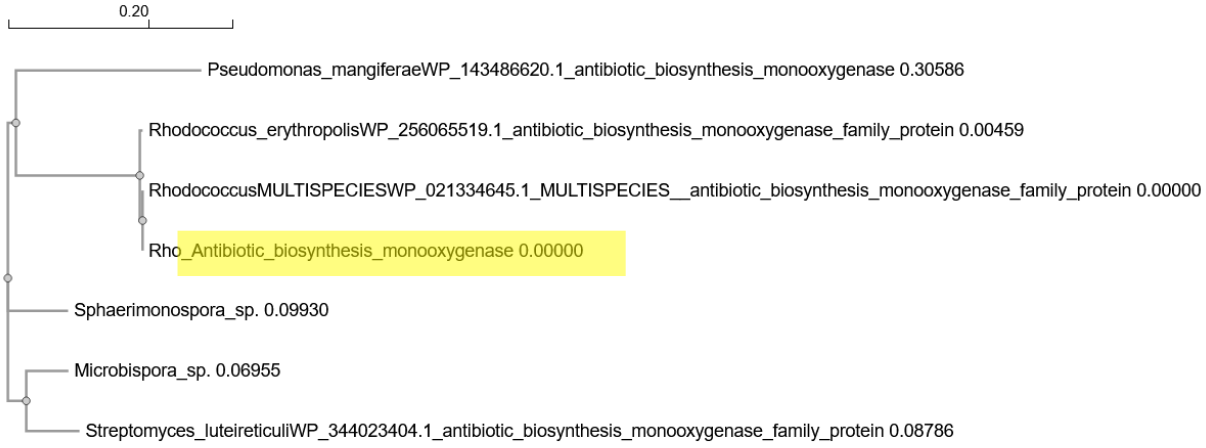

Multiple alignment output for the putative PhzA/B:

```
Pseudomonas_aeruginosa_HHW1969258.1_phenazine_biosynthesis_protein_PhzB ----------MLDNAIPQGFEDAVELRRKNRETVVKYMNTKG 32
Pseudomonas_sp.CMR5c_WP_053129818.1_PhzA/PhzB ----------MQNSAARQLNEHDTTELRRKNRATVEQYMHTKG 33
Pseudomonas_fluorescens_WP_214992101.1_PhzA/PhzB_family_protein ----------MPNSAALQLATRDTTELRRKNRATVEQYMRTKG 33
Pseudomonas_chlororaphis_WP_124339061.1_phenazine_biosynthesis_protein ----------MPNSATQQLTANDTTELRRKNRATVEQYMRTKG 33
Rhodococcus_qingshengii_WP_397525121.1_PhzA/PhzB_family_protein MRKANQNRCHSIIFPCVKHVHIPRGLAMYEVFG-----PEQEAIRSRNRSVVARYMNTRG 55
RhodococcusMULTISPECIES_WP_030537981.1_PhzA/PhzB_family_protein ----------MYEVFG-----PEQEAARSRNRSAVARYMQTRG 28
Rho_PhzB2_Phenazine_biosynthesis_protein ----------MYEVFG-----PEQEAARSRNRSVVARYMQTRG 28
Streptomyces_niveus_WP_359815293.1 ----------MSDDTQVREHNRAVVARYMNTRG 23
Streptomyces_marincola_WP_086157042.1_PhzA/PhzB_family_protein ----------MTDDIAPAHPPVDEKELRDHNRAIVEQYMNTRG 33
                                                          :   * :**  * :**.*:*

Pseudomonas_aeruginosa_HHW1969258.1_phenazine_biosynthesis_protein_PhzB QDRLRRHELFVEDGCGGLWTTDTGSPIVIRGKDKLAEHAVWSLKCFPDWEWYNIKVFDTD 92
Pseudomonas_sp.CMR5c_WP_053129818.1_PhzA/PhzB QDRLRRHELFTEDGSGGLWTTDTGAPIAINGKSKLAEHAVWSLKCFPDWEWYNIQIFETD 93
Pseudomonas_fluorescens_WP_214992101.1_PhzA/PhzB_family_protein KDRLRRHELFTEDGSGGLWTTDTGAPIVISGKAKLAEHAVWSLKCFPDWEWYNVKVFETD 93
Pseudomonas_chlororaphis_WP_124339061.1_phenazine_biosynthesis_protein QDRLRRHELFTEDGTGGLWTTDTGAPIVISGKAKLAEHAVWSLKCFPDWEWYNVKVFETD 93
Rhodococcus_qingshengii_WP_397525121.1_PhzA/PhzB_family_protein TDRLKRHELFTQDGEGGLWTTETGEPIMIKGRDRLAEHAVWSLECFPDWSWFNVEIFDTQ 115
RhodococcusMULTISPECIES_WP_030537981.1_PhzA/PhzB_family_protein LDRLRRHELFTQDGEGGLWTTETGEPIMIKGRDRLAEHAVWSLECFPDWSWFNIEIFDTQ 88
Rho_PhzB2_Phenazine_biosynthesis_protein LDRLRRHELFTQDGEGGLWTTETGEPIMIKGRDRLAEHAVWSLECFPDWSWFNIEIFDTQ 88
Streptomyces_niveus_WP_359815293.1 QDRLERHLLFTEDGTGGLWTTETGEPIVISGRDTLGEHAVWSLKCFPDWKWFNVEIFDTQ 83
Streptomyces_marincola_WP_086157042.1_PhzA/PhzB_family_protein QDRLRRHLLFTEDGTGGLWTTESGEPIVIRGRDRLGDHAVWSLKCFPDWAWINIEIFDTQ 93
                                                           ***.** **.:** ******::* ** * *:  *.:******:***** * *:::*:*:

Pseudomonas_aeruginosa_HHW1969258.1_phenazine_biosynthesis_protein_PhzB DPNHFWVECDGHGKILFPGYPEGYYENHFLHSFELDDGKIKRNREFMNVFQQLRALSIPV 152
Pseudomonas_sp.CMR5c_WP_053129818.1_PhzA/PhzB DPNHIWVECDGHGKILFPGYPEGYYENHFLHSFELQDGKIKQNREFMNVFQQLRALGIPV 153
Pseudomonas_fluorescens_WP_214992101.1_PhzA/PhzB_family_protein DPNHIWVECDGHGKILFPGYPEGYYENHFLHSFELEDGKVKRNREFMNVFQQLRALGIAV 153
Pseudomonas_chlororaphis_WP_124339061.1_phenazine_biosynthesis_protein DPNHFWVECDGHGKILFPGYPEGYYENHFLHSFELEDGKVKRNREFMNVFQQLRALGIPV 153
Rhodococcus_qingshengii_WP_397525121.1_PhzA/PhzB_family_protein DPDRFWVECDGAGIIRFAGYPEGRYENHFIHFFRFVDGKISQQREFMNPCQQFRALGIAV 175
RhodococcusMULTISPECIES_WP_030537981.1_PhzA/PhzB_family_protein DPDRFWVECDGAGIIRFTGYPEGRYENHFIHFFRFVDGKISQQREFMNPCQQFRALGIAV 148
Rho_PhzB2_Phenazine_biosynthesis_protein DPDRFWVECDGAGIIRFTGYPEGRYENHFIHFFRFVDGKISQQREFMNPCQQFRALGIAV 148
Streptomyces_niveus_WP_359815293.1 DPDRFWVECDGEGQIRFPGYPDGLYRNHFLHSFLFEDGKIKQQREFMNPCQQFRALGIDV 143
Streptomyces_marincola_WP_086157042.1_PhzA/PhzB_family_protein DPDRFWVECDGEGKILFPGYPEGHYRNHFLHSFLFEGGKIKQQREFMNPCQQFRALGIAV 153
                                                           **:::****** * * * ***:* *.***:* * : .**:.::*****  **:***.* *

Pseudomonas_aeruginosa_HHW1969258.1_phenazine_biosynthesis_protein_PhzB PQIKREGIPT 162
Pseudomonas_sp.CMR5c_WP_053129818.1_PhzA/PhzB PQIKREGIPT 163
Pseudomonas_fluorescens_WP_214992101.1_PhzA/PhzB_family_protein PQIKREGIPT 163
Pseudomonas_chlororaphis_WP_124339061.1_phenazine_biosynthesis_protein PQIKREGIPT 163
Rhodococcus_qingshengii_WP_397525121.1_PhzA/PhzB_family_protein PNVVREGIPT 185
RhodococcusMULTISPECIES_WP_030537981.1_PhzA/PhzB_family_protein PNVIREGIPT 158
Rho_PhzB2_Phenazine_biosynthesis_protein PNVIREGIPT 158
Streptomyces_niveus_WP_359815293.1 PAVRREGIPT 153
Streptomyces_marincola_WP_086157042.1_PhzA/PhzB_family_protein PEIRREGIPT 163
                                                           * : ******
```

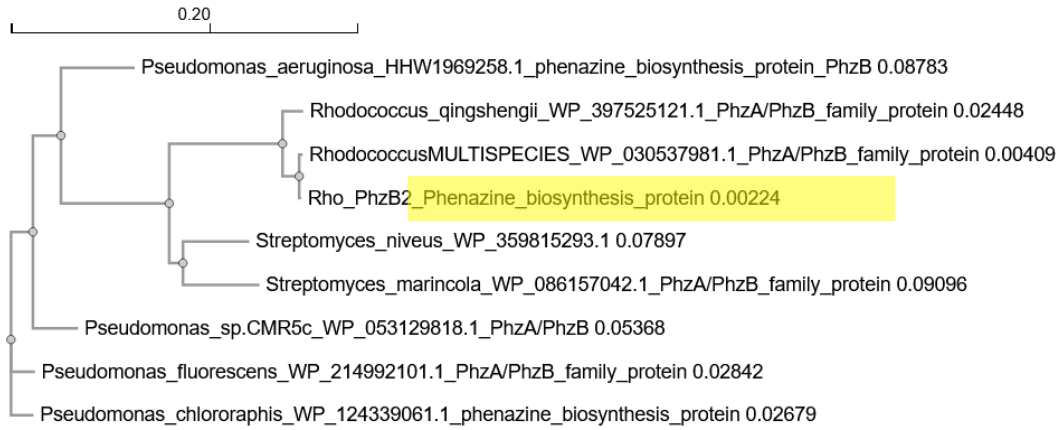

Multiple alignment output for the putative PhzC:

```
CLUSTAL O(1.2.4) multiple sequence alignment

Pseudomonas_shirazensis_WP_186698045.1_3-deoxy-7-phosphoheptulonate_synthase      MLTQGANVPDGPLAWSLNSWRDRSAAQQPLYHDQPALEQALAYLRQAPALVSRQSISLLT 60
Rhodococcus_erythropolis_WP_336505324.1_3-deoxy-7-phosphoheptulonate_synthase     --------------MIPSALTSMVNSHQPPWHDHPQLDLVRNVLETTTVIASPVEIDQLA 46
Rho_PhzC_Phospho-2-dehydro-3-deoxyheptonate_aldolase                              --------------MIPSALTSMVNSHQPPWHDHPQLDLVRNVLETTTVIASPVEIDQLA 46
Rhodococcus_qingshengii_KSU60285.1_hypothetical_protein_AS032_34340               ----------------------MVNSHQPPWHDHPQLDLVRNVLETTTVIASPVEIDQLA 38
Streptomyces_kutzneri_WP_314250358.1_3-deoxy-7-phosphoheptulonate_synthase        -----------MGNILADIERSQARHQPEWDNPPQVELVRAMLSSVTPLVTAAQVESLR 48
Pseudomonas_aeruginosa_WP_209098778.1_phenazine_biosynthesis_protein_PhzC         -----------MDDLLKRVRRCEALQQPEWGDPSRLRDVQAYLRGSPALIRAGDILALR 48
Pseudomonas_mangiferae_WP_143486210.1_3-deoxy-7-phosphoheptulonate_synthase       -----------MKDLLERVQNCEALQQPQWSEPSQLNDAQAYLRESPALVQLEDILALR 48
Streptomyces_variabilis_GAB2331875.1_phenazine_biosynthesis_protein_PhzC          -----------MTSLLDGCVDRPVLHQPLWEDRPELRCVTAELAQRPQLVSATDVARLR 48
Streptomyces_marincola_WP_226074269.1_3-deoxy-7-phosphoheptulonate_synthase       -----------MENTLLDIPPRSAPHQPDWEDPARVRWVRKELRARDPLVARDDVRALR 48
                                                                                             :** : :   :  .   *    :    .:  *

Pseudomonas_shirazensis_WP_186698045.1_3-deoxy-7-phosphoheptulonate_synthase      ALLAQAQQGRAFVLQGGDCAEGFTQTDQAALNRFVQLLQQMSQLLTRGVQRPVIKIGRLA 120
Rhodococcus_erythropolis_WP_336505324.1_3-deoxy-7-phosphoheptulonate_synthase     RRLRAVEAGHASILQMGDCAEDPAHCTPDHVHRKLDQLTASAGAVATPTGLPVVQVGRIA 106
Rho_PhzC_Phospho-2-dehydro-3-deoxyheptonate_aldolase                              RRLRAVEAGHASILQMGDCAEDPAHCTPDHVHRKLDQLTASAGAVATPTGLPVVQVGRIA 106
Rhodococcus_qingshengii_KSU60285.1_hypothetical_protein_AS032_34340               RRLRAVEAGHASILQMGDCAEDPAHCTPDHVHRKLDQLTASAGAVATPTGLPVVQVGRIA 98
Streptomyces_kutzneri_WP_314250358.1_3-deoxy-7-phosphoheptulonate_synthase        SHLAYVATGEMKVLQAGDCAEDPAECTAGHIQGKTGLIDLLAQNLETATGKQTLRVGRIA 108
Pseudomonas_aeruginosa_WP_209098778.1_phenazine_biosynthesis_protein_PhzC         ATLARVARGEALVVQCGDCAEDMDDHHAENVARKAAVLELLAGALRLAGRRPVIRVGRIA 108
Pseudomonas_mangiferae_WP_143486210.1_3-deoxy-7-phosphoheptulonate_synthase       AVLARVAAGEALVIQSGDCAEDMDEYEPGHVARKAAVLDLLAGAFRLVTEQPVVRVGRIA 108
Streptomyces_variabilis_GAB2331875.1_phenazine_biosynthesis_protein_PhzC          ALLARVAAGEAMVVQAGDCAEDPAECEPGSVARKAGLLDVLAGVLRMVTHRPVLRVGRIA 108
Streptomyces_marincola_WP_226074269.1_3-deoxy-7-phosphoheptulonate_synthase       ARLARVAAGEALVVQAGDCAEDPEECTAEHVARKAAVLDLLAGALRLITARPVLRVGRIA 108
                                                                                    *  .  *.  ::* *****.  .     :      :   :  .       .:::**:*

Pseudomonas_shirazensis_WP_186698045.1_3-deoxy-7-phosphoheptulonate_synthase      GQYAKPRPSDIETRDGLSLPVYRGDIVNQAEFRAAARRADPQRLLAAYAHSAATLRDIRT 180
Rhodococcus_erythropolis_WP_336505324.1_3-deoxy-7-phosphoheptulonate_synthase     GQFAKPRSKATETIGDREVVTYRGHMVNLPDSDEVSRTPDPLRILMGYLTSRQVAATIAG 166
Rho_PhzC_Phospho-2-dehydro-3-deoxyheptonate_aldolase                              GQFAKPRSKATETIGDREVVTYRGHMVNLPDSDEVSRTPDPLRILMGYLTSRQVAATIAG 166
Rhodococcus_qingshengii_KSU60285.1_hypothetical_protein_AS032_34340               GQFAKPRSKATETIGDREVVTYRGHMVNLPDSDEVSRTPDPLRILMGYLTSRQVAATIAG 158
Streptomyces_kutzneri_WP_314250358.1_3-deoxy-7-phosphoheptulonate_synthase        GQFSKPRSSQVEKLGDDELPSFFGHMINGPEPTHESRRPDPLRMLTGYMAARELTTQLGW 168
Pseudomonas_aeruginosa_WP_209098778.1_phenazine_biosynthesis_protein_PhzC         GQYAKPRSKPHEQVGEQTLPVYRGDMVNGREAHAEQRRADPQRILKGYAAARNIMRHLGW 168
Pseudomonas_mangiferae_WP_143486210.1_3-deoxy-7-phosphoheptulonate_synthase       GQFAKPRSKPSEVVGDVELPVYRGDMVNGREAHSGSRQHDAQRLVKGYNAARELMQHLGW 168
Streptomyces_variabilis_GAB2331875.1_phenazine_biosynthesis_protein_PhzC          GQFAKPRSNPTEMVGGIELPVFRGHMVNGPEPDPARRRPDPQRLLIGYAAAGEAMTHLGW 168
Streptomyces_marincola_WP_226074269.1_3-deoxy-7-phosphoheptulonate_synthase       GQYAKPRSKPTETVAGVELPVYRGHMINDPRPDADSRRPDPLRMLTGYMAAREVMRHLGW 168
                                                                                   **::*** .  *      :  : *.::*       *  *  *:: .*  :      :

Pseudomonas_shirazensis_WP_186698045.1_3-deoxy-7-phosphoheptulonate_synthase      LQGFMDSDGLCDQALFISHEALLLEYEQALTRQQDDGCWFNQSTHLPWIGLRTAQPDGAH 240
Rhodococcus_erythropolis_WP_336505324.1_3-deoxy-7-phosphoheptulonate_synthase     FNR----GRALEDRVWTSHEALLLDYEHPMMRQGSDERTYLTSTHWPWIGERTRNVDGPH 222
Rho_PhzC_Phospho-2-dehydro-3-deoxyheptonate_aldolase                              FNR----GRALEDRVWTSHEALLLDYEHPMMRPGSDERTYLTSTHWPWIGERTRNVDGPH 222
Rhodococcus_qingshengii_KSU60285.1_hypothetical_protein_AS032_34340               FNR----GRALEDRVWTSHEALLLDYEHPMMRPGSDERTYLTSTHWPWIGERTRNVDGPH 214
Streptomyces_kutzneri_WP_314250358.1_3-deoxy-7-phosphoheptulonate_synthase        VGST---PRLDGPVVWTSHEALLLDYEMSMLRELDGSRLLLSSTHWPWIGERTRQIDGPH 225
Pseudomonas_aeruginosa_WP_209098778.1_phenazine_biosynthesis_protein_PhzC         DA--ASGQEANASPVWTSHEMLLLDYELSMLREDEQRRVYLGSTHWPWIGERTRQVDGAH 226
Pseudomonas_mangiferae_WP_143486210.1_3-deoxy-7-phosphoheptulonate_synthase       MEDRATGAVLAGPPAWTSHEMLVLDYEVPLLREDGRGRVYLGSTHWPWIGERTRQEEGAH 228
Streptomyces_variabilis_GAB2331875.1_phenazine_biosynthesis_protein_PhzC          LSEP-R-WPGISPEVWTSHEALLLDYEIPMTRPTEDGGLLLASTHWPWIGERTRQVEGAH 226
Streptomyces_marincola_WP_226074269.1_3-deoxy-7-phosphoheptulonate_synthase       QPGGAA-ADGFDPRVWTSHEALLLDYEVPMLRRGGDGGLLLTSTHWPWIGERTRQVDGAH 227
                                                                                            : *** *:*:**  : *         *** **** ** : :* *
```

```
Pseudomonas_shirazensis_WP_186698045.1_3-deoxy-7-phosphoheptulonate_synthase      VEYLRGVSNPVAVKVGAETSASALLQLIKQLNPHNQPGRLTLIHRMGAALLEQHLGPLID 300
Rhodococcus_erythropolis_WP_336505324.1_3-deoxy-7-phosphoheptulonate_synthase     VATLAHIANPSACKVGPTATEDDLVALCSRLDPYREPGKLALITRMGAQHIRTGLPALMN 282
Rho_PhzC_Phospho-2-dehydro-3-deoxyheptonate_aldolase                              VATLAHIANPSACKVGPTATEDDLVALCSRLDPYREPGKLALITRMGAQHIRTGLPALMN 282
Rhodococcus_qingshengii_KSU60285.1_hypothetical_protein_AS032_34340               VATLAHIANPSACKVGPTATEDDLVALCSRLDPYREPGKLALITRMGAQHIRTGLPALMN 274
Streptomyces_kutzneri_WP_314250358.1_3-deoxy-7-phosphoheptulonate_synthase        VALLAQVANPVACKVGPSMTAGEIVELCDRLDPEREPGRLSLIVRMGADLVADRLPRLVE 285
Pseudomonas_aeruginosa_WP_209098778.1_phenazine_biosynthesis_protein_PhzC         VALLAEVLNPVACKVGPEIGRDQLLALCERLDPRREPGRLTLIARMGAQKVGERLPPLVE 286
Pseudomonas_mangiferae_WP_143486210.1_3-deoxy-7-phosphoheptulonate_synthase       VTLLSAVLNPVACKVGPNITPSQLLTLCERLDPRREPGRLTLIARMGASAVAERLPPLVK 288
Streptomyces_variabilis_GAB2331875.1_phenazine_biosynthesis_protein_PhzC          VDLLATVANPVACKVGPSMTPDELLALCERLDPPREPGRLTLISRMGADHVRERLPRLVS 286
Streptomyces_marincola_WP_226074269.1_3-deoxy-7-phosphoheptulonate_synthase       VSLLAGVANPVACKVGPSMEPDELLALCRRLDPRREPGRLTLISRMGADRVADALPPLVA 287
                                                                                  *  *  : ** * ***     . :: *  :*:* .:**:*:** ****  :   *  *:

Pseudomonas_shirazensis_WP_186698045.1_3-deoxy-7-phosphoheptulonate_synthase      AVEHAGARVLWLCDPMHGNTRTLPCGTKTRAFDDILAEIETAFAVHARHGSVLGGLHLEL 360
Rhodococcus_erythropolis_WP_336505324.1_3-deoxy-7-phosphoheptulonate_synthase     AVRAAGHRVLWICDPMHGNTLSTDDGTKTRVVDDVIAEMAGFVSVADQTGTRVHGLHLET 342
Rho_PhzC_Phospho-2-dehydro-3-deoxyheptonate_aldolase                              AVRAAGHRVLWICDPMHGNTLSTDDGTKTRVVDDVIAEMAGFVSVADQTGTRVHGLHLET 342
Rhodococcus_qingshengii_KSU60285.1_hypothetical_protein_AS032_34340               AVRAAGHRVLWICDPMHGNTLSTDDGTKTRVVDDVIAEMAGFVSVADQTGTRVHGLHLET 334
Streptomyces_kutzneri_WP_314250358.1_3-deoxy-7-phosphoheptulonate_synthase        AVQSAGHPVVWLSDPMHGNTDCAADGTKYRLVETVAREVRGFRRVLDLAGVPAGGLHLEA 345
Pseudomonas_aeruginosa_WP_209098778.1_phenazine_biosynthesis_protein_PhzC         AVRAAGHPVIWLSDPMHGNTIVAPCGNKTRLVRSIAEEVAAFRLAVSGSGGVAAGLHLET 346
Pseudomonas_mangiferae_WP_143486210.1_3-deoxy-7-phosphoheptulonate_synthase       AVREAGHPVIWLSDPMHGNTVVAPCGNKTRLVQTIAEEIAAFRQAVTAAGGVAGGLHLET 348
Streptomyces_variabilis_GAB2331875.1_phenazine_biosynthesis_protein_PhzC          AVKGAGHPVIWLTDPMHGNTVTTPDGLKTRLVETVLREVEGFQGAVRAAGGVAGGLHLET 346
Streptomyces_marincola_WP_226074269.1_3-deoxy-7-phosphoheptulonate_synthase       AVREAGHPVIWLTDPMHGNTVSVRGGIKTRFVATVAREVAAFHRAVTAAGGVAGGLHLET 347
                                                                                  **. **  *:*: *******     * * * .  :  *:     .    *    *****

Pseudomonas_shirazensis_WP_186698045.1_3-deoxy-7-phosphoheptulonate_synthase      TA-EAVTECLGGPSQLQPEDLHRCYLSKVDPRLNGEQAFALAQHLSRMPPCR-------- 411
Rhodococcus_erythropolis_WP_336505324.1_3-deoxy-7-phosphoheptulonate_synthase     THLTDVSECVWSSTDLAS---ARPSSSLCDPRLNPEQAAAVVEAWGEMLARHYRVSETTS 399
Rho_PhzC_Phospho-2-dehydro-3-deoxyheptonate_aldolase                              THLTDVSECVWSSTDLAS---ARPSSSLCDPRLNPEQAAAVVEAWGEMLARHYRGSETTS 399
Rhodococcus_qingshengii_KSU60285.1_hypothetical_protein_AS032_34340               THLTDVSECVWSSTDLAS---ARPSSSLCDPRLNPEQAAAVVEAWGEMLARHYRGSETTS 391
Streptomyces_kutzneri_WP_314250358.1_3-deoxy-7-phosphoheptulonate_synthase        TP-DDVTECVLDTAELG----SGPVTSLCDPRLNTAQAIKVVSAWSEY------------ 388
Pseudomonas_aeruginosa_WP_209098778.1_phenazine_biosynthesis_protein_PhzC         TP-DDVTECVADSSGLHQ--VSRHYTSLCDPRLNPWQALSAVMAWAGAEAIPSATFPLET 403
Pseudomonas_mangiferae_WP_143486210.1_3-deoxy-7-phosphoheptulonate_synthase       TP-DEVTECANDADALHQ--VASRYRSLCDPRLTPWQAITAVMAWNTSPQSPHTPS---- 401
Streptomyces_variabilis_GAB2331875.1_phenazine_biosynthesis_protein_PhzC          TP-DDVTECAQDDTHLAR--VGDTYTSLCDPRLNPEQAVAVVAAWQD------------- 390
Streptomyces_marincola_WP_226074269.1_3-deoxy-7-phosphoheptulonate_synthase       TP-DAVTECVADESAVDE--AGSVSTTFCDPRLTPDQAASVIAAWSR------------- 391
                                                                                  *    *:**  .   :          :  ****.  **

Pseudomonas_shirazensis_WP_186698045.1_3-deoxy-7-phosphoheptulonate_synthase      --   411
Rhodococcus_erythropolis_WP_336505324.1_3-deoxy-7-phosphoheptulonate_synthase     --   399
Rho_PhzC_Phospho-2-dehydro-3-deoxyheptonate_aldolase                              --   399
Rhodococcus_qingshengii_KSU60285.1_hypothetical_protein_AS032_34340               --   391
Streptomyces_kutzneri_WP_314250358.1_3-deoxy-7-phosphoheptulonate_synthase        --   388
Pseudomonas_aeruginosa_WP_209098778.1_phenazine_biosynthesis_protein_PhzC         VA   405
Pseudomonas_mangiferae_WP_143486210.1_3-deoxy-7-phosphoheptulonate_synthase       --   401
Streptomyces_variabilis_GAB2331875.1_phenazine_biosynthesis_protein_PhzC          --   390
Streptomyces_marincola_WP_226074269.1_3-deoxy-7-phosphoheptulonate_synthase       --   391
```

Multiple alignment output for the putative PhzD:

```
CLUSTAL O(1.2.4) multiple sequence alignment

Streptomyces_niveiscabiei_WP_055721456.1_isochorismatase_family_protein      ----MPGLPSISPYPMPTAESLPPRIPAWSVDPSRAVLLLHDLQRYFLRPLPDALRTELI   56
Pseudomonas_chlororaphis_WP_075121686.1_isochorismatase_family_protein       ----MTGIPSIVPYALPTSRDLPVNLAQWSIDPERAVLLVHDMQRYFLRPLPDALREAVV   56
Pseudomonas_aeruginosa_WP_203328712.1_isochorismatase_family_protein         ----MSRIPEITAYPLPTAQQLPANLARWSLEPRRAVLLVHDMQRYFLRPLPESLRAGLV   56
Pseudomonas_fluorescens_VEE46437.1_phenazine_biosynthesis_protein_PhzD       ----MSGIPEITAYPLPTAQQLPANLARWSLEPRRAVLLVHDMQRYFLRPLPESLRAGLV   56
Nocardia_aurantia_WP_153341071.1_isochorismatase_family_protein              MTIVPTPALQVQPYPLPSRTELPDNLVDWRVRPEQAVLLIHDMQQYFLATFPHALRSRLV   60
Rhodococcus_qingshengii_WP_217019070.1_isochorismatase_family_protein        ----MSRDLTVEPYLLPSPGEMPEALVDWDIRPRQATLLIHDMQRYFLSPFPDAMRPEIV   56
Rho_PhzD2_Phenazine_biosynthesis_protein                                     ----MSRDLTVEPYLLPSPGEMPEALVDWDIRPRQATLLIHDMQRYFLSPFPDAMRSEIV   56
Rhodococcus_erythropolis_WP_336505323.1_isochorismatase_family_protein       ----MSRDLTVEPYLLPSPGEMPEALVDWDIRPRQATLLIHDMQRYFLSPFPDAMRSEIV   56
                                                                                     :  * :*:  .:*  :  * : * :*.**:**:*:***  :*.::*  ::

Streptomyces_niveiscabiei_WP_055721456.1_isochorismatase_family_protein      GNAAELTSWARAGGVPVAYTAQPGGMTPQQRGLLKDFWGPGMRVDPADREVVEPVAPRDG   116
Pseudomonas_chlororaphis_WP_075121686.1_isochorismatase_family_protein       SNAARVRQWAADRGIPVAYTAQPGSMSEEQRGLLKDFWGPGMKASPADREVVDALAPMPD   116
Pseudomonas_aeruginosa_WP_203328712.1_isochorismatase_family_protein         ANAARLRRWCVEQGVQIAYTAQPGSMTEKQRGLLKDFWGPGMRASPADREVVEELAPGPD   116
Pseudomonas_fluorescens_VEE46437.1_phenazine_biosynthesis_protein_PhzD       ANAARLRRWCVEQGVQIAYTAQPGSMTEEQRGLLKDFWGPGMCASPADREVVEELAPGPD   116
Nocardia_aurantia_WP_153341071.1_isochorismatase_family_protein              GNAARLRKSCADRGVRIGYTAQPGRMTTADRGLLLDFWGPGMTTAEADRAIVAELTPETP   120
Rhodococcus_qingshengii_WP_217019070.1_isochorismatase_family_protein        GNVRDLHSWAQRVGAATAYTAQPGRMNVTDRGLLRDFWGPGMQTTDADRALVPELELGDD   116
Rho_PhzD2_Phenazine_biosynthesis_protein                                     GNVRDLHSWAQRVGAATAYTAQPGRMNVTDRGLLRDFWGPGMQTTDADRALVPELELGDD   116
Rhodococcus_erythropolis_WP_336505323.1_isochorismatase_family_protein       GNVRDLHSWAQRVGAATAYTAQPGRMNVTDRGLLRDFWGPGMQTTDTDRALVPELELGDD   116
                                                                             .*.  :   .   *   .****** *.  :**** ******* .  :** :*  :

Streptomyces_niveiscabiei_WP_055721456.1_isochorismatase_family_protein      DWLLTKWRYSAFFNTDLLQRMRDAGRDQLVVCGIYAHVGVLATCVEAYTHDIETFLVADA   176
Pseudomonas_chlororaphis_WP_075121686.1_isochorismatase_family_protein       DWLLTKWRYSAFFNSDLLERMRANGRDQLILCGVYAHVGVLISTVDAYSNDIQPFLVADA   176
Pseudomonas_aeruginosa_WP_203328712.1_isochorismatase_family_protein         DWLLTKWRYSAFFHSDLLQRMRAAGRDQLVLCGVYAHVGVLISTVDAYSNDIQPFLVADA   176
Pseudomonas_fluorescens_VEE46437.1_phenazine_biosynthesis_protein_PhzD       DWLLTKWRYSAFFHSDLLQRMRAAGRDQLVLCGVYAHVGVLISTVDAYSNDIQPFLVADA   176
Nocardia_aurantia_WP_153341071.1_isochorismatase_family_protein              DWTFTKWRYSAFHRSNLLGRMRAEGRDQLLLCGVYGHVGILATALEAYANDLQVFLIADA   180
Rhodococcus_qingshengii_WP_217019070.1_isochorismatase_family_protein        AWPFVKWRYSAFHRSDLLARMRKNGRTQLVLCGVYAHVGILATALDAYAHDIEVFLVGDA   176
Rho_PhzD2_Phenazine_biosynthesis_protein                                     AWPFVKWRYSAFHRSDLLARMRENGRTQLVLCGVYAHVGILATALDAYTHDIEVFLVGDA   176
Rhodococcus_erythropolis_WP_336505323.1_isochorismatase_family_protein       AWPFVKWRYSAFHRSDLLARMRENGRTQLVLCGVYAHVGILATALDAYTHDIEVFLVGDA   176
                                                                              * :.*******..::** ***  ** **:**:*.***:* : ::**::*:: **:.**

Streptomyces_niveiscabiei_WP_055721456.1_isochorismatase_family_protein      VADFGEGDHRMALEYAARCCAVVLPTKEVLG-   207
Pseudomonas_chlororaphis_WP_075121686.1_isochorismatase_family_protein       IADFSEEHHRMAIEYAASRCAMVVTTDEVVL-   207
Pseudomonas_aeruginosa_WP_203328712.1_isochorismatase_family_protein         IADFSEAHHRMALEYAASRCAMVVTTDEVLE-   207
Pseudomonas_fluorescens_VEE46437.1_phenazine_biosynthesis_protein_PhzD       IADFSEAHHRMALEYAASRCAMVVTTDEVLE-   207
Nocardia_aurantia_WP_153341071.1_isochorismatase_family_protein              IGDFSAEKHRFTLEYTASCCARITTVDEVLS-   211
Rhodococcus_qingshengii_WP_217019070.1_isochorismatase_family_protein        VADFTAADHRHTLEYTSRCCARVVATKWVTER   208
Rho_PhzD2_Phenazine_biosynthesis_protein                                     VADFTAADHRHTLEYTSRCCARVVATKWVTER   208
Rhodococcus_erythropolis_WP_336505323.1_isochorismatase_family_protein       VADFTAADHRHTLEYTSRCCARVVATKWVTER   208
                                                                             :.**   .** ::**::  ** :  .. *
```

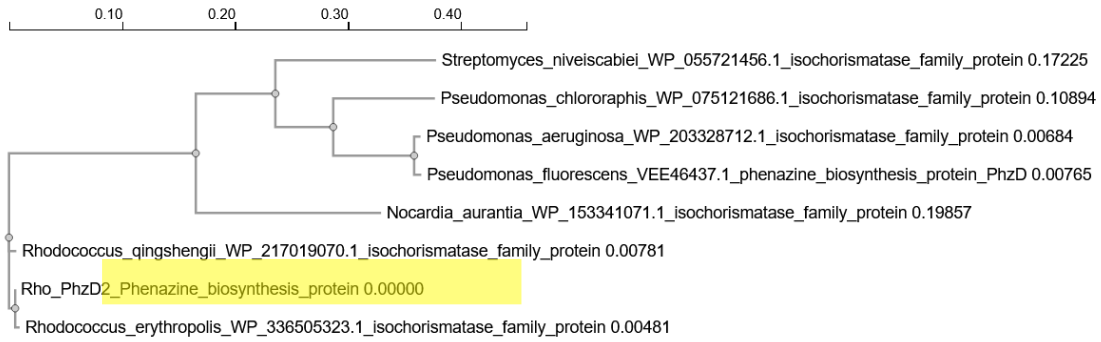

Multiple alignment output for the putative PhzE:

```
CLUSTAL O(1.2.4) multiple sequence alignment

Pseudomonas_fluorescens_VEE46436.1_phenazine_biosynthesis_protein_PhzE                ----------MNALPTSLLQRL-LERPAPFALLYRPESN-GPGLLDVIRGEALEL   43
Pseudomonas_chlororaphis_OLF51938.1                                                   ----------MNQAAARLMERILQPAPGPFALLYRPEST-GPGLLDVLIGDMSEP   44
Rho_PhzE_IsochorismatesynthaseMenF                                                    ----------MSPPLSTDLLTEILAGNRSVYALLCRADPATGARTVTALSGQLRQH   46
Rhodococcus_qingshengii_WP_047269922.1_anthranilate_synthase_family_protein           ----------MSPPLSTDLLTEILAGNRSVYALLCRADPATGARTVTALSGQLRQH   46
Rhodococcus_erythropolis_WP_336505322.1_anthranilate_synthase_family_protein          ----------MSPPLSTDLLTEILAGNCSVYALLCRADPATGARTVTALSGQLRQH   46
Nocardia_sp._BMG111209WP_026343200.1_anthranilate_synthase_family_protein             ----------MSGDLLGAVIDGSAGDFAIISRP-----GRDVTVLVGAAERP   37
Streptomyces_rubiginosohelvolus_WP_355064226.1_anthranilate_synthase_family_protein   ----------MTADLLDAVLDGTAGDYALICRSDEH--GRQVQVITGETGHP   40
Streptomyces_sp._NPDC002671MGW0882928.1_anthranilate_synthase_family_protein       MTDYNDPRKHTPHSPPAPAKSDLLQAVLDGSAENFAIVCRDGEH--GRDVQVFRGDVSQP   58
                                                                                                 *:  :       :*:: *         : .: *   .

Pseudomonas_fluorescens_VEE46436.1_phenazine_biosynthesis_protein_PhzE                HGLADLPLDEP-----GPGLPRHDLLALIPYRQIAERGFEALDDGTPLLALKVLEQELLP   98
Pseudomonas_chlororaphis_OLF51938.1                                                   QVLADIDLPAT-----SIGAPRLDVLALIPYRQIAERGFEAVDDQSPLLAMNITEQHSIS   99
Rho_PhzE_IsochorismatesynthaseMenF                                                    ELIEEI-------------STTADVFVLLPYRQIRERGYPAHDDGAPLLAIYIDEQQDYP   93
Rhodococcus_qingshengii_WP_047269922.1_anthranilate_synthase_family_protein           ELIEEI-------------STTADVFVLLPYRQIRERGYPAHDDGAPLLAIYIDEQQDYP   93
Rhodococcus_erythropolis_WP_336505322.1_anthranilate_synthase_family_protein          ELIEEI-------------STTADVFVLLPYRQIRERGYPAHDDGAPLLAIYIDEQQDYP   93
Nocardia_sp._BMG111209WP_026343200.1_anthranilate_synthase_family_protein             ESLAGIRLGGRG-------APGSEALVLIPYRQLTERGFPAPDDGAPLLALAVTGEERHP   90
Streptomyces_rubiginosohelvolus_WP_355064226.1_anthranilate_synthase_family_protein   ASLAAIDFAHRP----AVGAASSDMLIVVPYRQLVERGHPAVDDGAPLLAMRVTAEERHP   96
Streptomyces_sp._NPDC002671MGW0882928.1_anthranilate_synthase_family_protein       ASLDAIGLGQGGGSTGSARGEASTDVLVVVPYRQLAERGYPAPDDGTPLIAMAVTEEEHHA   118
                                                                                        :  :                : : ::****: ***. * ** :**:*: :  :.

Pseudomonas_fluorescens_VEE46436.1_phenazine_biosynthesis_protein_PhzE                LEQALALLPNQALELSEEGFDLDDEAYAEVVGRVIADEIGRGEGANFVIKRRFQARIDGY   158
Pseudomonas_chlororaphis_OLF51938.1                                                   IERVLGLLPNVPIQLNSERFDLSDASYAEIVSQVIANEIGSGEGANFVIKRTFLAEISEY   159
Rho_PhzE_IsochorismatesynthaseMenF                                                    LTSVLDKLPRRSFALTDGHFDSSDADYERKVAAIVSEEIGNGRGANFVIKREFSAECTPY   153
Rhodococcus_qingshengii_WP_047269922.1_anthranilate_synthase_family_protein           LTSVLDKLPRRSFALTDGHFDSSDADYERKVAAIVSEEIGNGRGANFVIKREFSAECTPY   153
Rhodococcus_erythropolis_WP_336505322.1_anthranilate_synthase_family_protein          LTSVLDKLPRRSFALTDGHFDSSDADYERKVAAIVSEEIGNGRGANFVIKREFSAECTPY   153
Nocardia_sp._BMG111209WP_026343200.1_anthranilate_synthase_family_protein             LGAVLARLPHRRVQLGEGGFDSDDAAYAATVRAIIDDEIGSGQGANFVIKRTYSAGIADY   150
Streptomyces_rubiginosohelvolus_WP_355064226.1_anthranilate_synthase_family_protein   VASVLGRLPDRQVRLEDGHFDADDDTYAKSVEAVLADEIGTGQGANFVIKRTYVADIADP   156
Streptomyces_sp._NPDC002671MGW0882928.1_anthranilate_synthase_family_protein       LSTVLERLPQHTVRLADGHFEPDDAAYAETVKAVLADEIGTGQGANFVIKRTYLADITDY   178
                                                                                      :  .*  **   . * .  *: .*  *   *  :: :*** *.******** : *

Pseudomonas_fluorescens_VEE46436.1_phenazine_biosynthesis_protein_PhzE                ATASALSFFRQLLLREKGAYWTFIVHTGERTLVGASPERHISVRDGLAVMNPISGTYRYP   218
Pseudomonas_chlororaphis_OLF51938.1                                                   GTDSALSFFRHLLEREKGAYWTFIIHTGSRTFVGASPERHISVKDGLAVMNPISGTYRYP   219
Rho_PhzE_IsochorismatesynthaseMenF                                                    NSTVPLSAFGELLDNERGAYWTFLVHTEGLVLVGASPEQHVVLDNGTAVMNPISGTYRYP   213
Rhodococcus_qingshengii_WP_047269922.1_anthranilate_synthase_family_protein           NSTVPLSAFGELLDNERGAYWTFLVHTEGLVLVGASPEQHVVLDNGTAVMNPISGTYRYP   213
Rhodococcus_erythropolis_WP_336505322.1_anthranilate_synthase_family_protein          NSTVPLSAFGELLDNERGAYWTFLVHTEGLVLVGASPEQHVVLDNGTAVMNPISGTYRYP   213
Nocardia_sp._BMG111209WP_026343200.1_anthranilate_synthase_family_protein             TPAMALAVLRELLAAERGAYWTFLVRVGDLTLVGASPERHVSLETGVLQMNPISGTYRYP   210
Streptomyces_rubiginosohelvolus_WP_355064226.1_anthranilate_synthase_family_protein   GPDAALSAFRQLLAAERGAYWTFLVRTAGSTIVGASPERHVGLIDDVVRMNPISGTYRYP   216
Streptomyces_sp._NPDC002671MGW0882928.1_anthranilate_synthase_family_protein       RPESALSAFRELLSRERGAYWTFLVRTRDVTLIGASPERHVSLADGVATMNPISGTYRYP   238
                                                                                           *: : .**  *:******:::.   .::*****:*: :  .   **********
```

```
Pseudomonas_fluorescens_VEE46436.1_phenazine_biosynthesis_protein_PhzE                PAGPNLAEVMEFLDNRKEADELYMVVDEELKMMARICEDGG-RVLGPYLKEMAHLAHTEY  277
Pseudomonas_chlororaphis_OLF51938.1                                                   PAGPNLTEVMDFLADRKEADELYMVVDEELKMMARICEDGG-HVLGPYLKEMAHLAHTEY  278
Rho_PhzE_IsochorismatesynthaseMenF                                                    PGGPTLDGVQQFLDDRKETDELYMVVDEELKMMCRICEPGTTRVHGPALKEMAWVAHTEY  273
Rhodococcus_qingshengii_WP_047269922.1_anthranilate_synthase_family_protein           PGGPTLDGVQQFLDDRKETDELYMVVDEELKMMCRICEPGTTRVHGPALKEMAWVAHTEY  273
Rhodococcus_erythropolis_WP_336505322.1_anthranilate_synthase_family_protein          PGGPTLDGVQQFLDDRKETDELYMVVDEELKMMCRICEPGTTRVHGPALKEMAWVAHTEY  273
Nocardia_sp._BMG111209WP_026343200.1_anthranilate_synthase_family_protein             AGGPTLDGVTAFLADRKETEELYMVVDEELKMMCRICEPGSTRMIGPFLKEMAWVAHTEY  270
Streptomyces_rubiginosohelvolus_WP_355064226.1_anthranilate_synthase_family_protein   ADGPTLSGVTAFLADRKEAEELYMVVDEELKMMCRLCLPGTVSVTGPHLKEMARVAHTEY  276
Streptomyces_sp._NPDC002671MGW0882928.1_anthranilate_synthase_family_protein       DGGPTLKGLTEFLADRKEAEELYMVVDEELKMMCRICEPGTVQVSGPHLKEMAKVAHTEY  298
                                                                                        **.*  :  ** :***::*************.*:*  *   : ** ***** :*****

Pseudomonas_fluorescens_VEE46436.1_phenazine_biosynthesis_protein_PhzE                FIEGQTSRDVREVLRETLFAPTVTGSPLESACRVIRRYEPQGRGYYSGVAALIGGDGQGG  337
Pseudomonas_chlororaphis_OLF51938.1                                                   FIEGRTRRDVREILRETLFAPTVTGSPLESACRVIQRYEPQGRAYYSGMAALIGSDGKGG  338
Rho_PhzE_IsochorismatesynthaseMenF                                                    FIEGQTRRDPREILRETMFAPTVTGSPVESATEVIARYETTGRGYYSGVAALITRSGGGA  333
Rhodococcus_qingshengii_WP_047269922.1_anthranilate_synthase_family_protein           FIEGQTRRDPREILRETMFAPTVTGSPVESATEVIARYETTGRGYYSGVAALITRSGGGA  333
Rhodococcus_erythropolis_WP_336505322.1_anthranilate_synthase_family_protein          FIEGQTRRDPREILRETMFAPTVTGSPVESATEVIARYETTGRGYYSGVAALITRSGGGA  333
Nocardia_sp._BMG111209WP_026343200.1_anthranilate_synthase_family_protein             HLEGRTRRDIRDVLRETMFAPTVTGSPVESAARVIRRYEPAGRGYYSGIIGLAGRDAQGE  330
Streptomyces_rubiginosohelvolus_WP_355064226.1_anthranilate_synthase_family_protein   HIEGRTDRGVPELLRETMFAPTVTGSPVESAARVIERYEPGGRRYYSGIIGLVGSDGAGR  336
Streptomyces_sp._NPDC002671MGW0882928.1_anthranilate_synthase_family_protein       HICGTANRDIPEVLRATMFAPTVTGSPVESAARVIERYEPDGRGYYSGIIGLAGTDKAGR  358
                                                                                      .: * : *.  ::** *:*********:*** .** ***  ** ****: .*   .  *

Pseudomonas_fluorescens_VEE46436.1_phenazine_biosynthesis_protein_PhzE                RTLDSAILIRTAEIEGD-GRLRIGVGSTIVRHSDPLGEAAESRAKASGLIAALKSQAP-Q  395
Pseudomonas_chlororaphis_OLF51938.1                                                   RSLDSAILIRTADIDDS-GQVRISVGSTIVRHSEPLAEAAESRAKAAGLIAALKDQAP-S  396
Rho_PhzE_IsochorismatesynthaseMenF                                                    PTLDSAILIRTAAIEPDCGRVRVAVGATLVRHSDPGAEVYETHAKAQSVLAAFGHSKPHA  393
Rhodococcus_qingshengii_WP_047269922.1_anthranilate_synthase_family_protein           PTLDSAILIRTAAIEPDCGRVRVAVGATLVRHSDPGAEVYETHAKAQSVLAAFGHSKPHA  393
Rhodococcus_erythropolis_WP_336505322.1_anthranilate_synthase_family_protein          PTLDSAILIRTAAIEPDCGRVRVAVGATLVRHSDPGAEVYETHAKAQSVLAAFGHSKPHA  393
Nocardia_sp._BMG111209WP_026343200.1_anthranilate_synthase_family_protein             PVLDSAILIRTASIEPA-GRLSISVGSTLVRHSDPLAEVAETQAKAAGLLAAFGAGA-GG  388
Streptomyces_rubiginosohelvolus_WP_355064226.1_anthranilate_synthase_family_protein   QTLDSAIVIRTAEIDPG-GRLSLSVGSTLVRHSDPLGEVAETRAKASALLAAFGEAEPRR  395
Streptomyces_sp._NPDC002671MGW0882928.1_anthranilate_synthase_family_protein       RTLDSAILIRTAVLEPS-GRLSISVGSTLVRHSDPQSEVAETRAKATALLEAFGECTPRR  417
                                                                                        *****:**** ::   *:: :.**:*:****:* .*. *::*** .:: *:

Pseudomonas_fluorescens_VEE46436.1_phenazine_biosynthesis_protein_PhzE                RLGSHPHVVAALASRNAPIADFWLRGASERQQLQADLSGREVLIVDAEDTFTSMIAKQLK  455
Pseudomonas_chlororaphis_OLF51938.1                                                   RFGSHLQVRAALASRNAYVSDFWLMDSQQRQQTQADFSGRQVLIVDAEDTFTSMIAKQLR  456
Rho_PhzE_IsochorismatesynthaseMenF                                                    RWNRHPMITTALAHRNDQIAGFWSPNYP-HDVRSRVLDGRKALVVDAEDTFTAMLDHQLR  452
Rhodococcus_qingshengii_WP_047269922.1_anthranilate_synthase_family_protein           RWNRHPMITTALAHRNDQIAGFWSPNYP-HDVRSRVLDGRKALVVDAEDTFTAMLDHQLR  452
Rhodococcus_erythropolis_WP_336505322.1_anthranilate_synthase_family_protein          SWNRHPMITTALAHRNDQIAGFWSPNYP-HDVRSRVLDGRKALVVDAEDTFTAMLDHQLR  452
Nocardia_sp._BMG111209WP_026343200.1_anthranilate_synthase_family_protein             EFADHPEVVAALRSRNDDIAAFWAGLTSS-ATRSERLHEHNALVIDAEDTFTAMLEHQLR  447
Streptomyces_rubiginosohelvolus_WP_355064226.1_anthranilate_synthase_family_protein   GFATHPEVLSSLSRRNEGIAGFWTMSGALGYARSKGLDGHKVLVVDAEDTFTSMLEHQLR  455
Streptomyces_sp._NPDC002671MGW0882928.1_anthranilate_synthase_family_protein       SPAQDPSVLASLRSRNEGIAGFWVGQDAGQGVSSRILNGRKALVIDAEDNFTSMLDHQLH  477
                                                                                        .  : ::*  **  :: **          .  :  ::.*::****.**:*: :**:
```

```
Pseudomonas_fluorescens_VEE46436.1_phenazine_biosynthesis_protein_PhzE                SLGLTVTVRGFQEPYSFDGYDLVIMGPGPGNPTEIGQPKIGHLHLAIRSLLSERRPFLAV   515
Pseudomonas_chlororaphis_OLF51938.1                                                   ALGLVVTVRSFNDEYSFDGYDLVIMGPGPGNPSDVQLPKIDHLHVAIRSLLSQQRPFLAV   516
Rho_PhzE_IsochorismatesynthaseMenF                                                    SLGLTVTVRRFDDMYTTSDHDLVIVGPGPGDPTDIDDEKIVHLRAQIDDLLSAQRPFLAI   512
Rhodococcus_qingshengii_WP_047269922.1_anthranilate_synthase_family_protein           SLGLTVTVRRFDDMYTTSDHDLVIVGPGPGDPTDIDDEKIVHLRAQIDDLLSAQRPFLAI   512
Rhodococcus_erythropolis_WP_336505322.1_anthranilate_synthase_family_protein          SLGLTVTVRRFDDMYTTSDHDLVIVGPGPGDPTDVDDEKIVHLRAQIDDLLSTQRPFLAI   512
Nocardia_sp._BMG111209WP_026343200.1_anthranilate_synthase_family_protein             MLGLSVTIRRFDEDFDLAGHDLVVVGPGPGDPCAADDPKIAKLAAVVDELLGSGRPFMAT   507
Streptomyces_rubiginosohelvolus_WP_355064226.1_anthranilate_synthase_family_protein   ALGLGVTVRRFDETYETRDHDLIVMGPGPGDPGDPGDPKIAALDAVVAELLAERRPMLAV   515
Streptomyces_sp._NPDC002671MGW0882928.1_anthranilate_synthase_family_protein           ALGLSVTVRRFDEPFETGDHDVVLLGPGPGDPRDTTHPKIAALDRVIGELLGERRPFVAV   537
                                                                                       *** **:* *:: :   .:*::::*****:*      **  *   : .**.  **::*

Pseudomonas_fluorescens_VEE46436.1_phenazine_biosynthesis_protein_PhzE                CLSHQVLSLCLGLDLQRRQEPNQGVQKQIDLFGAAERVGFYNTFAARALQDRIEIPEVGP   575
Pseudomonas_chlororaphis_OLF51938.1                                                   CLSHQVLSLCLGLELQRKAIPNQGVQKQIDLFGNAERVGFYNTFAAQSASDRLDINGIGT   576
Rho_PhzE_IsochorismatesynthaseMenF                                                    CLSHQILASRLGLPLTRRAEPNQGKQARVDVFGQSENVGFYNTFEARSAPGRIDVAGVGP   572
Rhodococcus_qingshengii_WP_047269922.1_anthranilate_synthase_family_protein           CLSHQILASRLGLPLTRRAEPNQGKQARVDVFGQSENVGFYNTFEARSAPGRIDVAGVGP   572
Rhodococcus_erythropolis_WP_336505322.1_anthranilate_synthase_family_protein          CLSHQILASRLGLPLTRRAEPNQGKQARVDVFGQSENVGFYNTFEARSAPGRIDVAGIGP   572
Nocardia_sp._BMG111209WP_026343200.1_anthranilate_synthase_family_protein             CLSHQVLSRRLGLPVLRRSLPNQGTQRWIDLFGSRERVGFYNTFSARSEHDRLDTWA-GA   566
Streptomyces_rubiginosohelvolus_WP_355064226.1_anthranilate_synthase_family_protein   CLSHQVLCRRLGLPVVRRARPNQGVQRQISLFGRPERVAFYNTFEARATADHRDTEAGGP   575
Streptomyces_sp._NPDC002671MGW0882928.1_anthranilate_synthase_family_protein           CLSHQVLCHRLGLPLVRREHPNQGTQRRIELFGNAERVGFYNTFEARSTTDRWKSAGGVQ   597
                                                                                       *****:*.  *** : *:  **** *  :.:**  *.*.***** *::  .: .

Pseudomonas_fluorescens_VEE46436.1_phenazine_biosynthesis_protein_PhzE                IEISRDRETGEVHALRGPRFASMQFHPESVLTREGPRIIADLLRHALVERRP--------   627
Pseudomonas_chlororaphis_OLF51938.1                                                   VEISRDSETGEVHALRGPSFASMQFHAESLLTQEGPRIIADLLRHALVHTPAENNASAAG   636
Rho_PhzE_IsochorismatesynthaseMenF                                                    VTVSADTATGAIHALEGPHFASVQFHPESILTVNGPRILAHMSERLLST-----------   621
Rhodococcus_qingshengii_WP_047269922.1_anthranilate_synthase_family_protein           VTVSADTATGAIHALEGPHFASVQFHPESILTVNGPRILAHMSERLLST-----------   621
Rhodococcus_erythropolis_WP_336505322.1_anthranilate_synthase_family_protein          VTVSADTATGAIHALEGPHFASVQFHPESILTVNGPRILAHMSERLLST-----------   621
Nocardia_sp._BMG111209WP_026343200.1_anthranilate_synthase_family_protein             VQVSRDPGTAEVHALRGPRFASVQFHPESLLTIDGPRILTGMAEGVLAQ-----------   615
Streptomyces_rubiginosohelvolus_WP_355064226.1_anthranilate_synthase_family_protein   VEITRDPDTGEVHALRGHRFASLQFHPESLLTVDGPRILTDMTEWVLGE-----------   624
Streptomyces_sp._NPDC002671MGW0882928.1_anthranilate_synthase_family_protein           VEISRDPVTSGVHALRGDRFASLQFHAESLLTVDGPRILTDMFEGVMTR-----------   646
                                                                                       : :: *  *. :***.*  ***:*** **:** :****:: : .  :

Pseudomonas_fluorescens_VEE46436.1_phenazine_biosynthesis_protein_PhzE                -      627
Pseudomonas_chlororaphis_OLF51938.1                                                   R      637
Rho_PhzE_IsochorismatesynthaseMenF                                                    -      621
Rhodococcus_qingshengii_WP_047269922.1_anthranilate_synthase_family_protein           -      621
Rhodococcus_erythropolis_WP_336505322.1_anthranilate_synthase_family_protein          -      621
Nocardia_sp._BMG111209WP_026343200.1_anthranilate_synthase_family_protein             -      615
Streptomyces_rubiginosohelvolus_WP_355064226.1_anthranilate_synthase_family_protein   -      624
Streptomyces_sp._NPDC002671MGW0882928.1_anthranilate_synthase_family_protein           -      646
```

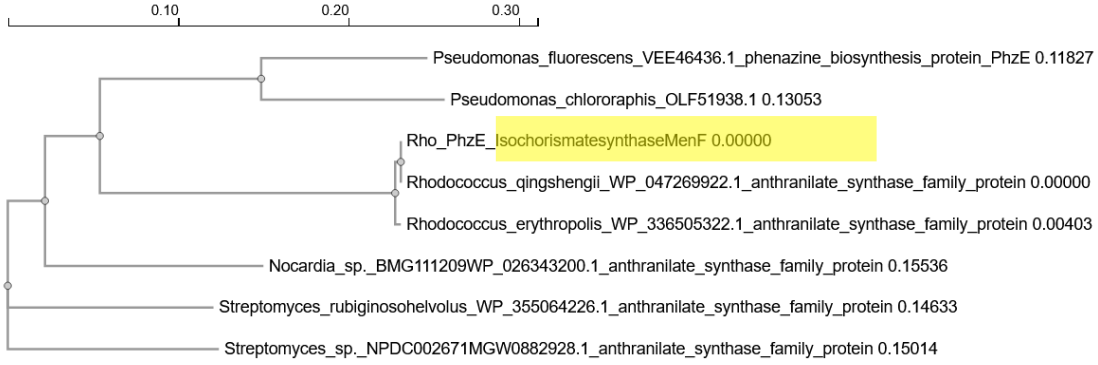

Multiple alignment output for the putative PhzF:

```
CLUSTAL O(1.2.4) multiple sequence alignment


Pseudomonas_fluorescens_WP_150770788.1_PhzF_family_phenazine_biosynthesis_protein               ------------------------------------------------------------   0
Rhodococcus_sp._C3VWP_276117756.1_PhzF_family_phenazine_biosynthesis_protein                    ---------MKLEYIMWDLQSDDDPSVTHLNELTDTAAVDAWRSVPGLAAKYWIHDRGSG   51
Rho_PhzF_hypotheticalprotein                                                                    ---------MKLEYIMWDLQSDDDPSVTHLNELTDTAAVDSWRSVPGLAAKYWIHDRGSG   51
Streptomyces_colonosanans_WP_071367550.1_PhzF_family_phenazine_biosynthesis_isomerase           ------------------------------------------------------------   0
Pseudomonas                                                                                     ------------------------------------------------------------   0
Pseudomonas_aeruginosa_WP_315558930.1_phenazine_biosynthesis_protein_PhzF                       ------------------------------------------------------------   0
Streptomyces_rubiginosohelvolus_WP_398714565.1_PhzF_family_phenazine_biosynthesis_isomerase     MNPTQKTNRMNLEIAWWDLENSFATVDDLERHLGEDGVVENWKEVGGLHEKYWIADRAGN   60
Nocardia_aurantia_WP_319942845.1_PhzF_family_phenazine_biosynthesis_protein                     ------MSPAALEIAWWDLDGSAVTVDRLTAQLADEDVPAGWRDVEGLDEKFWIADPDGC   54


Pseudomonas_fluorescens_WP_150770788.1_PhzF_family_phenazine_biosynthesis_protein               ---------------------------------------------------MLLDFVQVDA   10
Rhodococcus_sp._C3VWP_276117756.1_PhzF_family_phenazine_biosynthesis_protein                    QWGAILLWDDDRPAGVLPAGPALELLERERAHRKDFSVHALIGHRPESSRRSLRYCVVDA   111
Rho_PhzF_hypotheticalprotein                                                                    QWGAILIWDDDRPAGALPAGPALELLERERAHRKDFSVHALIEHRPESSRRSLRYCVVDA   111
Streptomyces_colonosanans_WP_071367550.1_PhzF_family_phenazine_biosynthesis_isomerase           ---------------------------------------------------MHTYVVVDA   9
Pseudomonas                                                                                     ---------------------------------------------------MHRYVIIDA   9
Pseudomonas_aeruginosa_WP_315558930.1_phenazine_biosynthesis_protein_PhzF                       ---------------------------------------------------MHRYVVIDA   9
Streptomyces_rubiginosohelvolus_WP_398714565.1_PhzF_family_phenazine_biosynthesis_isomerase     RWGAVMVWDGERPAE-LPENKAAQLIGGPVTHRERFEVQASVRGLARGRAASHRYIVVDA   119
Nocardia_aurantia_WP_319942845.1_PhzF_family_phenazine_biosynthesis_protein                     RWGAVMVWRGAKPAE-LPPNSALRLIGRPPTHRDRFEVRARVRGATR---PGHRYVVVDA   110
                                                                                                                                  :  :**


Pseudomonas_fluorescens_WP_150770788.1_PhzF_family_phenazine_biosynthesis_protein               FTNRPLYGNPAAVVFDGDELSTETMQRIARFMNLSETVFILKPTTPEADYRARIFTPMSE   70
Rhodococcus_sp._C3VWP_276117756.1_PhzF_family_phenazine_biosynthesis_protein                    FASTPLSGNPVAVFFGADSLSAEMMQRIAAELNLSEVTFVLSADSAESTARIRIFTPVNE   171
Rho_PhzF_hypotheticalprotein                                                                    FASTPLSGNPVAVFFGADSLSAETMQRIAAELNLSEVTFVLSADSAESTARIRIFTPVNE   171
Streptomyces_colonosanans_WP_071367550.1_PhzF_family_phenazine_biosynthesis_isomerase           FASEPLTGNPVAVYFEADSLSGEQMQRIAREMNLSETTFVLRPHRAGHDAHVRIFTPVNE   69
Pseudomonas                                                                                     FATQPLEGNPVAVFFDADDLSAEQMQRIGREMNLSEVTFVLKPRQG-GDALIRIFTPVNE   68
Pseudomonas_aeruginosa_WP_315558930.1_phenazine_biosynthesis_protein_PhzF                       FASEPLQGNPVAVFFDCDDLSGERMQRMAREMNLSESTFVLRPQQD-GDARIRIFTPVNE   68
Streptomyces_rubiginosohelvolus_WP_398714565.1_PhzF_family_phenazine_biosynthesis_isomerase     FASEPLRGNPVAVFFDADDLTADRMQRIAQEMNLSEVTFLLPPTTADADLRVRIFTPVNE   179
Nocardia_aurantia_WP_319942845.1_PhzF_family_phenazine_biosynthesis_protein                     FAREPLSGNPVAVFFDAGDLDGERMQRIAREMNLSEVVFLLPPTSDDADARVRIFTPVNE   170
                                                                                                *:  ** ***.** *  ..*  : ***:. *:**** .*:*          *****:.*


Pseudomonas_fluorescens_WP_150770788.1_PhzF_family_phenazine_biosynthesis_protein               LPFAGHPTVAAAHSVLARYPDKANATLLRQECGIGVVPVEVIPTGSGIL--LRMTQGSPE   128
Rhodococcus_sp._C3VWP_276117756.1_PhzF_family_phenazine_biosynthesis_protein                    LPFAGHPILGTAAAVAAQ----TGAKELAFETAVGLIPMTAEAV--DDYFRVTMDQPLPT   225
Rho_PhzF_hypotheticalprotein                                                                    LPFAGHPILGTAAAVAAQ----TGAKELAFETAVGLIPMTAEAV--DDYFRVTMDQPLPT   225
Streptomyces_colonosanans_WP_071367550.1_PhzF_family_phenazine_biosynthesis_isomerase           LPFAGHPLLGTAIALGAR----TKGDRLLIETAMGLVPFTLEREDG-KVLRASMRQPVPT   124
Pseudomonas                                                                                     LPFAGHPMLGTAIALGAE----TDSPQLRLETQMGTIAFQLERQNG-QVVACSMEQPIPT   123
Pseudomonas_aeruginosa_WP_315558930.1_phenazine_biosynthesis_protein_PhzF                       LPFAGHPLLGTAIALGAE----TDKDRLFLETRMGTVPFALXRQDG-KVVACSMQQPIPT   123
Streptomyces_rubiginosohelvolus_WP_398714565.1_PhzF_family_phenazine_biosynthesis_isomerase     LPFAGHPLQGTAVAVALD----SGRDRLRFETAMGVVPFEIVRAPGGETAHASMEQPIPE   235
Nocardia_aurantia_WP_319942845.1_PhzF_family_phenazine_biosynthesis_protein                     LPFAGHPLLGTAVAVGLE----RGVRRLRFETAMGTVPFEVG-PGGDEVAYVSMRQPIPR   225
                                                                                                *******  .:* ::           *  *  :* : .             * *  *
```

```
Pseudomonas_fluorescens_WP_150770788.1_PhzF_family_phenazine_biosynthesis_protein          YRETQLSRKTVAQMLGCAETEVADSPFEVVSTGVPWLIVELCSFEAISRLNPDQNLITRE  188
Rhodococcus_sp._C3VWP_276117756.1_PhzF_family_phenazine_biosynthesis_protein               WSP--MPDAEQRSLLAALGLDASALPIETYDNGPRHTIVTIDSIEALSALRPDHRALSEF  283
Rho_PhzF_hypotheticalprotein                                                               WSP--MPDAEQRSLLAALGLDTSALPIETYDNGPRHTIVTADSIEALSALRPDHRALSEF  283
Streptomyces_colonosanans_WP_071367550.1_PhzF_family_phenazine_biosynthesis_isomerase      WKP--FDRT--DELLEALGIRGSTLPVEIYRNGPRHVLVGLESIEALSKLDPDHRALARF  180
Pseudomonas                                                                                WSL--FDRT--PELLAALGIERSQYPVEIYRNGPRHVFVGLPDIASLSALHPDHRALSVF  179
Pseudomonas_aeruginosa_WP_315558930.1_phenazine_biosynthesis_protein_PhzF                  WEH--FSRP--AELLAALGLKGSTFPIEVYRNGPRHVFVGLESVAALSALHPDHRALCDF  179
Streptomyces_rubiginosohelvolus_WP_398714565.1_PhzF_family_phenazine_biosynthesis_isomerase WRP--YEHA--DALLAALGVDSSTLPVEIYRNGPRHVFVGLPDAAALNALHPDHRALAAF  291
Nocardia_aurantia_WP_319942845.1_PhzF_family_phenazine_biosynthesis_protein                WRR--FERG--EELLAALGITDSTLPVEIYRNGPRHVFAGLPDVDALSALRPDHRALAVF  281
                                                                                           :           :* .    :  *.*   .*    :.   .  ::. * **:. :

Pseudomonas_fluorescens_WP_150770788.1_PhzF_family_phenazine_biosynthesis_protein          CKALSAAGLTVFAECGDGA-PVRIRVRTFAPGEGVAEDPVCGSGNGSVAAYLARHKHVHE  247
Rhodococcus_sp._C3VWP_276117756.1_PhzF_family_phenazine_biosynthesis_protein               E----N----MAINCIAEDLDGVWRNRMFSPAYGVVEDAATGSAAGPIAIHLARHGRIEY  335
Rho_PhzF_hypotheticalprotein                                                               E----N----MAINCIAEDLDGVWRNRMFSPAYGVVEDAATGSAAGPIAIHLARHGRIEY  335
Streptomyces_colonosanans_WP_071367550.1_PhzF_family_phenazine_biosynthesis_isomerase      S----D----LATNCYAGE-GTSWRNRMFSPAYGVVEDAATGSAAGPIAIHLARYGLIEY  231
Pseudomonas                                                                                P----D----MAVNCFAGA-GRRWRSRMFSPAYGVVEDAATGSAAGPLAIHLARHGQATF  230
Pseudomonas_aeruginosa_WP_315558930.1_phenazine_biosynthesis_protein_PhzF                  P----D----LAVNCFAGA-GRHWRSRMFSPAYGVVEDAATGSAAGPLAIHLARHRQIPY  230
Streptomyces_rubiginosohelvolus_WP_398714565.1_PhzF_family_phenazine_biosynthesis_isomerase E----D----MAANCFAPD-GDHWQTRMFSPAYGVVEDAATGSAAGPLAIHLARYGRVPY  342
Nocardia_aurantia_WP_319942845.1_PhzF_family_phenazine_biosynthesis_protein                P----D----MAANCFAPA-DGHWRARMFSPAYGVVEDAATGSAAGPLAVHLARHGLADY  332
                                                                                                 :  :*         : * *:*. **.** . **. * :* :***:

Pseudomonas_fluorescens_WP_150770788.1_PhzF_family_phenazine_biosynthesis_protein          HSGSYVAEQGIEIGRDGEVQASWERD---GESLRVKIGGQAAVSASGQLHL---------  295
Rhodococcus_sp._C3VWP_276117756.1_PhzF_family_phenazine_biosynthesis_protein               -DHDLRIHQGVELGRHSVMHARASLDARTHDLISVQVGGDAITIAHATLYLGSDRGTDDE  394
Rho_PhzF_hypotheticalprotein                                                               -DHDLRIHQGVELGRHSVMHARASLDARTHNLTSVQVGGDAITIAHATLYLGSDRGTDDE  394
Streptomyces_colonosanans_WP_071367550.1_PhzF_family_phenazine_biosynthesis_isomerase      -GQHIQIVQGVEIGRPSPMGAVAHGEG--EHVAFVEVSGPGIQIIEGVLHV---------  279
Pseudomonas                                                                                -GQQIEILQGVEIGRPSLMFARAEARD--ERITRVEVSGNGALFGQGTIVI---------  278
Pseudomonas_aeruginosa_WP_315558930.1_phenazine_biosynthesis_protein_PhzF                  -GQQIEILQGVEIGRPSRMYARAEGAG--ERVSTVEVSGNGAAFAEGRAYL---------  278
Streptomyces_rubiginosohelvolus_WP_398714565.1_PhzF_family_phenazine_biosynthesis_isomerase -GRTVEIHQGVRLGRRSIMFADATVDTA-GEIARVRVGGHGVVAAEGTIRV---------  391
Nocardia_aurantia_WP_319942845.1_PhzF_family_phenazine_biosynthesis_protein                -GRTVEIHQGVEIGRRSVMFARATAAGS-GEITEVRVSGHGVVAAAGTLHV---------  381
                                                                                            .      **:.:** . : *             *.:.* .     .   :
```

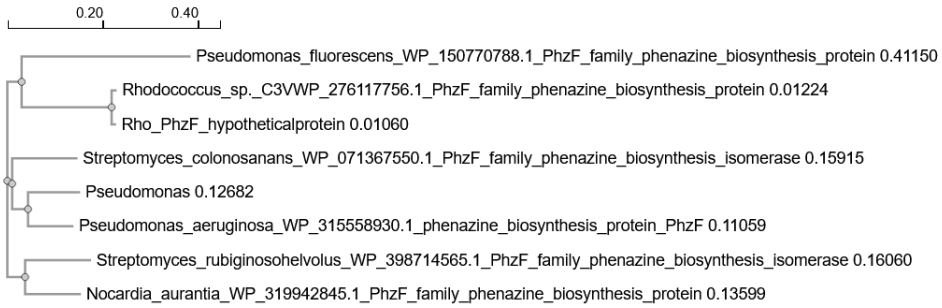

Multiple alignment output for the putative PhzG:

```
CLUSTAL O(1.2.4) multiple sequence alignment

Pseudomonas_sp._MWU13-2105WP_248798019.1_phenazine_biosynthesis_FMN-dependent_oxidase_PhzG          ---------MSAHLLSESLTGTIEAPFPEFATPPANPFIVLNNWLERARRYGVREPKALA     51
Pseudomonas_chlororaphis_WP_075121689.1_phenazine_biosynthesis_FMN-dependent_oxidase_PhzG           MNSSVQGQPLLGKGMSESLTGTLEAPFPEYQAPPANPMDVLHNWLERARRVGIREPRALA     60
Pseudomonas_aeruginosa_WP_128663115.1_phenazine                                                     --------MGVNANISESLTGTIEAPFPEFEAPPANPMEVLRNWLERARRYGVREPRALA     52
Rho_PhzG_Phenazine_biosynthesis_protein                                                             ----------MMSSQYETITGTAR-SFLEYSDPPPTPLDLFQVWIEQAEIAGVREPLALS     49
Rhodococcus_qingshengii_WP_217019068.1_pyridoxal_5'-phosphate_synthase                              ----------MSSQYETITGTAR-PFLEYSDPPPTPLDLFQVWIEQAEIAGVREPLASS     48
Streptomyces_albus_WP_173874215.1_phenazine_biosynthesis_FMN-dependent_oxidase_PhzG                 ----------MSSQYETLTGPADPDFPEYDNPPPEPLKLAAQWLASAIDTGVREPKALA     49
Streptomyces_rubiginosohelvolus_WP_355064222.1_phenazine_biosynthesis_FMN-dependent_oxidase_PhzG    ----------MSSELESITGAVDLDFPEYDNPPPEPMKPALAWLRTAVEGGVREPYALA     49
Microbispora_hainanensis_WP_328709570.1                                                             ----------MSSRFESLTGTIDPAFPEYDMPPAEPMDLARQWIAGAVEAGVREPLALA     49
                                                                                                                 *::**    * *:  **  *:    *:  *  *:*** * :

Pseudomonas_sp._MWU13-2105WP_248798019.1_phenazine_biosynthesis_FMN-dependent_oxidase_PhzG          LATADARGRPSTRIVVIAEVSDAGLVFSTHAGSQKGRELVENPWASGVLYWRETSQQIVL    111
Pseudomonas_chlororaphis_WP_075121689.1_phenazine_biosynthesis_FMN-dependent_oxidase_PhzG           LATVDDQGRPSTRIVVISEFSDRGVLFSTHAGSQKGRELAHNPWASGVLYWRESSQQIVL    120
Pseudomonas_aeruginosa_WP_128663115.1_phenazine                                                     LATVDGQGRPSTRIVVIAEXGERGVVFATHADSQKGRELAQNPWASGVLYWRESSQQIXL    112
Rho_PhzG_Phenazine_biosynthesis_protein                                                             LATTDSAGRCSQRTVAVTDISANGLSFSTHTTSRKARELQTNSWASGLFYWRELARQLIV    109
Rhodococcus_qingshengii_WP_217019068.1_pyridoxal_5'-phosphate_synthase                              LATTDSAGRCSQRTV--TDISASGLSFSTHTTSRKARELQTNSWASGLFYWRELARQLII    106
Streptomyces_albus_WP_173874215.1_phenazine_biosynthesis_FMN-dependent_oxidase_PhzG                 LATADRRGRPSSRTVVVLEIDQHGLRFSTHSTSRKGREIAENGWASGLLYWRETAQQLIF    109
Streptomyces_rubiginosohelvolus_WP_355064222.1_phenazine_biosynthesis_FMN-dependent_oxidase_PhzG    LATTDGAGRPSSRMVAVSDASAEGLLFTTHSTSRKGREIAGTGWASGLFYWRETARQLCF    109
Microbispora_hainanensis_WP_328709570.1                                                             LATADRGGRASTRMVAVIDVGDRGLVFTSHSTSRKGREIAQTGWASGLLYWRETARQLSL    109
                                                                                                    ***.*  ** * * *   : .  *: *::*: *:*.**:  . ****::**** ::*: .

Pseudomonas_sp._MWU13-2105WP_248798019.1_phenazine_biosynthesis_FMN-dependent_oxidase_PhzG          NGRAERLSDTRADVAWRGRPHVTHPMSAVSRQSEELTDVEALRARAKALSGTQAPLPRPD    171
Pseudomonas_chlororaphis_WP_075121689.1_phenazine_biosynthesis_FMN-dependent_oxidase_PhzG           NGQAVRLPDAKAEEAWLKRPYATHPMSSVSRQSEELEDIQAMRAAARELAEVQGPLPRPE    180
Pseudomonas_aeruginosa_WP_128663115.1_phenazine                                                     NGRAERLPDERADAQWLSRPYQTHPMSIASRQSETLADIHALRAEARRLAETDGPLPRPP    172
Rho_PhzG_Phenazine_biosynthesis_protein                                                             SGPVLKLNAAIADKVWDERAEPLKPMSTASHQSLHLGDPEVLLARSDSLG-LRTDLARPH    168
Rhodococcus_qingshengii_WP_217019068.1_pyridoxal_5'-phosphate_synthase                              SGPVLKLNAAIADKVWDERAEPLKPMSTASHQSLHLGDPEVLFARSESLG-LRTDLARPH    165
Streptomyces_albus_WP_173874215.1_phenazine_biosynthesis_FMN-dependent_oxidase_PhzG                 SGPVVRLDAAEADRHWEARPAPLRPMSTVSWQSDRLDDPEAMLKEAERLTPLQETLARPD    169
Streptomyces_rubiginosohelvolus_WP_355064222.1_phenazine_biosynthesis_FMN-dependent_oxidase_PhzG    SGPVVRLDDDENDRLWHSRAHGLHPMSAASRQSESLADPGRLQEEADLLAARDLPLPRPD    169
Microbispora_hainanensis_WP_328709570.1                                                             SGPVAMLPEPEAERLWDARPVPLHAMSVASRQSEPLEDVARLRSEAERLASYGTSLPRPA    169
                                                                                                    .* .  *    :  * *   : ** .* **  * *  :  :  *     * **

Pseudomonas_sp._MWU13-2105WP_248798019.1_phenazine_biosynthesis_FMN-dependent_oxidase_PhzG          GYCLFELRLESVEFWGNGQDRLHERLRYDRTPDGWAVRRLQP      213
Pseudomonas_chlororaphis_WP_075121689.1_phenazine_biosynthesis_FMN-dependent_oxidase_PhzG           GYCVFELRLESLEFWGNGQERLHERLRYDRSDSGWRVRRLQP      222
Pseudomonas_aeruginosa_WP_128663115.1_phenazine                                                     GYCLFELCLESVEFWGNGTERLHERLRYDRGEGGWKHRYLQP      214
Rho_PhzG_Phenazine_biosynthesis_protein                                                             RFAVYQLQPHRVEFWAADQSRLHRRLLYERSPRGWTVDRLQP      210
Rhodococcus_qingshengii_WP_217019068.1_pyridoxal_5'-phosphate_synthase                              RFAVYQLQPHRVEFWAADQSRLHRRLLYERSPLGWTVDRLQP      207
Streptomyces_albus_WP_173874215.1_phenazine_biosynthesis_FMN-dependent_oxidase_PhzG                 RFATYRLEPTSVEFWASSSSRLHRRLRYDLTEDGWRTVRLQP      211
Streptomyces_rubiginosohelvolus_WP_355064222.1_phenazine_biosynthesis_FMN-dependent_oxidase_PhzG    RFVGYRLQPHSVEFWSAAESRLHRRLRYELTDTGWQVSRLQP      211
Microbispora_hainanensis_WP_328709570.1                                                             RFAGYRLEPAAVEFWSADADRLHRRLRYDRTPSGWHISRLQP      211
                                                                                                     :  :.*    :***.   .***.** *:    **    ***
```

Multiple alignment output for the putative Baeyer-Villiger monooxygenase:

```
Pseudomonas_mangiferae_TRX76844.1                                --------MTKRSSIAQFDAIVIGAGLSGLYATHKLGNELGLKVLGLEKARSVGGTWYWN   52
Rhodococcus_multispecies_WP_011331502.1_flavin-containing_monooxygenase  ----------MEPDTSLDAIVIGAGFAGIYALHKLRNELGLAVRCFDKADGVGGTWHWN   49
Rho_putative_Baeyer-Villiger_monooxygenase                       ----------MEPDTSLDAIVIGAGFAGIYALHKLRNELGLAVRCFDKADGVGGTWHWN   49
Pseudomonas_fluorescens_WP_150644880.1_flavin-containing_monooxygenase  MTTTVLAKRSLGTDIIHYDAIIIGAGFAGIYMLKKLRDEMGLKVRAFDKAGGIGGTWYWN   60
Pseudomonas_aeruginosa_WP_420757901.1_flavin-containing_monooxygenase  ----------MVATKDFDAIVVGAGFGGLYMLKKLRDEQGLNVRVFDKAGDVGGTWYWN   49
Streptomyces_sp._S4.7WP_164247642.1_flavin-containing_monooxygenase  ----------MTQKTTHLDSLVIGAGFAGIYMLHKLRNELGLTARVFDKADGVGGTWYWN   50
Microbispora_sp._CSR-4WP_261985629.1_flavin-containing_monooxygenase  -MTDTTTDTTTGTTDTDFDAIVVGTGFAGIYMLHKLRNELGLRVRAFDRAGGVGGTWYWN   59
Streptomyces_luteireticuli_WP_344023394.1_flavin-containing_monooxygenase  ---------MNDTIETDFDAIVVGAGFAGIYMVHKLRNELGLTVRAFEKGSGVGGTWHWN   51
                                                                          *::::*:*:.*:*  :** :* ** .  :::. .:****:**

Pseudomonas_mangiferae_TRX76844.1                                RYPGVQADTDSFVYRYSFDREASPGWDMHARYQTGAQIRDYLENVASRNDLSRLYRFEVE   112
Rhodococcus_multispecies_WP_011331502.1_flavin-containing_monooxygenase  RYPGAKSDSEGFVYRYSFDKEMLQQWSWTNRYLEQAEVLEYLNAVVDRHDLRRDIQLETA   109
Rho_putative_Baeyer-Villiger_monooxygenase                       RYPGAKSDSEGFVYRYSFDKEMLQQWSWTNRYLEQAEVLEYLNAVVDRHDLRRDIQLETA   109
Pseudomonas_fluorescens_WP_150644880.1_flavin-containing_monooxygenase  RYPGALSDSESFVYCFSWDRELCQEWDITTRYLTQPQILSYLNHAVDRHDLRRDIQLETA   120
Pseudomonas_aeruginosa_WP_420757901.1_flavin-containing_monooxygenase  RYPGALSDTETHVYCYSWDKELLQEMDITSRYTTQPQILKYLEKVADRHDLRKDIQFNTG   109
Streptomyces_sp._S4.7WP_164247642.1_flavin-containing_monooxygenase  RYPGAAADVDSIVYRYSFDRELLQEWNWKNRYATQPEILAYLEHVVDRHDLREDIQLNTA   110
Microbispora_sp._CSR-4WP_261985629.1_flavin-containing_monooxygenase  RYPGAMSDVEGFVYRYSFDKQMLQEWNWTTKYTPQRELLAYLEAVVAKHDLGRDIQLNTG   119
Streptomyces_luteireticuli_WP_344023394.1_flavin-containing_monooxygenase  RYPGAMSDVEGFVYRYSFDKELLQEWNWTSRYTPQADVLAYLEKVVERHDLARDIQLNTA   111
                                                                 ****. :* :  ** :*:*::     .   :*    ::  **: .. ::** .  :::.

Pseudomonas_mangiferae_TRX76844.1                                AREATYDEADNLWRVKTSHGDVVTCRYLVNGVGVLSKPVAPKIEGLDDFKGRVVHTARWP   172
Rhodococcus_multispecies_WP_011331502.1_flavin-containing_monooxygenase  VTSARWDDSLARWEVRTDSSKVYRSKYLITALGVLSEPNTPEIPGIEQFSGQVVHTSRWP   169
Rho_putative_Baeyer-Villiger_monooxygenase                       VTSVRWDDSLARWEVRTDSSKVYRSKYLITALGVLSEPNTPEIPGIEQFSGQVVHTSRWP   169
Pseudomonas_fluorescens_WP_150644880.1_flavin-containing_monooxygenase  ITSAVFDEQTSRWLMSTDDGHRYSAKYLVTALGLLSATNVPKINGLDQFQGQMYHTANWP   180
Pseudomonas_aeruginosa_WP_420757901.1_flavin-containing_monooxygenase  ITAMHFNETTNLWEVHTDTGKSYTAKFIVTALGLLSATNIPKIKGLETFQRECYHTGNWP   169
Streptomyces_sp._S4.7WP_164247642.1_flavin-containing_monooxygenase  IESLAYDEESNLWTARTDGGEEVTARYVVGALGPLSTANFPDIPGRDTFAGPLVHTGAWP   170
Microbispora_sp._CSR-4WP_261985629.1_flavin-containing_monooxygenase  IESAVFDESRGVWTVGTDTGESFTARYVVTALGPLSTANIPDIKGRDRFRGRIVHTGSWP   179
Streptomyces_luteireticuli_WP_344023394.1_flavin-containing_monooxygenase  VESAVFDETRAIWTVTTSGGASHTARYVVTALGPLSKTNLPDIKGRDSFAGRLIHTGAWP   171
                                                                      :::    *   *. .    .:::: .:* **    *.* * : *     **. **

Pseudomonas_mangiferae_TRX76844.1                                EGLRIDGLRVGLLGTGSTGTQVAVAASKVASHLTVFQRSAQYVVPAGQRRHTDTEVDSFL   232
Rhodococcus_multispecies_WP_011331502.1_flavin-containing_monooxygenase  EGLDVAGRKVGVIGTGSTGTQFICTAAETAQQLTVFQRTAQYSIPSGNGPIDQEYLDRCR   229
Rho_putative_Baeyer-Villiger_monooxygenase                       EGLEVAGRKVGVIGTGSTGTQFICTAAETAQQLTVFQRTAQYSIPSGNGPIDQEYLDRCR   229
Pseudomonas_fluorescens_WP_150644880.1_flavin-containing_monooxygenase  ADAVLEGKRVGVIGTGSTGCQVITAIAPTVGHLTVFQRSAQYTVPVGNGPVSREYVDDIK   240
Pseudomonas_aeruginosa_WP_420757901.1_flavin-containing_monooxygenase  QDVQFEGKRVGVIGTGSTGTQVITAIAPQVEHLTVFQRSPQYSVPVGNGPVSREYVDNIK   229
Streptomyces_sp._S4.7WP_164247642.1_flavin-containing_monooxygenase  RDLDITGKRVGVVGTGSTGTQFICAAARTATHLTVFQRSAQYVVPSGDGPLSDAYLTECR   230
Microbispora_sp._CSR-4WP_261985629.1_flavin-containing_monooxygenase  DDLTIEGRRVGVVGTGSTGTQFACAAAKVAGHLTVFQRSAQYCVPSGHGPVTEEHVAEVR   239
Streptomyces_luteireticuli_WP_344023394.1_flavin-containing_monooxygenase  EGVTVHGKRVGVIGTGSTGTQFICEASRTAAHLTVFQRSPQYVVPSGNAPVTPEQVAAVK   231
                                                                  .  . * :**::****** *.    :  . :******: ** :* *.       :
```

```
Pseudomonas_mangiferae_TRX76844.1                                  SHFDENFREWRKTRLACGFEEPATSAAEASPEERKAVFEHAWNEGGGFGFMFGTFGDLVI  292
Rhodococcus_multispecies_WP_011331502.1_flavin-containing_monooxygenase  SNYDAIWDQVRNSIVGCGFEESTVSATSVSEAERTRVFEESWQRGNAFHFMFGTFNDIIF  289
Rho_putative_Baeyer-Villiger_monooxygenase                         SNYDAIWDQVRNSIVGCGFEESTVSATSVSEAERTRVFEESWQRGNAFHFMFGTFNDIIF  289
Pseudomonas_fluorescens_WP_150644880.1_flavin-containing_monooxygenase  RNYDAIWKEVRSSRLAFGFEESNIPTMSVSAPERKEIFQRAWDVGGGFRYMFQTFNDIAT  300
Pseudomonas_aeruginosa_WP_420757901.1_flavin-containing_monooxygenase  KNYDKIWEQVKNSMVAFGFEESTVPAMSVSDEERQAVFQKAWENGGGFRFMFETFCDIAT  289
Streptomyces_sp._S4.7WP_164247642.1_flavin-containing_monooxygenase  ETYDQIWDQVFNSRVGCGFKESEISATSVSPAERERLFQESWDAGNGFRFMFGIFSDIAF  290
Microbispora_sp._CSR-4WP_261985629.1_flavin-containing_monooxygenase  ASYDRIWEQVRNSRVACGFEESDVPAMSVSEEERRRVFQEYWDKGNGFRFMFGTFSDIAT  299
Streptomyces_luteireticuli_WP_344023394.1_flavin-containing_monooxygenase  ADYDRIWDQVRNSMVACGFEESTIPTMSVSPEERRRIFQEAWEEGNGFRFMFGTFCDIAV  291
                                                                     :*  : :  .: :. **:*    : ..*  **  :*:. *: *..* :**  * *:

Pseudomonas_mangiferae_TRX76844.1                                  NPDSNRAACEFIVGKIKQIVRDPETARRLTPSEPYAKRPVSVDGYYEAFNQPNVKLVSIQ  352
Rhodococcus_multispecies_WP_011331502.1_flavin-containing_monooxygenase  DPAANLAAADFVRDKIAAIVDDPDTARKLMPSGYYATRPIANKGYYETFNRPNVSLVSIK  349
Rho_putative_Baeyer-Villiger_monooxygenase                         DPAANLAAADFVRDKIAAIVDDPDTARKLMPSGYYATRPIANKGYYETFNRSNVSLVSIK  349
Pseudomonas_fluorescens_WP_150644880.1_flavin-containing_monooxygenase  NEEANVAAQDFVREKIAEIVKDPETARKLMPRDLYAKRPLCDSGYYATFNRDNVALVDVK  360
Pseudomonas_aeruginosa_WP_420757901.1_flavin-containing_monooxygenase  DERANKAAQDFIRSKIAEIVKDPETARKLTPNDLYAKRPLCDSGYYATYNRPNVSLLDVK  349
Streptomyces_sp._S4.7WP_164247642.1_flavin-containing_monooxygenase  NPAANEAAASFIKSKITQTVRDPETARKLMPTDYYAKRPICNSGYYETYNRDNVSLVSTK  350
Microbispora_sp._CSR-4WP_261985629.1_flavin-containing_monooxygenase  DPEANEAAAEFIRSKIREIVKDPETARKLTPSDFYAKRPICNPDYYEIFNRDNVSLVSIK  359
Streptomyces_luteireticuli_WP_344023394.1_flavin-containing_monooxygenase  DPAANKAAAEFIRSKIHEIVEDPETARKLTPTEYYAKRPICNAGYYEAYNRPNVSLVSIQ  351
                                                                     :  :* ** .*:  **   * **:***:* *   **.**:.  .**  :*: ** *:. :

Pseudomonas_mangiferae_TRX76844.1                                  ETPIVRVTENGILTADGVEHEIDILILATGFEAVEGAYRDFNVIGRNGRTLLDTWGEHPA  412
Rhodococcus_multispecies_WP_011331502.1_flavin-containing_monooxygenase  DNPITRLTENAVVTADGTEHEIDLLVLATGFD---AGYKKMHLTGRDGTPISELWNETTA  406
Rho_putative_Baeyer-Villiger_monooxygenase                         DNPITRLNENAVVTADGTEHEIDLLVLATGFDAVDGGYKKMHLTGRDGTPISDLWNETTA  409
Pseudomonas_fluorescens_WP_150644880.1_flavin-containing_monooxygenase  ANPIEEITATGIRTADGVEHELDVLVFATGFDAVDGNYKRIDIRGRDGVSMKDHWADGPS  420
Pseudomonas_aeruginosa_WP_420757901.1_flavin-containing_monooxygenase  ANPIAEITPKGVKTADGVEHELDMLIFATGFDAVDGNYTKIDIRGRKGLAIQDHWKAGPS  409
Streptomyces_sp._S4.7WP_164247642.1_flavin-containing_monooxygenase  ENPVVRITPAGVVTEDGTEHELDVLVFATGYEAMEGSYNRIGIQGRAGTTLRESWGDTPS  410
Microbispora_sp._CSR-4WP_261985629.1_flavin-containing_monooxygenase  ETPIKEITPTGVLTEDGVEHELDILVFATGFDAVDGSYKRMDIRGRDGVPILDHWDDGPT  419
Streptomyces_luteireticuli_WP_344023394.1_flavin-containing_monooxygenase  ENPIVEITPRGVITADGVEHELDILVFATGFEAVEGSYNQIDIRGRGGESIQDHWEDGPS  411
                                                                     .*: .:.  .: * **.***:*:*::***::   . *  : : ** *  : : *    :

Pseudomonas_mangiferae_TRX76844.1                                  AYLGLSTPGFPNLFTVLGPQGIFSNLAAGIEAEVNFIGDAIRWAEDRPGAAIEATPEALS  472
Rhodococcus_multispecies_WP_011331502.1_flavin-containing_monooxygenase  AYLGIATHQFPNMFMVYGPNSVFTNLPPGIETQVEWITELIRQAETQGSATVEADETAVR  466
Rho_putative_Baeyer-Villiger_monooxygenase                         AYLGIATHQFPNMFMVYGPNSVFTNLPPGIETQVEWITELIRQAETRGSAVVEVSETAVR  469
Pseudomonas_fluorescens_WP_150644880.1_flavin-containing_monooxygenase  SYMSVATANFPNMFMILGPNGPFTNLPPTIETEVEWVSELIGFMEENELACVETDPESER  480
Pseudomonas_aeruginosa_WP_420757901.1_flavin-containing_monooxygenase  SYLGVANANYPNMFMVLGPNGPFTNLPPSIETQVEWISDLIQDVNTKSLKTVEPTPEAEA  469
Streptomyces_sp._S4.7WP_164247642.1_flavin-containing_monooxygenase  SYLGVATHGFPNLFMVYGPNSVFCNLPPGIETQVEWISEMIGSARRRGITRIEATATAED  470
Microbispora_sp._CSR-4WP_261985629.1_flavin-containing_monooxygenase  SYLGVATHGFPNLFMVLGPNSAFSNLPPGIETQVEWIGDLIRTAEENGTTVIEATRDAED  479
Streptomyces_luteireticuli_WP_344023394.1_flavin-containing_monooxygenase  TYLGVATSGFPNLFMVLGPNSAFTNLPPGIETHVEWIAELVRTVENGGHSSIEATREAED  471
                                                                     :*:.::.  :**:* : **:. * **   **:.*::: : :   .      :*    :
```

```
Pseudomonas_mangiferae_TRX76844.1                                  TWSEQCSQMANYTVFAQVKSWIFGTNVHSNQPRVLFYFGGLKEYLSILDHERTHGFPGFT  532
Rhodococcus_multispecies_WP_011331502.1_flavin-containing_monooxygenase  TWAQLCDDIANASLFPKAHSWIFGANIPGKTSRALFYFAGLGNYRRVLADEADADYPNFT  526
Rho_putative_Baeyer-Villiger_monooxygenase                         AWAQLCDDIANASLFPKAHSWIFGANIPGKTSRALFYFAGLGNYRRVLADESDADYPNFT  529
Pseudomonas_fluorescens_WP_150644880.1_flavin-containing_monooxygenase  EWGATCQEIADQTLFAKADSWIFGANIPGKPNAVYFYMGGLGPFSEVLRSVKNDEYRGFK  540
Pseudomonas_aeruginosa_WP_420757901.1_flavin-containing_monooxygenase  FWTKTCQEIASTTLFPKAESWIFGANIPGKTNTVYFFLAGLGAYRQQLTEVRKQGYQGFQ  529
Streptomyces_sp._S4.7WP_164247642.1_flavin-containing_monooxygenase  EWTGMCREMAEQSLFAQTDSWIFGTNIPGRKRRTLFYFGGIGNYRQKLREVAAADYEGFS  530
Microbispora_sp._CSR-4WP_261985629.1_flavin-containing_monooxygenase  EWTETCRKLADYTLFPKVKSWIFGANIPGKKNRVMFYFAGLASYRLKLGEVAEAGYEGFD  539
Streptomyces_luteireticuli_WP_344023394.1_flavin-containing_monooxygenase  GWTETCREIAEQTLFAKIDSWIFGANIPGKEKRVLFYFGGLGAYRQKLREVAAADYDGFR  531
                                                                    *   * .:*. ::* : .*****:*: ..   . *::.*:  :   *       : .*

Pseudomonas_mangiferae_TRX76844.1                                  QAGSPSLTLVQSKADATDDEALRQRNYATVERYMHSLGQDRLTRHHLFQPDGICGLWTTE  592
Rhodococcus_multispecies_WP_011331502.1_flavin-containing_monooxygenase  FRSDDHTSLEREHASIPQ----------------------------------------  544
Rho_putative_Baeyer-Villiger_monooxygenase                         FHSDDHTSLEREHASIPQ*---------------------------------------  547
Pseudomonas_fluorescens_WP_150644880.1_flavin-containing_monooxygenase  FMVTEQYAQKVLY----------------------------------------------  553
Pseudomonas_aeruginosa_WP_420757901.1_flavin-containing_monooxygenase  FQ--------------------------------------------------------  531
Streptomyces_sp._S4.7WP_164247642.1_flavin-containing_monooxygenase  LEGQSSLTPA------------------------------------------------  540
Microbispora_sp._CSR-4WP_261985629.1_flavin-containing_monooxygenase  LHASPSLTPA------------------------------------------------  549
Streptomyces_luteireticuli_WP_344023394.1_flavin-containing_monooxygenase  LRGGVALAAA------------------------------------------------  541

Pseudomonas_mangiferae_TRX76844.1                                  TGKPIKIH 600
Rhodococcus_multispecies_WP_011331502.1_flavin-containing_monooxygenase  -------- 544
Rho_putative_Baeyer-Villiger_monooxygenase                         -------- 547
Pseudomonas_fluorescens_WP_150644880.1_flavin-containing_monooxygenase  -------- 553
Pseudomonas_aeruginosa_WP_420757901.1_flavin-containing_monooxygenase  -------- 531
Streptomyces_sp._S4.7WP_164247642.1_flavin-containing_monooxygenase  -------- 540
Microbispora_sp._CSR-4WP_261985629.1_flavin-containing_monooxygenase  -------- 549
Streptomyces_luteireticuli_WP_344023394.1_flavin-containing_monooxygenase  -------- 541
```

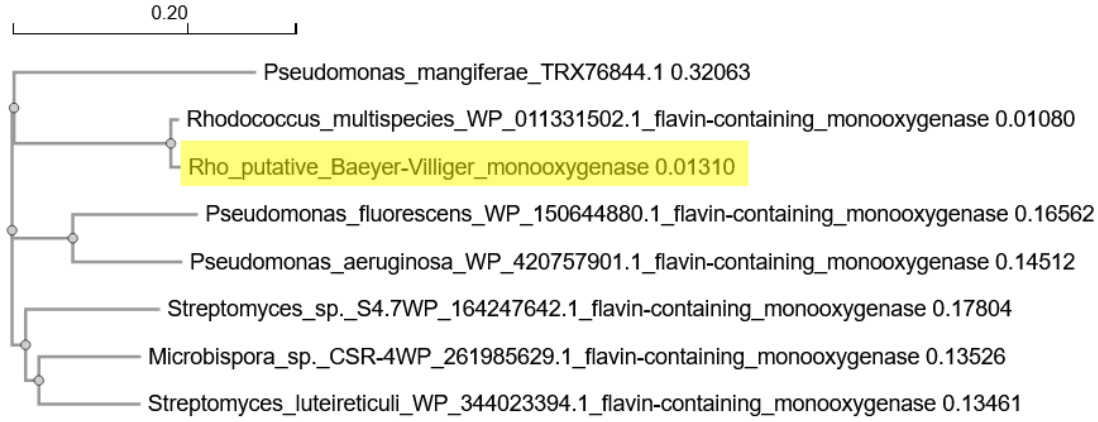

Circoletto analysis revealed the position of the genes in the three contigs identified in *Rhodococcus* sp. ef1 genome *(Figure 32)*. The operon mapping proposed in *Figure 31* was partially confirmed, with the exception of sequence G1, which was not detected by the tool. This may indicate that the G1 sequence

in *Rhodococcus* is distantly related to its counterpart in *Pseudomonas aeruginosa,* preventing its identification by Circoletto. Homologues of phzC and phzD were also identified in the main chromosome (contig 3). As previously hypothesised, PhzM and PhzH genes were not present in *Rhodococcus* sp. ef1.
In contrast, the same analysis performed on the genome of *Rhodococcus erythropolis* resulted in the absence of most of the phz genes, with only phzC1 and D1 detected in the main chromosome. These findings suggest that *Rhodococcus* sp. ef1 may have acquired the genes putatively involved in the synthesis of the pigment by a phenomenon of horizontal gene transfer (see discussion).

Pseudomonas aeruginosa

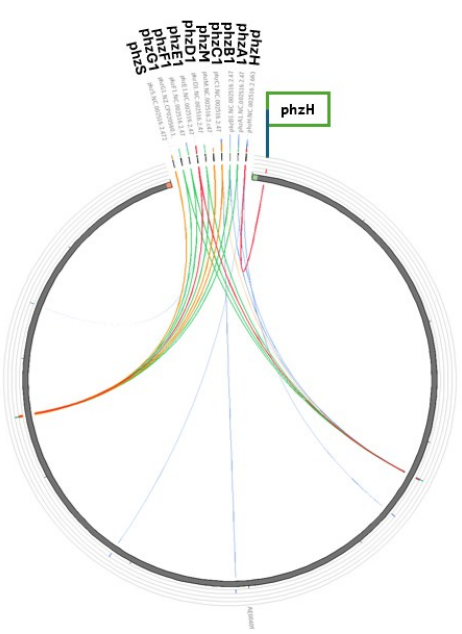

***Rhodococcus* sp. ef1**

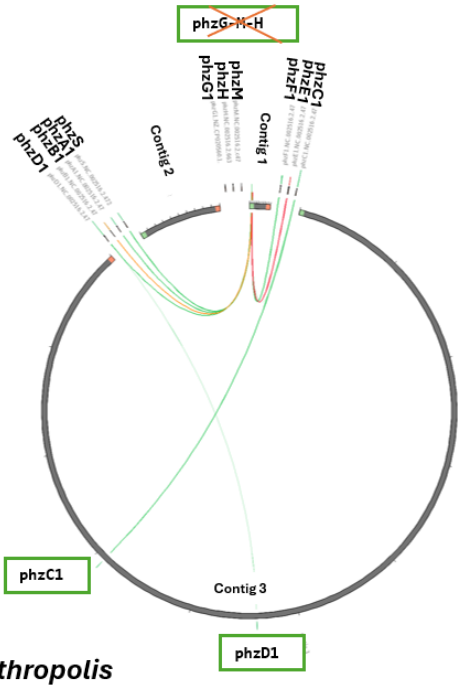

Rhodococcus erythropolis

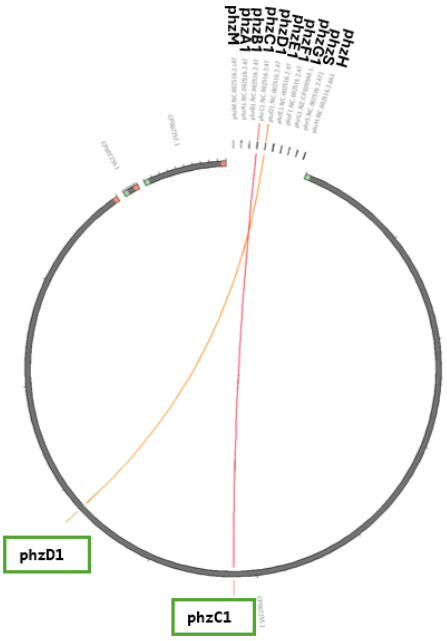

Figure 32 – Results of the Circoletto analysis.
Pseudomonas aeruginosa was used as a reference. Rhodococcus sp. ef1 exhibited all genes except phzM and phzH. Two copies of both phzC and phzD were identified, with one copy located on contig 1 and an additional copy located on contig 3. The genome of Rhodococcus erythropolis lacked most phz genes, with only phzC1 and D1 detected.

Antibiotic activity tests

Since preliminary results have shown that the pigment exhibits antimicrobial activity against Gram positive bacterial strain *Bacillus* sp, ef1 *(Figure 33)* and *S. aureus* (see the Chapter 3, *Figure 54*), other tests were conducted to further evaluate the potential against some common pathogenic species, including Gram negative, Gram-positive and yeast representatives. The tests didn't show significant antimicrobial efficacy *(Figure 34)*. This could be attributed to an insufficient concentration of the compound against the pathogens tested, to pH alteration after contact with the media (in some cases, the disks have changed their colour after being placed on the plates), or to the neutralization step performed, which may have altered the bioactivity of the molecule. Concerning this latter, a reduction of the antibacterial properties against *Bacillus* sp. ef1 was observed by comparing the pigment extracted at basic pH (from 10 to 12) with the pigment after neutralization process *(Figure 35)*.

Some pathogens were selected to repeat the test by performing microdilutions in broth. *P. aeruginosa, E. coli, K. pneumoniae, Candida albicans*, and *S. aureus* were chosen as they were easier to be maintained and manipulated. The results

showed that the pigment revealed antimicrobial effect only against *S. aureus* with a concentration of 600 µg/ml *(Figure 36)*.

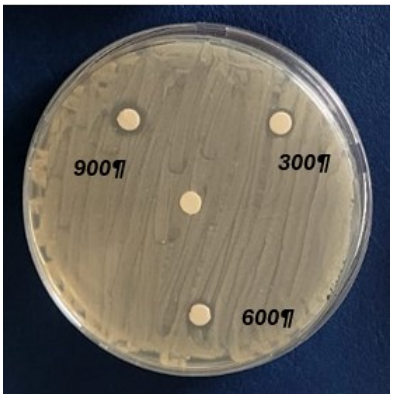
900¶
300¶
600¶

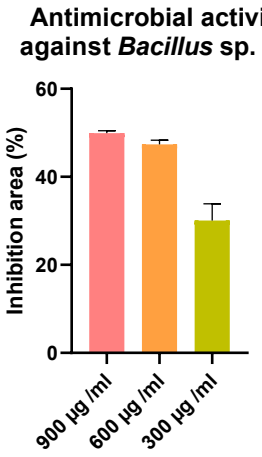
Antimicrobial activity
against *Bacillus* sp. ef1
Inhibition area (%)
60
40
20
0
900 µg /ml
600 µg /ml
300 µg /ml

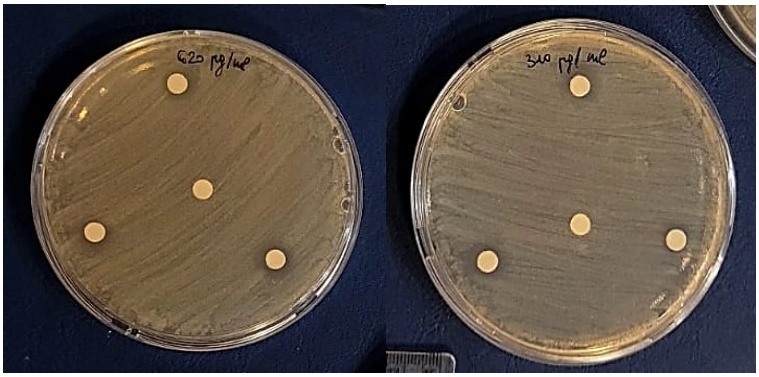


155 µg/ml

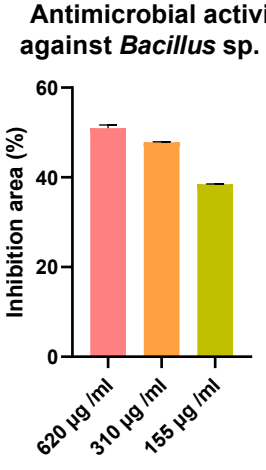
Antimicrobial activity
against *Bacillus* sp. ef1
Inhibition area (%)
60
40
20
0
620 µg /ml
310 µg /ml
155 µg /ml

Figure 33 – Antimicrobial activity against Bacillus sp. ef1 at different concentrations of the pigment.

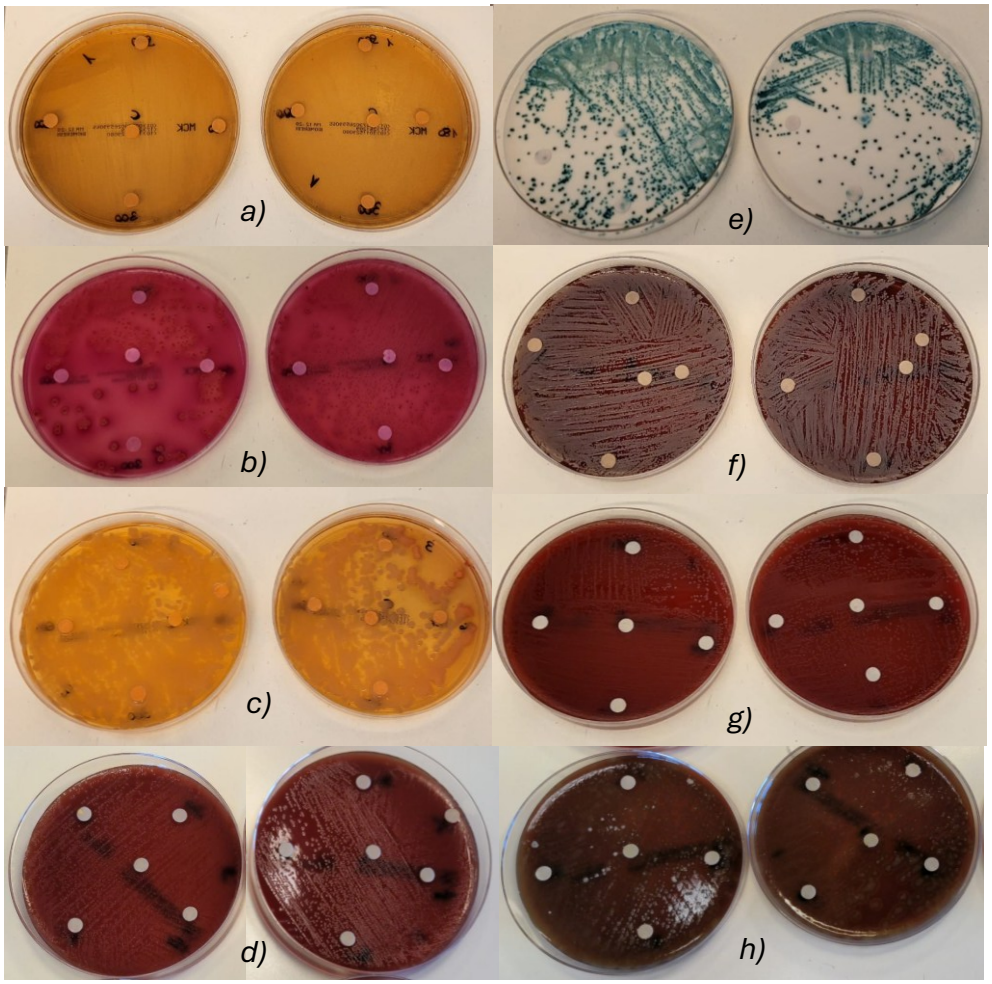

Figure 34 - Antibiotic activity tests against common pathogens. Each concentration (900, 600, 300, 150 µg/ml) of pyocyanin derivative was tested against the selected bacterial strains in duplicate. a) P. aeruginosa, b) E. coli, c) K. pneumoniae, d) Streptococcus pyogenes, e) Candida albicans, f) S. aureus, g) Enterococcus faecium, h) Streptococcus agalactiae.

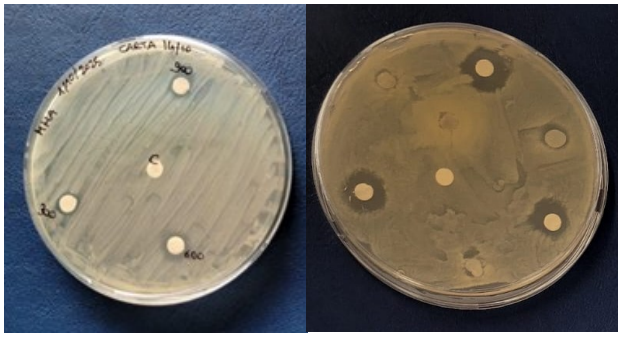

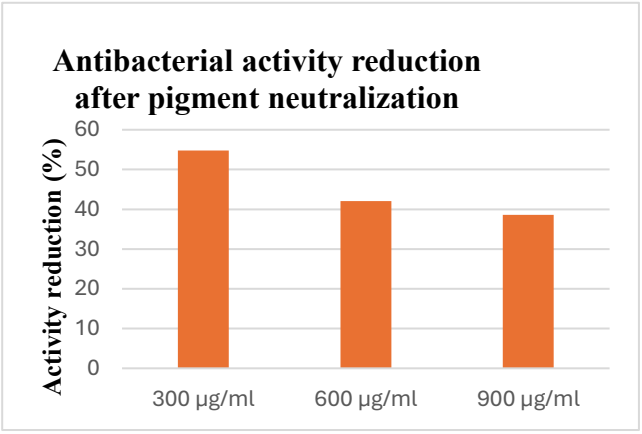

Figure 35 - Antibiotic potential reduction of pyocyanin derivative neutralized with HCl (a) compared with the pigment extracted at basic pH (b). (c) Graphical estimation of the residual effect of the antibacterial effect after the neutralization of the pigment at different concentrations.

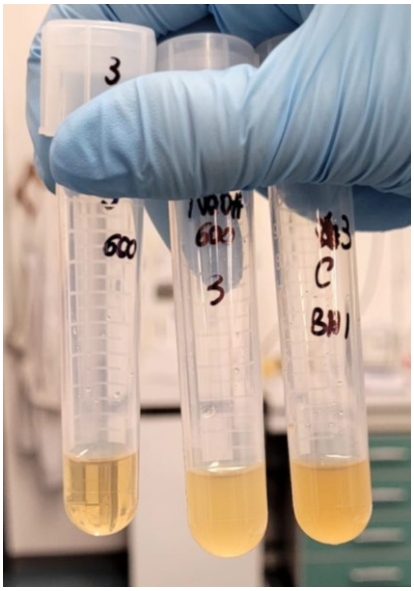

Figure 36 – The antibacterial activity test revealed efficacy against S. aureus at 600 µg/ml of pigment concentration. on the left: experimental sample with 600 µg/ml of pyocyanin derivative. in the middle: control with basic water (same pH of the pigment extracted). on the right: control sample with BHI without addition of the pigment.

Moreover, the activity was also evaluated by soaking bacterial cellulose (BC) produced by the Antarctic strain *Pseudomonas* sp. ef1 and the Kombucha. This was just a preliminary test to verify the possibility to combine different Antarctic bacteria-derived materials, with the final objective to produce an adsorbent coating of cellulose with antimicrobial properties to be applied in regenerative biomedicine. Also in this case, a reduction of the antimicrobial activity against *Bacillus* sp. ef1 was observed by comparing the pigment extracted at basic pH (from 10 to 12) with the pigment after neutralization process *(Figure 37)*.

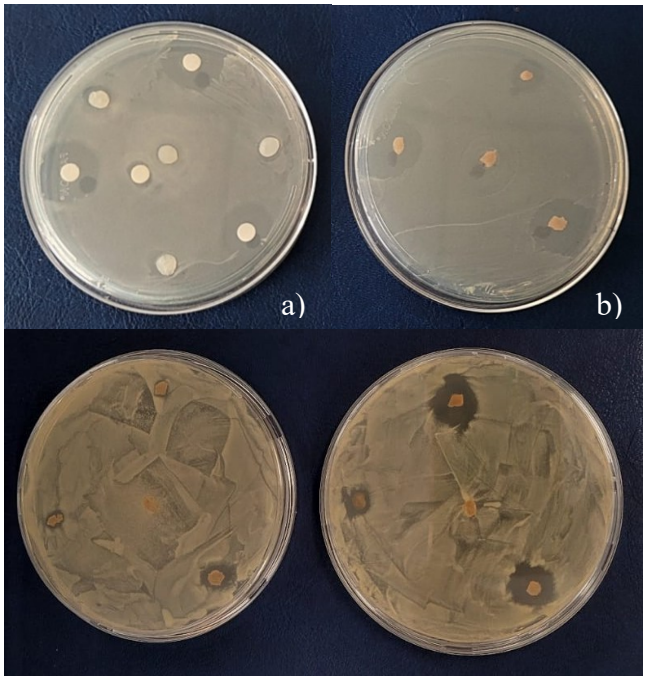

Figure 37 - Pigment antibacterial activity against Bacillus sp. ef1. On the left: a) filter paper and cellulose obtained from Kombucha and b) spherical cellulose from Pseudomonas sp. ef1 soaked with the pigment. On the right: *spherical cellulose from Pseudomonas sp. ef1 soaked with the pigment after neutralization (c) and extraction at basic pH (d).*

Discussion

This research work aimed to characterize and identify a novel pigment produced by the bacterial strain *Rhodococcus* sp. ef1 from Antarctica. Pigment production was obtained using a minimal medium with sodium citrate as sole carbon source. The synthesis was optimized by varying the sodium citrate concentration. In *Pseudomonas aeruginosa*, sodium citrate can affect bacterial growth, inhibiting biofilm formation and the expression of virulence factors in some contexts

(Khayat et al., 2022), while promoting the expression of specific virulence factors, including pyocyanin production, under defined conditions *(Mould et al., 2024)*. Thus, depending on the bacterial strain, culture conditions, and citrate concentration, it may play a significant role in the pigment biosynthetic pathway.

The estimated yield of the pyocyanin produced by *Rhodococcus* sp. ef1 was 31 mg/L, with an average productivity of 0.32 mg/L/h. The crude yield was calculated from the dry weight of the pigment recovered after chloroform extraction and solvent evaporation. The accuracy of this estimation could be affected by several factors, including incomplete chloroform extraction, possible residual impurities from cell debris and medium salts, errors associated with handling and weighing small quantities of dried pigment, and biological variability in pigment production due to the multiple parameters affecting biosynthesis.

Table 5 reports the characteristics of pyocyanin and its derivatives produced by *Pseudomonas* strains described in the literature or commercially available, including yield, productivity, and purity values where reported.

Table 5 – Characteristics of the pyocyanin produced from Pseudomonas strain.

Strain	**Pyocyanin or derivative name**	**Yield (mg/L)**	**Productivity (mg/L/h)**	**Purity**	**References**
P. chlororaphis H18	*1-hydroxyphenazine*	*3600*	*66.7 (54 h)*	*x*	*(Wan et al., 2021)*
P. aeruginosa (environmental isolate from sewage water)	*Pyocyanin*	*6*	*x*	*high*	*(Rashid & Andleeb, 2018)*
P. aeruginosa strain OG1	*Pyocyanin*	*33*	*0.46 (72 h)*	*94.2%*	*(Ozdal, 2019)*

P. aeruginosa DN9	*Pyocyanin*	*92.12*	*1,28 (72 h)*	*high*	*(Gahlout et al., 2021)*
P. chlororaphis Qlu-1	*Phenazine-1-carboxamide*	*11450*	*159, 02(72 h)*	*x*	*(L. Li et al., 2020a)*
P. aeruginosa PsC05 and PsE02	*Pyocyanin*	*10*	*x*	*x*	*(Shouman et al., 2023b)*
P. aeruginosa P8 and P9 (hospital wastewater isolates)	*Pyocyanin*	*14.34*	*0,20 (72 h)*	*x*	*(Rai et al., 2024)*
Pseudomonas sp. MPF-2	*Pyocyanin*	*31.35*	*0.435 (72 h)*	*-*	*(Eltarahony et al., 2025b)*
P. aeruginosa (Sigma-Aldrich)	*Pyocyanin*	*-*	*-*	*98%*	*https://www.sigmaaldrich.com*
P. aeruginosa (Cayman chemical)	*Pyocyanin*	*-*	*-*	*98%*	*https://www.caymanchem.com*
P. aeruginosa (MedChemExpress)	*Pyocyanin*	*-*	*-*	*99.23 %*	*https://www.medchemexpress.com*

As showed in *Table 5*, the yield of pyocyanin ranges between 6 and 11450 mg/L *(Eltarahony et al., 2025b; Gahlout et al., 2021; L. Li et al., 2020a; Ozdal, 2019; Rai et al., 2024; Shouman et al., 2023b; Wan et al., 2021)*. The highest values, 3600 and 11450 mg/L, were achieved by modifying gene expression of the producers and using fermenters *(L. Li et al., 2020b; Wan et al., 2021)*. Thus, although *Rhodococcus* sp. ef1 does not reach the highest production performances reported for *Pseudomonas*, its ability to synthesize pyocyanin at levels comparable to several native *Pseudomonas* isolates is remarkable, especially considering that *Rhodococcus* is not a canonical pyocyanin producer. This strain may represent an alternative producer, opening perspectives for

further optimization of culture conditions and investigation of its biosynthetic pathway.

Commercial pyocyanin standards are already available on the market as research-grade reagents, with a chromatographic purity of 98% to 99.23% and prices ranging from 52 to 143€ per 5 mg (Sigma-Aldrich, Cayman Chemical, MedChemExpress), reflecting the high production costs and the complexity of extraction and purification procedures *(Cheluvappa, 2014)*.

The molecule exhibited a very peculiar behaviour in terms of solubility and colour compared to the standard pyocyanin. Pyocyanin is reported to be soluble in organic solvents at normal and alkaline pH, assuming a distinctive blue colour, and in water at a lower pH, with a red-pink colour *(Abdelaziz et al., 2023)*. In contrast, the phenazine examined in this study behaved in the opposite manner, suggesting that it is a derivative with a different structure and/or redox state of the molecule.

Chemical characterization enabled the identification of the pigment as a novel pyocyanin derivative, named 3-amino-1,4-dihydroxy-5-methyl-1,4-dihydrophenazin-5-ium. Analytical profile revealed the presence of three peaks corresponding to three different forms of the compound coexisting in the sample. However, two of them were present in very low amounts and could not be isolated because of the limited sample availability. Therefore, the study focused on the most representative form of the molecule. Various spectrometric techniques showed that the molecule exhibits similar UV-Vis spectra and similar colours to pyocyanin. This pyocyanin derivative is soluble in chloroform and easily extractable in water. The compound itself is slightly acidic due to the presence of the phenolic group, and it remains stable in the dark with a

temperature of 4°C for several months. The photochemical characterization of the pigment revealed that this molecule degrades when exposed to UV light. When exposed to visible light, instead, it remains stable for a week, losing its characteristic blue colour after this period.

Phenazine biosynthesis is a complex and tightly regulated process *(Figure 38)*. Two similar operons, namely phz1 and phz2, have been identified as responsible for the synthesis of phenazine-1-carboxylic acid (PCA) starting from chorismic acid. They share 98% homology, and each includes seven core genes, phz A1B1C1D1E1F1G1 for phz1, and phz A2B2C2D2E2F2G2 for phz2. Three additional genes, phzM, phzS, and phzH, encode tailoring enzymes responsible for downstream chemical modifications. Specifically, PCA is converted to phenazine-1-carboxamide (PCN) by phzH and to 1-hydroxyphenazine (1-OH-PHZ) by phzS. PhzM mediates the conversion of PCA to 5-methylphenazine-1-carboxylic acid betaine, which can be subsequently converted to pyocyanin by phzS *(Higgins et al., 2018)*.

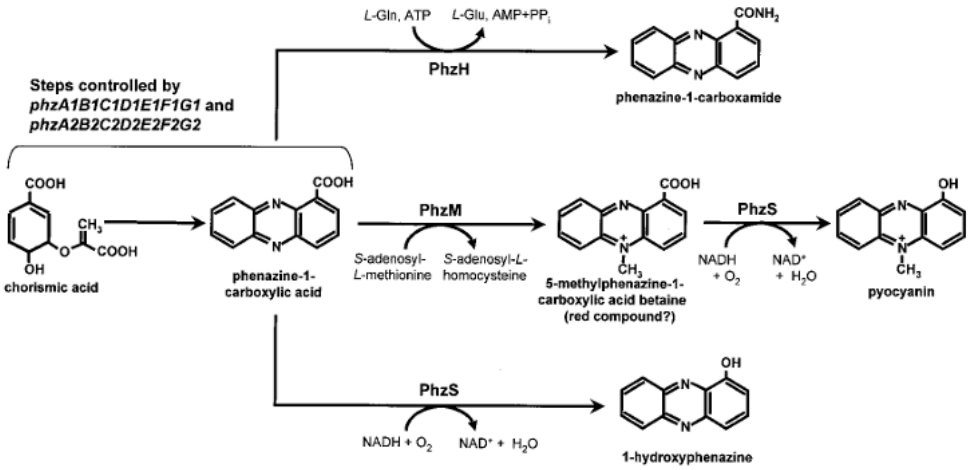

FIG. 4. Proposed mechanism for the synthesis of pyocyanin, 1-OH-PHZ, and PCN in *P. aeruginosa* PAO1.

Figure 38 -Mechanism for the synthesis of pyocyanin, 1-OH-PHZ, and PCN in P. aeruginosa PAO1 (Mavrodi et al., 2001)

According to the sequencing results, *Rhodococcus* sp. ef1 genome consists of a chromosome and two plasmids. A single gene with a pyridoxine/pyridoxamine 5'-phosphate oxidase domain was identified within the chromosome. The sequence could be potentially involved in the phenazine synthesis, although it also might simply encode a protein with a conserved domain which plays a role in other cellular processes, likely related to iron metabolism *(Richts et al., 2019)*. Six of the seven genes of the core of the phenazine operon, instead, were predicted to form a cluster within a single plasmid. Multiple alignments revealed that the proteins encoded by the putative phenazine related genes are conserved along different taxa including *Pseudomonas*, *Streptomyces* and other *Actinobacteria*. This is consistent with previous studies in the scientific literature, which indicated that phz pathways may have evolved via horizontal gene transfer in some bacterial lineages, involving *Streptomyces* and *Nocardiopsis* (Gram-positive Actinobacteria distantly related to *Rhodococcus* spp.), *Pseudomonas* spp., and *Burkholderia* spp. *(Mavrodi et al., 2010b)*.

To date, this is the first report of a *Rhodococcus* strain with evidence of phenazine production. A recent study conducted on *Rhodococcus qingshengii* F2-2 identified a plasmid carrying a cluster of genes (phzG, phzF, phzE, phzD, phzB, and phzS) putatively involved in phenazine biosynthesis. Similarly to *Rhodococcus* sp. ef1, no phenazine-modulating genes (phzO, phzH, phzM) nor regulatory genes (phzI and phzR) were detected. However, the functional role of the phz genes has not yet been elucidated. Analyses of the secondary metabolites produced by this strain suggested the possible production of a phenazine

derivative, although no definitive compound identification has been achieved so far *(Chayka et al., 2025)*. The absence of sequences encoding the tailoring enzymes PhzM and PhzH and the presence of an additional flavin containing-monooxygenase, potentially a Baeyer-Villiger monooxygenase, maybe responsible for the differences observed in the chemical structure of this novel pyocyanin derivative. In *Lysobacter antibioticus*, a Baeyer–Villiger-like flavin enzyme was identified as responsible of N-oxidation at both N5 and N10 of the phenazine core, converting 1,6-dihydroxyphenazine to 1,6-dihydroxyphenazine N5, N10-dioxide *(Jiang et al., 2018)*. This finding suggests that alternative enzymatic modifications in different strains are possible. The sequence putatively encoding an antibiotic biosynthesis monooxygenase (ABM) could be also involved in the biosynthetic of the phenazine derivative. In other systems, ABM proteins have been shown to influence pathway outcomes. In *Streptomyces formicae*, for instance, an ABM gene located in a polyketide biosynthetic cluster allowed the maintenance of biosynthetic pathway fidelity, ensuring the correct balance between shunt metabolites and the final product, whereas mutation of this gene disrupted this balance *(Z. Qin et al., 2019)*. In *Lysobacter antibioticus*, instead, an ABM gene located inside the phenazine operon was involved in a self-defence strategy performing myxin degradation *(J. Liu et al., 2021)*. These examples suggest that ABM like enzymes may participate to phenazine biosynthesis in a non-canonical way. However, transcriptomics analyses are required to verify these hypotheses and clarify which genes are truly involved in the synthesis of the phenazine derivative.

Several studies have investigated the antimicrobial activity of pyocyanin and its derivatives. The highest antibacterial effects are observed against Gram positive

organisms, with reported MIC values usually ranging from tens to just over a hundred μg/ml, whereas Gram negatives typically require higher concentrations, from hundred to several thousand of μg/ml *(Marey et al., 2024)*. The molecule exhibits a strong antibacterial activity against the methicillin-resistant *S. aureus* (MRSA) with a MIC value of 8 μg/ml, as well as biofilm eradicating and quorum sensing inhibitory activities *(Kamer et al., 2023a)*. However, many factors affecting the purity and the stability of the pigment may reduce the antimicrobial properties and the bioactivity of the molecule *(Abdelaziz et al., 2022)*.

In this research, the pyocyanin derivative exhibited antibacterial activity only against *S. aureus* and *Bacillus* sp. ef1, both Gram positive strains, whereas no effects were observed against the other tested pathogens. The selectivity may reflect a strain-specific mode of action, possibly reflecting the distinct molecular structure of this novel derivative. However, the limited activity could also result from reduced compound stability due to handling procedures. Prolonged manipulation, light exposure, suboptimal pH, or inappropriate temperature of storage may have compromised bioactivity *(Abdelaziz et al., 2022)*. The neutralization step, in particular, appeared to influence the behaviour of the molecule, likely reducing its efficacy. Additional assays should be performed to assess whether the tested concentrations were insufficient or whether pH and stability constraints affected the outcome of the analyses.

Conclusions

This study reports the synthesis of a novel pyocyanin derivative produced by *Rhodococcus* sp. ef1, an Antarctic bacterial strain recently isolated from a consortium associated with the Antarctic ciliate *E. focardii*. Culture conditions were optimized to achieve clear and rapid production of the compound. The

work provided chemical characterization and molecular identification of the pigment, as well as a preliminary assessment of its bioactivity. Furthermore, genome sequencing of *Rhodococcus* sp. ef1 offered insights into the organization of the putative operon involved in the biosynthesis of this compound. However, further studies are required to fully characterize the molecule and elucidate its biotechnological potential and the genes involved in its biosynthesis. Transcriptomic analyses, gene knockout and RNA silencing experiments are planned for future investigations.

References

Abdelaziz, A. A., Kamer, A. M. A., Al-Monofy, K. B., & Al-Madboly, L. A. (2022). A purified and lyophilized Pseudomonas aeruginosa derived pyocyanin induces promising apoptotic and necrotic activities against MCF-7 human breast adenocarcinoma. *Microbial Cell Factories*, *21*(1), 262. https://doi.org/10.1186/s12934-022-01988-x

Abdelaziz, A. A., Kamer, A. M. A., Al-Monofy, K. B., & Al-Madboly, L. A. (2023). Pseudomonas aeruginosa's greenish-blue pigment pyocyanin: its production and biological activities. *Microbial Cell Factories*, *22*(1), 110. https://doi.org/10.1186/s12934-023-02122-1

Agarwal, H., Bajpai, S., Mishra, A., Kohli, I., Varma, A., Fouillaud, M., Dufossé, L., & Joshi, N. C. (2023). Bacterial Pigments and Their Multifaceted Roles in Contemporary Biotechnology and Pharmacological Applications. *Microorganisms*, *11*(3), 614. https://doi.org/10.3390/microorganisms11030614

Anshi, Kapil, S., Goswami, L., & Sharma, V. (2024). Unveiling the Intricacies of Microbial Pigments as Sustainable Alternatives to Synthetic Colorants: Recent Trends and Advancements. *Micro*, *4*(4), 621–640. https://doi.org/10.3390/micro4040038

Biondini, M. C., Di Sessa, M., Vassallo, A., Chiappori, F., Zannotti, M., Mancini, A., Giovannetti, R., & Pucciarelli, S. (2025). Cellulose and Cellulose Synthase in a Marine Pseudomonas Strain from Antarctica: Characterization, Adaptive Implications, and Biotechnological Potential. *Marine Drugs*, *23*(10), 410. https://doi.org/10.3390/md23100410

Celedón, R. S., & Díaz, L. B. (2021). Natural Pigments of Bacterial Origin and Their Possible Biomedical Applications. *Microorganisms*, *9*(4), 739. https://doi.org/10.3390/microorganisms9040739

Chavan, A., Pawar, J., Kakde, U., Venkatachalam, M., Fouillaud, M., Dufossé, L., & Deshmukh, S. K. (2025). Pigments from Microorganisms: A Sustainable Alternative for Synthetic Food Coloring. *Fermentation*, *11*(7), 395. https://doi.org/10.3390/fermentation11070395

Chayka, N., Puntus, I., Zakharchenko, N., Rukavtsova, E., Anokhina, T., Pozdnyakova-Filatova, I., Akhmetov, L., Shutov, A., Delegan, Y., Bogun, A., Zvonarev, A., Kosheleva, I., & Filonov, A. (2025). Phytostimulating Properties of the Oil-Degrading Strain Rhodococcus qingshengii F2-2. *Environments*, *12*(12), 454. https://doi.org/10.3390/environments12120454

Cheluvappa, R. (2014). Standardized chemical synthesis of Pseudomonas aeruginosa pyocyanin. *MethodsX*, *1*, 67–73. https://doi.org/10.1016/j.mex.2014.07.001

Choi, S. Y., Lim, S., Yoon, K., Lee, J. I., & Mitchell, R. J. (2021). Biotechnological Activities and Applications of Bacterial Pigments Violacein and Prodigiosin. *Journal of Biological Engineering*, *15*(1), 10. https://doi.org/10.1186/s13036-021-00262-9

Eltarahony, M. M., Younis, S. S., Abdel Salam, S. A., & Arafa, F. M. (2025a). An insight into pyocyanin: production, characterization, and evaluation of its in vitro antibacterial, antifungal, antibiofilm and in vivo anti-schistosomal potency. *BMC Microbiology*, *25*(1), 532. https://doi.org/10.1186/s12866-025-04248-1

Gahlout, M., Chauhan, P. B., Prajapati, H., Tandel, N., Rana, S., Solanki, D., & Patel, N. (2021). Characterization, application and statistical optimization approach for

enhanced production of pyocyanin pigment by Pseudomonas aeruginosa DN9. *Systems Microbiology and Biomanufacturing*, *1*(4), 459–470. https://doi.org/10.1007/s43393-021-00033-z

Garcia-Lopez, E., Alcazar, P., & Cid, C. (2021). Identification of Biomolecules Involved in the Adaptation to the Environment of Cold-Loving Microorganisms and Metabolic Pathways for Their Production. *Biomolecules*, *11*(8), 1155. https://doi.org/10.3390/biom11081155

Higgins, S., Heeb, S., Rampioni, G., Fletcher, M. P., Williams, P., & Cámara, M. (2018). Differential Regulation of the Phenazine Biosynthetic Operons by Quorum Sensing in Pseudomonas aeruginosa PAO1-N. *Frontiers in Cellular and Infection Microbiology*, *8*. https://doi.org/10.3389/fcimb.2018.00252

Huang, W., Wan, Y., Zhang, S., Wang, C., Zhang, Z., Su, H., Xiong, P., & Hou, F. (2024). Recent Advances in Phenazine Natural Products: Chemical Structures and Biological Activities. *Molecules*, *29*(19), 4771. https://doi.org/10.3390/molecules29194771

Jiang, J., Guiza Beltran, D., Schacht, A., Wright, S., Zhang, L., & Du, L. (2018). Functional and Structural Analysis of Phenazine *O* -Methyltransferase LaPhzM from *Lysobacter antibioticus* OH13 and One-Pot Enzymatic Synthesis of the Antibiotic Myxin. *ACS Chemical Biology*, *13*(4), 1003–1012. https://doi.org/10.1021/acschembio.8b00062

John, M. S., Nagoth, J. A., Ramasamy, K. P., Mancini, A., Giuli, G., Miceli, C., & Pucciarelli, S. (2022). Synthesis of Bioactive Silver Nanoparticles Using New Bacterial Strains from an Antarctic Consortium. *Marine Drugs*, *20*(9), 558. https://doi.org/10.3390/md20090558

John, M. S., Nagoth, J. A., Zannotti, M., Giovannetti, R., Mancini, A., Ramasamy, K. P., Miceli, C., & Pucciarelli, S. (2021a). Biogenic Synthesis of Copper Nanoparticles Using Bacterial Strains Isolated from an Antarctic Consortium Associated to a Psychrophilic Marine Ciliate: Characterization and Potential Application as Antimicrobial Agents. *Marine Drugs*, *19*(5), 263. https://doi.org/10.3390/md19050263

John, M. S., Nagoth, J. A., Zannotti, M., Giovannetti, R., Mancini, A., Ramasamy, K. P., Miceli, C., & Pucciarelli, S. (2021b). Biogenic Synthesis of Copper Nanoparticles Using Bacterial Strains Isolated from an Antarctic Consortium Associated to a Psychrophilic Marine Ciliate: Characterization and Potential Application as Antimicrobial Agents. *Marine Drugs*, *19*(5), 263. https://doi.org/10.3390/md19050263

Kamer, A. M. A., Abdelaziz, A. A., Al-Monofy, K. B., & Al-Madboly, L. A. (2023). Antibacterial, antibiofilm, and anti-quorum sensing activities of pyocyanin against methicillin-resistant Staphylococcus aureus: in vitro and in vivo study. *BMC Microbiology*, *23*(1), 116. https://doi.org/10.1186/s12866-023-02861-6

Khan, S. R., Mavrodi, D. V., Jog, G. J., Suga, H., Thomashow, L. S., & Farrand, S. K. (2005). Activation of the *phz* Operon of *Pseudomonas fluorescens* 2-79 Requires the LuxR Homolog PhzR, *N* -(3-OH-Hexanoyl) - Homoserine Lactone Produced by the LuxI Homolog PhzI, and a *cis* -Acting *phz* Box. *Journal of Bacteriology*, *187*(18), 6517–6527. https://doi.org/10.1128/JB.187.18.6517-6527.2005

Khayat, M. T., Ibrahim, T. S., Khayyat, A. N., Alharbi, M., Shaldam, M. A., Mohammad, K. A., Khafagy, E.-S., El-damasy, D. A., Hegazy, W. A. H., & Abbas, H. A. (2022). Sodium Citrate Alleviates Virulence in Pseudomonas

aeruginosa. *Microorganisms*, *10*(5), 1046. https://doi.org/10.3390/microorganisms10051046

Koyun, M. T., Sirin, S., Erdem, S. A., & Aslim, B. (2022). Pyocyanin Isolated from Pseudomonas aeruginosa: Characterization, Biological Activity and Its Role in Cancer and Neurodegenerative Diseases. *Brazilian Archives of Biology and Technology*, *65*. https://doi.org/10.1590/1678-4324-2022210651

Li, L., Li, Z., Yao, W., Zhang, X., Wang, R., Li, P., Yang, K., Wang, T., & Liu, K. (2020a). Metabolic Engineering of *Pseudomonas chlororaphis* Qlu-1 for the Enhanced Production of Phenazine-1-carboxamide. *Journal of Agricultural and Food Chemistry*, *68*(50), 14832–14840. https://doi.org/10.1021/acs.jafc.0c05746

Liu, G. Y., & Nizet, V. (2009). Color me bad: microbial pigments as virulence factors. *Trends in Microbiology*, *17*(9), 406–413. https://doi.org/10.1016/j.tim.2009.06.006

Liu, J., Zhao, Y., Fu, Z. Q., & Liu, F. (2021). Monooxygenase LaPhzX is Involved in Self-Resistance Mechanisms during the Biosynthesis of *N* -Oxide Phenazine Myxin. *Journal of Agricultural and Food Chemistry*, *69*(45), 13524–13532. https://doi.org/10.1021/acs.jafc.1c05206

Marey, M. A., Abozahra, R., El-Nikhely, N. A., Kamal, M. F., Abdelhamid, S. M., & El-Kholy, M. A. (2024). Transforming microbial pigment into therapeutic revelation: extraction and characterization of pyocyanin from Pseudomonas aeruginosa and its therapeutic potential as an antibacterial and anticancer agent. *Microbial Cell Factories*, *23*(1), 174. https://doi.org/10.1186/s12934-024-02438-6

Mavrodi, D. V., Bonsall, R. F., Delaney, S. M., Soule, M. J., Phillips, G., & Thomashow, L. S. (2001). Functional Analysis of Genes for Biosynthesis of Pyocyanin and Phenazine-1-Carboxamide from *Pseudomonas aeruginosa* PAO1. *Journal of Bacteriology*, *183*(21), 6454–6465. https://doi.org/10.1128/JB.183.21.6454-6465.2001

Mavrodi, D. V., Peever, T. L., Mavrodi, O. V., Parejko, J. A., Raaijmakers, J. M., Lemanceau, P., Mazurier, S., Heide, L., Blankenfeldt, W., Weller, D. M., & Thomashow, L. S. (2010a). Diversity and Evolution of the Phenazine Biosynthesis Pathway. *Applied and Environmental Microbiology*, *76*(3), 866–879. https://doi.org/10.1128/AEM.02009-09

Mould, D. L., Finger, C. E., Conaway, A., Botelho, N., Stuut, S. E., & Hogan, D. A. (2024). Citrate cross-feeding by *Pseudomonas aeruginosa* supports *lasR* mutant fitness. *MBio*, *15*(2). https://doi.org/10.1128/mbio.01278-23

Mozzicafreddo, M., Pucciarelli, S., Swart, E. C., Piersanti, A., Emmerich, C., Migliorelli, G., Ballarini, P., & Miceli, C. (2021). The macronuclear genome of the Antarctic psychrophilic marine ciliate Euplotes focardii reveals new insights on molecular cold adaptation. *Scientific Reports*, *11*(1), 18782. https://doi.org/10.1038/s41598-021-98168-5

Mudaliar, S. B., & Bharath Prasad, A. S. (2024). A biomedical perspective of pyocyanin from Pseudomonas aeruginosa: its applications and challenges. *World Journal of Microbiology and Biotechnology*, *40*(3), 90. https://doi.org/10.1007/s11274-024-03889-0

Nagoth, J. A., John, M. S., Ramasamy, K. P., Mancini, A., Zannotti, M., Piras, S., Giovannetti, R., Rathnam, L., Miceli, C., Biondini, M. C., & Pucciarelli, S.

(2024). Synthesis of Bioactive Nickel Nanoparticles Using Bacterial Strains from an Antarctic Consortium. *Marine Drugs*, *22*(2), 89. https://doi.org/10.3390/md22020089

Nazari, M. T., Simon, V., Machado, B. S., Crestani, L., Marchezi, G., Concolato, G., Ferrari, V., Colla, L. M., & Piccin, J. S. (2022). Rhodococcus: A promising genus of actinomycetes for the bioremediation of organic and inorganic contaminants. *Journal of Environmental Management*, *323*, 116220. https://doi.org/10.1016/j.jenvman.2022.116220

Órdenes-Aenishanslins, N., Anziani-Ostuni, G., Vargas-Reyes, M., Alarcón, J., Tello, A., & Pérez-Donoso, J. M. (2016). Pigments from UV-resistant Antarctic bacteria as photosensitizers in Dye Sensitized Solar Cells. *Journal of Photochemistry and Photobiology B: Biology*, *162*, 707–714. https://doi.org/10.1016/j.jphotobiol.2016.08.004

Orlandi, V. T., Martegani, E., Giaroni, C., Baj, A., & Bolognese, F. (2022). Bacterial pigments: A colorful palette reservoir for biotechnological applications. *Biotechnology and Applied Biochemistry*, *69*(3), 981–1001. https://doi.org/10.1002/bab.2170

Ozdal, M. (2019). A new strategy for the efficient production of pyocyanin, a versatile pigment, in Pseudomonas aeruginosa OG1 via toluene addition. *3 Biotech*, *9*(10), 374. https://doi.org/10.1007/s13205-019-1907-1

Pierson, L. S., & Pierson, E. A. (2010). Metabolism and function of phenazines in bacteria: impacts on the behavior of bacteria in the environment and biotechnological processes. *Applied Microbiology and Biotechnology*, *86*(6), 1659–1670. https://doi.org/10.1007/s00253-010-2509-3

Pischedda, A., Ramasamy, K. P., Mangiagalli, M., Chiappori, F., Milanesi, L., Miceli, C., Pucciarelli, S., & Lotti, M. (2018). Antarctic marine ciliates under stress: superoxide dismutases from the psychrophilic Euplotes focardii are cold-active yet heat tolerant enzymes. *Scientific Reports*, *8*(1), 14721. https://doi.org/10.1038/s41598-018-33127-1

Price-Whelan, A., Dietrich, L. E. P., & Newman, D. K. (2007). Pyocyanin Alters Redox Homeostasis and Carbon Flux through Central Metabolic Pathways in *Pseudomonas aeruginosa* PA14. *Journal of Bacteriology*, *189*(17), 6372–6381. https://doi.org/10.1128/JB.00505-07

Pucciarelli, S., Devaraj, R. R., Mancini, A., Ballarini, P., Castelli, M., Schrallhammer, M., Petroni, G., & Miceli, C. (2015). Microbial Consortium Associated with the Antarctic Marine Ciliate Euplotes focardii: An Investigation from Genomic Sequences. *Microbial Ecology*, *70*(2), 484–497. https://doi.org/10.1007/s00248-015-0568-9

Pucciarelli, S., La Terza, A., Ballarini, P., Barchetta, S., Yu, T., Marziale, F., Passini, V., Methé, B., Detrich, H. W., & Miceli, C. (2009). Molecular cold-adaptation of protein function and gene regulation: The case for comparative genomic analyses in marine ciliated protozoa. *Marine Genomics*, *2*(1), 57–66. https://doi.org/10.1016/j.margen.2009.03.008

Qin, Z., Devine, R., Hutchings, M. I., & Wilkinson, B. (2019). A role for antibiotic biosynthesis monooxygenase domain proteins in fidelity control during aromatic polyketide biosynthesis. *Nature Communications*, *10*(1), 3611. https://doi.org/10.1038/s41467-019-11538-6

Rai, D., Sulthana, F., Neeksha, & Divyashree, M. (2024). Production and Antimicrobial Activities of Pyocyanin Extracts from Pseudomonas aeruginosa. *Journal of Pure and Applied Microbiology*, *18*(4), 2371–2379. https://doi.org/10.22207/JPAM.18.4.10

Rashid, M. I., & Andleeb, S. (2018). Pyocyanin yield improvement for enhancement of Pseudomonas aeruginosa inoculated Microbial Fuel Cell efficiency. *2018 International Conference on Power Generation Systems and Renewable Energy Technologies (PGSRET)*, 1–6. https://doi.org/10.1109/PGSRET.2018.8685940

Reis-Mansur, M. C. P. P., Cardoso-Rurr, J. S., Silva, J. V. M. A., de Souza, G. R., Cardoso, V. da S., Mansoldo, F. R. P., Pinheiro, Y., Schultz, J., Lopez Balottin, L. B., da Silva, A. J. R., Lage, C., dos Santos, E. P., Rosado, A. S., & Vermelho, A. B. (2019). Carotenoids from UV-resistant Antarctic Microbacterium sp. LEMMJ01. *Scientific Reports*, *9*(1), 9554. https://doi.org/10.1038/s41598-019-45840-6

Richts, B., Rosenberg, J., & Commichau, F. M. (2019). A Survey of Pyridoxal 5′-Phosphate-Dependent Proteins in the Gram-Positive Model Bacterium Bacillus subtilis. *Frontiers in Molecular Biosciences*, *6*. https://doi.org/10.3389/fmolb.2019.00032

Sandmann, G. (2019). Antioxidant Protection from UV- and Light-Stress Related to Carotenoid Structures. *Antioxidants*, *8*(7), 219. https://doi.org/10.3390/antiox8070219

Shouman, H., Said, H. S., Kenawy, H. I., & Hassan, R. (2023). Molecular and biological characterization of pyocyanin from clinical and environmental

Pseudomonas aeruginosa. *Microbial Cell Factories*, *22*(1), 166. https://doi.org/10.1186/s12934-023-02169-0

Venil, C. K., Dufossé, L., & Renuka Devi, P. (2020). Bacterial Pigments: Sustainable Compounds With Market Potential for Pharma and Food Industry. *Frontiers in Sustainable Food Systems*, *4*. https://doi.org/10.3389/fsufs.2020.00100

Visca, P., Imperi, F., & Lamont, I. L. (2007). Pyoverdine siderophores: from biogenesis to biosignificance. *Trends in Microbiology*, *15*(1), 22–30. https://doi.org/10.1016/j.tim.2006.11.004

Wan, Y., Liu, H., Xian, M., & Huang, W. (2021). Biosynthesis and metabolic engineering of 1-hydroxyphenazine in Pseudomonas chlororaphis H18. *Microbial Cell Factories*, *20*(1), 235. https://doi.org/10.1186/s12934-021-01731-y

Yang, G., De Santi, C., de Pascale, D., Pucciarelli, S., Pucciarelli, S., & Miceli, C. (2013). Characterization of the first eukaryotic cold-adapted patatin-like phospholipase from the psychrophilic Euplotes focardii: Identification of putative determinants of thermal-adaptation by comparison with the homologous protein from the mesophilic Euplotes crassus. *Biochimie*, *95*(9), 1795–1806. https://doi.org/10.1016/j.biochi.2013.06.008

Zannotti, M., Di Sessa, M., Biondini, M. C., Vassallo, A., Ferraro, S., Angeloni, S., Ricciutelli, M., Pucciarelli, S., & Giovannetti, R. (2026). Towards an easy production of novel pyoverdines by an antarctic Pseudomonas strain: a spectroscopic and HPLC-MS/MS characterization study. *Dyes and Pigments*, *244*, 113096. https://doi.org/10.1016/j.dyepig.2025.113096

CHAPTER 3

Antarctic microorganisms-derived compounds for human health protection

Abstract and project overview

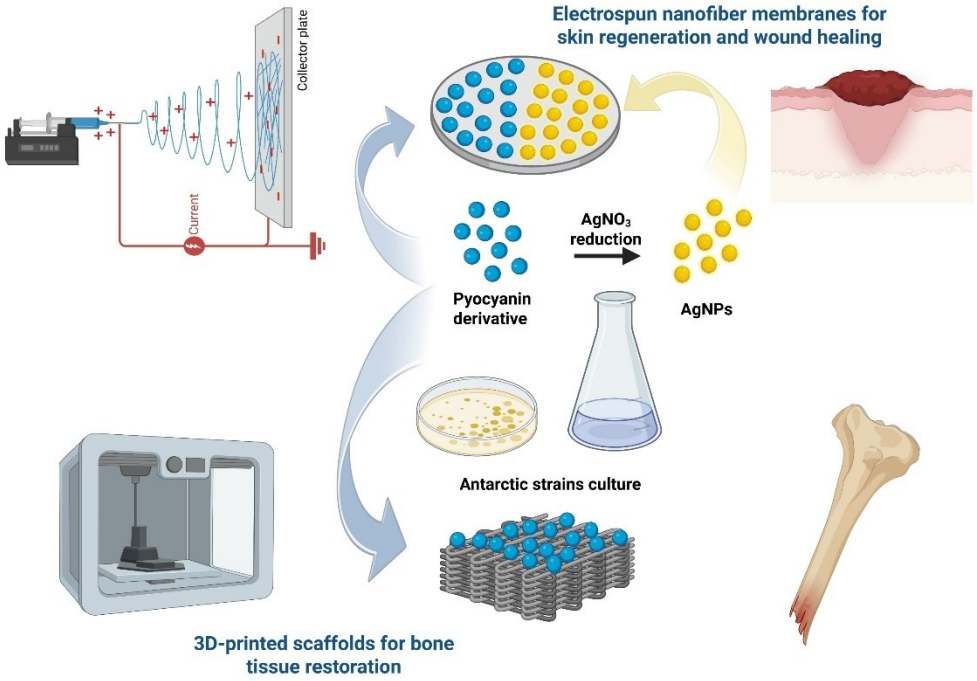

Figure 39 – Graphical Overview of the experimental section of this chapter. Created with BioRender.com. Publication license obtained.

This section of the experimental thesis is dedicated to the research activity carried out to explore the potential of Antarctic bacteria-derived metabolites for application in human health. Specifically, the new phenazine-derived molecule synthesized by the Antarctic microorganism *Rhodococcus* sp. ef1 was employed. Due to the very well-known antimicrobial and antioxidant properties of phenazines, this compound was incorporated into biomaterials aimed at promoting skin regeneration, wound healing, and bone regeneration. Moreover, a novel protocol for AgNPs synthesis was developed in collaboration with the

Chemistry Department. It involved the exploitation of the reducing ability of the microbial pigment, capable of promoting AgNPs formation starting from $AgNO_3$. Since AgNPs are well-established antimicrobial agents, they were also incorporated in biomaterials with the attempt to promote antibacterial effect. The research was mostly conducted abroad, at the University of Beira Interior (UBI) of Covilhã (Portugal), under the supervision of Professor Ilidio Correia. The experimental plan was articulated in several steps. Biomaterials production was performed in collaboration with David Pereira Lopes and Domenica Acosta, Master students at UBI, by using innovative technologies including electrospinning and 3D-printing. Various compositions were tested to optimize the physicochemical properties of the biomaterials and to develop new formulations. Optimization of production parameters and refinement of synthetic protocols and manipulation of Antarctic microorganisms-derived compounds were crucial steps to advance. Moreover, since the characterization of the pyocyanin derivative was still incomplete at that time, additional characterization analyses were performed to validate the preliminary results obtained in Italy. Subsequently, the bioactive compounds were incorporated within the regenerative biomaterials. Different incorporation strategies were tested, refining microbial-derived compounds concentration and distribution. After that, antimicrobial and biocompatibility properties were determined by preliminary assays. A major challenge was to achieve an effective antimicrobial activity while retaining biocompatibility with eukaryotic cells. Both the bioactive compounds and the regenerative biomaterials were obtained through innovative approaches, often starting from the ground up. Despite further experimental validation of the observed activities and refinement of the

optimization strategies are required, the results showed promising biomedical applications of the Antarctic bacteria-derived metabolites.

The following section reviews the essential characteristics of biomaterials and their applications in wound healing, skin regeneration and bone restoration. It examines strategies for biomaterial production and incorporation of both conventional and innovative antimicrobial agents, highlighting the advantages of microbial-derived metabolites, with a particular focus on the potential of Antarctic bacteria. Finally, future trends, perspectives, and limitations are discussed, emphasizing how my research relates to the current literature and offers significative insights that may support future advances.

State of the art

Biomaterials and tissue engineering: an overview

According to the National Institutes of Health (NIH), biomaterials are defined as "any natural or synthetic substance or combination of substances, other than drugs, which can be used to augment or partially or totally replace any tissue, organ or function of the body, in order to maintain or improve the quality of life of individual". Tissue engineering is an emerging biomedical field aimed at repairing and restoring damaged tissues by incorporating living cells into bioactive scaffolds. For this purpose, biomaterials must meet essential requirements: they should be biocompatible and stable, and they should possess controllable degradation and resorption rates, together with adequate mechanical properties and versatility in terms of shapes and size. In addition, they must be non-toxic and non-hazardous, non-inflammatory, non-carcinogenic, non-mutagenic, non-allergic, non-pyrogenic while mimicking the structure of the extracellular matrix (ECM) *(Shafiee & Atala, 2017)*. However, important challenges remain, including identifying appropriate cell sources, achieving adequate vascularization, designing scaffolds that effectively represent the ECM, reducing production time and costs *(Shafiee & Atala, 2017; Žiaran et al., 2025)*. Tissue engineering includes a broad range of applications. Among them, the regeneration and restoration of skin and bone tissues are of particular interest and constitute a pivotal area of focus in current and future development.

Bone regeneration and the emerging role of 3-D printed scaffolds

The high incidence of bone and joint-related diseases, including osteoporosis, arthritis, obesity, diabetes, and cancer, can significantly affect the integrity and function of skeletal tissues *(H. D. Kim et al., 2017)*.

Each year, more than four million operations worldwide involve the use of bone grafts or bone substitutes, rendering bone the second most transplanted tissue after blood. Despite their widespread application, these current treatments present critical limitations. Autografts are frequently associated with donor site morbidity, painful surgery and infection, whereas allografts carry risks of disease transmission, immune rejection and poor regenerative capacity *(Turnbull et al., 2018)*. Metallic-based implants have been explored as an alternative, but they often necessitate a secondary removal surgery following bone healing, increasing patient discomfort and morbidity. To address this drawback, biodegradable metals have been developed. Nonetheless, significant challenges persist, including the mismatch between metal degradation kinetics and bone regeneration rate, as well as premature loss of mechanical integrity due to rapid degradation *(De Pace et al., 2025)*.

Bone healing is a complex process that can be classified into primary (direct) and secondary (indirect) healing. Primary bone healing occurs when the fracture site is rigidly stabilized and the bone ends are closely approximated, allowing osteon-mediated bridging, similar to normal bone remodelling. This process involves minimal or no inflammatory response and may take months to years to complete *(Maruyama et al., 2020)*. Secondary bone healing is the most common form of fracture repair. It is structured into 3 partially overlapping phases: inflammatory, repair, and remodelling phase. The inflammatory phase begins

immediately after injury and is characterized by blood vessel disruption and hematoma formation at the fracture site. Immune cells and released cytokines play a pivotal role in promoting healing by recruiting other inflammatory cells, endothelial cells, fibroblasts and multipotent mesenchymal stem cells. Excessive or prolonged inflammation can impair healing, and anti-inflammatory cytokines help transition to the next phase. Bone repair involves vascular remodelling through angiogenesis and neovascularization, as well as recruitment of mesenchymal stem cells and osteoprogenitor cells. These cells differentiate into chondrocytes and osteoblasts contributing to the formation of a cartilaginous callus that is subsequently replaced by woven bone. During the remodelling phase, the bone's original structure and mechanical properties are restored and maintained through a balance between osteoblastic bone formation and osteoclastic resorption *(Bahney et al., 2019; Maruyama et al., 2020; G. Zhu et al., 2021)*.

In this context, bone tissue engineering emerged to support bone regeneration process at the defect sites, addressing the limitations of conventional approaches. Three-dimensional (3D) printing, also called rapid prototyping technology, is an innovative manufacturing technique that allows the fabrication of objects using computer-aided design through the sequential deposition of material layers. Originally introduced by Charles Hull in the 1980s, this technology has undergone continuous development finding numerous applications in biomedical research. In the context of bone tissue engineering, 3D printing offers several advantages such as high fabrication speed, precision, and possibility of patient-specific customization. These features enable the design and production of scaffolds tailored to the geometric and dimensional requirement of individual bone defects *(M. Wang et al., 2025)*.

Scaffolds are three-dimensional structures that mimic the extracellular matrix, designed to facilitate cell adhesion, proliferation and differentiation into osteoblasts, while promoting vascularization *(Bharadwaz & Jayasuriya, 2020)*. To serve these purposes, bone scaffolds must have adequate rigidity to support mechanical pressure, exhibit biocompatibility to prevent host tissue inflammation, and mimic the natural bone tissue microenvironment. In this regard, calcium phosphate-based materials have attracted considerable interest as they represent the main inorganic component of bone *(H. D. Kim et al., 2017)*. Among them, hydroxyapatite (HA), β-tricalcium phosphate (β-TCP), and their mixtures, known as biphasic calcium phosphates (BCP), are the most widely studied. HA implants, however, present several limitations, including poor bone stimulation and high chemical stability and crystallinity which make them non-resorbable in vivo, leading to risks of bone deformities and fractures. β-TCP, instead, is resorbable by osteoclasts. This property, combined with its strong osteoinductive ability and its high potential for functionalization with bactericidal and luminescent molecules, makes β-TCP one of the most promising bone graft substitute materials *(Bohner et al., 2020)*. Sodium alginate (SA), a natural polymer derived from the cell wall of various species of brown algae, has been recently investigated as organic component of regenerative bone scaffolds. Despite it exhibits poor mechanical strength and excessive swelling, SA is an attractive material due to its low cost, biodegradability, biocompatibility and low immunogenicity. Moreover, its ability to undergo ionotropic crosslinking in the presence of bivalent cations, such as calcium, enables stabilization of scaffold structures *(Arslan et al., 2023; Francisco et al., 2026)*.

Skin engineering: advances in electrospun nanofibers

Skin is the largest organ of the human body. It is essential to protect water-rich internal organs from the dry external environment, so maintenance of skin integrity and wound healing capacity is pivotal for surviving *(Almadani et al., 2021)*. Human skin wounds represent nowadays a major threat for public health *(S. Chen et al., 2017)*. Only in USA, chronic wounds affect 6.5 million patients, with increasing associated healthcare costs *(Sen et al., 2009)*. Wound healing is a dynamic, tightly regulated process consisting of three main stages. The inflammatory phase involves haemostasis and acute inflammation, during which cytokines and growth factors are released attracting leukocytes to the injured area. The proliferative phase is characterized by the migration and proliferation of keratinocytes, fibroblasts, endothelial cells, and leukocytes, with improved angiogenesis and re-epithelialization. In the remodelling phase, instead, the provisional extracellular matrix is reorganized by replacing collagen III with collagen I, conferring resistance and flexibility to the regenerated skin *(Gushiken et al., 2021)*.

Thus, considered the complexity of wound healing process and the related socio-economic implications, the development of new technologies is of crucial importance.

Several strategies have been tested over the past decade. Traditional dressings aimed at prevention and simple protective action have been progressively substituted by advanced dressings, that actively participate to the wound healing process *(Tottoli et al., 2020)*. Regenerative medicine offers many alternatives to promote wound healing. Among the emerging technologies, electrospun scaffolds represent promising skin substitutes, capable of resembling ECM. A

conventional electrospinning setup typically consists of a high-voltage power supply, a syringe pump, a spinneret and a collector. A potential difference is applied between the spinneret, usually positively charged, and the collector, oppositely charged *(Keirouz et al., 2020)*. In this technique, an electrically charged polymer solution is extruded through a nozzle under the influence of an electric field. Once a critical voltage is reached between the nozzle and the metallic collector, the liquid droplet at the nozzle becomes charged and opportunely stretched in a continuous jet. During its trajectory toward the collector, the jet solidifies through solvent evaporation, resulting in a deposited mat with a web-like fibrous structure. Electrospun scaffolds resemble native ECM design, and exhibit variable pore size, high surface area and oxygen permeability, making them suitable skin replacement materials *(Joseph et al., 2019; Tottoli et al., 2020)*. Moreover, the remarkable versatility of electrospinning, which allows control over surface conformation and functional modification, has enabled the use of electrospun nanofibers as drug delivery platforms and biosensors, as well as the development of tailored functionalities such as antimicrobial properties and enhanced cell adhesion *(Cleeton et al., 2019; C. Wang et al., 2024)*.

However, several challenges are associated with the use of this technique. The properties of the electrospinning solution, including viscosity, conductivity, polymers structures and concentrations, together with the processing parameters such as applied voltage, tip-to-collector distance, flow rate, temperature and relative humidity, critically influence the quality of the resulting fibres. As most of the parameters are interdependent, their optimization is highly complex. Therefore, proper control of the working variables is essential to achieve fibres with the desired morphological and biological properties *(Joseph et al., 2019)*.

Moreover, despite its scalability and cost-effectiveness, electrospinning based on conventional needle-syringes is limited by low production rates *(Keirouz et al., 2020)*.

A wide range of polymers has been employed in the electrospinning process. Among them, chitosan is particularly appreciated as it is a natural abundant material with intrinsic antibacterial and antifungal properties. However, its poor solubility – typically requiring acidic solvents – limits its use, since these solvents can be associated with toxicity and high costs. This challenge can be partially addressed considering that most of the solvent evaporates under safe conditions during electrospinning process and by combining chitosan with other polymers *(Mulholland, 2020)*.

Toward sustainable biomaterials: the potential of cellulose

Several natural biopolymers, including chitosan, collagen, silk fibroin, cellulose, alginate, and fucoidan, are currently employed in tissue engineering, alongside a wide range of synthetic materials, including polycaprolactone, polylactic acid, polyethylene glycol, and polyurethane *(Bharadwaz & Jayasuriya, 2020)*. Many authors agree that natural polymers present significant advantages over synthetic ones, enabling the design and fabrication of more complex structures that effectively represent living tissues and organs *(M. U. A. Khan et al., 2023)*. In recent years, increasing attention has also been directed toward the sustainability and biodegradability of biomaterials. This has driven interest in natural biopolymers biosynthesised by plants, fungi, arthropods, and microorganisms. In this context, cellulose and nanocellulose, on one hand, and chitin and chitosan, on the other, are emerging as key candidates. They represent the two most

abundant classes of natural biopolymers, with cellulose ranking first and chitin second in terms of availability *(Biswal et al., 2020)*.

Cellulose is an unbranched homopolysaccharide, made of long chains of β-d-glucopyranose joined by β (1→4) glycosidic bonds *(Etale et al., 2023)*. Cellulose-based nanoscaffolds are establishing themselves as valuable biomaterials across many biotechnological applications, including tissue engineering *(Alven & Aderibigbe, 2020)*. Their structure can mimic, indeed, the natural extracellular matrix in terms of morphology, fiber, pore diameter, and stiffness *(Ahn et al., 2018)*, thus enhancing cell proliferation and migration in vitro and promoting tissue regeneration in vivo *(Y. Wang et al., 2018)*.

Biomedical applications currently rely on the high purity, hydrophilic nature and biocompatibility of cellulose. Moreover, cellulose can be combined with other polymers of synthetic or natural origin to obtain hybrid biomaterials with superior properties. For example, cellulose can be integrated with other water-soluble polysaccharides, such as chitosan, chitin, pectin, alginate, agarose, etc. to increase the adsorbing capacity *(Rana et al., 2024)*. One study investigated a biomaterial constituted by human recombinant collagen and oxidized cellulose, demonstrating high wound healing efficacy due to its ability to bind and retain several growth factors at the wound site *(Alven & Aderibigbe, 2020)*.

Several studies have explored the potential of cellulose-based electrospun nanofibers, which can protect the wound and incorporate and release drugs or natural extracts that stimulate tissue reparation, such as nanoparticles, plant extracts, and essential oils. To overcome their limited solubility and poor mechanical properties, more importance has been given to the cellulose derivatives. Among them, cellulose acetate and nanocellulose are emerging as

promising candidates for wound healing applications *(Teixeira et al., 2020)*. In particular, bacterial cellulose (BC) is arousing great interest since it can be obtained through eco-friendly biosynthetic processes that exploit natural microbial metabolism. Interestingly, BC shows higher purity, water holding capacity, and tensile strength resistance compared to the plant-based one *(Gorgieva & Trček, 2019b; Skočaj, 2019)*. In addition, BC fibrils are about 100 times smaller than those of the vegetal counterpart *(I. G. R. da Silva et al., 2022)*. Thus, BC appears more able to mimic the extracellular matrix structure. It also exhibits good biocompatibility *(Sulaeva et al., 2015)*. Furthermore, by controlling parameters such as molecular weight, crystallinity, hydrophilicity, and eventually additional modifying agents, it is possible to vary the levels of BC biodegradability or biostability, to meet the requirements of different biomedical applications (Torgbo & Sukyai, 2020).

Biomaterials functionalization to enhance antimicrobial properties

Antimicrobial resistance and hospital-acquired infections represent major challenges in the context of biomaterials application. Since bacterial infection is a common complication in damaged tissues, its prevention and mitigation are of crucial importance *(Kalijaga et al., 2024)*. In wound healing, for example, Gram positive bacteria such as *S. aureus* dominate the early stages of chronic wound formation, followed by the invasion of Gram-negative species such as *E. coli* and *P. aeruginosa* which can be responsible for significant damages in deeper skin layers *(Liang et al., 2022)*.

In this regard, the use of traditional antibiotics is increasingly being replaced by novel antimicrobial compounds that are not associated with resistance

development. Among the most investigated emerging antimicrobial compounds, there are metal-based nanoparticles, antimicrobial peptides and bioactive natural compounds, such as plant extracts, curcumin, cinnamon, and ginger *(Takallu et al., 2024)*. These agents can target specific microbial pathways or act through multimodal mechanisms, reducing the likelihood of resistance development. Some limitations, however, remain, including the need to further elucidate their bactericidal mechanisms of action, the lack of sufficient in vivo studies, and concerns about potential long-term side effects and toxicity *(Rojo et al., 2022)*. Moreover, incorporating antimicrobial compounds into biomaterials can be challenging.

Currently, two main strategies are used to produce antimicrobial electrospun nanofibers.

The first, known as blend electrospinning, involves the incorporation of the antimicrobial agents directly into the polymer solution. The main limitation lies in the changes induced in the viscosity and conductivity of the solution during the electrospinning, which can affect the morphology and uniformity of the resultant biomaterial *(Hamdan et al., 2021)*. Since the integrity of the fibers is closely related to cell adhesion, migration and proliferation, these alterations may negatively impact their biological performance *(S. Agarwal et al., 2013)*. Nonetheless, the antimicrobial agents distribute homogeneously through the nanofibers. Variants of this strategy include the approach of emulsion electrospinning, in which the solvent is composed of two immiscible phases, polymers and antimicrobial agents, promoting core-shell encapsulation, and coaxial electrospinning, where two nozzles separately deliver the polymer solution and the antimicrobial agent *(de Faria et al., 2015; Hamdan et al., 2021)*. The properties of the fibers can be modulated by varying the concentration of

the antimicrobial compounds. Moreover, two miscible solvents may be combined, one to dissolve the polymer and the other to dissolve the nanoparticles, to help the dispersion and solubilization of the antimicrobial agent in the electrospinning solution (Maliszewska & Czapka, 2022).

The second strategy consists of the post-functionalization of the electrospun nanofibers with antimicrobial agents. This approach allows a more controlled and localized release and preserves the structural integrity of the fibers without directly affecting the electrospinning process *(Dong et al., 2008)***.** However, potential limitations include premature detachment of the antimicrobial coatings or accelerated release, which may compromise the antimicrobial efficacy and require additional optimization of surface attachment methods *(Chug & Brisbois, 2022)*.

Regarding 3D-printed scaffolds, the final constructs can be classified as well into two main categories: models incorporating antimicrobial agents directly within the material matrix, and models functionalized through antimicrobial coatings or post-printing loading. In this latter approach, after fabrication of the scaffolds through 3D-printing, the bioactive substances are introduced as surface coatings or by loading them into the micropores of the construct. The main challenges associated with this strategy are related to structural integrity and subsequent in vivo biocompatibility and bioactivity, since the performance of the scaffold and the biological activity of the antimicrobial agents should not affect each other *(Periferakis et al., 2024).*

Thus, further research is needed to address the limitations of the current strategies. In this context, efforts should be directed toward the identification of novel antimicrobial molecules capable of providing effective alternatives to

conventional antibiotics associated with the emergence of resistance. Ideally, these compounds should be readily incorporated into biomaterials, remain stable over time and be obtained through sustainable and reproducible protocols. In the following paragraph, an overview of metallic nanoparticles and natural compounds will be provided, with specific focus on silver nanoparticles and bacterial pigments.

Metallic nanoparticles

Metallic nanoparticles are characterized by large surface areas, lower toxicity, promising biocompatibility and long-lasting action *(Song et al., 2017)*. Having a range of dimensions between 1 and 100 nm, they can be easily taken up by the cells, being powerful tools in cancer treatment, biological imaging, and drug delivery *(Khursheed et al., 2022; W. Qin et al., 2022)*. They are very well-known antimicrobial agents, able to kill or at least inhibit a broad range of microbial species. This promotes tissue healing process and offers a valid alternative to the use of conventional antibiotics *(Luo et al., 2024)*. Their mechanism of action is based on different effects. First, positively charged nanoparticles can easily interact with the negatively charged membranes of both Gram-positive and Gram-negative strains. This causes cell wall disruption and increases the cell permeability, allowing metal ions that are released from the nanoparticles entering the cells and promoting the formation of reactive oxygen species (ROS). Therefore, biological processes are impaired and macromolecules and cellular structures are damaged *(Girma, 2023; Z. Li et al., 2019)*.

Different methods have been developed to synthesize metal-based nanoparticles. Chemical and physical approaches are well-established methods but present

limitations in terms of environmental impacts and of time and energy expenditure *(Jamkhande et al., 2019)*. Consequently, biological synthesis has recently gained more interest as a green nature-based solution, as it relies on the exploitation of natural metabolic processes of microorganisms, fungi, algae, and plants *(Karunakaran et al., 2023)*. Although further production optimization is required, biosynthetic metal nanoparticles exhibit superior stability, biocompatibility, and antimicrobial efficacy in comparison to nanoparticles synthesised with other methods *(John, Nagoth, Ramasamy, Mancini, et al., 2020; P. Singh et al., 2016)*. They are usually capped with non-toxic biomolecules which enhance their biocompatibility while preventing aggregation. However, complex purification steps are required after synthesis *(Campaña et al., 2023)*. Bacteria-mediated synthesis is an effective approach in terms of costs, time and biological activity *(John, Nagoth, Ramasamy, Mancini, et al., 2020)*, but residual salts from the culture medium may remain, making purification a crucial step *(Campaña et al., 2023)*. The development of new protocols based on bacterial metabolites, without involving the biomass, can address this limitation *(Campaña et al., 2023)*.

Among metallic nanoparticles, AuNPs, CuNPs, and AgNPs are the most used species due to their antimicrobial and anti-inflammatory activities, which can significantly enhance tissue regeneration *(Palani et al., 2024)*. These nanoparticles will be discussed in more detail in the following sections.

Gold nanoparticles (AuNPs)

Gold nanoparticles (AuNPs) are very promising biomedical tools as they have a broad spectrum of applications in drug delivery, cancer treatment, and diagnostic

imaging by virtue of their anticancer, anticoagulant, anti-inflammatory, and antibacterial activities *(Khursheed et al., 2022; K. R. Singh et al., 2021; Z. Wang et al., 2018)*. They have been recently employed successfully in tissue engineering and regeneration *(Peña et al., 2019)*. AuNPs, indeed, could promote fibroblasts adhesion, proliferation and migration and they allow collagen fibers regeneration *(J. Li et al., 2021; Xu et al., 2019; X. Zheng et al., 2020)*. It is believed that AuNPs anti-inflammatory activity occurs by increasing anti-inflammatory cytokine concentration, modulating the activity of transcription factors such as NF-kb, and lowering the expression of pro-inflammatory molecules such as ICAM-1 and TNFα *(Di Bella et al., 2021)*. The antimicrobial effect is mainly due to cell wall disruption, ROS generation, ATP levels reduction, and metabolism impair as for the other metallic nanoparticles *(Zhan et al., 2022)*. A study demonstrated that the efficacy of antimicrobial activity can be improved by lowering the size of AuNPs. Ultrasmall AuNCs (gold nanoclusters) with less than 2 nm-diameter showed great antimicrobial activity against a broad spectrum of microorganisms, killing more than 90% of bacterial population in a concentration of 0.1 mM *(K. Zheng et al., 2017)*. surface functionalized AuNPs also exhibit potent antimicrobial activity being effective against *E. coli*, *E. cloaca complex*, *P. aeruginosa* and *S. aureus* with MIC of 8-64 nM *(X. Li et al., 2014)*. AuNPs have been recently applied in wound dressings, with promising antibacterial and antifungal activities *(Dong et al., 2024; Hashem et al., 2022)*. Further studies are required in terms of toxicity of AuNPs, which likely depends on AuNPs size, shape, surface charge, coating, and dose. More investigations are needed for long term exposure and in vivo studies to cover the lack of information and to shed light on the contradictory results reported in many cases. If some studies propose a safe profile for AuNPs,

others highlight significant cellular responses, such as oxidative stress, inflammation, (Kadhim et al., 2021; Peng et al., 2024; Poomrattanangoon & Pissuwan, 2024)*t al., 2024; Poomrattanangoon & Pissuwan, 2024)*.

Copper nanoparticles (CuNPs)

Copper nanoparticles are garnering more attention in the field of tissue engineering as they possess antimicrobial, pro-angiogenic, and cell stimulating properties while improving the mechanical properties of biomaterials *(Krishna et al., 2024)*. Nanocomposites functionalized with CuNPs exhibit high tensile strength while favouring keratinocytes and fibroblasts proliferation, epithelialization, collagen synthesis, interleukin-2 production, short-time wound closure *(Eslaminezhad et al., 2024; Ghasemian Lemraski et al., 2021)*. Healing process and angiogenesis are promoted by CuNPs-mediated induction of hypoxia-induced factor-1-alpha *(Salvo & Sandoval, 2022)*. The antimicrobial activity relies on the mechanisms previously discussed for the metallic nanoparticles *(Girma, 2023)*. CuNPs are size, shape, and concentration-dependent antibacterial agents, with smaller CuNPs being more effective. For instance, 2 nm CuNPs disrupt and penetrate the bacterial membrane more efficiently than 30 nm CuNPs *(Ermini & Voliani, 2021)*. CuNPs incorporation in the electrospinning solvent enables uniform dispersion of nanoparticles within the nanofibers, conferring antibacterial activity against *B. cereus*, *S. aureus*, *E. coli*, and *P. aeruginosa*, with Gram positive bacteria being more sensitive. This trend is also observed with other metallic nanoparticles, and it is likely attributable to structural differences in bacterial cell wall *(Ghasemian Lemraski et al., 2021)*.

The potential toxic effect of CuNPs represents a major limitation in the use of these antimicrobial agents. Copper, indeed, can exert harmful effects on the liver and kidneys, and it has been associated with genotoxic, cytotoxic, and oxidative effects, as well as disruption of cell membrane integrity *(Ghasemian Lemraski et al., 2021)*. However, copper-based nanoparticles seem to have reduced toxicity compared to conventional copper-based materials, even though further studies are required to clarify this aspect *(J.-C. Kim et al., 2016; Letelier et al., 2010)*. Moreover, cytotoxicity is apparently influenced by CuNPs concentration and size, with 200 µg/ml CuNPs still able to improve cell proliferation *(Zhou et al., 2020)*. In addition, the toxic effect could be mitigated by combining CuNPs with other polymers, such as chitosan *(Worthington et al., 2013)*.

Silver nanoparticles (AgNPs)

Among the metallic nanoparticles, silver nanoparticles (AgNPs) are the most extensively studied since they possess unique physico-chemical properties and they are considered one of the most effective antimicrobial agents *(Tang & Zheng, 2018)*. The reduction of silver salts by reducing agents is the most common synthetic method *(W. Li et al., 2019)*. Green synthesis of AgNPs is now emerging as a cost-effective and environmentally friendly method that prevents the use of toxic solvents and produces nanoparticles with strong antibacterial activity *(John et al., 2022a)*.

AgNPs have been extensively incorporated into wound dressings, 3D-printed device and therapeutic formulations due to their potent antimicrobial properties, which contribute to the prevention of infections and the enhancement of wound healing *(C.-Y. Chen et al., 2020; Periferakis et al., 2024)*. For example, injured

animal models treated with AgNPs showed healed wound resembling normal skin, with a thin epidermis and hair follicles. The study also highlighted the anti-inflammatory activity of silver through the modulation of the cytokines involved in wound healing: IL-6 expression was decreased, whereas IL-10 and VEGF were significantly upregulated in the AgNPs treated group compared with the control group *(Tian et al., 2007)*.

Notably, AgNPs with smaller particle size exhibit superior antibacterial efficacy, attributed to their increased surface area to volume ratio, which facilitates stronger interactions with bacterial cell surfaces and more efficient membrane penetration *(Tang & Zheng, 2018)*. Accordingly, the synthesis of ultrasmall AgNPs is considered advantageous for maximizing bacterial eradication and for optimizing wound healing process *(Haidari et al., 2020, 2021)*. Moreover, AgNPs exhibit significant antibiofilm activity by inhibiting bacterial adhesion, suppressing extracellular polymeric substance (EPS) production, disrupting biofilm architecture, and downregulating biofilm and virulence-associated genes. They are able to penetrate biofilms via aqueous channels and release Ag^+ ions, affecting biofilm maturation and persistence especially in Gram-negative pathogens *(Mikhailova, 2024).*

AgNPs also proved themselves capable of inducing cell proliferation, fibroblasts differentiation into myofibroblasts, and of promoting angiogenesis by mediating the release of signalling molecules such as transforming growth factor beta (TGF-β) and vascular endothelial growth factor (VEGF) *(Munhoz et al., 2023)*.

For all these reasons, AgNPs are raising interest as antimicrobial agents to be incorporated in electrospun membranes for skin regeneration *(L. Zhu et al., 2022)*.

As for the other mentioned metallic nanoparticles, AgNPs toxicity remains a matter of ongoing debate *(Rajan et al., 2022)*. It is believed that silver ions are released by AgNPs surface, interacting with thiol groups of enzymes, which are subsequently inactivated. Moreover, they can enter the cell and be internalized, liberating silver ions inside the cells *(Abramenko et al., 2018)*.
Recent literature reports that AgNPs at concentrations ranging between 25–250 μg/mL effectively inhibit bacterial growth without inducing cytotoxicity *(Iurilli et al., 2025).* Moreover, it is generally accepted that biosynthetic AgNPs are considered safer since they are naturally capped molecules, being more stable and exhibiting less cytotoxicity *(Jassim et al., 2022)*. However, despite the significant advantages of biological green technology, concerns about potential toxicity remain *(Das & Paul, 2025)*. A study conducted on Wistar rats exposed to 0.5-10 mg/Kg for 14 days AgNPs reported minimal oxidative stress in the cortex and hippocampus, suggesting that green approaches reduce oxidative toxicity, but it does not fully prevent dose-dependent neurotoxicity *(Tareq et al., 2022)*. High doses (≥100 ppm) of AgNPs were also associated to anxiety, memory deficits, and oxidative stress in murine models *(Tarbali et al., 2022)*.

Nonetheless, biologically synthesized AgNPs may mitigate ecological toxicity. Although silver is one of the most hazardous pollutants, second only to mercury in aquatic systems, green-synthesised AgNPs show lower environmental impact due to their greater stability, reduced Ag+ release, and lower bioavailability. An estimated 63 tons of nanosilver are released annually into marine environments,

where they negatively impact aquatic organisms and accumulate intracellularly, entering the food chains and raising potential risks for human health *(Das & Paul, 2025; Domingo et al., 2019)*. In the terrestrial ecosystems, AgNPs contamination can also impair beneficial soil microbes and disrupt plant-microbe mutualistic interactions *(D. Huang et al., 2022)*. However, green production methods based on water or bio-derived solvents further minimize the environmental impact. In addition, AgNPs have potential in bioremediation, since they can effectively adsorb and eliminate toxic metal ions, including cobalt and lead, from contaminated water *(Das & Paul, 2025)*.

The role of bacterial pigments as natural antimicrobial agents

Among the emerging antimicrobial compounds, bacterial pigments have garnered considerable attention for their potential in wound healing and as bioactive agents in electrospun nanofibers *(Ramos et al., 2022)*. Notably, pigments such as violacein, prodigiosin, and melanin have been integrated into nanofibrous scaffolds to exploit their antimicrobial and antioxidant properties *(Devi et al., 2024)*. Compared to synthetic molecules, these natural bioactive compounds offer several advantages, including biodegradability, low toxicity, and non-*carcinogenicity (X. Huang et al., 2024; Numan et al., 2018)*. Moreover, they align with the growing demand for natural products derived from renewable and inexhaustible sources, whose synthetic processes do not generate toxic wastes *(Duarte et al., 2019)*. Recent research is focusing on enabling cost-effective production by exploring novel bacterial sources, utilizing low-cost substrates, and optimizing cultivation conditions *(Lopes & Ligabue-Braun, 2021)*.

Here, some examples of bacterial pigments employed as antimicrobial agents in biomaterials are presented.

Violacein is a violet pigment produced by several Gram-negative bacteria *(Park et al., 2021)*. This secondary metabolite exhibits a broad-spectrum of biological activities, including antibacterial, antiviral, antifungal, antitumoral and antioxidant activities *(Durán et al., 2021)*. Compared to synthetic antibiotic agents, studies indicate that it presents lower toxicity and better biocompatibility *(Choi et al., 2015)*. Moreover, the pigment has been reported to positively modulate the composition of the mammalian gut microbiota, even if further investigations are required *(Pauer et al., 2018)*. The mechanisms underlying its antimicrobial activity have not been fully elucidated yet. It is suggested that the molecule disrupts the integrity of the cell wall, leading to the efflux of ions, ATP, and proteins, thereby disturbing intracellular osmotic balance, inhibiting cell growth, and, ultimately, resulting in cell death *(Durán et al., 2021; J. Lee et al., 2022)*.

Electrospun nanofibrous membranes embedded with violacein possess enhanced antimicrobial efficacy and offer ultraviolet (UV) protection, paving the way towards applications in protective clothing and wound dressings *(J. Lee et al., 2022)*. Due to its low water solubility, violacein can be more uniformly dispersed in nanofibers when incorporated into hydrophobic polymer solutions(Ahmad et al., 2012). Moreover, violacein incorporation increases material porosity and improves protein adsorption, providing more cell attachment sites and improving cellular adhesion *(Chelminiak-Dudkiewicz et al., 2024)*.

Prodigiosin is a secondary metabolite mainly produced by *S. marcescens*, *Actinomycetes* and *Streptomyces (Williamson et al., 2006)*. This red alkaloid

pigment exhibits anti-cancer, anti-malarial, antifungal and antibacterial activity against Gram positives and Gram negatives, being a promising candidate for biomedical applications*(Díaz-Ruiz et al., 2001; Islan et al., 2022; John Jimtha et al., 2017; Lazaro et al., 2002)*. When incorporated into hydrogel dressings for tissue repair and regeneration, prodigiosin demonstrated potent antimicrobial activity against Multidrug resistant *Staphylococcus aureus* (MRSA) exhibiting a minimum inhibitory concentration (MIC) of 2 μg/mL, surpassing the efficacy of several well-known antibiotics *(X. Wang et al., 2024)*. This effective antibacterial activity is attributed to the pigment's ability to penetrate the outer membrane and disrupt the plasma membrane through a chaotropic-mediated mechanism *(Suryawanshi et al., 2017)*. In addition, prodigiosin could reduce wound inflammation and improved healing in mice models by inducing collagen synthesis, fibroblast growth, and angiogenesis. *(X. Wang et al., 2024)*. Prodigiosin was successfully used to functionalize composite materials based on oxidized-bacterial cellulose (BC) and poly(vinyl alcohol)-chitosan (PVA-CH) nanofibers produced by needleless electrospinning *(Amorim, Mouro, et al., 2022)*. Electrospun nanofiber scaffolds loaded with prodigiosin were developed for the treatment of triple-negative breast cancer. In this system, prodigiosin functioned as an anticancer agent, gradually diffusing from the nanofibers to induce apoptosis in cancer cells*(Akpan et al., 2020)*.

Bacterial melanin is another bacterial pigment produced by both Gram-positive and Gram-negative bacterial species *(Pavan et al., 2020)*. This dark brown polymer is characterized by biocompatibility, antioxidant capacity, and photoprotective properties *(Aghajanyan et al., 2005)*. Melanin incorporation into electrospun nanofibers can improve their mechanical properties while conferring

antimicrobial activity, thereby enhancing wound healing processes *(Avossa et al., 2021)*. Melanin-loaded polyacrylonitrile fibers exhibited high free radical scavenging activity and antimicrobial effects, in contrast with unmodified fibers which showed no activity *(García-García et al., 2025)*. Bacterial melanin derived from a mutant strain of *Bacillus thuringiensis* was successfully incorporated into nanofibrous scaffolds for nerve tissue engineering, leading to neurorestoration and central nervous system regeneration *(Nune et al., 2019)***.**

Flexirubin-type pigments have also been recently incorporated into electrospun biomaterials to impart antioxidant properties *(Amorim et al., 2024)*. This class of yellow-orange pigments has garnered growing interest due to its notable antioxidant, antimicrobial, anti-inflammatory, and anticancer activities *(Mogadem et al., 2021; Venil et al., 2014, 2017)*. Using a needleless electrospinning technique, researchers fabricated polyvinyl alcohol kefiran/polycaprolactone nanofibers loaded with flexirubin. The resulting nanofibers exhibited a smooth, defect-free, and homogeneous surface morphology, together with significant free radical scavenging activity, thus showing potential for food packaging applications *(Amorim, Fangueiro, et al., 2022)*. Despite further investigation is needed, the reported bioactivity and biocompatibility of flexirubin suggest its potential role in biomedical applications, particularly for supporting skin regeneration. *(Mogadem et al., 2022)*.

Pyocyanin has also demonstrated a broad spectrum of therapeutic potentials, particularly due to its ability to generate reactive oxygen species (ROS) *(Marey et al., 2024; Mudaliar & Bharath Prasad, 2024)*.

In a recent study, pyocyanin was incorporated at 10 wt% into a polyurethane/dextran electrospun membrane. The material exhibited potent antibacterial activity, displaying inhibition rates of 98.54% against *Escherichia coli* and 90.2% against *Staphylococcus aureus*. This effect was attributed to the rapid release of the bioactive pigment and the oxidative stress induced by ROS generation after its diffusion into bacterial membranes *(Sheet et al., 2018)*. However, this pigment has not been already entirely explored. In fact, numerous natural derivatives of this phenazine exist, many of which may hold significant therapeutical, environmental, and agricultural potential that remains to be systematically investigated *(W. Huang et al., 2024b)*.

Exploring extremophile bacteria as a source of novel molecules for biomedicine

In recent years, interest in microbial pigments has increased substantially due to their high potential in pharmaceutical, food, cosmetic, and textile industries. Following this trend, extremophiles have emerged as promising source of distinctive compounds with potent antioxidant, bioindicator, antimicrobial, antimalarial, antifungal, and anticancer activities *(Rather et al., 2023; T. R. e Silva et al., 2021)*. The increasing demand for natural ingredients in industrial and biomedical formulations has driven the scientific attention toward strains adapted to extreme environmental conditions. In particular, marine extremophiles coping with extreme pH and temperature have been reported to be especially rich in pigmented species. *(Rather et al., 2023)*. Among these environments, Antarctica offers a unique and largely unexplored reservoir of pigmented microorganisms. Notably, it has been reported that approximately

41,7% of Antarctic yeasts are producers of pigments and/or mycosporines. *(Duarte et al., 2019)*.

Pigment production is considered a key adaptive strategy that enables microorganisms to survive the harsh Antarctic conditions. In these environments, microorganisms are exposed to high UV radiation leading to increased generation of reactive oxygen species. Pigments can provide effective antioxidant defense and photoprotection *(Correa-Llantén et al., 2012)*. Moreover, microbial pigments can play a role in the regulation of membrane fluidity, particularly under low temperatures. The cryoprotection offered by carotenoids is well-established. Pigments have also been reported to protect against hypoosmotic shock at high NaCl concentrations. Overall, pigments produced by Antarctic bacteria are essentially intracellular and include carotenoids, violaceins, tetrapyrroles, indolic bichromes and heterocyclic biochromes, and other compounds. *(T. R. e Silva et al., 2021)*. Despite the difficult accessibility of Antarctic environments and the limited cultivability of several microorganisms, these extreme ecosystems represent a largely unexplored source of novel bioactive molecules with promising applications in many fields, including biomedicine and regenerative medicine *(Órdenes-Aenishanslins et al., 2016)*.

Overall, tissue engineering represents a dynamically developing field that continuously seeks innovative solutions. The need to prevent immune rejection and microbial infections together with the growing concerns over antibiotic resistance associated with many well-established compounds, has driven research toward novel alternatives. In this context, increasing attention has been directed toward natural sources. In particular, due to their versatility and their

distinctive properties, microbial-derived molecules have emerged as promising candidates for biomedical applications. In the following sections, the results of the research conducted abroad are presented, focusing on the application of novel metabolites derived from a recently isolated Antarctic bacterium in the field of human health.

Materials and Methods

Biosynthesis of the Antarctic pigment and characterization

Bacterial pigment was biosynthesised by *Rhodococcus* sp. ef1 in MMD medium and harvested as previously described. Briefly, bacterial suspension was centrifugated to collect the pellet. Extraction in chloroform and the subsequent solubilization in alkaline water allowed to collect the pigment. Neutralization of pH was achieved by gently adding HCl to the solution, until the pH dropped to 7. The pigment was stored at 4 °C until use, protected from the light.

Characterization was performed by UV-vis spectroscopy, Fourier transform infrared spectroscopy (FTIR) and scanning electron microscopy (SEM) approaches. UV-vis spectroscopy was performed using a Evolution 201 spectrophotometer supplied by Thermo Scientific, Waltham, USA. Spectra were collected after dilution of the sample to improve the resolution. FTIR was performed using a Nicolet iS10 model (Thermo Scientific, Waltham, USA). Each spectrum was collected as the average between 128 scans, in the range of 400-4000 cm^{-1}, with a resolution of 4 cm^{-1}. SEM analysis was conducted to get the elemental composition using a Hitachi S-3400N (Japan), operating with an accelerating voltage of 20 kV. Norm. C [wt.%] represented the normalised concentration in weight percent of the element, whereas C Atom. [at.%] the atomic weight percent, C Error (1 Sigma) [wt.%] the error in the weight percent concentration at the 1 sigma level.

Biosynthesis of silver nanoparticles and characterization

After MilliQ double distilled H_2O was pre-heated, 0.2%(V/V) of NaOH 2 M was added to obtain an alkaline pH, then 7% (V/V) of $AgNO_3$ (2.29 e^{-3}) was added.

Temperature was increased to 70 °C and 0.2 % (V/V) of the microbial pigment was added in the sample, representing the reducing agent responsible for the nanoparticles formation. The sample was covered from light and keep under agitation during all the synthetic process. UV-vis absorbance was constantly measured to monitor the AgNPs production. After the synthesis has occurred, AgNPs were stored for few days at 4 °C and in the dark until use.

Characterization of the synthetic AgNPs was performed by combining UV-vis spectroscopy, Fourier transform infrared spectroscopy (FTIR), transmission electron microscopy (TEM), and Dynamic Light Scattering (DLS) approaches.
FTIR was performed using a Nicolet iS10 model (Thermo Scientific, Waltham, USA). Each spectrum was collected as the average between 128 scans, in the range of 400-4000 cm^{-1}, with a resolution of 4 cm^{-1}.
TEM was performed by a Hitachi-HT7700 microscope, operating with an accelerating voltage of 80 kV. AgNPs were sonicated for 5 minutes to avoid aggregation, placed on a formvar-coated copper grid and dried at room temperature. DLS was performed to determine the hydrodynamic diameter by using a Zetasizer Nano ZS particle analyser (Malvern Instruments, Worcestershire, UK).

Nanofiber electrospinning

Nanofibrous membranes were produced using a conventional electrospinning apparatus, made of a high voltage source (Spellman SL40*10, 0-40 kV, obtained from Spellman, Corporate Headquarters USA), a precision syringe pump (KDS-100, acquired from Sigma-Aldrich, Sintra, Portugal), a plastic syringe with a stainless-steel needle (21 Gauge), and an aluminium disk connected to a copper

collector *(Miguel et al., 2019)*. The membranes were produced starting from a solution consisting of chitosan and polyethylene oxide (CS_PEO). The optimal polymer blend was identified as 60% chitosan (CS) and 40% polyethylene oxide (PEO), dissolved in a mixture of acetic acid (10% v/v) and ethanol (70% v/v) and stirred overnight. Then, the solution was loaded on a syringe and electrospun with constant flow rate of 0.5 ml/h, maintaining a working distance of 15 cm from the collector and an applied voltage of 2 kV, obtaining a membrane with a thickness resembling the epidermis layer of the human skin (around 0.05-1,5 mm).

3D-Scaffolds preparation and functionalization

The 3D-scaffolds were produced by 8RP rapid prototyping technique according with the protocols developed by the research team of the Host University *(Silva-Barroso et al., 2023)*. Briefly, a composite solution made of 30% alginate and 70% β-tricalcium phosphate (β-TCP) was prepared. Alginate was first dissolved in double deionized, filtered H_2O and homogenized with X10/25 Ultra-turrax (Ystral, Germany) for 7 minutes. Then, β-TCP was added to the solution and homogenized for additional 10 minutes. The prepared alginate/β-TCP mixture was subsequently loaded into a 10cc Luer Lock syringe and extruded using a Fab@home 3D printer. The 3D model, consisting of multiple layers, was designed with CAD/CAM software (OpenSCAD version 2014.3, ©2009-2014 Marius Kintel and Clifford Wolf). After printing, scaffolds were immersed in 3% $CaCl_2$ for 1 hour to promote crosslinking and finally dried at 37°C for 3 days. The resulting scaffolds were observed at SEM using a Hitachi S-3400N (Japan), operating with an accelerating voltage of 20 kV. The functionalization was performed by soaking the scaffolds into water-extracted pyocyanin derivative.

Incorporation of the pyocyanin derivative into the electrospun nanofibers

Pyocyanin derivative was incorporated following two strategies. In the first approach, the already elecrospun PEO/CS membrane was soaked into water-extracted pigment. In the second approach, the compound was directly incorporated in the electrospinning solution in chloroform phase. Volatile solvents, indeed, are considered optimal for the electrospinning process, whereas water-based solutions may cause electric shocks *(Ahmadi Bonakdar & Rodrigue, 2024)*. The solution was stirred overnight before initiating the electrospinning process. The resulting membranes were observed through scanning electron microscopy (SEM) to check membrane morphology, fibers size and orientation, and to detect the presence of beads. ImageJ software (provided by National Institutes of Health, Bethesda (MD), USA) was employed to determine the diameter distribution of the nanofibers in the electrospun membranes.

AgNPs incorporation into electrospun nanofibers

AgNPs were directly incorporated into the electrospun solution to promote a more homogeneous distribution within the final membrane.
The resulting nanofibers were analysed by SEM to characterize the surface morphology and the fiber orientation, while TEM analysis revealed the presence of AgNPs coating the nanofibers. Diameter distribution of the nanofibers was analysed by ImageJ software as mentioned above.

Antimicrobial activity test and antibiofilm properties evaluation

Antimicrobial activity of the Antarctic compounds was evaluated against *E. coli* (DH5α) and *S. aureus* (ATCC 25923), representing respectively the Gram

negative and Gram-positive bacterial models. The antimicrobial properties were investigated both as intrinsic characteristics of the Antarctic compounds, by soaking 8 mm sterile paper filter diffusion disks, and as functional properties when these compounds were applied to the biomaterials.

Each of the following steps was executed under sterile conditions. *E. coli* and *S. aureus* were revived from -80°C stocks by briefly thawing the bacteria at room temperature, followed by spreading 200 µl of microbial suspension on LBA plates. The microorganisms were incubated at 37 °C for 24 hours, to allow uniform bacterial growth. A small aliquot from each mother plate was transferred to fresh LBA plates and incubated under the same conditions to perform colony isolation. The colonies were then suspended in LB medium adjusting the final density to 0.5 McFarland units, before being uniformly spread on LBA plates. Filter papers and functionalized scaffolds and membranes, previously sterilized under UV light for 30 minutes, were subsequently placed on the inoculated plate surface.

After incubation at 37 °C for 24 hours, the antimicrobial activity was detected by visual inspection of an inhibition halo surrounding the samples. The area of the inhibition halo was measured to quantify the antimicrobial potential associated with different compounds concentrations. ImageJ software was used for this purpose.

The presence of bacterial biofilm on the tested biomaterials was evaluated by SEM analysis. After 24 hours of incubation in microbial culture plates, the discs were collected and immediately fixed by 2.5% of glutaraldehyde for 1 hour at room temperature. After that, the samples were rinsed with dH_2O and air dried for 30 minutes. The side of the membranes and of the scaffolds not in contact with bacteria was marked with varnish. Subsequently, the samples were

incubated at 4 °C for 30 minutes and then frozen at -80 °C for 1 hour. Lyophilization for 6 hours allowed to remove all the water content. The samples were store at room temperature, protected from humidity, and were finally examined by SEM for biofilm detection. Due to the limited time and materials available, SEM analysis was focused on the most representative samples and was performed in duplicate for each analysed condition.

Cellular assay

Cellular assays were conducted on human osteoblast cells (CRL-11372) acquired from the American Type Culture Collection (ATCC, VA, USA) and on normal human dermal fibroblasts (NHDF) cells acquired from PormoCell (Labclinics, S. A., Barcelona, Spain).

Scaffolds biocompatibility, with and without functionalization with the Antarctic pigment, was tested on osteoblasts, whereas skin regenerative membranes biocompatibility, with and without functionalization with AgNPs or the Antarctic pigment, were tested on fibroblasts.

Both cell types were cultured in 10 ml of Dulbecco's modified Eagle medium (DMEM F12), in a 75 cm^2 T-flasks. The medium was supplemented with 10% of heat-inactivated fetal bovine serum (FBS), 1% of antibiotics including penicillin, streptomycin and amphotericin B. Sterilization of the medium was ensured by vacuum filtration under a biological safety cabinet. Cell cultures were incubated under humidified conditions at 37ºC with a 5% CO_2 supply.
Once confluent, cells were detached by trypsinization. Briefly, 5 ml of trypsin were added to the culture flask. After incubation at 37 ° for 5 minutes, 5 ml of PBS were added to stop the reaction. Cells were harvested by centrifugation at

405 RCF for 5 minutes, and the resulting pellet was resuspended in 1 mL of fresh culture medium. After that, cellular density (number of cells/mL) was determined by the trypan blue exclusion method using a Neubauer Chamber. The total number of cells was calculated as follows:

$$\textbf{\textit{Total cell number}} = \frac{\textbf{\textit{counted cells}}}{\mathbf{4}} \times \mathbf{10} \times \mathbf{10\,000}$$

For biocompatibility evaluation at 24, 72, 168 hours, appropriate amounts of cells were seeded to obtain 20.000, 10.000, and 2.500 cells/well, respectively. Cells were plated in 12-well plates (1 ml/well) and cultured for 24 hours to promote their adhesion. After that, biomaterials were put in contact after a sterilization cycle of 30 minutes under UV light. The size of biomaterials did not exceed the 10% of the well capacity. Culture medium was renewed every 48 hours.

Cell viability was assessed via resazurin assay 24, 72, and 168 hours after contact with the biomaterials. Pictures of the cells were collected at each incubation time using Olympus CKX41 (Japan) connected to a camera. Then, the biomaterials were removed from each well, and the exhausted medium was replaced with fresh medium supplemented with 10% (V/V) resazurin. The cells were incubated at 37°C in humidified conditions with 5%CO_2 supply for 4 hours, protected from light. During this time, metabolically active cells reduce resazurin to resorufin, resulting in a visible colour change of the medium from blue to pink. Cell viability was quantified using a plate reader fluorimeter (Anthos 2020, Biochrom). Aliquots from each well were transferred into 96-well microplate for the analysis and diluted 1:5 with PBS to avoid signal saturation. Fluorescence was recorded at 570 and 600 nm.

Each experiment included proper controls. Cells cultured without biomaterials were used as the negative control, whereas cells exposed to 70% ethanol were used as the positive control. Five replicates were analysed for each incubation condition. Data were expressed as mean ± SD of biological replicates.

Toxicity assay

A range of pigment concentrations, including 133, 66,5, 33, 125, 16, 56, 8,28, 4,14, 2, 07, and 1,03 µg/ml, was tested on human osteoblasts. The assay was performed using the same cell culture conditions described for the viability test, with the only difference that cells were exposed to the solubilized molecule rather than to the biomaterials. Toxicity was evaluated after 24 and 72 hours by quantifying the resazurin-to-resorufin conversion as previously detailed. Cells cultured in absence of the pigment represented the negative control, whereas cells exposed to 70% ethanol were used as the positive control. Five replicates were analysed for each incubation condition, and data were presented as mean ± SD of biological replicates.

Results

Biosynthesis and characterization of the bacterial pigment

Pigment biosynthesis was achieved by culturing *Rhodococcus* sp. ef1 as previously discussed. As the following section of the research work was entirely conducted abroad, using the facilities of the host university of UBI (University of Beira Interior), the characterization studies were performed to verify that the pigment retained its characteristics and to validate the work conducted in Italy.

UV-vis spectrum was collected to verify the integrity of the sample after transportation and storage. The spectrum in alkaline aqueous medium showed the characteristic peaks previously obtained, with the main band at 303 nm and three lower absorption bands at 348, 360, and 617 nm, revealing that the sample has been correctly handled and it was ready to be used in the subsequent assays (*Figure 40)*.

FTIR spectrum showed many peaks and regions consistent with previous results (*Figure 41*). The peaks at approximately 3300 and 2900 cm^{-1} suggested the presence of an O-H and of a C-H aromatic bond, respectively. The region between 3300 and 3000 cm^{-1} indicating the presence of an amino group (NH_2), the peak at 1678 cm^{-1} representing a C-N bond, the absorption regions between 1500-1400 $cm^{-1}$and 1600-1585 cm^{-1} typical of the stretching vibrations of C-C bonds in the C-C aromatic ring, were also recognisable. The FTIR spectrum obtained was comparable with that obtained by the chemical characterization performed in Italy and confirmed that the pigment was a pyocyanin derivative *(Koyun et al., 2022)*.

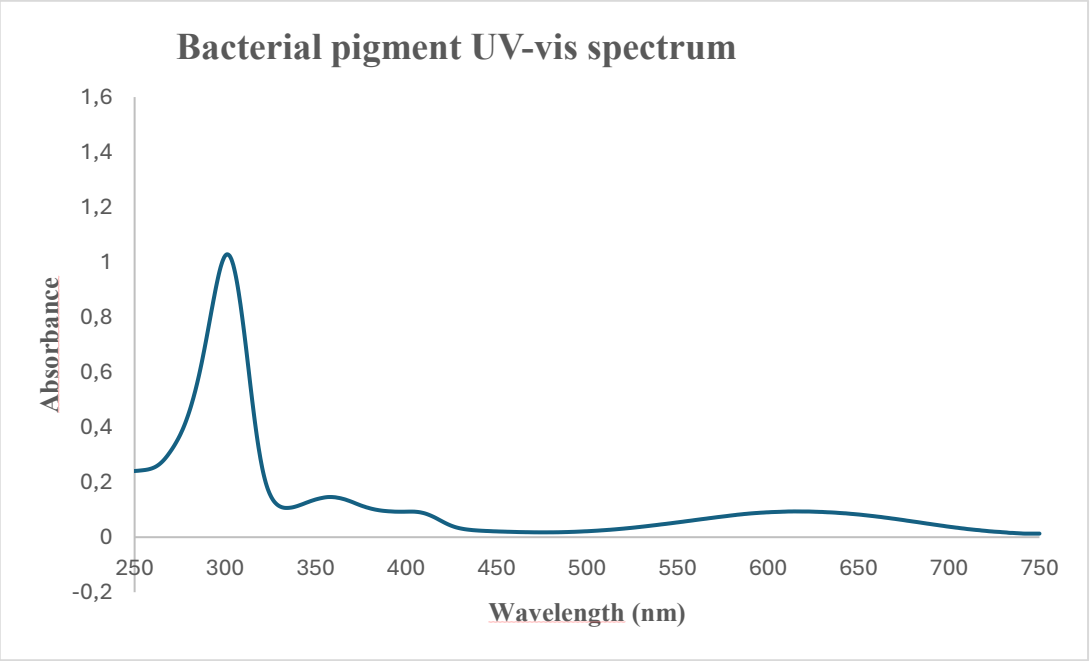

Figure 40 – UV-vis spectrum of the bacterial pigment revealed the characteristic peaks previously observed during the characterization studies in Italy. The main band was located at 303 nm, whereas three lower bands were detectable at at 348, 360, and 617 nm.

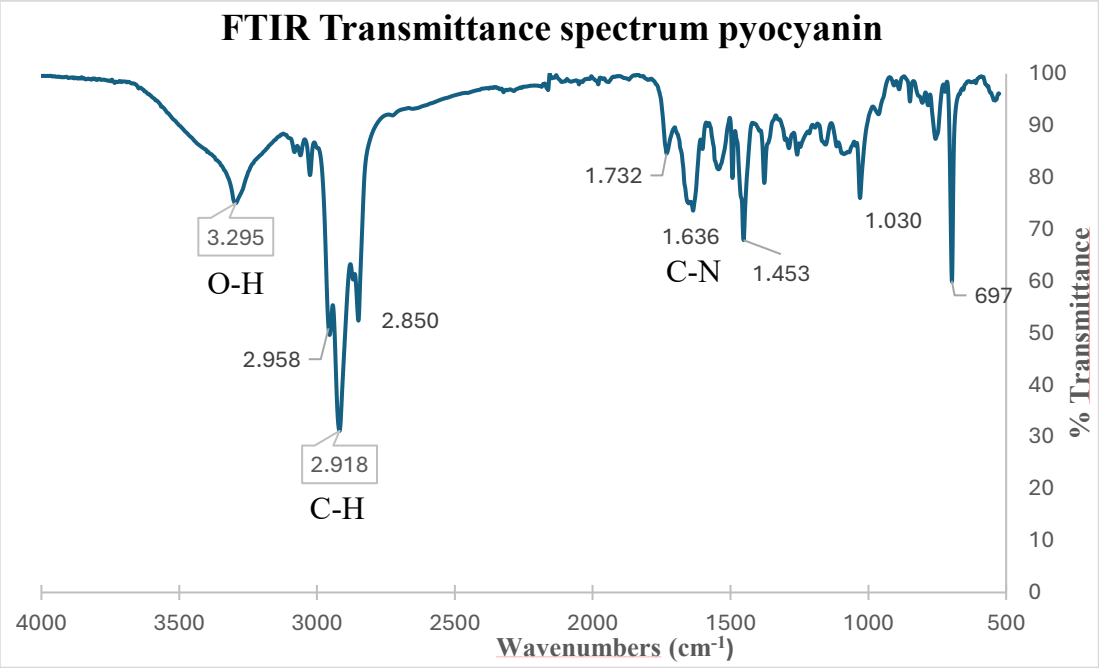

Figure 41 - FTIR spectrum of bacterial pigment showed the characteristic peaks of pyocyanin derivatives, confirming the previous results obtained during chemical characterization in Italy.

SEM analysis was conducted to assess the elemental composition of the sample (*Table 6*). Carbon, oxygen and nitrogen were the most represent elements in the sample, as expected from the molecular structure proposed for the compound. Silicon, phosphorus, potassium, and copper were also present in small traces. They likely corresponded to residuals from bacterial culture medium, or impurities.

Table 6 – Elemental analysis of the pyocyanin derivative sample

Element	***Norm. C [wt. %]***	***Atom C. [at. %]***	***Error (2 Sigma) [wt. %]***
Carbon	80,12	84,04	17,80
Nitrogen	5,38	4,84	2,51
Oxygen	13,78	10,85	4,15
Silicon	0,25	0,11	0,08
Phosphorus	0,19	0,08	0,07
Potassium	0,16	0,05	0,07
Copper	0,12	0,02	0,07

Synthesis and characterization of silver nanoparticles

A solution made with alkaline double distilled H_2O, $AgNO_3$, and the bacterial pigment as the reducing agent was stirred and kept under heating in the dark as previously discussed in Materials and Methods. A progressive change in colour of the solution toward far yellow revealed that the reduction of $AgNO_3$ had occurred (*Figure 42*). Moreover, AgNPs formation was monitored through UV-vis spectroscopy. After 30 minutes, UV-vis spectrum remained stable, showing AgNPs characteristic peak at around 400 nm, confirming that nanoparticles have been successfully formed (*Figure 43*). DLS analysis revealed that two population of AgNPs were present in the sample, with average diameters of

around 18 and 80 nm, respectively (*Figure 44*). TEM analysis, instead, showed that AgNPs size ranged between less than 5 to 25 nm, with the portion 10-15 nm most represented and an average diameter of 13,07 nm. The nanoparticles were surrounded by a halo likely corresponding to the capping layer (*Figure 45-46*).

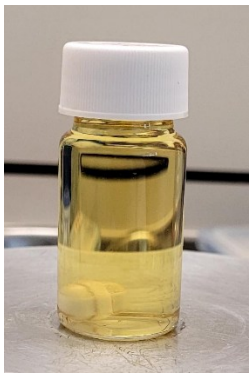

Figure 42 – After 30 minutes of incubation under stirring, AgNPs suspension assumed the typical far-yellow colour.

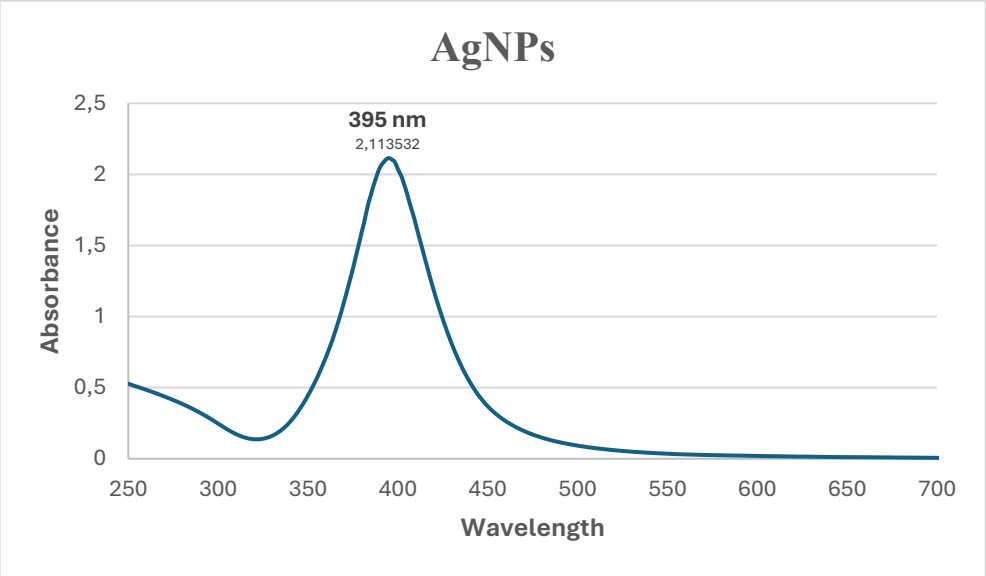

Figure 43 – AgNPs exhibited the characteristic absorption spectrum with a peak at around 395 nm, remaining stable over time.

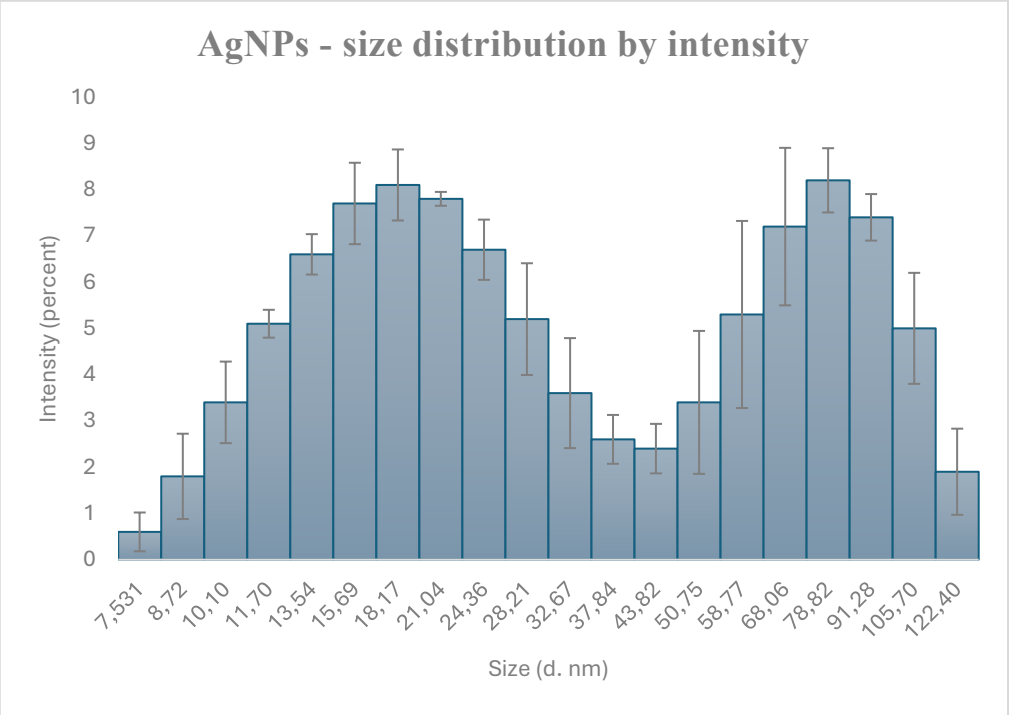

Figure 44 – DLS analysis revealed the presence of two populations of AgNPs, with an average diameter of around 18 nm and 80 nm, respectively.

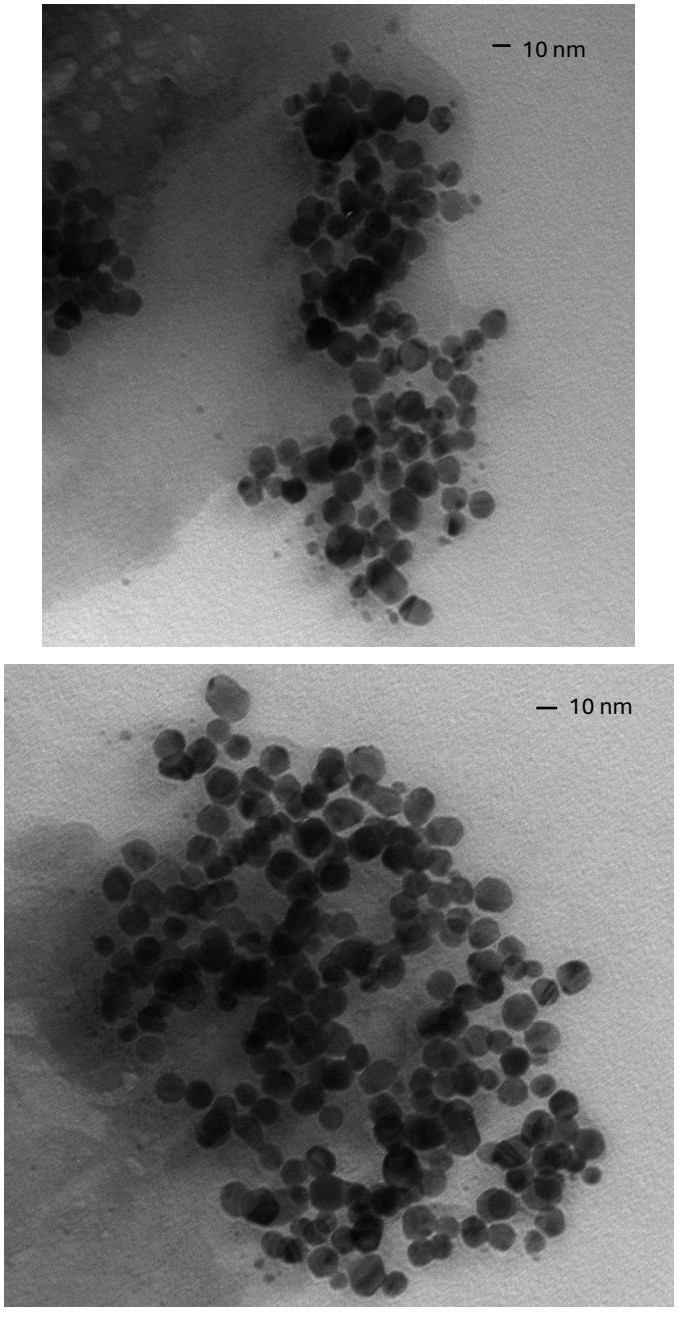

Figure 45 – TEM image of synthesised AgNPs.

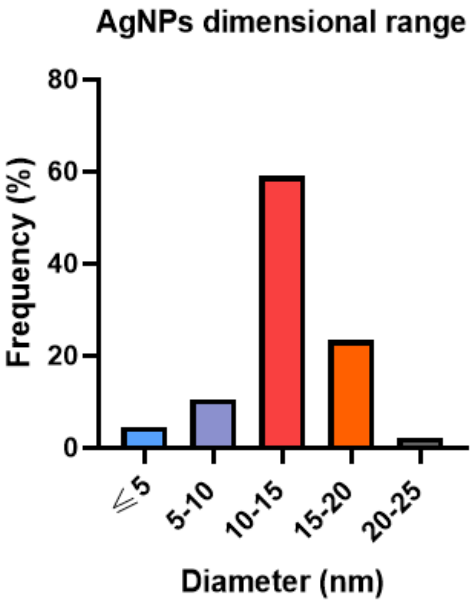

Figure 46 - Dimensional analysis of the AgNPs following TEM.

Incorporation of the bacterial pigment into the electrospun nanofibers

The bacterial pigment was incorporated in the polymer solution prior to electrospinning to favour a homogenous distribution within the final membrane. Initial attempts resulted in the pigment accumulating predominantly in the central portion of the membrane (*Figure 47a*). By optimizing the electrospinning parameters and improving sample homogenization, a more uniform distribution was achieved (*Figure 47b*).

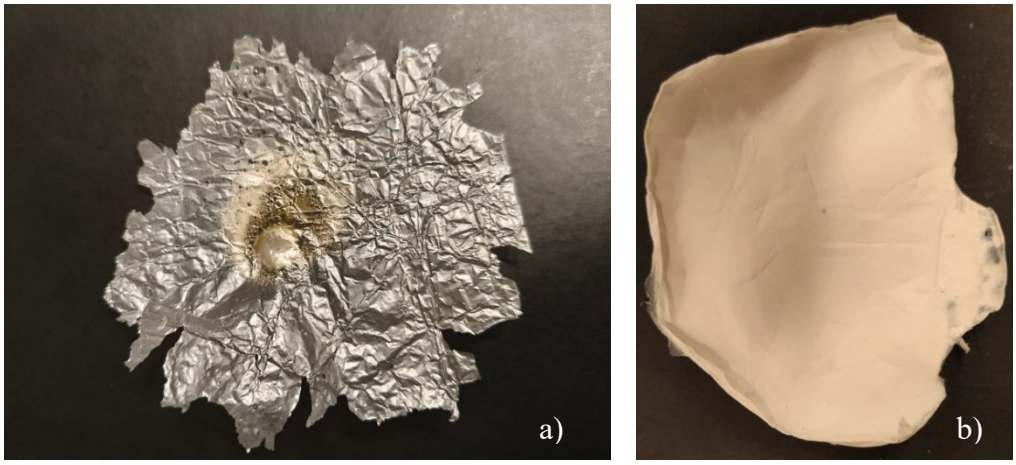

Figure 47 - ***Pigment-based skin regenerative membrane****. a) The first attempts resulted in a membrane with the pigment predominantly concentrated in the central portion. b) Optimization of the electrospinning working conditions and improved homogenization of the solution allowed a more uniform pigment distribution throughout the membrane.*

SEM analysis confirmed successful membrane formation, revealing the presence of a limited number of beads along the fibers. Although minor surface irregularities were observed, the membrane overall displayed a smooth morphology (*Figure 48a*). At higher magnification (*Figure 48b*), the fibers formed a reticular network, with an average diameter of approximately 90 nm, (*Figure 48c*) mimicking the structure of the native extracellular matrix.

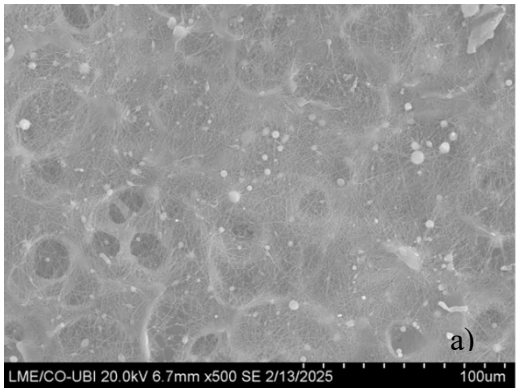

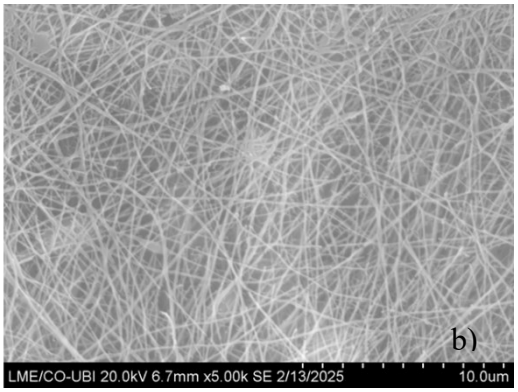

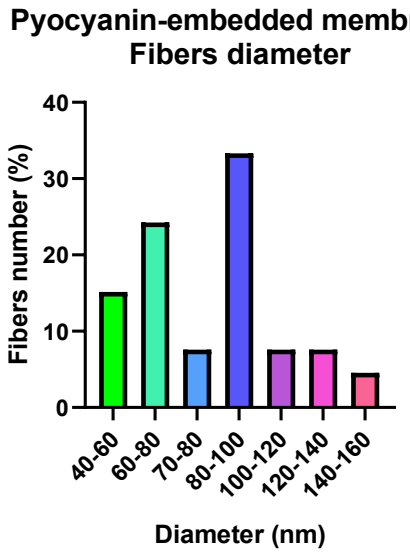

c)

Figure 48 – SEM images of pigment-based skin regenerative membrane at x500 (a) and of the relative nanofibers at x5.000 (b). c) % frequency distribution of the fibers diameter.

Incorporation of AgNPs into the electrospun nanofibers

AgNPs were also incorporated in the polymer solution prior to electrospinning to promote a homogenous distribution within the resulting membrane. The

obtained electrospun nanofiber showed AgNPs mostly localized in the central region of the membrane, appearing as darker dots on the membrane surface (*Figure 49*).

Figure 49 – Electrospun nanofiber with AgNPs incorporation

SEM pictures showed that the membrane generally exhibited a smooth morphology, with a limited number of beads (*Figure 50a*). At higher magnification, the nanofibers appeared organized in a reticular structure (*Figure 50b*), with an average diameter of approximately 150 nm (*Figure 50c*).

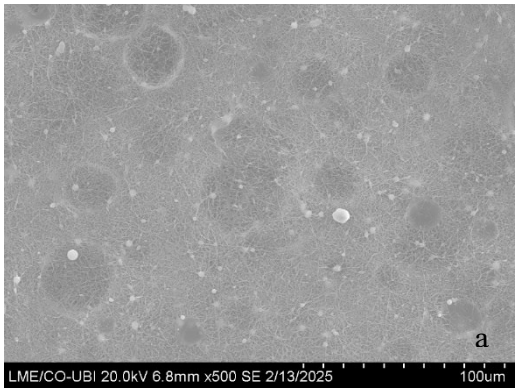

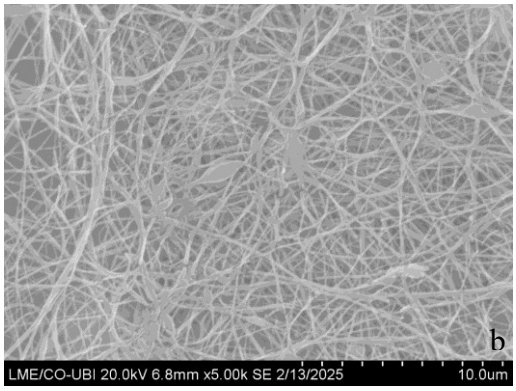

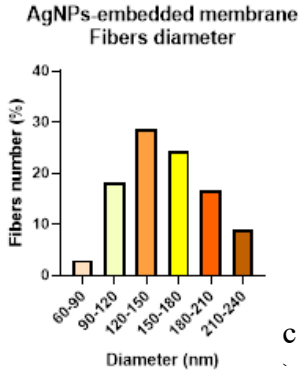

c

Figure 50 - ***SEM images of the nanofibers****. a) 500 X magnification revealed a quite homogeneous surface of the membrane, with few beads. b) 5.000 X magnification shows the presence of reticular nanofibers. c) frequency % distribution of the fibers diameter is reported.*

Finally, TEM analysis confirmed the presence of AgNPs coating the surface of the nanofibers (*Figure 51*).

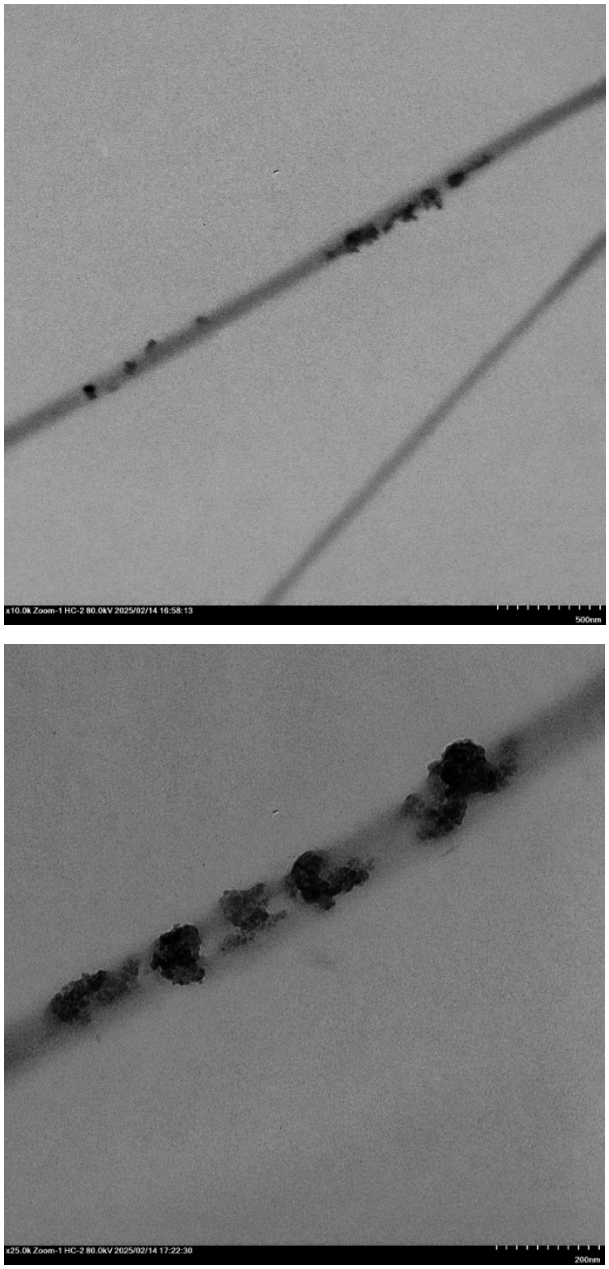

Figure 51 – TEM image of AgNPs coated nanofibers revealed the presence of AgNPs around the fibers.

3D scaffolds fabrication and functionalization with the pyocyanin derivative

The scaffolds were successfully obtained following the procedure described in the Material and Methods section. All samples showed comparable macroscopic features and regular geometry, highlighting the reproducibility of the fabrication process (*Figure 52a*). SEM analysis revealed a homogeneous reticular architecture across all the samples, with no structural defects (*Figure 52b and c*).

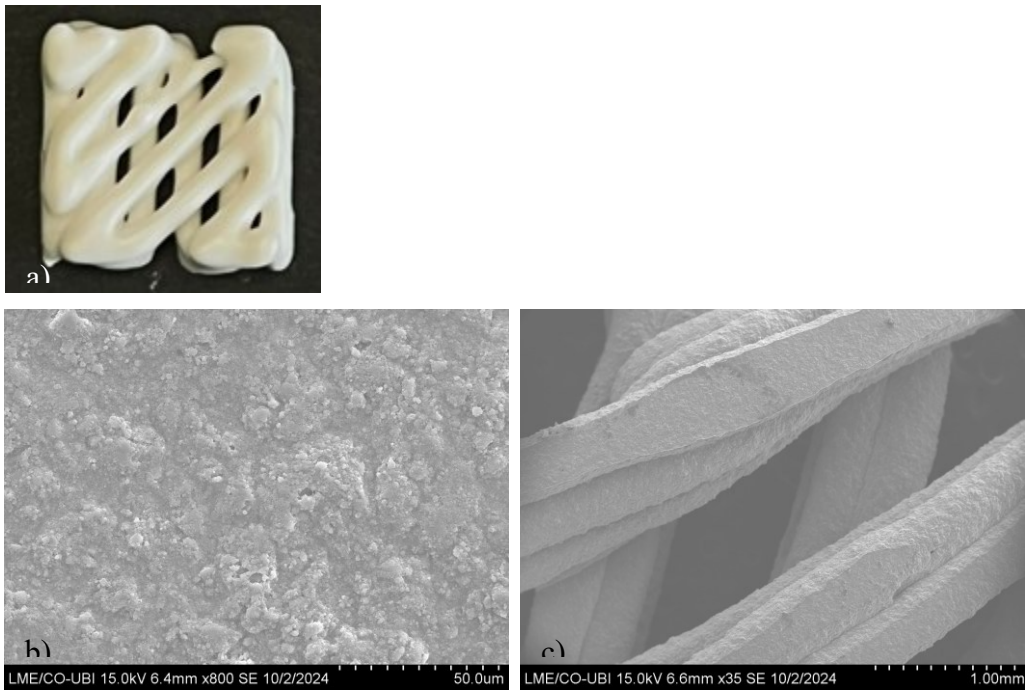

Figure 52 – ***3D-printed scaffolds for bone regeneration****.*

a) Macroscopic image of the scaffold exhibiting a regular geometry and structural integrity.

b) and c) SEM images of the scaffolds revealing a homogenous reticular architecture.

After functionalization with the pyocyanin derivative by immersion, no structural alteration was observed (*Figure 53*).

Figure 53 - 3D-printed scaffolds after functionalization with water-extracted pyocyanin derivative.

Antimicrobial activity assay

Antimicrobial activity of the Antarctic pigment

The antimicrobial activity of the pigment was evaluated both intrinsically and after functionalization of the biomaterials of interest. After extraction, the pigment concentration was estimated by evaporating the chloroform and determining the dry weight. The pyocyanin derivative was then solubilized in water and diluted to the desired concentration. Different concentrations were tested, including 29, 58, 145, and 290 μg/ml. The antimicrobial activity of the Antarctic pigment was first evaluated using filter papers to assess its intrinsic behaviour (*Figure 54*).

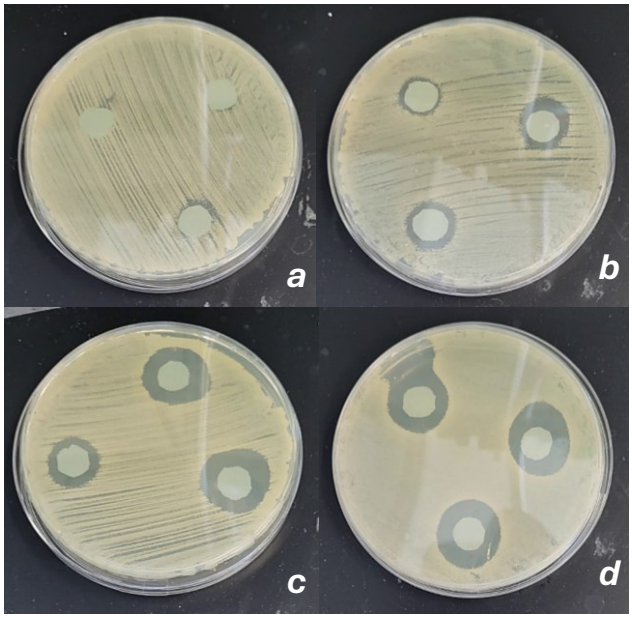
a
b
c
d

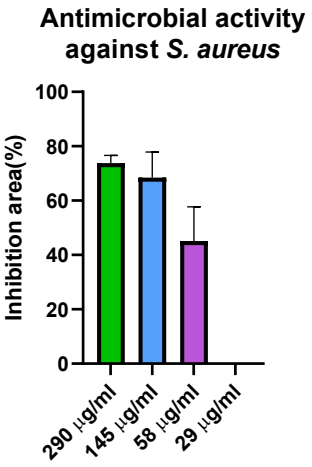
Antimicrobial activity against S. aureus
Inhibition area(%)
100
80
60
40
20
0
290 µg/ml
145 µg/ml
58 µg/ml
29 µg/ml

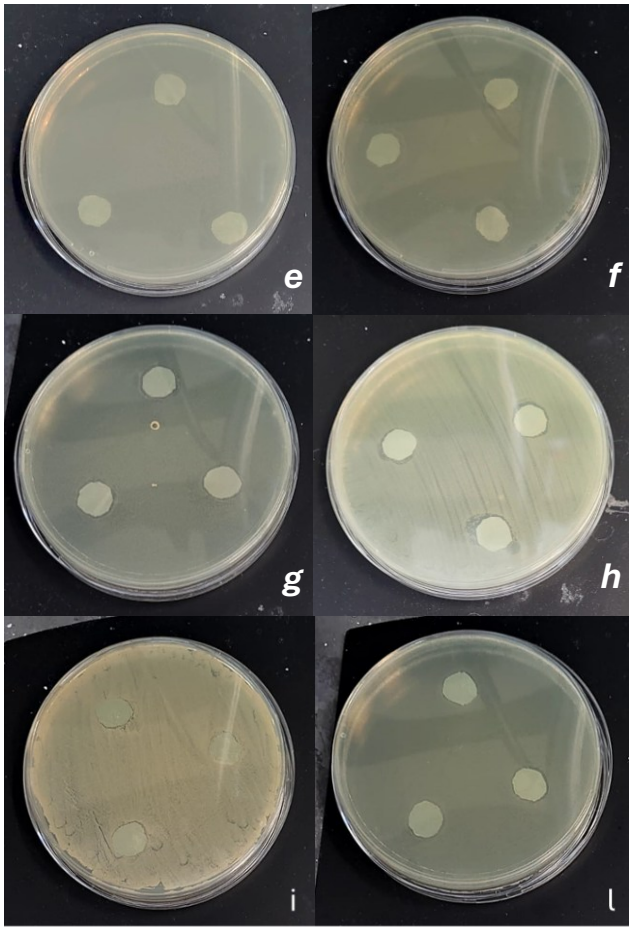

Figure 54 - The results showed the antimicrobial activity of the Antarctic pigment at estimated concentrations of 29, 58, 145, 290 µg/ml, against S. aureus (a, b, c, d, respectively), and against E. coli (e, f, g, h, respectively). Panels i and l represent the control samples of E. coli and S. aureus, respectively, immersed in the aqueous solution used to solubilize the pyocyanin derivative.

The results of antimicrobial activity test suggested that the compound is more effective against Gram positive (*Figure 54 a, b, c, d*) than Gram negative microorganisms (*Figure 54 e, f, g, h*). This can be explained by the different

structure of the microbial membrane that can reduce the efficacy of the molecule *(Epand et al., 2016)*. While inhibition halos were obtained even at the estimated concentration of 58 μg/ml against *S. aureus*, no clear inhibition was detectable against *E. coli*, suggesting that higher concentrations are required.

Antimicrobial property's stability over time was evaluated by comparing the activity of a freshly synthesised sample of the Antarctic pigment with that of the compound stored for 2 months at 4°C, protected from light. After two months, the Antarctic pigment still retained 95% of its antimicrobial effect against *S. aureus (Figure 55)*.

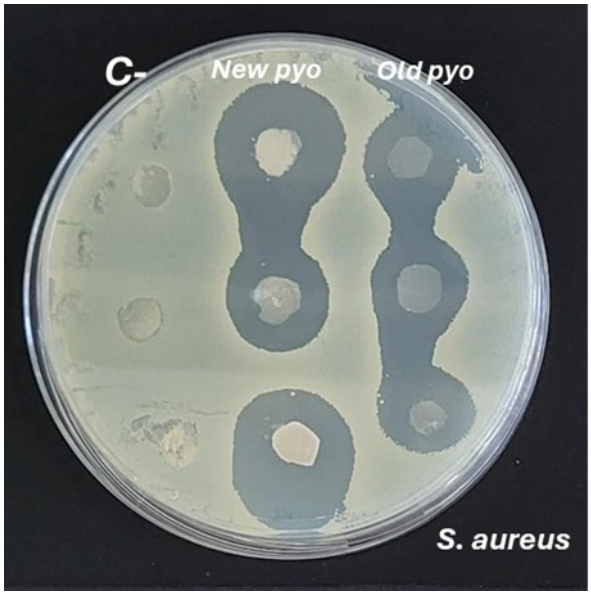

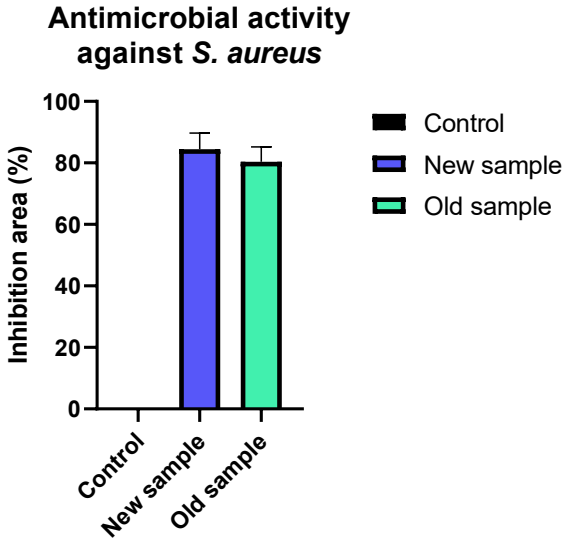

Figure 55 - Antibacterial activity of a freshly synthesized pyocyanin derivative against a sample stored for 2 months in the dark at 4 °C. The oldest sample retained 95% of the efficacy compared to the new sample.

Antarctic pigment was also applied to the wound dressing membranes to assess its antimicrobial properties. Two approaches were considered. The first was based on impregnation of the membrane with the compound after elettrospinning, the other was based on pigment incorporation within the

polymer solution prior to elettrospinning. *Figure 56* showed the results of the antimicrobial activity test.

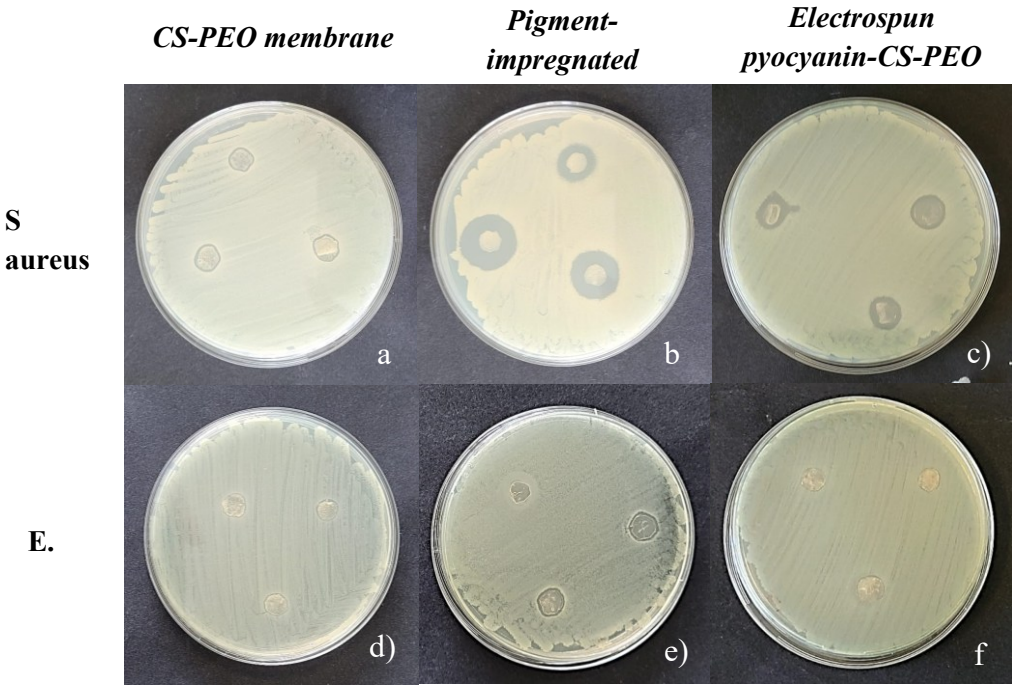
CS-PEO membrane
Pigment-impregnated
Electrospun pyocyanin-CS-PEO
S aureus
E.
a
b
c)
d)
e)
f

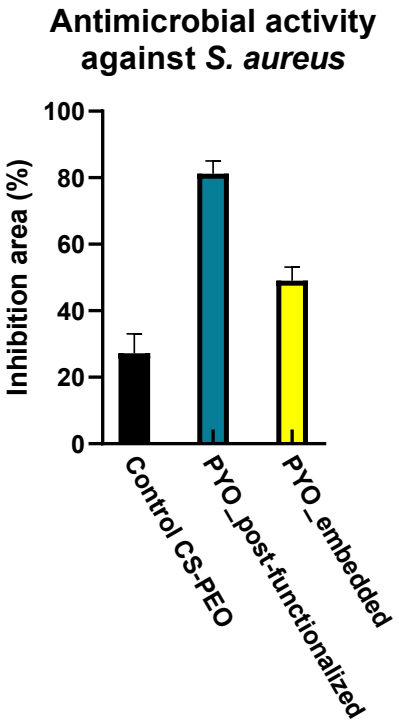

Figure 56 – ***Antimicrobial activity of skin regenerative membranes functionalized with the pyocyanin derivative.***

The figure shows the results of pigment-impregnated membranes against S. aureus (b) and E. coli (e) and of pigment-embedded membranes prior electrospinning against S. aureus (c) and E. coli (f) compared to their non-functionalized controls made of chitosan and polyethylene oxide (a) against S. aureus and d) against E. coli, respectively). Below, the values of the inhibition areas associated with the different functionalization strategies tested are reported.

As shown in the results, the activity is effective against *S. aureus*, suggesting that the compound primarily affects Gram-positive organisms (*Figure 56, a, b,*

c). A stronger effect was observed for the pyocyanin-impregnated membranes (*Figure 56 b*) compared to the pyocyanin-incorporated ones (*Figure 56 c*), likely due to a higher effective concentration at the membrane surface. The values of inhibition area (%) are, respectively, 27,20% for the CS-PEO control membrane, 81, 23% for the phenazine-derivative impregnated membrane, and 49, 06% for the phenazine-derivative embedded membrane.

The antimicrobial property of pyacyanin was also evaluated when the pigment was applied to 3D-printed scaffolds for bone regeneration (*Figure 57*).

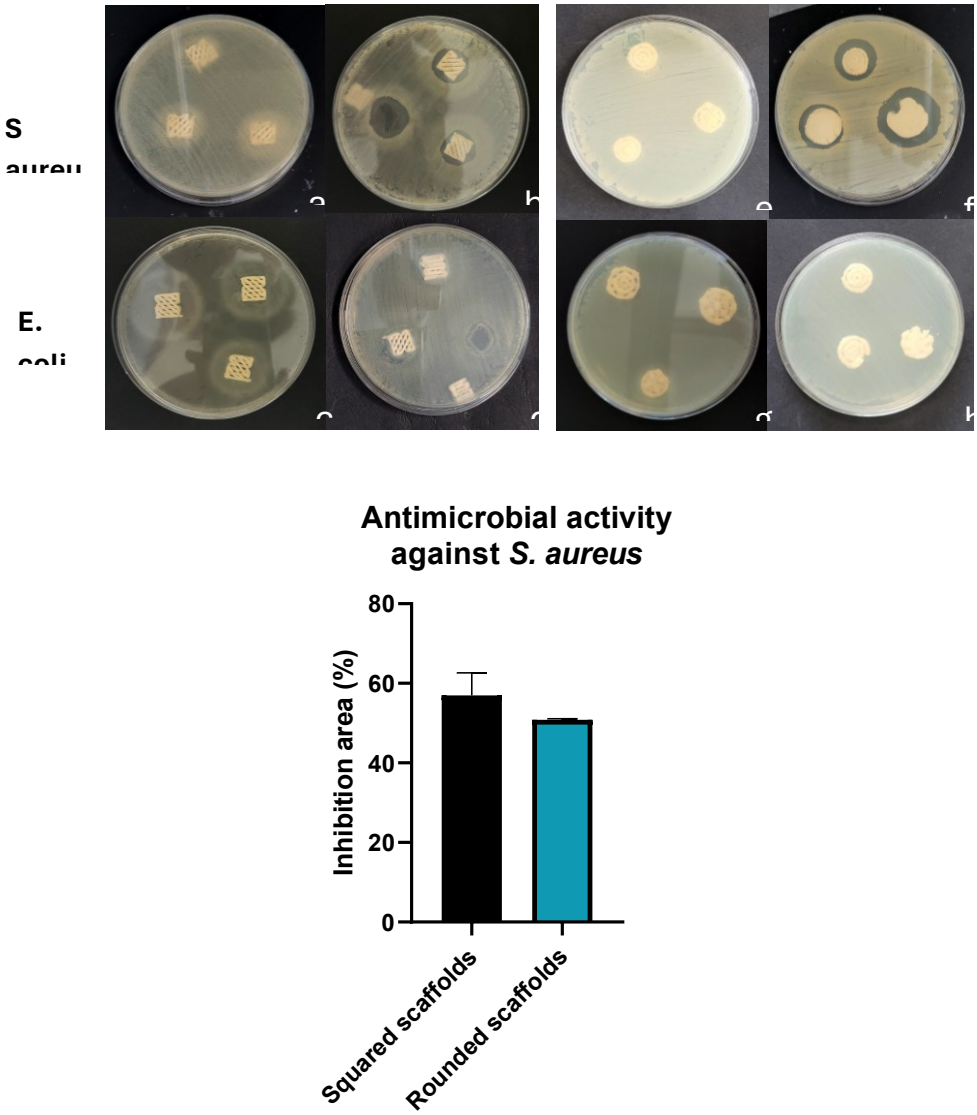

Figure 57 – ***Antimicrobial activity of pyocyanin-impregnated 3D scaffolds.*** *Square-shaped (on the left) and circle-shaped scaffolds (on the right) were tested. Specifically, (a), (b), (e) and (f) show the antimicrobial activity exhibited by pyocyanin-impregnated scaffolds (b, f)) compared with control scaffolds (a, e) against S. aureus. (c), (d), (g) and (h), instead, show the activity of pyocyanin*

impregnated scaffolds (d, h) compared to control scaffolds (c, g) against E. coli. Below, the values of the inhibition area (%) against S. aureus (corresponding to the plates b and f of the picture) are reported.

The results showed that the Antarctic pigment exhibited the antimicrobial activity only against *S. aureus (Figure 57 b and f)*, in agreement with the previous results.

Antimicrobial activity of the AgNPs

Electrospun membranes functionalized with AgNPs prior to electrospinning were tested against *S. aureus* and *E. coli* to enhance the antimicrobial activity of the CS-PEO wound dressing. As showed by the results in *Figure 58*, AgNPs provided a slight antimicrobial effect against both *S. aureus (Figure 58 b)* and *E. coli (Figure 58 d)*.

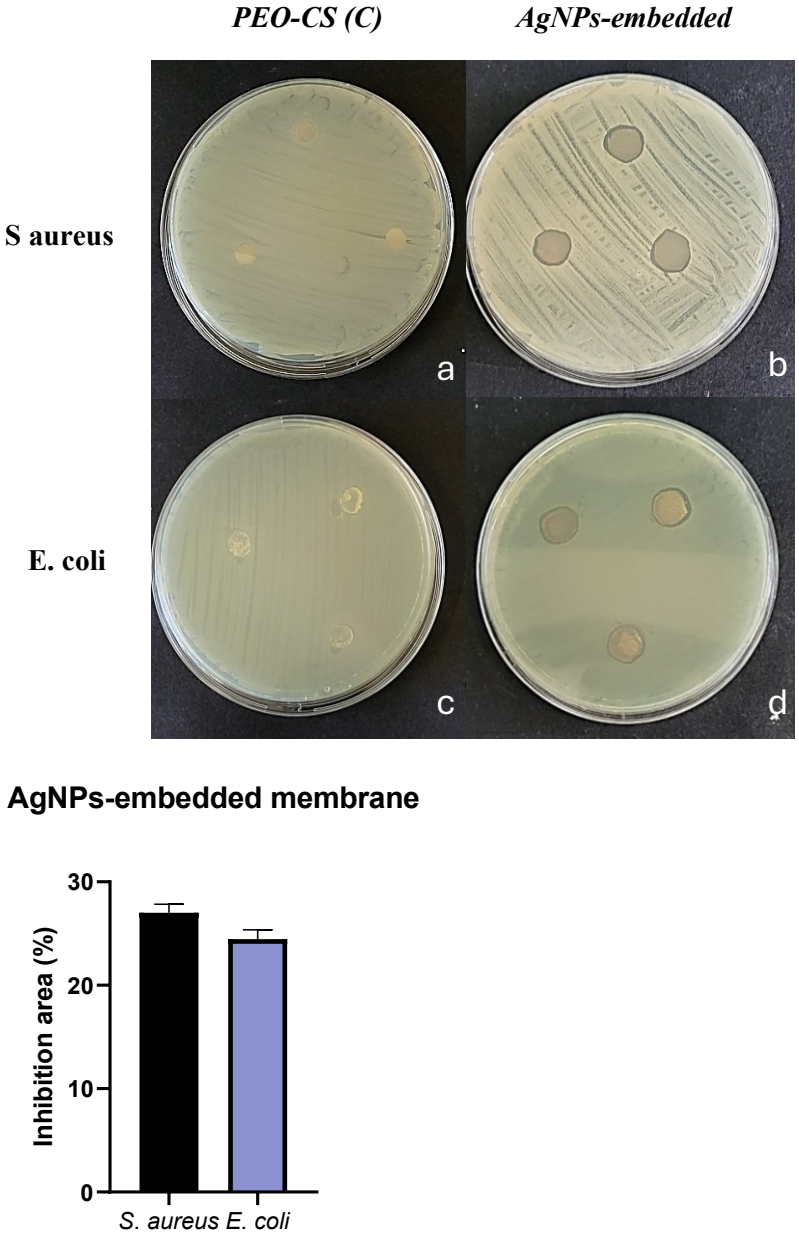

Figure 58 ***-Antimicrobial activity of AgNPs incorporated electrospun membranes****.*

The results showed the antimicrobial activity exhibited by PEO-CS skin regenerative membranes functionalized with AgNPs against S. aureus (b) and E. coli (d) compared to their control PEO-CS wound dressings (a and c, respectively). The inhibition area (%) is also reported.

Biofilm formation

The antibiofilm activity of the biomaterials was qualitatively evaluated by SEM analysis of the samples after 24 hours of incubation with *E. coli* and *S. aureus*, to detect the presence of bacterial cells and biofilm formation on the surfaces in contact with the prokaryotic cells (*Figure 59*). *E. coli* cells were observed on pyocyanin derivative-functionalized electrospun membranes (*Figure 59, e and f*), whereas only a limited number of rounded bodies, likely corresponding to *S. aureus* cells, were observed. They were highlighted in red in *Figure 59, d*. No clear evidence of *S. aureus* adhesion was observed on the functionalized scaffolds (*Figure 59 g and h)*. Detection of *S. aureus* cells was particularly challenging due to the presence of spherical beads on the membranes and to the irregular morphology at the surface of the scaffolds. A limited number of cells were also observed in case of AgNPs-functionalized membranes in contact with *E. coli (Figure 59, a and b)*.

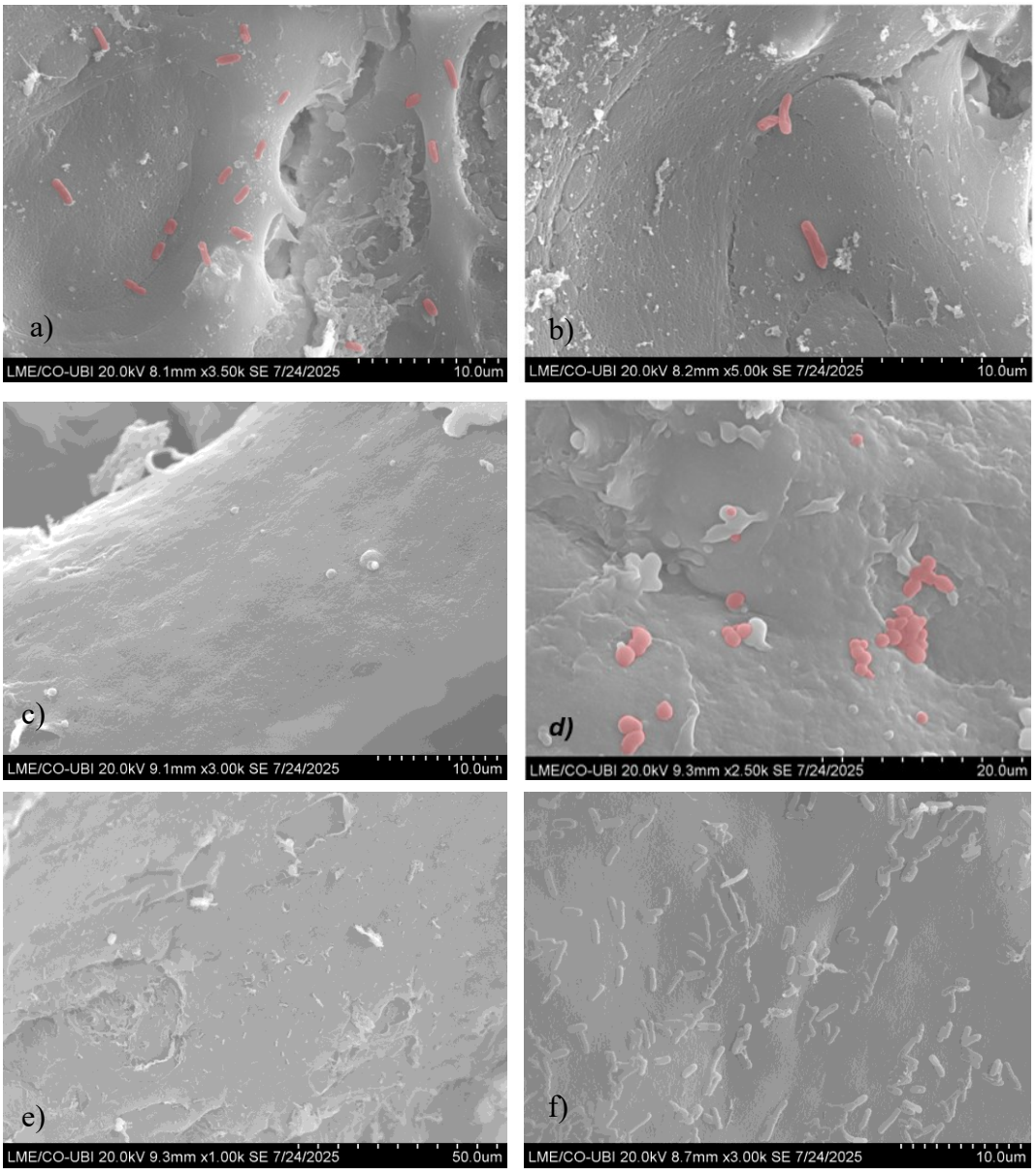
a)
LME/CO-UBI 20.0kV 8.1mm x3.50k SE 7/24/2025
10.0um
b)
LME/CO-UBI 20.0kV 8.2mm x5.00k SE 7/24/2025
10.0um
c)
LME/CO-UBI 20.0kV 9.1mm x3.00k SE 7/24/2025
10.0um
d)
LME/CO-UBI 20.0kV 9.3mm x2.50k SE 7/24/2025
20.0um
e)
LME/CO-UBI 20.0kV 9.3mm x1.00k SE 7/24/2025
50.0um
f)
LME/CO-UBI 20.0kV 8.7mm x3.00k SE 7/24/2025
10.0um

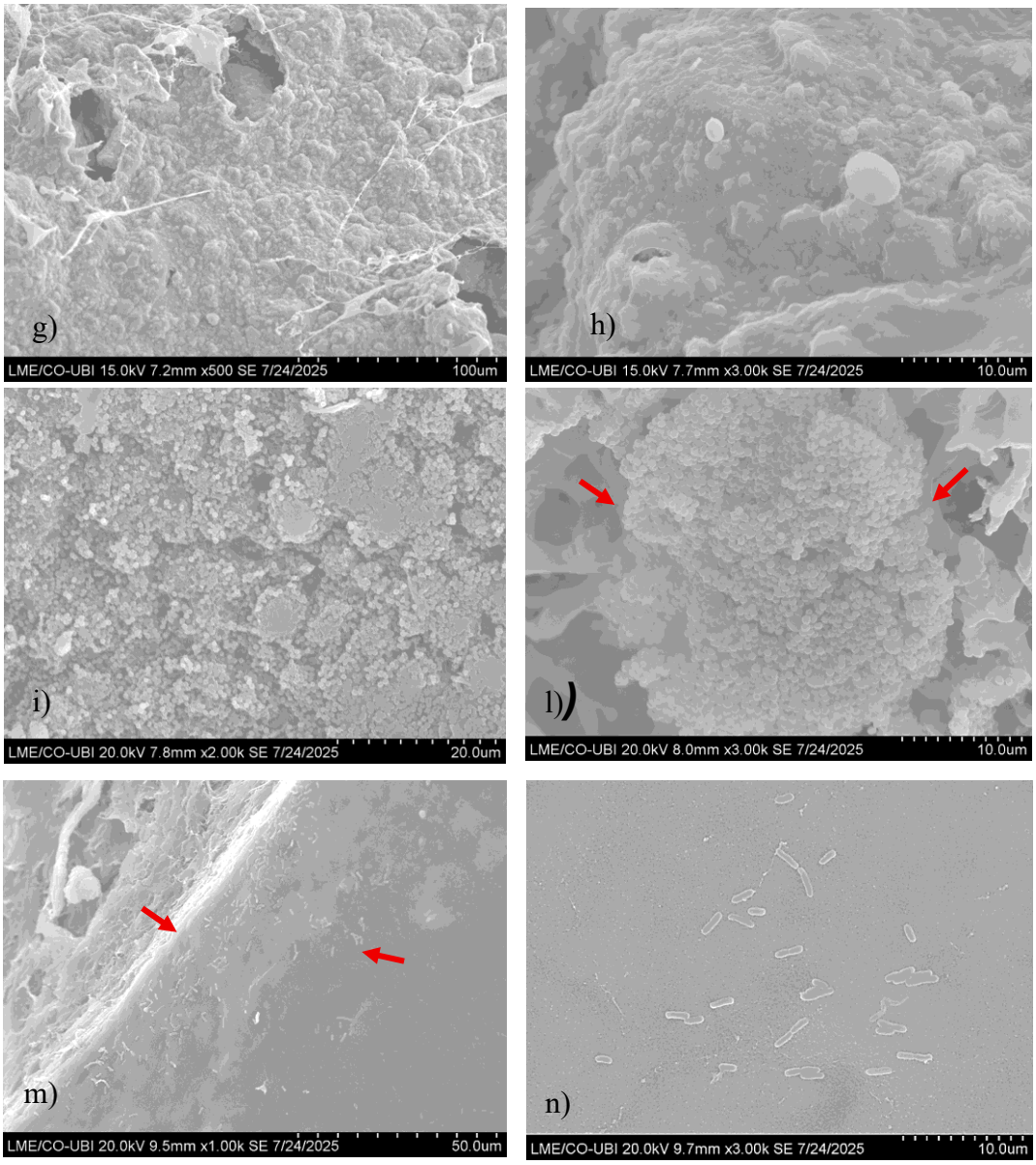

Figure 59 - ***SEM images of the antibiofilm activity of functionalized biomaterials and their controls.***

a, b) nanofiber membranes functionalized with AgNPs tested against E. coli

c, d) nanofiber membranes functionalized with the pyocyanin derivative tested against S. aureus
e, f) nanofiber membranes functionalized with the pyocyanin derivative tested against E. coli
g, h) scaffolds functionalized with the pyocyanin derivative against S. aureus
i, l) non-functionalized membrane (control) tested against S. aureus
m, n) non-functionalized membrane (control) tested against E. coli

Biocompatibility assay

Biocompatibility was evaluated after 24, 72, and 168 hours of incubation of the cells with the biomaterials, as previously described in the Materials and Methods.
Biocompatibility of the PEO-CS electrospun membranes functionalized for skin regeneration and wound healing was evaluated using human fibroblasts. In a first experiment, cells cultured in contact with membranes functionalized with AgNPs showed viability values above 70% over the entire observation period (*Figure 60*).
In a second experiment, human fibroblasts exposed to membranes functionalized with AgNPs and the pyocyanin derivative exhibited viability values above the 70% threshold at 24 and 168 hours, whereas a decrease was observed at 72 hours. Additionally, biological replicates of the pigment-functionalized membranes displayed some variability, resulting in high standard deviations (*Figure 61*). This variability can be attributed to uneven interactions between the pigment and the membrane and to structural heterogeneity across different membrane regions. Control membranes exhibited a good biocompatibility throughout the entire observation period (*Figure 60-61, pink*).

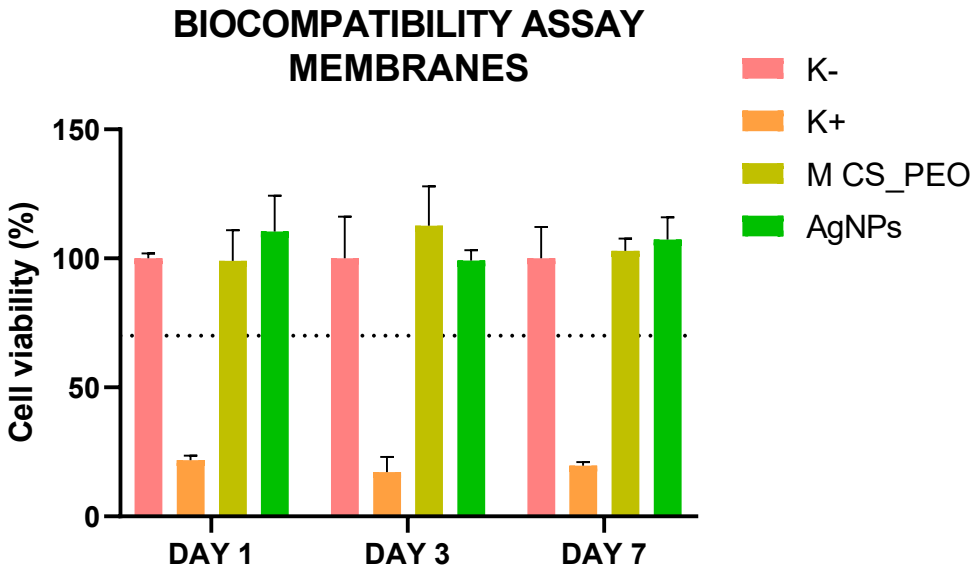

Figure 60 ***- Biocompatibility assay on human fibroblasts in contact with electrospun membranes for skin regeneration and wound healing.***

The threshold was set at 70%. K^- = cells not in contact with biomaterials (negative control). K^+ = cells treated with ethanol 70% (positive control). M = membranes not functionalized with bioactive compounds (control samples). AgNPs = membranes functionalized with AgNPs. Data are expressed as mean ± SD of biological replicates.

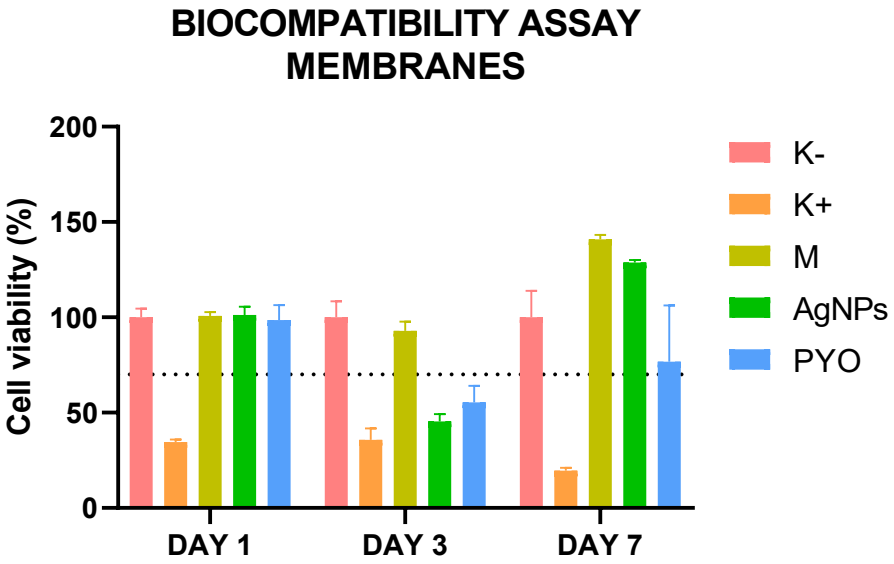

*Figure 61 – **Biocompatibility assay on fibroblasts in contact with the electrospun membranes for skin regeneration and wound healing**.*
The threshold was set at 70%. K^- = cells not in contact with biomaterials (negative controls). K^+ = cells treated with ethanol 70% (positive controls). M = membranes not functionalized with bioactive compounds (control samples). AgNPs = membranes functionalized with AgNPs. PYO = membranes impregnated in phenazine-derivative. Data are expressed as mean ± SD of biological replicates.

Biocompatibility of the scaffolds for bone tissue restoration impregnated with the phenazine derivative was evaluated using human osteoblasts. Cells in contact with the pigment-impregnated scaffolds exhibited viability values above the 70% threshold after 24 hours; however, viability markedly decreased after 72 and 168 hours (*Figure 62*). Control samples (scaffolds without pigment

impregnation) also showed very low compatibility, even at 24 hours. Therefore, it cannot be conclusively stated that the pigment itself lacks biocompatibility, but more analyses should be performed after optimization of the scaffold composition.

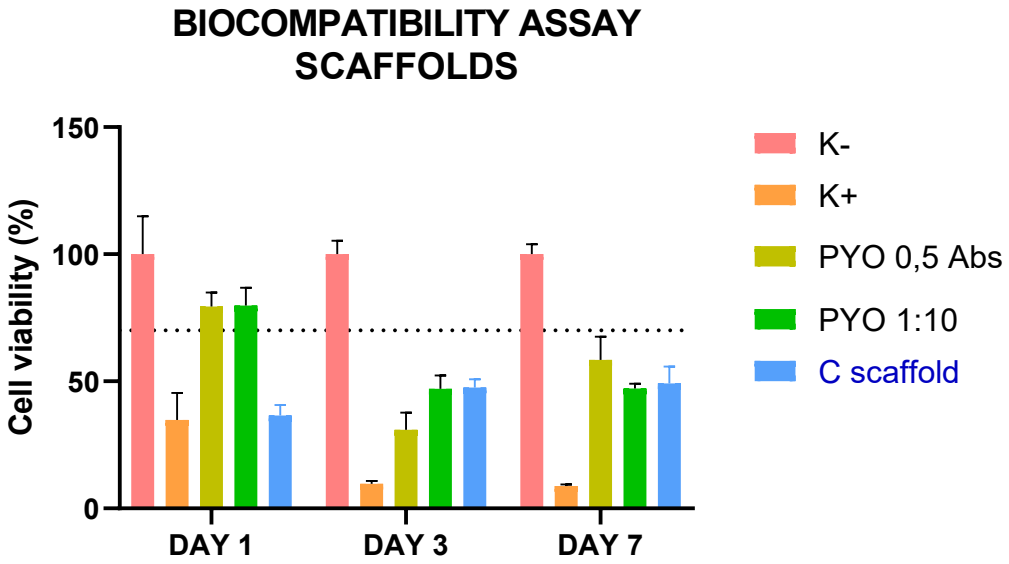

Figure 62 – ***Biocompatibility assay on osteoblasts: preliminary results****.*
The threshold was set at 70%. K^+ = cells treated with ethanol 70% (positive controls). K^- = cells not in contact with biomaterials (negative controls). PYO = scaffolds impregnated in phenazine-derivative. C scaffolds = scaffolds not impregnated into phenazine-derivative (control samples). Data are expressed as mean ± SD of biological replicates.

Toxicity test

Toxicity of the pyocyanin derivative was evaluated on human osteoblasts after 24 and 72 hours of exposure. A range of pigment concentrations from 132,5 to 1,03 µg/ml was tested. Each concentration was compared with a corresponding control containing the same amount of solvent used to solubilize the pigment, to exclude any solvent-derived toxicity. As shown by the results (*Figure 63, a*), cell viability after 24 hours remained above 70% at all tested concentrations, reaching approximately 73% and 78% at 132,5 and 66,25 µg/ml, respectively, and exceeding 85% for the other lower concentrations. After 72 hours (*Figure 63, b*), cell viability remained close to 100% in all cases, suggesting that the molecule did not exert any detectable cytotoxic effect.

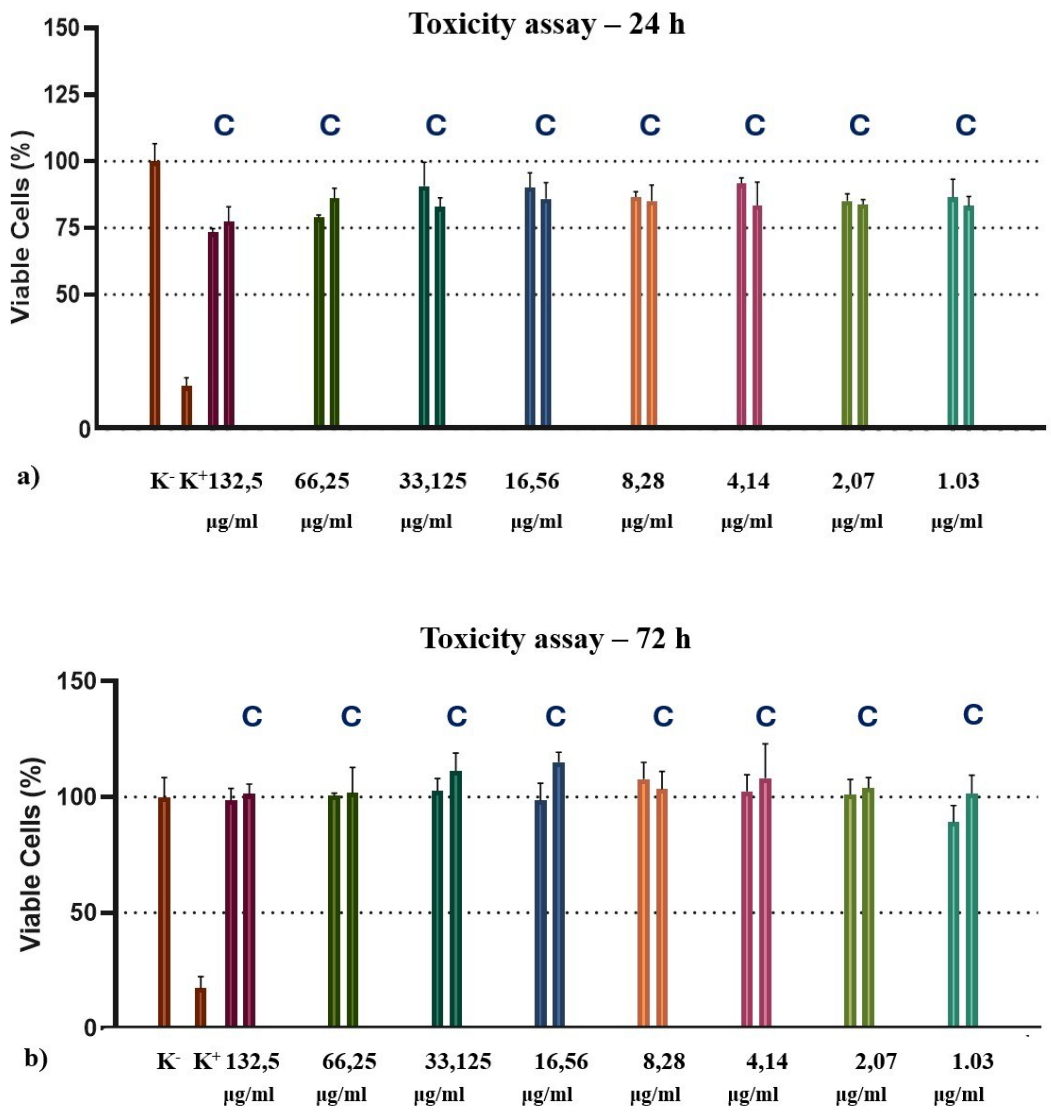

Figure 63 - ***Toxicity assay of the pyocyanin derivative on human osteoblasts after 24 (a) and 72 hours (b) of exposure****.*

A concentration range from 132,5 to 1,03 µg/ml of the pyocyanin derivative was tested. For each concentration, the second bar, indicated with a "C" above,

represents the corresponding control prepared with the same amount of solvent used to solubilize the pigment. K^- = cells not treated with the pigment (negative control). K^+ = cells treated with ethanol 70% (positive control). Data are expressed as mean ± SD of biological replicates.

Discussion

Biomaterials with innovative compositions and fabrication techniques were successfully developed.

The bacterial-derived metabolites were employed for biomaterials functionalization. The chemical characterization of the Antarctic pigment was consistent with the preliminary results obtained in Italy and with the molecular structure of a novel pyocyanin derivative, further confirming its identity *(Koyun et al., 2022)*. Moreover, a novel protocol for AgNPs synthesis was developed using the pyocyanin derivative as reducing agent. The nanoparticles displayed high purity and exhibited an average diameter of 13,07 nm in TEM analyses. The small size of AgNPs is associated with enhanced antimicrobial activity, since particles of approximately 10 nm can penetrate microbial cells and interfere with essential cellular functions *(Mikhailova, 2024)*. In contrast, DLS analysis revealed the presence of two distinct AgNPs populations, with average diameters of 18 nm and 80 nm, respectively, possibly indicating a non-homogenous size distribution or the presence of aggregates that could lead to an overestimation of particle size *(Farkas & Kramar, 2021)*. TEM images also showed a halo surrounding the AgNPs, likely representing the capping layer, a feature known to improve nanoparticles stabilization and biocompatibility *(Cinteza et al., 2018)*.

The electrospun nanofiber membranes generally exhibited a smooth morphology with a limited presence of beads. The nanofibers were organized in a reticular structure, closely resembling the native ECM architecture, which in the dermis is characterized by fibrils typically ranging from 60 to 120 nm *(Sui et al., 2025)*. Despite their potential in wound healing and skin regeneration, further optimization is still required to improve production time and reproducibility of membrane morphology. Standardization of working parameters (humidity, temperature, flow rate, etc.), together with automation of the fabrication workflow could help to address these issues *(Joseph et al., 2019; Keirouz et al., 2020)*.

Only few cases of functionalization using bacterial metabolites have been reported in the literature *(Akpan et al., 2020; Amorim, Fangueiro, et al., 2022; Devi et al., 2024; García-García et al., 2025; J. Lee et al., 2022; Ramos et al., 2022; Sheet et al., 2018)*. The electrospun CS/PEO membranes functionalized with the Antarctic pyocyanin derivative acquired antibacterial activity against *S. aureus*, suggesting efficacy against Gram positive bacteria. This selective effect might be attributed to structural differences in the bacterial membrane that could reduce susceptibility in some species *(Epand et al., 2016)*. A study recently demonstrated that incorporation of 10 wt% of pyocyanin into a polyurethane/dextran electrospun membrane produced a material that displayed high inhibition rates against both *Escherichia coli* and *Staphylococcus aureus (Sheet et al., 2018)*, suggesting that higher concentrations of the molecule could also be effective against Gram-negative species. Functionalization with AgNPs resulted in a limited activity against both *S. aureus* and *E. coli*, indicating a possible effect against a broader spectrum of microorganisms. The antibacterial activity of AgNPs is mediated by their adhesion to bacterial cell walls and

membranes though electrostatic interactions, leading to membrane disruption, increased permeability, ROS production, and cell death. Gram negative bacteria generally exhibit higher susceptibility due to thinner peptidoglycan layers, negatively charged lipopolysaccharides, and the presence of porins facilitating AgNPs entry.*(Mikhailova, 2024)*. Thus, optimization of concentration and handling of the metabolites prior to and during electrospinning will be crucial to enhance bioactivity of the final product. This was also reflected in the preliminary results obtained in the antibiofilm activity assay. Biofilm formation by the tested bacterial species was reduced after functionalization of the biomaterials, although total eradication was not achieved. It has been demonstrated that AgNPs alone exhibit significant antibiofilm activity particularly against Gram-negative pathogens, in a concentration-dependent manner: while low concentrations of AgNPs are insufficient to inhibit microbial growth, concentrations above 100 μg/ml, in contrast, completely block biofilm formation *(Mikhailova, 2024)*.

A study on pyocyanin demonstrated a reduction in bacterial viability of approximately 82% and a decrease in biofilm thickness of approximately 60%, even in resistant pathogens *(Kamer et al., 2023a).* Despite necessity of testing adequate concentrations and optimizing the interactions of the molecule with the biomaterials, the incomplete biofilm reduction could also reflect technical issues during sample manipulation, especially when removing the biomaterials from the agar plates, where accidental scratching of bacterial colonies or cross-contamination between samples may have occurred. However, the antibiofilm activity test should be repeated including all the samples and the proper controls in the analysis.

Scaffolds were successfully fabricated through 3D printing. While various surface functionalization techniques have been developed typically involving growth factors, coatings and nanoparticles, to date, no studies have reported the functionalization of scaffolds with microbial-derived antibacterial agents *(Y. S. Kim & Shin, 2024)*. Functionalization was achieved only by post-printing immersion in the pyocyanin derivative, since attempts to incorporate the pigment into the printing solution were impeded by low residual sample amount. Antimicrobial and antibiofilm assay results were consistent with those obtained for the electrospun membranes.

For both types of tested biomaterials, the biocompatibility assay requires further validation through additional experiments. Different concentrations of AgNPs and the phenazine-derivative should be considered to identify the optimal balance between antimicrobial efficacy and promotion of cell growth and proliferation. This aspect is particularly relevant for pyocyanin-derived compounds, as commercial product data sheets attribute to pyocyanin antibacterial, anti-inflammatory and immunomodulatory activities *(Castañeda-Tamez et al., 2018; Hong et al., 2016; Kamer et al., 2023b)*. However, the reported properties should be interpreted with caution, since pyocyanin is also an established redox-active virulence factor of *P. aeruginosa*, associated with oxidative stress induction, depletion of intracellular antioxidant defenses, accelerated neutrophil apoptosis and cytotoxic effects on host cells *(Arora et al., 2018)*. Moreover, the phenazine derivative investigated in this work was produced by an environmental *Rhodococcus* strain, and this different biological origin may result in distinct functional and toxicological properties. Therefore, the biological effects of pyocyanin-related compounds remain highly dependent

on concentration and biological context, making experimental validation essential for biomedical applications.

Human fibroblasts cultured in contact with membranes functionalized with AgNPs and the phenazine derivative showed viability values above the 70% threshold at 24 and 168 hours. In contrast, cellular viability declined after 72 hours in one experiment. The variability displayed by pyocyanin derivative-functionalized membranes may be attributed to an uneven distribution of the compound across the membrane surface and to structural heterogeneity of the wound dressing material. Variability between replicates has been reported in other studies involving AgNPs-functionalized materials, together with differences in cell viability observed at intermediate time points of incubation *(Iurilli et al., 2025).* The control membranes exhibited high viability values, confirming the overall biocompatibility of the CS_PEO formulation.

In the case of the 3D-printed scaffolds impregnated with the phenazine derivative, results were inconclusive. The osteoblast viability, indeed, decreased markedly even in the untreated control scaffolds, raising concerns regarding the compatibility of the specific formulation used for scaffold fabrication. A work recently demonstrated that 3D-printed scaffolds with 10% alginate/β-tricalcium phosphate exhibited good printability, swelling capability, biocompatibility and nutrient diffusion *(Wu et al., 2024)*. Therefore, optimizing the ratio between the two components, as well as the incorporation strategy of the pyocyanin derivative, may contribute to overcoming the observed limitations. However, preliminary results on osteoblasts suggest that the pyocyanin derivative did not exert any detectable cytotoxic effect within the concentration range of 132,5 and 1,03 μg/ml. These findings are consistent with previous studies that showed no

pyocyanin cytotoxicity at doses ranging from 6,25 and 100 µg/ml *(Shouman et al., 2023)* and cytotoxicity was specifically directed against cancer cells *(Abdelaziz et al., 2022)*..

Several technical challenges emerged during the experimental study, including issues related to cellular conversion of resazurin into resorufin, the limited availability of the pyocyanin derivative compared to the large amounts required for the assays, the prolonged time needed for the fabrication of the electrospun membranes, which had to be repeated several times to improve the synthetic protocol. These issues were further compounded by the limited timeframe available and the need to work in an unfamiliar research environment and field. Despite these challenges, the results presented here should be considered as promising initial steps into an unexplored research area with considerable potential. Further investigation will be essential to fully assess the suitability of these functionalized biomaterials for biomedical applications.

Conclusions

Overall, this research demonstrated that a novel pyocyanin derivative can play a relevant role in the functionalization of polymeric wound dressings and 3D-printed scaffolds. Moreover, it can mediate the biological synthesis of AgNPs with favourable size, capping properties, and antibacterial potential. The promising antimicrobial and putative antioxidant properties of the Antarctic pigment and AgNPs should be further investigated, especially in combination with biomaterials. The biocompatibility of the functionalized biomaterials, particularly the 3D-printed scaffolds, requires further validation.

In conclusion, this research is the result of an important international collaboration that enabled the integration of multidisciplinary expertise and knowledge and development of a highly innovative project. With appropriate follow-up experiments, these functionalized biomaterials could represent a valuable advancement in the field of wound healing and tissue regeneration.

References

Abdelaziz, A. A., Kamer, A. M. A., Al-Monofy, K. B., & Al-Madboly, L. A. (2022). A purified and lyophilized Pseudomonas aeruginosa derived pyocyanin induces promising apoptotic and necrotic activities against MCF-7 human breast adenocarcinoma. *Microbial Cell Factories*, *21*(1), 262. https://doi.org/10.1186/s12934-022-01988-x

Abramenko, N. B., Demidova, T. B., Abkhalimov, E. V., Ershov, B. G., Krysanov, E. Yu., & Kustov, L. M. (2018). Ecotoxicity of different-shaped silver nanoparticles: Case of zebrafish embryos. *Journal of Hazardous Materials*, *347*, 89–94. https://doi.org/10.1016/j.jhazmat.2017.12.060

Agarwal, S., Greiner, A., & Wendorff, J. H. (2013). Functional materials by electrospinning of polymers. *Progress in Polymer Science*, *38*(6), 963–991. https://doi.org/10.1016/j.progpolymsci.2013.02.001

Aghajanyan, A. E., Hambardzumyan, A. A., Hovsepyan, A. S., Asaturian, R. A., Vardanyan, A. A., & Saghiyan, A. A. (2005). Isolation, purification and physicochemical characterization of water-soluble Bacillus thuringiensis melanin. *Pigment Cell Research*, *18*(2), 130–135. https://doi.org/10.1111/j.1600-0749.2005.00211.x

Ahmad, W. A., Yusof, N. Z., Nordin, N., Zakaria, Z. A., & Rezali, M. F. (2012). Production and Characterization of Violacein by Locally Isolated Chromobacterium violaceum Grown in Agricultural Wastes. *Applied Biochemistry and Biotechnology*, *167*(5), 1220–1234. https://doi.org/10.1007/s12010-012-9553-7

Ahmadi Bonakdar, M., & Rodrigue, D. (2024). Electrospinning: Processes, Structures, and Materials. *Macromol*, *4*(1), 58–103. https://doi.org/10.3390/macromol4010004

Ahn, S., Chantre, C. O., Gannon, A. R., Lind, J. U., Campbell, P. H., Grevesse, T., O'Connor, B. B., & Parker, K. K. (2018). Soy Protein/Cellulose Nanofiber Scaffolds Mimicking Skin Extracellular Matrix for Enhanced Wound Healing. *Advanced Healthcare Materials*, *7*(9). https://doi.org/10.1002/adhm.201701175

Akpan, U. M., Pellegrini, M., Obayemi, J. D., Ezenwafor, T., Browl, D., Ani, C. J., Yiporo, D., Salifu, A., Dozie-Nwachukwu, S., Odusanya, S., Freeman, J., & Soboyejo, W. O. (2020). Prodigiosin-loaded electrospun nanofibers scaffold for localized treatment of triple negative breast cancer. *Materials Science and Engineering: C*, *114*, 110976. https://doi.org/10.1016/j.msec.2020.110976

Almadani, Y. H., Vorstenbosch, J., Davison, P. G., & Murphy, A. M. (2021). Wound Healing: A Comprehensive Review. *Seminars in Plastic Surgery*, *35*(03), 141–144. https://doi.org/10.1055/s-0041-1731791

Alven, S., & Aderibigbe, B. A. (2020). Chitosan and Cellulose-Based Hydrogels for Wound Management. *International Journal of Molecular Sciences*, *21*(24), 9656. https://doi.org/10.3390/ijms21249656

Amorim, L. F. A., Fangueiro, R., & Gouveia, I. C. (2022). Novel functional material incorporating flexirubin-type pigment in polyvinyl alcohol_kefiran/polycaprolactone nanofibers. *Journal of Applied Polymer Science*, *139*(48). https://doi.org/10.1002/app.53208

Amorim, L. F. A., Mouro, C., & Gouveia, I. C. (2024). Electrospun fiber materials based on polysaccharides and natural colorants for food packaging applications. *Cellulose*, *31*(10), 6043–6069. https://doi.org/10.1007/s10570-024-05956-z

Amorim, L. F. A., Mouro, C., Riool, M., & Gouveia, I. C. (2022). Antimicrobial Food Packaging Based on Prodigiosin-Incorporated Double-Layered Bacterial Cellulose and Chitosan Composites. *Polymers*, *14*(2), 315. https://doi.org/10.3390/polym14020315

Arora, D., Hall, S., Anoopkumar-Dukie, S., Morrison, R., McFarland, A., Perkins, A. V., Davey, A. K., & Grant, G. D. (2018). Pyocyanin induces systemic oxidative stress, inflammation and behavioral changes *in vivo*. *Toxicology Mechanisms and Methods*, *28*(6), 410–414. https://doi.org/10.1080/15376516.2018.1429038

Arslan, A. K., Aydoğdu, A., Tolunay, T., Basat, Ç., Bircan, R., & Demirbilek, M. (2023). The effect of alginate scaffolds on bone healing in defects formed with drilling model in rat femur diaphysis. *Journal of Biomedical Materials Research Part B: Applied Biomaterials*, *111*(6), 1299–1308. https://doi.org/10.1002/jbm.b.35233

Avossa, J., Pota, G., Vitiello, G., Macagnano, A., Zanfardino, A., Di Napoli, M., Pezzella, A., D'Errico, G., Varcamonti, M., & Luciani, G. (2021). Multifunctional mats by antimicrobial nanoparticles decoration for bioinspired smart wound dressing solutions. *Materials Science and Engineering: C*, *123*, 111954. https://doi.org/10.1016/j.msec.2021.111954

Bahney, C. S., Zondervan, R. L., Allison, P., Theologis, A., Ashley, J. W., Ahn, J., Miclau, T., Marcucio, R. S., & Hankenson, K. D. (2019). Cellular biology of

fracture healing. *Journal of Orthopaedic Research*, *37*(1), 35–50. https://doi.org/10.1002/jor.24170

Bharadwaz, A., & Jayasuriya, A. C. (2020). Recent trends in the application of widely used natural and synthetic polymer nanocomposites in bone tissue regeneration. *Materials Science and Engineering: C*, *110*, 110698. https://doi.org/10.1016/j.msec.2020.110698

Biswal, T., BadJena, S. K., & Pradhan, D. (2020). Sustainable biomaterials and their applications: A short review. *Materials Today: Proceedings*, *30*, 274–282. https://doi.org/10.1016/j.matpr.2020.01.437

Bohner, M., Santoni, B. L. G., & Döbelin, N. (2020). β-tricalcium phosphate for bone substitution: Synthesis and properties. *Acta Biomaterialia*, *113*, 23–41. https://doi.org/10.1016/j.actbio.2020.06.022

Campaña, A. L., Saragliadis, A., Mikheenko, P., & Linke, D. (2023). Insights into the bacterial synthesis of metal nanoparticles. *Frontiers in Nanotechnology*, *5*. https://doi.org/10.3389/fnano.2023.1216921

Castañeda-Tamez, P., Ramírez-Peris, J., Pérez-Velázquez, J., Kuttler, C., Jalalimanesh, A., Saucedo-Mora, M. Á., Jiménez-Cortés, J. G., Maeda, T., González, Y., Tomás, M., Wood, T. K., & García-Contreras, R. (2018). Pyocyanin Restricts Social Cheating in Pseudomonas aeruginosa. *Frontiers in Microbiology*, *9*. https://doi.org/10.3389/fmicb.2018.01348

Chelminiak-Dudkiewicz, D., Wujak, M., Mlynarczyk, D. T., Dlugaszewska, J., Mylkie, K., Smolarkiewicz-Wyczachowski, A., & Ziegler-Borowska, M. (2024). Enhancing the porosity of chitosan sponges with CBD by adding antimicrobial

violacein. *Heliyon*, *10*(15), e35389. https://doi.org/10.1016/j.heliyon.2024.e35389

Chen, C.-Y., Yin, H., Chen, X., Chen, T.-H., Liu, H.-M., Rao, S.-S., Tan, Y.-J., Qian, Y.-X., Liu, Y.-W., Hu, X.-K., Luo, M.-J., Wang, Z.-X., Liu, Z.-Z., Cao, J., He, Z.-H., Wu, B., Yue, T., Wang, Y.-Y., Xia, K., … Xie, H. (2020). Ångstrom-scale silver particle–embedded carbomer gel promotes wound healing by inhibiting bacterial colonization and inflammation. *Science Advances*, *6*(43). https://doi.org/10.1126/sciadv.aba0942

Chen, S., Liu, B., Carlson, M. A., Gombart, A. F., Reilly, D. A., & Xie, J. (2017). Recent Advances in Electrospun Nanofibers for Wound Healing. *Nanomedicine*, *12*(11), 1335–1352. https://doi.org/10.2217/nnm-2017-0017

Choi, S. Y., Yoon, K., Lee, J. Il, & Mitchell, R. J. (2015). Violacein: Properties and Production of a Versatile Bacterial Pigment. *BioMed Research International*, *2015*, 1–8. https://doi.org/10.1155/2015/465056

Chug, M. K., & Brisbois, E. J. (2022). Recent Developments in Multifunctional Antimicrobial Surfaces and Applications toward Advanced Nitric Oxide-Based Biomaterials. *ACS Materials Au*, *2*(5), 525–551. https://doi.org/10.1021/acsmaterialsau.2c00040

Cinteza, L. O., Scomoroscenco, C., Voicu, S. N., Nistor, C. L., Nitu, S. G., Trica, B., Jecu, M.-L., & Petcu, C. (2018). Chitosan-Stabilized Ag Nanoparticles with Superior Biocompatibility and Their Synergistic Antibacterial Effect in Mixtures with Essential Oils. *Nanomaterials*, *8*(10), 826. https://doi.org/10.3390/nano8100826

Cleeton, C., Keirouz, A., Chen, X., & Radacsi, N. (2019). Electrospun Nanofibers for Drug Delivery and Biosensing. *ACS Biomaterials Science & Engineering*, *5*(9), 4183–4205. https://doi.org/10.1021/acsbiomaterials.9b00853

Correa-Llantén, D. N., Amenábar, M. J., & Blamey, J. M. (2012). Antioxidant capacity of novel pigments from an Antarctic bacterium. *Journal of Microbiology*, *50*(3), 374–379. https://doi.org/10.1007/s12275-012-2029-1

Das, D., & Paul, P. (2025). Environmental impact of silver nanoparticles and its sustainable mitigation by novel approach of green chemistry. *Plant Nano Biology*, *14*, 100210. https://doi.org/10.1016/j.plana.2025.100210

de Faria, A. F., Perreault, F., Shaulsky, E., Arias Chavez, L. H., & Elimelech, M. (2015). Antimicrobial Electrospun Biopolymer Nanofiber Mats Functionalized with Graphene Oxide–Silver Nanocomposites. *ACS Applied Materials & Interfaces*, *7*(23), 12751–12759. https://doi.org/10.1021/acsami.5b01639

De Pace, R., Molinari, S., Mazzoni, E., & Perale, G. (2025). Bone Regeneration: A Review of Current Treatment Strategies. *Journal of Clinical Medicine*, *14*(6), 1838. https://doi.org/10.3390/jcm14061838

Devi, M., Ramakrishnan, E., Deka, S., & Parasar, D. P. (2024). Bacteria as a source of biopigments and their potential applications. *Journal of Microbiological Methods*, *219*, 106907. https://doi.org/10.1016/j.mimet.2024.106907

Di Bella, D., Ferreira, J. P. S., Silva, R. de N. O., Echem, C., Milan, A., Akamine, E. H., Carvalho, M. H., & Rodrigues, S. F. (2021). Gold nanoparticles reduce inflammation in cerebral microvessels of mice with sepsis. *Journal of Nanobiotechnology*, *19*(1), 52. https://doi.org/10.1186/s12951-021-00796-6

Díaz-Ruiz, C., Montaner, B., & Pérez-Tomás, R. (2001). Prodigiosin induces cell death and morphological changes indicative of apoptosis in gastric cancer cell line HGT-1. *Histology and Histopathology*, *16*(2), 415–421. https://doi.org/10.14670/HH-16.415

Dong, H., Feng, C., Zhu, J., Gu, X., Cai, X., Qian, H., Gao, Y., Tan, Z., Cao, Y., Xie, W., Lu, X., Zhou, Y., Xu, J., Ma, S., Yang, S., Shi, Y., Shi, M., Yu, H., Jiang, D., … Wu, L. (2024). Ultrasmall gold Nanoparticles/Carboxymethyl chitosan composite hydrogel: Tough, restorable, biocompatible antimicrobial dressing for wound healing. *Applied Materials Today*, *38*, 102206. https://doi.org/10.1016/j.apmt.2024.102206

Dong, H., Wang, D., Sun, G., & Hinestroza, J. P. (2008). Assembly of Metal Nanoparticles on Electrospun Nylon 6 Nanofibers by Control of Interfacial Hydrogen-Bonding Interactions. *Chemistry of Materials*, *20*(21), 6627–6632. https://doi.org/10.1021/cm801077p

Duarte, A. W. F., de Menezes, G. C. A., e Silva, T. R., Bicas, J. L., Oliveira, V. M., & Rosa, L. H. (2019). Antarctic Fungi as Producers of Pigments. In *Fungi of Antarctica* (pp. 305–318). Springer International Publishing. https://doi.org/10.1007/978-3-030-18367-7_14

Durán, N., Nakazato, G., Durán, M., Berti, I. R., Castro, G. R., Stanisic, D., Brocchi, M., Fávaro, W. J., Ferreira-Halder, C. V., Justo, G. Z., & Tasic, L. (2021). Multi-target drug with potential applications: violacein in the spotlight. *World Journal of Microbiology and Biotechnology*, *37*(9), 151. https://doi.org/10.1007/s11274-021-03120-4

Epand, R. M., Walker, C., Epand, R. F., & Magarvey, N. A. (2016). Molecular mechanisms of membrane targeting antibiotics. *Biochimica et Biophysica Acta (BBA) - Biomembranes*, *1858*(5), 980–987. https://doi.org/10.1016/j.bbamem.2015.10.018

Ermini, M. L., & Voliani, V. (2021). Antimicrobial Nano-Agents: The Copper Age. *ACS Nano*, *15*(4), 6008–6029. https://doi.org/10.1021/acsnano.0c10756

Eslaminezhad, S., Moradi, F., & Hojjati, M. R. (2024). Evaluation of the wound healing efficacy of new antibacterial polymeric nanofiber based on polyethylene oxide coated with copper nanoparticles and defensin peptide: An in-vitro to in-vivo assessment. *Heliyon*, *10*(8), e29542. https://doi.org/10.1016/j.heliyon.2024.e29542

Etale, A., Onyianta, A. J., Turner, S. R., & Eichhorn, S. J. (2023). Cellulose: A Review of Water Interactions, Applications in Composites, and Water Treatment. *Chemical Reviews*, *123*(5), 2016–2048. https://doi.org/10.1021/acs.chemrev.2c00477

Farkas, N., & Kramar, J. A. (2021). Dynamic light scattering distributions by any means. *Journal of Nanoparticle Research*, *23*(5), 120. https://doi.org/10.1007/s11051-021-05220-6

Francisco, M. J., Cabral, C. S. D., Ferreira, P., Correia, I. J., & Moreira, A. F. (2026). Beeswax-enriched tricalcium phosphate/hydroxyapatite/sodium alginate/thymol 3D-printed scaffolds for application in bone tissue engineering. *Biomaterials Advances*, *178*, 214440. https://doi.org/10.1016/j.bioadv.2025.214440

García-García, M., Jaime-Ferrer, J. S., Medrano-Lango, F. N., Quintana-Rodríguez, E., Campos-García, T., Rodríguez-Sevilla, E., & Orona-Tamayo, D. (2025).

Electrospun Membranes Loaded with Melanin Derived from Pecan Nutshell (Carya illinoinensis) Residues for Skin-Care Applications. *Membranes*, *15*(2), 44. https://doi.org/10.3390/membranes15020044

Ghasemian Lemraski, E., Jahangirian, H., Dashti, M., Khajehali, E., Sharafinia, Mis. S., Rafiee-Moghaddam, R., & Webster, T. J. (2021). Antimicrobial Double-Layer Wound Dressing Based on Chitosan/Polyvinyl Alcohol/Copper: In vitro and in vivo Assessment. *International Journal of Nanomedicine*, *Volume 16*, 223–235. https://doi.org/10.2147/IJN.S266692

Girma, A. (2023). Alternative mechanisms of action of metallic nanoparticles to mitigate the global spread of antibiotic-resistant bacteria. *The Cell Surface*, *10*, 100112. https://doi.org/10.1016/j.tcsw.2023.100112

Gorgieva, S., & Trček, J. (2019). Bacterial Cellulose: Production, Modification and Perspectives in Biomedical Applications. *Nanomaterials*, *9*(10), 1352. https://doi.org/10.3390/nano9101352

Gushiken, L. F. S., Beserra, F. P., Bastos, J. K., Jackson, C. J., & Pellizzon, C. H. (2021). Cutaneous Wound Healing: An Update from Physiopathology to Current Therapies. *Life*, *11*(7), 665. https://doi.org/10.3390/life11070665

Haidari, H., Bright, R., Strudwick, X. L., Garg, S., Vasilev, K., Cowin, A. J., & Kopecki, Z. (2021). Multifunctional ultrasmall AgNP hydrogel accelerates healing of S. aureus infected wounds. *Acta Biomaterialia*, *128*, 420–434. https://doi.org/10.1016/j.actbio.2021.04.007

Haidari, H., Kopecki, Z., Bright, R., Cowin, A. J., Garg, S., Goswami, N., & Vasilev, K. (2020). Ultrasmall AgNP-Impregnated Biocompatible Hydrogel with Highly

Effective Biofilm Elimination Properties. *ACS Applied Materials & Interfaces*, *12*(37), 41011–41025. https://doi.org/10.1021/acsami.0c09414

Hamdan, N., Yamin, A., Hamid, S. A., Khodir, W. K. W. A., & Guarino, V. (2021). Functionalized Antimicrobial Nanofibers: Design Criteria and Recent Advances. *Journal of Functional Biomaterials*, *12*(4), 59. https://doi.org/10.3390/jfb12040059

Hashem, A. H., Shehabeldine, A. M., Ali, O. M., & Salem, S. S. (2022). Synthesis of Chitosan-Based Gold Nanoparticles: Antimicrobial and Wound-Healing Activities. *Polymers*, *14*(11), 2293. https://doi.org/10.3390/polym14112293

Hong, Y., Chen, C., Guo, W., Zhao, L., Mei, F., Xiang, M., & Wang, W. (2016). Effects of Castanospermine on Inflammatory Response in a Rat Model of Experimental Severe Acute Pancreatitis. *Archives of Medical Research*, *47*(6), 436–445. https://doi.org/10.1016/j.arcmed.2016.11.007

Huang, D., Dang, F., Huang, Y., Chen, N., & Zhou, D. (2022). Uptake, translocation, and transformation of silver nanoparticles in plants. *Environmental Science: Nano*, *9*(1), 12–39. https://doi.org/10.1039/D1EN00870F

Huang, W., Wan, Y., Zhang, S., Wang, C., Zhang, Z., Su, H., Xiong, P., & Hou, F. (2024). Recent Advances in Phenazine Natural Products: Chemical Structures and Biological Activities. *Molecules*, *29*(19), 4771. https://doi.org/10.3390/molecules29194771

Huang, X., Gan, L., He, Z., Jiang, G., & He, T. (2024). Bacterial Pigments as a Promising Alternative to Synthetic Colorants: From Fundamentals to Applications. *Journal of Microbiology and Biotechnology*, *34*(11), 2153–2165. https://doi.org/10.4014/jmb.2404.04018

Islan, G. A., Rodenak-Kladniew, B., Noacco, N., Duran, N., & Castro, G. R. (2022). Prodigiosin: a promising biomolecule with many potential biomedical applications. *Bioengineered*, *13*(6), 14227–14258. https://doi.org/10.1080/21655979.2022.2084498

Iurilli, M., Porrelli, D., Turco, G., Lagatolla, C., Camurri Piloni, A., Medagli, B., Nicolin, V., & Papa, G. (2025). Electrospun Collagen-Coated Nanofiber Membranes Functionalized with Silver Nanoparticles for Advanced Wound Healing Applications. *Membranes*, *15*(2), 39. https://doi.org/10.3390/membranes15020039

Jamkhande, P. G., Ghule, N. W., Bamer, A. H., & Kalaskar, M. G. (2019). Metal nanoparticles synthesis: An overview on methods of preparation, advantages and disadvantages, and applications. *Journal of Drug Delivery Science and Technology*, *53*, 101174. https://doi.org/10.1016/j.jddst.2019.101174

Jassim, A. Y., Wang, J., Chung, K. W., Loosli, F., Chanda, A., Scott, G. I., & Baalousha, M. (2022). Comparative assessment of the fate and toxicity of chemically and biologically synthesized silver nanoparticles to juvenile clams. *Colloids and Surfaces B: Biointerfaces*, *209*, 112173. https://doi.org/10.1016/j.colsurfb.2021.112173

John Jimtha, C., Jishma, P., Sreelekha, S., Chithra, S., & Radhakrishnan, EK. (2017). Antifungal properties of prodigiosin producing rhizospheric Serratia sp. *Rhizosphere*, *3*, 105–108. https://doi.org/10.1016/j.rhisph.2017.02.003

John, M. S., Nagoth, J. A., Ramasamy, K. P., Mancini, A., Giuli, G., Miceli, C., & Pucciarelli, S. (2022). Synthesis of Bioactive Silver Nanoparticles Using New

Bacterial Strains from an Antarctic Consortium. *Marine Drugs*, *20*(9), 558. https://doi.org/10.3390/md20090558

John, M. S., Nagoth, J. A., Ramasamy, K. P., Mancini, A., Giuli, G., Natalello, A., Ballarini, P., Miceli, C., & Pucciarelli, S. (2020). Synthesis of Bioactive Silver Nanoparticles by a Pseudomonas Strain Associated with the Antarctic Psychrophilic Protozoon Euplotes focardii. *Marine Drugs*, *18*(1), 38. https://doi.org/10.3390/md18010038

Joseph, B., Augustine, R., Kalarikkal, N., Thomas, S., Seantier, B., & Grohens, Y. (2019). Recent advances in electrospun polycaprolactone based scaffolds for wound healing and skin bioengineering applications. *Materials Today Communications*, *19*, 319–335. https://doi.org/10.1016/j.mtcomm.2019.02.009

Kadhim, R. J., Karsh, E. H., Taqi, Z. J., & Jabir, M. S. (2021). Biocompatibility of gold nanoparticles: In-vitro and In-vivo study. *Materials Today: Proceedings*, *42*, 3041–3045. https://doi.org/10.1016/j.matpr.2020.12.826

Kalijaga, M. H. A., Nurrochman, A., Annur, D., Sari, W. R., Sumboja, A., & Prajatelistia, E. (2024). CeO2-loaded PVA/GelMA core-shell nanofiber membrane to promote wound healing. *Polymer*, *307*, 127320. https://doi.org/10.1016/j.polymer.2024.127320

Kamer, A. M. A., Abdelaziz, A. A., Al-Monofy, K. B., & Al-Madboly, L. A. (2023a). Antibacterial, antibiofilm, and anti-quorum sensing activities of pyocyanin against methicillin-resistant Staphylococcus aureus: in vitro and in vivo study. *BMC Microbiology*, *23*(1), 116. https://doi.org/10.1186/s12866-023-02861-6

Karunakaran, G., Sudha, K. G., Ali, S., & Cho, E.-B. (2023). Biosynthesis of Nanoparticles from Various Biological Sources and Its Biomedical Applications. *Molecules*, *28*(11), 4527. https://doi.org/10.3390/molecules28114527

Keirouz, A., Chung, M., Kwon, J., Fortunato, G., & Radacsi, N. (2020). 2D and 3D electrospinning technologies for the fabrication of nanofibrous scaffolds for skin tissue engineering: A review. *WIREs Nanomedicine and Nanobiotechnology*, *12*(4). https://doi.org/10.1002/wnan.1626

Khan, M. U. A., Aslam, M. A., Bin Abdullah, M. F., Hasan, A., Shah, S. A., & Stojanović, G. M. (2023). Recent perspective of polymeric biomaterial in tissue engineering– a review. *Materials Today Chemistry*, *34*, 101818. https://doi.org/10.1016/j.mtchem.2023.101818

Khursheed, R., Dua, K., Vishwas, S., Gulati, M., Jha, N. K., Aldhafeeri, G. M., Alanazi, F. G., Goh, B. H., Gupta, G., Paudel, K. R., Hansbro, P. M., Chellappan, D. K., & Singh, S. K. (2022). Biomedical applications of metallic nanoparticles in cancer: Current status and future perspectives. *Biomedicine & Pharmacotherapy*, *150*, 112951. https://doi.org/10.1016/j.biopha.2022.112951

Kim, H. D., Amirthalingam, S., Kim, S. L., Lee, S. S., Rangasamy, J., & Hwang, N. S. (2017). Biomimetic Materials and Fabrication Approaches for Bone Tissue Engineering. *Advanced Healthcare Materials*, *6*(23). https://doi.org/10.1002/adhm.201700612

Kim, J.-C., Lee, I.-C., Ko, J.-W., Park, S.-H., Lim, J.-O., Shin, I.-S., Moon, C., Kim, S.-H., & Her, J.-D. (2016). Comparative toxicity and biodistribution of copper nanoparticles and cupric ions in rats. *International Journal of Nanomedicine*, 2883. https://doi.org/10.2147/IJN.S106346

Kim, Y. S., & Shin, Y. S. (2024). Surface Functionalization of 3D-Printed Bio-Inspired Scaffolds for Biomedical Applications: A Review. *Biomimetics*, *9*(11), 703. https://doi.org/10.3390/biomimetics9110703

Koyun, M. T., Sirin, S., Erdem, S. A., & Aslim, B. (2022). Pyocyanin Isolated from Pseudomonas aeruginosa: Characterization, Biological Activity and Its Role in Cancer and Neurodegenerative Diseases. *Brazilian Archives of Biology and Technology*, *65*. https://doi.org/10.1590/1678-4324-2022210651

Krishna, D. V., Sankar, M. R., Sarma, P. V. G. K., & Samundeshwari, E. L. (2024). Copper nanoparticles loaded gelatin/ polyvinyl alcohol/ guar gum-based 3D printable multimaterial hydrogel for tissue engineering applications. *International Journal of Biological Macromolecules*, *276*, 133866. https://doi.org/10.1016/j.ijbiomac.2024.133866

Lazaro, J. E. H., Nitcheu, J., Predicala, R. Z., Mangalindan, G. C., Nesslany, F., Marzin, D., Concepcion, G. P., & Diquet, B. (2002). Heptyl prodigiosin, a bacterial metabolite, is antimalarial in vivo and non-mutagenic in vitro. *Journal of Natural Toxins*, *11*(4), 367–377.

Lee, J., Bae, J., Youn, D.-Y., Ahn, J., Hwang, W.-T., Bae, H., Bae, P. K., & Kim, I.-D. (2022). Violacein-embedded nanofiber filters with antiviral and antibacterial activities. *Chemical Engineering Journal*, *444*, 136460. https://doi.org/10.1016/j.cej.2022.136460

Letelier, M. E., Sánchez-Jofré, S., Peredo-Silva, L., Cortés-Troncoso, J., & Aracena-Parks, P. (2010). Mechanisms underlying iron and copper ions toxicity in biological systems: Pro-oxidant activity and protein-binding effects. *Chemico-*

Biological Interactions, *188*(1), 220–227. https://doi.org/10.1016/j.cbi.2010.06.013

Li, J., Wang, Y., Yang, J., & Liu, W. (2021). Bacteria activated-macrophage membrane-coated tough nanocomposite hydrogel with targeted photothermal antibacterial ability for infected wound healing. *Chemical Engineering Journal*, *420*, 127638. https://doi.org/10.1016/j.cej.2020.127638

Li, W., Cao, Z., Liu, R., Liu, L., Li, H., Li, X., Chen, Y., Lu, C., & Liu, Y. (2019). AuNPs as an important inorganic nanoparticle applied in drug carrier systems. *Artificial Cells, Nanomedicine, and Biotechnology*, *47*(1), 4222–4233. https://doi.org/10.1080/21691401.2019.1687501

Li, X., Robinson, S. M., Gupta, A., Saha, K., Jiang, Z., Moyano, D. F., Sahar, A., Riley, M. A., & Rotello, V. M. (2014). Functional Gold Nanoparticles as Potent Antimicrobial Agents against Multi-Drug-Resistant Bacteria. *ACS Nano*, *8*(10), 10682–10686. https://doi.org/10.1021/nn5042625

Li, Z., Zhang, Q., Jiang, Q., Zhan, G., & Li, D. (2019). The enhancement of iron fuel cell on bio-cathode denitrification and its mechanism as well as the microbial community analysis of bio-cathode. *Bioresource Technology*, *274*, 1–8. https://doi.org/10.1016/j.biortech.2018.11.070

Liang, Y., Liang, Y., Zhang, H., & Guo, B. (2022). Antibacterial biomaterials for skin wound dressing. *Asian Journal of Pharmaceutical Sciences*, *17*(3), 353–384. https://doi.org/10.1016/j.ajps.2022.01.001

Lopes, F. C., & Ligabue-Braun, R. (2021). Agro-Industrial Residues: Eco-Friendly and Inexpensive Substrates for Microbial Pigments Production. *Frontiers in Sustainable Food Systems*, *5*. https://doi.org/10.3389/fsufs.2021.589414

Luo, L., Huang, W., Zhang, J., Yu, Y., & Sun, T. (2024). Metal-Based Nanoparticles as Antimicrobial Agents: A Review. *ACS Applied Nano Materials*, *7*(3), 2529–2545. https://doi.org/10.1021/acsanm.3c05615

Maliszewska, I., & Czapka, T. (2022). Electrospun Polymer Nanofibers with Antimicrobial Activity. *Polymers*, *14*(9), 1661. https://doi.org/10.3390/polym14091661

Marey, M. A., Abozahra, R., El-Nikhely, N. A., Kamal, M. F., Abdelhamid, S. M., & El-Kholy, M. A. (2024). Transforming microbial pigment into therapeutic revelation: extraction and characterization of pyocyanin from Pseudomonas aeruginosa and its therapeutic potential as an antibacterial and anticancer agent. *Microbial Cell Factories*, *23*(1), 174. https://doi.org/10.1186/s12934-024-02438-6

Maruyama, M., Rhee, C., Utsunomiya, T., Zhang, N., Ueno, M., Yao, Z., & Goodman, S. B. (2020). Modulation of the Inflammatory Response and Bone Healing. *Frontiers in Endocrinology*, *11*. https://doi.org/10.3389/fendo.2020.00386

Miguel, S. P., Simões, D., Moreira, A. F., Sequeira, R. S., & Correia, I. J. (2019). Production and characterization of electrospun silk fibroin based asymmetric membranes for wound dressing applications. *International Journal of Biological Macromolecules*, *121*, 524–535. https://doi.org/10.1016/j.ijbiomac.2018.10.041

Mikhailova, E. O. (2024). Green Silver Nanoparticles: An Antibacterial Mechanism. *Antibiotics*, *14*(1), 5. https://doi.org/10.3390/antibiotics14010005

Mogadem, A., Almamary, M. A., Mahat, N. A., Jemon, K., Ahmad, W. A., & Ali, I. (2021). Antioxidant Activity Evaluation of FlexirubinType Pigment from

Chryseobacterium artocarpi CECT 8497 and Related Docking Study. *Molecules*, *26*(4), 979. https://doi.org/10.3390/molecules26040979

Mogadem, A., Naqvi, A., Almamary, M. A., Ahmad, W. A., Jemon, K., & El-Alfy, S. H. (2022). Hepatoprotective effects of flexirubin, a novel pigment from Chryseobacterium artocarpi, against carbon tetrachloride-induced liver injury: An in vivo study and molecular modeling. *Toxicology and Applied Pharmacology*, *444*, 116022. https://doi.org/10.1016/j.taap.2022.116022

Mudaliar, S. B., & Bharath Prasad, A. S. (2024). A biomedical perspective of pyocyanin from Pseudomonas aeruginosa: its applications and challenges. *World Journal of Microbiology and Biotechnology*, *40*(3), 90. https://doi.org/10.1007/s11274-024-03889-0

Mulholland, E. J. (2020). Electrospun Biomaterials in the Treatment and Prevention of Scars in Skin Wound Healing. *Frontiers in Bioengineering and Biotechnology*, *8*. https://doi.org/10.3389/fbioe.2020.00481

Munhoz, L. L. S., Alves, M. T. O., Alves, B. C., Nascimento, M. G. F. S., Sábio, R. M., Manieri, K. F., Barud, H. S., Esquisatto, M. A. M., Aro, A. A., de Roch Casagrande, L., Silveira, P. C. L., Santos, G. M. T., Andrade, T. A. M., & Caetano, G. F. (2023). Bacterial cellulose membrane incorporated with silver nanoparticles for wound healing in animal model. *Biochemical and Biophysical Research Communications*, *654*, 47–54. https://doi.org/10.1016/j.bbrc.2023.02.058

Numan, M., Bashir, S., Mumtaz, R., Tayyab, S., Rehman, N. U., Khan, A. L., Shinwari, Z. K., & Al-Harrasi, A. (2018). Therapeutic applications of bacterial

pigments: a review of current status and future opportunities. *3 Biotech*, *8*(4), 207. https://doi.org/10.1007/s13205-018-1227-x

Nune, M., Manchineella, S., T., G., & K.S., N. (2019). Melanin incorporated electroactive and antioxidant silk fibroin nanofibrous scaffolds for nerve tissue engineering. *Materials Science and Engineering: C*, *94*, 17–25. https://doi.org/10.1016/j.msec.2018.09.014

Órdenes-Aenishanslins, N., Anziani-Ostuni, G., Vargas-Reyes, M., Alarcón, J., Tello, A., & Pérez-Donoso, J. M. (2016). Pigments from UV-resistant Antarctic bacteria as photosensitizers in Dye Sensitized Solar Cells. *Journal of Photochemistry and Photobiology B: Biology*, *162*, 707–714. https://doi.org/10.1016/j.jphotobiol.2016.08.004

Palani, N., Vijayakumar, P., Monisha, P., Ayyadurai, S., & Rajadesingu, S. (2024). Electrospun nanofibers synthesized from polymers incorporated with bioactive compounds for wound healing. *Journal of Nanobiotechnology*, *22*(1), 211. https://doi.org/10.1186/s12951-024-02491-8

Park, H., Park, S., Yang, Y.-H., & Choi, K.-Y. (2021). Microbial synthesis of violacein pigment and its potential applications. *Critical Reviews in Biotechnology*, *41*(6), 879–901. https://doi.org/10.1080/07388551.2021.1892579

Pauer, H., Hardoim, C. C. P., Teixeira, F. L., Miranda, K. R., Barbirato, D. da S., Carvalho, D. P. de, Antunes, L. C. M., Leitão, Á. A. da C., Lobo, L. A., & Domingues, R. M. C. P. (2018). Impact of violacein from Chromobacterium violaceum on the mammalian gut microbiome. *PLOS ONE*, *13*(9), e0203748. https://doi.org/10.1371/journal.pone.0203748

Pavan, M. E., López, N. I., & Pettinari, M. J. (2020). Correction to: Melanin biosynthesis in bacteria, regulation and production perspectives. *Applied Microbiology and Biotechnology*, *104*(4), 1821–1822. https://doi.org/10.1007/s00253-019-10331-1

Peña, B., Maldonado, M., Bonham, A. J., Aguado, B. A., Dominguez-Alfaro, A., Laughter, M., Rowland, T. J., Bardill, J., Farnsworth, N. L., Alegret Ramon, N., Taylor, M. R. G., Anseth, K. S., Prato, M., Shandas, R., McKinsey, T. A., Park, D., & Mestroni, L. (2019). Gold Nanoparticle-Functionalized Reverse Thermal Gel for Tissue Engineering Applications. *ACS Applied Materials & Interfaces*, *11*(20), 18671–18680. https://doi.org/10.1021/acsami.9b00666

Peng, J., Liu, C., Mo, M., Huang, Y., Lu, Y., Xiao, M., Zhao, X., Ruan, Q., & Ti, H. (2024). Construction of multifunctional hydrogel containing pH-responsive gold nanozyme for bacteria-infected wound healing. *International Journal of Biological Macromolecules*, *283*, 137746. https://doi.org/10.1016/j.ijbiomac.2024.137746

Periferakis, A., Periferakis, A.-T., Troumpata, L., Dragosloveanu, S., Timofticiuc, I.-A., Georgatos-Garcia, S., Scheau, A.-E., Periferakis, K., Caruntu, A., Badarau, I. A., Scheau, C., & Caruntu, C. (2024). Use of Biomaterials in 3D Printing as a Solution to Microbial Infections in Arthroplasty and Osseous Reconstruction. *Biomimetics*, *9*(3), 154. https://doi.org/10.3390/biomimetics9030154

Poomrattanangoon, S., & Pissuwan, D. (2024). Gold nanoparticles coated with collagen-I and their wound healing activity in human skin fibroblast cells. *Heliyon*, *10*(13), e33302. https://doi.org/10.1016/j.heliyon.2024.e33302

Qin, W., Wu, Y., Liu, J., Yuan, X., & Gao, J. (2022). A Comprehensive Review of the Application of Nanoparticles in Diabetic Wound Healing: Therapeutic Potential and Future Perspectives. *International Journal of Nanomedicine*, *Volume 17*, 6007–6029. https://doi.org/10.2147/IJN.S386585

Rajan, R., Huo, P., Chandran, K., Manickam Dakshinamoorthi, B., Yun, S.-I., & Liu, B. (2022). A review on the toxicity of silver nanoparticles against different biosystems. *Chemosphere*, *292*, 133397. https://doi.org/10.1016/j.chemosphere.2021.133397

Ramos, S. dos P., Trindade, L. G. da, Mazzo, T. M., Longo, E., Bonsanto, F. P., de Rosso, V. V., & Braga, A. R. C. (2022). Electrospinning Composites as Carriers of Natural Pigment: Screening of Polymeric Blends. *Processes*, *10*(12), 2737. https://doi.org/10.3390/pr10122737

Rana, A. K., Gupta, V. K., Hart, P., & Thakur, V. K. (2024). Cellulose-alginate hydrogels and their nanocomposites for water remediation and biomedical applications. *Environmental Research*, *243*, 117889. https://doi.org/10.1016/j.envres.2023.117889

Rather, L. J., Mir, S. S., Ganie, S. A., Shahid-ul-Islam, & Li, Q. (2023). Research progress, challenges, and perspectives in microbial pigment production for industrial applications - A review. *Dyes and Pigments*, *210*, 110989. https://doi.org/10.1016/j.dyepig.2022.110989

Rojo, L., García-Fernández, L., Aguilar, M. R., & Vázquez-Lasa, B. (2022). Antimicrobial polymeric biomaterials based on synthetic, nanotechnology, and biotechnological approaches. *Current Opinion in Biotechnology*, *76*, 102752. https://doi.org/10.1016/j.copbio.2022.102752

Salvo, J., & Sandoval, C. (2022). Role of copper nanoparticles in wound healing for chronic wounds: literature review. *Burns & Trauma*, *10*. https://doi.org/10.1093/burnst/tkab047

Sen, C. K., Gordillo, G. M., Roy, S., Kirsner, R., Lambert, L., Hunt, T. K., Gottrup, F., Gurtner, G. C., & Longaker, M. T. (2009). Human skin wounds: A major and snowballing threat to public health and the economy. *Wound Repair and Regeneration*, *17*(6), 763–771. https://doi.org/10.1111/j.1524-475X.2009.00543.x

Shafiee, A., & Atala, A. (2017). Tissue Engineering: Toward a New Era of Medicine. *Annual Review of Medicine*, *68*(1), 29–40. https://doi.org/10.1146/annurev-med-102715-092331

Sheet, S., Vinothkannan, M., Balasubramaniam, S., Subramaniyan, S. A., Acharya, S., & Lee, Y. S. (2018). Highly Flexible Electrospun Hybrid (Polyurethane/Dextran/Pyocyanin) Membrane for Antibacterial Activity via Generation of Oxidative Stress. *ACS Omega*, *3*(11), 14551–14561. https://doi.org/10.1021/acsomega.8b01607

Shouman, H., Said, H. S., Kenawy, H. I., & Hassan, R. (2023). Molecular and biological characterization of pyocyanin from clinical and environmental Pseudomonas aeruginosa. *Microbial Cell Factories*, *22*(1), 166. https://doi.org/10.1186/s12934-023-02169-0

Silva, I. G. R. da, Pantoja, B. T. dos S., Almeida, G. H. D. R., Carreira, A. C. O., & Miglino, M. A. (2022). Bacterial Cellulose and ECM Hydrogels: An Innovative Approach for Cardiovascular Regenerative Medicine. *International Journal of Molecular Sciences*, *23*(7), 3955. https://doi.org/10.3390/ijms23073955

Silva, T. R. e, Silva, L. C. F., de Queiroz, A. C., Alexandre Moreira, M. S., de Carvalho Fraga, C. A., de Menezes, G. C. A., Rosa, L. H., Bicas, J., de Oliveira, V. M., & Duarte, A. W. F. (2021). Pigments from Antarctic bacteria and their biotechnological applications. *Critical Reviews in Biotechnology*, *41*(6), 809–826. https://doi.org/10.1080/07388551.2021.1888068

Silva-Barroso, A. S., Cabral, C. S. D., Ferreira, P., Moreira, A. F., & Correia, I. J. (2023). Lignin-enriched tricalcium phosphate/sodium alginate 3D scaffolds for application in bone tissue regeneration. *International Journal of Biological Macromolecules*, *239*, 124258. https://doi.org/10.1016/j.ijbiomac.2023.124258

Singh, K. R., Nayak, V., Singh, J., Singh, A. K., & Singh, R. P. (2021). Potentialities of bioinspired metal and metal oxide nanoparticles in biomedical sciences. *RSC Advances*, *11*(40), 24722–24746. https://doi.org/10.1039/D1RA04273D

Singh, P., Kim, Y.-J., Zhang, D., & Yang, D.-C. (2016). Biological Synthesis of Nanoparticles from Plants and Microorganisms. *Trends in Biotechnology*, *34*(7), 588–599. https://doi.org/10.1016/j.tibtech.2016.02.006

Skočaj, M. (2019). Bacterial nanocellulose in papermaking. *Cellulose*, *26*(11), 6477–6488. https://doi.org/10.1007/s10570-019-02566-y

Song, K., Wu, Q., Qi, Y., & Kärki, T. (2017). Electrospun nanofibers with antimicrobial properties. In *Electrospun Nanofibers* (pp. 551–569). Elsevier. https://doi.org/10.1016/B978-0-08-100907-9.00020-9

Sui, J., Pragnere, S., & Kurniawan, N. A. (2025). Revisiting the biophysical aspects of extracellular-matrix-mimicking hydrogels: what cells see *vs.* what cells feel. *Biomaterials Science*, *13*(19), 5297–5324. https://doi.org/10.1039/D5BM00210A

Sulaeva, I., Henniges, U., Rosenau, T., & Potthast, A. (2015). Bacterial cellulose as a material for wound treatment: Properties and modifications. A review. *Biotechnology Advances*, *33*(8), 1547–1571. https://doi.org/10.1016/j.biotechadv.2015.07.009

Suryawanshi, R. K., Patil, C. D., Koli, S. H., Hallsworth, J. E., & Patil, S. V. (2017). Antimicrobial activity of prodigiosin is attributable to plasma-membrane damage. *Natural Product Research*, *31*(5), 572–577. https://doi.org/10.1080/14786419.2016.1195380

Takallu, S., Mirzaei, E., Zakeri Bazmandeh, A., Ghaderi Jafarbeigloo, H. R., & Khorshidi, H. (2024). Addressing Antimicrobial Properties in Guided Tissue/Bone Regeneration Membrane: Enhancing Effectiveness in Periodontitis Treatment. *ACS Infectious Diseases*, *10*(3), 779–807. https://doi.org/10.1021/acsinfecdis.3c00568

Tang, S., & Zheng, J. (2018). Antibacterial Activity of Silver Nanoparticles: Structural Effects. *Advanced Healthcare Materials*, *7*(13). https://doi.org/10.1002/adhm.201701503

Tarbali, S., Karami Mehrian, S., & Khezri, S. (2022). Toxicity effects evaluation of green synthesized silver nanoparticles on intraperitoneally exposed male Wistar rats. *Toxicology Mechanisms and Methods*, *32*(7), 488–500. https://doi.org/10.1080/15376516.2022.2049412

Tareq, M., Khadrawy, Y. A., Rageh, M. M., & Mohammed, H. S. (2022). Dose-dependent biological toxicity of green synthesized silver nanoparticles in rat's brain. *Scientific Reports*, *12*(1), 22642. https://doi.org/10.1038/s41598-022-27171-1

Teixeira, M. A., Paiva, M. C., Amorim, M. T. P., & Felgueiras, H. P. (2020). Electrospun Nanocomposites Containing Cellulose and Its Derivatives Modified with Specialized Biomolecules for an Enhanced Wound Healing. *Nanomaterials*, *10*(3), 557. https://doi.org/10.3390/nano10030557

Tian, J., Wong, K. K. Y., Ho, C., Lok, C., Yu, W., Che, C., Chiu, J., & Tam, P. K. H. (2007). Topical Delivery of Silver Nanoparticles Promotes Wound Healing. *ChemMedChem*, *2*(1), 129–136. https://doi.org/10.1002/cmdc.200600171

Torgbo, S., & Sukyai, P. (2020). Biodegradation and thermal stability of bacterial cellulose as biomaterial: The relevance in biomedical applications. *Polymer Degradation and Stability*, *179*, 109232. https://doi.org/10.1016/j.polymdegradstab.2020.109232

Tottoli, E. M., Dorati, R., Genta, I., Chiesa, E., Pisani, S., & Conti, B. (2020). Skin Wound Healing Process and New Emerging Technologies for Skin Wound Care and Regeneration. *Pharmaceutics*, *12*(8), 735. https://doi.org/10.3390/pharmaceutics12080735

Turnbull, G., Clarke, J., Picard, F., Riches, P., Jia, L., Han, F., Li, B., & Shu, W. (2018). 3D bioactive composite scaffolds for bone tissue engineering. *Bioactive Materials*, *3*(3), 278–314. https://doi.org/10.1016/j.bioactmat.2017.10.001

Venil, C. K., Khasim, A. R., Aruldass, C. A., & Ahmad, W. A. (2017). Safety evaluation of flexirubin from Chryseobacterium artocarpi CECT 8497: Acute, sub-acute toxicity and mutagenicity studies. *Process Safety and Environmental Protection*, *112*, 362–370. https://doi.org/10.1016/j.psep.2017.02.022

Venil, C. K., Zakaria, Z. A., Usha, R., & Ahmad, W. A. (2014). Isolation and characterization of flexirubin type pigment from Chryseobacterium sp. UTM-

3T. *Biocatalysis and Agricultural Biotechnology*, *3*(4), 103–107. https://doi.org/10.1016/j.bcab.2014.02.006

Wang, C., Su, Y., & Xie, J. (2024). Advances in Electrospun Nanofibers: Versatile Materials and Diverse Biomedical Applications. *Accounts of Materials Research*, *5*(8), 987–999. https://doi.org/10.1021/accountsmr.4c00145

Wang, M., Xu, Y., Cao, L., Xiong, L., Shang, D., Cong, Y., Zhao, D., Wei, X., Li, J., Fu, D., Lian, H., & Zhao, Z. (2025). Mechanical and biological properties of 3D printed bone tissue engineering scaffolds. *Frontiers in Bioengineering and Biotechnology*, *13*. https://doi.org/10.3389/fbioe.2025.1545693

Wang, X., Meng, G., Zhang, Z., Zhao, J., Wang, S., Hua, D., JingZhang, & Zhang, J. (2024). Prodigiosin hydrogel to promote healing of trauma-infected multidrug-resistant Staphylococcus aureus mice wounds. *International Journal of Pharmaceutics: X*, *8*, 100306. https://doi.org/10.1016/j.ijpx.2024.100306

Wang, Y., Yuan, X., Yu, K., Meng, H., Zheng, Y., Peng, J., Lu, S., & Liu, X. (2018). Corrigendum to “Fabrication of nanofibrous microcarriers mimicking extracellular matrix for functional microtissue formation and cartilage regeneration” [Biomaterials 171 (2018) 118–132]. *Biomaterials*, *183*, 171–172. https://doi.org/10.1016/j.biomaterials.2018.08.051

Wang, Z., Chen, L., Chu, Z., Huang, C., Huang, Y., & Jia, N. (2018). Gemcitabine-loaded gold nanospheres mediated by albumin for enhanced anti-tumor activity combining with CT imaging. *Materials Science and Engineering: C*, *89*, 106–118. https://doi.org/10.1016/j.msec.2018.03.025

Williamson, N. R., Fineran, P. C., Leeper, F. J., & Salmond, G. P. C. (2006). The biosynthesis and regulation of bacterial prodiginines. *Nature Reviews Microbiology*, *4*(12), 887–899. https://doi.org/10.1038/nrmicro1531

Worthington, K. L. S., Adamcakova-Dodd, A., Wongrakpanich, A., Mudunkotuwa, I. A., Mapuskar, K. A., Joshi, V. B., Allan Guymon, C., Spitz, D. R., Grassian, V. H., Thorne, P. S., & Salem, A. K. (2013). Chitosan coating of copper nanoparticles reduces *in vitro* toxicity and increases inflammation in the lung. *Nanotechnology*, *24*(39), 395101. https://doi.org/10.1088/0957-4484/24/39/395101

Wu, Y.-F., Wen, Y.-T., Salamanca, E., Moe Aung, L., Chao, Y.-Q., Chen, C.-Y., Sun, Y.-S., & Chang, W.-J. (2024). 3D-bioprinted alginate-based bioink scaffolds with β-tricalcium phosphate for bone regeneration applications. *Journal of Dental Sciences*, *19*(2), 1116–1125. https://doi.org/10.1016/j.jds.2023.12.023

Xu, W., Qi, M., Li, X., Liu, X., Wang, L., Yu, W., Liu, M., A, L., Zhou, Y., & Song, Y. (2019). TiO2 nanotubes modified with Au nanoparticles for visible-light enhanced antibacterial and anti-inflammatory capabilities. *Journal of Electroanalytical Chemistry*, *842*, 66–73. https://doi.org/10.1016/j.jelechem.2019.04.062

Zhan, X., Yan, J., Tang, H., Xia, D., & Lin, H. (2022). Antibacterial Properties of Gold Nanoparticles in the Modification of Medical Implants: A Systematic Review. *Pharmaceutics*, *14*(12), 2654. https://doi.org/10.3390/pharmaceutics14122654

Zheng, K., Setyawati, M. I., Leong, D. T., & Xie, J. (2017). Antimicrobial Gold Nanoclusters. *ACS Nano*, *11*(7), 6904–6910. https://doi.org/10.1021/acsnano.7b02035

Zheng, X., Sun, J., Li, W., Dong, B., Song, Y., Xu, W., Zhou, Y., & Wang, L. (2020). Engineering nanotubular titania with gold nanoparticles for antibiofilm enhancement and soft tissue healing promotion. *Journal of Electroanalytical Chemistry*, *871*, 114362. https://doi.org/10.1016/j.jelechem.2020.114362

Zhou, W., Zi, L., Cen, Y., You, C., & Tian, M. (2020). Copper Sulfide Nanoparticles-Incorporated Hyaluronic Acid Injectable Hydrogel With Enhanced Angiogenesis to Promote Wound Healing. *Frontiers in Bioengineering and Biotechnology*, *8*. https://doi.org/10.3389/fbioe.2020.00417

Zhu, G., Zhang, T., Chen, M., Yao, K., Huang, X., Zhang, B., Li, Y., Liu, J., Wang, Y., & Zhao, Z. (2021). Bone physiological microenvironment and healing mechanism: Basis for future bone-tissue engineering scaffolds. *Bioactive Materials*, *6*(11), 4110–4140. https://doi.org/10.1016/j.bioactmat.2021.03.043

Zhu, L., Zhu, W., Hu, X., Lin, Y., Machmudah, S., Wahyudiono, Kanda, H., & Goto, M. (2022). PVP/Highly Dispersed AgNPs Nanofibers Using Ultrasonic-Assisted Electrospinning. *Polymers*, *14*(3), 599. https://doi.org/10.3390/polym14030599

CHAPTER 4

Biosynthesis of a novel pyoverdine using the Antarctic bacterium *Pseudomonas* sp. ef1

This chapter is extensively based on the following publication, to which I contributed in terms of validation, investigation, formal analysis, and data curation:

Zannotti, M., Di Sessa, M., Biondini, M. C., Vassallo, A., Ferraro, S., Angeloni, S., Ricciutelli, M., Pucciarelli, S., & Giovannetti, R. (2026). Towards an easy production of novel pyoverdines by an Antarctic Pseudomonas strain: a spectroscopic and HPLC-MS/MS characterization study. https://doi.org/10.1016/j.dyepig.2025.113096

Abstract

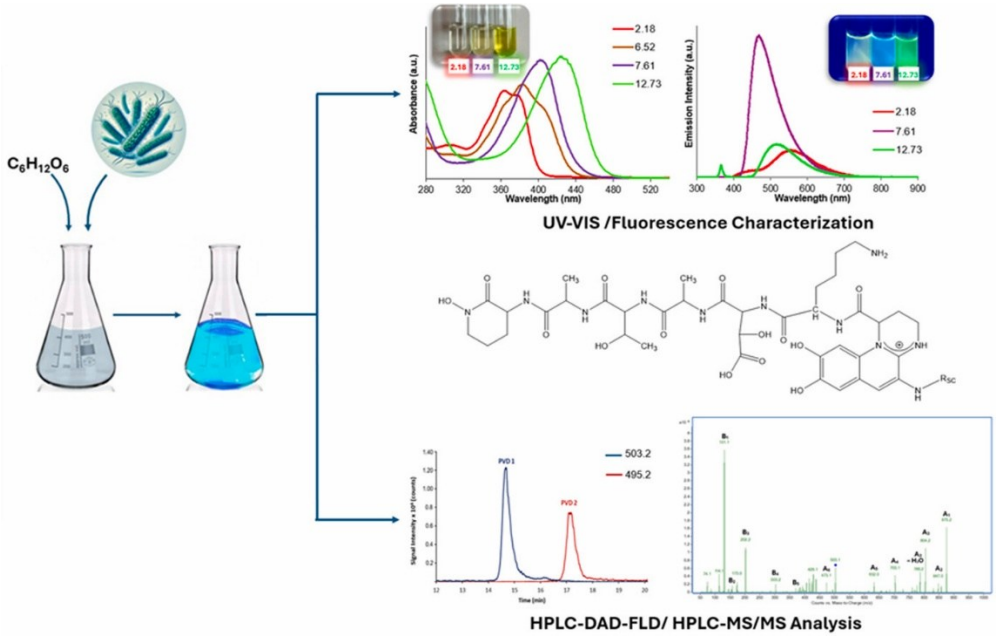

Figure 64 - Graphical abstract of pyoverdine production and chemical characterization

Bacterial secondary metabolites are fundamental molecules not only in several microbial processes, but also in various sectors of today's economy, especially in human health and agriculture. Siderophores are important secondary metabolites produced by various bacterial strains, including *Pseudomonas* species, under iron-deficient conditions. Pyoverdines are fluorescent types of siderophores with molecular mass between 889 and 1764 Da that have strong affinity to iron and other metals.

In this study, *Pseudomonas* sp. ef1, isolated from a consortium associated with the Antarctic psychrophilic ciliate *Euplotes focardii*, was cultured under iron-

deficiency conditions to induce pyoverdine production, in the presence of 1% w/v glucose as a sole carbon source. The produced pyoverdines were purified and characterized by UV–Vis, fluorescence spectroscopy and HPLC-MS/MS analysis. The isolated and characterized compounds were represented by two different Group 1 Pyoverdines, both containing six amino acids peptide chain, with the following sequence: cOHOrn-Ala-Thr-Ala-OHAsp-Lys. The two pyoverdines differ only in the sidechain dicarboxylic acid, called R_{SC}, that usually consists either of succinic/malic acid or their monoamide analogues, or glutamic/α-ketoglutaric acid. One of the two pyoverdines produced by *Pseudomonas* sp. ef1 is reported for the first time. The study of novel pyoverdines contribute to understand the role of secondary metabolites in modulating bacterial consortia. Furthermore, it opens new perspective in different possible applications.

State of the art

Secondary metabolites produced by microorganisms have attracted considerable attention in recent years due to their structural diversity and biological activities. Bacterial secondary metabolites display great potential as antibiotics and other bioactive agents *(Newman & Cragg, 2016; Ramírez-Rendon et al., 2022; Vollenweider et al., 2024)*. Within microbial communities, these molecules mediate interspecies interactions and responses to environmental stressors *(Chevrette et al., 2022).*

Among bacterial secondary metabolites, siderophores are gaining increasing interest within the scientific community. They represent natural molecules characterized by a strong affinity for iron ions and other metal ions *(Hider & Kong, 2010)*. Iron has a pivotal role in numerous cellular processes, including

oxygen reduction for ATP synthesis, DNA replication and repair, oxygen transport, carbon metabolism, and regulation of gene expression *(Dell'Anno et al., 2022; Swayambhu et al., 2021)*. Despite its high natural abundance, iron bioavailability is often limited under physiological conditions because of ferric hydroxide, $Fe(OH)_3$, reduced solubility *(Cezard et al., 2014a, 2014b)*. Therefore, to overcome iron limitation, microorganisms synthesize a wide variety of siderophores. Depending on their chemical structure, siderophores are categorized into catecholates and phenolates, hydroxamates, carboxylates, and mixed type siderophores. Pyoverdine (PVDs) belongs to the latter group and may simultaneously contain two or even three siderophore classes, such as catecholate and hydroxamate moieties, showing exceptionally high affinity for iron chelation *(Hider & Kong, 2010; Saha et al., 2016; Timofeeva et al., 2022)*.
Pyoverdines are yellow-green, water-soluble fluorescent pigments produced by a subgroup of *Pseudomonas* genus, commonly referred to as "fluorescent *Pseudomonads*". This group includes both pathogenic and non-pathogenic species, such as *P. aeruginosa*, *P. putida*, *P. syringae*, and *P. fluorescens*. These bacterial pigments were discovered in 1892 and originally termed fluorescins, before being subsequently renamed pyoverdines *(Ringel & Brüser, 2018)*.
In pathogenic species such as *P. aeruginosa*, pyoverdines play a key role during bacterial infection. They function as siderophores that scavenge iron from the host proteins and act as signaling molecules regulating the production of two major virulence factors, exotoxin A and the endo-proteinase PrpL *(Bonneau et al., 2020)*. Pyoverdine can transiently enter host cells and remove significant amounts of ferric iron. As a consequence, mitochondria function is impaired, with compromised electron transfer and ATP production, ultimately activating mitochondrial turnover *(H. Budzikiewicz et al., 2007).*

PVDs typically exhibit molecular masses approximately in the range of 889-1764 Da *(Meyer et al., 2008).* They are characterized by two main absorption bands at 232 and 400 nm at UV-vis spectroscopy. In addition, they are known to be susceptible to discolouration induced by acidification, a reversible process in which their distinctive colour can be restored upon neutralization*(Dane et al., 2016a)*.

From a molecular point of view, pyoverdines consist of three distinct structural parts: i) a dihydroxyquinoline chromophore responsible for their characteristic fluorescence, ii) a peptide chain composed of 6 to 12 aminoacids, covalently linked to the chromophore, and iii) a small dicarboxylic acid amidically bound to the NH_2 – group of the chromophore. This latter component, also termed the sidechain (RSC), may consists of succinic/malic acid, their monoamide analogues, or glutamic/-α ketoglutaric acid. Notably, several pyoverdines differ only in the nature of this acid moiety *(Budzikiewicz et al., 2006; Hannauer et al., 2012; Meyer et al., 2008; Owen & Ackerley, 2011; Ruangviriyachai et al., 2004; Scholz et al., 2018; Visca et al., 2007b; Wei & Aristilde, 2015)*.
The peptide chain differs in length and amino acid composition among strains, in accordance with the substrate specificities of the transport systems involved in the uptake of iron-bound PVDs. The peptide sequences are not directly encoded by genomic DNA; their core structure, instead, is biosynthesized by non-ribosomal peptide synthetases (NRPSs) *(Ochiai et al., 2025).*
Both the chromophore and the peptide chains are involved in the bonding to ferric ion Fe^{+3} *(Budzikiewicz, 2001).* Over 60 pyoverdines were reported and analysed in different studies *(Schalk & Guillon, 2013)*. Pyoverdines produced by fluorescent *Pseudomonas* species can be classified into four groups based on the

structural properties of their peptide chains. In Group 1, the most prevalent pyoverdines possess a linear peptide chain terminating with cyclo-N-hydroxyornithine; some variants feature a tetrahydropyrimidine ring resulting from the condensation of diaminobutyric acid (Dab) with the preceding amino acid. Group 2 is characterized by a peptide chain with a C-terminal cyclic structure comprising three to four amino acids, formed through an amide bond between the terminal amino acid and an in-chain lysine. Group 3 includes a minority of pyoverdines whose peptide chains end with a C-terminal cyclodepsipeptidic substructure, produced by an ester bond between the terminal amino acid and an internal serine or threonine. Group 4 is distinguished by a free C-terminal carboxyl group, typically representing hydrolysis products of Group 3 cyclic esters, which are readily hydrolysed at pH levels of 9 or higher *(Gu et al., 2020a; Schalk et al., 2020).*

PVD biosynthesis is a complex tightly regulated process involving different steps *(Figure 65) (Ringel & Brüser, 2018)*. The biosynthetic process begins in the cytoplasm with the assembly of acylated ferribactin, a peptide precursor, by NRPSs and auxiliary enzymes, named MbtH, PvdG, PvdH, PvdA, PvdF, and PvdD. These biosynthetic components are organized in membrane-associated complexes commonly referred to as siderosomes. The enzyme PvdL synthesizes and acylates the conserved N-terminal tripeptide, while the remaining NRPS elongate the peptide chain and differ among strains. After its synthesis, the acylated ferribactin is transported to the periplasm most likely due to the activity of PvdE; once there, it is deacylated by the N- terminal nucleophile hydrolase PvdQ. Subsequently, PvdP catalyses the oxidative cyclization, leading to dihydropyoverdine. PvdO, possibly in conjunction with other proteins, mediates

a final oxidation reaction, obtaining the characteristic pyoverdine chromophore. Subsequently, the original L-glutamic acid side chain is transformed into the succinamide by PvdN or the α-ketoglutarate thanks to PtaA. The modified pyoverdines are exported to the extracellular environment by transport systems such as PvdRT-OmpQ, where they chelate ferric iron. The resulting complex is recognised by the outer membrane receptor FpvA and internalized by TonB. Iron is then released through reduction and dechelation mediated by FpvF and FpvC,. Lastly, iron is taken up by the FpvDE transporter and the iron-free pyoverdine is finally recycled *(Ringel & Brüser, 2018).*

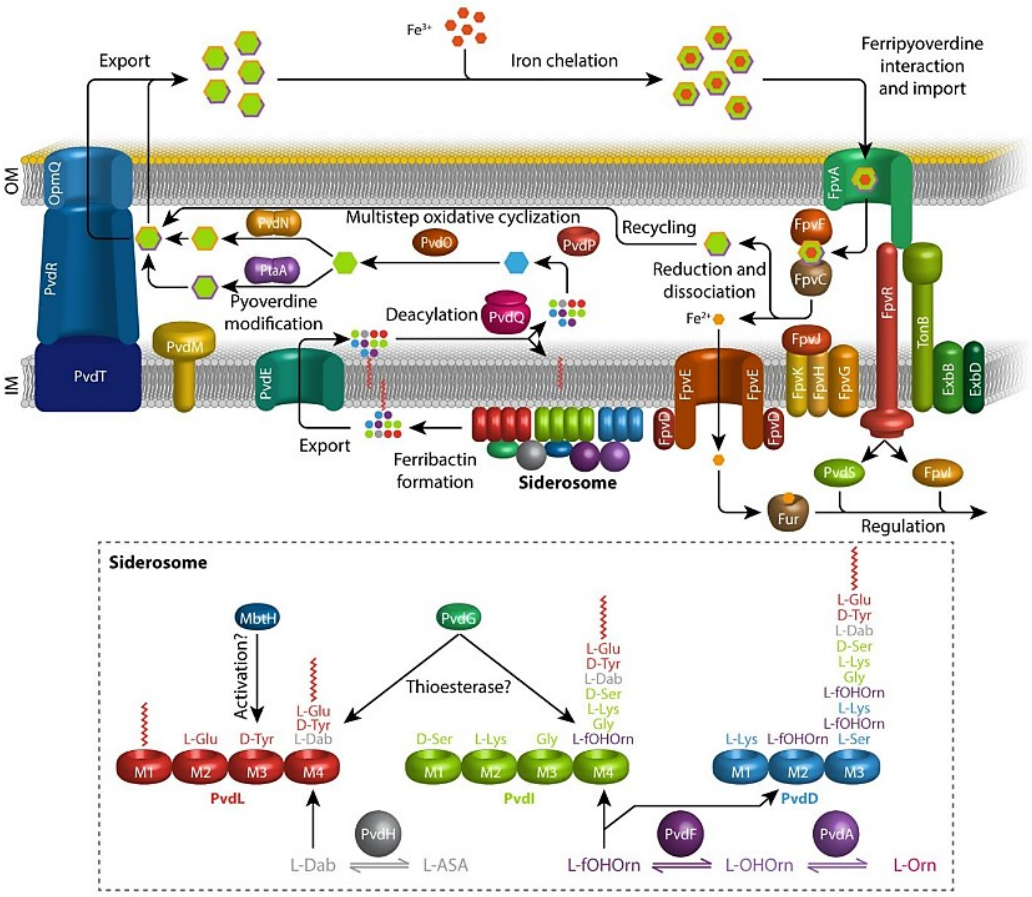

Figure 65 - Biosynthesis, secretion, uptake and recycling of pyoverdines in P. fluorescens A506 (Ringel & Brüser, 2018).

PVD molecules can be used in different fields of applications from medicines to agriculture *(Saha et al., 2016)*. Being a virulence factor, PVD is a promising target to detect pathogens and can be used to protect plants from infections *(Gu et al., 2020b)*. The strong chelating ability of pyoverdines, indeed, subtract iron to phytopathogens, thus promoting plant growth *(Xiao & Kisaalita, 1995a)*. Furthermore, PVDs can provide nutrients to plants, triggering selectively the

mobilization of specific metal ions, for example by increasing the bioavailability of nickel respect of cadmium in hydroponics *(Dell'Anno et al., 2022; Ferret et al., 2015)*. The ability to bind metal by PVDs can be exploited for bioremediation by removing iron from asbestos fibres or efficiently removing iron from chrysotile-gypsum and amosite-gypsum, as examples *(David, Fritsch, et al., 2020; David, Ihiawakrim, et al., 2020).* In addition, pyoverdines have been employed in the synthesis of silver nanoparticles using $AgNO_3$ as a precursor *(Dane et al., 2016b)*. One study investigated AgNPs synthesis mediated by siderophores produced by *Pseudomonas* spp. and proposed a photoreduction mechanism driven by natural sunlight. In this process, negatively charged functional groups of PVD bound Ag^+ ions at neutral pH, while PVD chromophore promoted the generation of superoxide free radicals from dissolved oxygen under photolytic activity, inducing monovalent Ag^+ ions reduction to Ag^0. This mechanism could also occur in natural environments, explaining the presence of AgNPs traces in marine and other aquatic systems *(Jacques et al., 1995)*. Finally, PVDs can form strong and stable complexes with actinides metals like U, Cm and Np, showing strong chelator ability *(Hazotte et al., 2016).* The fluorescence behaviour can be also used for their use in sensor applications for the detection of metals and organic compounds *(Nosrati et al., 2018a; Yin et al., 2014a)*.

For the characterization of PVD compounds and their congeners, they are analysed using tandem mass spectrometry (MS/MS) that shows the highest level of confidence, and by interpretating the fragmentation of the pseudo-molecular target ion, $[M+2H]^{2+}$, that commonly is the most abundant. In the double charged ion $[M+2H]^{2+}$, one proton is reasonably located on the chromophore

due to its ability to delocalize the positive charge; the second proton, according to the "mobile proton" model, can be present on the different amide groups in the peptide chain favouring the cleavages in the near vicinity, giving useful information about the amino acid sequence of the pyoverdine structure *(Budzikiewicz et al., 2007; Georgias et al., 1999a; Meyer et al., 2008; Rehm et al., 2022, 2023; Ruangviriyachai et al., 2004; Scholz et al., 2018; Sultana et al., 2000a; Tappe et al., 1993; Weber et al., 2000; Wei & Aristilde, 2015)*.

In this study, the ability of the Antarctic bacteria *Pseudomonas* sp. ef1, isolated from a consortium associated to the Antarctic psychrophilic *Euplotes focardii* to biosynthesize pyoverdines under iron-deficient conditions, using 1 % w/v glucose as the sole carbon source, has been reported. The produced PVD compounds were deeply characterized by UV–Vis, fluorescence spectroscopy and by HPLC-MS/MS and the structure of two different PVDs has been identified, one of these never reported before.

Materials and methods

Bacterial culture, growth conditions and pyoverdine production

The bacterial strain reported in this work was isolated from a consortium associated with the Antarctic psychrophilic ciliate *E. focardii* and named as *Pseudomonas* sp. ef1. After isolation, the strain was stored at −80 °C in glycerol stock and spread on LB agar plates (10 g/L Tryptone, 5 g/L yeast extract, 5 g/L NaCl, 15 g/L bacto-agar) and let grown at 21 °C. For pyoverdine production, the bacterial cells from the overnight-grown culture were inoculated in 500 mL of M9 medium, supplemented with 1% w/v glucose as a sole carbon source, and incubated at 21 °C in a 2 L-Erlenmeyer flask under shaking (180 rpm).

Composition of M9 medium is as follows: Na_2HPO_4 6 g/L, KH_2PO_4 3 g/L, NaCl 0.5 g/L, NH_4Cl 1 g/L, $MgSO_4$ 2 mM, $CaCl_2$ 0.1 mM. Solutions of $MgSO_4$, $CaCl_2$ and glucose (1 %w/v) were separately sterilized by autoclave and added just before use. The pH was adjusted to 7.4 with NaOH before sterilization. The bacterial growth was monitored by measuring the optical density at 600 nm (OD600) using a NanoDrop (Thermo Scientific™) spectrophotometer. Three replicates for each test were measured. In addition, the growth of the bacteria at 21°C was also monitored in presence of $FeCl_3$ salt in M9 agar plates supplemented with 1% glucose. All the media, reagents and salts used were provided by Merck (Milan, Italy) and used without further purification.
The produced pyoverdine was dried in a vacuum oven at 50 °C and weighed to determine yield and productivity.

Sample preparation and UV–Vis characterization

The bacterial culture was centrifuged at 8000×g for 10 min at room temperature and the supernatant was filtrated by PTFE sterile ReliaPrep Syringe™ filters (0.22 mm, Ahlstrom) to completely remove bacterial cells from samples to obtain a water solution containing the yellow pigment.
SPE purification was performed using a Strata-XL 100 μm polymeric reversed-phase column (Phenomenex, Torrance, CA, USA) to purify the sample and remove excess salts by selectively eluting only the fluorescent fraction.
The SPE column was initially conditioned with methanol 1 mL with a successive equilibration with 1 ml of ultrapure water. The sample was then loaded (1 mL) and washed two times with water (2×300 μL). The elution was finally made using H_2O/MeOH(70/30) + 0.1% of formic acid (2×300μL).

The yellow pigment was then characterized by UV–Vis spectroscopy using an Agilent 8454 Cary UV–Visible Diode Array Spectrophotometer (Agilent, Santa Clara, USA). The UV–Vis spectral change at different pH was monitored by micro-additions of HCl and NaOH 1 M (Carlo Erba reagents, Cornaredo, MI, Italy). The emission spectrum of the samples was monitored using an Ocean HDX Fluorimeter (Ocean Insight), equipped with a monochromatic laser at 365 nm.

Liquid chromatography and mass-spectrometry analysis

The yellow pigment was analysed by HPLC 1260 Infinity (Agilent, Santa Clara, USA) equipped with a diode Array (DAD) and fluorescent (FLD) detectors. The separation was performed using an isocratic elution, the mobile phase was composed by water (A, 90%) and methanol (B, 10%), both with formic acid 0.1% with a flow rate of 1 mL/min. The analysis was achieved using a C18 Kinetex (250×4.60 mm, particles size 5 μm) from Phenomenex (Torrance, CA, USA). The injection volume was 5 μL; the temperature of the column was set at 30 °C. The monitored wavelengths were 306, 364, 377 nm using DAD, while for FL, the wavelengths monitored were 464, 514, 555 nm (excitation 365nm).
HPLC-MS/MS analysis were performed using an HPLC Agilent 1290 Infinity coupled with a Triple Quadrupole 6420 (Agilent, Santa Clara, USA) with an electrospray (ESI) source operating in positive mode. The column and the operative conditions of the separation were the same used for HPLC-DAD-FLD analysis. The source parameters were set as follow: the temperature of the drying gas was 350 °C; the gas flow was 12 L/min^{-1}; the nebulizer pressure was 55 psi; and the capillary voltage was 4000 V. The acquisitions were performed in scan mode and once identified some interesting precursor ions the acquisitions were

carried out in product ion scan mode. For each selected precursor ion, the fragmentation of the investigated compounds was monitored at different collision energy: 16, 30 and 40 eV.

For all the analysis, the sample was filtered through a 0.2 µm single use syringe filter from Phenomenex (Bologna, Italy).

Results and Discussion

Pseudomonas sp. ef1 growth and pyoverdine production

The bacterial growth of the *Pseudomonas* sp. ef1 in M9 supplemented with 1 % w/v glucose as sole carbon source has been monitored at 4 °C and 22 °C, that represent respectively the ideal growing temperature of the Antarctic *E. focardii* ciliate host *(Ramasamy et al., 2019)* and that of the isolated *Pseudomonas* sp. ef1 *(John, Nagoth, Ramasamy, Mancini, et al., 2020)*. In *Figure 66*, the optical density at 600 nm (OD600) is reported as function of time: *Pseudomonas* can growth in this medium at both 4 °C and 22 °C, but at 22 °C the bacterial culture reaches the plateau earlier than at 4 °C. At both temperatures, the culture becomes fluorescent once reached the plateau. The fluorescent bioproduct was purified as described under Material and Methods for further analysis. *Pseudomonas* sp. ef1 growth was also estimated at 22 °C in M9 agar plates supplemented with 1% glucose in the presence or absence of $FeCl_3$, demonstrating that, in the presence of iron, the cultures are not fluorescent (*Figure S1, Supplementary Materials available at https://ars.els-cdn.com/content/image/1-s2.0-S0143720825004668-mmc1.docx*), suggesting that the bioproduct is a siderophore.

The estimated yield of pyoverdine production was 200 mg/L, with a productivity of 2.08 mg/L/h. A recent publication reported a pyoverdine concentration of 108 µmol/L after 144 h in rhizospheric *Pseudomonas*. Depending on the molecular weight assumed for the molecule, this corresponds to an estimated concentration of approximately 160 mg/L, with an estimated productivity of 1,11 mg/L/h *(Lozano-González et al., 2023)*. The large-scale production of pyoverdines is currently limited by the low availability and high production costs. To date, only pyoverdines from *Pseudomonas fluorescens* are commercially available, with a high purity within the range 90-95% (HPLC) and at remarkably high costs (242-279 €/mg according to Sigma-Aldrich and Cayman Chemical), due to the low production yields achieved in native strains. Production optimization through heterologous systems and bioengineering are still under development. Therefore, the development of non-pathogenic *Pseudomonas* strains could represent a promising strategy to enable an efficient and economically feasible production of pyoverdines *(Dell'Anno et al., 2022)*.

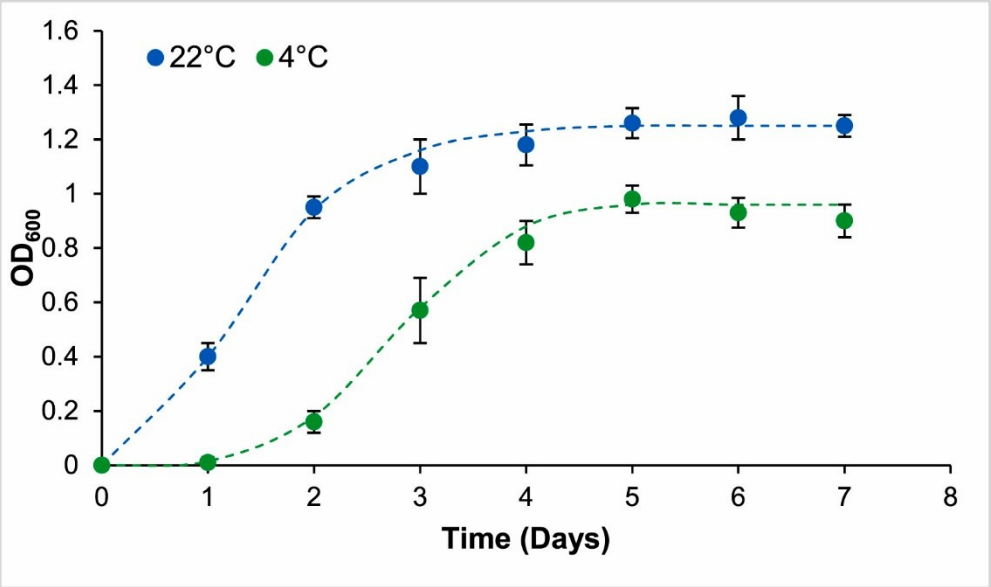

Figure 66 - Growth curves of Pseudomonas sp. ef1 in M9 medium supplemented with 1% (w/v) of glucose at 4°C (blue dash line) and 22°C (blue line). The experimental data represents a mean ± standard deviation of three replicates.

Spectroscopic characterization of the fluorescent pigment

The bacterial fluorescent pigment was characterized by UV–Vis spectroscopy at different pH values (*Figure 67*). At pH 2.18, the colour of the pigment solution was pale-yellow, almost transparent, and the spectrum shows two mainly bands at 364 and 378 nm. Increasing the pH, the absorption band at 364 nm started to decrease, while the band at 378 nm increased and red-shifted to higher wavelength; in addition, a new absorption band at 406 nm started to increase after pH 3.53. At pH 7.61, the band at 364 completely disappeared and, towards alkaline pH, the band at 406 nm increase up to a pH about 8.19; after this value, the band at 406 nm decrease and red shift-shifted to 426 nm, as broadened band

at pH of 12.73. At alkaline pH the sample shows an intense green-yellow colour as reported in the inset of *Figure 67*. The observed UV–Vis spectral behaviour is consistent with the presence of pyoverdine compounds in the solution *(Albrecht-Gary et al., 1994; Boukhalfa et al., 2006; Xiao & Kisaalita, 1995b).*

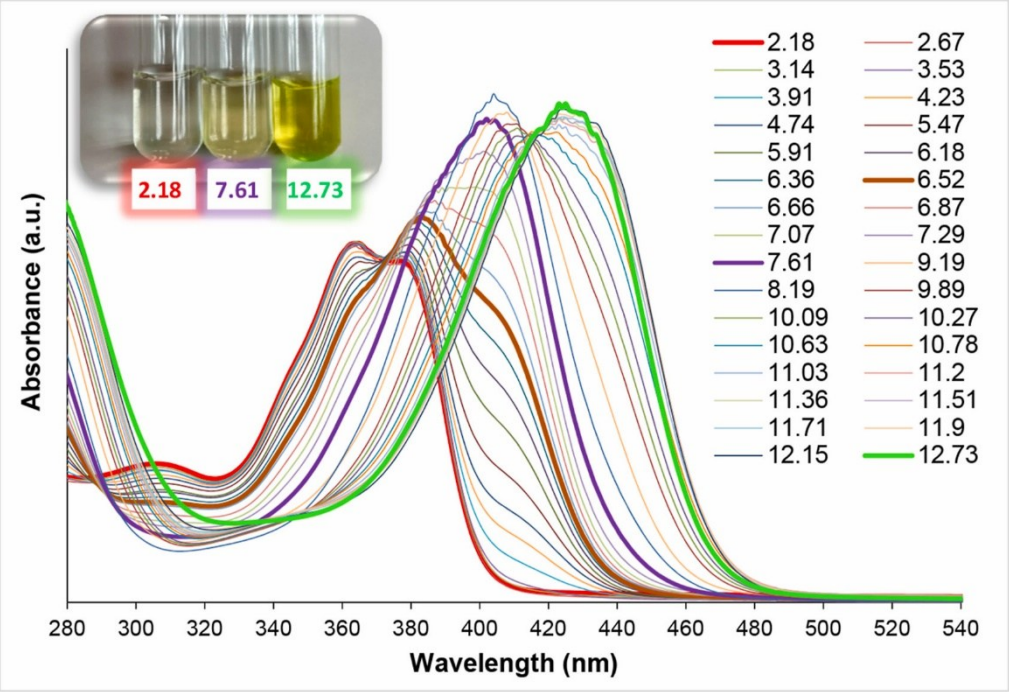

Figure 67 - UV–Vis spectral change of pyoverdine compounds in the pH range between 2.18 and 12.73; in the inset the colour variation of the pigment at acid, neutral and alkaline pH conditions.

Typical structure of pyoverdine is reported in *Figure 68*, where the dihydroxyquinoline chromophore, responsible for the fluorescence, is directly linked by amide bond to the peptide chain sequence, that consists of 6–12 amino acids, and to a dicarboxylic acid side chain (R_{SC}), that usually consist of succinic/malic acid or the monoamide analogues, or glutamic/α-ketoglutaric acid

(Budzikiewicz et al., 2006; Hannauer et al., 2012; Meyer et al., 2008; Ruangviriyachai et al., 2004; Scholz et al., 2018; Visca et al., 2007a; Wei & Aristilde, 2015).

As first described by Albrecht-Garry et al. *(Albrecht-Gary et al., 1994)*, the spectral changes reported in *Figure 68*, which correspond to pH variations, can be correlated with the first and second deprotonation of the –OH groups in the dihydroxyquinoline chromophore, as well as with the acid-base properties of the RSC moieties present in the pyoverdine structure.

The spectral changes, corresponding to the pH variation, can be correlated to the first and the second deprotonation of the –OH groups of the di-hydroxyquinoline chromophore, and about the RSC moieties acid- base features, present in the pyoverdine's structure, as reported in *Figure 68*.

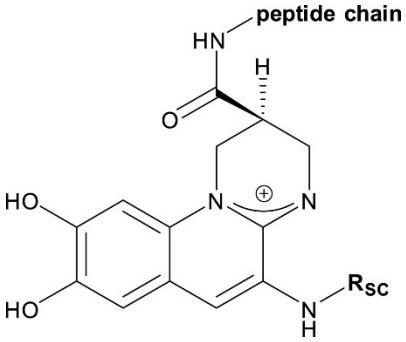

Figure 68 - Typical structure of Pyoverdine.

Analysing the absorbance of the characteristic wavelengths at 364 nm and 426 nm as function of the pH (*Figure 69*), an estimation of the pKas values can be calculated from the first derivative of the data, associated to the flex points, as it is possible to observe in the plot of *Figure 69*. From the calculation of the first derivative four pKas values have been find.

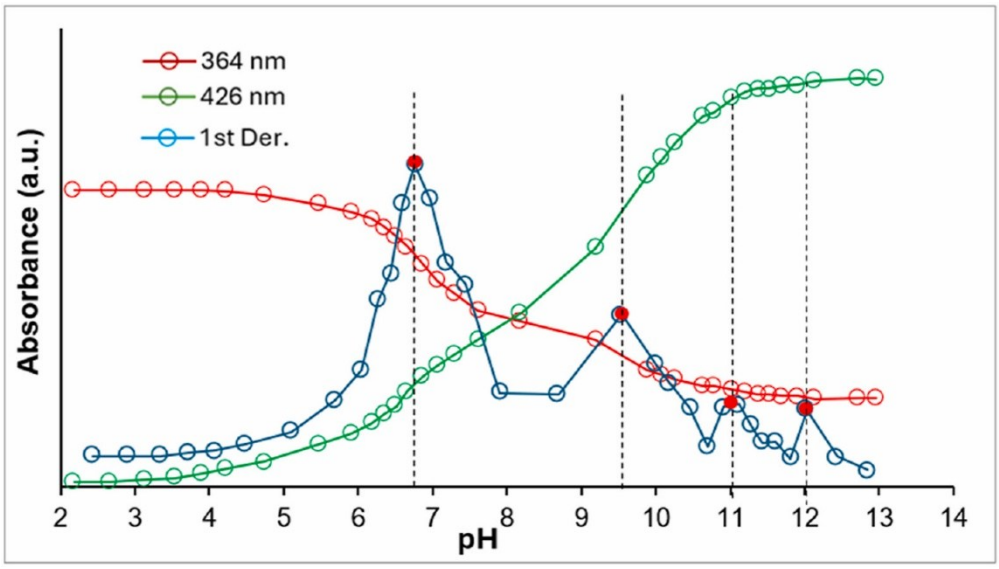

Figure 69 - Absorbance changes at 364 and 426 nm, and 1st derivative calculation at different pHs.

The pK_{a1} at around 6.7 can be attributable to the first –OH group (pK_{a1}) on the dihydroxiquinoline structure and about 11 for the second –OH (pK_{a3}) *(Mozzicafreddo et al., 2021; Pucciarelli et al., 2015; Ramasamy et al., 2019)*. An additional pK_a can be estimated from the absorption profile and it was detected at around pH 9.5 (pK_{a2}); this can be due to the presence of an amino group in the vicinity of the chromophore that influence its absorption behaviour. An additional maximum peak has been calculated at pH 12; in that case can be traced to the deprotonation of an additional –OH group on the R_{SC} side chain (pK_{a4}), as example for the presence of hydroxy succinic amide, that is an R_{SC} reported as pyoverdine dicarboxylic side chain in pyoverdine compounds produced by *Pseudomonas* sp. ef1.

The emission spectra have been also investigated at different pH values and the obtained fluorescence spectra are reported in *Figure 70*. The emission behaviour depends on the pyoverdine's form. In fact, at acidic pH in water solutions, the protonated form of pyoverdine shows a typical emission peak centred at 554 nm of lower intensity, while, increasing the pH, the emission intensity strongly increases and blue-shifts to 466 nm; the maximum emission intensity was detected for the pH 7.6. After the last reported value, a further increase in pH leads to a decrease of the emission intensity that red-shift to 520 nm for the strongest alkaline pyoverdine's solution at pH 12.73.

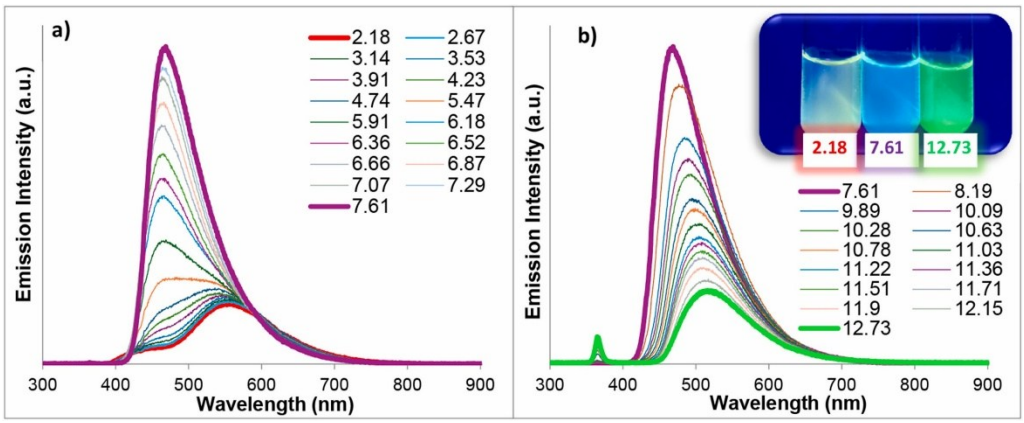

Figure 70 - Emission spectra of the pigment (Excitation = 365 nm) at different pH values: a)2.17–7.61 and b) 7.61–12.73.

Characterization by HPLC-DAD-FLD analysis

Since it is known that these bacteria generally do not produce a single pyoverdine molecule but instead a group of different pyoverdines *(Meyer et al., 2008; Rehm et al., 2023)*, to verify the number and types of pyoverdines produced by

Pseudomonas sp. ef1, HPLC analysis with DAD and FLD detectors has been performed to analyse the yellow pigment.

In *Figure 71a* are reported the superimposed HPLC DAD/FLD chromatograms by using H_2O/MeOH (90/10), both with formic acid 0.1 % as the mobile phase. The results confirm the presence of two strong peaks with high fluorescence that eluted at 14.6 and 17.3 min. In *Figure 71b and c* are reported the UV–Vis and fluorescence spectra that are consistent with different pyoverdines compounds in acidic pH.

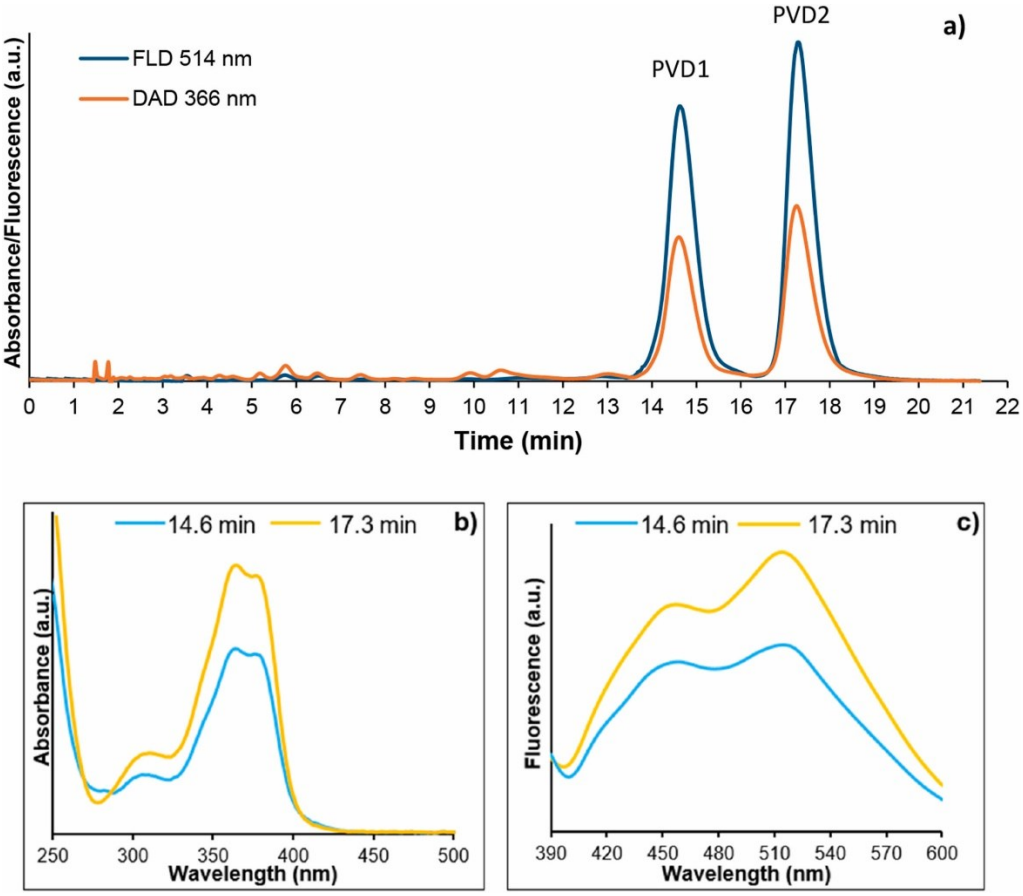

Figure 71 - a) HPLC-DAD-FLD chromatogram, by isocratic elution H_2O/MeOH (90/10) with formic acid 0.1%, of the pigment and the relative b) UV-VIS and (c) emission spectra of the PVDs eluted at 14.6 and 17.3 min.

Characterization by HPLC-MS/MS analysis

To detect and characterize the different PVDs and evaluate their respective molecular weights, these have been analysed by HPLC-MS and tandem HPLC-MS/MS by using the same analytical protocol. The total ion current chromatogram (TIC) reported in the supplementary figure *Figure S2*, available

at https://ars.els-cdn.com/content/image/1-s2.0-S0143720825004668-mmc1.docx, shows two main distinct peaks at around 14.6 min and 17.3 min corresponding to the retention times of the analytes under investigation.

Analysing the MS-spectrum of the two peaks investigated, reported in *Figure 72 a and b*, for both the compounds, four characteristic ion species have been detected: the pseudo-molecular ion $[M+H]^+$ at m/z 1005.3 and 989.3, for PVD1 and PVD2 respectively, the double and triple charged ions $[M+2H]^{2+}$ and $[M+3H]^{3+}$ and, in addition, the adduct with potassium $[M+H+K]^{2+}$. All the results obtained from HPLC-MS analysis in scan mode are reported in *Table 7*.

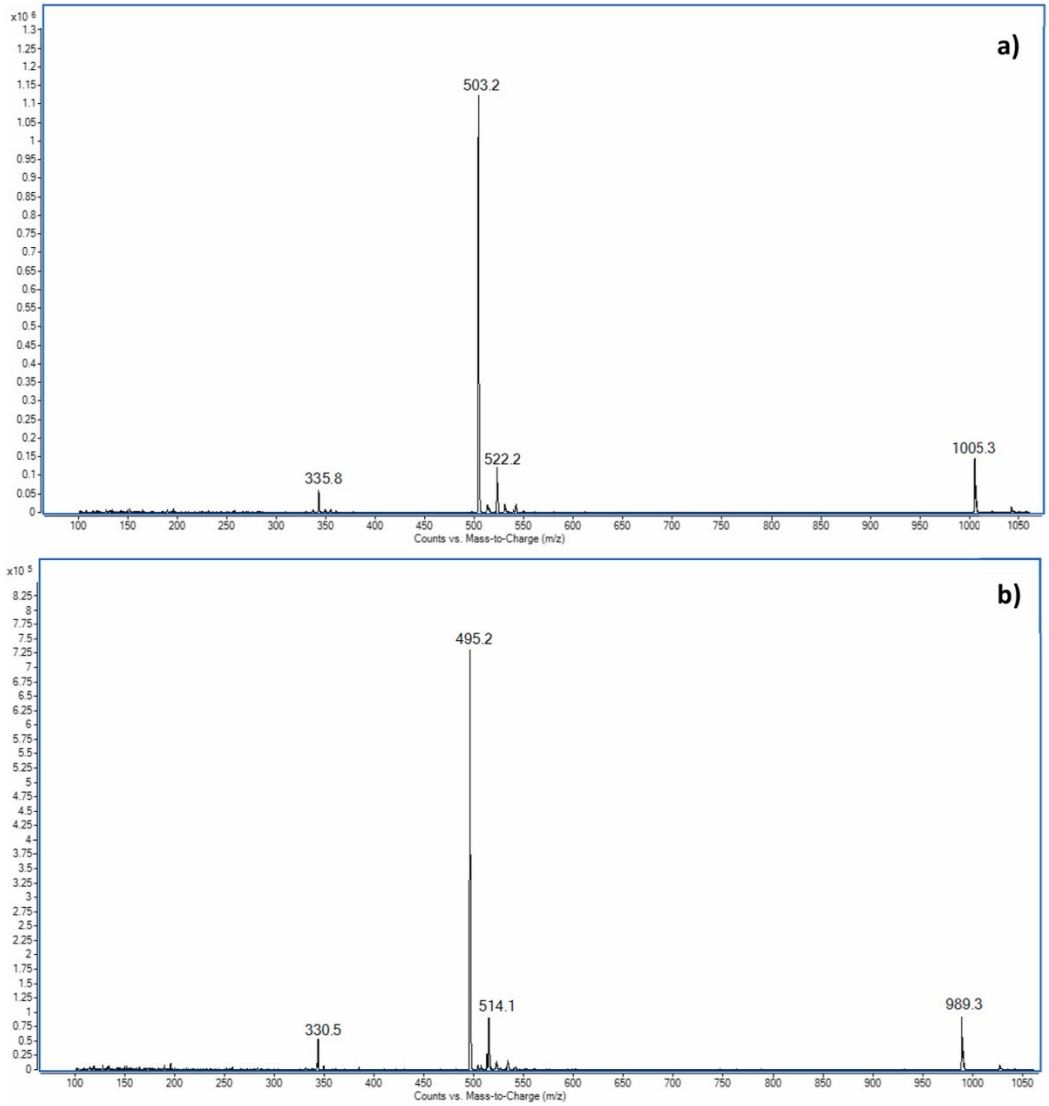

Figure 72 - MS-spectrum of the PVDs detected at a) 14.3 and b) 17.3 min by HPLC-MS analysis.

Table 7 - Molecular mass and the related *m/z* corresponding to the different PVDs.

PVD	$[M+3H]^{3+}$	$[M+H+K]^{2+}$	$[M+2H]^{2+}$	$[M+H]^{+}$	M
1	335.8	522.2	503.2	1005.3	1004.3
2	330.5	514.1	495.2	989.3	988.3

Figure 73 reports the extracted ion chromatograms (EIC) of the two most abundant adduct ions $[M+2H]^{2+}$ at m/z 503.2, and 495.2 for the two distinctive PVDs compounds confirming that the reported m/z ions are specific of the two selected peaks at 14.6 and 17.3 min.

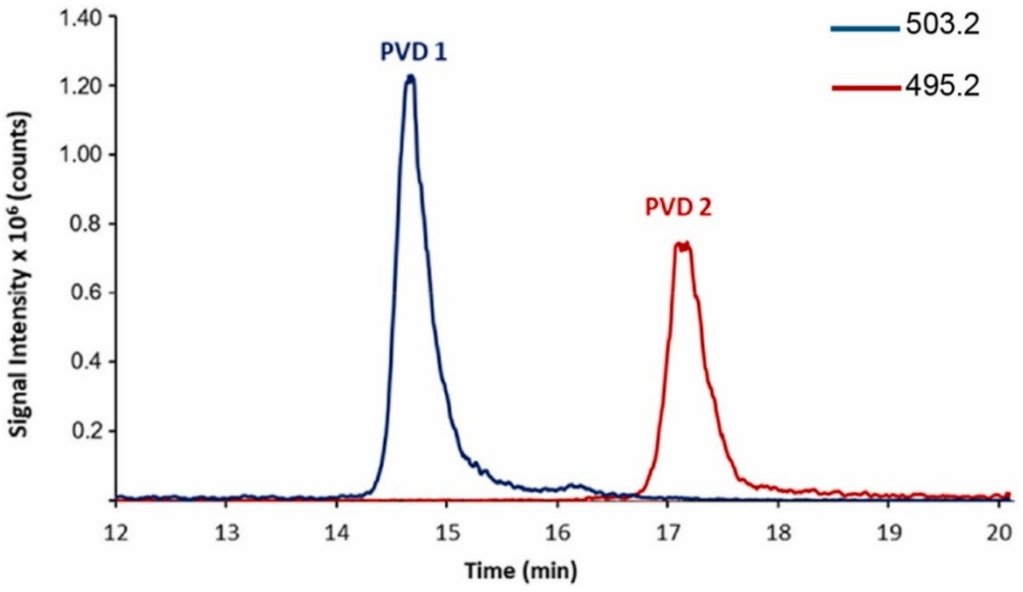

Figure 73 - Extracted ion chromatograms (EIC) of the pigment produced by Pseudomonas sp. ef1.

Successively, the $[M+2H]^{2+}$ ions of the two PVD molecules have been fragmented using various collision energies, in order to confirms the presence of the characteristic fragments and to have information about the amino acid sequence *(Georgias et al., 1999b; Hannauer et al., 2012; Meyer et al., 2008; Nosrati et al., 2018b; Ruangviriyachai et al., 2004; Schalk et al., 2020; Sultana et al., 2000b; Wei & Aristilde, 2015; Yin et al., 2014b)*

In *Figure 74*, *Figure 75* are reported the MS/MS spectrum of the PVD1 and PVD2 at 16 and 40 eV, respectively.

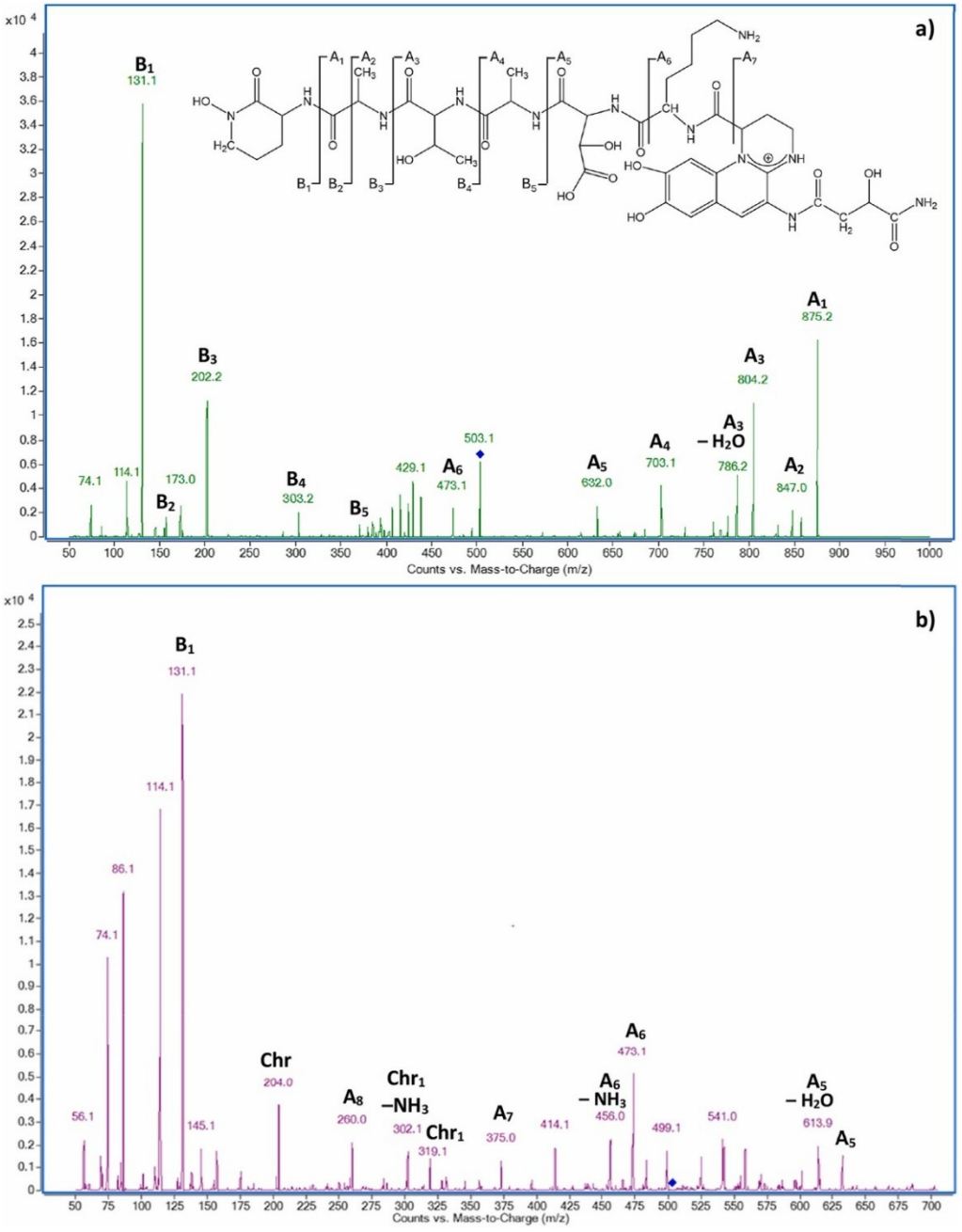

Figure 74 - MS/MS spectra of the $[M+2H]^{2+}$ (m/z 503.1) at a) 16 and b) 40 eV of collision energy. In the inset of a) reported the fragmentation scheme.

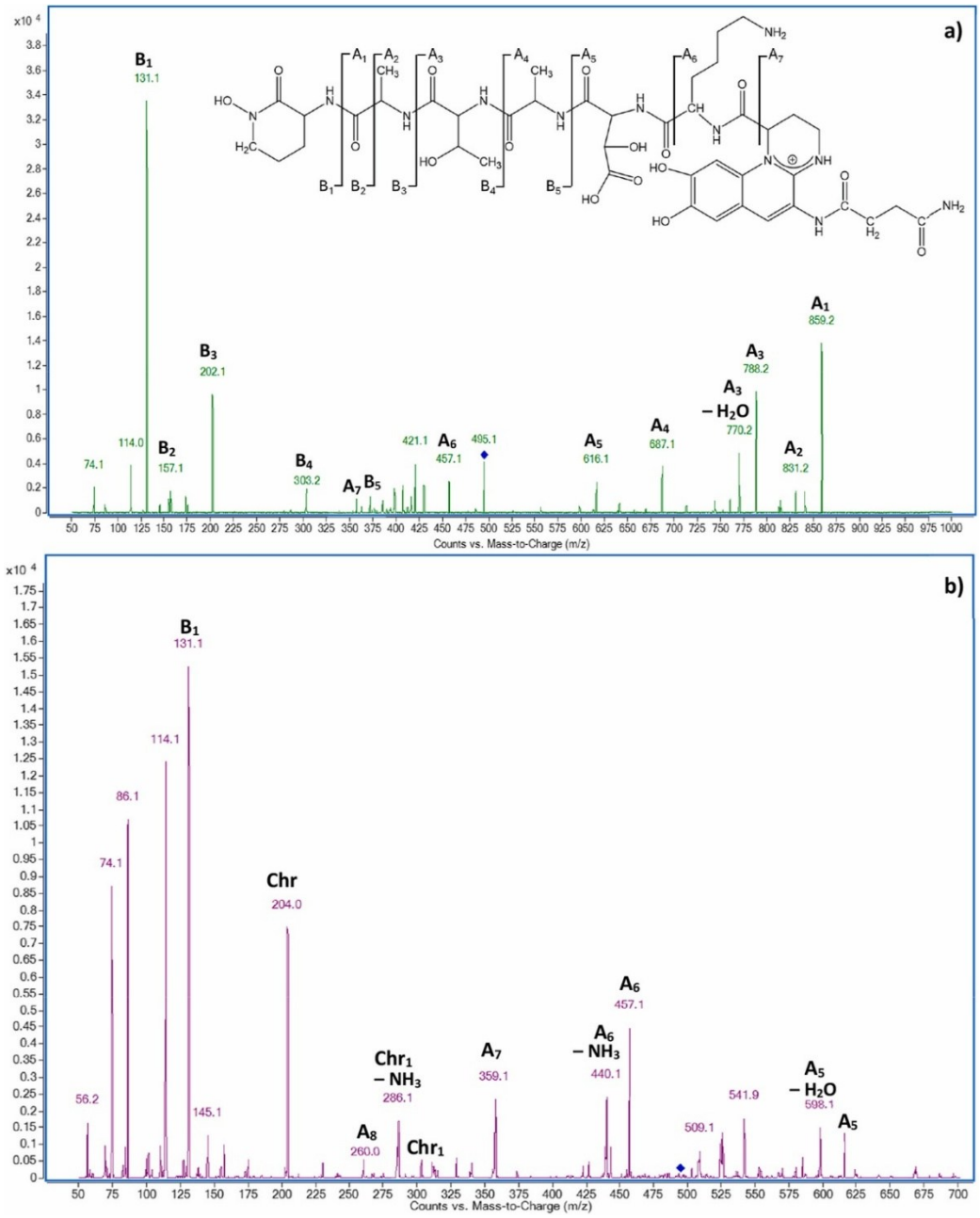

Figure 75 - MS/MS spectra of the $[M+2H]^{2+}$ (m/z 495.1) at a) 16 and b) 40 eV of collision energy. In the inset of a) is reported the fragmentation scheme.

The ion $[M+2H]^{2+}$ is typically used as a precursor for the fragmentation due to its higher abundance with respect the monocharged ion $[M+H]^{+}$ (*Figure 72*); in addition, in the double charged ion, the second proton, following the mobile proton scheme, can lies at the different peptide bonds and promote the cleavage of the peptide chain, giving the information about the amino acids sequence *(Wei & Aristilde, 2015)*. The fragmentation scheme is reported in *Figure 74*, *Figure 75.*

For both the compounds, in the MS/MS spectra (*Figure 74*, *Figure 75a*), at lower m/z value, high-intensity signals at m/z 131.1, accompanied by a lower m/z signal at 114, have been detected; these fragments signals are relative to the terminal N-hydroxyl(cyclo)Ornithine (cOHOrn), that is the last amino acid on the peptide chain, indicated as B_1. This confirms that both PVDs belong to Group 1.

All the fragments detected by HPLC-MS/MS relative to the PVD1 and PVD2 following the fragmentation scheme showed in *Figure 74*, *Figure 75*, are reported in *Table 8.*

Table 8 - Ion fragments detected by HPLC-MS/MS of the PVD1 and PVD2 and the relative *m/z* signals.

Fragments	**Ion/Ion fragments**	**PVD 2** ***m/z***	**PVD 1** ***m/z***
$[M+H]^{+}$	[cOHOrn-Ala-Thr-Ala-OHAsp-Lys-Chr–NH–R_{sc} + H]$^{+}$	989.3	1005.3
A_1	$[M - cOHOrn + H]^{+}$	859.2	875.2
A_2	$[M - B_2 + H]^{+}$	831.2	847.0

Fragments	Ion/Ion fragments	PVD 2 *m/z*	PVD 1 *m/z*
A_3	$[M - cOHOrn - Ala + H]^+$	788.2	804.2
$A_3 - H_2O$	$[A_3 - H_2O]^+$	770.2	786.2
A_4	$[M - cOHOrn - Ala - Thr + H]^+$	687.1	703.1
A_5	$[M - cOHOrn - Ala\text{-}Thr\text{-}Ala + H]^+$	616.1	632.0
$A_5 - H_2O$	$[A_5 - H_2O]^+$	598.1	613.9
A_6	$[Lys\text{-}Chr\text{–}NH\text{–}Rsc + H]^+$	457.1	473.1
$A_6 - NH_3$	$[A_6 - NH_3]^+$	440.1	456.0
A_7	$[Chr\text{–}NH\text{–}R_{sc} + H]^+$	359.1	375.0
A_8	$[Chr\text{-}NH_2 + H]^+$	260.0	260.0
Chr_1	After RDA from A_6	303.1	319.1
$Chr_1 - NH_3$	$[Chr_1 - NH_3 + H]^+$	286.1	302.1
Chr	$[Chr_1 - R_{sc} + H]^+$	204.0	204.0
B_1	$[cOHOrn + H]^+$	131.1	131.1
B_2	$[cOHOrn\text{-}COH + H]^+$	157.1	157.1
B_3	$[cOHOrn\text{-}Ala + H]^+$	202.1	202.1
B_4	$[cOHOrn\text{-}Ala\text{-}Thr + H]^+$	303.2	303.2
B_5	$[cOHOrn\text{-}Ala\text{-}Thr\text{-}Ala + H]^+$	374.2	374.2

At higher collision energy (40eV) for both the PVDs *(Figure 74*, *Figure 75*), high intensity peak of the fragment ions at m/z86.1, 114.1 and 131.1 for the terminal cOHOrn has been always detected.

In addition, at high collision energy, the fragments A_6, that corresponds to the chromophore bind to the L-Lysine and the R_{SC} moiety, can be clearly detected at 473.1and 457.1m/z, for PVD1 and PVD2, respectively. In Fig. is reported the fragmentation pattern starting from the ion fragment A_6 with the related ions and m/z. The fragment A_7, relative to the loss of the L-lysine from $A_6$are detected at 375.1 and 359.1 m/z, for PVD 1 and PVD 2, respectively. Therefore, in this study, the only difference between the two pyoverdine produced by Pseudomonas sp. ef1 is due to the different R_{SC} moieties bind to the chromophore, that for PVD1 is the hydroxy succinic acid amide and, for the PVD2, is the succinic acid amide, as reported in *Scheme 1.* The fragment ions related to chromophore after the loss of the dicarboxylic side chain (R_{SC}) at m/z 260.0 (*Scheme 1*) can be also detected for both PVD1 and PVD2 at 40eV, as reported in the MS/MS spectra (*Figure 74, Figure 75b*) *(Ruangviriyachai et al., 2004)*.

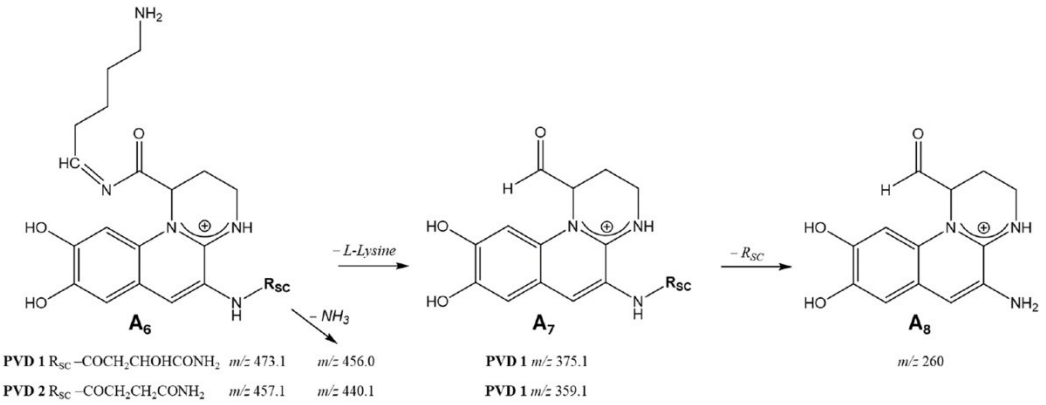

Scheme 1 - Fragmentation of the A_6 ions and the formation of the ions A_8 at m/z 260.0.

The fundamental fragment ion at m/z 204.0 (Chr), that corresponds to the characteristic 2-3-diamino-6,7-dihydroxyquinoline chromophore of the pyoverdine *(Budzikiewicz et al., 2006, 2007; H. Budzikiewicz et al., 2007; Rehm et al., 2022)* and confirms its presence, has been not detected at low collision energy (16eV), but for both the compounds is identified at high collision energy at 40eV. This ion species arises from the retro Diels-Alder reaction of the chromophore, reported in *Scheme 2*, where R_{SC} is relative to the dicarboxylic side chain. The intermediate fragment ions (Chr_1), relative to the dihydroxyquinoline chromophore bind to the R_{SC} side chain, can be detected at 319.1 and 303.1 m/z for PVD1 and PVD2, respectively, with the corresponding fragment ions at m/z 286.1 and 302.1 relative to the ions after the loss of NH_3 (*Figure 74, Figure 75b*).

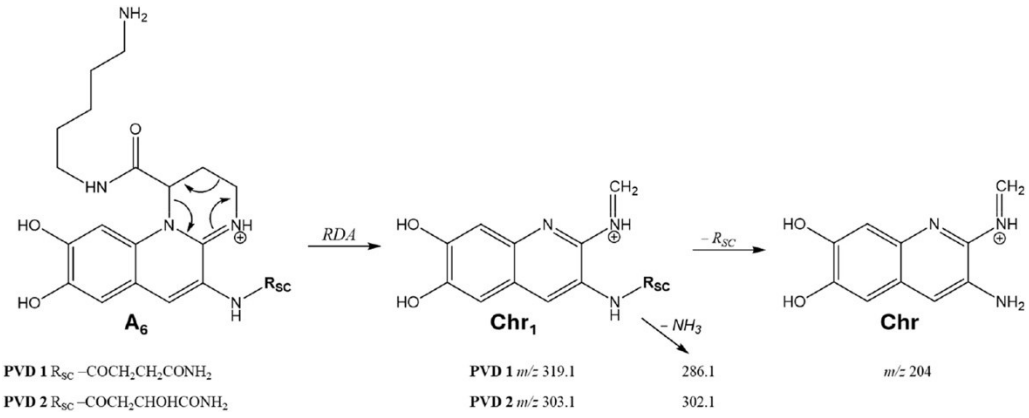

Scheme 2 - Fragmentation of the pyoverdine chromophore by Retro-Diels Alder reaction.

These fragmentation pattern has been also confirmed by the precursor ion scan chromatogram, reported in *Figure 76* , showing that the m/z fragments at 204.0 and 260.0 (set as product ions in the precursor ion scan acquisitions) are in

common between the two pyoverdines; in this case the precursor ion scan chromatogram also include the m/z 131.1 of the terminal cOHOrn amino acid.

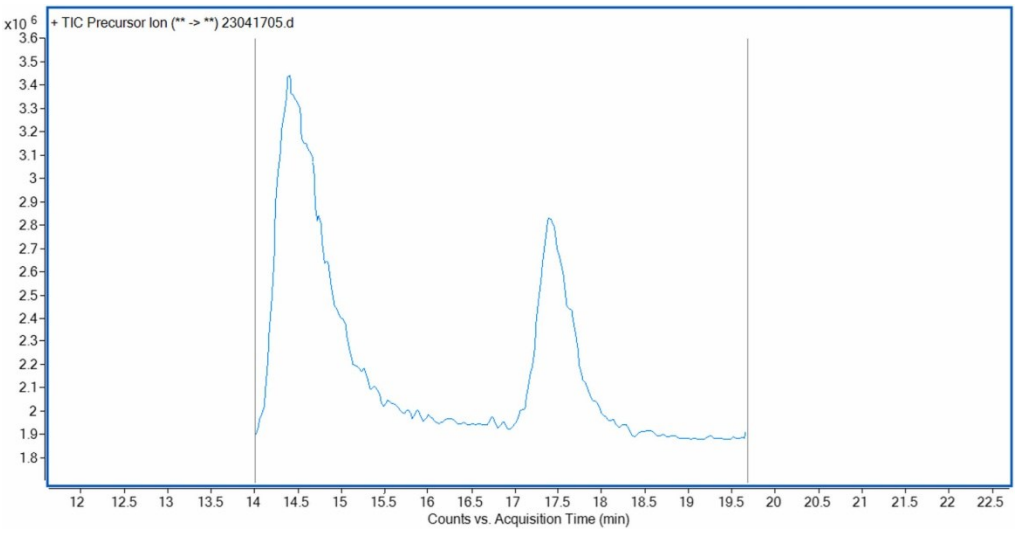

Figure 76 - Precursor ion chromatogram for the m/z precursor ions at 131.1, 204.0 and 260.0.

In addition, analysing the peak at m/z 202.1 and 204.0, relative to the B_3 fragment ions and to the chromophore (Chr), it is interesting to observe their intensity ratio evolution as function of the collision energies, as reported in *Figure 77*. At three different collision energies 16, 30 and 40eV, at lower energy the ion at m/z 202.1 (B_3) is the predominant while, increasing the energy, the ion relative to the chromophore is the predominant, confirming the presence of the dihydroxyquinoline chromophore, indicating that, for the detection of pyoverdine chromophore using ESI-MS/MS, it is necessary to operate at higher collision energies.

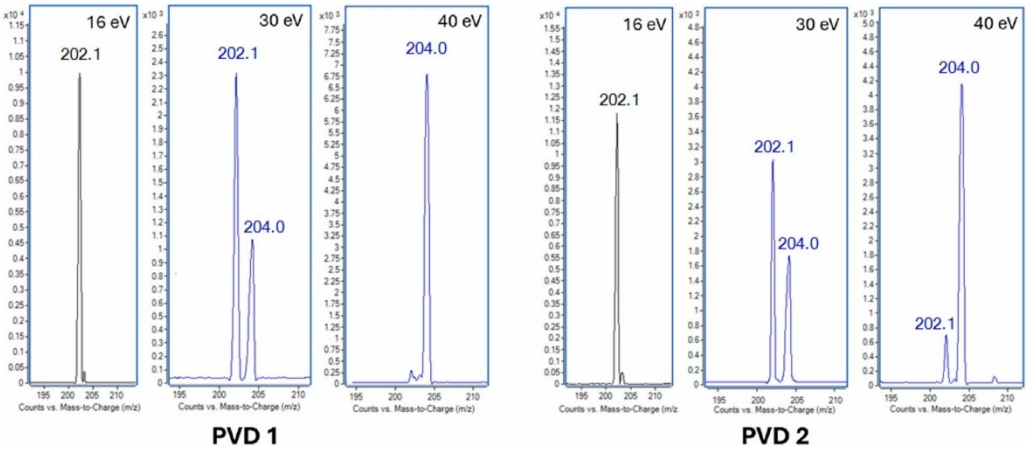

Figure 77 - MS/MS spectra of PVD1 and PVD2 at different collision energies (16, 30 and 40eV).

In conclusion, the Antarctic bacteria *Pseudomonas* sp. ef1 biosynthesized two different pyoverdines composed of the same peptide chain sequence of six amino acids: cOHOrn-Ala-Thr-Ala-OHAsp-Lys, with the cOHOrn as terminal amino acid. The two PVDs differs only in the R_{SC} moiety bind to the chromophore, that for PVD1 is the hydroxy succinic acid amide and, for the PVD2, is the succinic acid amide. Specifically, the PVD1 is characterized for the first time, no evidence it is reported in literature, as is possible to observe in *Table 9*, that reports the PVDs produced by different *Pseudomonas* bacteria with peptide chain sequence of six amino acids.

The identification of a novel pyoverdine-producing strain may contribute to expanding the currently available repertoire of microbial siderophores. Considering the growing interest in pyoverdines for applications in agriculture, bioremediation, and antimicrobial delivery, the exploration of new microbial producers and structurally diverse pyoverdines may support the development of

innovative and economically sustainable biotechnological processes *(David, Ihiawakrim, et al., 2020; Ferret et al., 2015; Gu et al., 2020a; Saha et al., 2016)*. In this context, Antarctic bacteria may represent a promising source of unexplored siderophores.

Table 9 - Group 1 pyoverdines, characterized by a six-amino-acid peptide chain, biosynthesized by different *Pseudomonas* bacteria reported in literature.

Peptide chain sequence	$[M+H]^+$	R_{SC}	REFERENCES
Lys-OHAsp-Ala-Thr-Ala-cOHOrn	989	Succinic acid amide	*(Rehm et al., 2023; Teintze et al., 1981)*
Lys-OHAsp-Ser-Ser-Ser-cOHOrn	1007	Succinic acid amide	*(Meyer et al., 2008)*
Ser-Lys-OHHis-Thr-Ser-cOHOrn	1043	Hydroxy succinic acid amide	*(Budzikiewicz et al., 1997)*
Ala-Lys-Thr-Ser-AcOHOrn-cOHOrn	1046	Succinic acid	*(Budzikiewicz et al., 1992; Rehm et al., 2023)*
Asp-Ala-Asp-AcOHOrn-Ser-cOHOrn	1047	Succinic acid	*(Jacques et al., 1995; Rehm et al., 2023)*
Lys-OHAsp-Ala-Thr-Ala-cOHOrn	989.3	Succinic acid amide	This study
Lys-OHAsp-Ala-Thr-Ala-cOHOrn	**1005.3**	**Hydroxy succinic acid amide**	**This study (NEW)**

R_{SC}: dicarboxylic side chain.

Conclusions

In this study, a yellow, fluorescent pigment produced by an Antarctic *Pseudomonas* sp. ef1 in the presence of only glucose as carbon source was purified and subsequently characterized. The obtained pigment showed

absorbance and fluorescence profiles typical of pyoverdine compounds. For its characterization, an analytical method using HPLC-DAD-FLD and HPLC-MS/MS was developed. The analysis demonstrated that the pigment is a mixture of two Group 1 PVDs composed by the following sequence of six amino acids: cOHOrn-Ala-Thr-Ala-OHAsp-Lys.

The two PVDs differ to each other only in the R_{SC} moiety, and one of these is characterized for the first time. This implies that the Antarctic bacterium *Pseudomonas* sp. ef1 is as source of a novel PVD characterized for the first time in this work.

Microbial communities influence the health of every ecosystem on Earth, including humans. Microbes have a role in biogeochemical cycles and to determine the difference between host health and disease. Microbiomes are often highly complex, in part due to their biodiversity and metabolic responses that they display. The discovery of novel secondary metabolites, especially from a bacterial strain associated with an Antarctic consortium, may provide new insight in understanding their role in mediating microbial interactions and mechanisms of environmental adaptation.

References

Albrecht-Gary, A.-M., Blanc, S., Rochel, N., Ocaktan, A. Z., & Abdallah, M. A. (1994). Bacterial Iron Transport: Coordination Properties of Pyoverdin PaA, a Peptidic Siderophore of Pseudomonas aeruginosa. *Inorganic Chemistry*, *33*(26), 6391–6402. https://doi.org/10.1021/ic00104a059

Bonneau, A., Roche, B., & Schalk, I. J. (2020). Iron acquisition in Pseudomonas aeruginosa by the siderophore pyoverdine: an intricate interacting network including periplasmic and membrane proteins. *Scientific Reports*, *10*(1), 120. https://doi.org/10.1038/s41598-019-56913-x

Boukhalfa, H., Reilly, S. D., Michalczyk, R., Iyer, S., & Neu, M. P. (2006). Iron(III) Coordination Properties of a Pyoverdin Siderophore Produced by *Pseudomonas putida* ATCC 33015. *Inorganic Chemistry*, *45*(14), 5607–5616. https://doi.org/10.1021/ic060196p

Budzikiewicz, H. (2001). Siderophores of the Human Pathogenic Fluorescent Pseudomonads. *Current Topics in Medicinal Chemistry*, *1*(1), 1–6. https://doi.org/10.2174/1568026013395560

Budzikiewicz, H., Kilz, S., Taraz, K., & Meyer, J.-M. (1997). Identical Pyoverdines from Pseudomonas fluorescens 9AW and from Pseudomonas putida 9BW. *Zeitschrift Für Naturforschung C*, *52*(11–12), 721–728. https://doi.org/10.1515/znc-1997-11-1202

Budzikiewicz, H., Schäfer, M., Fernández, D. U., Matthijs, S., & Cornelis, P. (2007). Characterization of the chromophores of pyoverdins and related siderophores by

electrospray tandem mass spectrometry. *BioMetals*, *20*(2), 135–144. https://doi.org/10.1007/s10534-006-9021-3

Budzikiewicz, H., Schäfer, M., Fernández, D. U., & Meyer, J.-M. (2006). Structure Proposal for a New Pyoverdin from Pseudomonas sp. PS 6.10. *Zeitschrift Für Naturforschung C*, *61*(11–12), 815–820. https://doi.org/10.1515/znc-2006-11-1208

Budzikiewicz, H., Schröder, H., & Taraz, K. (1992). Zur Biogenese der Pseudomonas-Siderophore: Der Nachweis analoger Strukturen eines Pyoverdin-Desferriferribactin-Paares [1] / The Biogenesis of Pseudomonas Siderophores: The Proof of Analogous Structures of a Pyoverdin/Desferriferribactin Pair [1]. *Zeitschrift Für Naturforschung C*, *47*(1–2), 26–32. https://doi.org/10.1515/znc-1992-1-206

Cezard, C., Farvacques, N., & Sonnet, P. (2014). Chemistry and Biology of Pyoverdines, Pseudomonas Primary Siderophores. *Current Medicinal Chemistry*, *22*(2), 165–186. https://doi.org/10.2174/09298673216661410111946 24

Chevrette, M. G., Thomas, C. S., Hurley, A., Rosario-Meléndez, N., Sankaran, K., Tu, Y., Hall, A., Magesh, S., & Handelsman, J. (2022). Microbiome composition modulates secondary metabolism in a multispecies bacterial community. *Proceedings of the National Academy of Sciences*, *119*(42). https://doi.org/10.1073/pnas.2212930119

Dane, P. R., Pawar, S. P., Kankariya, R. A., & Chaudhari, B. L. (2016a). Pyoverdin mediated sunlight induced green synthesis of silver nanoparticles. *RSC Advances*, *6*(10), 8503–8510. https://doi.org/10.1039/C5RA20856D

David, S. R., Fritsch, S., Forster, A., Ihiawakrim, D., & Geoffroy, V. A. (2020). Flocking asbestos waste, an iron and magnesium source for Pseudomonas. *Science of The Total Environment*, *709*, 135936. https://doi.org/10.1016/j.scitotenv.2019.135936

David, S. R., Ihiawakrim, D., Regis, R., & Geoffroy, V. A. (2020). Efficiency of pyoverdines in iron removal from flocking asbestos waste: An innovative bacterial bioremediation strategy. *Journal of Hazardous Materials*, *394*, 122532. https://doi.org/10.1016/j.jhazmat.2020.122532

Dell'Anno, F., Vitale, G. A., Buonocore, C., Vitale, L., Palma Esposito, F., Coppola, D., Della Sala, G., Tedesco, P., & de Pascale, D. (2022). Novel Insights on Pyoverdine: From Biosynthesis to Biotechnological Application. *International Journal of Molecular Sciences*, *23*(19), 11507. https://doi.org/10.3390/ijms231911507

Ferret, C., Cornu, J. Y., Elhabiri, M., Sterckeman, T., Braud, A., Jezequel, K., Lollier, M., Lebeau, T., Schalk, I. J., & Geoffroy, V. A. (2015). Effect of pyoverdine supply on cadmium and nickel complexation and phytoavailability in hydroponics. *Environmental Science and Pollution Research*, *22*(3), 2106–2116. https://doi.org/10.1007/s11356-014-3487-2

Georgias, H., Taraz, K., Budzikiewicz, H., Geoffroy, V., & Meyer, J.-M. (1999). The Structure of the Pyoverdin from Pseudomonas fluorescens 1.3. Structural and Biological Relationships of Pyoverdins from Different Strains. *Zeitschrift Für Naturforschung C*, *54*(5–6), 301–308. https://doi.org/10.1515/znc-1999-5-602

Gu, S., Wei, Z., Shao, Z., Friman, V.-P., Cao, K., Yang, T., Kramer, J., Wang, X., Li, M., Mei, X., Xu, Y., Shen, Q., Kümmerli, R., & Jousset, A. (2020). Competition

for iron drives phytopathogen control by natural rhizosphere microbiomes. *Nature Microbiology*, *5*(8), 1002–1010. https://doi.org/10.1038/s41564-020-0719-8

H. Budzikiewicz, M. Schafer, & J.-M. Meyer. (2007). Siderotyping of Fluorescent Pseudomonads - Problems in the Determination of Molecular Masses by Mass Spectrometry. *Mini-Reviews in Organic Chemistry*, *4*(3), 246–253. https://doi.org/10.2174/157019307781369968

Hannauer, M., Schäfer, M., Hoegy, F., Gizzi, P., Wehrung, P., Mislin, G. L. A., Budzikiewicz, H., & Schalk, I. J. (2012). Biosynthesis of the pyoverdine siderophore of *Pseudomonas aeruginosa* involves precursors with a myristic or a myristoleic acid chain. *FEBS Letters*, *586*(1), 96–101. https://doi.org/10.1016/j.febslet.2011.12.004

Hazotte, A. A., Peron, O., Abdelouas, A., Montavon, G., & Lebeau, T. (2016). Microbial mobilization of cesium from illite: The role of organic acids and siderophores. *Chemical Geology*, *428*, 8–14. https://doi.org/10.1016/j.chemgeo.2016.02.024

Hider, R. C., & Kong, X. (2010). Chemistry and biology of siderophores. *Natural Product Reports*, *27*(5), 637. https://doi.org/10.1039/b906679a

Jacques, Ph., Ongena, M., Gwose, I., Seinsche, D., Schröder, H., Delfosse, Ph., Thonart, Ph., Taraz, K., & Budzikiewicz, H. (1995). Structure and Characterization of Isopyoverdin from Pseudomonas putida BTP1 and Its Relation to the Biogenetic Pathway Leading to Pyoverdins. *Zeitschrift Für Naturforschung C*, *50*(9–10), 622–629. https://doi.org/10.1515/znc-1995-9-1005

John, M. S., Nagoth, J. A., Ramasamy, K. P., Mancini, A., Giuli, G., Natalello, A., Ballarini, P., Miceli, C., & Pucciarelli, S. (2020). Synthesis of Bioactive Silver Nanoparticles by a Pseudomonas Strain Associated with the Antarctic Psychrophilic Protozoon Euplotes focardii. *Marine Drugs*, *18*(1), 38. https://doi.org/10.3390/md18010038

Lozano-González, J. M., Valverde, S., Montoya, M., Martín, M., Rivilla, R., Lucena, J. J., & López-Rayo, S. (2023). Evaluation of Siderophores Generated by Pseudomonas Bacteria and Their Possible Application as Fe Biofertilizers. *Plants*, *12*(23), 4054. https://doi.org/10.3390/plants12234054

Meyer, J.-M., Gruffaz, C., Raharinosy, V., Bezverbnaya, I., Schäfer, M., & Budzikiewicz, H. (2008). Siderotyping of fluorescent Pseudomonas: molecular mass determination by mass spectrometry as a powerful pyoverdine siderotyping method. *BioMetals*, *21*(3), 259–271. https://doi.org/10.1007/s10534-007-9115-6

Mozzicafreddo, M., Pucciarelli, S., Swart, E. C., Piersanti, A., Emmerich, C., Migliorelli, G., Ballarini, P., & Miceli, C. (2021). The macronuclear genome of the Antarctic psychrophilic marine ciliate Euplotes focardii reveals new insights on molecular cold adaptation. *Scientific Reports*, *11*(1), 18782. https://doi.org/10.1038/s41598-021-98168-5

Newman, D. J., & Cragg, G. M. (2016). Natural Products as Sources of New Drugs from 1981 to 2014. *Journal of Natural Products*, *79*(3), 629–661. https://doi.org/10.1021/acs.jnatprod.5b01055

Nosrati, R., Dehghani, S., Karimi, B., Yousefi, M., Taghdisi, S. M., Abnous, K., Alibolandi, M., & Ramezani, M. (2018a). Siderophore-based biosensors and nanosensors; new approach on the development of diagnostic systems.

Biosensors and Bioelectronics, *117*, 1–14. https://doi.org/10.1016/j.bios.2018.05.057

Nosrati, R., Dehghani, S., Karimi, B., Yousefi, M., Taghdisi, S. M., Abnous, K., Alibolandi, M., & Ramezani, M. (2018b). Siderophore-based biosensors and nanosensors; new approach on the development of diagnostic systems. *Biosensors and Bioelectronics*, *117*, 1–14. https://doi.org/10.1016/j.bios.2018.05.057

Ochiai, E., Kawabe, T., Shionyu, M., & Hasegawa, M. (2025). Molecular Structure and Biosynthesis of Pyoverdines Produced by Pseudomonas fulva. *Microorganisms*, *13*(6), 1409. https://doi.org/10.3390/microorganisms13061409

Owen, J. G., & Ackerley, D. F. (2011). Characterization of pyoverdine and achromobactin in Pseudomonas syringae pv. phaseolicola 1448a. *BMC Microbiology*, *11*(1), 218. https://doi.org/10.1186/1471-2180-11-218

Pucciarelli, S., Devaraj, R. R., Mancini, A., Ballarini, P., Castelli, M., Schrallhammer, M., Petroni, G., & Miceli, C. (2015). Microbial Consortium Associated with the Antarctic Marine Ciliate Euplotes focardii: An Investigation from Genomic Sequences. *Microbial Ecology*, *70*(2), 484–497. https://doi.org/10.1007/s00248-015-0568-9

Ramasamy, K. P., Telatin, A., Mozzicafreddo, M., Miceli, C., & Pucciarelli, S. (2019). Draft Genome Sequence of a New Pseudomonas sp. Strain, ef1, Associated with the Psychrophilic Antarctic Ciliate Euplotes focardii. *Microbiology Resource Announcements*, *8*(41). https://doi.org/10.1128/MRA.00867-19

Ramírez-Rendon, D., Passari, A. K., Ruiz-Villafán, B., Rodríguez-Sanoja, R., Sánchez, S., & Demain, A. L. (2022). Impact of novel microbial secondary

metabolites on the pharma industry. *Applied Microbiology and Biotechnology*, *106*(5–6), 1855–1878. https://doi.org/10.1007/s00253-022-11821-5

Rehm, K., Vollenweider, V., Kümmerli, R., & Bigler, L. (2022). A comprehensive method to elucidate pyoverdines produced by fluorescent Pseudomonas spp. by UHPLC-HR-MS/MS. *Analytical and Bioanalytical Chemistry*, *414*(8), 2671–2685. https://doi.org/10.1007/s00216-022-03907-w

Rehm, K., Vollenweider, V., Kümmerli, R., & Bigler, L. (2023). Rapid identification of pyoverdines of fluorescent Pseudomonas spp. by UHPLC-IM-MS. *BioMetals*, *36*(1), 19–34. https://doi.org/10.1007/s10534-022-00454-w

Ringel, M. T., & Brüser, T. (2018). The biosynthesis of pyoverdines. *Microbial Cell*, *5*(10), 424–437. https://doi.org/10.15698/mic2018.10.649

Ruangviriyachai, C., Uría Fernández, D., Schäfer, M., & Budzikiewicz, H. (2004). Structure proposal for a new pyoverdin from a Thai *Pseudomonas putida* strain [1]. *Journal of Spectroscopy*, *18*(3), 453–458. https://doi.org/10.1155/2004/394872

Saha, M., Sarkar, S., Sarkar, B., Sharma, B. K., Bhattacharjee, S., & Tribedi, P. (2016). Microbial siderophores and their potential applications: a review. *Environmental Science and Pollution Research*, *23*(5), 3984–3999. https://doi.org/10.1007/s11356-015-4294-0

Schalk, I. J., & Guillon, L. (2013). Pyoverdine biosynthesis and secretion in *Pseudomonas aeruginosa* : implications for metal homeostasis. *Environmental Microbiology*, *15*(6), 1661–1673. https://doi.org/10.1111/1462-2920.12013

Schalk, I. J., Rigouin, C., & Godet, J. (2020). An overview of siderophore biosynthesis among fluorescent Pseudomonads and new insights into their complex cellular organization. *Environmental Microbiology*, *22*(4), 1447–1466. https://doi.org/10.1111/1462-2920.14937

Scholz, K., Tiso, T., Blank, L. M., & Hayen, H. (2018). Mass spectrometric characterization of siderophores produced by Pseudomonas taiwanensis VLB120 assisted by stable isotope labeling of nitrogen source. *BioMetals*, *31*(5), 785–795. https://doi.org/10.1007/s10534-018-0122-6

Sultana, R., Siddiqui, B. S., Taraz, K., Budzikiewicz, H., & Meyer, J.-M. (2000a). A pyoverdine from Pseudomonas putida CFML 90-51 with a Lys ε-amino link in the peptide chain. *Biometals*, *13*(2), 147–152. https://doi.org/10.1023/A:1009212729408

Swayambhu, G., Bruno, M., Gulick, A. M., & Pfeifer, B. A. (2021). Siderophore natural products as pharmaceutical agents. *Current Opinion in Biotechnology*, *69*, 242–251. https://doi.org/10.1016/j.copbio.2021.01.021

Tappe, R., Taraz, K., Budzikiewicz, H., Meyer, J.-M., & Lef□vre, J. F. (1993). Structure elucidation of a Pyoverdin Produced byPseudomonas aeruginosa ATCC 27 853. *Journal F□r Praktische Chemie/Chemiker-Zeitung*, *335*(1), 83–87. https://doi.org/10.1002/prac.19933350113

Teintze, M., Hossain, M. B., Barnes, C. L., Leong, J., & Van der Helm, D. (1981). Structure of ferric pseudobactin: a siderophore from a plant growth promoting Pseudomonas. *Biochemistry*, *20*(22), 6446–6457. https://doi.org/10.1021/bi00525a025

Timofeeva, A. M., Galyamova, M. R., & Sedykh, S. E. (2022). Bacterial Siderophores: Classification, Biosynthesis, Perspectives of Use in Agriculture. *Plants*, *11*(22), 3065. https://doi.org/10.3390/plants11223065

Visca, P., Imperi, F., & Lamont, I. L. (2007a). Pyoverdine siderophores: from biogenesis to biosignificance. *Trends in Microbiology*, *15*(1), 22–30. https://doi.org/10.1016/j.tim.2006.11.004

Vollenweider, V., Roncoroni, F., & Kümmerli, R. (2024). Pyoverdine–antibiotic combination treatment: its efficacy and effects on resistance evolution in *Escherichia coli*. *MicroLife*, *5*. https://doi.org/10.1093/femsml/uqae021

Weber, M., Taraz, K., Budzikiewicz, H., Geoffroy, V., & Meyer, J.-M. (2000). The structure of a pyoverdine from Pseudomonas sp. CFML 96.188 and its relation to other pyoverdines with a cyclic C-terminus. *Biometals*, *13*(4), 301–309. https://doi.org/10.1023/A:1009235421503

Wei, H., & Aristilde, L. (2015). Structural characterization of multiple pyoverdines secreted by two Pseudomonas strains using liquid chromatography-high resolution tandem mass spectrometry with varying dissociation energies. *Analytical and Bioanalytical Chemistry*, *407*(16), 4629–4638. https://doi.org/10.1007/s00216-015-8659-5

Xiao, R., & Kisaalita, W. S. (1995a). Purification of Pyoverdines of Pseudomonas fluorescens 2-79 by Copper-Chelate Chromatography. *Applied and Environmental Microbiology*, *61*(11), 3769–3774. https://doi.org/10.1128/aem.61.11.3769-3774.1995

Yin, K., Zhang, W., & Chen, L. (2014b). Pyoverdine secreted by Pseudomonas aeruginosa as a biological recognition element for the fluorescent detection of

furazolidone. *Biosensors and Bioelectronics*, *51*, 90–96. https://doi.org/10.1016/j.bios.2013.07.038

CHAPTER 5

Isolation of novel bacterial species spp. belonging to the *Halomonadaceae* family

Abstract

This chapter offers insights into a population of isolates belonging to the family *Halomonadaceae* identified in a consortium associated with their ciliate host *E. focardii*.

As the experimental work is still ongoing, preliminary results are reported. Several colonies of previously uncharacterized bacterial strains were isolated from *E. focardii*. These strains were cultured and characterized in terms of their biotechnological potential by evaluating the ability to produce BC, silver NPs, pigments, resin-like materials and bioplastics. In addition, 16S rDNA sequencing was performed to determine the taxonomic collocation of the isolates. Finally, genomic sequencing of the most promising strain, selected for its ease of cultivation and biotechnological potential, was performed using a Nanopore sequencing approach.

State of the art

Halophiles are extremophilic microorganisms that naturally inhabit hypersaline environments and have attracted considerable interest due to their unique physiological adaptations. The family *Halomonadaceae* represents one of the most widespread groups of halophilic bacteria, with more than 160 described species *(de la Haba et al., 2023)*. To cope with extreme salinity conditions, these microorganisms have evolved specialized metabolic strategies, including the production of distinctive enzymes and biomolecules. *Vreelandella titanicae* is a recently established species that was previously classified within the genus *Halomonas* as *Halomonas titanicae (Oren & Göker, 2024)*. This species was originally isolated from a microbial consortium associated with rusticle samples

collected from the RMS Titanic wreck site during the Akademic Keldysh expedition in 1991. *Halomonas titanicae* was first described as a Gram-negative, heterotrophic, aerobic, non-sporulating, motile bacterium with peritrichous flagella. It exhibits moderate halophily, being capable of growing in salt concentrations between 0.5 and 25% (w/v) NaCl, with optimal growth observed in the range 2–8% (w/v) NaCl *(Sánchez-Porro et al., 2010).* The genus *Halomonas* represented the 15th largest genus within prokaryotes, encompassing numerous species primarily isolated from marine, hypersaline, and alkaline environments. Members of this genus share important genomic features linked to metal corrosion processes; among them, metal-dependent and -binding genes, iron reductases, iron uptake regulators, ferrochelases, iron transporters, and metallopeptidases *(Sánchez-Porro et al., 2013).* However, the high degree of heterogeneity observed within this genus, reflected in a wide DNA G + C content range (51.4–74.3 mol%), led to a comprehensive taxonomic re-evaluation and subsequent reclassification *(Oren & Göker, 2024; Sánchez-Porro et al., 2010)*.
The genus *Vreelandella* comprises slightly to moderately halophilic bacteria capable of growth over a broad salinity range (0–27% w/v NaCl), with optimal growth observed between 0 and 15% (w/v) NaCl. Members of this genus are mesophilic or psychrotolerant, displaying survival across a wide temperature spectrum (from −5 to 60°C), with optimal proliferation in the temperature range 20–37°C. Species within *Vreelandella* are generally alkaliphilic or alkalitolerant, and exhibit a DNA G + C content ranging from 52.1 to 63.8 mol%. Colonies display phenotypic variability, appearing translucent, beige, black, cream, glistening-coloured, ochre, orange, pale-pink, reddish-brown, white, or yellow pigmented. Among these species, *Vreelandella titanicae* is characterized

by a genome size of approximately 5.34 Mbp and a DNA G + C content of 54.6 mol% *(de la Haba et al., 2023)*.

Members of the family *Halomonadaceae* show remarkable biotechnological potential.

Most species belonging to the *Halomonas* genus have been reported to produce ectoine, a compatible solute functioning as an osmoprotective agent with diverse biotechnological applications, including its use as hydrating and protective ingredient in cosmetics formulations *(M. Liu et al., 2021; Ye & Chen, 2021)*. *Halomonas* spp. can also synthesise enzymes of industrial relevance, including thermostable and alkali resistant lipases and halotolerant cellulases. Furthermore, several biopolymers synthesised by *Halomonas* spp. such as extracellular polysaccharides (EPS), have attracted interest due to their potential use as adhesives, jellifying agents and emulsifier, and for their reported antioxidant, cytotoxic, anti-tumour and cell proliferative activities. These bacteria are also known to produce biosurfactants and pigments involved in crude oil recovery, as well as siderophores under iron limitation conditions. Moreover, these microorganisms were reported to be able to detoxify Cr(VI) and other heavy metals and to remove a wide range of hydrocarbons *(Biswas et al., 2023)*. Additionally, *Halomonas* species present several advantages over conventional organisms currently used in industrial applications such as *Escherichia coli* and *Corynebacterium glutamicum*. These include enhanced resistance to contamination, rapid growth rates, the ability to use inexpensive seawater-based media and metabolic versatility toward a wide range of substrates. Notably, the production of some of *Halomonas*-derived products

have already been scaled up to bioreactors with working volumes of at least 5000 litres, suggesting industrial feasibility *(Ye & Chen, 2021)*.
Vreelandella species were also demonstrated capable of producing ectoine, biosurfactants, and exopolysaccharides with promising antioxidant activity, to detoxify environmental pollutants and carcinogen substances, and to degrade organic compounds and heavy metals in saline environments *(Daga-Quisbert et al., 2024; Darden et al., 2025; Lautert-Dutra et al., 2025; Sabroso et al., 2025).*

Among the natural products attracting increasing interest is the ability of these microorganisms to produce polyhydroxyalkanoates (PHAs).
Polyhydroxyalkanoates are natural polymers synthesized by different bacterial species under imbalanced nutrient conditions. PHA accumulation represents a microbial strategy for storing energy and carbon under conditions of excess carbon availability and low access to nitrogen, phosphorous, and oxygen *(Obulisamy & Mehariya, 2021)*. They are accumulated in cytoplasmic granules which are insoluble in water to levels up to 90% (w/w) of the dry cell mass (Steinbüchel & Lütke-Eversloh, 2003). PHAs include a variety of biopolymers. Among them, poly(3-hydroxybutyric acid) (PHB), poly(3-hydroxyvalerate) (PHV) and their copolymer poly(3-hydroxybutyrate-co-3-hydroxyvalerate) (PHBV) represent the most extensively studied *(Volova et al., 2003).* These compounds are commonly referred to as bioplastics, since they exhibit similar properties to polypropylene, paving the way for plastic replacement *(Naser et al., 2021)*. In everyday life, disposable plastics are consumed in enormous quantities, especially in the medical and food-packaging sectors. Their extensive use contributes significantly to fossil fuels depletion, climate change, and environmental pollution, as approximately 90% of plastic waste ultimately ends

up in landfills, contaminating soil and groundwater and threatening ecosystems *(Bhatia et al., 2021; J. Lee et al., 2021)*. For these reasons, PHAs have emerged as valuable eco-friendly alternatives to conventional plastics, with a market that is continuously expanding *(Sirohi et al., 2021)*.

PHAs have already found a broad range of applications in food packaging, textile industries, and in the biomedical sectors (*Figure 78*) *(Pulingam et al., 2022)*, owing to their non-toxic, biodegradable and biocompatible nature *(Cywar et al., 2023; Rekhi et al., 2022)*. PHAs application in the electrospinning has been recently explored, revealing potential for improving bone and skin regeneration *(Kitsara et al., 2017; Lim et al., 2017; Sanhueza et al., 2019; Zhao et al., 2021)*. However, several limitations hinder their large-scale application, mainly due to low yields and high production costs *(Y. Wang et al., 2014)*. To mitigate these issues, the use of inexpensive media and waste recycling have been proposed to improve the economic feasibility of PHA production *(M. Ullah et al., 2025)*. Moreover, the employment of highly productive microorganisms, such as halophilic species belonging to the genera *Halomonas* and *Vreelandella,* offers a valuabe alternative for developing cost-effective and scalable PHA production processes.

PHA-related genes are generally organized into clusters, but their genomic arrangements are highly diversified. In halophilic microorganisms, a conserved PHA gene cluster containing maoC-phaR-phaP-phaE-phaC genes have been reported and is functionally associated with the classical enzymes β-ketothiolase (PhaA), β-ketoacyl-CoA reductase (PhaB) and PHA synthase (PhaC) *(Mitra et al., 2020)*. However, studies on some *Halomonas* species have shown that PHA-related genes are not always organized within a single operon but may instead be distributed across distant genomic regions *(Biswas et al., 2023)*.

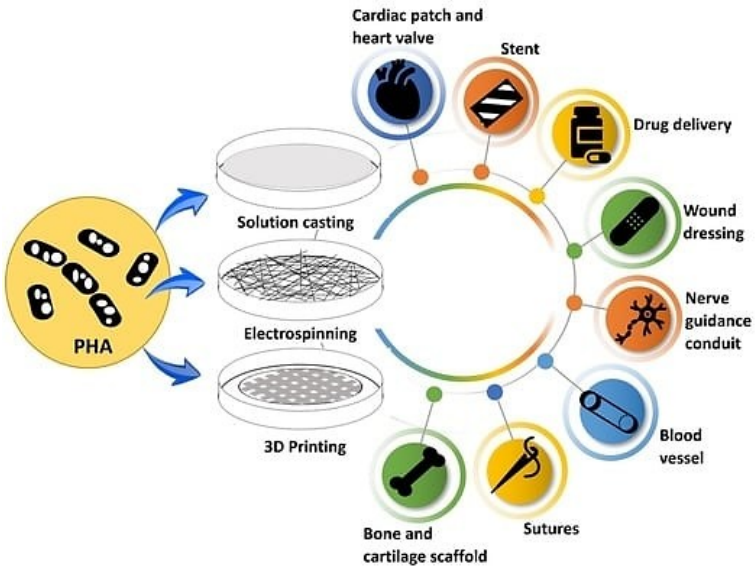

Figure 78 - Biomedical applications of PHAs. From Pulingam et al., 2022 https://doi.org/10.3390/polym14112141).

In this research work, several isolates were identified within a consortium associated with the protozoan *E. focardii*. Based on the 16S rDNA gene sequence, a close phylogenetic relationship with the genera *Halomonas* and *Vreelandella*, including *Vreelandella titanicae*, emerged. The biotechnological potential of the isolates, including their ability to synthesize AgNPs, PHAs, pigments, and cellulose-like biofilms, was investigated. Whole genome sequencing of isolate #12, which emerged as the most promising strain in terms of biomolecule production and growth rate, was performed to enable detailed genomic characterization.

Materials and Methods

Bacterial colonies isolation starting from *E. focardii*

Two samples of the marine ciliate *E. focardii* suspended in seawater were collected respectively before and after sonication treatment. The sonicated sample was kept on ice during the procedure to keep the temperature low, as the optimal living temperature for this organism is set at 4 °C *(Pucciarelli et al., 2015)*. Sonication occurred applying ultrasounds at 20 kHz for 3 seconds, intermitted by a 10 second stop and again repeated for 3 more seconds using Misonix Sonicator 3000. Both samples were centrifuged at 14.000 rpm for 10 min. The pellets were resuspended in 100 µl Minimal Medium and seeded in MacConkey Agar plates. This latter represents a selective and differential medium able to discriminate between lactose and non-lactose fermenters Gram negative bacterial species. The initial objective of the research was to isolate strains of *Marinomonas* genus, previously identified in the consortium *(John, Nagoth, Ramasamy, Ballarini, et al., 2020)* and recognized as lactose fermenters. Aliquots of both samples were seeded on LB Agar plates as control medium. Incubation occurred at 4 °C to favour the growth of Antarctic bacterial species over non-Antarctic possible contaminants. Each colony was then scooped and plated in a LBA plate to encourage the growth of the isolates.

Two independent screenings were performed using this approach. In the first screening, 14 colonies emerged from the sonicated sample, whereas no colonies were recovered from the non-sonicated sample. The isolates #1, #2, #7, #10, #12, and #14 were selected for further analyses. Among them, the isolate #12 was considered the most promising strain and was characterized more in detail, as illustrated in the following sections. In the second screening, 25 colonies

emerged from the sonicated sample, while only two colonies emerged from the non-sonicated sample. In this case, the isolates #2CG, #3CG, #4CG, #15CG, were selected for further analyses.

RAPD analysis

RAPD technique allowed to detect the presence of different haplotypes in the sample, in order to understand if the emerging bacterial colonies belonged to different strains and species. Only the colonies that reached a sufficient growth on LBA medium were tested. This test was performed on the isolates collected during the second screening.

Two RAPD analyses were executed according to the protocol provided by Castronovo et al. *(Castronovo et al., 2020)*. The first was performed using a primer with the sequence CACCCCAGTCI on 21 selected isolates, named 1, 2, 3, 4, 5, 6, 7, 8, 11, 12, 13, 14, 15, 16, 18, 19, 20, 23, 24, 26, 27. Another analysis was performed using a primer with the sequence TCACGGGAC on isolates 3, 4, 7, 26, 27 to better clarify their haplotype.

Briefly, colonies from the isolates grown in LBA plates were picked with a sterile toothpick and resuspended in 20 µl of DNA-free H_2O. Cell lysis was achieved by incubating the tubes at 95°C for 10 minutes, and then on ice for 5 minutes. The tubes were centrifuged at 15.000 rpm for 5 minutes, and the supernatant was collected with a micropipette.

Each PCR reaction contained 50 µl of solution with the following composition:

Reagents	*Volume/sample*	*Final concentration*
H_2O	*39.7 µl*	
Buffer 10X	*5 µl*	*1X*
dNTPs 10 mM	*1 µl*	*200 µM*
DNA	*2 µl*	*1-500 ng*

Primer	*1 µl*	*1 µg*
Taq DNA Polymerase	*0.3 µl*	*1 U*

PCR samples were mixed by pipetting up-and-down. PCR cycles were set up as follow:

I. Initial denaturation: 90 °C for 1 minute

II. Denaturation: 95 °C for 30 seconds

III. Annealing: 36 °C for 1 minute

IV. Extension: 72 °C for 2 minutes

V. Final elongation: 72 °C for 10 minutes

VI. Final incubation at 60 °C for 10 minutes

Steps II, III and IV were repeated for 45 cycles on BIOMETRA T-Personal thermal cycler. The PCR products were then analysed by electrophoresis on a 1% agarose gel at 50 V, to verify the fragment size and observe the pattern of the bands.

The assignment of different isolates to the same haplotype group was determined based on the fingerprint pattern of each RAPD product, comparing them for the presence/absence of bands *(Castronovo et al., 2020)*.

DNA purification and 16S rDNA sequencing

The bacterial isolates belonging to different strains based on the RAPD test results were selected for DNA amplification, performed by PCR using the universal primers 27F and 1492R that anneal near the ends of the 16S rDNA sequence, as shown in *Figure 79*. The PCR products were purified and sent to BMR Genomics (Padua), to be sequenced using the Sanger method.

Colonies of the isolates grown in LBA plates were picked with a sterile toothpick and resuspended in 20 µl of DNA-free H_2O. Cell lysis was achieved by incubating the tubes at 95°C for 10 minutes, and then on ice for 5 minutes. The tubes were centrifuged at 15.000 rpm for 5 minutes, and the supernatant was collected with a micropipette. DNA from *Pseudomonas* sp. ef1, amplified with *Pseudomonas* sp. ef1 16S-specific primers was used as a positive control, whereas DNA-free water amplified with the universal 16S primers served as the negative control.

The sequences for both forward and reverse primers are reported in the following table:

Primer's name	*Sequence*
27F (forward)	*AGAGTTTGATCMTGGCTCAG*
1492R (reverse)	*TACGGYTACCTTGTTACGACTT*

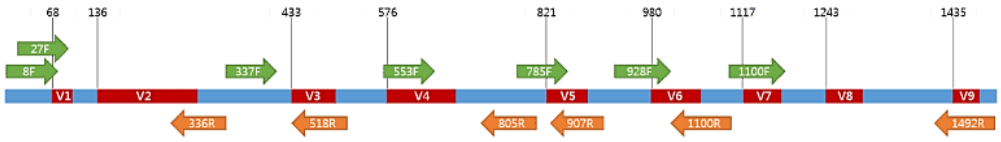

Figure 79 – Schematic representation of 16S rDNA gene and the universal couple of primers used for its amplification. The amplicon using the couple 27F and 1492R has an approximate length of 1400 bp. Image taken from https://help.ezbiocloud.net/16s-rrna-and-16s-rrna-gene/.

Each PCR reaction contained 50 µl of solution with the following composition:

Reagents	*Volume/sample*	*Final concentration*
H_2O	*39.7 µl*	

Buffer 10X	*5 µl*	*1X*
dNTPs 10 mM	*1 µl*	*200 µM*
DNA	*2 µl*	*1-500 ng*
Primer Forward 10 µM	*1 µl*	*0.2 µM*
Primer Reverse 10 µM	*1 µl*	*0.2 µM*
Taq DNA Polymerase	*0.3 µl*	*1 U*

PCR samples were mixed by pipetting up-and-down. PCR cycles were set up as follow:

I. Initial denaturation: 95 °C for 1 minute

II. Denaturation: 95 °C for 30 seconds

III. Annealing: 52 °C for 1 minute

IV. Extension: 72 °C for 1 minute

V. Final elongation: 72 °C for 5 minutes

Steps II, III and IV were repeated for 30 cycles on BIOMETRA T-Personal thermal cycler. The PCR products were then analysed by electrophoresis on a 1% agarose gel at 50 V, to verify the fragment size. After DNA amplification, the PCR products were purified using the NucleoSpin ® Gel and PCR Clean-up kit according to the instructions of the manufacturer.

The purity of the sample was subsequently evaluated using a Nanodrop spectrophotometer. The concentration of dsDNA was adjusted according to the guidelines provided by BMR Genomics.

The 16 rDNA sequences were analysed using BLASTn to identify the most closely related taxa, and were subsequently compared though multiple sequence alignment using Clustal Omega.

Biotechnological characterisation

Bacterial cellulose production

Bacterial strains were inoculated in HS medium (pH 6.5) supplemented with 2% (v/v) of glucose, lactose or sucrose to determine the optimal conditions for BC production. *Brevundimonas* sp. #2 was used as a positive control, as it already proved significant cellulose synthesis ability.

AgNPs production

The bacterial strains were grown in LB medium at 22°C for 24 hours. Cells were harvested by centrifugation at 3,000 rpm for 20 minutes using a Beckam Model J2-21 centrifuge. The pellet was then washed twice with deionized water to remove residual salts from the culture medium. The biomass was quantified by weighing the pellet after centrifugation. Bacterial cells were resuspended in deionized water to obtain a final concentration of 200 mg/ml. AgNPs synthesis was performed by adding silver nitrate ($AgNO_3$) 1 mM to the bacterial suspension, carefully mixing it with the micropipette. The reaction mixtures were placed on ArgoLab M2-A magnetic stirrer for 24 hours, protected from light. Visual inspection of the suspension allowed to preliminary assess the formation of AgNPs, indicated by a colour change of the suspension from white to brown. The synthesis of AgNPs was further confirmed by UV-visible spectroscopic analysis.

PHAs production

The accumulation of polyhydroxyalkanoates was monitored by a viable-colony staining using Nile Red, a lipophilic dye able to distinguish between PHA-producing and non-producing strains *(Spiekermann et al., 1999)*. Nile Red was

dissolved in DMSO and was directly added to the previously sterilized MMD (Davis Minimal Medium) Agar with a final concentration of 0.5 µg ml^{-1}. 25 ml of MMD Agar supplemented with Nile Red were poured in each plate. Plates without Nile Red were used as negative controls. To identify the optimal conditions for PHA synthesis, different sugars were included in the solid medium at a final concentration of 1% (w/v), including glucose, sucrose, and lactose. In addition, plates containing no added carbon source other than agar were used to assess the ability of the organisms to synthesize PHAs in absence of supplemented sugars.

Bacterial isolates #1, #2, #10, #12, previously grown overnight in LBA were then plated in the MMD Agar plates. *Rhodococcus* sp. ef1 and *Pseudomonas* sp. ef1 were used as positive controls as they have been previously shown to be capable of accumulating PHAs. *Bacillus* sp. ef1, instead, served as a negative control.

Accumulation of PHAs was monitored daily by exposing the plates to UV light (312 nm). Orange fluorescence was expected in case of PHA-positive strains.

In another experiment, bacteria were grown in nutrient broth (NB, containing peptone 5.0 g/L, yeast extract 2.0 g/L, NaCl 5.0 g/L, Meat extract 1.0 g/L) overnight and subsequently cultured in a liquid NB-seawater medium (1:1 volume ratio) supplemented with 1% (w/v) of sucrose to favour the synthesis of PHAs. Different bacterial isolates were tested: #2, #7, #10, #12, and #14. *Rhodococcus* sp. ef1 was used as a positive control as it was previously demonstrated to produce PHAs. *Bacillus* sp. ef1 was used as the negative control as it is not able to synthesize this biopolymer. PHA production was monitored daily by collecting an aliquot from each bacterial suspension which was then

plated in the solid MMD Agar plates. Agar plates were exposed to ultraviolet light (312 nm) to detect accumulation of PHAs.

Pigment production

The isolates were cultured in MMD supplemented with 1% lactose and M9 (Na_2HPO_4 6 g/L, KH_2PO_4 3 g/L, NaCl 0,5 g/L, NH_4Cl 1 g/L, $MgSO_4$ 2 mM, $CaCl_2$ 0,1 mM), supplemented with either glucose or lactose 1% to test their ability to produce pigments. The isolate #2 CG was also incubated in a culture medium containing NB and seawater (1:1 v/v), and 1% (v/v) of soy oil. Pigment production was assessed by visual inspection and by exposure to UV light. UV-visible absorption spectra were collected to allow a preliminary characterization of the produced pigments.

Additional tests

To assess biodegradation capability and bioremediation potential, isolate #2 was grown in a minimal medium (M9) modified by doubling salt concentrations (Na_2HPO_4 12 g/L, KH_2PO_4 6 g/L, NaCl 1 g/L, NH_4Cl 2 g/L, $MgSO_4$ 2 mM, $CaCl_2$ 0,1 mM), supplemented with 1% diesel (v/v) as the sole carbon source. In parallel, the isolate was cultured in a NB-seawater (1:1 v/v) medium supplemented with 1% soy oil as the sole carbon source.

Sequencing of isolate #12

Isolate #12 was grown overnight in 10 mL of LB (10 g/L tryptone, 5 g/L yeast extract, 10 g/L NaCl) at 23°C under shaking. Cells were harvested by centrifugation and DNA was extracted by using the 'DNeasy PowerSoil Pro Kit' (Qiagen), following the protocol provided by the manufacturer. Genomic DNA

was sequenced with Oxford Nanopore technology using a GridION equipped with a R 10.4 flow cell though a native barcoding approach. Basecalling was performed with MinKNOW v23.11.3 using the super accurate model. A minimum Q score of 10 and a minimum read length of 200 b were applied as filtering criteria. Sequencing reads were assembled using EPI2ME v5.1.8 and the workflow 'wf-bacterial-genomes' v1.0.0. The putative coding regions (CDSs) were annotated by the software PROKKA (version 1.14.5).

Results

Bacterial colonies isolation starting from *E. focardii*

Two independent screenings were performed starting from *E. focardii* containing sample. In the first screening, 14 colonies emerged from the sonicated sample, whereas no colonies were recovered from the non-sonicated sample. The isolates #1, #2, #7, #10, #12, and #14 were selected for further analyses (*Figure 80*). Among them, the isolate #12 was considered the most promising strain and was characterized more in detail, as illustrated in the following sections. In the second screening, 25 colonies emerged from the sonicated sample (*Figure 81*), while only two colonies emerged from the non-sonicated sample. In this case, the isolates #2CG, #3CG, #4CG, #15CG, were selected for further analyses.
In both cases, the colonies arose after two weeks at 4 °C.
The aim of this investigation was to better understand the relationship between the endosymbiont microorganisms and the ciliate host, in order to see whether the bacteria were associated to the external membrane or live inside their host. This outcome suggests that the bacterial symbionts are mostly inside the ciliate hosts.

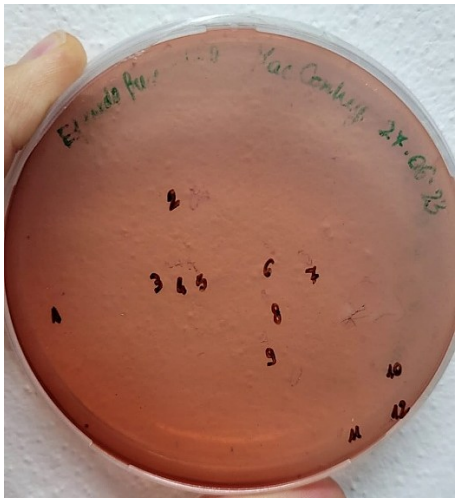

FIGURE 80 - ***Bacterial colonies emerging from sonicated E. focardii on MacConkey agar plate (first screening)****. A total of 14 colonies were observed. In contrast, no colony emerged from the non-sonicated sample (picture not shown).*

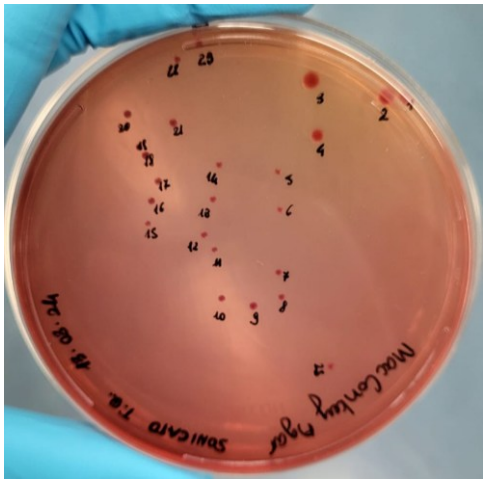

FIGURE 81 - ***Bacterial colonies emerging from sonicated E. focardii on MacConkey agar plate (second screening)****. A total of 25 colonies were*

observed. In contrast, only two colonies emerged from the non-sonicated sample (picture not shown).

RAPD analysis

The first RAPD screening revealed the presence of at least 3 different haplotypes, as shown in *Figure 82*. One haplotype included the isolate #2, a second haplotype comprised the isolates #5, #6, #8, #12, #13, #14, #15, #16, #18, #19, #20, #23, possibly corresponding to the previously identified *Halomonas* sp. #12, a third haplotype included the isolates #1, #3, #4, #7, #26, #27. For isolate #7, it was unclear whether it shared the same haplotype of the last group or if it belonged to a distinct one.

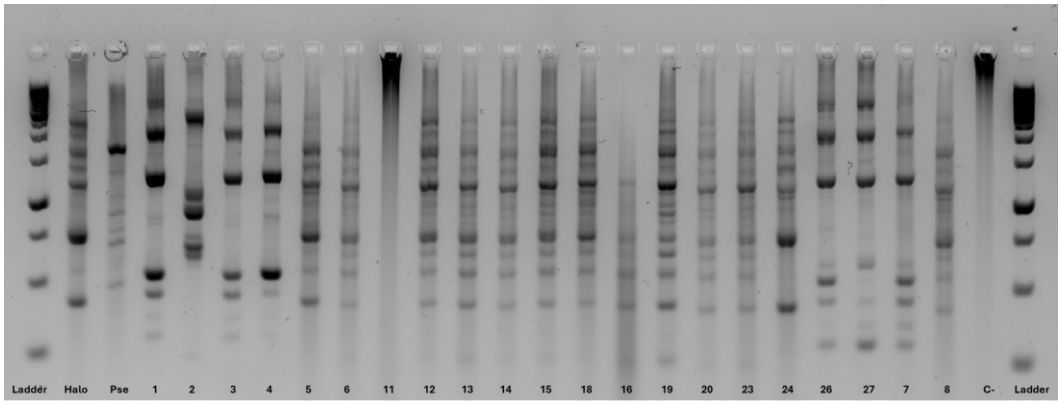

*Figure 82 – **RAPD results obtained using the primer CACCCCAGTCI**. Variations in the RAPD band patterns suggest the presence of different haplotypes, likely indicating the coexistence of multiple bacterial strains in the sample.*

To obtain further clarification, RAPD analysis was repeated on isolates #3, #4, #7, #20, and #27, using a different primer sequence.

The results (*Figure 83*) suggested that the isolate #3 belongs to a distinct haplotype, likely representing a different bacterial strain.

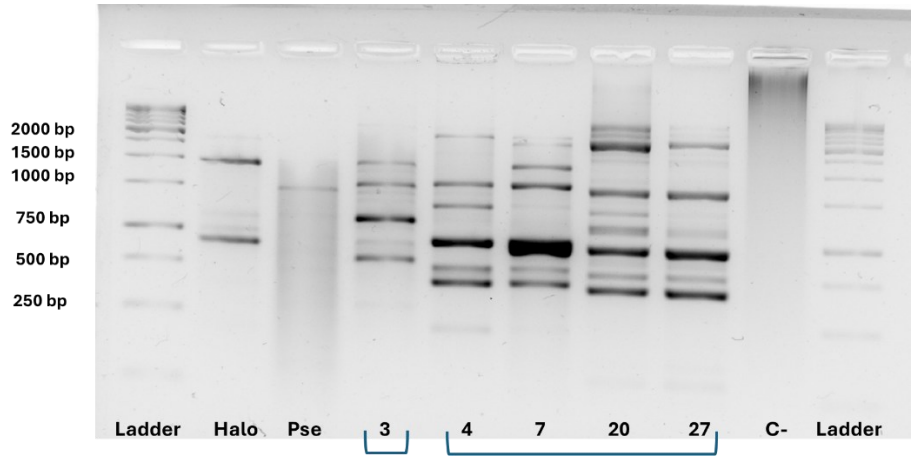

*Figure 83 – **RAPD results obtained using the primer TCACGGGAC**. Two distinct haplotypes were detected, one associated with isolate #3 and another shared by the isolates #4, #7, #20, #27, which likely represent different bacterial strains.*

Biotechnological potential of the selected isolates

The selected isolates were characterised in terms of biotechnological potential, investigating their ability to produce AgNPs, BC, bioplastic, and pigments. *Table 10* resumes the main preliminary results obtained.

Table 10 – Biotechnological characterization of the selected isolates in terms of AgNPS, BC, pigments and bioplastic production. N. i. = not investigated.

Strain	***AgNPs production***	***BC production***	***Pigment production***	***Bioplastics production***	***Other features***

#1	✓	✓	✓, *fluorescent, yellow*	✓	
#2 CG	✓	✓	✓, *fluorescent, pink*	✓, *PHB*	*Capable of growing in a NB-seawater medium (1:1 v/v) supplemented with 1% (v/v) soy oil as sole carbon source, producing a pink pigment*
#2	✓	✓	✓, *fluorescent*	✓	*Capable of growing into a minimal medium (M9) containing 1% (v/v) diesel as sole carbon source and to produce a resin-like material*
#3	*N. i.*	*N. i.*	*N. i.*	*N. i.*	
#4	*N. i.*	*N. i.*	*N. i.*	*N. i.*	
#7	✓	✓	*X*	✓	
#10	✓		*N. i.*	✓	
#12	✓	✓	✓, *fluorescent, yellow-red*	✓	
#14	✓	✓	*X*	✓	
#15	*N. i.*	*N. i.*	*N. i.*	*N. i.*	

AgNPs

The isolates #1, #2, #2 CG, #7, #10, #12, and #14 could produce AgNPs. As shown in *Figure 84*, after 24 hours of stirring, a change in the colour of the suspension from white to dark brown was observed, indicating the reduction of $AgNO_3$ in AgNPs, which is attributable to the excitation of the surface plasmon resonance of AgNPs *(John, Nagoth, Ramasamy, Mancini, et al., 2020)*. The AgNPs were purified using a purification column containing G50 resin to remove residual salts. Each sample was analysed by UV-vis spectroscopy in the range 300-800 nm, to confirm the presence of nanoparticles.

The spectra showed a peak at between 400-500 nm, consistent with surface plasmon resonance of AgNPs, whereas absorption peaks in the 200-300 nm range could be attributed to residual salts and the presence of capping proteins.

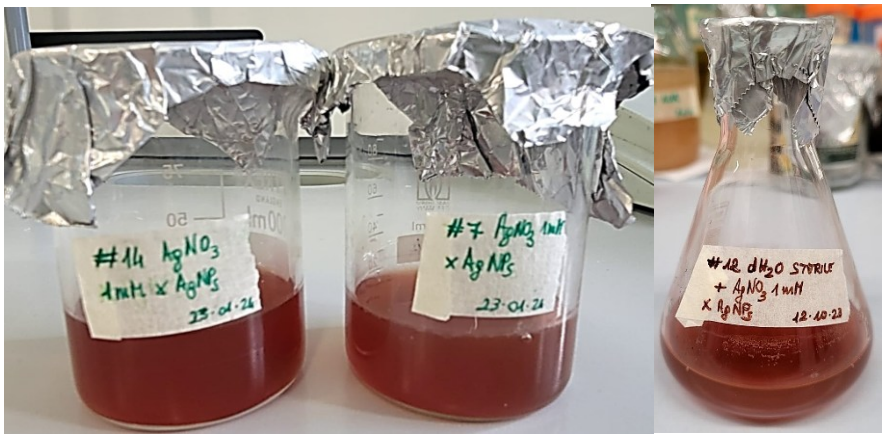

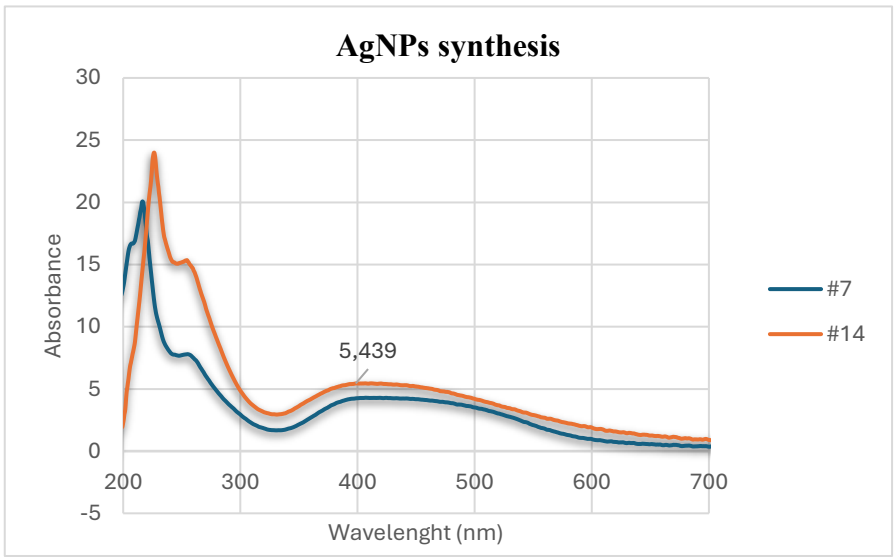

Figure 84 – AgNPs produced by the isolates #14, #7, and #12. Below, the absorption spectrum of the AgNPs produced by isolates #7 and #14 is reported as example.

Bacterial cellulose synthesis

Isolates #1, #2, #2 CG, #7, #12, and #14 cultivated in HS medium produced cellulose-like biofilms after one week incubation in both static and agitated

conditions. The biopolymers exhibited different morphologies, including loose sheets, dispersed or filamentous forms, pellets, and star-shaped aggregates (*Figure 85*).

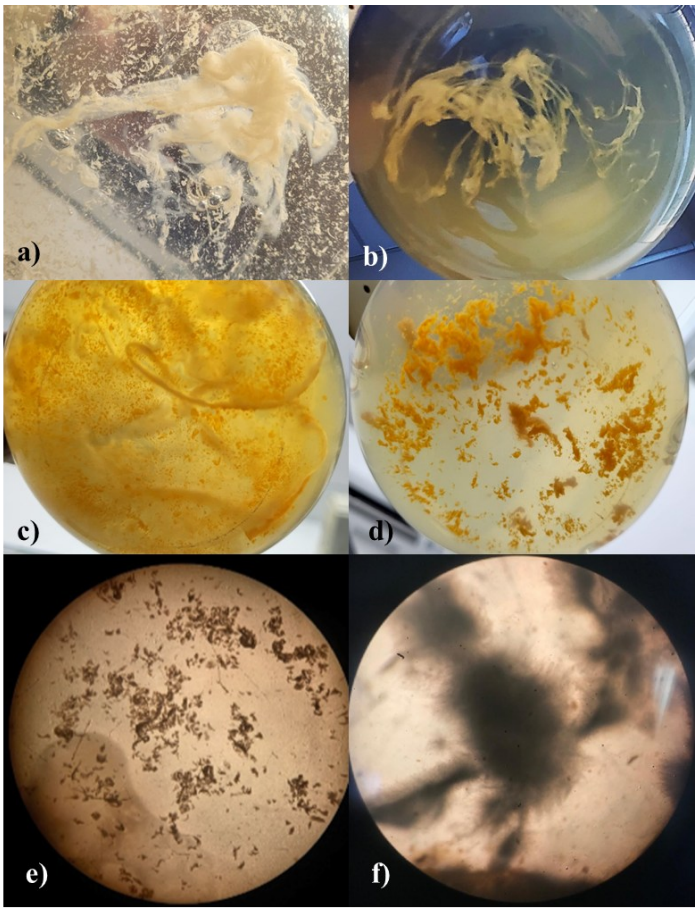

Figure 85 – ***BC-like biofilms synthesised by the isolates #1, #2, #2 CG, #7, #12, and #14****. Different morphologies can be recognised, including loose sheets (a) dispersed (b) or filamentous* forms *(c), pellets (d, e), and star-shaped* aggregates *(f).*

The FTIR spectrum obtained from the BC-like biofilm produced by the isolate #12 (image not shown) confirmed that the peaks were consistent to those of bacterial cellulose.

Bioplastic production

Production of polyhydroxyalkanoates was monitored daily using a viable colony staining assay relying on the use of Nile Red, a sensitive fluorescent dye able to discriminate between PHAs-negative and PHAs-positive strains, these latter exhibiting a distinctive orange fluorescence *(Spiekermann et al., 1999)*. In all the experiments, *Rhodococcus* sp. ef1 was used as a positive control, since this strain was previously demonstrated to be a PHAs producer, as reported in the Supplementary Materials – Chapter V, *Figure 99*.

The first experiments were conducted on isolates #1, #2, #10, and #12. After three days of incubation on solid medium in absence of additional sugars, a weak orange fluorescence was detected for all the isolates, with isolate #1 showing the strongest signal (*Figure 86*). This suggests either autonomous PHA synthesis or the ability to metabolize solid medium components, such as agar.

Nile Red⁻ MMD Agar plate *Nile Red⁺ MMD Agar plate*

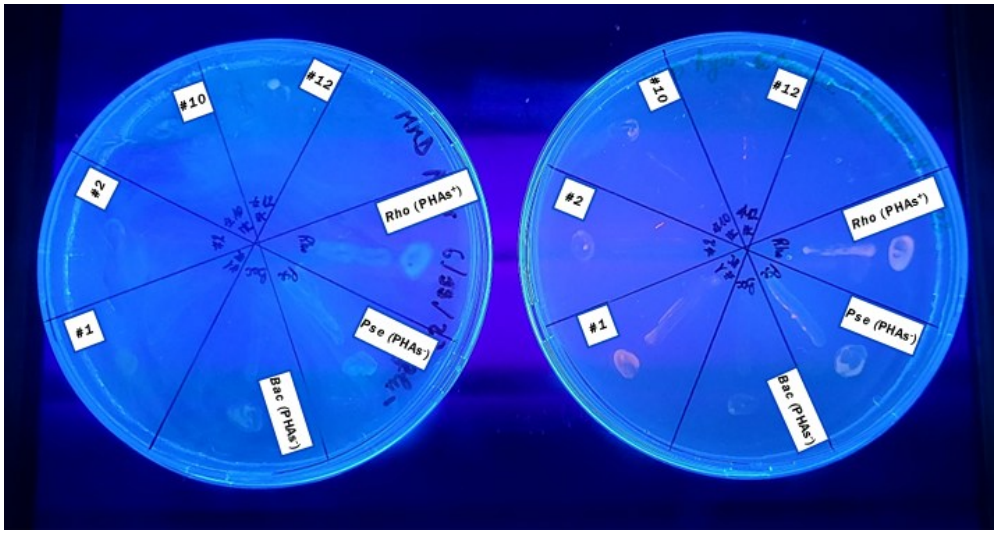

Figure 86 – ***Screening for PHAs production using isolates #1, #2, #10, #12 in absence of supplemental sugars****.*
Rhodococcus sp. ef1 and Pseudomonas sp. ef1, indicated as Rho (PHAs⁺) and as Pse (PHAs⁺), respectively, were used as the positive control, whereas Bacillus sp. ef1, indicated as Bac (PHAs⁻), served as a negative control. Orange fluorescence on the right column showing the Nile Red⁺ plates indicates that the strains are PHAs producers.

Further investigations explored the influence of different types of carbon sources on PHA production, including lactose, sucrose, and glucose. Among them. lactose and glucose resulted particularly effective (*Figure 87*), as the orange fluorescence was detectable after two days of bacterial incubation, suggesting that the synthesis occurs quickly under favorable culture conditions.

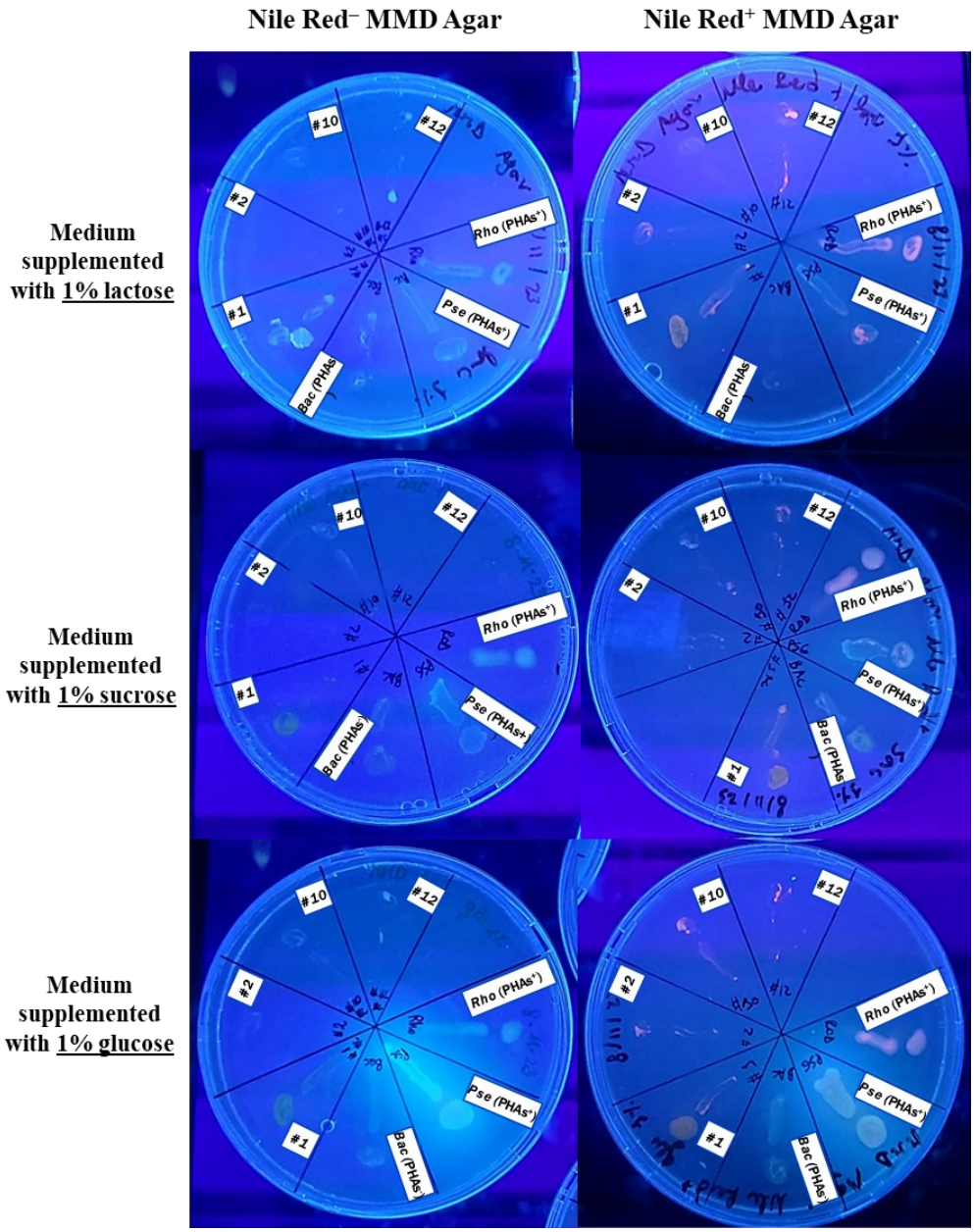

Figure 87 – ***Screening for PHAs production using isolates #1, #2, #10, #12 with different supplemental carbon sources****.*

1% (w/v) of lactose, sucrose, and glucose were tested as supplemental sugars. Rhodococcus sp. ef1 and Pseudomonas sp. ef1 (indicated as Rho (PHAs$^+$) and as Pse (PHAs$^+$), respectively) were used as the positive control, whereas Bacillus sp. ef1 (indicated as Bac (PHAs$^-$) served as a negative control. Orange fluorescence on the right column showing the Nile Red$^+$ plates indicates that the strains are PHAs producers.

In another experiment, PHAs production was assessed in liquid culture using an NB-seawater medium (1:1, v/v) supplemented with 1% (w/v) of sucrose. In this case, isolates #2, #7, #12, and #14 were tested. The role of sucrose was investigated as it represents a more economical carbon source than lactose or glucose and could contribute to cut the production costs. PHA production was monitored daily by collecting an aliquot from each bacterial suspension which was then plated in the solid MMD Agar plates. Agar plates were exposed to ultraviolet light (312 nm) to detect accumulation of PHAs. Day four emerged as the most productive timepoint for most of the isolates, suggesting that the optimal PHA synthesis is achieved after approximately 90 hours of incubation (*Figure 88*).

Overall, these findings offer valuable insights to improve the microbial production of polyhydroxyalkanoates.

Nile Red⁺ MMD Agar *Nile Red⁻ MMD Agar*

Day 0

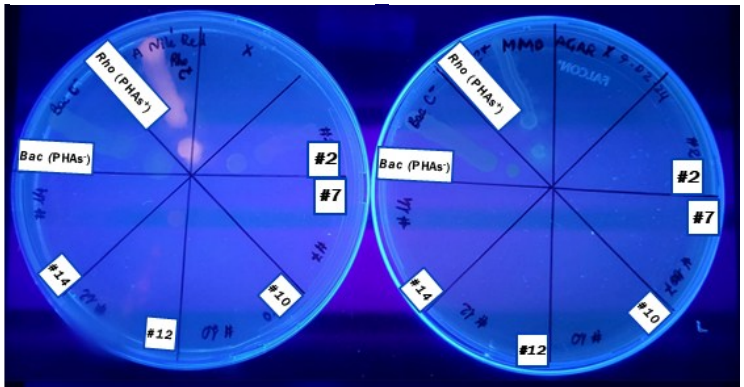

Day 1

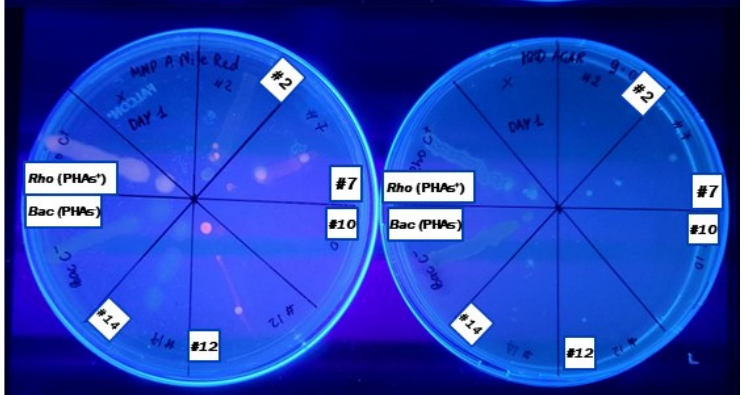

Day 3

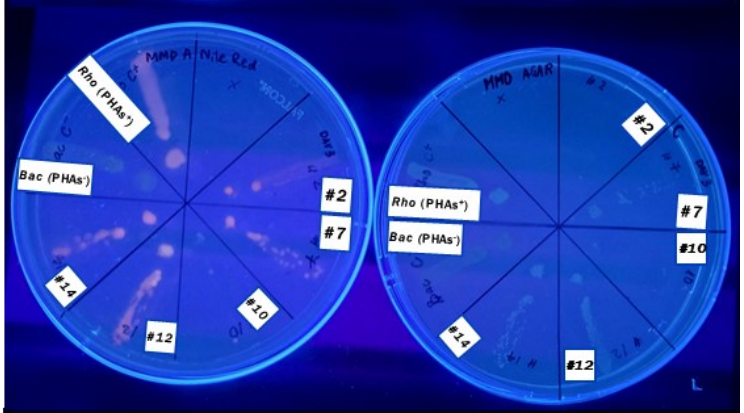

Day 4

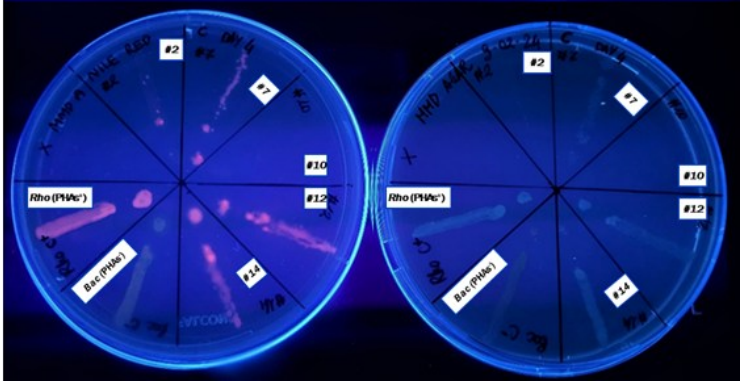

Figure 88 - ***PHAs screening results using the isolates #2, #7, #12, and #14 after 4 days of bacterial culture in NB-liquid seawater medium***. *Rhodococcus sp. ef1 was used as positive control (PHA^+) while Bacillus sp. ef1 served as the negative control (PHA^-). Orange fluorescence on the left plates in the image, representing the Nile Red^+ plates, indicates that the strains are PHAs producers.*

Lastly, the isolate #2 CG cultured in M9 supplemented with either 1% of glucose or 1% of lactose produced a pellicle identified as polyhydroxybutyrate (PHB) at FTIR analysis (*Figure 89*), according with the literature *(Trakunjae et al., 2021).*

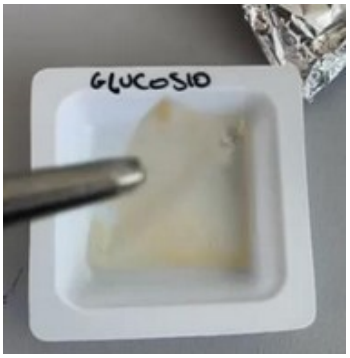

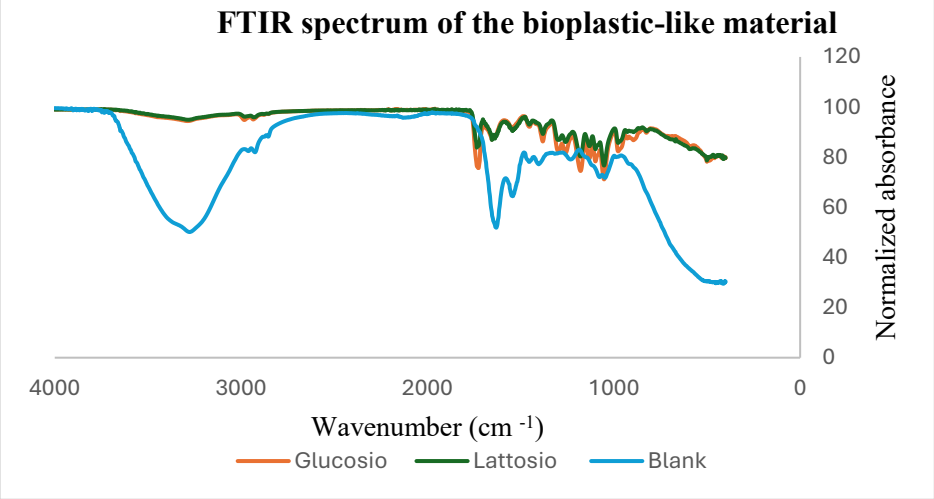

Figure 89 – Pellicular material produced by the isolate #2 CG cultured in M9 supplemented with glucose 1%. FTIR spectrum of both the pellicles obtained with M9 supplemented with 1% glucose or 1% lactose suggest that the polymer is a polyhydroxybutyrate.

Pigments

Isolates #1, #2, #12, #2 CG were capable of producing fluorescent pigments in minimal media (MMD or M9). UV-vis analysis of the pigment produced by isolate #12 revealed a characteristic peak at 254 nm (*Figure 90*). However,

additional studies and chemical characterization are required to identify the molecules involved.

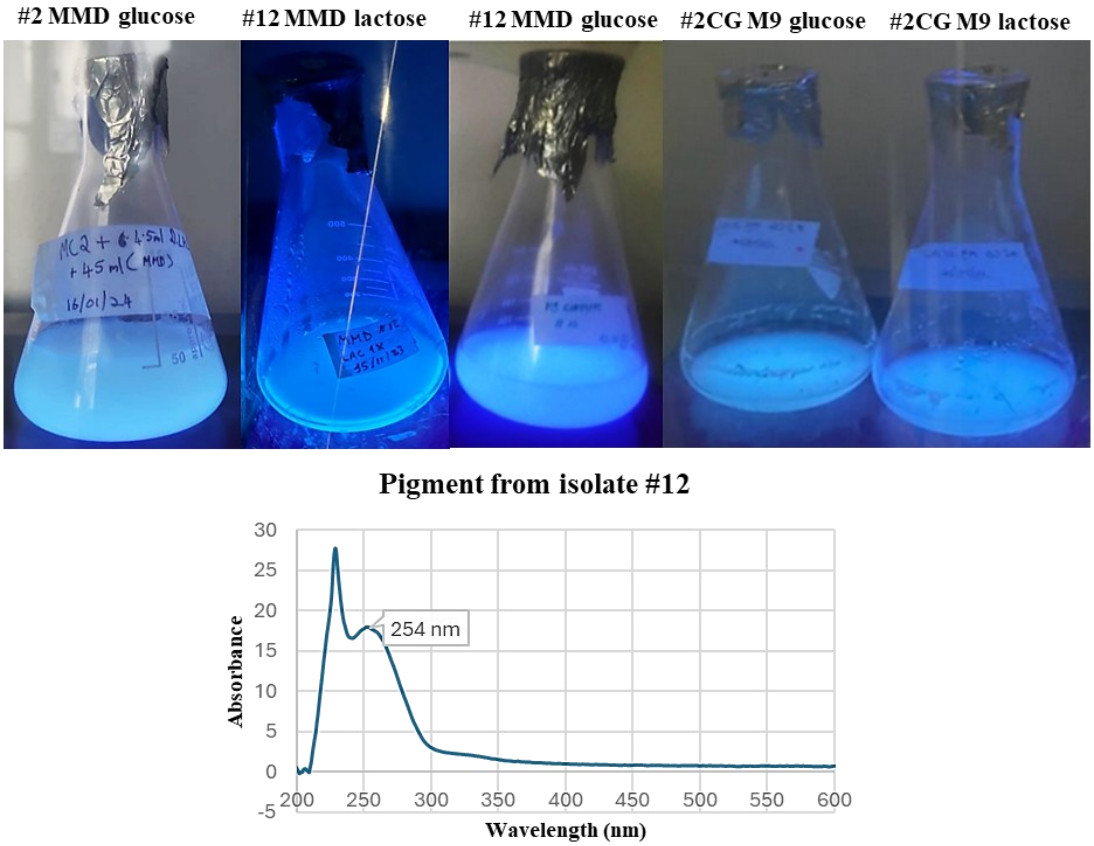

Figure 90 – Fluorescent pigments produced by the strain #2, #12, and #2CG. the UV-visible spectrum of the pigment synthesised by isolate #12 revealed a characteristic peak at around 254 nm.

Moreover, the isolate #2CG incubated in NB, seawater, and 1% (v/v) of soy oil, produced a pink pigment that still requires characterization (*Figure 91*).

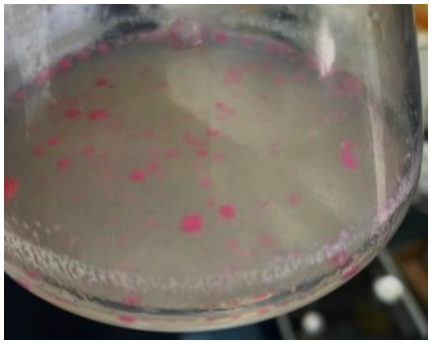

Figure 91 – The isolate #2CG produced a pigment when cultured in NB-seawater (1:1 v/v) supplemented with soy oil 1% (v/v).

Additional bioremediation tests

To assess biodegradation capability and bioremediation potential, isolate #2 was grown in a minimal medium (M9) with doubled salt concentrations (Na_2 HPO_4 12 g/L, KH_2PO_4 6 g/L, NaCl 1 g/L, NH_4Cl 2 g/L, $MgSO_4$ 2 mM, $CaCl_2$ 0,1 mM), supplemented with 1% diesel (v/v) as the sole carbon source. In parallel, this isolate was cultivated in a NB-seawater (1:1 v/v) medium supplemented with 1% soy oil as the sole carbon source. The isolate exhibited efficient growth in both media, producing a resin-like material in the soy oil-supplemented medium (images not shown).

16S rDNA sequencing results

The 16S rDNA gene sequences of each analysed strain are reported in the Supplementary Material – Chapter V. The electropherogram showed overall evenly spaced peaks with minimal baseline noise, indicating that the obtained sequences are reliable. A BLASTn search was performed to identify microbial species that are phylogenetically closest to the isolates. The most relevant results

are summarized in the *Table 11*. As can be observed, most matches were represented by *Halomonas* sp., *Vreelandella titanicae*, and uncultured bacteria closely related to these two taxa.

Table 11 – Most relevant matches of each isolate's 16S rDNA gene sequence obtained by BLASTn analysis. The table reports the three most similar aligned specie, together with alignment parameters, including query coverage, E value, % of identities and of gaps, and the accession number of each sequence. In the column "Accession number", the sequence IDs belonging to the same organism are highlighted with the same colour.

Bacterial isolate	Most relevant BLAST alignments	Query cover	E value	% identities	% gaps	Accession number
#1	uncultured bacterium	100%	0.0	99.79%	0%	JQ032039.1
	Vreelandella titanicae	100%	0.0	99.79%	0%	MT645895.1
	Halomonas sp.	100%	0.0	99.79%	0%	MT653345.1
#2	*Vreelandella titanicae*	100%	0.0	99.93%	0%	CP177050.1
	Halomonas sp. PA16-9	100%	0.0	99.87%	0%	CP040451.1
	uncultured *Halomonas* sp.	100%	0.0	99.93%	0%	MH894279.1
#2CG	*Halomonas* sp. BB65	100%	0.0	99.38%	0%	FR693337.1

	Halomonas sp. MH184	100%	0.0	99.38%	0%	**EU052736.1**
	Halomonas sp. BG-3a	100%	0.0	99.38%	0%	**KM404161.1**
#3	uncultured bacterium	100%	0.0	99.06%	0%	**JQ032242.1**
	uncultured *Halomonas* sp.	00%	0.0	98.94%	0%	**KU961748.1**
	Halomonas sp. ZXY12VA01	100%	0.0	98.94%	0%	**KT274805.1**
#4	*Halomonas* sp. BB65	100%	0.0	99.38%	0%	**FR693337.1**
	Halomonas sp. MH184	100%	0.0	99.38%	0%	**EU052736.1**
	Halomonas sp. BG-3a	100%	0.0	99.38%	0%	**KM404161.1**
#7	*Halomonas* sp.	100%	0.0	99.90%	0%	**PP330012.1**
	uncultured bacterium	100%	0.0	99.90%	0%	**JQ032039.1**
	Vreelandella titanicae	100%	0.0	99.90%	0%	**MT645895.1**
#10	uncultured bacterium	100%	0.0	99.80%	1396	**JQ032039.1**
	Vreelandella titanicae	100%	0.0	99.80%	1404	**MT645895.1**

	Halomonas sp.	100%	0.0	99.80%	1407	**MT653345.1**
#12	uncultured bacterium	100%	0.0	98.68%	1%	**JQ032039.1**
	Vreelandella titanicae	100%	0.0	98.68%	1%	**MT645895.1**
	Halomonas sp.	100%	0.0	98.68%	1%	**MT653345.1**
#14	uncultured bacterium	100%	0.0	99.16%	0%	**JQ032039.1**
	Vreelandella titanicae	100%	0.0	99.16%	0%	**MT645895.1**
	Halomonas sp.	100%	0.0	99.16%	0%	**MT653345.1**
#15	uncultured bacterium	100%	0.0	98.60%	1396	**JQ032039.1**
	Vreelandella titanicae	100%	0.0	98.60%	1404	**MT645895.1**
	Halomonas sp.	100%	0.0	98.60%	1407	**MT653345.1**

The 16S rDNA sequences were then aligned with Clustal Omega. The output of the alignment with colours is provided below, together with the phylogenetic tree (*Figure 92*).

```
Isolate#4       ----------------------------------------GGCCTAACACATGCAAGTCG   20
Isolate#2CG     ----------------------------------------GGCCTAACACATGCAAGTCG   20
Isolate#12      ---------------------------------------GGCCTAAACATGCAAGTCG   19
Isolate#14      ----------------------------------------GG-CCTAAACATGCAAGTCG   19
Isolate#1       ----------------------------------------GGCCTAACACATGCAAGTCG   20
Isolate#3       ----------------------------------------GGCCTAACACATGCAAGTCG   20
Isolate#2       TGAAGAGTTTGATCATGGCTCAGATTGAACGCTGGCGGCAGGCCTAACACATGCAAGTCG   60
Isolate#7       ---------------------------------------GCCTACACATGCAAGTCG   18
Isolate#15      ----------------------------------------GGCCTAACACATGCAAGTCG   20
Isolate#10      -----------------------------------GGCAGGCCTAACACATGCAAGTCG   24
                                                    * :*.************

Isolate#4       AGCGGTAACAGGAGGTAGCTTGCTACCTCGCTGACGAGCGGCGGACGGGTGAGTAATGCA   80
Isolate#2CG     AGCGGTAACAGGAGGTAGCTTGCTACCTCGCTGACGAGCGGCGGACGGGTGAGTAATGCA   80
Isolate#12      AGCGGTAACAGGAGGTAGCTTGCTACCTCGCTGACGAGCGGCGGACGGGTGAGTAATGCA   79
Isolate#14      AGCGGTAACAGG-GGTAGCTTGCTAC-CCGCTGACGAGCGGCGGACGGGTGAGTAATGCA   77
Isolate#1       AGCGGTAACAGG-GGTAGCTTGCTAC-CCGCTGACGAGCGGCGGACGGGTGAGTAATGCA   78
Isolate#3       AGCGGTAACAGGATGTAGCTTGCTACATCGCTGACGAGCGGCGGACGGGTGAGTAATGCA   80
Isolate#2       AGCGGTAACAGGG-GTAGCTTGCTAC-CCGCTGACGAGCGGCGGACGGGTGAGTAATGCA   118
Isolate#7       AGCGGTAACAG-GGGTAGCTTGCTAC-CCGCTGACGAGCGGCGGACGGGTGAGTAATGCA   76
Isolate#15      AGCGGTAACANGGGGTAGCTTGCTAC-CCGCTGACGAGCGGCGGACGGGTGAGTAATGCA   79
Isolate#10      AGCGGTAACAG-GGGTAGCTTGCTAC-CCGCTGACGAGCGGCGGACGGGTGAGTAATGCA   82
                **********.   ************  ********************************

Isolate#4       TAGGAATCTGCCCGGTAGTGGGGGATAACCTGGGGAAACCCAGGCTAATACCGCATACGT   140
Isolate#2CG     TAGGAATCTGCCCGGTAGTGGGGGATAACCTGGGGAAACCCAGGCTAATACCGCATACGT   140
Isolate#12      TAGGAATCTGCCCGATAGTGGGGGATAACCTGGGGAAACCCAGGCTAATACCGCATACGT   139
Isolate#14      TAGGAATCTGCCCGATAGTGGGGGATAACCTGGGGAAACCCAGGCTAATACCGCATACGT   137
Isolate#1       TAGGAATCTGCCCGATAGTGGGGGATAACCTGGGGAAACCCAGGCTAATACCGCATACGT   138
Isolate#3       TAGGAATCTGCCCGATAGTGGGGGATAACCTGGGGAAACCCAGGCTAATACCGCATACGT   140
Isolate#2       TAGGAATCTGCCCGATAGTGGGGGATAACCTGGGGAAACCCAGGCTAATACCGCATACGT   178
Isolate#7       TAGGAATCTGCCCGATAGTGGGGGATAACCTGGGGAAACCCAGGCTAATACCGCATACGT   136
Isolate#15      TAGGAATCTGCCCGATAGTGGGGGATAACCTGGGGAAACCCAGGCTAATACCGCATACGT   139
Isolate#10      TAGGAATCTGCCCGATAGTGGGGGATAACCTGGGGAAACCCAGGCTAATACCGCATACGT   142
                **************.*********************************************

Isolate#4       CCTACGGGAGAAAGGGGGCTTCGGCTCCCGCTATTGGATGAGCCTATGTCGGATTAGCTA   200
Isolate#2CG     CCTACGGGAGAAAGGGGGCTTCGGCTCCCGCTATTGGATGAGCCTATGTCGGATTAGCTA   200
Isolate#12      CCTACGGGAGAAAGGGGGCTTCGGCTCCCGCTATTGGATGAGCCTATGTCGGATTAGCTA   199
Isolate#14      CCTACGGGAGAAAGGGGGCTTCGGCTCCCGCTATTGGATGAGCCTATGTCGGATTAGCTA   197
Isolate#1       CCTACGGGAGAAAGGGGGCTTCGGCTCCCGCTATTGGATGAGCCTATGTCGGATTAGCTA   198
Isolate#3       CCTACGGGAGAAAGGGGGCTCCGGCTCCCGCTATTGGATGAGCCTATGTCGGATTAGCTA   200
Isolate#2       CCTACGGGAGAAAGGGGGCTCCGGCTCCCGCTATTGGATGAGCCTATGTCGGATTAGCTA   238
Isolate#7       CCTACGGGAGAAAGGGGGCTTCGGCTCCCGCTATTGGATGAGCCTATGTCGGATTAGCTA   196
Isolate#15      CCTACGGGAGAAAGGGGGCTTCGGCTCCCGCTATTGGATGAGCCTATGTCGGATTAGCTA   199
Isolate#10      CCTACGGGAGAAAGGGGGCTTCGGCTCCCGCTATTGGATGAGCCTATGTCGGATTAGCTA   202
                ******************** ************************************
```

```
Isolate#2CG      GTTGGTGAGGTAATGGCTCACCAAGGCAACGATCCGTAGCTGGTCTGAGAGGATGATCAG   260
Isolate#12       GTTGGTAAGGTAATGGCTTACCAAGGCAACGATCCGTAGCTGGTCTGAGAGGATGATCAG   259
Isolate#14       GTTGGTAAGGTAATGGCTTACCAAGGCAACGATCCGTAGCTGGTCTGAGAGGATGATCAG   257
Isolate#1        GTTGGTAAGGTAATGGCTTACCAAGGCAACGATCCGTAGCTGGTCTGAGAGGATGATCAG   258
Isolate#3        GTTGGTGAGGTAATGGCTCACCAAGGCAACGATCCGTAGCTGGTCTGAGAGGATGATCAG   260
Isolate#2        GTTGGTAAGGTAATGGCTTACCAAGGCAACGATCCGTAGCTGGTCTGAGAGGATGATCAG   298
Isolate#7        GTTGGTAAGGTAATGGCTTACCAAGGCAACGATCCGTAGCTGGTCTGAGAGGATGATCAG   256
Isolate#15       GTTGGTAAGGTAATGGCTTACCAAGGCAACGATCCGTAGCTGGTCTGAGAGGATGATCAG   259
Isolate#10       GTTGGTAAGGTAATGGCTTACCAAGGCAACGATCCGTAGCTGGTCTGAGAGGATGATCAG   262
                 ******.*********** ****************************************

Isolate#4        CCACATCGGGACTGAGACACGGCCCGAACTCCTACGGGAGGCAGCAGTGGGGAATATTGG   320
Isolate#2CG      CCACATCGGGACTGAGACACGGCCCGAACTCCTACGGGAGGCAGCAGTGGGGAATATTGG   320
Isolate#12       CCACATCGGGACTGAGACACGGCCCGAACTCCTACGGGAGGCAGCAGTGGGGAATATTGG   319
Isolate#14       CCACATCGGGACTGAGACACGGCCCGAACTCCTACGGGAGGCAGCAGTGGGGAATATTGG   317
Isolate#1        CCACATCGGGACTGAGACACGGCCCGAACTCCTACGGGAGGCAGCAGTGGGGAATATTGG   318
Isolate#3        CCACATCGGGACTGAGACACGGCCCGAACTCCTACGGGAGGCAGCAGTGGGGAATATTGG   320
Isolate#2        CCACATCGGGACTGAGACACGGCCCGAACTCCTACGGGAGGCAGCAGTGGGGAATATTGG   358
Isolate#7        CCACATCGGGACTGAGACACGGCCCGAACTCCTACGGGAGGCAGCAGTGGGGAATATTGG   316
Isolate#15       CCACATCGGGACTGAGACACGGCCCGAACTCCTACGGGAGGCAGCAGTGGGGAATATTGG   319
Isolate#10       CCACATCGGGACTGAGACACGGCCCGAACTCCTACGGGAGGCAGCAGTGGGGAATATTGG   322
                 ************************************************************

Isolate#4        ACAATGGGGGCAACCCTGATCCAGCCATGCCGCGTGTGTGAAGAAGGCCCTCGGGTTGTA   380
Isolate#2CG      ACAATGGGGGCAACCCTGATCCAGCCATGCCGCGTGTGTGAAGAAGGCCCTCGGGTTGTA   380
Isolate#12       ACAATGGGGGCAACCCTGATCCAGCCATGCCGCGTGTGTGAAGAAGGCCCTCGGGTTGTA   379
Isolate#14       ACAATGGGGGCAACCCTGATCCAGCCATGCCGCGTGTGTGAAGAAGGCCCTCGGGTTGTA   377
Isolate#1        ACAATGGGGGCAACCCTGATCCAGCCATGCCGCGTGTGTGAAGAAGGCCCTCGGGTTGTA   378
Isolate#3        ACAATGGGGGCAACCCTGATCCAGCCATGCCGCGTGTGTGAAGAAGGCCCTCGGGTTGTA   380
Isolate#2        ACAATGGGGGCAACCCTGATCCAGCCATGCCGCGTGTGTGAAGAAGGCCCTCGGGTTGTA   418
Isolate#7        ACAATGGGGGCAACCCTGATCCAGCCATGCCGCGTGTGTGAAGAAGGCCCTCGGGTTGTA   376
Isolate#15       ACAATGGGGGCAACCCTGATCCAGCCATGCCGCGTGTGTGAAGAAGGCCCTCGGGTTGTA   379
Isolate#10       ACAATGGGGGCAACCCTGATCCAGCCATGCCGCGTGTGTGAAGAAGGCCCTCGGGTTGTA   382
                 ************************************************************

Isolate#4        AAGCACTTTCAGCGAGGAAGAACGCCTATTGGTTAATACCCATTAGGAAAGACATCACTC   440
Isolate#2CG      AAGCACTTTCAGCGAGGAAGAACGCCTAGTGGTTAATACCCATTAGGAAAGACATCACTC   440
Isolate#12       AAGCACCTTCAGCGAGGAAGAACGCCTATCGGTTAATACCCGGTAGGAAAGACATCACTC   439
Isolate#14       AAGCACTTTCAGCGAGGAAGAACGCCTATCGGTTAATACCCGGTAGGAAAGACATCACTC   437
Isolate#1        AAGCACTTTCAGCGAGGAAGAACGCCTATCGGTTAATACCCGGTAGGAAAGACATCACTC   438
Isolate#3        AAGCACTTTCAGCGAGGAAGAACGCCTATCGGTTAATACCCGGTAGGAAAGACATCACTC   440
Isolate#2        AAGCACTTTCAGCGAGGAAGAACGCCTATCGGTTAATACCCGTTAGGAAAGACATCACTC   478
Isolate#7        AAGCACTTTCAGCGAGGAAGAACGCCTATCGGTTAATACCCGGTAGGAAAGACATCACTC   436
Isolate#15       AAGCACTTTCAGCGAGGAAGAACGCCTATCGGTTAATACCCGGTAGGAAAGACATCACTC   439
Isolate#10       AAGCACTTTCAGCGAGGAAGAACGCCTATCGGTTAATACCCGGTAGGAAAGACATCACTC   442
                 ****** ********************  ***********. *****************
```

```
Isolate#4       GCAGAAGAAGCACCGGCTAACTCCGTGCCAGCAGCCGCGGTAATACGGAGGGTGCAAGCG   500
Isolate#2CG     GCAGAAGAAGCACCGGCTAACTCCGTGCCAGCAGCCGCGGTAATACGGAGGGTGCAAGCG   500
Isolate#12      GCAGAAGAAGCACCGGCTAACTCCGTGCCAGCAGCCGCGGTAATACGGAGGGTGCAAGCG   499
Isolate#14      GCAGAAGAAGCACCGGCTAACTCCGTGCCAGCAGCCGCGGTAATACGGAGGGTGCAAGCG   497
Isolate#1       GCAGAAGAAGCACCGGCTAACTCCGTGCCAGCAGCCGCGGTAATACGGAGGGTGCAAGCG   498
Isolate#3       GCAGAAGAAGCACCGGCTAACTCCGTGCCAGCAGCCGCGGTAATACGGAGGGTGCAAGCG   500
Isolate#2       GCAGAAGAAGCACCGGCTAACTCCGTGCCAGCAGCCGCGGTAATACGGAGGGTGCAAGCG   538
Isolate#7       GCAGAAGAAGCACCGGCTAACTCCGTGCCAGCAGCCGCGGTAATACGGAGGGTGCAAGCG   496
Isolate#15      GCAGAAGAAGCACCGGCTAACTCCGTGCCAGCAGCCGCGGTAATACGGAGGGTGCAAGCG   499
Isolate#10      GCAGAAGAAGCACCGGCTAACTCCGTGCCAGCAGCCGCGGTAATACGGAGGGTGCAAGCG   502
                ************************************************************

Isolate#4       TTAATCGGAATTACTGGGCGTAAAGCGCGCGTAGGTGGCTTGATAAGCCGGTTGTGAAAG   560
Isolate#2CG     TTAATCGGAATTACTGGGCGTAAAGCGCGCGTAGGTGGCTTGATAAGCCGGTTGTGAAAG   560
Isolate#12      TTAATCGGAATTACTGGGCGTAAAGCGCGCGTAGGTGGCTTGATAAGCCGGTTGTGAAAG   559
Isolate#14      TTAATCGGAATTACTGGGCGTAAAGCGCGCGTAGGTGGCTTGATAAGCCGGTTGTGAAAG   557
Isolate#1       TTAATCGGAATTACTGGGCGTAAAGCGCGCGTAGGTGGCTTGATAAGCCGGTTGTGAAAG   558
Isolate#3       TTAATCGGAATTACTGGGCGTAAAGCGCGCGTAGGTGGCTTGATAAGCCGGTTGTGAAAG   560
Isolate#2       TTAATCGGAATTACTGGGCGTAAAGCGCGCGTAGGTGGCTTGATAAGCCGGTTGTGAAAG   598
Isolate#7       TTAATCGGAATTACTGGGCGTAAAGCGCGCGTAGGTGGCTTGATAAGCCGGTTGTGAAAG   556
Isolate#15      TTAATCGGAATTACTGGGCGTAAAGCGCGCGTAGGTGGCTTGATAAGCCGGTTGTGAAAG   559
Isolate#10      TTAATCGGAATTACTGGGCGTAAAGCGCGCGTAGGTGGCTTGATAAGCCGGTTGTGAAAG   562
                ************************************************************

Isolate#4       CCCCG-GGCTCAACCTGGGAACGGCATCCGGAACTGTCAGGC-TAGAGTGCAGGAGAGGA   618
Isolate#2CG     CCCCG-GGCTCAACCTGGGAACGGCATCCGGAACTGTCAGGC-TAGAGTGCAGGAGAGGA   618
Isolate#12      CCCCG-GGCTCAACCTGGGAACGGCATCCGGAACTGTCAGGC-TAGAGTGCAGGAGAGGA   617
Isolate#14      CCCCG-GGCTCAACCTGGGAACGGCATCCGGAACTGTCAGGC-TAGAGTGCAGGAGAGGA   615
Isolate#1       CCCCG-GGCTCAACCTGGGAACGGCATCCGGAACTGTCAGGC-TAGAGTGCAGGAGAGGA   616
Isolate#3       CCCTG-GGCTCAACCTGGGAACGGCATCCGGAACTGTCAGGC-TAGAGTGCAGGAGAGGA   618
Isolate#2       CCCCG-GGCTCAACCTGGGAACGGCATCCGGAACTGTCAGGC-TAGAGTGCAGGAGAGGA   656
Isolate#7       CCCCG-GGCTCAACCTGGGAACGGCATCCGGAACTGTCAGGC-TAGAGTGCAGGAGAGGA   614
Isolate#15      CCCCGGGGCTCAACCTGGGAACGGCATCCGGAACTGTCAGGCCTANAGTGCAGGAGAGGA   619
Isolate#10      CCCCG-GGCTCAACCTGGGAACGGCATCCGGAACTGTCAGGC-TAGAGTGCAGGAGAGGA   620
                *** * ********************************** **.**************

Isolate#4       AGGTAGAATTCCCGGTGTAGCGGTGAAATGCGTAGAGATCGGGAGGAATACCAGTGGCGA   678
Isolate#2CG     AGGTAGAATTCCCGGTGTAGCGGTGAAATGCGTAGAGATCGGGAGGAATACCAGTGGCGA   678
Isolate#12      AGGTAGAATTCCCGGTGTAGCGGTGAAATGCGTAGAGATCGGGAGGAATACCAGTGGCGA   677
Isolate#14      AGGTAGAATTCCCGGTGTAGCGGTGAAATGCGTAGAGATCGGGAGGAATACCAGTGGCGA   675
Isolate#1       AGGTAGAATTCCCGGTGTAGCGGTGAAATGCGTAGAGATCGGGAGGAATACCAGTGGCGA   676
Isolate#3       AGGTAGAATTCCCGGTGTAGCGGTGAAATGCGTAGAGATCGGGAGGAATACCAGTGGCGA   678
Isolate#2       AGGTAGAATTCCCGGTGTAGCGGTGAAATGCGTAGAGATCGGGAGGAATACCAGTGGCGA   716
Isolate#7       AGGTAGAATTCCCGGTGTAGCGGTGAAATGCGTAGAGATCGGGAGGAATACCAGTGGCGA   674
Isolate#15      AGGTAGAATTCCCGGTGTAGCGGTGAAATGCGTAGAGATCGGGAGGAATACCAGTGGCGA   679
Isolate#10      AGGTAGAATTCCCGGTGTAGCGGTGAAATGCGTAGAGATCGGGAGGAATACCAGTGGCGA   680
                ************************************************************
```

```
Isolate#4       AGGCGGCCTTCTG-GACTGACACTGACACTGAGGTGCGAAAGCGTGG-GTAGCAAACAGG   736
Isolate#2CG     AGGCGGCCTTCTG-GACTGACACTGACACTGAGGTGCGAAAGCGTGG-GTAGCAAACAGG   736
Isolate#12      AGGCGGCCTTCTGGGACTGACACTGACACTGAGGTGCGAAAGCGTGGGGTAGCAAACAGG   737
Isolate#14      AGGCGGCCTTCTG-GACTGACACTGACACTGAGGTGCGAAAGCGTGGGGTAGCAAACAGG   734
Isolate#1       AGGCGGCCTTCTG-GACTGACACTGACACTGAGGTGCGAAAGCGTGG-GTAGCAAACAGG   734
Isolate#3       AGGCGGCCTTCTG-GACTGACACTGACACTGAGGTGCGAAAGCGTGG-GTAGCAAACAGG   736
Isolate#2       AGGCGGCCTTCTG-GACTGACACTGACACTGAGGTGCGAAAGCGTGG-GTAGCAAACAGG   774
Isolate#7       AGGCGGCCTTCTG-GACTGACACTGACACTGAGGTGCGAAAGCGTGG-GTAGCAAACAGG   732
Isolate#15      AGGCGGGCTTTTG-GACTGACACTGACACTGAGGTGCGAAAGCGTGG-GTAGCAAACAGG   737
Isolate#10      AGGCGGCCTTCTG-GACTGACACTGACACTGAGGTGCGAAAGCGTGG-GTAGCAAACAGG   738
                ****** *** ** ********************************* ************

Isolate#4       ATTAGATACCCTG-GTAGTCCACGCCGTAA-ACGAT-GTCGACCAGCCGTT-GGGTGCCT   792
Isolate#2CG     ATTAGATACCCTG-GTAGTCCACGCCGTAA-ACGAT-GTCGACCAGCCGTT-GGGTGCCT   792
Isolate#12      ATTAGATACCCTGGGTAGTCCACGCCGTAA-ACGAT-GTCGACCAGCCGTTTGGGTGCCT   795
Isolate#14      ATTAGATACCCTG-GTAGTCCACGCCGTAA-ACGAT-GTCGACCAGCCGTTTGGGTGCCT   791
Isolate#1       ATTAGATACCCTG-GTAGTCCACGCCGTAA-ACGAT-GTCGACCAGCCGTT-GGGTGCCT   790
Isolate#3       ATTAGATACCCTGG-TAGT-CACGCCG-TAAACGATG-TCGACCAGCCGTT-GGGTGCCT   791
Isolate#2       ATTAGATACCCTGG-TAGTCCACGCCG-TAAACGATG-TCGACCAGCCGTT-GGGTGCCT   830
Isolate#7       ATTAGATACCCTGG-TAGTCCACGCC-GTAAACGATG-TCGACCAGCCGTT-GGGTGCCT   788
Isolate#15      ATTATATACCCTTGTTAGTCCACGCCCGTAAACGATGTTCGACCAG--------------   783
Isolate#10      ATTAGATACCCTGG-TAGTCCACGCC-GTAAACGATG-TCGACCAGCCGTT-GGGTGCCT   794
                **** *******   **** ******  :* *****  ********

Isolate#4       AGAGCACTTTGTG-GCGAAGTTAACGCGATAAGTCGACCGCCTGG-GGAGTACGGCCGCA   850
Isolate#2CG     AGAGCACTTTGTG-GCGAAGTTAACGCGATAAGTCGACCGCCTGG-GGAGTACGGCCGCA   850
Isolate#12      AGAGCACTTTGTGGCCGAAGTTAACGCGATAAGTCGACCGCCTGGGGGAGTACGGCCGCA   855
Isolate#14      AGAGCACTTTGTGGGCGAAGTTAACGCGATAAGTCGACCGCCTGG-GGAGTACGGCCGCA   850
Isolate#1       AGAGCACTTTGTG-GCGAAGTTAACGCGATAAGTCGACCGCCTGG-GGAGTACGGCCGCA   848
Isolate#3       AGCGCACTTTGTG-GCGAAGTTAACGCGATAAGTCGACCGCCTGG-GGAGTACNGCCGCA   849
Isolate#2       AGAGCACTTTGTG-GCGAAGTTAACGCGATAAGTCGACCGCCTGG-GGAGTACGGCCGCA   888
Isolate#7       AGAGCACTTTGTG-GCGAAGTTAACGCGATAAGTCGACCGCCTGG-GGAGTACGGCCGCA   846
Isolate#15      ------------------------------------------------------------   783
Isolate#10      AGAGCACTTTGTG-GCGAAGTTAACGCGATAAGTCGACCGCCTGG-GGAGTACGGCCGCA   852

Isolate#4       AGGTTAAAACTCAAATGAATTGACGGGGGCCCGCACAAGCGGTGGAGCATGTGG-TTTAA   909
Isolate#2CG     AGGTTAAAACTCAAATGAATTGACGGGGGCCCGCACAAGCGGTGGAGCATGTGGGTTTAA   910
Isolate#12      AGGTTAAAACTCAAATGATTTGACGGGGGCCCGCACAAGCGGTGA-GCATGG--------   906
Isolate#14      AGGTTAAAACTCAAATGAATTGACGG-GGCCCGCACAAGCGGTGGAGCATGGTGGTTTAA   909
Isolate#1       AGGTTAAAACTCAAATGAATTGACGGGGGCCCGCACAAGCGGTGGAGCATGT-GGTTTAA   907
Isolate#3       ------------------------------------------------------------   849
Isolate#2       AGGTTAAAACTCAAATGAATTGACGGGGGCCCGCACAAGCGGTGGAGCATGTGGTT-TAA   947
Isolate#7       AGGTTAAAACTCAAATGAATTGACGGGGGCCCGCACAAGCGGTGGAGCATGTGGTT-TAA   905
Isolate#15      ------------------------------------------------------------   783
Isolate#10      AGGTTAAAACTCAAATGAATTGACGGGGGCCCGCACAAGCGGTGGAGCATGTGGTT-TAA   911
```

```
Isolate#4       TTCGATGCAACGCGAAGAACCTTACCTACCCTTGACATCTACAGAAGCCCGGAGGAGATT   969
Isolate#2CG     TTCGATGCAACGCGAAGAACCTTACCTACCCTTGACATCTACAGANCCC-GGA-------   962
Isolate#12      ------------------------------------------------------------   906
Isolate#14      TTCGATGC-ACGCGAAGA-CCTTACCTACCCTTGACATCTAC------------------   949
Isolate#1       TTCGATGCAACGCGAAGACCCTTACCTACCCTTGACATCTACAGAGCCG-GA--------   958
Isolate#3       ------------------------------------------------------------   849
Isolate#2       TTCGATGCAACGCGAAGAACCTTACCTACCCTTGACATCTACAGAAGCCGGAAG-AGATT   1006
Isolate#7       TTCGATGCAACGCGAAGAACCTTACCTACCCTTGACATCTACAGAAGCCGGAAG-AGATT   964
Isolate#15      ------------------------------------------------------------   783
Isolate#10      TTCGATGCAACGCGAAGAACCTTACCTACCCTTGACATCTACAGAAGCCGGAAG-AGATT   970


Isolate#4       ------------------------------------------------------------   969
Isolate#2CG     ------------------------------------------------------------   962
Isolate#12      ------------------------------------------------------------   906
Isolate#14      ------------------------------------------------------------   949
Isolate#1       ------------------------------------------------------------   958
Isolate#3       ------------------------------------------------------------   849
Isolate#2       CTGGTGTGCCTTCGGGAACTGTAAGACAGGTGCTGCATGGCTGTCGTCAGCTCGTGTTGT   1066
Isolate#7       CTGGTGTGCCTTCGGGAACTGTAAGACAGGTGCTGCATGGCTGTCGTCAGCTCGTGTTGT   1024
Isolate#15      ------------------------------------------------------------   783
Isolate#10      CTGGTGTGCCTTCGGNAACTGTAGA-CAG----------------------------------   998


Isolate#4       ------------------------------------------------------------   969
Isolate#2CG     ------------------------------------------------------------   962
Isolate#12      ------------------------------------------------------------   906
Isolate#14      ------------------------------------------------------------   949
Isolate#1       ------------------------------------------------------------   958
Isolate#3       ------------------------------------------------------------   849
Isolate#2       GAAATGTTGGGTTAAGTCCCGTAACGAGCGCAACCCTTGTCCTTATTTGCCAGCGAGTAA   1126
Isolate#7       GAAAT--------------------------------------------------------   1029
Isolate#15      ------------------------------------------------------------   783
Isolate#10      ------------------------------------------------------------   998


Isolate#4       ------------------------------------------------------------   969
Isolate#2CG     ------------------------------------------------------------   962
Isolate#12      ------------------------------------------------------------   906
Isolate#14      ------------------------------------------------------------   949
Isolate#1       ------------------------------------------------------------   958
Isolate#3       ------------------------------------------------------------   849
Isolate#2       TGTCGGGAACTCTAAGGAGACTGCCGGTGACAAACCGGAGGAAGGTGGGGACGACGTCAA   1186
Isolate#7       ------------------------------------------------------------   1029
Isolate#15      ------------------------------------------------------------   783
Isolate#10      ------------------------------------------------------------   998
```

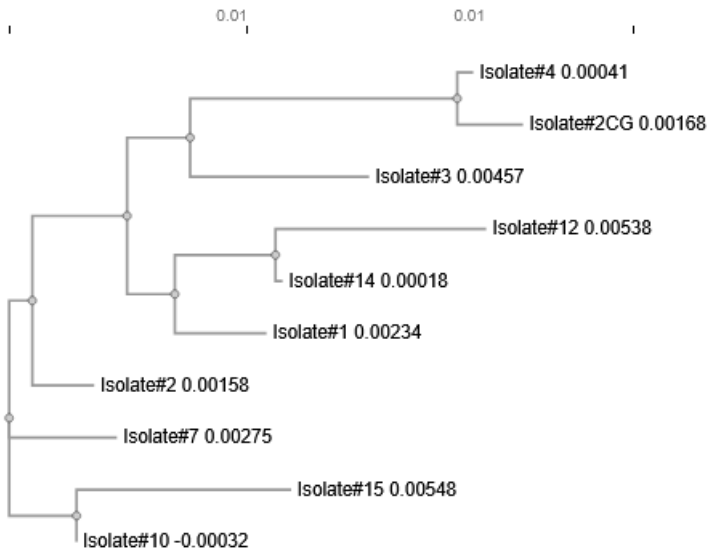

Figure 92 – Phylogenetic tree output from Clustal Omega.

Isolate #12 genomic sequencing results

DNA was successfully extracted and purified with a concentration of 1159,5 ng/µl. The purity of the sample was adequate for the following analyses, with an A_{260}/A_{280} ratio of 1.89 and an A_{260}/A_{230} ratio of 2.01 (*Figure 93*).

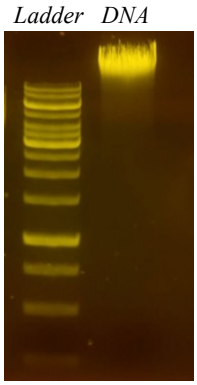

Figure 93 – DNA run in agorose gel 1% after extraction and purification.

From genome sequencing, a unique circular contig of 5,268,113 bp was obtained. The *Table 12* resumes the main information:

Table 12 – Data from genome sequencing of isolate #12.

Average CG content	***54.69%***
CDS	***4792***
Repeat region	***2***
rRNA	***18***
tRNA	***61***
tmRNA	***1***

By analysing the annotated sequences, few sequences putatively involved in the synthesis of polyhydroxyalkanoates and two sequences potentially involved in cellulose biosynthesis were identified. They are reported in the section Supplementary Material – Chapter V. Here, instead, the BLASTp search results for each sequence are reported.

The protein sequence annotated by PROKKA as PHAC1 matched a class I poly(R)-hydroxyalkanoic acid synthase from *Vreelandella neptunia* (accession number **WP_240718533.1**), with an e value of 0.0, identities of 93%, and gaps of 0%. A conservative domain was detected and reported as a poly(R)-hydroxyalkanoic acid synthase, class I (*Figure 94*).

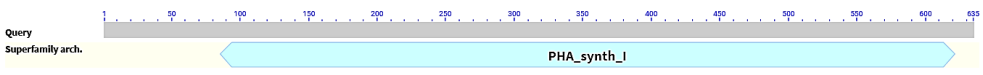

Name	Accession	Description	Interval	E-value
+ PHA_synth_I	TIGR01838	poly(R)-hydroxyalkanoic acid synthase, class I	86-621	0

Figure 94 – Conservative domain identified for the sequence PHAC1.

The protein sequence annotated by PROKKA as PHAC2 matched a PHA/PHB synthase family protein from *Vreelandella titanicae* (accession number WP_342584044.1), with an e value of $5e^{-168}$, identities of 100%, and gaps of 0%. A conservative domain was detected and reported as a poly-beta-hydroxybutyrate synthase (*Figure 95*).

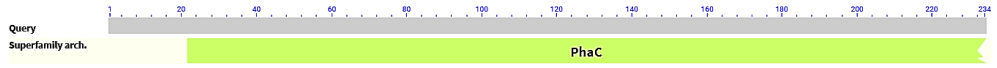

Name	Accession	Description	Interval	E-value
+ PhaC	COG3243	Poly-beta-hydroxybutyrate synthase [Lipid transport and metabolism]	22-234	4.35×10^{-81}

Figure 95 - Conservative domain identified for the sequence PHAC2.

The protein sequence annotated by PROKKA as PHAC3 matched a PHA/PHB synthase family protein from *Vreelandella titanicae* (accession number WP_342584044.1, as for the previous illustrated sequence), with an e value of 0.0, identities of 99%, and gaps of 0%. A conservative domain was detected and reported as a poly-beta-hydroxybutyrate synthase (*Figure 96*).

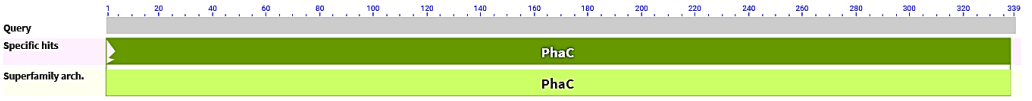

Name	Accession	Description	Interval	E-value
+ PhaC	COG3243	Poly-beta-hydroxybutyrate synthase [Lipid transport and metabolism]	1-337	0

Figure 96 - Conservative domain identified for the sequence PHAC3.

The protein sequence annotated by PROKKA as Glucans biosynthesis protein G matched a glucan biosynthesis protein G from *Halomonas* sp. FeN2 (accession number WP_227404297.1) with an e value of 0.0, identities of 94%, and gaps of

0%. A conservative domain was detected and reported as a glucan biosynthesis protein G (*Figure 97*), belonging to the MdoG superfamily. This family includes protein involved in the synthesis of periplasmic glucans, whose functions are not fully understood. It has been suggested that it may catalyse the addition of branches to a linear glucan backbone.

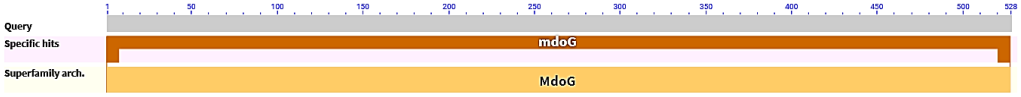

Name	Accession	Description	Interval	E-value
+ mdoG	PRK13274	glucan biosynthesis protein G	1-527	0

Figure 97 - Conservative domain identified for the sequence glucans biosynthesis protein G.

The protein sequence annotated by PROKKA as Glucans biosynthesis glucosyltransferase H matched a glucans biosynthesis glucosyltransferase MdoH from an unclassified *Halomonas* (accession number WP_226250177.1) with an e value of 0.0, identities of 94%, and gaps of 0%. A conservative domain was detected and reported as a membrane glycosyltransferase (*Figure 98*), belonging to the MdoH superfamily, involved in carbohydrate transport and metabolism.

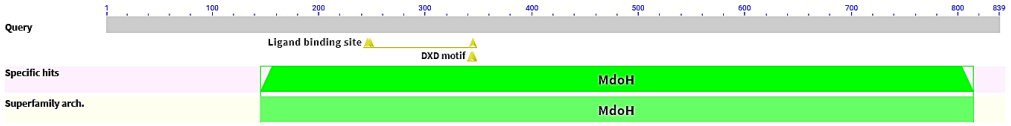

Name	Accession	Description	Interval	E-value
+ MdoH	COG2943	Membrane glycosyltransferase [Cell wall/membrane/ envelope biogenesis, Carbohydrate transport and metabolism]	146-814	0

Figure 98 - Conservative domain identified for the sequence glucans biosynthesis glucosyltransferase H.

Interestingly, 6 rDNA 16 S sequences were identified and annotated by PROKKA. They are reported in the section Supplementary Materials – Chapter V. A BLASTn search was performed to identify microbial species that are phylogenetically closest to the isolates. The most relevant results are summarized in the *Table 13*. As can be observed, most matches were represented by *Vreelandella titanicae* and *Halomonas* species.

Table 13 - Most relevant matches of each 16S rDNA gene sequence obtained by BLASTn analysis. The table reports the most similar aligned specie, together with alignment parameters, including query coverage, E value, % of identities and of gaps, and the accession number of each sequence. In the column "Accession number", the sequence IDs belonging to the same organism are highlighted using the same colour.

rDNA 16 S sequence position	Most relevant BLAST alignments	Query cover	E value	% identities	% gaps	Accession number
200839-202366	*Halomonas* sp. PA16-9	100%	0.0	99.93%	0%	CP040452.1

(Complement)						
237470-238997 (Complement)	*Vreelandella titanicae*	100%	0.0	99.93%	0%	CP177050.1
	uncultured *Halomonas* sp.	100%	0.0	99.93%	0%	MH894279.1
1403092-1404619	*Vreelandella titanicae*	100%	0.0	100%	0%	CP177050.1
	Halomonas sp. PA16-9	100%	0.0	100%	0%	CP040451.1
2314791-2316318	*Vreelandella titanicae*	100%	0.0	100%	0%	CP177050.1
	Halomonas sp. PA16-9	100%	0.0	100%	0%	CP040451.1
2708522-2710049	*Vreelandella titanicae*	100%	0.0	99.93%	0%	CP177050.1
	Halomonas sp. PA16-9	100%	0.0	99.87%	0%	CP040451.1
5083810-5085337	*Vreelandella titanicae*	100%	0.0	100%	0%	CP177050.1
	Halomonas sp. PA16-9	100%	0.0	100%	0%	CP040451.1

The 16S rDNA sequences were then aligned with Clustal Omega. The sequences resulted very similar differing only in few positions. The output of the alignment with colours is provided below.

```
rDNA16S_complement_[200839..202366]       TGAAGAGTTTGATCATGGCTCAGATTGAACGCTGGCGGCAGGCCTAACACATGCAAGTCG 60
rDNA16S_complement[237470..238997]        TGAAGAGTTTGATCATGGCTCAGATTGAACGCTGGCGGCAGGCCTAACACATGCAAGTCG 60
rDNA16S_2708522..2710049                  TGAAGAGTTTGATCATGGCTCAGATTGAACGCTGGCGGCAGGCCTAACACATGCAAGTCG 60
rDNA16S_1403092..1404619                  TGAAGAGTTTGATCATGGCTCAGATTGAACGCTGGCGGCAGGCCTAACACATGCAAGTCG 60
rDNA16S_2314791..2316318                  TGAAGAGTTTGATCATGGCTCAGATTGAACGCTGGCGGCAGGCCTAACACATGCAAGTCG 60
rDNA16S_complement_[5083810..5085337]     TGAAGAGTTTGATCATGGCTCAGATTGAACGCTGGCGGCAGGCCTAACACATGCAAGTCG 60
                                          ************************************************************

rDNA16S_complement_[200839..202366]       AGCGGTAACAGATCTAGCTTGCTAGATGCTGACGAGCGGCGGACGGGTGAGTAATGCATA 120
rDNA16S_complement[237470..238997]        AGCGGTAACAGGGGTAGCTTGCTACCCGCTGACGAGCGGCGGACGGGTGAGTAATGCATA 120
rDNA16S_2708522..2710049                  AGCGGTAACAGGGGTAGCTTGCTACCCGCTGACGAGCGGCGGACGGGTGAGTAATGCATA 120
rDNA16S_1403092..1404619                  AGCGGTAACAGGGGTAGCTTGCTACCCGCTGACGAGCGGCGGACGGGTGAGTAATGCATA 120
rDNA16S_2314791..2316318                  AGCGGTAACAGGGGTAGCTTGCTACCCGCTGACGAGCGGCGGACGGGTGAGTAATGCATA 120
rDNA16S_complement_[5083810..5085337]     AGCGGTAACAGGGGTAGCTTGCTACCGCTGACGAGCGGCGGACGGGTGAGTAATGCATA 120
                                          **********.  ********** . ********************************

rDNA16S_complement_[200839..202366]       GGAATCTGCCCGATAGTGGGGGATAACCTGGGGAAACCCAGGCTAATACCGCATACGTCC 180
rDNA16S_complement[237470..238997]        GGAATCTGCCCGATAGTGGGGGATAACCTGGGGAAACCCAGGCTAATACCGCATACGTCC 180
rDNA16S_2708522..2710049                  GGAATCTGCCCGATAGTGGGGGATAACCTGGGGAAACCCAGGCTAATACCGCATACGTCC 180
rDNA16S_1403092..1404619                  GGAATCTGCCCGATAGTGGGGGATAACCTGGGGAAACCCAGGCTAATACCGCATACGTCC 180
rDNA16S_2314791..2316318                  GGAATCTGCCCGATAGTGGGGGATAACCTGGGGAAACCCAGGCTAATACCGCATACGTCC 180
rDNA16S_complement_[5083810..5085337]     GGAATCTGCCCGATAGTGGGGGATAACCTGGGGAAACCCAGGCTAATACCGCATACGTCC 180
                                          ************************************************************

rDNA16S_complement_[200839..202366]       TACGGGAGAAAGGGGGCTTCGGCTCCCGCTATTGGATGAGCCTATGTCGGATTAGCTAGT 240
rDNA16S_complement[237470..238997]        TACGGGAGAAAGGGGGCTCCGGCTCCCGCTATTGGATGAGCCTATGTCGGATTAGCTAGT 240
rDNA16S_2708522..2710049                  TACGGGAGAAAGGGGGCTCCGGCTCCCGCTATTGGATGAGCCTATGTCGGATTAGCTAGT 240
rDNA16S_1403092..1404619                  TACGGGAGAAAGGGGGCTTCGGCTCCCGCTATTGGATGAGCCTATGTCGGATTAGCTAGT 240
rDNA16S_2314791..2316318                  TACGGGAGAAAGGGGGCTTCGGCTCCCGCTATTGGATGAGCCTATGTCGGATTAGCTAGT 240
rDNA16S_complement_[5083810..5085337]     TACGGGAGAAAGGGGGCTTCGGCTCCCGCTATTGGATGAGCCTATGTCGGATTAGCTAGT 240
                                          ****************** ****************************************

rDNA16S_complement_[200839..202366]       TGGTAAGGTAATGGCTTACCAAGGCAACGATCCGTAGCTGGTCTGAGAGGATGATCAGCC 300
rDNA16S_complement[237470..238997]        TGGTAAGGTAATGGCTTACCAAGGCAACGATCCGTAGCTGGTCTGAGAGGATGATCAGCC 300
rDNA16S_2708522..2710049                  TGGTAAGGTAATGGCTTACCAAGGCAACGATCCGTAGCTGGTCTGAGAGGATGATCAGCC 300
rDNA16S_1403092..1404619                  TGGTAAGGTAATGGCTTACCAAGGCAACGATCCGTAGCTGGTCTGAGAGGATGATCAGCC 300
rDNA16S_2314791..2316318                  TGGTAAGGTAATGGCTTACCAAGGCAACGATCCGTAGCTGGTCTGAGAGGATGATCAGCC 300
rDNA16S_complement_[5083810..5085337]     TGGTAAGGTAATGGCTTACCAAGGCAACGATCCGTAGCTGGTCTGAGAGGATGATCAGCC 300
                                          ************************************************************

rDNA16S_complement_[200839..202366]       ACATCGGGACTGAGACACGGCCCGAACTCCTACGGGAGGCAGCAGTGGGGAATATTGGAC 360
rDNA16S_complement[237470..238997]        ACATCGGGACTGAGACACGGCCCGAACTCCTACGGGAGGCAGCAGTGGGGAATATTGGAC 360
rDNA16S_2708522..2710049                  ACATCGGGACTGAGACACGGCCCGAACTCCTACGGGAGGCAGCAGTGGGGAATATTGGAC 360
rDNA16S_1403092..1404619                  ACATCGGGACTGAGACACGGCCCGAACTCCTACGGGAGGCAGCAGTGGGGAATATTGGAC 360
rDNA16S_2314791..2316318                  ACATCGGGACTGAGACACGGCCCGAACTCCTACGGGAGGCAGCAGTGGGGAATATTGGAC 360
rDNA16S_complement_[5083810..5085337]     ACATCGGGACTGAGACACGGCCCGAACTCCTACGGGAGGCAGCAGTGGGGAATATTGGAC 360
                                          ************************************************************

rDNA16S_complement_[200839..202366]       AATGGGGGCAACCCTGATCCAGCCATGCCGCGTGTGTGAAGAAGGCCCTCGGGTTGTAAA 420
rDNA16S_complement[237470..238997]        AATGGGGGCAACCCTGATCCAGCCATGCCGCGTGTGTGAAGAAGGCCCTCGGGTTGTAAA 420
rDNA16S_2708522..2710049                  AATGGGGGCAACCCTGATCCAGCCATGCCGCGTGTGTGAAGAAGGCCCTCGGGTTGTAAA 420
rDNA16S_1403092..1404619                  AATGGGGGCAACCCTGATCCAGCCATGCCGCGTGTGTGAAGAAGGCCCTCGGGTTGTAAA 420
rDNA16S_2314791..2316318                  AATGGGGGCAACCCTGATCCAGCCATGCCGCGTGTGTGAAGAAGGCCCTCGGGTTGTAAA 420
rDNA16S_complement_[5083810..5085337]     AATGGGGGCAACCCTGATCCAGCCATGCCGCGTGTGTGAAGAAGGCCCTCGGGTTGTAAA 420
                                          ************************************************************

rDNA16S_complement_[200839..202366]       GCACTTTCAGCGAGGAAGAACGCCTATCGGTTAATACCCGTTAGGAAAGACATCACTCGC 480
rDNA16S_complement[237470..238997]        GCACTTTCAGCGAGGAAGAACGCCTATCGGTTAATACCCGTTAGGAAAGACATCACTCGC 480
rDNA16S_2708522..2710049                  GCACTTTCAGCGAGGAAGAACGCCTATCGGTTAATACCCGTTAGGAAAGACATCACTCGC 480
rDNA16S_1403092..1404619                  GCACTTTCAGCGAGGAAGAACGCCTATCGGTTAATACCCGGTAGGAAAGACATCACTCGC 480
rDNA16S_2314791..2316318                  GCACTTTCAGCGAGGAAGAACGCCTATCGGTTAATACCCGGTAGGAAAGACATCACTCGC 480
rDNA16S_complement_[5083810..5085337]     GCACTTTCAGCGAGGAAGAACGCCTATCGGTTAATACCCGGTAGGAAAGACATCACTCGC 480
                                          ****************************************** ******************
```

```
rDNA16S_complement_[200839..202366]       AGAAGAAGCACCGGCTAACTCCGTGCCAGCAGCCGCGGTAATACGGAGGGTGCAAGCGTT 540
rDNA16S_complement[237470..238997]        AGAAGAAGCACCGGCTAACTCCGTGCCAGCAGCCGCGGTAATACGGAGGGTGCAAGCGTT 540
rDNA16S_2708522..2710049                  AGAAGAAGCACCGGCTAACTCCGTGCCAGCAGCCGCGGTAATACGGAGGGTGCAAGCGTT 540
rDNA16S_1403092..1404619                  AGAAGAAGCACCGGCTAACTCCGTGCCAGCAGCCGCGGTAATACGGAGGGTGCAAGCGTT 540
rDNA16S_2314791..2316318                  AGAAGAAGCACCGGCTAACTCCGTGCCAGCAGCCGCGGTAATACGGAGGGTGCAAGCGTT 540
rDNA16S_complement_[5083810..5085337]     AGAAGAAGCACCGGCTAACTCCGTGCCAGCAGCCGCGGTAATACGGAGGGTGCAAGCGTT 540
                                          ************************************************************

rDNA16S_complement_[200839..202366]       AATCGGAATTACTGGGCGTAAAGCGCGCGTAGGTGGCTTGATAAGCCGGTTGTGAAAGCC 600
rDNA16S_complement[237470..238997]        AATCGGAATTACTGGGCGTAAAGCGCGCGTAGGTGGCTTGATAAGCCGGTTGTGAAAGCC 600
rDNA16S_2708522..2710049                  AATCGGAATTACTGGGCGTAAAGCGCGCGTAGGTGGCTTGATAAGCCGGTTGTGAAAGCC 600
rDNA16S_1403092..1404619                  AATCGGAATTACTGGGCGTAAAGCGCGCGTAGGTGGCTTGATAAGCCGGTTGTGAAAGCC 600
rDNA16S_2314791..2316318                  AATCGGAATTACTGGGCGTAAAGCGCGCGTAGGTGGCTTGATAAGCCGGTTGTGAAAGCC 600
rDNA16S_complement_[5083810..5085337]     AATCGGAATTACTGGGCGTAAAGCGCGCGTAGGTGGCTTGATAAGCCGGTTGTGAAAGCC 600
                                          ************************************************************

rDNA16S_complement_[200839..202366]       CCGGGCTCAACCTGGGAACGGCATCCGGAACTGTCAGGCTAGAGTGCAGGAGAGGAAGGT 660
rDNA16S_complement[237470..238997]        CCGGGCTCAACCTGGGAACGGCATCCGGAACTGTCAGGCTAGAGTGCAGGAGAGGAAGGT 660
rDNA16S_2708522..2710049                  CCGGGCTCAACCTGGGAACGGCATCCGGAACTGTCAGGCTAGAGTGCAGGAGAGGAAGGT 660
rDNA16S_1403092..1404619                  CCGGGCTCAACCTGGGAACGGCATCCGGAACTGTCAGGCTAGAGTGCAGGAGAGGAAGGT 660
rDNA16S_2314791..2316318                  CCGGGCTCAACCTGGGAACGGCATCCGGAACTGTCAGGCTAGAGTGCAGGAGAGGAAGGT 660
rDNA16S_complement_[5083810..5085337]     CCGGGCTCAACCTGGGAACGGCATCCGGAACTGTCAGGCTAGAGTGCAGGAGAGGAAGGT 660
                                          ************************************************************

rDNA16S_complement_[200839..202366]       AGAATTCCCGGTGTAGCGGTGAAATGCGTAGAGATCGGGAGGAATACCAGTGGCGAAGGC 720
rDNA16S_complement[237470..238997]        AGAATTCCCGGTGTAGCGGTGAAATGCGTAGAGATCGGGAGGAATACCAGTGGCGAAGGC 720
rDNA16S_2708522..2710049                  AGAATTCCCGGTGTAGCGGTGAAATGCGTAGAGATCGGGAGGAATACCAGTGGCGAAGGC 720
rDNA16S_1403092..1404619                  AGAATTCCCGGTGTAGCGGTGAAATGCGTAGAGATCGGGAGGAATACCAGTGGCGAAGGC 720
rDNA16S_2314791..2316318                  AGAATTCCCGGTGTAGCGGTGAAATGCGTAGAGATCGGGAGGAATACCAGTGGCGAAGGC 720
rDNA16S_complement_[5083810..5085337]     AGAATTCCCGGTGTAGCGGTGAAATGCGTAGAGATCGGGAGGAATACCAGTGGCGAAGGC 720
                                          ************************************************************

rDNA16S_complement_[200839..202366]       GGCCTTCTGGACTGACACTGACACTGAGGTGCGAAAGCGTGGGTAGCAAACAGGATTAGA 780
rDNA16S_complement[237470..238997]        GGCCTTCTGGACTGACACTGACACTGAGGTGCGAAAGCGTGGGTAGCAAACAGGATTAGA 780
rDNA16S_2708522..2710049                  GGCCTTCTGGACTGACACTGACACTGAGGTGCGAAAGCGTGGGTAGCAAACAGGATTAGA 780
rDNA16S_1403092..1404619                  GGCCTTCTGGACTGACACTGACACTGAGGTGCGAAAGCGTGGGTAGCAAACAGGATTAGA 780
rDNA16S_2314791..2316318                  GGCCTTCTGGACTGACACTGACACTGAGGTGCGAAAGCGTGGGTAGCAAACAGGATTAGA 780
rDNA16S_complement_[5083810..5085337]     GGCCTTCTGGACTGACACTGACACTGAGGTGCGAAAGCGTGGGTAGCAAACAGGATTAGA 780
                                          ************************************************************
```

```
rDNA16S_complement_[200839..202366]       TACCCTGGTAGTCCACGCCGTAAACGATGTCGACCAGCCGTTGGGTGCCTAGAGCACTTT 840
rDNA16S_complement[237470..238997]        TACCCTGGTAGTCCACGCCGTAAACGATGTCGACCAGCCGTTGGGTGCCTAGAGCACTTT 840
rDNA16S_2708522..2710049                  TACCCTGGTAGTCCACGCCGTAAACGATGTCGACCAGCCGTTGGGTGCCTAGAGCACTTT 840
rDNA16S_1403092..1404619                  TACCCTGGTAGTCCACGCCGTAAACGATGTCGACCAGCCGTTGGGTGCCTAGAGCACTTT 840
rDNA16S_2314791..2316318                  TACCCTGGTAGTCCACGCCGTAAACGATGTCGACCAGCCGTTGGGTGCCTAGAGCACTTT 840
rDNA16S_complement_[5083810..5085337]     TACCCTGGTAGTCCACGCCGTAAACGATGTCGACCAGCCGTTGGGTGCCTAGAGCACTTT 840
                                          ************************************************************

rDNA16S_complement_[200839..202366]       GTGGCGAAGTTAACGCGATAAGTCGACCGCCTGGGGAGTACGGCCGCAAGGTTAAAACTC 900
rDNA16S_complement[237470..238997]        GTGGCGAAGTTAACGCGATAAGTCGACCGCCTGGGGAGTACGGCCGCAAGGTTAAAACTC 900
rDNA16S_2708522..2710049                  GTGGCGAAGTTAACGCGATAAGTCGACCGCCTGGGGAGTACGGCCGCAAGGTTAAAACTC 900
rDNA16S_1403092..1404619                  GTGGCGAAGTTAACGCGATAAGTCGACCGCCTGGGGAGTACGGCCGCAAGGTTAAAACTC 900
rDNA16S_2314791..2316318                  GTGGCGAAGTTAACGCGATAAGTCGACCGCCTGGGGAGTACGGCCGCAAGGTTAAAACTC 900
rDNA16S_complement_[5083810..5085337]     GTGGCGAAGTTAACGCGATAAGTCGACCGCCTGGGGAGTACGGCCGCAAGGTTAAAACTC 900
                                          ************************************************************

rDNA16S_complement_[200839..202366]       AAATGAATTGACGGGGGCCCGCACAAGCGGTGGAGCATGTGGTTTAATTCGATGCAACGC 960
rDNA16S_complement[237470..238997]        AAATGAATTGACGGGGGCCCGCACAAGCGGTGGAGCATGTGGTTTAATTCGATGCAACGC 960
rDNA16S_2708522..2710049                  AAATGAATTGACGGGGGCCCGCACAAGCGGTGGAGCATGTGGTTTAATTCGATGCAACGC 960
rDNA16S_1403092..1404619                  AAATGAATTGACGGGGGCCCGCACAAGCGGTGGAGCATGTGGTTTAATTCGATGCAACGC 960
rDNA16S_2314791..2316318                  AAATGAATTGACGGGGGCCCGCACAAGCGGTGGAGCATGTGGTTTAATTCGATGCAACGC 960
rDNA16S_complement_[5083810..5085337]     AAATGAATTGACGGGGGCCCGCACAAGCGGTGGAGCATGTGGTTTAATTCGATGCAACGC 960
                                          ************************************************************

rDNA16S_complement_[200839..202366]       GAAGAACCTTACCTACCCTTGACATCTACAGAAGCCGGAAGAGATTCTGGTGTGCCTTCG 1020
rDNA16S_complement[237470..238997]        GAAGAACCTTACCTACCCTTGACATCTACAGAAGCCGGAAGAGATTCTGGTGTGCCTTCG 1020
rDNA16S_2708522..2710049                  GAAGAACCTTACCTACCCTTGACATCTACAGAAGCCGGAAGAGATTCTGGTGTGCCTTCG 1020
rDNA16S_1403092..1404619                  GAAGAACCTTACCTACCCTTGACATCTACAGAAGCCGGAAGAGATTCTGGTGTGCCTTCG 1020
rDNA16S_2314791..2316318                  GAAGAACCTTACCTACCCTTGACATCTACAGAAGCCGGAAGAGATTCTGGTGTGCCTTCG 1020
rDNA16S_complement_[5083810..5085337]     GAAGAACCTTACCTACCCTTGACATCTACAGAAGCCGGAAGAGATTCTGGTGTGCCTTCG 1020
                                          ************************************************************

rDNA16S_complement_[200839..202366]       GGAACTGTAAGACAGGTGCTGCATGGCTGTCGTCAGCTCGTGTTGTGAAATGTTGGGTTA 1080
rDNA16S_complement[237470..238997]        GGAACTGTAAGACAGGTGCTGCATGGCTGTCGTCAGCTCGTGTTGTGAAATGTTGGGTTA 1080
rDNA16S_2708522..2710049                  GGAACTGTAAGACAGGTGCTGCATGGCTGTCGTCAGCTCGTGTTGTGAAATGTTGGGTTA 1080
rDNA16S_1403092..1404619                  GGAACTGTAAGACAGGTGCTGCATGGCTGTCGTCAGCTCGTGTTGTGAAATGTTGGGTTA 1080
rDNA16S_2314791..2316318                  GGAACTGTAAGACAGGTGCTGCATGGCTGTCGTCAGCTCGTGTTGTGAAATGTTGGGTTA 1080
rDNA16S_complement_[5083810..5085337]     GGAACTGTAAGACAGGTGCTGCATGGCTGTCGTCAGCTCGTGTTGTGAAATGTTGGGTTA 1080
                                          ************************************************************
```

```
rDNA16S_complement_[200839..202366]       AGTCCCGTAACGAGCGCAACCCTTGTCCTTATTTGCCAGCGAGTAATGTCGGGAACTCTA 1140
rDNA16S_complement[237470..238997]        AGTCCCGTAACGAGCGCAACCCTTGTCCTTATTTGCCAGCGAGTAATGTCGGGAACTCTA 1140
rDNA16S_2708522..2710049                  AGTCCCGTAACGAGCGCAACCCTTGTCCTTATTTGCCAGCGAGTAATGTCGGGAACTCTA 1140
rDNA16S_1403092..1404619                  AGTCCCGTAACGAGCGCAACCCTTGTCCTTATTTGCCAGCGAGTAATGTCGGGAACTCTA 1140
rDNA16S_2314791..2316318                  AGTCCCGTAACGAGCGCAACCCTTGTCCTTATTTGCCAGCGAGTAATGTCGGGAACTCTA 1140
rDNA16S_complement_[5083810..5085337]     AGTCCCGTAACGAGCGCAACCCTTGTCCTTATTTGCCAGCGAGTAATGTCGGGAACTCTA 1140
                                          ************************************************************

rDNA16S_complement_[200839..202366]       AGGAGACTGCCGGTGACAAACCGGAGGAAGGTGGGGACGACGTCAAGTCATCATGGCCCT 1200
rDNA16S_complement[237470..238997]        AGGAGACTGCCGGTGACAAACCGGAGGAAGGTGGGGACGACGTCAAGTCATCATGGCCCT 1200
rDNA16S_2708522..2710049                  AGGAGACTGCCGGTGACAAACCGGAGGAAGGTGGGGACGACGTCAAGTCATCATGGCCCT 1200
rDNA16S_1403092..1404619                  AGGAGACTGCCGGTGACAAACCGGAGGAAGGTGGGGACGACGTCAAGTCATCATGGCCCT 1200
rDNA16S_2314791..2316318                  AGGAGACTGCCGGTGACAAACCGGAGGAAGGTGGGGACGACGTCAAGTCATCATGGCCCT 1200
rDNA16S_complement_[5083810..5085337]     AGGAGACTGCCGGTGACAAACCGGAGGAAGGTGGGGACGACGTCAAGTCATCATGGCCCT 1200
                                          ************************************************************

rDNA16S_complement_[200839..202366]       TACGGGTAGGGCTACACACGTGCTACAATGGCCGGTACAAAGGGCTGCGAGCTCGCGAGA 1260
rDNA16S_complement[237470..238997]        TACGGGTAGGGCTACACACGTGCTACAATGGCCGGTACAAAGGGCTGCGAGCTCGCGAGA 1260
rDNA16S_2708522..2710049                  TACGGGTAGGGCTACACACGTGCTACAATGGCCGGTACAAAGGGCTGCGAGCTCGCGAGA 1260
rDNA16S_1403092..1404619                  TACGGGTAGGGCTACACACGTGCTACAATGGCCGGTACAAAGGGCTGCGAGCTCGCGAGA 1260
rDNA16S_2314791..2316318                  TACGGGTAGGGCTACACACGTGCTACAATGGCCGGTACAAAGGGCTGCGAGCTCGCGAGA 1260
rDNA16S_complement_[5083810..5085337]     TACGGGTAGGGCTACACACGTGCTACAATGGCCGGTACAAAGGGCTGCGAGCTCGCGAGA 1260
                                          ************************************************************

rDNA16S_complement_[200839..202366]       GTCAGCGAATCCCTTAAAGCCGGTCTCAGTCCGGATCGGAGTCTGCAACTCGACTCCGTG 1320
rDNA16S_complement[237470..238997]        GTCAGCGAATCCCTTAAAGCCGGTCTCAGTCCGGATCGGAGTCTGCAACTCGACTCCGTG 1320
rDNA16S_2708522..2710049                  GTCAGCGAATCCCTTAAAGCCGGTCTCAGTCCGGATCGGAGTCTGCAACTCGACTCCGTG 1320
rDNA16S_1403092..1404619                  GTCAGCGAATCCCTTAAAGCCGGTCTCAGTCCGGATCGGAGTCTGCAACTCGACTCCGTG 1320
rDNA16S_2314791..2316318                  GTCAGCGAATCCCTTAAAGCCGGTCTCAGTCCGGATCGGAGTCTGCAACTCGACTCCGTG 1320
rDNA16S_complement_[5083810..5085337]     GTCAGCGAATCCCTTAAAGCCGGTCTCAGTCCGGATCGGAGTCTGCAACTCGACTCCGTG 1320
                                          ************************************************************

rDNA16S_complement_[200839..202366]       AAGTCGGAATCGCTAGTAATCGTGAATCAGAATGTCACGGTGAATACGTTCCCGGGCCTT 1380
rDNA16S_complement[237470..238997]        AAGTCGGAATCGCTAGTAATCGTGAATCAGAATGTCACGGTGAATACGTTCCCGGGCCTT 1380
rDNA16S_2708522..2710049                  AAGTCGGAATCGCTAGTAATCGTGAATCAGAATGTCACGGTGAATACGTTCCCGGGCCTT 1380
rDNA16S_1403092..1404619                  AAGTCGGAATCGCTAGTAATCGTGAATCAGAATGTCACGGTGAATACGTTCCCGGGCCTT 1380
rDNA16S_2314791..2316318                  AAGTCGGAATCGCTAGTAATCGTGAATCAGAATGTCACGGTGAATACGTTCCCGGGCCTT 1380
rDNA16S_complement_[5083810..5085337]     AAGTCGGAATCGCTAGTAATCGTGAATCAGAATGTCACGGTGAATACGTTCCCGGGCCTT 1380
                                          ************************************************************

rDNA16S_complement_[200839..202366]       GTACACACCGCCCGTCACACCATGGGAGTGGACTGCACCAGAAGTGGTTAGCCTAACGCA 1440
rDNA16S_complement[237470..238997]        GTACACACCGCCCGTCACACCATGGGAGTGGACTGCACCAGAAGTGGTTAGCCTAACGCA 1440
rDNA16S_2708522..2710049                  GTACACACCGCCCGTCACACCATGGGAGTGGACTGCACCAGAAGTGGTTAGCCTAACGCA 1440
rDNA16S_1403092..1404619                  GTACACACCGCCCGTCACACCATGGGAGTGGACTGCACCAGAAGTGGTTAGCCTAACGCA 1440
rDNA16S_2314791..2316318                  GTACACACCGCCCGTCACACCATGGGAGTGGACTGCACCAGAAGTGGTTAGCCTAACGCA 1440
rDNA16S_complement_[5083810..5085337]     GTACACACCGCCCGTCACACCATGGGAGTGGACTGCACCAGAAGTGGTTAGCCTAACGCA 1440

rDNA16S_complement_[200839..202366]       AGAGGGCGATCACCACGGTGTGGTTCATGACTGGGGTGAAGTCGTAACAAGGTAGCCGTA 1500
rDNA16S_complement[237470..238997]        AGAGGGCGATCACCACGGTGTGGTTCATGACTGGGGTGAAGTCGTAACAAGGTAGCCGTA 1500
rDNA16S_2708522..2710049                  AGAGGGCGATCACCACGGTGTGGTTCATGACTGGGGTGAAGTCGTAACAAGGTAGCCGTA 1500
rDNA16S_1403092..1404619                  AGAGGGCGATCACCACGGTGTGGTTCATGACTGGGGTGAAGTCGTAACAAGGTAGCCGTA 1500
rDNA16S_2314791..2316318                  AGAGGGCGATCACCACGGTGTGGTTCATGACTGGGGTGAAGTCGTAACAAGGTAGCCGTA 1500
rDNA16S_complement_[5083810..5085337]     AGAGGGCGATCACCACGGTGTGGTTCATGACTGGGGTGAAGTCGTAACAAGGTAGCCGTA 1500
                                          ************************************************************

rDNA16S_complement_[200839..202366]       GGGGAACCTGCGGCTGGATCACCTCCTT 1528
rDNA16S_complement[237470..238997]        GGGGAACCTGCGGCTGGATCACCTCCTT 1528
rDNA16S_2708522..2710049                  GGGGAACCTGCGGCTGGATCACCTCCTT 1528
rDNA16S_1403092..1404619                  GGGGAACCTGCGGCTGGATCACCTCCTT 1528
rDNA16S_2314791..2316318                  GGGGAACCTGCGGCTGGATCACCTCCTT 1528
rDNA16S_complement_[5083810..5085337]     GGGGAACCTGCGGCTGGATCACCTCCTT 1528
                                          ****************************
```

Discussion

In this research work, several isolates were identified within a consortium associated with the protozoan *E. focardii*. Analysis of 16S rDNA gene sequences of the isolates revealed a close relationship with the taxa *Halomonas* and *Vreelandella titanicae*. *Vreelandella titanicae* is a recently discovered species closely related to *Halomonas* and previously identified as *Halomonas titanicae (Oren & Göker, 2024)*. This latter consists of a Gram-negative strain isolated from a microbial consortium associated with rusticle samples collected at the RMS Titanic wreck site *(Sánchez-Porro et al., 2010). V. titanicae* was already characterized as a versatile Gram negative bacterium with considerable biotechnological potential, including the ability to produce ectoine, biosurfactants, exopolysaccharides, and polyhydroxyalkanoates, to detoxify environmental pollutants and toxic substances, and to degrade organic compounds and heavy metals in saline environments *(Daga-Quisbert et al., 2024; Darden et al., 2025; Lautert-Dutra et al., 2025; Sabroso et al., 2025).* Its capacity for metal degradation is supported by the presence of numerous metal-interacting genes in its genome, including those encoding iron reductases, iron uptake regulators, chelators, and transporters *(Sánchez-Porro et al., 2013).* The wide potential associated with this taxon is consistent with the observed capability of the selected isolates to form cellulose-like biofilms, synthesize AgNPs, produce fluorescent pigments, and accumulate bioplastics.

Halomonas spp. have been reported to form biofilms though the secretion of extracellular polymeric substances (EPS), which exert a similar function to

cellulose-like matrices, facilitating surface attachment and protection under high salinity and stress conditions. These biofilms enhance water-holding capacity, structural stability, and interactions with metal ions, contributing to environmental stress tolerance *(Sabroso et al., 2025).* Although there is no direct evidence of bacterial cellulose production by *Halomonas* or *Vreelandella* species in literature, preliminary characterization analyses of cellulose-like biofilms produced by isolate #12 suggests the possible synthesis of cellulose-containing polysaccharide matrices. The presence of glucans biosynthesis glucosyltransferase H and glucans biosynthesis protein G, identified in the genome of isolate #12, may indicate that these proteins are involved in this biosynthetic process, since they have been previously reported to be associated with the synthesis and transport of EPS *(Heng et al., 2011; Melamed & Brockhausen, 2021)*. These findings may open new perspectives for biotechnological applications.

Extremophiles, including halophiles, have shown potential for metal ions reduction as an adaptation strategy. Their genome indeed comprises genes encoding heavy metal transporters and reductases, as well as genes related to heavy metal resistance and efflux systems *(Du et al., 2022).* These genomic features are consistent with the $AgNO_3$ reduction and synthesis of silver nanoparticles observed in several isolates considered in this study (*Table 9*).

Several *Halomonas* isolates have been reported to produce carotenoid-like pigments, highlighting their genetic and metabolic capacity for the synthesis of colourful secondary metabolites with potential antioxidant activity *(Athmika et al., 2021; Patkar et al., 2021).* In addition, unique siderophores have been identified in *Halomonas* species, supporting their role in iron acquisition under

nutrient-limited conditions and potentially contributing to fluorescence and pigmentation phenotypes *(Figueroa et al., 2015)*. Isolates #1 and #12 were observed to produce yellow-orange pigments which still requires characterization. In addition, isolates #1, #2, #2MC, #12 exhibited the production of fluorescent pigments when grown in minimal media. A preliminary UV-vis characterization of the compound produced by isolate #12 revealed a major absorption peak at approximately 254 nm, indicating the presence of aromatic or conjugated metabolites *(Burke et al., 2000)*. Additional analyses are required to fully elucidate the nature of these fluorescent compounds.

Polyhydroxyalkanoates represent biodegradable polymer offering an eco-friendly alternative to synthetic plastics and are characterized by high biocompatibility and biodegradability *(Cywar et al., 2023; Naser et al., 2021; Rekhi et al., 2022)*. *Halomonas* and *Vreelandella* spp. have been extensively reported as promising bioplastics producers *(Christensen et al., 2025; Hendy et al., 2025; Obulisamy & Mehariya, 2021)*, which is consistent with the observed production of polyhydroxyalkanoates by several screened isolates. FTIR spectrum of the pellicle produced by isolate #2CG matched with that reported in literature for polyhydroxybutyrate (PHB), the most commonly synthesized PHA. PHB has been widely investigated due to its physicochemical properties which make it a suitable candidate for applications in agriculture, food, and medicine *(Trakunjae et al., 2021).* In contrast, chemical characterization of the bioplastics produced by other isolates still needs to be completed and will be addressed in the near future. Screening results obtained using the Nile Red staining approach suggest that the synthesis of PHAs occurs between 2 and 4 days of bacterial

cultivation. This observation is consistent with data reported in literature, indicating that PHA accumulation's peak is reached during the late exponential or early stationary growth phase, occurring between 24 and108 hours depending on the strain considered *(Adhikari et al., 2025)*. Optimization of cultivation parameters, including carbon and nitrogen source types and concentrations and fermentation conditions has been shown to significantly enhance PHB yields *(Hendy et al., 2025)*.

Studies on *Halomonas* species have shown that PHA-related genes are not always organized within a single operon but may instead be distributed across distant genomic regions *(Biswas et al., 2023).*

Polyhydroxybutyrate biosynthetic pathway can be activated by the activity of three enzymes, namely β-ketothiolase, β-ketoacyl-CoA reductase, and PHA synthase, also known as PhaA, PhaB, and PhaC and encoded by the genes phaA, phaB, and phaC, respectively *(Mitra et al., 2020)*. Briefly, two molecules of acetyl-CoA are condensed by PhaA, followed by reduction to (R)-3-hydroxybutyryl-CoA performed by PhaB, which is subsequently polymerized into PHB by PhaC *(Christensen et al., 2025).* Consistent with this pathway, genome analysis of isolate #12 revealed the presence of all three pha genes.

The metabolic versatility of halophilic bacteria is further supported by genomic analyses of *Halomonas titanicae* strain TAT1, which presented a large repertoire of genes involved in the degradation of aromatic compounds, including benzoate, biphenyl, gentisate, and N-heterocyclic aromatic compounds *(Grouzdev et al., 2020).* For this reason, these bacteria are increasingly applied in bioremediation sector due to their ability to degrade hydrocarbons and pollutants under saline conditions *(Bogale & Aragaw, 2025; Mnif et al., 2009)*.

In this context, preliminary observations indicated efficient growth of isolate #2 in minimal medium supplemented with diesel as the sole carbon source and in the soy oil-supplemented medium, with contextual production of a resin-like material. Moreover, the release of a pink pigment dissolved in soy oil was observed for isolate #2 CG, suggesting the possible transformation of hydrocarbons into secondary metabolites, although exhaustive chemical characterization is required to fully assess the nature of the bioproduct and potential applications.

Finally, the ability of *Halomonadaceae* to thrive under high osmotic pressure is associated with the accumulation of compatible solutes, such as glycine betaine, ectoine, and hydroxyectoine, which represent another distinctive adaptation strategy *(Du et al., 2022)*. Investigations on the ability of the isolates to synthesize these osmoprotectants could enhance their biotechnological value and open additional application perspectives.

Conclusions

Several isolates likely belonging to the *Halomonas* or *Vreelandella* genera were identified within a consortium associated with the ciliate organism *Euplotes focardii*. The isolates that were easiest to cultivate were selected for amplification and subsequent sequencing of the 16S rDNA gene in order to determine their taxonomic assignment. A preliminary characterization of the biotechnological potential was also carried out by evaluating the ability of the strains to produce AgNPs, BC, pigments, PHAs, and resin-like materials in some cases. Among the isolates, the strain #12 was selected to perform whole genome sequencing using Nanopore technology, as it proved to be the easiest to maintain

in culture and the most promising strain in terms of biotechnological potential. Overall, the identification of novel strains represents a preliminary step toward the exploration of new microbial resources that may be further investigated for potential applications in the development of environmentally friendly materials and bioprocesses.

References

Adhikari, S., Bhattarai, S., Shrestha, R., Shah, S. S., & Kunwar, U. (2025). Analysis and optimization of polyhydroxyalkanoates production by environmental bacterial isolates from Nepal. *BMC Microbiology*, *25*(1), 548. https://doi.org/10.1186/s12866-025-04314-8

Athmika, Ghate, S. D., Arun, A. B., Rao, S. S., Kumar, S. T. A., Kandiyil, M. K., Saptami, K., & Rekha, P. D. (2021). Genome analysis of a halophilic bacterium Halomonas malpeensis YU-PRIM-29T reveals its exopolysaccharide and pigment producing capabilities. *Scientific Reports*, *11*(1), 1749. https://doi.org/10.1038/s41598-021-81395-1

Bhatia, S. K., Otari, S. V., Jeon, J.-M., Gurav, R., Choi, Y.-K., Bhatia, R. K., Pugazhendhi, A., Kumar, V., Rajesh Banu, J., Yoon, J.-J., Choi, K.-Y., & Yang, Y.-H. (2021). Biowaste-to-bioplastic (polyhydroxyalkanoates): Conversion technologies, strategies, challenges, and perspective. *Bioresource Technology*, *326*, 124733. https://doi.org/10.1016/j.biortech.2021.124733

Biswas, J., Jana, S. K., & Mandal, S. (2023). Biotechnological impacts of *Halomonas* : a promising cell factory for industrially relevant biomolecules. *Biotechnology and Genetic Engineering Reviews*, *39*(2), 348–377. https://doi.org/10.1080/02648725.2022.2131961

Bogale, F. M., & Aragaw, T. A. (2025). The genus Halomonas: A promising haloalkaliphilic bacterium for dye biodegradation in dyeing industry wastewater. *Journal of Hazardous Materials Advances*, *19*, 100825. https://doi.org/10.1016/j.hazadv.2025.100825

Burke, L. T., Dixon, D. J., Ley, S. V., & Rodríguez, F. (2000). A Short Stereoselective Total Synthesis of the Fusarium Toxin Equisetin. *Organic Letters*, *2*(23), 3611–3613. https://doi.org/10.1021/ol006493u

Castronovo, L. M., Calonico, C., Ascrizzi, R., Del Duca, S., Delfino, V., Chioccioli, S., Vassallo, A., Strozza, I., De Leo, M., Biffi, S., Bacci, G., Bogani, P., Maggini, V., Mengoni, A., Pistelli, L., Lo Nostro, A., Firenzuoli, F., & Fani, R. (2020). The Cultivable Bacterial Microbiota Associated to the Medicinal Plant Origanum vulgare L.: From Antibiotic Resistance to Growth-Inhibitory Properties. *Frontiers in Microbiology*, *11*. https://doi.org/10.3389/fmicb.2020.00862

Christensen, M., Chiciudean, I., Lascu, I., Jablonski, P., Shapaval, V., Zimmermann, B., Tanase, A.-M., & Hansen, H. (2025). Halomonas sp. MC140, a polyhydroxyalkanoate (PHA) producer isolated from the Arctic environment. *Scientific Reports*, *15*(1), 23744. https://doi.org/10.1038/s41598-025-06898-7

Cywar, R. M., Ling, C., Clarke, R. W., Kim, D. H., Kneucker, C. M., Salvachúa, D., Addison, B., Hesse, S. A., Takacs, C. J., Xu, S., Demirtas, M. U., Woodworth, S. P., Rorrer, N. A., Johnson, C. W., Tassone, C. J., Allen, R. D., Chen, E. Y.-X., & Beckham, G. T. (2023). Elastomeric vitrimers from designer polyhydroxyalkanoates with recyclability and biodegradability. *Science Advances*, *9*(47). https://doi.org/10.1126/sciadv.adi1735

Daga-Quisbert, J., Mendieta, D., Rajarao, G. K., van Maris, A. J. A., & Quillaguamán, J. (2024). Production of ectoine by Vreelandella boliviensis using non-aseptic repeated-batch and continuous cultivations in an air-lift bioreactor. *International Microbiology*, *28*(6), 1385–1394. https://doi.org/10.1007/s10123-024-00626-3

Darden, B., Johnson, G., Busch, G., & Sharma, I. (2025). Draft genome sequence of *Vreelandella neptunia* strain 04GJ23 isolated from the underwater Hawaii seamounts. *Microbiology Resource Announcements*, *14*(6). https://doi.org/10.1128/mra.00882-24

de la Haba, R. R., Arahal, D. R., Sánchez-Porro, C., Chuvochina, M., Wittouck, S., Hugenholtz, P., & Ventosa, A. (2023). A long-awaited taxogenomic investigation of the family Halomonadaceae. *Frontiers in Microbiology*, *14*. https://doi.org/10.3389/fmicb.2023.1293707

Du, R., Gao, D., Wang, Y., Liu, L., Cheng, J., Liu, J., Zhang, X.-H., & Yu, M. (2022). Heterotrophic Sulfur Oxidation of Halomonas titanicae SOB56 and Its Habitat Adaptation to the Hydrothermal Environment. *Frontiers in Microbiology*, *13*. https://doi.org/10.3389/fmicb.2022.888833

Figueroa, L. O. S., Schwarz, B., & Richards, A. M. (2015). Structural characterization of amphiphilic siderophores produced by a soda lake isolate, Halomonas sp. SL01, reveals cysteine-, phenylalanine- and proline-containing head groups. *Extremophiles*, *19*(6), 1183–1192. https://doi.org/10.1007/s00792-015-0790-x

Grouzdev, D. S., Sokolova, D. S., Poltaraus, A. B., & Nazina, T. N. (2020). Draft Genome Sequence of Halomonas titanicae Strain TAT1, a Hydrocarbon-Oxidizing Halophilic Bacterium Isolated from a Petroleum Reservoir in Russia. *Microbiology Resource Announcements*, *9*(48). https://doi.org/10.1128/MRA.01255-20

Hendy, M. H., Shehabeldine, A. M., Hashem, A. H., El-Sayed, A. F., & El-Sheikh, H. H. (2025). Optimization and characterization of polyhydroxybutyrate produced

by Vreelandella piezotolerans using orange peel waste. *Scientific Reports*, *15*(1), 25873. https://doi.org/10.1038/s41598-025-10899-x

Heng, S. S. J., Chan, O. Y. W., Keng, B. M. H., & Ling, M. H. T. (2011). Glucan Biosynthesis Protein G Is a Suitable Reference Gene in *Escherichia coli* K-12. *ISRN Microbiology*, *2011*, 1–6. https://doi.org/10.5402/2011/469053

John, M. S., Nagoth, J. A., Ramasamy, K. P., Ballarini, P., Mozzicafreddo, M., Mancini, A., Telatin, A., Liò, P., Giuli, G., Natalello, A., Miceli, C., & Pucciarelli, S. (2020). Horizontal gene transfer and silver nanoparticles production in a new Marinomonas strain isolated from the Antarctic psychrophilic ciliate Euplotes focardii. *Scientific Reports*, *10*(1), 10218. https://doi.org/10.1038/s41598-020-66878-x

John, M. S., Nagoth, J. A., Ramasamy, K. P., Mancini, A., Giuli, G., Natalello, A., Ballarini, P., Miceli, C., & Pucciarelli, S. (2020). Synthesis of Bioactive Silver Nanoparticles by a Pseudomonas Strain Associated with the Antarctic Psychrophilic Protozoon Euplotes focardii. *Marine Drugs*, *18*(1), 38. https://doi.org/10.3390/md18010038

Kitsara, M., Agbulut, O., Kontziampasis, D., Chen, Y., & Menasché, P. (2017). Fibers for hearts: A critical review on electrospinning for cardiac tissue engineering. *Acta Biomaterialia*, *48*, 20–40. https://doi.org/10.1016/j.actbio.2016.11.014

Lautert-Dutra, W., dos Santos, F. M., Pasinato Napp, A., & Lovato Melo, C. (2025). Draft genome sequence of *Vreelandella stevensii* strain BS235 isolated from hypersaline lakes from Brazilian pantanal. *Microbiology Resource Announcements*, *14*(4). https://doi.org/10.1128/mra.00748-24

Lee, J., Park, H. J., Moon, M., Lee, J.-S., & Min, K. (2021). Recent progress and challenges in microbial polyhydroxybutyrate (PHB) production from CO2 as a sustainable feedstock: A state-of-the-art review. *Bioresource Technology*, *339*, 125616. https://doi.org/10.1016/j.biortech.2021.125616

Lim, J., You, M., Li, J., & Li, Z. (2017). Emerging bone tissue engineering via Polyhydroxyalkanoate (PHA)-based scaffolds. *Materials Science and Engineering: C*, *79*, 917–929. https://doi.org/10.1016/j.msec.2017.05.132

Liu, M., Liu, H., Shi, M., Jiang, M., Li, L., & Zheng, Y. (2021). Microbial production of ectoine and hydroxyectoine as high-value chemicals. *Microbial Cell Factories*, *20*(1), 76. https://doi.org/10.1186/s12934-021-01567-6

Melamed, J., & Brockhausen, I. (2021). Biosynthesis of Bacterial Polysaccharides. In *Comprehensive Glycoscience* (pp. 143–178). Elsevier. https://doi.org/10.1016/B978-0-12-819475-1.00097-3

Mitra, R., Xu, T., Xiang, H., & Han, J. (2020). Current developments on polyhydroxyalkanoates synthesis by using halophiles as a promising cell factory. *Microbial Cell Factories*, *19*(1), 86. https://doi.org/10.1186/s12934-020-01342-z

Mnif, S., Chamkha, M., & Sayadi, S. (2009). Isolation and characterization of *Halomonas* sp. strain C2SS100, a hydrocarbon-degrading bacterium under hypersaline conditions. *Journal of Applied Microbiology*, *107*(3), 785–794. https://doi.org/10.1111/j.1365-2672.2009.04251.x

Naser, A. Z., Deiab, I., & Darras, B. M. (2021). Poly(lactic acid) (PLA) and polyhydroxyalkanoates (PHAs), green alternatives to petroleum-based plastics:

a review. *RSC Advances*, *11*(28), 17151–17196. https://doi.org/10.1039/D1RA02390J

Obulisamy, P. K., & Mehariya, S. (2021). Polyhydroxyalkanoates from extremophiles: A review. *Bioresource Technology*, *325*, 124653. https://doi.org/10.1016/j.biortech.2020.124653

Oren, A., & Göker, M. (2024). Validation List no. 216. Valid publication of new names and new combinations effectively published outside the IJSEM. *International Journal of Systematic and Evolutionary Microbiology*, *74*(3). https://doi.org/10.1099/ijsem.0.006229

Patkar, S., Shinde, Y., Chindarkar, P., & Chakraborty, P. (2021). Evaluation of antioxidant potential of pigments extracted from Bacillus spp. and Halomonas spp. isolated from mangrove rhizosphere. *BioTechnologia*, *102*(2), 157–169. https://doi.org/10.5114/bta.2021.106522

Pucciarelli, S., Devaraj, R. R., Mancini, A., Ballarini, P., Castelli, M., Schrallhammer, M., Petroni, G., & Miceli, C. (2015). Microbial Consortium Associated with the Antarctic Marine Ciliate Euplotes focardii: An Investigation from Genomic Sequences. *Microbial Ecology*, *70*(2), 484–497. https://doi.org/10.1007/s00248-015-0568-9

Pulingam, T., Appaturi, J. N., Parumasivam, T., Ahmad, A., & Sudesh, K. (2022). Biomedical Applications of Polyhydroxyalkanoate in Tissue Engineering. *Polymers*, *14*(11), 2141. https://doi.org/10.3390/polym14112141

Rekhi, P., Goswami, M., Ramakrishna, S., & Debnath, M. (2022). Polyhydroxyalkanoates biopolymers toward decarbonizing economy and

sustainable future. *Critical Reviews in Biotechnology*, *42*(5), 668–692. https://doi.org/10.1080/07388551.2021.1960265

Sabroso, E., Martínez, J. M., Sánchez-León, E., Rodríguez, N., Amils, R., & Abrusci, C. (2025). Production and Characterisation of an Exopolysaccharide by Vreelandella titanicae Zn11_249 Isolated from Salar de Uyuni (Bolivia). *Polymers*, *17*(17), 2362. https://doi.org/10.3390/polym17172362

Sánchez-Porro, C., de la Haba, R. R., Cruz-Hernández, N., González, J. M., Reyes-Guirao, C., Navarro-Sampedro, L., Carballo, M., & Ventosa, A. (2013). Draft Genome of the Marine Gammaproteobacterium Halomonas titanicae. *Genome Announcements*, *1*(2). https://doi.org/10.1128/genomeA.00083-13

Sánchez-Porro, C., Kaur, B., Mann, H., & Ventosa, A. (2010). Halomonas titanicae sp. nov., a halophilic bacterium isolated from the RMS Titanic. *International Journal of Systematic and Evolutionary Microbiology*, *60*(12), 2768–2774. https://doi.org/10.1099/ijs.0.020628-0

Sanhueza, C., Acevedo, F., Rocha, S., Villegas, P., Seeger, M., & Navia, R. (2019). Polyhydroxyalkanoates as biomaterial for electrospun scaffolds. *International Journal of Biological Macromolecules*, *124*, 102–110. https://doi.org/10.1016/j.ijbiomac.2018.11.068

Sirohi, R., Kumar Gaur, V., Kumar Pandey, A., Jun Sim, S., & Kumar, S. (2021). Harnessing fruit waste for poly-3-hydroxybutyrate production: A review. *Bioresource Technology*, *326*, 124734. https://doi.org/10.1016/j.biortech.2021.124734

Spiekermann, P., Rehm, B. H. A., Kalscheuer, R., Baumeister, D., & Steinbüchel, A. (1999). A sensitive, viable-colony staining method using Nile red for direct

screening of bacteria that accumulate polyhydroxyalkanoic acids and other lipid storage compounds. *Archives of Microbiology*, *171*(2), 73–80. https://doi.org/10.1007/s002030050681

Steinbüchel, A., & Lütke-Eversloh, T. (2003). Metabolic engineering and pathway construction for biotechnological production of relevant polyhydroxyalkanoates in microorganisms. *Biochemical Engineering Journal*, *16*(2), 81–96. https://doi.org/10.1016/S1369-703X(03)00036-6

Trakunjae, C., Boondaeng, A., Apiwatanapiwat, W., Kosugi, A., Arai, T., Sudesh, K., & Vaithanomsat, P. (2021). Enhanced polyhydroxybutyrate (PHB) production by newly isolated rare actinomycetes Rhodococcus sp. strain BSRT1-1 using response surface methodology. *Scientific Reports*, *11*(1), 1896. https://doi.org/10.1038/s41598-021-81386-2

Ullah, M., Wahab, A., Hussain, W., Mingyuan, C., Ma, F., Sun, S., & Xie, S. (2025). Wastes valorization to polyhydroxyalkanoate: Key concepts and strategies to overcome potential challenges. *Journal of Environmental Chemical Engineering*, *13*(2), 115779. https://doi.org/10.1016/j.jece.2025.115779

Volova, T., Shishatskaya, E., Sevastianov, V., Efremov, S., & Mogilnaya, O. (2003). Results of biomedical investigations of PHB and PHB/PHV fibers. *Biochemical Engineering Journal*, *16*(2), 125–133. https://doi.org/10.1016/S1369-703X(03)00038-X

Wang, Y., Yin, J., & Chen, G.-Q. (2014). Polyhydroxyalkanoates, challenges and opportunities. *Current Opinion in Biotechnology*, *30*, 59–65. https://doi.org/10.1016/j.copbio.2014.06.001

Ye, J.-W., & Chen, G.-Q. (2021). *Halomonas* as a chassis. *Essays in Biochemistry*, *65*(2), 393–403. https://doi.org/10.1042/EBC20200159

Zhao, X., Niu, Y., Mi, C., Gong, H., Yang, X., Cheng, J., Zhou, Z., Liu, J., Peng, X., & Wei, D. (2021). Electrospinning nanofibers of microbial polyhydroxyalkanoates for applications in medical tissue engineering. *Journal of Polymer Science*, *59*(18), 1994–2013. https://doi.org/10.1002/pol.20210418

Conclusions

Overall, Antarctic microorganisms represent a valuable source of nature-based solutions for biomedical and industrial applications.

Several Antarctic microbial strains were capable of producing bacterial cellulose, a biomaterial with promising potential for coatings and sustainable packaging. Depending on the protocols and culture conditions adopted, BC with different morphologies can be produced. In the case of *Pseudomonas* sp. ef1, the genomic analysis revealed a putative cellulose synthase subunit A with an unusual extracellular domain belonging to the Exo-beta-1,3-glucanase family, likely contributing to the unique organization and water solubility of the BC produced by this strain. The application of BC as a coating aimed at developing an innovative packaging material was explored in collaboration with the paper industry.

Furthermore, novel Antarctic microbial compounds have been identified and characterized, including pyocyanin, pyoverdine, and AgNPs synthesised through an innovative protocol. These molecules may serve as antimicrobial agents and protectors against UV and oxidative stress and may find applications in the bioremediation sector. Specifically, the pyocyanin derivative and AgNPs were employed as functionalizing agents in polymeric wound dressings and 3D-printed scaffolds. Despite further validation is required, these molecules show promise in supporting wound healing, skin, and bone regeneration. Moreover, genome sequencing of *Rhodococcus* sp. ef1 offered insights into the organization of the putative operon involved in the biosynthesis of this compound.

Several isolates, likely belonging to the *Halomonas* and *Vreelandella* genera, were identified within the microbial consortium associated with *Euplotes focardii.* Among other valuable metabolic features, preliminary characterization of their biotechnological potential suggest that most strains can produce polyhydroxyalkanoates. As the easiest culturable strain, isolate #12 was selected for whole genome sequencing using Nanopore technology, providing further insights into its metabolic and biotechnological capabilities.

Further studies are required to upscale the production processes of the compounds of interest, to fully characterize their bioactivity, to assess their eventual toxicity, and to validate the preliminary results obtained from initial application studies and genomic analyses. The projects conducted during this research are still ongoing, with a long-term future perspective of exploring the transition of scientific findings into industrial applications beyond the academic context. Additional projects, not presented in this work, are also under development, including the evaluation of CO_2 capture and utilization by the Antarctic strains, their ability to reduce sulphates and other contaminants from wastewater, and investigations into the contribution of each individual strain within the consortium to survival under increasing temperatures by exposing the community to progressively higher temperatures, according with the climate change scenarios. Together, these follow-up experiments and additional studies will contribute to expanding our understanding of these extremophilic organisms and to fully unlocking their biotechnological potential.

Supplementary Materials

Chapter I

In this section, the protein sequences identified as putative cellulose synthase subunits involved in BC biosynthesis are reported for each analyzed strain.

Bacillus sp. ef1

>PROKKA_02205_Cellulose_synthase_catalytic_subunit_[UDP-forming]
MSFITTYYPLFMLCMLSLLYMIYRIQPMASTVKKVIIVLCVLTNAAYIC
WRLFFTLPHEGTFNVVMGILLVVCECIGFIQLLVFYTLVWKPSNRKQV
MISDLERLPTVDIFIATYNEPIEVLKRTVAGCLNLSYPKESVQIYLCDDG
NREAVEQLASAFGVHYLTRTDNRFAKAGNLNHAMSQTDGELILTLDA
DMVPLPSFLEKTVPYFHDGATAFVQVPQAFYNEDPFQYNMFSKDRIPN
EQDFFMQTLQAGKDRFNAVMYVGSNTVFRRTALDEIGGFATGVITED
MATGMLLQGKFKSVSVGEVLAVGLAPESWLDLLKQRDRWSRGNIQC
ARKFNPLKVRGLTLMQRVLYLDGIVYWFNGLFKMIYILTPILFLLFGIQ
SFWADFQSVFMFWLPAFFSSYLAFKLVSNQKRSMFWSHIYESSMAFHL
AGVALSELFLKKRVEFLVTPKGIQTDKRHFHLKTMIPHLIFLLLSLLALV
KIGYDVKVNGTMNADLMLINIFWVLYNGAGLFMALLVAFDRPRYRKS
ERFVIEKEGHFRSDHQDQSIACFLLDMSDSGARLSIPLDQASSLYQGQT
QLFFQENESVSCDVVWSYPEGDKLMVGVAFTDTKKSEYLSLIRFLFIRE
HVAMTDREKKSHAVRTFLRFLRETEKVPKALRRKWMRRPLQGVTGTI
AYEDRLEEKVPVIIHDISLSGCKIEFEDSIELNGKVLITIDTESLTDQPAIA
VWTSQKRRRTMAGLKFVQPEIKQIEEREGVVS

>PROKKA_03481_cellulose_synthase_regulator_protein

MKSLKWLIYILGLSLAIQPFFMAGQAMAQSNRIQVKDDWVQSSKESKT
KTQHLSEDVVTLYGQEDRTEFTYQVDQEKTESSTLTFNIEASPLLISPSS
FTVMIDGEIEKTIPVSGKNQKKSIQIKLNKAQLKKGTHRIQVTFYGVLK
EGVCINQETPANWLKVYPESELTFKGIQTKDFTLDSFPSPFIQTGDQKEQ
TDIVIPNSPDAAELEAAIKVYRTLKNKDRQKEIKLIQEKDIKQVAHPTIA
VGAKGSWDGRMKTIEQAAGIKTKSNHLTLAMRTLTAKKTEQPILFVTA
EKPVTIAEKINVLTQSELTDQLTGTDLVLQKAAAQTSKPSHKIHLKDFG
GDDVTVGTNKTASDHYYYPKALLANQKSGAKLNLSFKKSETAASKTE
RLTVMINDEPHDVPLTKLGSKDANGFYHVSIPVDSKILQKNEYIDLQFV
TSGFKNMESCRHTDEEGWIFIDKNSSLQIPEGTTSEKPDLAAWPLPFTSK
NTLIIIPDQIKREIINQMAMLTESFSQPEVAQYHLIKASQVTNEQLKNHPL
IFIGGIQTFSLLKEKAADLVVPVKKDQYDVSSFGMINETTARIVWTQPS
VWNKEQTMTVFSGMTAAEANVSNKVMQFLQTNTEKATVAIESKNKG
VFTNHQSVSSTSNSLKTSEKQSSSESWIYFVCIAALILFVLVMIVYFVRK
NRKKTEF

Brevundimonas sp. ef1:

>PROKKA_00029_Cellulose_1,4-beta-cellobiosidase_precursor
MNKRLVTTVAVLALTAAFGAAHAEPAAVAVRMSQVGFETQGPKTAT
VEDHAARPLPWRIVDLSGAVVAQGASKVFGQDAASGQSVHTVDFQSL
QTDGEGYRLIVGSHESRPFSIQQHPHARLKYDALAYFYQNRAGVPILA
DHVARPDLARAAGHAHEVAACFSGADTAGVVWPGCDYTLDVTGGW
YDAGDHGKYVVNGGISIWMLLNAYERAMTKSGPRASAFADGKVDIPE
AGNGVNDLLDEARYEIEFLLKMQIADGVKLKVPVGAQAPGQPLTLTEI
DAGGMVHHKVHDAQWTGLPMAPADDPQPRLLYPPSTAATLNLAAVG
AQCARIWRDIDPAFARQCLTASQRAFRAALRNRDVRAGENFAGGGAY

GDNDFSDEFYWATAELLATTRNPAYLTALKTSPYYLGGPLSGKSATGD
PGFSWTASLGSLTLATVPDVLPPEDLVTVRANIVAAARAYVDAGYGQ
GYGLPVAGEKYEWGSNGALMSRAVILGSAFDYTGDWNFRNAVIWSL
DYVLGRNPMDRSYVTGYGDRPVQNPHHRFWAHQADPAYPLPPAGAL
SGGPNNQAMIDDVAKTLVGKCAAQTCWADDINAYALNEVAINWNAP
LVWVAAFIDDH

>PROKKA_01815_cellulose_synthase_subunit_BcsC
MIASRSRLFAASLTVLAVALAGHASAQDTTPPAPTPDTHPPAVILEPGQ
TAPGKGTPSQVPTQAAPDPHIIITDTPATPAIPAVWAPIPTNAEGRSAYG
LYLAGKLALMQGEGATGSDYLAQAERLTPEQPRVREQAFTSALLTGD
LDVAAALAPTDATASPAFVEGGRLVRLVQDFVRGDARTPNAELARQPI
GAPHARAGLLVAPWIAAAAGDWTRALQPVPTAGDPLTLAFARINRAA
LLEKRRDYAEAEVELKTASEVAGVGALFKRPYGEFLERRGRRDDAVA
LYETAMAVQPVDPGVARALQRLKDGGRPPALPDFREGAAQGLITAAA
QASAERGNEFAAVYLRLAQNLHDDDETEYQLAQVLSRAGLKSAARNA
LSRVGTADPKLYAAARAQLAVALEEDGQSQEALTELRRAAAASPDDR
QIALVLAGQLMQLKQHDEALALLDGPLLNTADQGASVHFLRGAAYEA
LGRVPEAEAELWAALQTAPNDADMLNYLGYLWVDKGLRVQEGAEMI
ARAHALEPDNGNIQDSLGWAQFKQGQYETAVNTLEEAVDKEPSNAEI
NDHLGDAYWKVGRQREAVWLWNRVLVLEPEPERRAEVERKIANGLD
SALSAKGVAQ

Pseudomonas sp. ef1:

>PROKKA_00265_Cellulose_synthase_1
MSSRKFGLNLVVVLAIAALFTGFWALVNRPVTAPNWPQQISGFSYSPF
QQGQFPQKDQYPSDDEMRRDLEIMSKLTDNIRIYSVDGSLGDIPKLAEE

FGLRVTLGIWISPDQERNEREITKAIELANTSRSVVRVVVGNEALFREEI
TPEALIVLLDRVRAAVKVPVTTSEQWHIWEKYPQLAKHVDLIAAHVLP
YWEFIPVDKAGQFVFDRARDLKKLFPKKPLLLSEVGWPSNGRMRGGA
DASPADQAIYLRTLVNKLNRQGFNYFVIEAFDQPWKASDEGSVGAYW
GVFNAARQQKFNFEGPVVAIPQWRVLAIGSVVLALLSLTLLMIDGSAL
RQRGRTFLTFIAFLCGSVLVYIGYDYSQQYSTWFSLTVGFLLALGALGV
FIVLLTEAHELAEAVWIHKRRREFLPVLGDSDYRPKVSIHVPCYNEPPE
MVKQTLDALAALDYPDFEVLIIDNNTKDPAVWEPVRDYCATLGPRFKF
FHVSPLAGFKGGALNYLIPHTAKDAEVIAVIDSDYCVHPNWLKHMVPH
FADPKIAVVQSPQDYRDQNESTFKKLCYAEYKGFFHIGMVTRNDRDAI
IQHGTMTMTRRSVLEELGWADWCICEDAELGLRVFEKGLSAAYYHDS
YGKGLMPDTFIDFKKQRFRWAYGAIQIIKRHTRSLLRGKDTELTRGQR
YHFLAGWLPWVADGMNIFFTVGALLWSAAMIIVPQRVDPPLLIFAIPPL
ALFVFKVGKIIFLYRRAVGVNLKDAFCAALAGLALSHTIAKAVLYGFF
TTSIPFFRTPKNADNHGFWVAISEAREELFIMLLLWGAALGIFLVQGIPS
NDMRFWVTMLLVQSLPYLAALIMAFLSSLPKPAAKAEPAPVV

Chapter II

These are the sequences used in the multiple alignment of putative **PhzS** from *Rhodococcus* sp. ef1:

>WP_100882555.1 pyocyanin biosynthetic protein [*Pseudomonas aeruginosa*]
MSEPIDILIAGAGIGGLSCALALHQAGIGKVTLLESSSEIRPLGVGINIQP
AAVEALAELGLGPALAATAIPTHELRYIDQSGATVWSEPRGVEAGNAY
PQYSIHRGELQMILLAAVRERLGQQAVRTDLGVERIEERDGRVLIGARD

GHGKPQALGADVLVGADGIHSAVRAHLHPDQGPLSHGGITMWRGVTE
LDRFLDGKTMIVANDEHWSRLVAYPISARHAAEGKSLVNWVCMVPSA
AVGQLDNEADWNRDGRLEDVLPFFADWDLGWFDIRDLLTRNQLILQY
PMVDRDPLPHWGRGRITLLGDAAHLMYPMGANGASQAILDGIELAAA
LARNADVAAALREYEEARRPTANKIILANREREKEEWAAASRPKTEKS
AALEAITGSYRNQVERPR

>WP_097866731.1 FAD-dependent monooxygenase [*Streptomyces sp. rh34*]
MSKAAQTAIVIAGAGIGGLTAALALHARGLPATVLETAAEIRPLGVGIN
IQPTAVAELIGLGLGDALAATGIPTREHRYLNHRGATLWTEPRGAAAG
HAAPQYSLHRGELQMLLLEAVKERLGARAIRTATEVRGFHQAGDRVF
VHTTTPSGEAEVAEADVLIGADGLRSAVRSQLHPDEPPLRTTAVRMWR
GLTELPAFIDGRTMIIAADDRAGRFVAYPCSRRHAERGTVLLNWVCLA
AVEGGDPGSGVEPGRLEDLLPHFADWEFDWLDIRGTLAASPEILHYPM
VDRDPLPTWGDSRVTILGDAAHPMYPIGANGASQAVLDGVAVAAELS
GGGDPAAALHRYEAARRPATTAIVEANRAMDRSERALAERLDGDVSA
ELRTITDDYRAAVERS

>WP_372409467.1 FAD-dependent monooxygenase [*Streptomyces luteireticuli*]
MTTADTAGFVIAGAGIGGLTAALALHARGIGATVLEAAEEILPLGVGIN
IQPAAIAELTALGFADALAATGIATREHLYVDHRGTTLWTEPRGLAAG
YGHPQYSLHRGELQMMLLDAVRERLGPGAVRTGLRVHGFERTADGV
RVEARDPSDSAVLLEATALIGADGVRSTVRDRLHPGRSGLSTGGTRM
WRGLTELDGFLDGRTMIVAADDRATRLIAYPVSTRAAARGKALLNWV
CLVPDPAGGAAGDPRLSRPGDPEEVLPHLAHWSFDWLDLRAMVLGSP
QILHYPMVDRDPLDRWGDGRVTLLGDAAHLMYPIGANGASQAVLDA

AALADHCAEHADPAVALERYEAVRRPATTAIVLANREMDHAEKALAA
RPDGDKSATLAEVTTAYRTTVERRPSAGR

>VEE50093.1 putative flavin-containing monooxygenase [*Pseudomonas fluorescens*]
MSEPIDILIAGAGIGGLSCALALHQAGIGKVTLLESSSEIRPLGVGINIQP
AAVEALAELGLGPALAATAIPTHELRYIDQSGATVWSEPRGVEAGNAY
PQYSIHRGELQMILLAAVRERLGQQAVRTGLGVERIEERDGRVLIGARD
GHGKPLALGGDVLVGADGIHSAVRAHLHPDQGPLSHGGITMWRGVTE
FDRFLDGKTMIVANDEHWSRLVAYPISARHAAEGKSLVNWVCMVPSA
AVGQLDNEADWNRNGRLEDVLPFFADWDLGWFDIRDLLTRNQLILQY
PMVDRDPLPHWGRGRITLLGDAAHLMYPMGANGASQAILDGIELAAA
LARNADVAAALREYEEARRPTANKIILANREREKEEWAAASRPKTEKS
AALEAITGSYRNQVERPR

>WP_256065518.1 FAD-dependent monooxygenase [*Rhodococcus erythropolis*]
MASKDLTTTRPPISIAGAGIGGLSAALALHERGHEAALFESAPEIVPLGV
GINVQPTAIAELSRLGLADQLARIGVATQAHRYVDHRGRTLWTEPRGI
AAGHDYPQYSVHRGHLQMMLLDAVTERLGPGAVHSDARLSNISGSGE
TAIQLTVVNSDGRSRTLDTDVLVGADGLHSTVRRWLHPDEAPVSVAG
TTMWRGLADLPYTFLDGVTMIIANDGTGTRLVAYPCSEQASVEGRTLL
NWVCLTPSDRRSPSEDERTGLVNALAEWDFDWFDLTELAARSPQVSV
YPMVDRDPLSHWGSGRVTLLGDAAHPMYPIGANGASQAIIDAGALAE
CFTRATDPVSALRSYEAMRIIPTTSIVEANRAMNESEKKTASRAGDPAA
APARRLREITTEYRTVVDRSTAR

>WP_217019072.1 FAD-dependent monooxygenase [*Rhodococcus qingshengii*]
MASKDLTTIRPPISTTTRPPISIAGAGIGGLSAALALHERGHEAALFESAP
EIVPLGVGINVQPTAIAELSRLGLADQLARIGVATQAHRYVDHRGRTL
WTEPRGIAAGHDYPQYSVHRGHLQMMLLDAVTERLGPGAVHSDARL
SNISGSGETAIRLTVVNSDGRSRILDTDVLVGADGLHSTVRRWLHPDEA
PVSVAGTTMWRGLADLPYTFLDGVTMIIANDGTGTRMVAYPCSEQAS
VEGRTLLNWVCLTPPDRRSPSEDERTGLVNALAEWDFDWFALTELAA
RSPQVSVYPMVDRDPLSHWGSGRVTLLGDAAHPMYPIGANGASQAIID
AGALAECFTRATDPVSALRSYEAMRIIPTTSIVEANRAMNESEKKTASR
AGDPASAPARRLREITTEYRTVVDRSTAR

These are the sequences used in the multiple alignment of putative antibiotic biosynthesis monooxygenase from *Rhodococcus* sp. ef1:

>*Rhodococcus*_erythropolis_WP_256065519.1_antibiotic_biosynthesis_monooxygenase_family_protein
MTETVIREGDKVATFINILELKDPAKQQDLIDVLNEGTEKVIKHQPGFIS
VNLFASRDGSRVVNLAQWSSPDDIKAVATNPDAQAFAKKAAELATPA
PGPYSVASVTQA

>*Microbispora*_sp._CA-102843_WP_433107589.1_antibiotic_biosynthesis_monooxygenase
MSETVIRVGDQVATFINVFDVDPSQQQELIGILNEGAEKVMRHRPGFIS
VNILASADGTRVVNLAQWRSPDDIKATAGDPEAQVFAKRAAEIAKAA
PQPYKVVSVYHA

>*Sphaerimonospora*_sp._CA-214678WP_433496940.1_antibiotic_biosynthesis_monooxygenase
MSETVIRVEDQVVTFINILDVDPTKQQELIDVLNEGTEKVMSHRPGFVSVNILASLDGTRVVNLAQWRSLDDIKATMSDPEAQTFAKRTAEIAKAAPSPYRVVSVHHA

>*Streptomyces_luteireticuli*_WP_344023404.1_antibiotic_biosynthesis_monooxygenase_family_protein
MSETVIRVGDEVATLINVFDVEPSKQQELIAVLNEGTEKVMRHRPGFISVNLLASADGTRVVNYAQWRSPDDIKATLGDPEAGAFAKRAAELAKAAPLVYKVVAVHHA

>*Rhodococcus*MULTISPECIESWP_021334645.1_MULTISPECIES:antibiotic_biosynthesis_monooxygenase_family_protein
MTETVIREGDKVATFINILELKDPAKQQDLIDVLNEGTEKVIKHQPGFISVNLFASRDGSRVVNLAQWSSPDDIKAVATNPDAQVFAKKAAELATPAPGPYSVASVTQA

>*Pseudomonas_mangiferae*_WP_143486620.1_antibiotic_biosynthesis_monooxygenase family protein
MSGSEVTFINVIDVDPSKQAEVIKLLQEGTESVISKRPGFVSVTLLASKDGSRVVNIAKWKSAADIQATQGDPAAAEFAKRTAALAKASPGIFEVVGEYSA

These are the sequences used in the multiple alignment of putative **PhzA/B** from *Rhodococcus* sp. ef1:

>*Rhodococcus_qingshengii*_WP_397525121.1_PhzA/PhzB_family_protein

MRKANQNRCHSIIFPCVKHVHIPRGLAMYEVFGPEQEAIRSRNRSVVA
RYMNTRGTDRLKRHELFTQDGEGGLWTTETGEPIMIKGRDRLAEHAV
WSLECFPDWSWFNVEIFDTQDPDRFWVECDGAGIIRFAGYPEGRYENH
FIHFFRFVDGKISQQREFMNPCQQFRALGIAVPNVVREGIPT

>*Rhodococcus*MULTISPECIES_WP_030537981.1_PhzA/PhzB_family_protei
n
MYEVFGPEQEAARSRNRSAVARYMQTRGLDRLRRHELFTQDGEGGL
WTTETGEPIMIKGRDRLAEHAVWSLECFPDWSWFNIEIFDTQDPDRFW
VECDGAGIIRFTGYPEGRYENHFIHFFRFVDGKISQQREFMNPCQQFRA
LGIAVPNVIREGIPT

>*Streptomyces_niveus*_WP_359815293.1 PhzA/PhzB family protein
MSDDTQVREHNRAVVARYMNTRGQDRLERHLLFTEDGTGGLWTTET
GEPIVISGRDTLGEHAVWSLKCFPDWKWFNVEIFDTQDPDRFWVECDG
EGQIRFPGYPDGLYRNHFLHSFLFEDGKIKQQREFMNPCQQFRALGIDV
PAVRREGIPT

>*Streptomyces_marincola*_WP_086157042.1_PhzA/PhzB_family_protein
MTDDIAPAHPPVDEKELRDHNRAIVEQYMNTRGQDRLRRHLLFTEDG
TGGLWTTESGEPIVIRGRDRLGDHAVWSLKCFPDWAWINIEIFDTQDPD
RFWVECDGEGKILFPGYPEGHYRNHFLHSFLFEGGKIKQQREFMNPCQ
QFRALGIAVPEIRREGIPT

>*Pseudomonas*_sp.CMR5c_WP_053129818.1_PhzA/PhzB family protein
MQNSAARQLNEHDTTELRRKNRATVEQYMHTKGQDRLRRHELFTED
GSGGLWTTDTGAPIAINGKSKLAEHAVWSLKCFPDWEWYNIQIFETDD

PNHIWVECDGHGKILFPGYPEGYYENHFLHSFELQDGKIKQNREFMNV
FQQLRALGIPVPQIKREGIPT

>*Pseudomonas_fluorescens*_WP_214992101.1_PhzA/PhzB_family_protein
MPNSAALQLATRDTTELRRKNRATVEQYMRTKGKDRLRRHELFTEDG
SGGLWTTDTGAPIVISGKAKLAEHAVWSLKCFPDWEWYNVKVFETDD
PNHIWVECDGHGKILFPGYPEGYYENHFLHSFELEDGKVKRNREFMNV
FQQLRALGIAVPQIKREGIPT

>*Pseudomonas_chlororaphis*_WP_124339061.1_phenazine_biosynthesis_prot
ein
MPNSATQQLTANDTTELRRKNRATVEQYMRTKGQDRLRRHELFTEDG
TGGLWTTDTGAPIVISGKAKLAEHAVWSLKCFPDWEWYNVKVFETDD
PNHFWVECDGHGKILFPGYPEGYYENHFLHSFELEDGKVKRNREFMN
VFQQLRALGIPVPQIKREGIPT

>*Pseudomonas_aeruginosa*_HHW1969258.1_phenazine_biosynthesis_protein
_PhzB
MLDNAIPQGFEDAVELRRKNRETVVKYMNTKGQDRLRRHELFVEDGC
GGLWTTDTGSPIVIRGKDKLAEHAVWSLKCFPDWEWYNIKVFDTDDP
NHFWVECDGHGKILFPGYPEGYYENHFLHSFELDDGKIKRNREFMNVF
QQLRALSIPVPQIKREGIPT

These are the sequences used in the multiple alignment with the putative **PhzC** from *Rhodococcus* sp. ef1:

>*Rhodococcus_erythropolis*_WP_336505324.1_3-deoxy-7-
phosphoheptulonate_synthase

MIPSALTSMVNSHQPPWHDHPQLDLVRNVLETTTVIASPVEIDQLARRL
RAVEAGHASILQMGDCAEDPAHCTPDHVHRKLDQLTASAGAVATPTG
LPVVQVGRIAGQFAKPRSKATETIGDREVVTYRGHMVNLPDSDEVSRT
PDPLRILMGYLTSRQVAATIAGFNRGRALEDRVWTSHEALLLDYEHPM
MRQGSDERTYLTSTHWPWIGERTRNVDGPHVATLAHIANPSACKVGP
TATEDDLVALCSRLDPYREPGKLALITRMGAQHIRTGLPALMNAVRAA
GHRVLWICDPMHGNTLSTDDGTKTRVVDDVIAEMAGFVSVADQTGTR
VHGLHLETTHLTDVSECVWSSTDLASARPSSSLCDPRLNPEQAAAVVE
AWGEMLARHYRVSETTS

>*Rhodococcus_qingshengii*_KSU60285.1_hypothetical_protein_AS032_34340
MVNSHQPPWHDHPQLDLVRNVLETTTVIASPVEIDQLARRLRAVEAGH
ASILQMGDCAEDPAHCTPDHVHRKLDQLTASAGAVATPTGLPVVQVG
RIAGQFAKPRSKATETIGDREVVTYRGHMVNLPDSDEVSRTPDPLRILM
GYLTSRQVAATIAGFNRGRALEDRVWTSHEALLLDYEHPMMRPGSDE
RTYLTSTHWPWIGERTRNVDGPHVATLAHIANPSACKVGPTATEDDLV
ALCSRLDPYREPGKLALITRMGAQHIRTGLPALMNAVRAAGHRVLWIC
DPMHGNTLSTDDGTKTRVVDDVIAEMAGFVSVADQTGTRVHGLHLET
THLTDVSECVWSSTDLASARPSSSLCDPRLNPEQAAAVVEAWGEMLA
RHYRGSETTS

>*Streptomyces_variabilis*_GAB2331875.1_phenazine_biosynthesis_protein_P
hzC
MTSLLDGCVDRPVLHQPLWEDRPELRCVTAELAQRPQLVSATDVARL
RALLARVAAGEAMVVQAGDCAEDPAECEPGSVARKAGLLDVLAGVL
RMVTHRPVLRVGRIAGQFAKPRSNPTEMVGGIELPVFRGHMVNGPEPD
PARRRPDPQRLLIGYAAAGEAMTHLGWLSEPRWPGISPEVWTSHEALL

LDYEIPMTRPTEDGGLLLASTHWPWIGERTRQVEGAHVDLLATVANPV
ACKVGPSMTPDELLALCERLDPPREPGRLTLISRMGADHVRERLPRLVS
AVKGAGHPVIWLTDPMHGNTVTTPDGLKTRLVETVLREVEGFQGAVR
AAGGVAGGLHLETTPDDVTECAQDDTHLARVGDTYTSLCDPRLNPEQ
AVAVVAAWQD

>*Streptomyces_marincola*_WP_226074269.1_3-deoxy-7-phosphoheptulonate_synthase
MENTLLDIPPRSAPHQPDWEDPARVRWVRKELRARDPLVARDDVRAL
RARLARVAAGEALVVQAGDCAEDPEECTAEHVARKAAVLDLLAGAL
RLITARPVLRVGRIAGQYAKPRSKPTETVAGVELPVYRGHMINDPRPD
ADSRRPDPLRMLTGYMAAREVMRHLGWQPGGAAADGFDPRVWTSH
EALLLDYEVPMLRRGGDGGLLLTSTHWPWIGERTRQVDGAHVSLLAG
VANPVACKVGPSMEPDELLALCRRLDPRREPGRLTLISRMGADRVADA
LPPLVAAVREAGHPVIWLTDPMHGNTVSVRGGIKTRFVATVAREVAA
FHRAVTAAGGVAGGLHLETTPDAVTECVADESAVDEAGSVSTTFCDP
RLTPDQAASVIAAWSR

>*Streptomyces_kutzneri*_WP_314250358.1_3-deoxy-7-phosphoheptulonate_synthase
MGNILADIERSQARHQPEWDNPPQVELVRAMLSSVTPLVTAAQVESLR
SHLAYVATGEMKVLQAGDCAEDPAECTAGHIQGKTGLIDLLAQNLET
ATGKQTLRVGRIAGQFSKPRSSQVEKLGDDELPSFFGHMINGPEPTHES
RRPDPLRMLTGYMAAREITTQLGWVGSTPRLDGPVVWTSHEALLLDY
EMSMLRELDGSRLLLSSTHWPWIGERTRQIDGPHVALLAQVANPVAC
KVGPSMTAGEIVELCDRLDPEREPGRLSLIVRMGADLVADRLPRLVEA
VQSAGHPVVWLSDPMHGNTDCAADGTKYRLVETVAREVRGFRRVLD

LAGVPAGGLHLEATPDDVTECVLDTAELGSGPVTSLCDPRLNTAQAIK
VVSAWSEY

>*Pseudomonas_aeruginosa*_WP_209098778.1_phenazine_biosynthesis_protei
n_PhzC
MDDLLKRVRRCEALQQPEWGDPSRLRDVQAYLRGSPALIRAGDILALR
ATLARVARGEALVVQCGDCAEDMDDHHAENVARKAAVLELLAGALR
LAGRRPVIRVGRIAGQYAKPRSKPHEQVGEQTLPVYRGDMVNGREAH
AEQRRADPQRILKGYAAARNIMRHLGWDAASGQEANASPVWTSHEM
LLLDYELSMLREDEQRRVYLGSTHWPWIGERTRQVDGAHVALLAEVL
NPVACKVGPEIGRDQLLALCERLDPRREPGRLTLIARMGAQKVGERLP
PLVEAVRAAGHPVI

WLSDPMHGNTIVAPCGNKTRLVRSIAEEVAAFRLAVSGSGGVAAGLH
LETTPDDVTECVADSSGLHQVSRHYTSLCDPRLNPWQALSAVMAWAG
AEAIPSATFPLETVA

>*Pseudomonas_mangiferae*_WP_143486210.1_3-deoxy-7-
phosphoheptulonate_synthase
MKDLLERVQNCEALQQPQWSEPSQLNDAQAYLRESPALVQLEDILAL
RAVLARVAAGEALVIQSGDCAEDMDEYEPGHVARKAAVLDLLAGAF
RLVTEQPVVRVGRIAGQFAKPRSKPSEVVGDVELPVYRGDMVNGREA
HSGSRQHDAQRLVKGYNAAREIMQHLGWMEDRATGA

VLAGPPAWTSHEMLVLDYEVPLLREDGRGRVYLGSTHWPWIGERTRQ
EEGAHVTLLSAVLNPVACKVGPNITPSQLLTLCERLDPRREPGRLTLIA
RMGASAVAERLPPLVKAVREAGHPVIWLSDPMHGNTVVAPCGNKTRL

VQTIAEEIAAFRQAVTAAGGVAGGLHLETTPDEVTECANDADALHQV
ASRYRSLCDPRLTPWQAITAVMAWNTSPQSPHTPS

>*Pseudomonas_shirazensis*_WP_186698045.1_3-deoxy-7-phosphoheptulonate_synthase
MLTQGANVPDGPLAWSLNSWRDRSAAQQPLYHDQPALEQALAYLRQ
APALVSRQSISLLTALLAQAQQGRAFVLQGGDCAEGFTQTDQAALNRF
VQLLQQMSQLLTRGVQRPVIKIGRLAGQYAKPRPSDIETRDGLSLPVYR
GDIVNQAEFRAAARRADPQRLLAAYAHSAATLRDIRTLQGFMDSDGL
CDQALFISHEALLLEYEQALTRQQDDGCWFNQSTHLPWIGLRTAQPDG
AHVEYLRGVSNPVAVKVGAETSASALLQLIKQLNPHNQPGRLTLIHRM
GAALLEQHLGPLIDAVEHAGARVLWLCDPMHGNTRTLPCGTKTRAFD
DILAEIETAFAVHARHGSVLGGLHLELTAEAVTECLGGPSQLQPEDLHR
CYLSKVDPRLNGEQAFALAQHLSRMPPCR

These are the sequences used in the multiple alignment with the putative **PhzD** from *Rhodococcus* sp. ef1:

>*Rhodococcus_erythropolis*_WP_336505323.1_isochorismatase_family_protein
MSRDLTVEPYLLPSPGEMPEALVDWDIRPRQATLLIHDMQRYFLSPFPD
AMRSEIVGNVRDLHSWAQRVGAATAYTAQPGRMNVTDRGLLRDFWG
PGMQTTDTDRALVPELELGDDAWPFVKWRYSAFHRSDLLARMRENG
RTQLVLCGVYAHVGILATALDAYTHDIEVFLVGDAVADFTAADHRHT
LEYTSRCCARVVATKWVTER

>*Rhodococcus_qingshengii*_WP_217019070.1_isochorismatase_family_protein

MSRDLTVEPYLLPSPGEMPEALVDWDIRPRQATLLIHDMQRYFLSPFPD
AMRPEIVGNVRDLHSWAQRVGAATAYTAQPGRMNVTDRGLLRDFWG
PGMQTTDADRALVPELELGDDAWPFVKWRYSAFHRSDLLARMRKNG
RTQLVLCGVYAHVGILATALDAYAHDIEVFLVGDAVADFTAADHRHT
LEYTSRCCARVVATKWVTER

>*Nocardia_aurantia*_WP_153341071.1_isochorismatase_family_protein
MTIVPTPALQVQPYPLPSRTELPDNLVDWRVRPEQAVLLIHDMQQYFL
ATFPHALRSRLVGNAARLRKSCADRGVRIGYTAQPGRMTTADRGLLL
DFWGPGMTTAEADRAIVAELTPETPDWTFTKWRYSAFHRSNLLGRMR
AEGRDQLLLCGVYGHVGILATALEAYANDLQVFLIADAIGDFSAEKHR
FTLEYTASCCARITTVDEVLS

>*Streptomyces_niveiscabiei*_WP_055721456.1_isochorismatase_family_protei
n
MPGLPSISPYPMPTAESLPPRIPAWSVDPSRAVLLLHDLQRYFLRPLPDA
LRTELIGNAAELTSWARAGGVPVAYTAQPGGMTPQQRGLLKDFWGPG
MRVDPADREVVEPVAPRDGDWLLTKWRYSAFFNTDLLQRMRDAGRD
QLVVCGIYAHVGVLATCVEAYTHDIETFLVADAVADFGEGDHRMALE
YAARCCAVVLPTKEVLG

>*Pseudomonas_aeruginosa*_WP_203328712.1_isochorismatase_family_protei
n
MSRIPEITAYPLPTAQQLPANLARWSLEPRRAVLLVHDMQRYFLRPLPE
SLRAGLVANAARLRRWCVEQGVQIAYTAQPGSMTEKQRGLLKDFWG
PGMRASPADREVVEELAPGPDDWLLTKWRYSAFFHSDLLQRMRAAG

RDQLVLCGVYAHVGVLISTVDAYSNDIQPFLVADAIADFSEAHHRMAL
EYAASRCAMVVTTDEVLE

>*Pseudomonas_fluorescens*_VEE46437.1_phenazine_biosynthesis_protein_Ph
zD
MSGIPEITAYPLPTAQQLPANLARWSLEPRRAVLLVHDMQRYFLRPLPE
SLRAGLVANAARLRRWCVEQGVQIAYTAQPGSMTEEQRGLLKDFWG
PGMCASPADREVVEELAPGPDDWLLTKWRYSAFFHSDLLQRMRAAG
RDQLVLCGVYAHVGVLISTVDAYSNDIQPFLVADAIADFSEAHHRMAL
EYAASRCAMVVTTDEVLE

>*Pseudomonas_chlororaphis*_WP_075121686.1_isochorismatase_family_prot
ein
MTGIPSIVPYALPTSRDLPVNLAQWSIDPERAVLLVHDMQRYFLRPLPD
ALREAVVSNAARVRQWAADRGIPVAYTAQPGSMSEEQRGLLKDFWG
PGMKASPADREVVDALAPMPDDWLLTKWRYSAFFNSDLLERMRANG
RDQLILCGVYAHVGVLISTVDAYSNDIQPFLVADAIADFSEEHHRMAIE
YAASRCAMVVTTDEVVL

These are the sequences used in the multiple alignment with the putative **PhzE** from *Rhodococcus* sp. ef1:

>*Streptomyces_rubiginosohelvolus*_WP_355064226.1_anthranilate_synthase_f
amily_protein
MTADLLDAVLDGTAGDYALICRSDEHGRQVQVITGETGHPASLAAIDF
AHRPAVGAASSDMLIVVPYRQLVERGHPAVDDGAPLLAMRVTAEERH
PVASVLGRLPDRQVRLEDGHFDADDDTYAKSVEAVLADEIGTGQGAN
FVIKRTYVADIADPGPDAALSAFRQLLAAERGAYWTFLVRTAGSTIVG

ASPERHVGLIDDVVRMNPISGTYRYPADGPTLSGVTAFLADRKEAEEL
YMVVDEELKMMCRLCLPGTVSVTGPHLKEMARVAHTEYHIEGRTDR
GVPELLRETMFAPTVTGSPVESAARVIERYEPGGRRYYSGIIGLVGSDG
AGRQTLDSAIVIRTAEIDPGGRLSLSVGSTLVRHSDPLGEVAETRAKAS
ALLAAFGEAEPRRGFATHPEVLSSLSRRNEGIAGFWTMSGALGYARSK
GLDGHKVLVVDAEDTFTSMLEHQLRALGLGVTVRRFDETYETRDHDL
IVMGPGPGDPGDPGDPKIAALDAVVAELLAERRPMLAVCLSHQVLCRR
LGLPVVRRARPNQGVQRQISLFGRPERVAFYNTFEARATADHRDTEAG
GPVEITRDPDTGEVHALRGHRFASLQFHPESLLTVDGPRILTDMTEWVL
GE

>*Streptomyces*_sp._NPDC002671_MGW0882928.1_anthranilate_synthase_fa
mily_protein
MTDYNDPRKHTPHSPPAPAKSDLLQAVLDGSAENFAIVCRDGEHGRD
VQVFRGDVSQPASLDAIGLGQGGSTGSARGEASTDVLVVVPYRQLAER
GYPAPDDGTPLIAMAVTEEEHHALSTVLERLPQHTVRLADGHFEPDDA
AYAETVKAVLADEIGTGQGANFVIKRTYLADITDYRPESALSAFRELLS
RERGAYWTFLVRTRDVTLIGASPERHVSLADGVATMNPISGTYRYPDG
GPTLKGLTEFLADRKEAEELYMVVDEELKMMCRICEPGTVQVSGPHL
KEMAKVAHTEYHICGTANRDIPEVLRATMFAPTVTGSPVESAARVIER
YEPDGRGYYSGIIGLAGTDKAGRRTLDSAILIRTAVLEPSGRLSISVGST
LVRHSDPQSEVAETRAKATALLEAFGECTPRRSPAQDPSVLASLRSRNE
GIAGFWVGQDAGQGVSSRILNGRKALVIDAEDNFTSMLDHQLHALGL
SVTVRRFDEPFETGDHDVVLLGPGPGDPRDTTHPKIAALDRVIGELLGE
RRPFVAVCLSHQVLCHRLGLPLVRREHPNQGTQRRIELFGNAERVGFY

NTFEARSTTDRWKSAGGVQVEISRDPVTSGVHALRGDRFASLQFHAES
LLTVDGPRILTDMFEGVMTR

>*Nocardia_sp._BMG111209*_WP_026343200.1_anthranilate_synthase_family
_protein
MSGDLLGAVIDGSAGDFAIISRPGRDVTVLVGAAERPESLAGIRLGGRG
APGSEALVLIPYRQLTERGFPAPDDGAPLLALAVTGEERHPLGAVLARL
PHRRVQLGEGGFDSDDAAYAATVRAIIDDEIGSGQGANFVIKRTYSAGI
ADYTPAMALAVLRELLAAERGAYWTFLVRVGDLTLVGASPERHVSLE
TGVLQMNPISGTYRYPAGGPTLDGVTAFLADRKETEELYMVVDEELK
MMCRICEPGSTRMIGPFLKEMAWVAHTEYHLEGRTRRDIRDVLRETM
FAPTVTGSPVESAARVIRRYEPAGRGYYSGIIGLAGRDAQGEPVLDSAI
LIRTASIEPAGRLSISVGSTLVRHSDPLAEVAETQAKAAGLLAAFGAGA
GGEFADHPEVVAALRSRNDDIAAFWAGLTSSATRSERLHEHNALVIDA
EDTFTAMLEHQLRMLGLSVTIRRFDEDFDLAGHDLVVVGPGPGDPCA
ADDPKIAKLAAVVDELLGSGRPFMATCLSHQVLSRRLGLPVLRRSLPN
QGTQRWIDLFGSRERVGFYNTFSARSEHDRLDTWAGAVQVSRDPGTA
EVHALRGPRFASVQFHPESLLTIDGPRILTGMAEGVLAQ

>*Rhodococcus_erythropolis*_WP_336505322.1_anthranilate_synthase_family_
protein
MSPPLSTDLLTEILAGNCSVYALLCRADPATGARTVTALSGQLRQHELI
EEISTTADVFVLLPYRQIRERGYPAHDDGAPLLAIYIDEQQDYPLTSVLD
KLPRRSFALTDGHFDSSDADYERKVAAIVSEEIGNGRGANFVIKREFSA
ECTPYNSTVPLSAFGELLDNERGAYWTFLVHTEGLVLVGASPEQHVVL
DNGTAVMNPISGTYRYPPGGPTLDGVQQFLDDRKETDELYMVVDEEL
KMMCRICEPGTTRVHGPALKEMAWVAHTEYFIEGQTRRDPREILRETM

FAPTVTGSPVESATEVIARYETTGRGYYSGVAALITRSGGGAPTLDSAIL
IRTAAIEPDCGRVRVAVGATLVRHSDPGAEVYETHAKAQSVLAAFGHS
KPHASWNRHPMITTALAHRNDQIAGFWSPNYPHDVRSRVLDGRKALV
VDAEDTFTAMLDHQLRSLGLTVTVRRFDDMYTTSDHDLVIVGPGPGD
PTDVDDEKIVHLRAQIDDLLSTQRPFLAICLSHQILASRLGLPLTRRAEP
NQGKQARVDVFGQSENVGFYNTFEARSAPGRIDVAGIGPVTVSADTAT
GAIHALEGPHFASVQFHPESILTVNGPRILAHMSERLLST

>*Rhodococcus_qingshengii*_WP_047269922.1_anthranilate_synthase_family_protein
MSPPLSTDLLTEILAGNRSVYALLCRADPATGARTVTALSGQLRQHELI
EEISTTADVFVLLPYRQIRERGYPAHDDGAPLLAIYIDEQQDYPLTSVLD
KLPRRSFALTDGHFDSSDADYERKVAAIVSEEIGNGRGANFVIKREFSA
ECTPYNSTVPLSAFGELLDNERGAYWTFLVHTEGLVLVGASPEQHVVL
DNGTAVMNPISGTYRYPPGGPTLDGVQQFLDDRKETDELYMVVDEEL
KMMCRICEPGTTRVHGPALKEMAWVAHTEYFIEGQTRRDPREILRETM
FAPTVTGSPVESATEVIARYETTGRGYYSGVAALITRSGGGAPTLDSAIL
IRTAAIEPDCGRVRVAVGATLVRHSDPGAEVYETHAKAQSVLAAFGHS
KPHARWNRHPMITTALAHRNDQIAGFWSPNYPHDVRSRVLDGRKALV
VDAEDTFTAMLDHQLRSLGLTVTVRRFDDMYTTSDHDLVIVGPGPGD
PTDIDDEKIVHLRAQIDDLLSAQRPFLAICLSHQILASRLGLPLTRRAEPN
QGKQARVDVFGQSENVGFYNTFEARSAPGRIDVAGVGPVTVSADTAT
GAIHALEGPHFASVQFHPESILTVNGPRILAHMSERLLST

>*Pseudomonas_fluorescens*_VEE46436.1_phenazine_biosynthesis_protein_PhzE

MNALPTSLLQRLLERPAPFALLYRPESNGPGLLDVIRGEALELHGLADL
PLDEPGPGLPRHDLLALIPYRQIAERGFEALDDGTPLLALKVLEQELLPL
EQALALLPNQALELSEEGFDLDDEAYAEVVGRVIADEIGRGEGANFVIK
RRFQARIDGYATASALSFFRQLLLREKGAYWTFIVHTGERTLVGASPER
HISVRDGLAVMNPISGTYRYPPAGPNLAEVMEFLDNRKEADELYMVV
DEELKMMARICEDGGRVLGPYLKEMAHLAHTEYFIEGQTSRDVREVL
RETLFAPTVTGSPLESACRVIRRYEPQGRGYYSGVAALIGGDGQGGRTL
DSAILIRTAEIEGDGRLRIGVGSTIVRHSDPLGEAAESRAKASGLIAALKS
QAPQRLGSHPHVVAALASRNAPIADFWLRGASERQQLQADLSGREVLI
VDAEDTFTSMIAKQLKSLGLTVTVRGFQEPYSFDGYDLVIMGPGPGNP
TEIGQPKIGHLHLAIRSLLSERRPFLAVCLSHQVLSLCLGLDLQRRQEPN
QGVQKQIDLFGAAERVGFYNTFAARALQDRIEIPEVGPIEISRDRETGEV
HALRGPRFASMQFHPESVLTREGPRIIADLLRHALVERRP

>*Pseudomonas_chlororaphis*_OLF51938.1 phenazine-specific_anthranilate_synthase_component

MNQAAARLMERILQPAPGPFALLYRPESTGPGLLDVLIGDMSEPQVLA
DIDLPATSIGAPRLDVLALIPYRQIAERGFEAVDDQSPLLAMNITEQHSIS
IERVLGLLPNVPIQLNSERFDLSDASYAEIVSQVIANEIGSGEGANFVIKR
TFLAEISEYGTDSALSFFRHLLEREKGAYWTFIIHTGSRTFVGASPERHIS
VKDGLAVMNPISGTYRYPPAGPNLTEVMDFLADRKEADELYMVVDEE
LKMMARICEDGGHVLGPYLKEMAHLAHTEYFIEGRTRRDVREILRETL
FAPTVTGSPLESACRVIQRYEPQGRAYYSGMAALIGSDGKGGRSLDSAI
LIRTADIDDSGQVRISVGSTIVRHSEPLAEAAESRAKAAGLIAALKDQAP
SRFGSHLQVRAALASRNAYVSDFWLMDSQQRQQTQADFSGRQVLIVD
AEDTFTSMIAKQLRALGLVVTVRSFNDEYSFDGYDLVIMGPGPGNPSD

VQLPKIDHLHVAIRSLLSQQRPFLAVCLSHQVLSLCLGLELQRKAIPNQ
GVQKQIDLFGNAERVGFYNTFAAQSASDRLDINGIGTVEISRDSETGEV
HALRGPSFASMQFHAESLLTQEGPRIIADLLRHALVHTPAENNASAAGR

These are the sequences used in the multiple alignment with the putative **PhzF** from *Rhodococcus* sp. ef1:

>*Rhodococcus*_sp._C3V_WP_276117756.1_PhzF_family_phenazine_biosynthesis_protein
MKLEYIMWDLQSDDDPSVTHLNELTDTAAVDAWRSVPGLAAKYWIH
DRGSGQWGAILLWDDDRPAGVLPAGPALELLERERAHRKDFSVHALI
GHRPESSRRSLRYCVVDAFASTPLSGNPVAVFFGADSLSAEMMQRIAA
ELNLSEVTFVLSADSAESTARIRIFTPVNELPFAGHPILGTAAAVAAQTG
AKELAFETAVGLIPMTAEAVDDYFRVTMDQPLPTWSPMPDAEQRSLL
AALGLDASALPIETYDNGPRHTIVTIDSIEALSALRPDHRALSEFENMAI
NCIAEDLDGVWRNRMFSPAYGVVEDAATGSAAGPIAIHLARHGRIEYD
HDLRIHQGVELGRHSVMHARASLDARTHDLISVQVGGDAITIAHATLY
LGSDRGTDDE

>*Streptomyces_rubiginosohelvolus*_WP_398714565.1_PhzF_family_phenazine_biosynthesis_isomerase
MNPTQKTNRMNLEIAWWDLENSFATVDDLERHLGEDGVVENWKEVG
GLHEKYWIADRAGNRWGAVMVWDGERPAELPENKAAQLIGGPVTHR
ERFEVQASVRGLARGRAASHRYIVVDAFASEPLRGNPVAVFFDADDLT
ADRMQRIAQEMNLSEVTFLLPPTTADADLRVRIFTPVNELPFAGHPLQG
TAVAVALDSGRDRLRFETAMGVVPFEIVRAPGGETAHASMEQPIPEWR
PYEHADALLAALGVDSSTLPVEIYRNGPRHVFVGLPDAAALNALHPDH

RALAAFEDMAANCFAPDGDHWQTRMFSPAYGVVEDAATGSAAGPLA
IHLARYGRVPYGRTVEIHQGVRLGRRSIMFADATVDTAGEIARVRVGG
HGVVAAEGTIRV

>*Streptomyces_colonosanans*_WP_071367550.1_PhzF_family_phenazine_bio
synthesis_isomerase
MHTYVVVDAFASEPLTGNPVAVYFEADSLSGEQMQRIAREMNLSETTF
VLRPHRAGHDAHVRIFTPVNELPFAGHPLLGTAIALGARTKGDRLLIET
AMGLVPFTLEREDGKVLRASMRQPVPTWKPFDRTDELLEALGIRGSTL
PVEIYRNGPRHVLVGLESIEALSKLDPDHRALARFSDLATNCYAGEGTS
WRNRMFSPAYGVVEDAATGSAAGPIAIHLARYGLIEYGQHIQIVQGVEI
GRPSPMGAVAHGEGEHVAFVEVSGPGIQIIEGVLHV

>*Nocardia_aurantia*_WP_319942845.1_PhzF_family_phenazine_biosynthesis
_protein
MSPAALEIAWWDLDGSAVTVDRLTAQLADEDVPAGWRDVEGLDEKF
WIADPDGCRWGAVMVWRGAKPAELPPNSALRLIGRPPTHRDRFEVRA
RVRGATRPGHRYVVVDAFAREPLSGNPVAVFFDAGDLDGERMQRIAR
EMNLSEVVFLLPPTSDDADARVRIFTPVNELPFAGHPLLGTAVAVGLER
GVRRLRFETAMGTVPFEVGPGGDEVAYVSMRQPIPRWRRFERGEELLA
ALGITDSTLPVEIYRNGPRHVFAGLPDVDALSALRPDHRALAVFPDMA
ANCFAPADGHWRARMFSPAYGVVEDAATGSAAGPLAVHLARHGLAD
YGRTVEIHQGVEIGRRSVMFARATAAGSGEITEVRVSGHGVVAAAGTL
HV

>*Pseudomonas*
*mangiferae*_WP_143486207.1_PhzF_family_phenazine_biosynthesis_protein

MHRYVIIDAFATQPLEGNPVAVFFDADDLSAEQMQRIGREMNLSEVTF
VLKPRQGGDALIRIFTPVNELPFAGHPMLGTAIALGAETDSPQLRLETQ
MGTIAFQLERQNGQVVACSMEQPIPTWSLFDRTPELLAALGIERSQYPV
EIYRNGPRHVFVGLPDIASLSALHPDHRALSVFPDMAVNCFAGAGRRW
RSRMFSPAYGVVEDAATGSAAGPLAIHLARHGQATFGQQIEILQGVEIG
RPSLMFARAEARDERITRVEVSGNGALFGQGTIVI

>*Pseudomonas_aeruginosa*_WP_315558930.1_phenazine_biosynthesis_protei
n_PhzF
MHRYVVIDAFASEPLQGNPVAVFFDCDDLSGERMQRMAREMNLSEST
FVLRPQQDGDARIRIFTPVNELPFAGHPLLGTAIALGAETDKDRLFLETR
MGTVPFALXRQDGKVVACSMQQPIPTWEHFSRPAELLAALGLKGSTFP
IEVYRNGPRHVFVGLESVAALSALHPDHRALCDFPDLAVNCFAGAGRH
WRSRMFSPAYGVVEDAATGSAAGPLAIHLARHRQIPYGQQIEILQGVEI
GRPSRMYARAEGAGERVSTVEVSGNGAAFAEGRAYL

>*Pseudomonas_fluorescens*_WP_150770788.1_PhzF_family_phenazine_biosy
nthesis_protein
MLLDFVQVDAFTNRPLYGNPAAVVFDGDELSTETMQRIAREMNLSET
VFILKPTTPEADYRARIFTPMSELPFAGHPTVAAAHSVLARYPDKANAT
LLRQECGIGVVPVEVIPTGSGILLRMTQGSPEYRETQLSRKTVAQMLGC
AETEVADSPFEVVSTGVPWLIVELCSFEAISRLNPDQNLITRECKALSAA
GLTVFAECGDGAPVRIRVRTFAPGEGVAEDPVCGSGNGSVAAYLARH
KHVHEHSGSYVAEQGIEIGRDGEVQASWERDGESLRVKIGGQAAVSAS
GQLHL

These are the sequences used in the multiple alignment with the putative **PhzG** from *Rhodococcus* sp. ef1:

>*Pseudomonas_chlororaphis*_WP_075121689.1_phenazine_biosynthesis_FMN-dependent_oxidase_PhzG
MNSSVQGQPLLGKGMSESLTGTLEAPFPEYQAPPANPMDVLHNWLERARRVGIREPRALALATVDDQGRPSTRIVVISEFSDRGVLFSTHAGSQKGRELAHNPWASGVLYWRESSQQIVLNGQAVRLPDAKAEEAWLKRPYATHPMSSVSRQSEELEDIQAMRAAARELAEVQGPLPRPEGYCVFELRLESLEFWGNGQERLHERLRYDRSDSGWRVRRLQP

>*Pseudomonas_aeruginosa*_WP_128663115.1_phenazine_biosynthesis_FMN-dependent_oxidase_PhzG
MGVNANISESLTGTIEAPFPEFEAPPANPMEVLRNWLERARRYGVREPRALALATVDGQGRPSTRIVVIAEXGERGVVFATHADSQKGRELAQNPWASGVLYWRESSQQIXLNGRAERLPDERADAQWLSRPYQTHPMSIASRQSETLADIHALRAEARRLAETDGPLPRPPGYCLFELCLESVEFWGNGTERLHERLRYDRGEGGWKHRYLQP

>*Pseudomonas*_sp._MWU13-2105_WP_248798019.1_phenazine_biosynthesis_FMN-dependent_oxidase_PhzG
MSAHLLSESLTGTIEAPFPEFATPPANPFIVLNNWLERARRYGVREPKALALATADARGRPSTRIVVIAEVSDAGLVFSTHAGSQKGRELVENPWASGVLYWRETSQQIVLNGRAERLSDTRADVAWRGRPHVTHPMSAVSRQSEELTDVEALRARAKALSGTQAPLPRPDGYCLFELRLESVEFWGNGQDRLHERLRYDRTPDGWAVRRLQP

>*Rhodococcus_qingshengii*_WP_217019068.1_pyridoxal_5'-phosphate_synthase
MSSQYETITGTARPFLEYSDPPPTPLDLFQVWIEQAEIAGVREPLASSLA
TTDSAGRCSQRTVTDISASGLSFSTHTTSRKARELQTNSWASGLFYWRE
LARQLIISGPVLKLNAAIADKVWDERAEPLKPMSTASHQSLHLGDPEVL
FARSESLGLRTDLARPHRFAVYQLQPHRVEFWAADQSRLHRRLLYERS
PLGWTVDRLQP

>*Streptomyces_rubiginosohelvolus*_WP_355064222.1_phenazine_biosynthesis_FMN-dependent_oxidase_PhzG
MSSELESITGAVDLDFPEYDNPPPEPMKPALAWLRTAVEGGVREPYAL
ALATTDGAGRPSSRMVAVSDASAEGLLFTTHSTSRKGREIAGTGWASG
LFYWRETARQLCFSGPVVRLDDDENDRLWHSRAHGLHPMSAASRQSE
SLADPGRLQEEADLLAARDLPLPRPDRFVGYRLQPHSVEFWSAAESRL
HRRLRYELTDTGWQVSRLQP

>*Microbispora_hainanensis*_WP_328709570.1_phenazine_biosynthesis_FMN-dependent_oxidase_PhzG
MSSRFESLTGTIDPAFPEYDMPPAEPMDLARQWIAGAVEAGVREPLAL
ALATADRGGRASTRMVAVIDVGDRGLVFTSHSTSRKGREIAQTGWAS
GLLYWRETARQLSLSGPVAMLPEPEAERLWDARPVPLHAMSVASRQS
EPLEDVARLRSEAERLASYGTSLPRPARFAGYRLEPAAVEFWSADADR
LHRRLRYDRTPSGWHISRLQP

>*Streptomyces_albus*_WP_173874215.1_phenazine_biosynthesis_FMN-dependent_oxidase_PhzG

MSSQYETLTGPADPDFPEYDNPPPEPLKLAAQWLASAIDTGVREPKAL
ALATADRRGRPSSRTVVVLEIDQHGLRFSTHSTSRKGREIAENGWASG
LLYWRETAQQLIFSGPVVRLDAAEADRHWEARPAPLRPMSTVSWQSD
RLDDPEAMLKEAERLTPLQETLARPDRFATYRLEPTSVEFWASSSSRLH
RRLRYDLTEDGWRTVRLQP

These are the sequences used in the multiple alignment with the putative **Baeyer Villiger monooxygenase** from *Rhodococcus* sp. ef1:

>*Rhodococcus*_multispecies_WP_011331502.1_flavin-containing_monooxygenase
MEPDTSLDAIVIGAGFAGIYALHKLRNELGLAVRCFDKADGVGGTWH
WNRYPGAKSDSEGFVYRYSFDKEMLQQWSWTNRYLEQAEVLEYLNA
VVDRHDLRRDIQLETAVTSARWDDSLARWEVRTDSSKVYRSKYLITA
LGVLSEPNTPEIPGIEQFSGQVVHTSRWPEGLDVAGRKVGVIGTGSTGT
QFICTAAETAQQLTVFQRTAQYSIPSGNGPIDQEYLDRCRSNYDAIWDQ
VRNSIVGCGFEESTVSATSVSEAERTRVFEESWQRGNAFHFMFGTFNDI
IFDPAANLAAADFVRDKIAAIVDDPDTARKLMPSGYYATRPIANKGYY
ETFNRPNVSLVSIKDNPITRLTENAVVTADGTEHEIDLLVLATGFDAGY
KKMHLTGRDGTPISELWNETTAAYLGIATHQFPNMFMVYGPNSVFTN
LPPGIETQVEWITELIRQAETQGSATVEADETAVRTWAQLCDDIANASL
FPKAHSWIFGANIPGKTSRALFYFAGLGNYRRVLADEADADYPNFTFR
SDDHTSLEREHASIPQ

>*Streptomyces*_sp._S4.7_WP_164247642.1_flavin-containing_monooxygenase

MTQKTTHLDSLVIGAGFAGIYMLHKLRNELGLTARVFDKADGVGGTW
YWNRYPGAAADVDSIVYRYSFDRELLQEWNWKNRYATQPEILAYLEH
VVDRHDLREDIQLNTAIESLAYDEESNLWTARTDGGEEVTARYVVGAL
GPLSTANFPDIPGRDTFAGPLVHTGAWPRDLDITGKRVGVVGTGSTGT
QFICAAARTATHLTVFQRSAQYVVPSGDGPLSDAYLTECRETYDQIWD
QVFNSRVGCGFKESEISATSVSPAERERLFQESWDAGNGFRFMFGIFSDI
AFNPAANEAAASFIKSKITQTVRDPETARKLMPTDYYAKRPICNSGYYE
TYNRDNVSLVSTKENPVVRITPAGVVTEDGTEHELDVLVFATGYEAME
GSYNRIGIQGRAGTTLRESWGDTPSSYLGVATHGFPNLFMVYGPNSVF
CNLPPGIETQVEWISEMIGSARRRGITRIEATATAEDEWTGMCREMAEQ
SLFAQTDSWIFGTNIPGRKRRTLFYFGGIGNYRQKLREVAAADYEGFSL
EGQSSLTPA

>*Microbispora*_sp._CSR-4_WP_261985629.1_flavin-containing_monooxygenase

MTDTTTDTTTGTTDTDFDAIVVGTGFAGIYMLHKLRNELGLRVRAFDR
AGGVGGTWYWNRYPGAMSDVEGFVYRYSFDKQMLQEWNWTTKYTP
QRELLAYLEAVVAKHDLGRDIQLNTGIESAVFDESRGVWTVGTDTGES
FTARYVVTALGPLSTANIPDIKGRDRFRGRIVHTGSWPDDLTIEGRRVG
VVGTGSTGTQFACAAAKVAGHLTVFQRSAQYCVPSGHGPVTEEHVAE
VRASYDRIWEQVRNSRVACGFEESDVPAMSVSEEERRRVFQEYWDKG
NGFRFMFGTFSDIATDPEANEAAAEFIRSKIREIVKDPETARKLTPSDFY
AKRPICNPDYYEIFNRDNVSLVSIKETPIKEITPTGVLTEDGVEHELDILV
FATGFDAVDGSYKRMDIRGRDGVPILDHWDDGPTSYLGVATHGFPNL
FMVLGPNSAFSNLPPGIETQVEWIGDLIRTAEENGTTVIEATRDAEDEW

TETCRKLADYTLFPKVKSWIFGANIPGKKNRVMFYFAGLASYRLKLGE
VAEAGYEGFDLHASPSLTPA

>*Streptomyces_luteireticuli*_WP_344023394.1_flavin-
containing_monooxygenase
MNDTIETDFDAIVVGAGFAGIYMVHKLRNELGLTVRAFEKGSGVGGT
WHWNRYPGAMSDVEGFVYRYSFDKELLQEWNWTSRYTPQADVLAY
LEKVVERHDLARDIQLNTAVESAVFDETRAIWTVTTSGGASHTARYVV
TALGPLSKTNLPDIKGRDSFAGRLIHTGAWPEGVTVHGKRVGVIGTGS
TGTQFICEASRTAAHLTVFQRSPQYVVPSGNAPVTPEQVAAVKADYDR
IWDQVRNSMVACGFEESTIPTMSVSPEERRRIFQEAWEEGNGFRFMFG
TFCDIAVDPAANKAAAEFIRSKIHEIVEDPETARKLTPTEYYAKRPICNA
GYYEAYNRPNVSLVSIQENPIVEITPRGVITADGVEHELDILVFATGFEA
VEGSYNQIDIRGRGGESIQDHWEDGPSTYLGVATSGFPNLFMVLGPNS
AFTNLPPGIETHVEWIAELVRTVENGGHSSIEATREAEDGWTETCREIA
EQTLFAKIDSWIFGANIPGKEKRVLFYFGGLGAYRQKLREVAAADYDG
FRLRGGVALAAA

>*Pseudomonas_fluorescens*_WP_150644880.1_flavin-
containing_monooxygenase
MTTTVLAKRSLGTDIIHYDAIIIGAGFAGIYMLKKLRDEMGLKVRAFDK
AGGIGGTWYWNRYPGALSDSESFVYCFSWDRELCQEWDITTRYLTQP
QILSYLNHAVDRHDLRRDIQLETAITSAVFDEQTSRWLMSTDDGHRYS
AKYLVTALGLLSATNVPKINGLDQFQGQMYHTANWPADAVLEGKRV
GVIGTGSTGCQVITAIAPTVGHLTVFQRSAQYTVPVGNGPVSREYVDDI
KRNYDAIWKEVRSSRLAFGFEESNIPTMSVSAPERKEIFQRAWDVGGG
FRYMFQTFNDIATNEEANVAAQDFVREKIAEIVKDPETARKLMPRDLY

AKRPLCDSGYYATFNRDNVALVDVKANPIEEITATGIRTADGVEHELD
VLVFATGFDAVDGNYKRIDIRGRDGVSMKDHWADGPSSYMSVATAN
FPNMFMILGPNGPFTNLPPTIETEVEWVSELIGFMEENELACVETDPESE
REWGATCQEIADQTLFAKADSWIFGANIPGKPNAVYFYMGGLGPFSEV
LRSVKNDEYRGFKFMVTEQYAQKVLY

>*Pseudomonas_aeruginosa*_WP_420757901.1_flavin-
containing_monooxygenase
MVATKDFDAIVVGAGFGGLYMLKKLRDEQGLNVRVFDKAGDVGGT
WYWNRYPGALSDTETHVYCYSWDKELLQEMDITSRYTTQPQILKYLE
KVADRHDLRKDIQFNTGITAMHFNETTNLWEVHTDTGKSYTAKFIVTA
LGLLSATNIPKIKGLETFQRECYHTGNWPQDVQFEGKRVGVIGTGSTGT
QVITAIAPQVEHLTVFQRSPQYSVPVGNGPVSREYVDNIKKNYDKIWE
QVKNSMVAFGFEESTVPAMSVSDEERQAVFQKAWENGGGFRFMFETF
CDIATDERANKAAQDFIRSKIAEIVKDPETARKLTPNDLYAKRPLCDSG
YYATYNRPNVSLLDVKANPIAEITPKGVKTADGVEHELDMLIFATGFD
AVDGNYTKIDIRGRKGLAIQDHWKAGPSSYLGVANANYPNMFMVLGP
NGPFTNLPPSIETQVEWISDLIQDVNTKSLKTVEPTPEAEAFWTKTCQEI
ASTTLFPKAESWIFGANIPGKTNTVYFFLAGLGAYRQQLTEVRKQGYQ
GFQFQ

>*Pseudomonas_mangiferae*_TRX76844.1_NAD[P]/FAD-
dependent_oxidoreductase
MTKRSSIAQFDAIVIGAGLSGLYATHKLGNELGLKVLGLEKARSVGGT
WYWNRYPGVQADTDSFVYRYSFDREASPGWDMHARYQTGAQIRDYL
ENVASRNDLSRLYRFEVEAREATYDEADNLWRVKTSHGDVVTCRYLV
NGVGVLSKPVAPKIEGLDDFKGRVVHTARWPEGLRIDGLRVGLLGTGS

TGTQVAVAASKVASHLTVFQRSAQYVVPAGQRRHTDTEVDSFLSHFD
ENFREWRKTRLACGFEEPATSAAEASPEERKAVFEHAWNEGGGFGFM
FGTFGDLVINPDSNRAACEFIVGKIKQIVRDPETARRLTPSEPYAKRPVS
VDGYYEAFNQPNVKLVSIQETPIVRVTENGILTADGVEHEIDILILATGF
EAVEGAYRDFNVIGRNGRTLLDTWGEHPAAYLGLSTPGFPNLFTVLGP
QGIFSNLAAGIEAEVNFIGDAIRWAEDRPGAAIEATPEALSTWSEQCSQ
MANYTVFAQVKSWIFGTNVHSNQPRVLFYFGGLKEYLSILDHERTHGF
PGFTQAGSPSLTLVQSKADATDDEALRQRNYATVERYMHSLGQDRLT
RHHLFQPDGICGLWTTETGKPIKIH

Here are reported the protein sequences of the six genes of the core, followed by the protein sequences likely corresponding to the tailoring enzymes:

>Rho_**PhzA/B**_Phenazine_biosynthesis_protein
MYEVFGPEQEAARSRNRSVVARYMQTRGLDRLRRHELFTQDGEGGL
WTTETGEPIMIKGRDRLAEHAVWSLECFPDWSWFNIEIFDTQDPDRFW
VECDGAGIIRFTGYPEGRYENHFIHFFRFVDGKISQQREFMNPCQQFRA
LGIAVPNVIREGIPT

>Rho_**PhzC**_Phospho-2-dehydro-3-deoxyheptonate aldolase
MIPSALTSMVNSHQPPWHDHPQLDLVRNVLETTTVIASPVEIDQLARRL
RAVEAGHASILQMGDCAEDPAHCTPDHVHRKLDQLTASAGAVATPTG
LPVVQVGRIAGQFAKPRSKATETIGDREVVTYRGHMVNLPDSDEVSRT
PDPLRILMGYLTSRQVAATIAGFNRGRALEDRVWTSHEALLLDYEHPM
MRPGSDERTYLTSTHWPWIGERTRNVDGPHVATLAHIANPSACKVGPT
ATEDDLVALCSRLDPYREPGKLALITRMGAQHIRTGLPALMNAVRAA
GHRVLWICDPMHGNTLSTDDGTKTRVVDDVIAEMAGFVSVADQTGTR

VHGLHLETTHLTDVSECVWSSTDLASARPSSSLCDPRLNPEQAAAVVE
AWGEMLARHYRGSETTS

>Rho_**PhzD**_Phenazine_biosynthesis_protein
MSRDLTVEPYLLPSPGEMPEALVDWDIRPRQATLLIHDMQRYFLSPFPD
AMRSEIVGNVRDLHSWAQRVGAATAYTAQPGRMNVTDRGLLRDFWG
PGMQTTDADRALVPELELGDDAWPFVKWRYSAFHRSDLLARMRENG
RTQLVLCGVYAHVGILATALDAYTHDIEVFLVGDAVADFTAADHRHT
LEYTSRCCARVVATKWVTER

>Rho_**PhzE**_IsochorismatesynthaseMenF
MSPPLSTDLLTEILAGNRSVYALLCRADPATGARTVTALSGQLRQHELI
EEISTTADVFVLLPYRQIRERGYPAHDDGAPLLAIYIDEQQDYPLTSVLD
KLPRRSFALTDGHFDSSDADYERKVAAIVSEEIGNGRGANFVIKREFSA
ECTPYNSTVPLSAFGELLDNERGAYWTFLVHTEGLVLVGASPEQHVVL
DNGTAVMNPISGTYRYPPGGPTLDGVQQFLDDRKETDELYMVVDEEL
KMMCRICEPGTTRVHGPALKEMAWVAHTEYFIEGQTRRDPREILRETM
FAPTVTGSPVESATEVIARYETTGRGYYSGVAALITRSGGGAPTLDSAIL
IRTAAIEPDCGRVRVAVGATLVRHSDPGAEVYETHAKAQSVLAAFGHS
KPHARWNRHPMITTALAHRNDQIAGFWSPNYPHDVRSRVLDGRKALV
VDAEDTFTAMLDHQLRSLGLTVTVRRFDDMYTTSDHDLVIVGPGPGD
PTDIDDEKIVHLRAQIDDLLSAQRPFLAICLSHQILASRLGLPLTRRAEPN
QGKQARVDVFGQSENVGFYNTFEARSAPGRIDVAGVGPVTVSADTAT
GAIHALEGPHFASVQFHPESILTVNGPRILAHMSERLLST

>Rho_**PhzF**_hypotheticalprotein

MKLEYIMWDLQSDDDPSVTHLNELTDTAAVDSWRSVPGLAAKYWIH
DRGSGQWGAILIWDDDRPAGALPAGPALELLERERAHRKDFSVHALIE
HRPESSRRSLRYCVVDAFASTPLSGNPVAVFFGADSLSAETMQRIAAEL
NLSEVTFVLSADSAESTARIRIFTPVNELPFAGHPILGTAAAVAAQTGAK
ELAFETAVGLIPMTAEAVDDYFRVTMDQPLPTWSPMPDAEQRSLLAAL
GLDTSALPIETYDNGPRHTIVTADSIEALSALRPDHRALSEFENMAINCI
AEDLDGVWRNRMFSPAYGVVEDAATGSAAGPIAIHLARHGRIEYDHD
LRIHQGVELGRHSVMHARASLDARTHNLTSVQVGGDAITIAHATLYLG
SDRGTDDE

>Rho_**PhzG**_Phenazine_biosynthesis_protein_(plasmid)
MMSSQYETITGTARSFLEYSDPPPTPLDLFQVWIEQAEIAGVREPLALSL
ATTDSAGRCSQRTVAVTDISANGLSFSTHTTSRKARELQTNSWASGLF
YWRELARQLIVSGPVLKLNAAIADKVWDERAEPLKPMSTASHQSLHL
GDPEVLLARSDSLGLRTDLARPHRFAVYQLQPHRVEFWAADQSRLHR
RLLYERSPRGWTVDRLQP

>Rho_**PhzS**_5-methylphenazine-1-carboxylate1-monooxygenase
MASKDLTTTRPPISIAGAGIGGLSAALALHERGHEAALFESAPEIVPLGV
GINVQPTAIAELSRLGLADQLARIGVATQAHRYVDHRGRTLWTEPRGI
AAGHDYPQYSVHRGHLQMMLLDAVTERLGPGAVHSDARLSNISGSGE
TAIQLTVVNSDGRSRILDTDVLVGADGLHSTVRRWLHPDEAPVSVAGT
TMWRGLADLPYIFLDGVTMIIANDGTGTRLVAYPCSEQASVEGRTLLN
WVCLTPSDRRSPSEDERTGLVNALAEWDFDWFDLTELAARSPQVSVY
PMVDRDPLSHWGSGRVTLLGDAAHPMYPIGANGASQAIIDAGALAEC
FTRATDPVSALRSYEAMRIIPTTSIVEANRAMNESEKKTASRAGDPAAA
PVRRLREITTEYRTVVDRSTAR

>Rho_**Antibiotic_biosynthesis_monooxygenase**
MTETVIREGDKVATFINILELKDPAKQQDLIDVLNEGTEKVIKHQPGFIS
VNLFASRDGSRVVNLAQWSSPDDIKAVATNPDAQVFAKKAAELATPA
PGPYSVASVTQA*

>Rho_**Baeyer-Villiger_monooxygenase**
MEPDTSLDAIVIGAGFAGIYALHKLRNELGLAVRCFDKADGVGGTWH
WNRYPGAKSDSEGFVYRYSFDKEMLQQWSWTNRYLEQAEVLEYLNA
VVDRHDLRRDIQLETAVTSVRWDDSLARWEVRTDSSKVYRSKYLITA
LGVLSEPNTPEIPGIEQFSGQVVHTSRWPEGLEVAGRKVGVIGTGSTGT
QFICTAAETAQQLTVFQRTAQYSIPSGNGPIDQEYLDRCRSNYDAIWDQ
VRNSIVGCGFEESTVSATSVSEAERTRVFEESWQRGNAFHFMFGTFNDI
IFDPAANLAAADFVRDKIAAIVDDPDTARKLMPSGYYATRPIANKGYY
ETFNRSNVSLVSIKDNPITRLNENAVVTADGTEHEIDLLVLATGFDAVD
GGYKKMHLTGRDGTPISDLWNETTAAYLGIATHQFPNMFMVYGPNSV
FTNLPPGIETQVEWITELIRQAETRGSAVVEVSETAVRAWAQLCDDIAN
ASLFPKAHSWIFGANIPGKTSRALFYFAGLGNYRRVLADESDADYPNF
TFHSDDHTSLEREHASIPQ*

The protein sequence of the gene identified in the contig3 as phzG1, potentially responsible for encoding the enzyme PhzG, is reported below:

>Rho_**PhzG**_1_Phenazine_biosynthesis_protein_(chromosome)
MVDADFSLPDVRTWIRGIPALTGTPPPAPEHFPEKPGELFLDWLRAAVA
FGVVEPHVCALSTVDGDGMPDSRFLILKDVTEGGFWFSGSAASPKGVE
LKENPRASLAFYWRETGQQVRIRGLVREGDDAIRTRDFVERSVTARAV
ATASKQSEVLEDSGAYETSVAAAEARIGGDPGFVSKDWRAWCLEPES
VEFWQADSGRRHQRWLYRRGSDRAWTRAVLWP

Chapter V

Bioplastic production from *Rhodococcus* sp. ef1

Rhodococcus sp. was previously characterised as a polyhydroxyalkanoate producer through Nile Red screening assay and fluorescence microscopy (*Figure 99*).

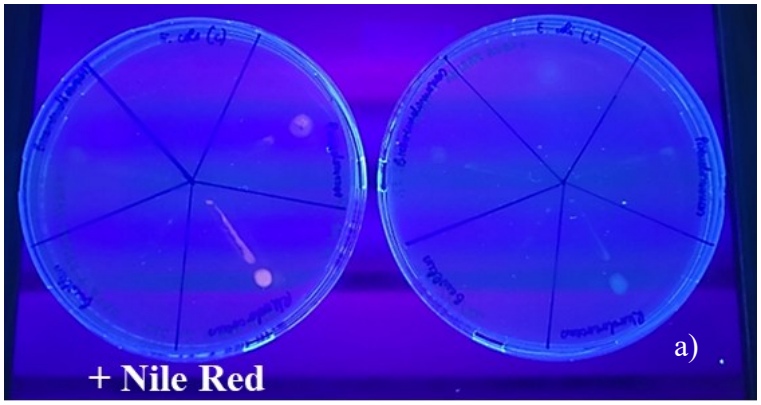

Bacillus *sp. ef1 (C⁻)* Rhodococcus *sp. ef1*

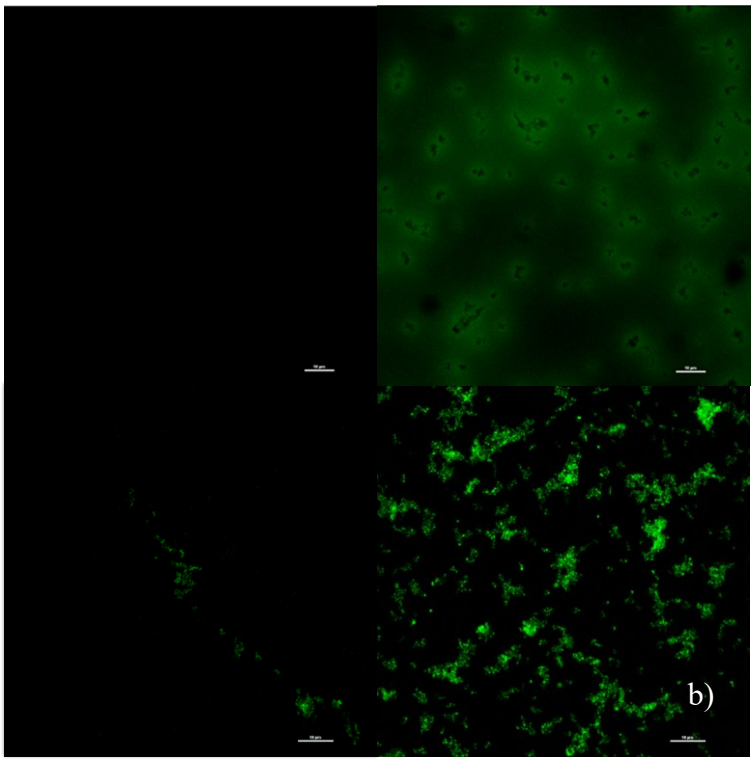

Figure 99 – Rhodococcus sp. ef1 exhibited orange fluorescence in the presence of Nile Red in the MMD agar medium, suggesting that this strain is a polyhydroxyalkanoate producer (panel a). Fluorescence spectroscopy

confirmed the presence of PHA granules, whereas Bacillus sp. ef1, used as a negative control, didn't show any comparable fluorescent signal (panel b).

16S rDNA sequences

The high-quality 16S rDNA sequences obtained by Sanger sequencing are reported below for each strain, followed by their corresponding quality assessment.

>Isolate**#1**

GGCCTAACACATGCAAGTCGAGCGGTAACAGGGGTAGCTTGCTACC
CGCTGACGAGCGGCGGACGGGTGAGTAATGCATAGGAATCTGCCCG
ATAGTGGGGGATAACCTGGGGAAACCCAGGCTAATACCGCATACGT
CCTACGGGAGAAAGGGGGCTTCGGCTCCCGCTATTGGATGAGCCTA
TGTCGGATTAGCTAGTTGGTAAGGTAATGGCTTACCAAGGCAACGA
TCCGTAGCTGGTCTGAGAGGATGATCAGCCACATCGGGACTGAGAC
ACGGCCCGAACTCCTACGGGAGGCAGCAGTGGGGAATATTGGACA
ATGGGGGCAACCCTGATCCAGCCATGCCGCGTGTGTGAAGAAGGCC
CTCGGGTTGTAAAGCACTTTCAGCGAGGAAGAACGCCTATCGGTTA
ATACCCGGTAGGAAAGACATCACTCGCAGAAGAAGCACCGGCTAA
CTCCGTGCCAGCAGCCGCGGTAATACGGAGGGTGCAAGCGTTAATC
GGAATTACTGGGCGTAAAGCGCGCGTAGGTGGCTTGATAAGCCGGT
TGTGAAAGCCCCGGGCTCAACCTGGGAACGGCATCCGGAACTGTCA
GGCTAGAGTGCAGGAGAGGAAGGTAGAATTCCCGGTGTAGCGGTG
AAATGCGTAGAGATCGGGAGGAATACCAGTGGCGAAGGCGGCCTT
CTGGACTGACACTGACACTGAGGTGCGAAAGCGTGGGTAGCAAAC
AGGATTAGATACCCTGGTAGTCCACGCCGTAAACGATGTCGACCAG

CCGTTGGGTGCCTAGAGCACTTTGTGGCGAAGTTAACGCGATAAGT
CGACCGCCTGGGGAGTACGGCCGCAAGGTTAAAACTCAAATGAATT
GACGGGGGCCCGCACAAGCGGTGGAGCATGTGGTTTAATTCGATGC
AACGCGAAGACCCTTACCTACCCTTGACATCTACAGAGCCGGA

Quality Analyse					
High Sequence quality from 20 to 977 (quality average= 46.8) 20 977 -|----------|---------- Length sequence 1223					
Basis Type			Quality average= 39.3		
AT	GC	Other	< 20	>20	>40
512	660	51	264	959	655

Figure 100 - Quality assessment of the 16S rDNA sequence of the isolate #1

>Isolate**#2**
TGAAGAGTTTGATCATGGCTCAGATTGAACGCTGGCGGCAGGCCTA
ACACATGCAAGTCGAGCGGTAACAGGGGTAGCTTGCTACCCGCTGA
CGAGCGGCGGACGGGTGAGTAATGCATAGGAATCTGCCCGATAGTG
GGGGATAACCTGGGGAAACCCAGGCTAATACCGCATACGTCCTACG
GGAGAAAGGGGGCTCCGGCTCCCGCTATTGGATGAGCCTATGTCGG
ATTAGCTAGTTGGTAAGGTAATGGCTTACCAAGGCAACGATCCGTA
GCTGGTCTGAGAGGATGATCAGCCACATCGGGACTGAGACACGGCC
CGAACTCCTACGGGAGGCAGCAGTGGGGAATATTGGACAATGGGG
GCAACCCTGATCCAGCCATGCCGCGTGTGTGAAGAAGGCCCTCGGG
TTGTAAAGCACTTTCAGCGAGGAAGAACGCCTATCGGTTAATACCC
GTTAGGAAAGACATCACTCGCAGAAGAAGCACCGGCTAACTCCGTG

CCAGCAGCCGCGGTAATACGGAGGGTGCAAGCGTTAATCGGAATTA
CTGGGCGTAAAGCGCGCGTAGGTGGCTTGATAAGCCGGTTGTGAAA
GCCCCGGGCTCAACCTGGGAACGGCATCCGGAACTGTCAGGCTAGA
GTGCAGGAGAGGAAGGTAGAATTCCCGGTGTAGCGGTGAAATGCGT
AGAGATCGGGAGGAATACCAGTGGCGAAGGCGGCCTTCTGGACTG
ACACTGACACTGAGGTGCGAAAGCGTGGGTAGCAAACAGGATTAG
ATACCCTGGTAGTCCACGCCGTAAACGATGTCGACCAGCCGTTGGG
TGCCTAGAGCACTTTGTGGCGAAGTTAACGCGATAAGTCGACCGCC
TGGGGAGTACGGCCGCAAGGTTAAAACTCAAATGAATTGACGGGG
GCCCGCACAAGCGGTGGAGCATGTGGTTTAATTCGATGCAACGCGA
AGAACCTTACCTACCCTTGACATCTACAGAAGCCGGAAGAGATTCT
GGTGTGCCTTCGGGAACTGTAAGACAGGTGCTGCATGGCTGTCGTC
AGCTCGTGTTGTGAAATGTTGGGTTAAGTCCCGTAACGAGCGCAAC
CCTTGTCCTTATTTGCCAGCGAGTAATGTCGGGAACTCTAAGGAGA
CTGCCGGTGACAAACCGGAGGAAGGTGGGGACGACGTCAAGTCAT
CATGGCCCTTACGGGTAGGGCTACACACGTGCTACAATGGCCGGTA
CAAAGGGCTGCGAGCTCGCGAGAGTCAGCGAATCCCTTAAAGCCGG
TCTCAGTCCGGATCGGAGTCTGCAACTCGACTCCGTGAAGTCGGAA
TCGCTAGTAATCGTGAATCAGAATGTCACGGTGAATACGTTCCCGG
GCCTTGTACACACCGCCCGTCACACCATGGGAGTGGACTGCACCAG
AAGTGGTTAGCCTAACGCAAGAGGGCGATCACCACGGTGTGGTTCA
TGACTGGGGTGAAGTCGTAACAAGGTAGCCGTAGGGGAACCTGCG
GCTGGATCACCTCCTT

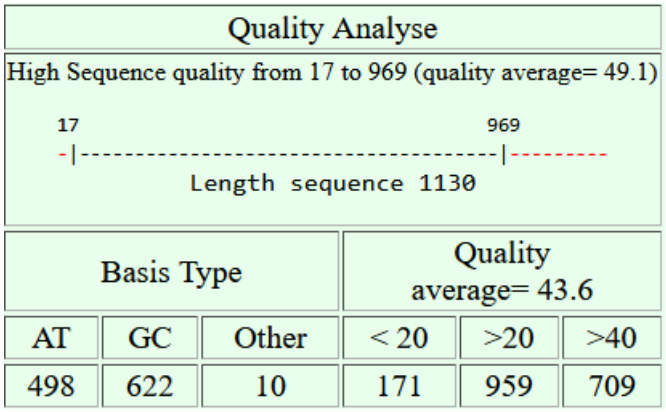

Figure 101 - Quality assessment of the 16S rDNA sequence of the isolate #2.

>Isolate**#2CG**

GGCCTAACACATGCAAGTCGAGCGGTAACAGGAGGTAGCTTGCTAC
CTCGCTGACGAGCGGCGGACGGGTGAGTAATGCATAGGAATCTGCC
CGGTAGTGGGGGATAACCTGGGGAAACCCAGGCTAATACCGCATAC
GTCCTACGGGAGAAAGGGGGCTTCGGCTCCCGCTATTGGATGAGCC
TATGTCGGATTAGCTAGTTGGTGAGGTAATGGCTCACCAAGGCAAC
GATCCGTAGCTGGTCTGAGAGGATGATCAGCCACATCGGGACTGAG
ACACGGCCCGAACTCCTACGGGAGGCAGCAGTGGGGAATATTGGA
CAATGGGGGCAACCCTGATCCAGCCATGCCGCGTGTGTGAAGAAGG
CCCTCGGGTTGTAAAGCACTTTCAGCGAGGAAGAACGCCTAGTGGT
TAATACCCATTAGGAAAGACATCACTCGCAGAAGAAGCACCGGCTA
ACTCCGTGCCAGCAGCCGCGGTAATACGGAGGGTGCAAGCGTTAAT
CGGAATTACTGGGCGTAAAGCGCGCGTAGGTGGCTTGATAAGCCGG
TTGTGAAAGCCCCGGGCTCAACCTGGGAACGGCATCCGGAACTGTC
AGGCTAGAGTGCAGGAGAGGAAGGTAGAATTCCCGGTGTAGCGGT
GAAATGCGTAGAGATCGGGAGGAATACCAGTGGCGAAGGCGGCCT

TCTGGACTGACACTGACACTGAGGTGCGAAAGCGTGGGTAGCAAAC
AGGATTAGATACCCTGGTAGTCCACGCCGTAAACGATGTCGACCAG
CCGTTGGGTGCCTAGAGCACTTTGTGGCGAAGTTAACGCGATAAGT
CGACCGCCTGGGGAGTACGGCCGCAAGGTTAAAACTCAAATGAATT
GACGGGGGCCCGCACAAGCGGTGGAGCATGTGGGTTTAATTCGATG
CAACGCGAAGAACCTTACCTACCCTTGACATCTACAGANCCCGGA

Quality Analyse					
High Sequence quality from 18 to 979 (quality average= 48.0) 18 979 -|----------|---------- Length sequence 1218					
Basis Type			Quality average= 40.0		
AT	GC	Other	< 20	>20	>40
506	635	77	279	939	682

Figure 102 - Quality assessment of the 16S rDNA sequence of the isolate #2 CG

>Isolate#**3**

GGCCTAACACATGCAAGTCGAGCGGTAACAGGATGTAGCTTGCTAC
ATCGCTGACGAGCGGCGGACGGGTGAGTAATGCATAGGAATCTGCC
CGATAGTGGGGGATAACCTGGGGAAACCCAGGCTAATACCGCATAC
GTCCTACGGGAGAAAGGGGGCTCCGGCTCCCGCTATTGGATGAGCC
TATGTCGGATTAGCTAGTTGGTGAGGTAATGGCTCACCAAGGCAAC
GATCCGTAGCTGGTCTGAGAGGATGATCAGCCACATCGGGACTGAG
ACACGGCCCGAACTCCTACGGGAGGCAGCAGTGGGGAATATTGGA
CAATGGGGGCAACCCTGATCCAGCCATGCCGCGTGTGTGAAGAAGG
CCCTCGGGTTGTAAAGCACTTTCAGCGAGGAAGAACGCCTATCGGT

TAATACCCGGTAGGAAAGACATCACTCGCAGAAGAAGCACCGGCT
AACTCCGTGCCAGCAGCCGCGGTAATACGGAGGGTGCAAGCGTTAA
TCGGAATTACTGGGCGTAAAGCGCGCGTAGGTGGCTTGATAAGCCG
GTTGTGAAAGCCCTGGGCTCAACCTGGGAACGGCATCCGGAACTGT
CAGGCTAGAGTGCAGGAGAGGAAGGTAGAATTCCCGGTGTAGCGG
TGAAATGCGTAGAGATCGGGAGGAATACCAGTGGCGAAGGCGGCC
TTCTGGACTGACACTGACACTGAGGTGCGAAAGCGTGGGTAGCAAA
CAGGATTAGATACCCTGGTAGTCACGCCGTAAACGATGTCGACCAG
CCGTTGGGTGCCTAGCGCACTTTGTGGCGAAGTTAACGCGATAAGT
CGACCGCCTGGGGAGTACNGCCGCA

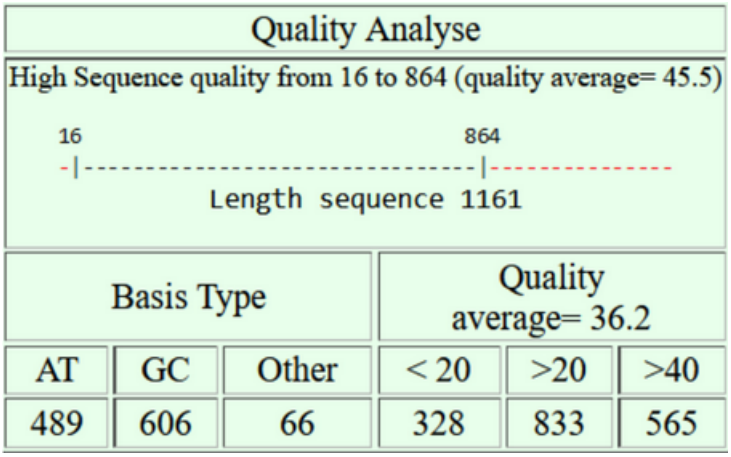

Figure 103 - Quality assessment of the 16S rDNA sequence of the isolate #3

>Isolate#**4**

GGCCTAACACATGCAAGTCGAGCGGTAACAGGAGGTAGCTTGCTAC
CTCGCTGACGAGCGGCGGACGGGTGAGTAATGCATAGGAATCTGCC
CGGTAGTGGGGGATAACCTGGGGAAACCCAGGCTAATACCGCATAC
GTCCTACGGGAGAAAGGGGGCTTCGGCTCCCGCTATTGGATGAGCC

TATGTCGGATTAGCTAGTTGGTGAGGTAATGGCTCACCAAGGCAAC
GATCCGTAGCTGGTCTGAGAGGATGATCAGCCACATCGGGACTGAG
ACACGGCCCGAACTCCTACGGGAGGCAGCAGTGGGGAATATTGGA
CAATGGGGGCAACCCTGATCCAGCCATGCCGCGTGTGTGAAGAAGG
CCCTCGGGTTGTAAAGCACTTTCAGCGAGGAAGAACGCCTATTGGT
TAATACCCATTAGGAAAGACATCACTCGCAGAAGAAGCACCGGCTA
ACTCCGTGCCAGCAGCCGCGGTAATACGGAGGGTGCAAGCGTTAAT
CGGAATTACTGGGCGTAAAGCGCGCGTAGGTGGCTTGATAAGCCGG
TTGTGAAAGCCCCGGGCTCAACCTGGGAACGGCATCCGGAACTGTC
AGGCTAGAGTGCAGGAGAGGAAGGTAGAATTCCCGGTGTAGCGGT
GAAATGCGTAGAGATCGGGAGGAATACCAGTGGCGAAGGCGGCCT
TCTGGACTGACACTGACACTGAGGTGCGAAAGCGTGGGTAGCAAAC
AGGATTAGATACCCTGGTAGTCCACGCCGTAAACGATGTCGACCAG
CCGTTGGGTGCCTAGAGCACTTTGTGGCGAAGTTAACGCGATAAGT
CGACCGCCTGGGGAGTACGGCCGCAAGGTTAAAACTCAAATGAATT
GACGGGGGCCCGCACAAGCGGTGGAGCATGTGGTTTAATTCGATGC
AACGCGAAGAACCTTACCTACCCTTGACATCTACAGAAGCCCGGAG
GAGATT

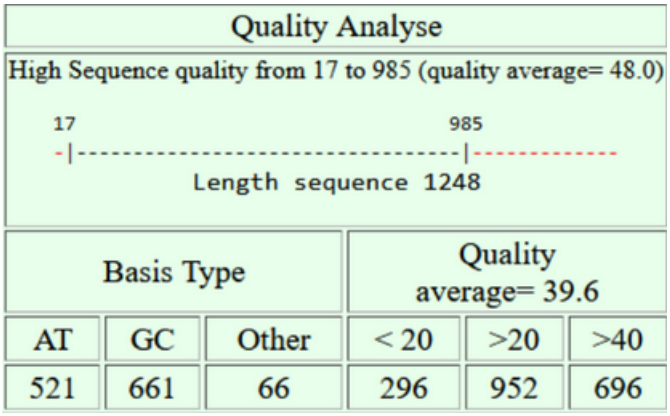

Quality Analyse

High Sequence quality from 17 to 985 (quality average= 48.0)

17 985

Length sequence 1248

Basis Type			Quality average= 39.6		
AT	GC	Other	< 20	>20	>40
521	661	66	296	952	696

Figure 104 - Quality assessment of the 16S rDNA sequence of the isolate #4

>Isolate#**7**

GCCTACACATGCAAGTCGAGCGGTAACAGGGGTAGCTTGCTACCCG
CTGACGAGCGGCGGACGGGTGAGTAATGCATAGGAATCTGCCCGAT
AGTGGGGGATAACCTGGGGAAACCCAGGCTAATACCGCATACGTCC
TACGGGAGAAAGGGGGCTTCGGCTCCCGCTATTGGATGAGCCTATG
TCGGATTAGCTAGTTGGTAAGGTAATGGCTTACCAAGGCAACGATC
CGTAGCTGGTCTGAGAGGATGATCAGCCACATCGGGACTGAGACAC
GGCCCGAACTCCTACGGGAGGCAGCAGTGGGGAATATTGGACAAT
GGGGGCAACCCTGATCCAGCCATGCCGCGTGTGTGAAGAAGGCCCT
CGGGTTGTAAAGCACTTTCAGCGAGGAAGAACGCCTATCGGTTAAT
ACCCGGTAGGAAAGACATCACTCGCAGAAGAAGCACCGGCTAACT
CCGTGCCAGCAGCCGCGGTAATACGGAGGGTGCAAGCGTTAATCGG
AATTACTGGGCGTAAAGCGCGCGTAGGTGGCTTGATAAGCCGGTTG
TGAAAGCCCCGGGCTCAACCTGGGAACGGCATCCGGAACTGTCAGG
CTAGAGTGCAGGAGAGGAAGGTAGAATTCCCGGTGTAGCGGTGAA
ATGCGTAGAGATCGGGAGGAATACCAGTGGCGAAGGCGGCCTTCTG

GACTGACACTGACACTGAGGTGCGAAAGCGTGGGTAGCAAACAGG
ATTAGATACCCTGGTAGTCCACGCCGTAAACGATGTCGACCAGCCG
TTGGGTGCCTAGAGCACTTTGTGGCGAAGTTAACGCGATAAGTCGA
CCGCCTGGGGAGTACGGCCGCAAGGTTAAAACTCAAATGAATTGAC
GGGGGCCCGCACAAGCGGTGGAGCATGTGGTTTAATTCGATGCAAC
GCGAAGAACCTTACCTACCCTTGACATCTACAGAAGCCGGAAGAGA
TTCTGGTGTGCCTTCGGGAACTGTAAGACAGGTGCTGCATGGCTGTC
GTCAGCTCGTGTTGTGAAAT

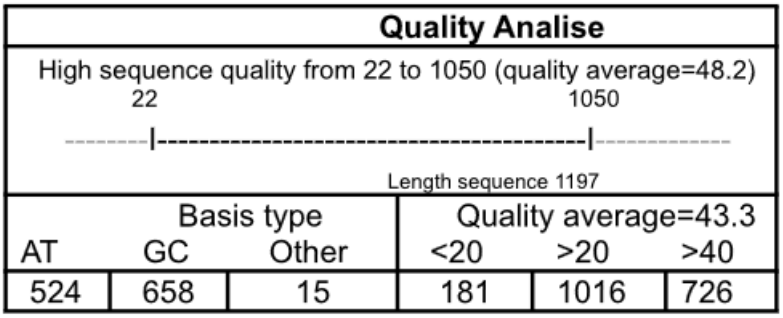

Figure 105 – Quality assessment of the 16S rDNA sequence of the isolate #7.

>Isolate#**10**

GGCAGGCCTAACACATGCAAGTCGAGCGGTAACAGGGGTAGCTTGC
TACCCGCTGACGAGCGGCGGACGGGTGAGTAATGCATAGGAATCTG
CCCGATAGTGGGGGATAACCTGGGGAAACCCAGGCTAATACCGCAT
ACGTCCTACGGGAGAAAGGGGGCTTCGGCTCCCGCTATTGGATGAG
CCTATGTCGGATTAGCTAGTTGGTAAGGTAATGGCTTACCAAGGCA
ACGATCCGTAGCTGGTCTGAGAGGATGATCAGCCACATCGGGACTG
AGACACGGCCCGAACTCCTACGGGAGGCAGCAGTGGGGAATATTG
GACAATGGGGGCAACCCTGATCCAGCCATGCCGCGTGTGTGAAGAA

GGCCCTCGGGTTGTAAAGCACTTTCAGCGAGGAAGAACGCCTATCG
GTTAATACCCGGTAGGAAAGACATCACTCGCAGAAGAAGCACCGG
CTAACTCCGTGCCAGCAGCCGCGGTAATACGGAGGGTGCAAGCGTT
AATCGGAATTACTGGGCGTAAAGCGCGCGTAGGTGGCTTGATAAGC
CGGTTGTGAAAGCCCCGGGCTCAACCTGGGAACGGCATCCGGAACT
GTCAGGCTAGAGTGCAGGAGAGGAAGGTAGAATTCCCGGTGTAGC
GGTGAAATGCGTAGAGATCGGGAGGAATACCAGTGGCGAAGGCGG
CCTTCTGGACTGACACTGACACTGAGGTGCGAAAGCGTGGGTAGCA
AACAGGATTAGATACCCTGGTAGTCCACGCCGTAAACGATGTCGAC
CAGCCGTTGGGTGCCTAGAGCACTTTGTGGCGAAGTTAACGCGATA
AGTCGACCGCCTGGGGAGTACGGCCGCAAGGTTAAAACTCAAATGA
ATTGACGGGGGCCCGCACAAGCGGTGGAGCATGTGGTTTAATTCGA
TGCAACGCGAAGAACCTTACCTACCCTTGACATCTACAGAAGCCGG
AAGAGATTCTGGTGTGCCTTCGGNAACTGTAGACAG

Quality Analyse					
High Sequence quality from 14 to 1011 (quality average= 48.6) 14 1011 -|----------|--------- Length sequence 1152					
Basis Type			Quality average= 43.9		
AT	GC	Other	< 20	>20	>40
499	633	20	170	982	721

Figure 106 – Quality assessment of the 16S rDNA sequence of the isolate #10.

>Isolate#**12**

GGCCTAAACATGCAAGTCGAGCGGTAACAGGAGGTAGCTTGCTACC
TCGCTGACGAGCGGCGGACGGGTGAGTAATGCATAGGAATCTGCCC
GATAGTGGGGGATAACCTGGGGAAACCCAGGCTAATACCGCATAC
GTCCTACGGGAGAAAGGGGGCTTCGGCTCCCGCTATTGGATGAGCC
TATGTCGGATTAGCTAGTTGGTAAGGTAATGGCTTACCAAGGCAAC
GATCCGTAGCTGGTCTGAGAGGATGATCAGCCACATCGGGACTGAG
ACACGGCCCGAACTCCTACGGGAGGCAGCAGTGGGGAATATTGGA
CAATGGGGGCAACCCTGATCCAGCCATGCCGCGTGTGTGAAGAAGG
CCCTCGGGTTGTAAAGCACCTTCAGCGAGGAAGAACGCCTATCGGT
TAATACCCGGTAGGAAAGACATCACTCGCAGAAGAAGCACCGGCT
AACTCCGTGCCAGCAGCCGCGGTAATACGGAGGGTGCAAGCGTTAA
TCGGAATTACTGGGCGTAAAGCGCGCGTAGGTGGCTTGATAAGCCG
GTTGTGAAAGCCCCGGGCTCAACCTGGGAACGGCATCCGGAACTGT
CAGGCTAGAGTGCAGGAGAGGAAGGTAGAATTCCCGGTGTAGCGG
TGAAATGCGTAGAGATCGGGAGGAATACCAGTGGCGAAGGCGGCC
TTCTGGGACTGACACTGACACTGAGGTGCGAAAGCGTGGGGTAGCA
AACAGGATTAGATACCCTGGGTAGTCCACGCCGTAAACGATGTCGA
CCAGCCGTTTGGGTGCCTAGAGCACTTTGTGGCCGAAGTTAACGCG
ATAAGTCGACCGCCTGGGGGAGTACGGCCGCAAGGTTAAAACTCAA
ATGATTTGACGGGGGCCCGCACAAGCGGTGAGCATGG

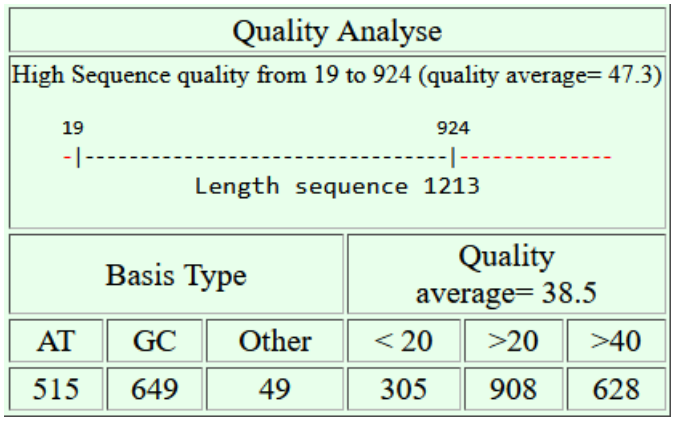

Quality Analyse

High Sequence quality from 19 to 924 (quality average= 47.3)

19 924

-|----------|----------

Length sequence 1213

Basis Type			Quality average= 38.5		
AT	GC	Other	< 20	>20	>40
515	649	49	305	908	628

Figure 107 - Quality assessment of the 16S rDNA sequence of the isolate #12.

>Isolate**#14**

GGCCTAAACATGCAAGTCGAGCGGTAACAGGGGTAGCTTGCTACCC
GCTGACGAGCGGCGGACGGGTGAGTAATGCATAGGAATCTGCCCG
ATAGTGGGGGATAACCTGGGGAAACCCAGGCTAATACCGCATACGT
CCTACGGGAGAAAGGGGGCTTCGGCTCCCGCTATTGGATGAGCCTA
TGTCGGATTAGCTAGTTGGTAAGGTAATGGCTTACCAAGGCAACGA
TCCGTAGCTGGTCTGAGAGGATGATCAGCCACATCGGGACTGAGAC
ACGGCCCGAACTCCTACGGGAGGCAGCAGTGGGGAATATTGGACA
ATGGGGGCAACCCTGATCCAGCCATGCCGCGTGTGTGAAGAAGGCC
CTCGGGTTGTAAAGCACTTTCAGCGAGGAAGAACGCCTATCGGTTA
ATACCCGGTAGGAAAGACATCACTCGCAGAAGAAGCACCGGCTAA
CTCCGTGCCAGCAGCCGCGGTAATACGGAGGGTGCAAGCGTTAATC
GGAATTACTGGGCGTAAAGCGCGCGTAGGTGGCTTGATAAGCCGGT
TGTGAAAGCCCCGGGCTCAACCTGGGAACGGCATCCGGAACTGTCA
GGCTAGAGTGCAGGAGAGGAAGGTAGAATTCCCGGTGTAGCGGTG
AAATGCGTAGAGATCGGGAGGAATACCAGTGGCGAAGGCGGCCTT

CTGGACTGACACTGACACTGAGGTGCGAAAGCGTGGGGTAGCAAA
CAGGATTAGATACCCTGGTAGTCCACGCCGTAAACGATGTCGACCA
GCCGTTTGGGTGCCTAGAGCACTTTGTGGGCGAAGTTAACGCGATA
AGTCGACCGCCTGGGGAGTACGGCCGCAAGGTTAAAACTCAAATGA
ATTGACGGGGCCCGCACAAGCGGTGGAGCATGGTGGTTTAATTCGA
TGCACGCGAAGACCTTACCTACCCTTGACATCTAC

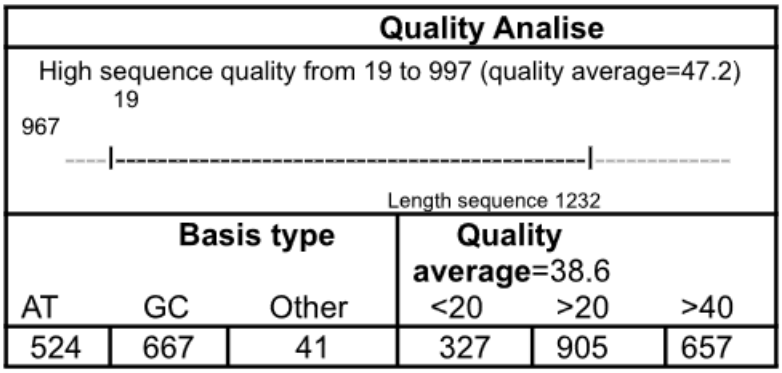

Figure 108 - Quality assessment of the 16S rDNA sequence of the isolate #14.

>Isolate#**15**

GGCCTAACACATGCAAGTCGAGCGGTAACANGGGGTAGCTTGCTAC
CCGCTGACGAGCGGCGGACGGGTGAGTAATGCATAGGAATCTGCCC
GATAGTGGGGGATAACCTGGGGAAACCCAGGCTAATACCGCATAC
GTCCTACGGGAGAAAGGGGGCTTCGGCTCCCGCTATTGGATGAGCC
TATGTCGGATTAGCTAGTTGGTAAGGTAATGGCTTACCAAGGCAAC
GATCCGTAGCTGGTCTGAGAGGATGATCAGCCACATCGGGACTGAG
ACACGGCCCGAACTCCTACGGGAGGCAGCAGTGGGGAATATTGGA
CAATGGGGGCAACCCTGATCCAGCCATGCCGCGTGTGTGAAGAAGG
CCCTCGGGTTGTAAAGCACTTTCAGCGAGGAAGAACGCCTATCGGT

TAATACCCGGTAGGAAAGACATCACTCGCAGAAGAAGCACCGGCT
AACTCCGTGCCAGCAGCCGCGGTAATACGGAGGGTGCAAGCGTTAA
TCGGAATTACTGGGCGTAAAGCGCGCGTAGGTGGCTTGATAAGCCG
GTTGTGAAAGCCCCGGGGCTCAACCTGGGAACGGCATCCGGAACTG
TCAGGCCTANAGTGCAGGAGAGGAAGGTAGAATTCCCGGTGTAGC
GGTGAAATGCGTAGAGATCGGGAGGAATACCAGTGGCGAAGGCGG
GCTTTTGGACTGACACTGACACTGAGGTGCGAAAGCGTGGGTAGCA
AACAGGATTATATACCCTTGTTAGTCCACGCCCGTAAACGATGTTCG
ACCAG

Quality Analyse

High Sequence quality from 17 to 799 (quality average= 44.1)

17 799

-|----------|--

Length sequence 804

Basis Type			Quality average= 43.1		
AT	GC	Other	< 20	>20	>40
348	449	7	111	693	493

Figure 109 - Quality assessment of the 16S rDNA sequence of the isolate #15

Sequences putatively involved in polyhydroxyalkanoate synthesis in isolate #12

For isolate #12, the protein sequences putatively involved in the synthesis of polyhydroxyalkanoates are reported below.

>PhaC1_Poly(3-hydroxyalkanoate)_polymerase_subunit_PhaC

MQSAWHNPFQAISQGLSDSLSEGLSQGLPEGLSPEEIEAWNNQLKEISE
QYQGLMQDLLSRIAPSEAADSIYSDMRESFEAGAQSLMQNPTLLWETQ
NRLLQDQWLLWQQALRGMAGEKMTPLITPAKSDRRFKDEAWTQDPH
YMAIMQQYLLFSQMVEELVENLSGLDETQKRNLMFYARQLVNAMAPT
NFITTNPEVMRRTIETRGQNLVDGLARLREDLGNSGEGINVRMTDRAA
FGVGENIAVTPGSVVYENELIQLIQYTPTTEKTFKTPLLMVPPWINKYYI
LDLREDNSMVKWLVDQGHTVFLISWRNPGPEQRDITWADYMQMGPIS
AIEAIEQACGEKSVNLLSYCVGGTLTASTVAYLTSTRRGRKVKSVTYMA
TLQDFRDPGDIGVFLNERVVEGIEQTLEAKGYLDGRSMAYTFNLLREN
DLFWSFYINNYLKGETPAAFDLLYWNTDGTNLTAGTHAWYLRHMYLE
NRLVEPGGIELDGVKIDLRKVSAPSYFISTKEDHIAKWNSTYYGALLPK
GPVTFVLGGSGHIAGIVNPPHKNKYSYWTNDTLPESHEEWLAGATAQE
GSWWPHWQAWMTDNGYANSEKMVPVRQPGDGELNIIEPAPGRYVKM
TIPEVLGEIPSSS

>PhaC2_Poly(3-hydroxyalkanoate)_polymerase_subunit_PhaC
MIYDEAQHQNIDRLVRASLARLTLGISPASAMLTYLDWLSSLQLSPGTQ
AHLLQKATKKHLRLLIWASHSALDPDAKPCIAPLPQDRRFRDPAWRYFP
YNLLYQGFLLQQQWWHNATTGPRGLSPHHEQAVEFGARQWLDVFSPS
NFLLTNPTVLKKTFESAGGNLIQGLQHYCEDIQNHYLGKRSAGTEKYV
VGKNVAITPGKVIYRNHLVELIQYTPTTEEVHAAPMLIVPA

>PhaC3_ Poly(3-hydroxyalkanoate)_polymerase_subunit_PhaC
MKYYILDLSPHNSLVRYLVDHGHTVFMISWRNPTSEDCDIGMDDYRQQ
GIMASLDIIEHLFPSQKIHAVGYCLGGTLLAITASAMARNSDNRLASMT
LFAAQTDFREAGELMLFIDEKQLAFLEDLMWAQGILDTKQMSGVFQIL
RSNDLIWSRVVNEYLLGTRQPINDLLAWNADATRMPYRMHSEYLRNLF

LNNDLAEGRLRVDGRPIALSDIQIPIFCVGTEWDHVAPWRSTYRLHLIA
DAPEITFLLTSGGHNAGIISPPEQSHRHYRVATAFEGDSYIDPDTWLKRTA
IKPGSWWAAWQSWLATRSGSLIKAPDVGSQTYPPLEDAPGSYVRKA

The protein sequences potentially involved in the synthesis of bacterial cellulose are reported below.

>Glucans_biosynthesis_protein_G
MSGSTRLSKFSSCKGFFSVAVLGGLLVGSIPLEAFAFGFDDVARKAEELA
QQGYRAPETSLPDELRELSYMEYSQIQFKRDRDVWSGKGAPFTLSFIHE
GMHYDSAIQLNSVDQEGGVHGFAYNPDDFTYGDLGISDEVKNSDGIGI
AGVRINHALNEGDRKDEVMVFLGASYFRAIGEGQVYGLSGRGLAVDT
GLPSGEEFPRFKEIWIVEPGPESQYLTIFALLDSPSVTGAYRFVLRPGEDT
IVDVQSRLYLRRAVEKLGIAPLTSMYLYGPEQPSSTQHYIPAIHDSNGLLI
NDAQNGWLWRPLANPARLMMNRHATPQFRGYGLMQRGHNFSDYQDI
AARYDLRPSAWVEPQNEWGAGSVELIQIPTDNETNDNIVSMWLSDEPH
EPGTPLAFDYRITFTTNESRHLDPQLAWVEETRRSRGEVMRDNLVREPD
GTLAFVLDFIGPSLSGIGSDANMTVEASVGDNGELATSRVVHNPATNG
WRVFVNVKRNNGSQPLDIRAKLMLDGKQMSETWYYRLPANG

>Glucans_biosynthesis_glucosyltransferase_H
MAEMMSSSQATPTDIYLERLALETQNRKERYKLLVGDLDKHDMASLH
AALSEDSDGDGNWQRGDNSDPAALSVGRRLALAYAEPPLAPPDVLSTD
TSGITRLQTAPPMKRTPLAPQQWSTNPFVNIGRRFKRWANGDFRRRRRE
SPSASWKWVATRRRWVLLVLIFGQSIIAANQMRTVLPGQGLQWLEIAIL
SLFVLLFAWVSAGFWTALMGFFQLLRSHDRYAIDNEVGDEPIDDEARTA
LLVPICNEDVARVFAGVRATLESLRSTGNDRHFDIFVLSDTSDPDIAIQET
YAWLVLCRDLDAFGQVFYRRRQRRVKRKSGNLDDFCRRWGALYRYM

VVLDADSVMSGKCLTRLVQMMEVHSRVGIIQTAPRASGRLNLYARMQ
QFATRVYGPLFTAGLHFWQLGESHYWGHNAIIRLAPFMQHCILAPLPGK
GSMSGEILSHDFVEAALMRRAGWGVWIAYKLEGSFEEMPPNLLDELN
RDRRWCHGNLMNFRLFFSQGIHPVHRAVFLTGLMSYLSAPLWCLFLVL
STALLAVHTFSTPDYFPEPGMLFPVWPQWNPTLAVGLFGVTALLLFLPK
LLSVLLVWIQGSRQFGGPLKVLESMILESLFSMLLAPVRMLFHTRFVLT
SLMGWAVQWRSPSRENSDTTWGDAFRAHWSQTLIGAVWAAGVYYVME
PTFLWWLSPIVVALMLSIPVSALSSRVSLGWFCFQKRLFRIPEETQPPRVL
RRMVRLLSHMNTGMAAPSFAQMVVDPVPNALATALGTSRHTDAEPIR
QRRAERVARGVRMGPAAMSKLERLDFLDDPVMMSQLHYHVWEDSKA
HHSWFDCGLPGRESKHLPTFN

rDNA16S sequences annotated in PROKKA

>rDNA16S_complement_(200839..202366)
TGAAGAGTTTGATCATGGCTCAGATTGAACGCTGGCGGCAGGCCTA
ACACATGCAAGTCGAGCGGTAACAGATCTAGCTTGCTAGATGCTGA
CGAGCGGCGGACGGGTGAGTAATGCATAGGAATCTGCCCGATAGTG
GGGGATAACCTGGGGAAACCCAGGCTAATACCGCATACGTCCTACG
GGAGAAAGGGGGCTTCGGCTCCCGCTATTGGATGAGCCTATGTCGG
ATTAGCTAGTTGGTAAGGTAATGGCTTACCAAGGCAACGATCCGTA
GCTGGTCTGAGAGGATGATCAGCCACATCGGGACTGAGACACGGCC
CGAACTCCTACGGGAGGCAGCAGTGGGGAATATTGGACAATGGGG
GCAACCCTGATCCAGCCATGCCGCGTGTGTGAAGAAGGCCCTCGGG
TTGTAAAGCACTTTCAGCGAGGAAGAACGCCTATCGGTTAATACCC
GTTAGGAAAGACATCACTCGCAGAAGAAGCACCGGCTAACTCCGTG
CCAGCAGCCGCGGTAATACGGAGGGTGCAAGCGTTAATCGGAATTA

CTGGGCGTAAAGCGCGCGTAGGTGGCTTGATAAGCCGGTTGTGAAA
GCCCCGGGCTCAACCTGGGAACGGCATCCGGAACTGTCAGGCTAGA
GTGCAGGAGAGGAAGGTAGAATTCCCGGTGTAGCGGTGAAATGCGT
AGAGATCGGGAGGAATACCAGTGGCGAAGGCGGCCTTCTGGACTG
ACACTGACACTGAGGTGCGAAAGCGTGGGTAGCAAACAGGATTAG
ATACCCTGGTAGTCCACGCCGTAAACGATGTCGACCAGCCGTTGGG
TGCCTAGAGCACTTTGTGGCGAAGTTAACGCGATAAGTCGACCGCC
TGGGGAGTACGGCCGCAAGGTTAAAACTCAAATGAATTGACGGGG
GCCCGCACAAGCGGTGGAGCATGTGGTTTAATTCGATGCAACGCGA
AGAACCTTACCTACCCTTGACATCTACAGAAGCCGGAAGAGATTCT
GGTGTGCCTTCGGGAACTGTAAGACAGGTGCTGCATGGCTGTCGTC
AGCTCGTGTTGTGAAATGTTGGGTTAAGTCCCGTAACGAGCGCAAC
CCTTGTCCTTATTTGCCAGCGAGTAATGTCGGGAACTCTAAGGAGA
CTGCCGGTGACAAACCGGAGGAAGGTGGGGACGACGTCAAGTCAT
CATGGCCCTTACGGGTAGGGCTACACACGTGCTACAATGGCCGGTA
CAAAGGGCTGCGAGCTCGCGAGAGTCAGCGAATCCCTTAAAGCCGG
TCTCAGTCCGGATCGGAGTCTGCAACTCGACTCCGTGAAGTCGGAA
TCGCTAGTAATCGTGAATCAGAATGTCACGGTGAATACGTTCCCGG
GCCTTGTACACACCGCCCGTCACACCATGGGAGTGGACTGCACCAG
AAGTGGTTAGCCTAACGCAAGAGGGCGATCACCACGGTGTGGTTCA
TGACTGGGGTGAAGTCGTAACAAGGTAGCCGTAGGGGAACCTGCG
GCTGGATCACCTCCTT

>rDNA16S_complement(237470..238997)
TGAAGAGTTTGATCATGGCTCAGATTGAACGCTGGCGGCAGGCCTA
ACACATGCAAGTCGAGCGGTAACAGGGGTAGCTTGCTACCCGCTGA

CGAGCGGCGGACGGGTGAGTAATGCATAGGAATCTGCCCGATAGTG
GGGGATAACCTGGGGAAACCCAGGCTAATACCGCATACGTCCTACG
GGAGAAAGGGGGCTCCGGCTCCCGCTATTGGATGAGCCTATGTCGG
ATTAGCTAGTTGGTAAGGTAATGGCTTACCAAGGCAACGATCCGTA
GCTGGTCTGAGAGGATGATCAGCCACATCGGGACTGAGACACGGCC
CGAACTCCTACGGGAGGCAGCAGTGGGGAATATTGGACAATGGGG
GCAACCCTGATCCAGCCATGCCGCGTGTGTGAAGAAGGCCCTCGGG
TTGTAAAGCACTTTCAGCGAGGAAGAACGCCTATCGGTTAATACCC
GTTAGGAAAGACATCACTCGCAGAAGAAGCACCGGCTAACTCCGTG
CCAGCAGCCGCGGTAATACGGAGGGTGCAAGCGTTAATCGGAATTA
CTGGGCGTAAAGCGCGCGTAGGTGGCTTGATAAGCCGGTTGTGAAA
GCCCCGGGCTCAACCTGGGAACGGCATCCGGAACTGTCAGGCTAGA
GTGCAGGAGAGGAAGGTAGAATTCCCGGTGTAGCGGTGAAATGCGT
AGAGATCGGGAGGAATACCAGTGGCGAAGGCGGCCTTCTGGACTG
ACACTGACACTGAGGTGCGAAAGCGTGGGTAGCAAACAGGATTAG
ATACCCTGGTAGTCCACGCCGTAAACGATGTCGACCAGCCGTTGGG
TGCCTAGAGCACTTTGTGGCGAAGTTAACGCGATAAGTCGACCGCC
TGGGGAGTACGGCCGCAAGGTTAAAACTCAAATGAATTGACGGGG
GCCCGCACAAGCGGTGGAGCATGTGGTTTAATTCGATGCAACGCGA
AGAACCTTACCTACCCTTGACATCTACAGAAGCCGGAAGAGATTCT
GGTGTGCCTTCGGGAACTGTAAGACAGGTGCTGCATGGCTGTCGTC
AGCTCGTGTTGTGAAATGTTGGGTTAAGTCCCGTAACGAGCGCAAC
CCTTGTCCTTATTTGCCAGCGAGTAATGTCGGGAACTCTAAGGAGA
CTGCCGGTGACAAACCGGAGGAAGGTGGGGACGACGTCAAGTCAT
CATGGCCCTTACGGGTAGGGCTACACACGTGCTACAATGGCCGGTA
CAAAGGGCTGCGAGCTCGCGAGAGTCAGCGAATCCCTTAAAGCCGG

TCTCAGTCCGGATCGGAGTCTGCAACTCGACTCCGTGAAGTCGGAA
TCGCTAGTAATCGTGAATCAGAATGTCACGGTGAATACGTTCCCGG
GCCTTGTACACACCGCCCGTCACACCATGGGAGTGGACTGCACCAG
AAGTGGTTAGCCTAACGCAAGAGGGCGATCACCACGGTGTGGTTCA
TGACTGGGGTGAAGTCGTAACAAGGTAGCCGTAGGGGAACCTGCG
GCTGGATCACCTCCTT

>rDNA16S_1403092..1404619

TGAAGAGTTTGATCATGGCTCAGATTGAACGCTGGCGGCAGGCCTA
ACACATGCAAGTCGAGCGGTAACAGGGGTAGCTTGCTACCCGCTGA
CGAGCGGCGGACGGGTGAGTAATGCATAGGAATCTGCCCGATAGTG
GGGGATAACCTGGGGAAACCCAGGCTAATACCGCATACGTCCTACG
GGAGAAAGGGGGCTTCGGCTCCCGCTATTGGATGAGCCTATGTCGG
ATTAGCTAGTTGGTAAGGTAATGGCTTACCAAGGCAACGATCCGTA
GCTGGTCTGAGAGGATGATCAGCCACATCGGGACTGAGACACGGCC
CGAACTCCTACGGGAGGCAGCAGTGGGGAATATTGGACAATGGGG
GCAACCCTGATCCAGCCATGCCGCGTGTGTGAAGAAGGCCCTCGGG
TTGTAAAGCACTTTCAGCGAGGAAGAACGCCTATCGGTTAATACCC
GGTAGGAAAGACATCACTCGCAGAAGAAGCACCGGCTAACTCCGT
GCCAGCAGCCGCGGTAATACGGAGGGTGCAAGCGTTAATCGGAATT
ACTGGGCGTAAAGCGCGCGTAGGTGGCTTGATAAGCCGGTTGTGAA
AGCCCCGGGCTCAACCTGGGAACGGCATCCGGAACTGTCAGGCTAG
AGTGCAGGAGAGGAAGGTAGAATTCCCGGTGTAGCGGTGAAATGC
GTAGAGATCGGGAGGAATACCAGTGGCGAAGGCGGCCTTCTGGACT
GACACTGACACTGAGGTGCGAAAGCGTGGGTAGCAAACAGGATTA
GATACCCTGGTAGTCCACGCCGTAAACGATGTCGACCAGCCGTTGG

GTGCCTAGAGCACTTTGTGGCGAAGTTAACGCGATAAGTCGACCGC
CTGGGGAGTACGGCCGCAAGGTTAAAACTCAAATGAATTGACGGG
GGCCCGCACAAGCGGTGGAGCATGTGGTTTAATTCGATGCAACGCG
AAGAACCTTACCTACCCTTGACATCTACAGAAGCCGGAAGAGATTC
TGGTGTGCCTTCGGGAACTGTAAGACAGGTGCTGCATGGCTGTCGT
CAGCTCGTGTTGTGAAATGTTGGGTTAAGTCCCGTAACGAGCGCAA
CCCTTGTCCTTATTTGCCAGCGAGTAATGTCGGGAACTCTAAGGAG
ACTGCCGGTGACAAACCGGAGGAAGGTGGGGACGACGTCAAGTCA
TCATGGCCCTTACGGGTAGGGCTACACACGTGCTACAATGGCCGGT
ACAAAGGGCTGCGAGCTCGCGAGAGTCAGCGAATCCCTTAAAGCCG
GTCTCAGTCCGGATCGGAGTCTGCAACTCGACTCCGTGAAGTCGGA
ATCGCTAGTAATCGTGAATCAGAATGTCACGGTGAATACGTTCCCG
GGCCTTGTACACACCGCCCGTCACACCATGGGAGTGGACTGCACCA
GAAGTGGTTAGCCTAACGCAAGAGGGCGATCACCACGGTGTGGTTC
ATGACTGGGGTGAAGTCGTAACAAGGTAGCCGTAGGGGAACCTGC
GGCTGGATCACCTCCTT

>rDNA16S_2314791..2316318
TGAAGAGTTTGATCATGGCTCAGATTGAACGCTGGCGGCAGGCCTA
ACACATGCAAGTCGAGCGGTAACAGGGGTAGCTTGCTACCCGCTGA
CGAGCGGCGGACGGGTGAGTAATGCATAGGAATCTGCCCGATAGTG
GGGGATAACCTGGGGAAACCCAGGCTAATACCGCATACGTCCTACG
GGAGAAAGGGGGCTTCGGCTCCCGCTATTGGATGAGCCTATGTCGG
ATTAGCTAGTTGGTAAGGTAATGGCTTACCAAGGCAACGATCCGTA
GCTGGTCTGAGAGGATGATCAGCCACATCGGGACTGAGACACGGCC
CGAACTCCTACGGGAGGCAGCAGTGGGGAATATTGGACAATGGGG

GCAACCCTGATCCAGCCATGCCGCGTGTGTGAAGAAGGCCCTCGGG
TTGTAAAGCACTTTCAGCGAGGAAGAACGCCTATCGGTTAATACCC
GGTAGGAAAGACATCACTCGCAGAAGAAGCACCGGCTAACTCCGT
GCCAGCAGCCGCGGTAATACGGAGGGTGCAAGCGTTAATCGGAATT
ACTGGGCGTAAAGCGCGCGTAGGTGGCTTGATAAGCCGGTTGTGAA
AGCCCCGGGCTCAACCTGGGAACGGCATCCGGAACTGTCAGGCTAG
AGTGCAGGAGAGGAAGGTAGAATTCCCGGTGTAGCGGTGAAATGC
GTAGAGATCGGGAGGAATACCAGTGGCGAAGGCGGCCTTCTGGACT
GACACTGACACTGAGGTGCGAAAGCGTGGGTAGCAAACAGGATTA
GATACCCTGGTAGTCCACGCCGTAAACGATGTCGACCAGCCGTTGG
GTGCCTAGAGCACTTTGTGGCGAAGTTAACGCGATAAGTCGACCGC
CTGGGGAGTACGGCCGCAAGGTTAAAACTCAAATGAATTGACGGG
GGCCCGCACAAGCGGTGGAGCATGTGGTTTAATTCGATGCAACGCG
AAGAACCTTACCTACCCTTGACATCTACAGAAGCCGGAAGAGATTC
TGGTGTGCCTTCGGGAACTGTAAGACAGGTGCTGCATGGCTGTCGT
CAGCTCGTGTTGTGAAATGTTGGGTTAAGTCCCGTAACGAGCGCAA
CCCTTGTCCTTATTTGCCAGCGAGTAATGTCGGGAACTCTAAGGAG
ACTGCCGGTGACAAACCGGAGGAAGGTGGGGACGACGTCAAGTCA
TCATGGCCCTTACGGGTAGGGCTACACACGTGCTACAATGGCCGGT
ACAAAGGGCTGCGAGCTCGCGAGAGTCAGCGAATCCCTTAAAGCCG
GTCTCAGTCCGGATCGGAGTCTGCAACTCGACTCCGTGAAGTCGGA
ATCGCTAGTAATCGTGAATCAGAATGTCACGGTGAATACGTTCCCG
GGCCTTGTACACACCGCCCGTCACACCATGGGAGTGGACTGCACCA
GAAGTGGTTAGCCTAACGCAAGAGGGCGATCACCACGGTGTGGTTC
ATGACTGGGGTGAAGTCGTAACAAGGTAGCCGTAGGGGAACCTGC
GGCTGGATCACCTCCTT

>rDNA16S_2708522..2710049

TGAAGAGTTTGATCATGGCTCAGATTGAACGCTGGCGGCAGGCCTA
ACACATGCAAGTCGAGCGGTAACAGGGGTAGCTTGCTACCCGCTGA
CGAGCGGCGGACGGGTGAGTAATGCATAGGAATCTGCCCGATAGTG
GGGGATAACCTGGGGAAACCCAGGCTAATACCGCATACGTCCTACG
GGAGAAAGGGGGCTCCGGCTCCCGCTATTGGATGAGCCTATGTCGG
ATTAGCTAGTTGGTAAGGTAATGGCTTACCAAGGCAACGATCCGTA
GCTGGTCTGAGAGGATGATCAGCCACATCGGGACTGAGACACGGCC
CGAACTCCTACGGGAGGCAGCAGTGGGGAATATTGGACAATGGGG
GCAACCCTGATCCAGCCATGCCGCGTGTGTGAAGAAGGCCCTCGGG
TTGTAAAGCACTTTCAGCGAGGAAGAACGCCTATCGGTTAATACCC
GTTAGGAAAGACATCACTCGCAGAAGAAGCACCGGCTAACTCCGTG
CCAGCAGCCGCGGTAATACGGAGGGTGCAAGCGTTAATCGGAATTA
CTGGGCGTAAAGCGCGCGTAGGTGGCTTGATAAGCCGGTTGTGAAA
GCCCCGGGCTCAACCTGGGAACGGCATCCGGAACTGTCAGGCTAGA
GTGCAGGAGAGGAAGGTAGAATTCCCGGTGTAGCGGTGAAATGCGT
AGAGATCGGGAGGAATACCAGTGGCGAAGGCGGCCTTCTGGACTG
ACACTGACACTGAGGTGCGAAAGCGTGGGTAGCAAACAGGATTAG
ATACCCTGGTAGTCCACGCCGTAAACGATGTCGACCAGCCGTTGGG
TGCCTAGAGCACTTTGTGGCGAAGTTAACGCGATAAGTCGACCGCC
TGGGGAGTACGGCCGCAAGGTTAAAACTCAAATGAATTGACGGGG
GCCCGCACAAGCGGTGGAGCATGTGGTTTAATTCGATGCAACGCGA
AGAACCTTACCTACCCTTGACATCTACAGAAGCCGGAAGAGATTCT
GGTGTGCCTTCGGGAACTGTAAGACAGGTGCTGCATGGCTGTCGTC
AGCTCGTGTTGTGAAATGTTGGGTTAAGTCCCGTAACGAGCGCAAC
CCTTGTCCTTATTTGCCAGCGAGTAATGTCGGGAACTCTAAGGAGA

CTGCCGGTGACAAACCGGAGGAAGGTGGGGACGACGTCAAGTCAT
CATGGCCCTTACGGGTAGGGCTACACACGTGCTACAATGGCCGGTA
CAAAGGGCTGCGAGCTCGCGAGAGTCAGCGAATCCCTTAAAGCCGG
TCTCAGTCCGGATCGGAGTCTGCAACTCGACTCCGTGAAGTCGGAA
TCGCTAGTAATCGTGAATCAGAATGTCACGGTGAATACGTTCCCGG
GCCTTGTACACACCGCCCGTCACACCATGGGAGTGGACTGCACCAG
AAGTGGTTAGCCTAACGCAAGAGGGCGATCACCACGGTGTGGTTCA
TGACTGGGGTGAAGTCGTAACAAGGTAGCCGTAGGGGAACCTGCG
GCTGGATCACCTCCTT

>rDNA16S_complement_(5083810..5085337)
TGAAGAGTTTGATCATGGCTCAGATTGAACGCTGGCGGCAGGCCTA
ACACATGCAAGTCGAGCGGTAACAGGGGTAGCTTGCTACCCGCTGA
CGAGCGGCGGACGGGTGAGTAATGCATAGGAATCTGCCCGATAGTG
GGGGATAACCTGGGGAAACCCAGGCTAATACCGCATACGTCCTACG
GGAGAAAGGGGGCTTCGGCTCCCGCTATTGGATGAGCCTATGTCGG
ATTAGCTAGTTGGTAAGGTAATGGCTTACCAAGGCAACGATCCGTA
GCTGGTCTGAGAGGATGATCAGCCACATCGGGACTGAGACACGGCC
CGAACTCCTACGGGAGGCAGCAGTGGGGAATATTGGACAATGGGG
GCAACCCTGATCCAGCCATGCCGCGTGTGTGAAGAAGGCCCTCGGG
TTGTAAAGCACTTTCAGCGAGGAAGAACGCCTATCGGTTAATACCC
GGTAGGAAAGACATCACTCGCAGAAGAAGCACCGGCTAACTCCGT
GCCAGCAGCCGCGGTAATACGGAGGGTGCAAGCGTTAATCGGAATT
ACTGGGCGTAAAGCGCGCGTAGGTGGCTTGATAAGCCGGTTGTGAA
AGCCCCGGGCTCAACCTGGGAACGGCATCCGGAACTGTCAGGCTAG
AGTGCAGGAGAGGAAGGTAGAATTCCCGGTGTAGCGGTGAAATGC

GTAGAGATCGGGAGGAATACCAGTGGCGAAGGCGGCCTTCTGGACT
GACACTGACACTGAGGTGCGAAAGCGTGGGTAGCAAACAGGATTA
GATACCCTGGTAGTCCACGCCGTAAACGATGTCGACCAGCCGTTGG
GTGCCTAGAGCACTTTGTGGCGAAGTTAACGCGATAAGTCGACCGC
CTGGGGAGTACGGCCGCAAGGTTAAAACTCAAATGAATTGACGGG
GGCCCGCACAAGCGGTGGAGCATGTGGTTTAATTCGATGCAACGCG
AAGAACCTTACCTACCCTTGACATCTACAGAAGCCGGAAGAGATTC
TGGTGTGCCTTCGGGAACTGTAAGACAGGTGCTGCATGGCTGTCGT
CAGCTCGTGTTGTGAAATGTTGGGTTAAGTCCCGTAACGAGCGCAA
CCCTTGTCCTTATTTGCCAGCGAGTAATGTCGGGAACTCTAAGGAG
ACTGCCGGTGACAAACCGGAGGAAGGTGGGGACGACGTCAAGTCA
TCATGGCCCTTACGGGTAGGGCTACACACGTGCTACAATGGCCGGT
ACAAAGGGCTGCGAGCTCGCGAGAGTCAGCGAATCCCTTAAAGCCG
GTCTCAGTCCGGATCGGAGTCTGCAACTCGACTCCGTGAAGTCGGA
ATCGCTAGTAATCGTGAATCAGAATGTCACGGTGAATACGTTCCCG
GGCCTTGTACACACCGCCCGTCACACCATGGGAGTGGACTGCACCA
GAAGTGGTTAGCCTAACGCAAGAGGGCGATCACCACGGTGTGGTTC
ATGACTGGGGTGAAGTCGTAACAAGGTAGCCGTAGGGGAACCTGC
GGCTGGATCACCTCCTT